CARDIAC FIBROSIS, FROM LINEAGE TRACING TO THERAPEUTIC APPLICATION

EDITED BY: Gianluigi Pironti, Claudio de Lucia, Markus Wallner and Domenico Corradi
PUBLISHED IN: Frontiers in Physiology and Frontiers in Pharmacology

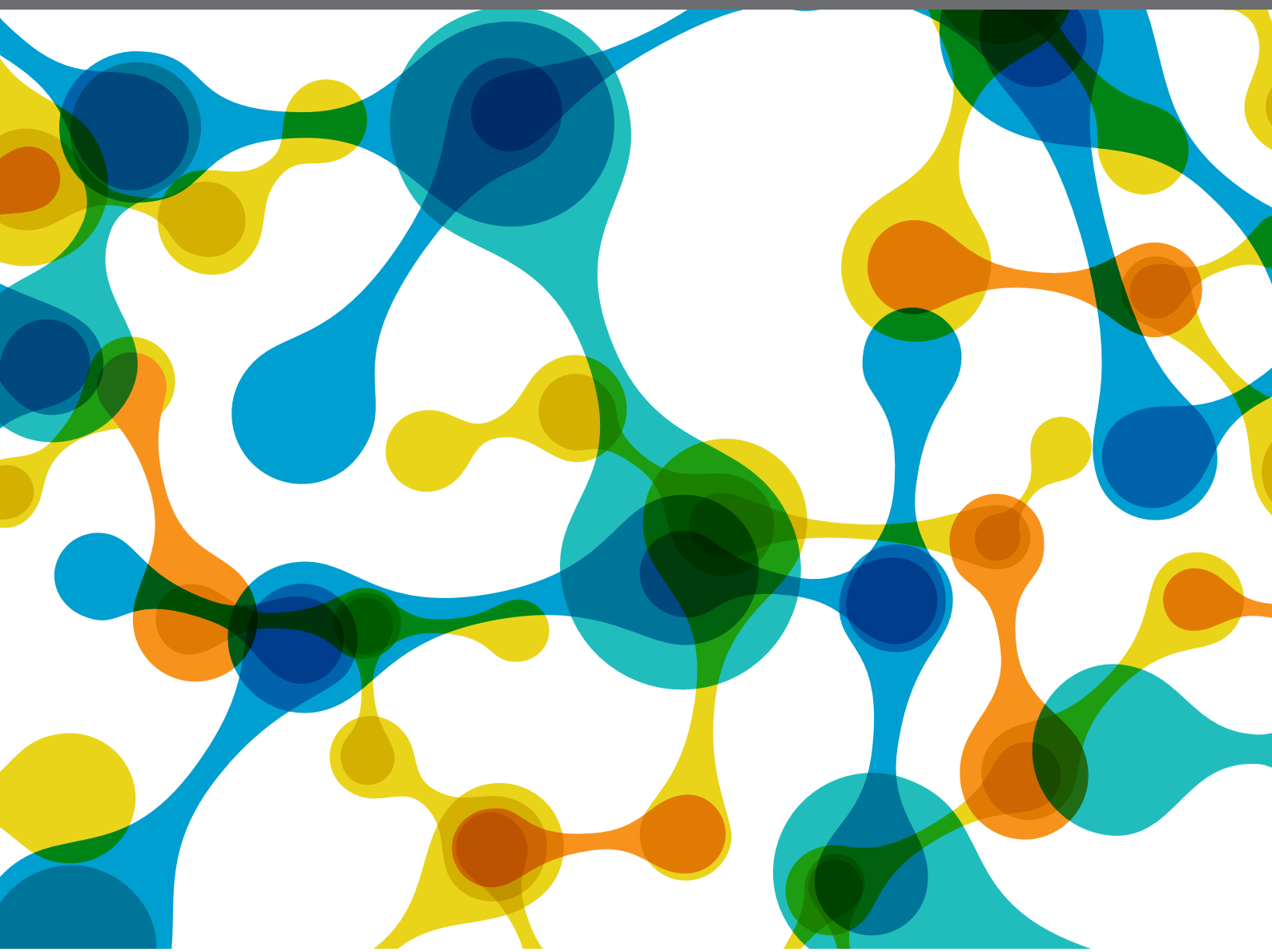

frontiers Research Topics

frontiers

ISSN 1664-8714
ISBN 978-2-88966-526-6
DOI 10.3389/978-2-88966-526-6

About Frontiers

Frontiers is more than just an open-access publisher of scholarly articles: it is a pioneering approach to the world of academia, radically improving the way scholarly research is managed. The grand vision of Frontiers is a world where all people have an equal opportunity to seek, share and generate knowledge. Frontiers provides immediate and permanent online open access to all its publications, but this alone is not enough to realize our grand goals.

Frontiers Journal Series

The Frontiers Journal Series is a multi-tier and interdisciplinary set of open-access, online journals, promising a paradigm shift from the current review, selection and dissemination processes in academic publishing. All Frontiers journals are driven by researchers for researchers; therefore, they constitute a service to the scholarly community. At the same time, the Frontiers Journal Series operates on a revolutionary invention, the tiered publishing system, initially addressing specific communities of scholars, and gradually climbing up to broader public understanding, thus serving the interests of the lay society, too.

Dedication to Quality

Each Frontiers article is a landmark of the highest quality, thanks to genuinely collaborative interactions between authors and review editors, who include some of the world's best academicians. Research must be certified by peers before entering a stream of knowledge that may eventually reach the public - and shape society; therefore, Frontiers only applies the most rigorous and unbiased reviews.
Frontiers revolutionizes research publishing by freely delivering the most outstanding research, evaluated with no bias from both the academic and social point of view. By applying the most advanced information technologies, Frontiers is catapulting scholarly publishing into a new generation.

What are Frontiers Research Topics?

Frontiers Research Topics are very popular trademarks of the Frontiers Journals Series: they are collections of at least ten articles, all centered on a particular subject. With their unique mix of varied contributions from Original Research to Review Articles, Frontiers Research Topics unify the most influential researchers, the latest key findings and historical advances in a hot research area! Find out more on how to host your own Frontiers Research Topic or contribute to one as an author by contacting the Frontiers Editorial Office: frontiersin.org/about/contact

CARDIAC FIBROSIS, FROM LINEAGE TRACING TO THERAPEUTIC APPLICATION

Topic Editors:
Gianluigi Pironti, Karolinska Institutet (KI), Sweden
Claudio de Lucia, Temple University, United States
Markus Wallner, Medical University of Graz, Austria
Domenico Corradi, University of Parma, Italy

Citation: Pironti, G., de Lucia, C., Wallner, M., Corradi, D., eds. (2021). Cardiac Fibrosis, from Lineage Tracing to Therapeutic Application. Lausanne: Frontiers Media SA. doi: 10.3389/978-2-88966-526-6

Table of Contents

04 ***Editorial: Cardiac Fibrosis, From Lineage Tracing to Therapeutic Application***
Claudio de Lucia, Markus Wallner, Domenico Corradi and Gianluigi Pironti

08 ***Choline Attenuates Cardiac Fibrosis by Inhibiting p38MAPK Signaling Possibly by Acting on M_3 Muscarinic Acetylcholine Receptor***
Lihui Zhao, Tingting Chen, Pengzhou Hang, Wen Li, Jing Guo, Yang Pan, Jingjing Du, Yuyang Zheng and Zhimin Du

20 ***Elevated β1-Adrenergic Receptor Autoantibody Levels Increase Atrial Fibrillation Susceptibility by Promoting Atrial Fibrosis***
Luxiang Shang, Ling Zhang, Mengjiao Shao, Min Feng, Jia Shi, Zhenyu Dong, Qilong Guo, Jiasuoer Xiaokereti, Ran Xiang, Huaxin Sun, Xianhui Zhou and Baopeng Tang

33 ***Icariin Ameliorates Diabetic Cardiomyopathy Through Apelin/Sirt3 Signalling to Improve Mitochondrial Dysfunction***
Tingjuan Ni, Na Lin, Xingxiao Huang, Wenqiang Lu, Zhenzhu Sun, Jie Zhang, Hui Lin, Jufang Chi and Hangyuan Guo

43 ***The Role of Membrane Capacitance in Cardiac Impulse Conduction: An Optogenetic Study With Non-excitable Cells Coupled to Cardiomyocytes***
Stefano Andrea De Simone, Sarah Moyle, Andrea Buccarello, Christian Dellenbach, Jan Pavel Kucera and Stephan Rohr

59 ***Leukocyte-Dependent Regulation of Cardiac Fibrosis***
Ama Dedo Okyere and Douglas G. Tilley

72 ***Isoproterenol Increases Left Atrial Fibrosis and Susceptibility to Atrial Fibrillation by Inducing Atrial Ischemic Infarction in Rats***
Shiyu Ma, Jin Ma, Qingqiang Tu, Chaoyang Zheng, Qiuxiong Chen and Weihui Lv

83 ***Minimal Invasive Pericardial Perfusion Model in Swine: A Translational Model for Cardiac Remodeling After Ischemia/Reperfusion Injury***
Stefanie Marek-Iannucci, Amandine Thomas and Roberta A. Gottlieb

91 ***Cardiac Fibrosis and Cardiac Fibroblast Lineage-Tracing: Recent Advances***
Xing Fu, Qianglin Liu, Chaoyang Li, Yuxia Li and Leshan Wang

105 ***PTX3 Predicts Myocardial Damage and Fibrosis in Duchenne Muscular Dystrophy***
Andrea Farini, Chiara Villa, Dario Di Silvestre, Pamela Bella, Luana Tripodi, Rossana Rossi, Clementina Sitzia, Stefano Gatti, Pierluigi Mauri and Yvan Torrente

120 ***Extracellular Vesicles as Therapeutic Agents for Cardiac Fibrosis***
Russell G. Rogers, Alessandra Ciullo, Eduardo Marbán and Ahmed G. Ibrahim

130 ***Notch3 Modulates Cardiac Fibroblast Proliferation, Apoptosis, and Fibroblast to Myofibroblast Transition via Negative Regulation of the RhoA/ROCK/Hif1α Axis***
Jianli Shi, Peilin Xiao, Xiaoli Liu, Yunlin Chen, Yanping Xu, Jinqi Fan and Yuehui Yin

143 ***The Dynamic Interplay Between Cardiac Inflammation and Fibrosis***
Toby P. Thomas and Laurel A. Grisanti

frontiers in Physiology

EDITORIAL
published: 20 January 2021
doi: 10.3389/fphys.2020.641771

Editorial: Cardiac Fibrosis, From Lineage Tracing to Therapeutic Application

Claudio de Lucia[1], *Markus Wallner*[2,3,4], *Domenico Corradi*[5] *and Gianluigi Pironti*[6]*

[1] Center for Translational Medicine, Temple University, Philadelphia, PA, United States, [2] Division of Cardiology, Medical University of Graz, Graz, Austria, [3] Cardiovascular Research Center, Temple University, Philadelphia, PA, United States, [4] Center for Biomarker Research in Medicine, CBmed GmbH, Graz, Austria, [5] Unit of Pathology, Department of Medicine and Surgery, University of Parma, Parma, Italy, [6] Cardiology Research Unit, Department of Medicine, Karolinska Institute Stockholm, Solna, Sweden

Keywords: cardiac fibrosis, myofibroblast, cardiac fibroblast, reparative fibrosis, reactive fibrosis, anti-fibrotic therapy, lineage tracing

Editorial on the Research Topic

Cardiac Fibrosis, From Lineage Tracing to Therapeutic Application

WHAT IS CARDIAC FIBROSIS?

Roughly 6% of healthy myocardium is composed of pure extracellular matrix (ECM) such as collagen fibers and, to a lesser extent, elastic fibers. This interstitial extracellular mixture—mainly synthesized by fibroblast and myofibroblasts—creates a three-dimensional cardiac skeleton which allows the cardiomyocytes to perform their contractile functions (Ten Tusscher and Panfilov, 2007). An excessive deposition of collagen fibers in the myocardium is commonly referred to as "fibrosis," which is regulated by ECM production, activity of matrix metalloproteinases (MMPs) and their endogenous inhibitors (TIMPs) (De Boer et al., 2019; Frangogiannis, 2019). Various subsets of leukocytes play an important modulatory role determining the characteristics of the fibrotic response and cardiac remodeling post-injury (Frangogiannis, 2019). Disproportionate amounts of ECM (either focal or diffuse, scar-like, thin around single or small groups of muscle cells) represents an interstitial encumbrance which may lower myocardial compliance, decrease ventricular filling, interfere with electrical coupling, predispose to rhythm disturbances and ultimately lead to depressed cardiac function (Sharma and Kass, 2014; Nattel, 2017). Schematically, fibrosis may be secondary to two different—but not mutually exclusive—pathogenic mechanisms: (1). "reparative" fibrosis which replaces myocardial areas where cardiomyocytes have undergone cell death (i.e., ischemic events); and/or (2). "reactive" fibrosis which is driven by a series of stimuli (e.g., pressure overload, inflammation, metabolic dysfunction, aging) and mediators (e.g., AngII, PDGF, TGF-β, and CTGF) (Hanna et al., 2004; Corradi et al., 2008; De Boer et al., 2019; Frangogiannis, 2019) (**Figure 1**).

WHICH CELL IS TO BLAME?

The process of cardiac fibrosis can be schematically divided into three phases based on the cell type mainly involved: (i) resident quiescent cardiac fibroblasts inhabit myocardial tissue; (ii) during myocardial injury (MI), fibroblasts differentiate into myofibroblasts, which actively proliferate and secrete ECM until the injury is resolved; (iii) finally the site of injury is populated by not proliferative and terminally differentiated matrifibrocytes secreting ECM in order to maintain the integrity of the scar (Eschenhagen, 2018; Fu et al., 2018) (**Figure 1**).

OPEN ACCESS

Edited and reviewed by:
Geoffrey A. Head, Baker Heart and Diabetes Institute, Australia

***Correspondence:**
Gianluigi Pironti
gianluigi.pironti@ki.se
orcid.org/0000-0001-9401-3029

Specialty section:
This article was submitted to Integrative Physiology, a section of the journal Frontiers in Physiology

Received: *14 December 2020*
Accepted: *22 December 2020*
Published: *20 January 2021*

Citation:
de Lucia C, Wallner M, Corradi D and Pironti G (2021) Editorial: Cardiac Fibrosis, From Lineage Tracing to Therapeutic Application. Front. Physiol. 11:641771. doi: 10.3389/fphys.2020.641771

Fu et al. described state-of-the-art techniques to trace the lineage of fibrogenic cells following cardiac injury, providing tools to specifically trace the different stages of cardiac fibrosis. Although the high grade of plasticity makes the lineage tracing of cardiac fibroblasts quite challenging, some biomarkers are known to uniquely identify fibroblasts (i.e., Tcf21), activated myofibroblasts (i.e., Periostin), and matrifibrocytes (i.e., ACTA2) (Fu et al., 2018). In terms of cellular signaling the activation of TGF-β receptor Smad2-3 pathway seems to be the principal mediator of myofibroblast activation and ECM accumulation.

Shi et al. demonstrated that Notch3 is involved in the regulation of cardiac fibrosis influencing fibroblast proliferation and myofibroblast transition/apoptosis via RhoA/ROCK/Hif1-α signaling pathway inhibition.

Ni et al. discovered that diabetic cardiomyopathy might benefit from icariin (a flavonoid monomer isolated from the herb Epimedium) treatment, which reduced cardiac fibrosis and ameliorated cardiomyocytes mitochondrial function through Apelin/Sirt3 pathway. Zhao et al. described how muscarinic acetylcholine receptor 3 (M3R) signaling after choline activation represents another important axes that controls cardiac fibrosis through TGF-β1/Smad2-3/p38 MAPK pathway.

Thomas and Grisanti reviewed the extensive crosstalk between inflammation and cardiac fibrosis contributing to the progression of heart failure (HF). Following myocardial injury and cardiomyocytes death, local inflammatory cells (i.e., mast cells, B and T cells and macrophages) infiltrate the site of injury and secrete pro-inflammatory mediators (i.e., TNF-α, IL-1-β, IL-6), which play an important regulatory role in the transition from quiescent resident fibroblasts into active and proliferative myofibroblasts, initiating the production of ECM components. Narrowing the focus to one specific mediator in the crosstalk between the inflammatory response and development of fibrosis, Okyere and Tilley described the role of leukocytes in the regulation of cardiac remodeling. Both innate and adaptive leukocytes critically influence pathological fibrotic remodeling.

Interestingly, cardiac fibrosis is regulated over an organized intercellular communication, where extracellular vehicles (EVs) play a crucial role. The interplay among macrophages, fibroblasts, and endothelial cells represents a major driving force of myocardial fibrosis. Rogers et al. described a cell-free therapeutic application based on EVs secreted from stem/progenitor cells that can directly stimulate the trans-differentiation of pro-inflammatory M1 macrophages to anti-inflammatory M2 macrophages(Silva et al., 2017), thereby reducing fibrosis in preclinical models of heart failure.

Marek-Iannucci et al. established a minimally invasive and cost-effective model of cooling pericardial perfusion in swine, which highlights the potential therapeutic effects of hypothermia post-ischemia/reperfusion injury in reducing cardiac fibrosis, inflammation and immune cell recruitment.

Abbreviations: TIMPs, tissue inhibitors of metalloproteases; AngII, Angiotensin type II; PDGF, Platelet derived grow factor; TGF-β, Transforming grow factor β; CTGF, connective tissue grow factor; TNF-α, Tumor necrosis factor α; IL-1-β, Interleukin 1 β; IL-6, Interleukin 6; Tcf21, transcription factor 21; Acta2, smooth muscle actin alpha 2.

Farini et al. showed that cardiac expression of the inflammatory mediator Pentraxin 3 (PTX3) influences inflammatory/fibrotic pathways in an animal model of Duchenne Muscular Dystrophy and may be an interesting therapeutic target.

WHEN IS THE RIGHT TIME TO BLOCK FIBROSIS?

Degradation of large areas of replacement fibrosis could be catastrophic unless accompanied by robust cardiac regeneration, due to the negligible endogenous regenerative potential of the adult heart. Upon cardiac injury, the compensatory but maladaptive fibrotic response mediated by cardiac fibroblast can vary significantly among different injury types (Khalil et al., 2019). While the beneficial effect of fibrotic tissue may outweigh its deleterious effect after an acute injury that causes massive cardiomyocyte death (i.e., reparative fibrosis in a myocardial infarction), the effects of reactive interstitial fibrosis in chronic conditions may be largely detrimental. The timing is of utmost importance since a too early intervention can cause adverse effects on wound healing, enhancing LV rupture and increasing the mortality rate in HF patients. Based on this, any medical and surgical treatment should be aimed at blocking/mitigating the excessive ECM deposition between single cardiomyocytes and/or the fine interstitial fibrosis around scar-like sclerotic areas replacing significant cardiomyocytes necrotic cell losses.

Ma et al. described a preclinical model of left atria (LA) fibrosis with increased arrhythmogenesis following isoproterenol (ISO) injections for 5 weeks in rats. The anti-fibrotic and anti-inflammatory agent pirfenidone administered 1 week after completion of ISO decreased LA fibrosis and arrhythmia leading to an improvement in cardiac function.

De Simone et al. showed that cardiac myofibroblast are not excitable cells, electronically coupled to cardiomyocytes and their function is not limited solely to ECM production and protecting the architecture of the heart, but is also important for regulating the cardiac electrical conduction. After excessive collagen deposition, only scarce cellular structures populate the sclerotic area, which likely is not capable of creating electrically efficient fibroblast/cardiomyocyte couplings and causing arrhythmogenesis(Callegari et al., 2020).

Shang et al. presented preclinical and clinical evidences linking together elevated levels of β1AR autoantibodies, circulating fibrosis markers and atrial remodeling in patients with paroxysmal atrial fibrillation (AF). Overexpressing β1AR antibodies, which act as βAR agonists, impacted electrophysiological properties in terms of atrial effective refractory period (AERP), AF inducibility, and electrical conduction in rabbits.

CONCLUSIONS

The implication of early delivery of therapies post-MI will most certainly differ from the treatment for non-ischemic diastolic dysfunction with a stiff left ventricle and even more so from

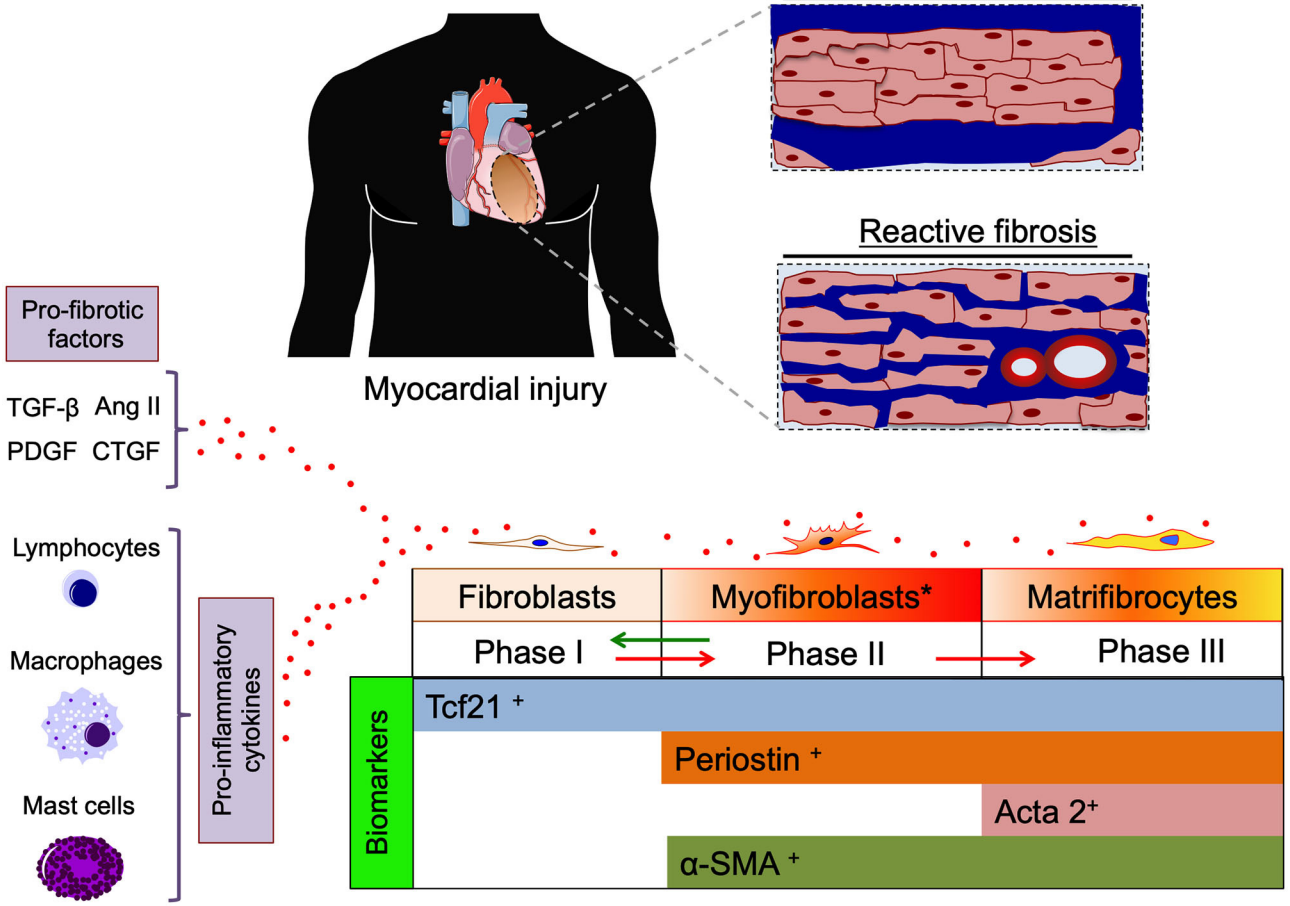

FIGURE 1 | Cartoon depicting two pathogenic mechanisms of cardiac fibrosis, "reparative" (replacing dead cardiomyocytes) and "reactive" (interstitial and perivascular) cardiac fibrosis (blue color). Pro-fibrotic factors (TGF-β, AngII, PDGF, and CTGF) and cytokines released from inflammatory cells promote differentiation of fibroblasts toward activated myofibroblasts and matrifibrocytes actively producing extracellular matrix (ECM). Specific biomarkers of different stages of cardiac fibroblast differentiation are indicated on the bottom. TGF-β, transforming grow factor β; Ang II, angiotensin type II; PDGF, platelet derived grow factor; CTGF, connective tissue grow factor; Tcf21, transcription factor 21(biomarker for cardiac fibroblasts); Periostin, (biomarker of activated myofibroblasts) Acta2, smooth muscle actin alpha 2 (biomarker of matrifibrocytes); α-SMA, α smooth muscle actin.

the treatment of end-stage heart failure with more pronounced fibrosis. While the fibrotic response following myocardial injury may initially be compensatory, could eventually be maladaptive if the large cardiac functional reserve is compromised. Therapeutic intervention in this setting should aim to prevent the fine sclerotic tissue deposition between the cardiomyocytes. This could be implemented with personalized anti-fibrotic therapy with specific timing of the intervention and tailoring it to the type of injury rather than completely blocking the fibrosis pathway.

AUTHOR CONTRIBUTIONS

GP substantially contributed to the conception and design of the editorial, literature search, drafting the article, and revising the article critically for important intellectual content. CL contributed in literature search, drafting the article, and revising the article critically for important intellectual content. MW contributed in literature search, drafting the article, and revising the article critically for important intellectual content. DC contributed in literature search and drafting the article and revising the article critically for important intellectual content. All the authors approved the final version of the article to be published.

ACKNOWLEDGMENTS

We sincerely thank the authors who have contributed to the success of this Research Topic. Their articles have definitely implemented the current knowledge on this Research Topic.

REFERENCES

Callegari, S., Macchi, E., Monaco, R., Magnani, L., Tafuni, A., Croci, S., et al. (2020). Clinicopathological bird's-eye view of left atrial myocardial fibrosis in 121 patients with persistent atrial fibrillation: developing architecture and main cellular players. *Circ. Arrhythm. Electrophysiol.* 13:e007588. doi: 10.1161/CIRCEP.119.007588

Corradi, D., Callegari, S., Maestri, R., Benussi, S., and Alfieri, O. (2008). Structural remodeling in atrial fibrillation. *Nat. Clin. Pract. Cardiovasc. Med.* 5, 782–796. doi: 10.1038/ncpcardio1370

De Boer, R. A., De Keulenaer, G., Bauersachs, J., Brutsaert, D., Cleland, J. G., Diez, J., et al. (2019). Towards better definition, quantification and treatment of fibrosis in heart failure. A scientific roadmap by the Committee of Translational Research of the Heart Failure Association (HFA) of the European Society of Cardiology. *Eur. J. Heart Fail* 21, 272–285. doi: 10.1002/ejhf.1406

Eschenhagen, T. (2018). A new concept of fibroblast dynamics in post-myocardial infarction remodeling. *J. Clin. Invest.* 128, 1731–1733. doi: 10.1172/JCI121079

Frangogiannis, N. G. (2019). Can myocardial fibrosis be reversed? *J. Am. Coll. Cardiol.* 73, 2283–2285. doi: 10.1016/j.jacc.2018.10.094

Fu, X., Khalil, H., Kanisicak, O., Boyer, J. G., Vagnozzi, R. J., Maliken, B. D., et al. (2018). Specialized fibroblast differentiated states underlie scar formation in the infarcted mouse heart. *J. Clin. Invest.* 128, 2127–2143. doi: 10.1172/JCI98215

Hanna, N., Cardin, S., Leung, T. K., and Nattel, S. (2004). Differences in atrial versus ventricular remodeling in dogs with ventricular tachypacing-induced congestive heart failure. *Cardiovasc. Res.* 63, 236–244. doi: 10.1016/j.cardiores.2004.03.026

Khalil, H., Kanisicak, O., Vagnozzi, R. J., Johansen, A. K., Maliken, B. D., Prasad, V., et al. (2019). Cell-specific ablation of Hsp47 defines the collagen-producing cells in the injured heart. *JCI Insight* 4:e128722. doi: 10.1172/jci.insight.128722

Nattel, S. (2017). Molecular and cellular mechanisms of atrial fibrosis in atrial fibrillation. *JACC Clin. Electrophysiol.* 3, 425–435. doi: 10.1016/j.jacep.2017.03.002

Sharma, K., and Kass, D. A. (2014). Heart failure with preserved ejection fraction: mechanisms, clinical features, and therapies. *Circ. Res.* 115, 79–96. doi: 10.1161/CIRCRESAHA.115.302922

Silva, A. M., Teixeira, J. H., Almeida, M. I., Goncalves, R. M., Barbosa, M. A., and Santos, S. G. (2017). Extracellular Vesicles: Immunomodulatory messengers in the context of tissue repair/regeneration. *Eur. J. Pharm. Sci.* 98, 86–95. doi: 10.1016/j.ejps.2016.09.017

Ten Tusscher, K. H., and Panfilov, A. V. (2007). Influence of diffuse fibrosis on wave propagation in human ventricular tissue. *Europace* 9 (Suppl. 6), vi38–45. doi: 10.1093/europace/eum206

Conflict of Interest: MW was employed by the company Center for Biomarker Research in Medicine, CBmed GmbH, Austria.

The remaining authors declare that the research was conducted in the absence of any commercial or financial relationships that could be construed as a potential conflict of interest.

frontiers in Pharmacology

ORIGINAL RESEARCH
published: 21 November 2019
doi: 10.3389/fphar.2019.01386

Choline Attenuates Cardiac Fibrosis by Inhibiting p38MAPK Signaling Possibly by Acting on M_3 Muscarinic Acetylcholine Receptor

Lihui Zhao[1,2†], Tingting Chen[1,2†], Pengzhou Hang[1,2], Wen Li[1,2], Jing Guo[1,2], Yang Pan[1,2], Jingjing Du[1,2], Yuyang Zheng[1,2] and Zhimin Du[1,2,3]*

[1] Institute of Clinical Pharmacology, the Second Affiliated Hospital of Harbin Medical University (The University Key Laboratory of Drug Research, Heilongjiang Province), Harbin, China, [2] Department of Clinical Pharmacology, College of Pharmacy, Harbin Medical University, Harbin, China, [3] State Key Laboratory of Quality Research in Chinese Medicines, Macau University of Science and Technology, Macau, China

OPEN ACCESS

Edited by:
Gianluigi Pironti,
Karolinska Institutet (KI),
Sweden

Reviewed by:
Jaromir Myslivecek,
Charles University,
Czechia
JoAnn Trial,
Baylor College of Medicine,
United States

***Correspondence:**
Zhimin Du
dzm1956@126.com

†These authors have contributed equally to this work

Specialty section:
This article was submitted to Cardiovascular and Smooth Muscle Pharmacology, a section of the journal Frontiers in Pharmacology

Received: 10 July 2019
Accepted: 31 October 2019
Published: 21 November 2019

Citation:
Zhao L, Chen T, Hang P, Li W, Guo J, Pan Y, Du J, Zheng Y and Du Z (2019) Choline Attenuates Cardiac Fibrosis by Inhibiting p38MAPK Signaling Possibly by Acting on M_3 Muscarinic Acetylcholine Receptor. Front. Pharmacol. 10:1386. doi: 10.3389/fphar.2019.01386

Choline has been reported to produce a variety of cellular functions including cardioprotection *via* activating M_3 muscarinic acetylcholine receptor (M_3R) under various insults. However, whether choline offers similar beneficial effects *via* the same mechanism in cardiac fibrosis remained unexplored. The present study aimed to investigate the effects of choline on cardiac fibrosis and the underlying signaling mechanisms, particularly the possible involvement of M_3R. Transverse aortic constriction (TAC) mouse model was established to simulate the cardiac fibrosis. Transforming growth factor (TGF)-β1 treatment was employed to induce proliferation of cardiac fibroblasts *in vitro*. Choline chloride and M_3R antagonist 4-diphenylacetoxy-*N*-methylpiperidine methiodide (4-DAMP) were used to unravel the potential role of M_3R. Cardiac function was assessed by echocardiography and interstitial fibrosis was quantified by Masson staining. Protein levels of collagens I and III were determined by Western blot analysis. The role of M_3R in the proliferation cardiac fibroblasts was validated by silencing M_3R with specific small interference RNA (siRNA). Furthermore, the mitogen-activated protein kinase (MAPK) signaling pathway including p38MAPK and ERK1/2 as well as the TGF-β1/Smad pathway were analyzed. M_3R protein was found abundantly in cardiac fibroblasts. M_3R protein level, as identified by Western blotting, was higher in mice with excessive cardiac fibrosis and in TGF-β1-induced cardiac fibrosis as well. Choline significantly inhibited interstitial fibrosis, and this beneficial action was reversed by 4-DAMP. Production of collagens I and III was reduced after choline treatment but restored by 4-DAMP. Expression silence of endogenous M_3R using siRNA increased the level of collagen I. Furthermore, the TGF-β1/Smad2/3 and the p38MAPK pathways were both suppressed by choline. In summary, choline produced an anti-fibrotic effect both *in vivo* and *in vitro* by regulating the TGF-β1/Smad2/3 and p38MAPK pathways. These findings unraveled a novel pharmacological property of choline linked to M_3R, suggesting that choline regulates cardiac fibrosis and the associated heart diseases possibly by acting on M_3R.

Keywords: M_3 receptor, cardiac fibrosis, choline, collagen, p38MAPK

INTRODUCTION

There are plenty of receptors that play an opposite or synergistic role in heart function (Pfleger et al., 2019). In the view of muscarinic acetylcholine receptors (MR), there are major subtypes (M_2) and minor subtypes (M_1, M_3, maybe M_5) in the heart, and the physiological and pathophysiological roles of these receptors have been uncovered (Colecraft et al., 1998; Shi et al., 1999; Hellgren et al., 2000; Brodde et al., 2001; Hardouin et al., 2002; Hang et al., 2013; Saternos et al., 2018). It has been reported that choline has some effects on M_3 muscarinic acetylcholine receptor (M_3R) in cardiac myocytes (Shi et al., 1999). This compound has been used as an agonist of muscarinic receptor in numerous published studies (Hang et al., 2009; Wang et al., 2009; Zhao et al., 2010; Liu L, 2017; Xu et al., 2019). Previous studies by our laboratory and others have demonstrated that activation of M_3R protected against cardiac ischemia, cardiac hypertrophy, and arrhythmias (Pan et al., 2012; Liu et al., 2013). Specifically, activation of M_3R by choline or overexpression of M_3R in transgenic mice inhibits cardiac apoptosis, inflammation, calcium overload, and ion channel dysfunction (Yang et al., 2005; Liu et al., 2008; Liu et al., 2011; Wang et al., 2018). It is known that in the late phase of cardiac ischemia or hypertrophy, cardiac fibroblasts play an essential role in cardiac remodeling characterized by collagen overproduction and accumulation leading to cardiac interstitial fibrosis (Kong et al., 2014). While these studies primarily focused on the effects of M_3R in cardiomyocytes, the function of M_3R in cardiac fibroblasts and its potential role in cardiac fibrosis has not been exploited. Intriguingly, it has been documented that selective activation of M_3R attenuates hepatic collagen deposition, bile ductule proliferation, and liver fibrosis (Khurana et al., 2013). In contrast, a study reported that cholinergic stimuli mediated by muscarinic receptors induced the proliferation of fibroblasts and myofibroblasts in airway (Pieper et al., 2007). A study reported by Organ et al. demonstrated that the inbred mice fed with choline has significantly enhanced cardiac fibrosis in a transverse aortic constriction (TAC) model (Organ et al., 2016). Another study conducted in a model of myocardial infarction reported that choline promotes cardiac fibrosis (Yang et al., 2019). All these studies suggest that M_3R participates in the proliferation of fibroblasts and collagen production. However, the role of M_3R in cardiac fibrosis remained controversial and inadequately addressed.

It has been well recognized that transforming growth factor (TGF)-β1/Smad cascade governs cardiac fibroblast proliferation and collagen secretion. For example, activation of the TGF-β1/Smad pathway promotes the growth of cardiac fibroblasts and collagen production (Zhang et al., 2016). In contrast, inhibition of TGF-β1/Smad limits the progression of cardiac fibrosis (Pan et al., 2011). In addition, many other signaling pathways have also been uncovered to participate in the development and progress of cardiac fibrosis. Among them, the mitogen-activated protein kinase (MAPK) pathway constituted by p38MAPK, ERK, and JNK is crucial to cardiac fibrosis and structural remodeling (Wang et al., 2016). Importantly, modulation of the MAPK pathway controls the pathological changes of cardiac fibrosis (Pan et al., 2011).

Taken together the above background information, we set up the present study focusing on the role of M_3R in cardiac fibrosis and the underlying mechanisms. Our results demonstrated for the first time that choline significantly inhibits cardiac fibroblast proliferation and collagen secretion, and this anti-fibrotic property is likely ascribed to the inhibition of the TGF-β1/Smad and MAPK pathways.

MATERIALS AND METHODS

Animals

Male Kunming mice and neonatal Sprague Dawley rats were purchased from the Animal Center of the Second Affiliated Hospital of Harbin Medical University (Harbin, China). The mice were maintained under standard animal room conditions (temperature, 21 ± 1°C; humidity, 55 to 60%), with food and water *ad libitum*. This study was conducted in strict accordance with the recommendations of the National Institutes of Health's "Guidelines for the Care and Use of Laboratory Animals" (NIH publication, revised 2011). The protocol was approved by the Animal Care and Use Committee of Harbin Medical University.

A total of 32 mice of 20~25 g were used in our study. The mice were anesthetized with 2,2,2-tribromoethanol (270 mg/kg) and TAC model with excessive cardiac fibrosis was established (Liu Y, 2017). The sham-operated control mice underwent the same surgical procedures without ligation of the aortic bundle. Three days after TAC, the mice were divided into four experimental groups (n = 8): sham, TAC, TAC + choline (14 mg/kg), TAC + choline + 4-DAMP (4-diphenylacetoxy-*N*-methyl-piperidine, 14 mg/kg choline, 0.7 μg/kg 4-DAMP). For co-administration of choline and 4-DAMP, 4-DAMP was injected 30 min before choline treatment and the administration method was intraperitoneal injection. After 8 weeks, cardiac function of the survived mice was examined by echocardiography. For molecular biology studies, the hearts were isolated and then quickly striped, cleared in cold buffer, and weighed after drying. The left ventricle preparations were stored frozen in a −80°C freezer for subsequent Western blot experiments.

Cell Culture and Treatment

Hearts of neonatal SD rats (1–3 days) were cut into pieces and gathered in 50 ml centrifugal tube with 0.25% trypsin. The cell suspensions was collected in Dulbecco's modified Eagle's medium (DMEM, Corning, USA) supplemented with 10% fetal bovine serum, 100 U/ml penicillin, and 100 μg/ml streptomycin. It was then incubated in culture flasks for 2 h, to allow for fibroblasts to adhere to the bottom of the culture flasks. Unattached cardiomyocytes and other cells were removed. Isolated fibroblasts were incubated at 37°C in a humidified atmosphere of 5% CO_2 and 95% air and nourished at an interval of every 2–3 days. The purity of cardiac fibroblasts used in our study was validated by staining specific marker vimentin using immunofluorescence (**Figure S1**). The cardiac fibroblasts were pre-treated with 3 nM 4-DAMP in the presence or absence of choline (1, 5, or 10 mM) for 1 h and then incubated with 20 ng/ml TGF-β1 for 48 h. 4-DAMP was dissolved in dimethyl sulfoxide (DMSO)

and diluted to a final concentration of DMSO < 0.1%. The dose/concentration of M_3 receptor 4-DAMP was selected according to previous studies (Wang et al., 2012; Zhao et al., 2013).

Echocardiography and Histological Analysis

Mice were anesthetized mice before echocardiography. Both two-dimensional M-mode and three-dimensional Doppler echocardiography were performed by using the Vevo 770 imaging system (VisualSonics, Toronto, Canada) to evaluate cardiac diameter and the function of heart.

Echocardiographic parameters included left ventricular ejection fraction (LVEF), left ventricular shortening score (LVFS), the left ventricular end-diastolic diameter (LVIDd), and left ventricular end-systole diameter (LVIDs) For histological analysis, the hearts were fixed with 4% paraformaldehyde (pH 7.4) for 48 h. The tissue was soaked in paraffin, cut into 5-μm sections, and stained with Masson trichrome. Collagen deposition was quantified by Image-Pro Plus software (Media Cybernetics, Silver Spring, USA).

Western Blot

Total protein samples were extracted from cardiac tissues and cardiac fibroblasts using lysis buffer. Protein sample (100 μg) was fractionated by sodium dodecyl sulfate polyacrylamide gel electrophoresis (10% polyacrylamide gels) and transferred to nitrocellulose membrane. The membrane was blocked with 5% nonfat milk at room temperature for 2 h. The membrane was then incubated with primary antibodies for collagen I (1:500), collagen III (1:500), M_3R (1;500), TGF-β1 (1:500), total Smad2/3 (t-Smad2/3; 1:1,000), phosphorylated Smad1/3 (p-Smad2/3; 1:1,000), t-ERK (1:1,000), p-ERK (1:1,000), t-P38 (1:1,000), p-p38 (1:1,000), and glyceraldehyde 3-phosphate dehydrogenase (GAPDH) (1:1,000) on a shaking bed at 4°C overnight. The membrane was washed with PBS-Tween (0.5%) for three times and then incubated with secondary antibodies in the dark at room temperature for 1 h. Finally, the membranes were rinsed with PBS-T three times before being scanned by Imaging System (LI-COR Biosciences, Lincoln, NE, USA).

Ribonucleic Acid Extraction and Real-Time Reverse Transcription Polymerase Chain Reaction

Total RNA (0.5 μg) was extracted from cardiac fibroblasts by using TRIzol™ Reagent (Thermo, USA) according to the manufacturer's protocol. RNA concentration was measured and then reversely transcribed into complementary DNA. The messenger RNA (mRNA) levels of collagen I, collagen III, and TGF-β1 were determined using SYBR Green I incorporation method on LC480 Real-time PCR system (Roche, USA), with GAPDH as an internal control. The sequences of the primer pairs used in our study are as follow. Collagen I: forward (F): 5'-ATCAGCCCAAACCCCAAGGAGA-3' and reverse (R): 5'-CGCAGGAAGGTCAGCTGGATAG-3,' TGF-β1: F: 5'-CGCCTGCAGAGATTCAAGTCAAC-3' and R: 5'-GTATCAGTGGGGGTCAGCAGCC-3,' and GAPDH: F: 5'-TCCCTCAAGATTGTCAGCAA-3' and R: 5'-AGATCCACAACGGATACATT-3.'

Immunofluorescence

Cardiac fibroblasts were cultured in an incubator for 48 h, then washed with PBS. Next, the cells were fixed with 4% paraformaldehyde solution for 20 min, permeabilized with 1% Triton X-100 (prepared by PBS) at room temperature for 60 min, and incubated with goat serum (Solarbio, Beijing, China) at 37°C for 30 min, following three washes with PBS. Subsequently, the cells were incubated with collagen I antibody (1:500) at 4°C overnight, followed by incubation with fluorescence secondary antibody (1:500) and Alexa Fluor® 488-conjugated goat anti-rabbit IgG (H + L) secondary antibody (Life Technologies) as a control in the dark at room temperature for 1 h. 4′,6-Diamidino-2-phenylindole (DAPI) (10 mg/ml, Beyotime, Haimen, China) was used for nuclear staining. Images were obtained using an Olympus microscope (Japan).

Small Interference Ribonucleic Acid Transfection

Cardiac fibroblasts were transfected with an M_3R small interference RNA (siRNA) or a scramble negative control (CTL) siRNA. Three siRNAs were used to screen the most potent sequence which was then used in subsequent experiments. The sequence of selected M_3R siRNA was 5′-GCUACUGGCUGUGCUAUAUTTAUAUAGCACAGCCAGUAGCTT-3.′ Cells were transfected with 50 nM of siRNA using Lipofectamine 2000 (Invitrogen) for 6 h, before replacing with the medium containing 1% bovine serum. The cells were cultured for another 48 h. At 48 h after transfection, the cells were stimulated with TGF-β1 for 24 h and choline for an additional 24 h. The siRNA was constructed by GenePharma and transfected into cells according to the manufacturer's instructions.

Reagents

The recombinant human TGF-β1 was purchased from PeproTech (#100-21, NJ, USA). Choline chloride was purchased from Sigma (C7527, ≧98% purity, USA). 4-DAMP was purchased from Abcam (ab120144, USA). Anti-M_3 receptor antibody was provided by Alomone (AMR-006; Israel). Antibodies against t-Smad2/3 (#8685), p-Smad2/3 (#8828), TGF-β1 (#3711), p38MAPK (#9212), p-p38MAPK (#9211), t-ERK1/2 (#4695), and p-ERK1/2 (#4370) were purchased from Cell Signaling Technology (CST, USA). Anti-collagen I antibody was purchased from Abcam (ab34710; Abcam, USA). Antibody against collagen III was purchased from Proteintech (13548-AP; Wuhan, China). Antibody against GAPDH was provided by ZSGB (TA-08; Beijing, China). Fluorescent secondary antibodies were purchased from LI-COR Biosciences (Lincoln, NE, USA).

Statistical Analysis

Data are presented as mean ± SEM. Comparison between two groups was performed using an unpaired Student's t-test. Comparisons among multiple groups were determined by

one-way ANOVA followed by a *post hoc* Tukey test. The randomized block ANOVA (repeated measures ANOVA) was used for western blot data with a control value of 1 and no SEM as described previously (Lew, 2007). A value of $p < 0.05$ was considered statistically significant.

RESULTS

Protein Level of M_3 Muscarinic Acetylcholine Receptor in Transforming Growth Factor Beta 1-Induced Cardiac Fibroblasts

Previous studies demonstrated that M_3R is expressed in cardiomyocytes; however, whether this subtype of MR is also expressed in cardiac fibroblasts remained unknown. We therefore firstly detected protein level of M_3R in cardiac fibroblasts using cardiomyocytes as a positive control group. As shown in **Figure 1A**, protein level of M_3R in cardiac fibroblasts was within the same range as that in cardiomyocytes. We then treated cardiac fibroblasts with 20 ng/ml TGF-β1 for 48 h to promote their proliferation. The mRNA levels of TGF-β1 and collagen I were significantly higher in TGF-β1-treated cells than in non-treated control cells (**Figures 1B**, **C**). Moreover, TGF-β1 markedly elevated the protein level of M_3R (**Figure 1D**). These findings support that M_3R is expressed in cardiac fibroblasts and can be activated in response to TGF-β1 stimulation.

Effects of Choline on Protein Levels of Collagen in Cardiac Fibroblasts

In order to investigate the effects of M_3R on the proliferation of cardiac fibroblasts, we measured the protein levels of collagen I after treatment with a muscarinic acetylcholine receptor agonist choline at concentrations of 1, 5, and 10 mM. Both western blot and immunofluorescence results showed that collagen I was significantly decreased by 1 mM choline (**Figures 2A**, **B**). And higher concentration of choline (5 and 10 mM) did not impose further inhibitory effects on collagen I levels. We therefore used 1 mM choline for subsequent experiments. As shown in **Figures 2C**, **D**, compared with the TGF-β1 group, collagens I and III were significantly decreased by 1 mM choline, and this effect was abolished by adding 4-DAMP, a specific antagonist of M_3R. These data suggested that activation of M_3R significantly inhibits the secretion of collagen in cardiac fibroblasts.

Furthermore, the protein level of M_3R was further up-regulated by choline in cardiac fibroblasts pretreated with TGF-β1, which was partially but significantly reversed by 4-DAMP (**Figure 2E**). These results suggest that M_3R up-regulation and M_3R activation are both involved in inhibiting collagen production in TGF-β1-treated cardiac fibroblasts.

Because choline and 4-DAMP are not highly specific ligands for M_3R, siRNA of M_3R siRNA was used by transfection to specifically silence the expression of M_3R, and to validate the effects of M_3R on the proliferation of cardiac fibroblasts. We examined three M_3R siRNAs and selected the one with the highest silencing efficacy from them for subsequent experiments (**Figure 2F**). As expected, silence of M_3R promoted collagen production in cardiac fibroblasts treated with M_3R siRNA compared with the control group (**Figure 2G**).

Effects of Choline on Transverse Aortic Constriction-Induced Cardiac Dysfunction in Mice

As shown in **Figure 3A**, the heart size of TAC mice was obviously larger than sham control mice but was markedly reduced by choline. The effect of choline was abrogated by 4-DAMP. Consistently, both the ratios of heart weight to body weight and left ventricular weight to body weight of TAC mice were decreased by choline, which was

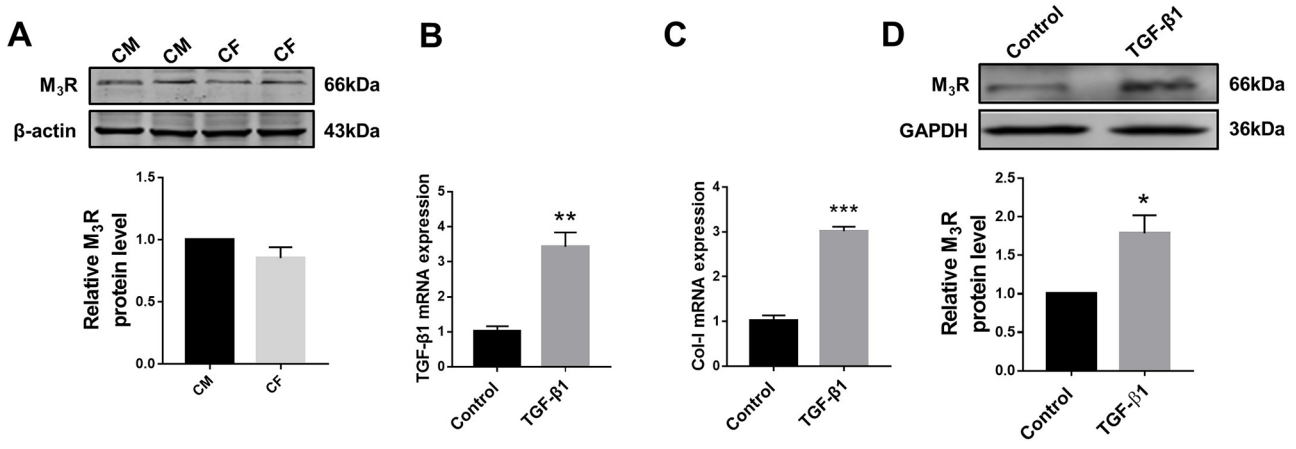

FIGURE 1 | Protein level of M3 muscarinic acetylcholine receptor (M3R) in transforming growth factor beta 1 (TGF-β1)-induced cardiac fibroblasts (CF). **(A)** Protein level of M3R in CF and cardiomyocytes (CM). n = 3. **(B)** Effect of TGF-β1 (20 ng/ml, 48 h) on messenger RNA level of TGF-β1. $^{**}p < 0.01$ *vs.* Ctrl, n = 3. **(C)** Effect of TGF-β1 (20 ng/ml, 48 h) on mRNA level of collagen I. $^{***}p < 0.001$ *vs.* Ctrl, n = 3. **(D)** Effect of TGF-β1 (20 ng/ml, 48 h) on protein level of M_3R in CF. $^{*}p < 0.05$ *vs.* Ctrl, n = 4.

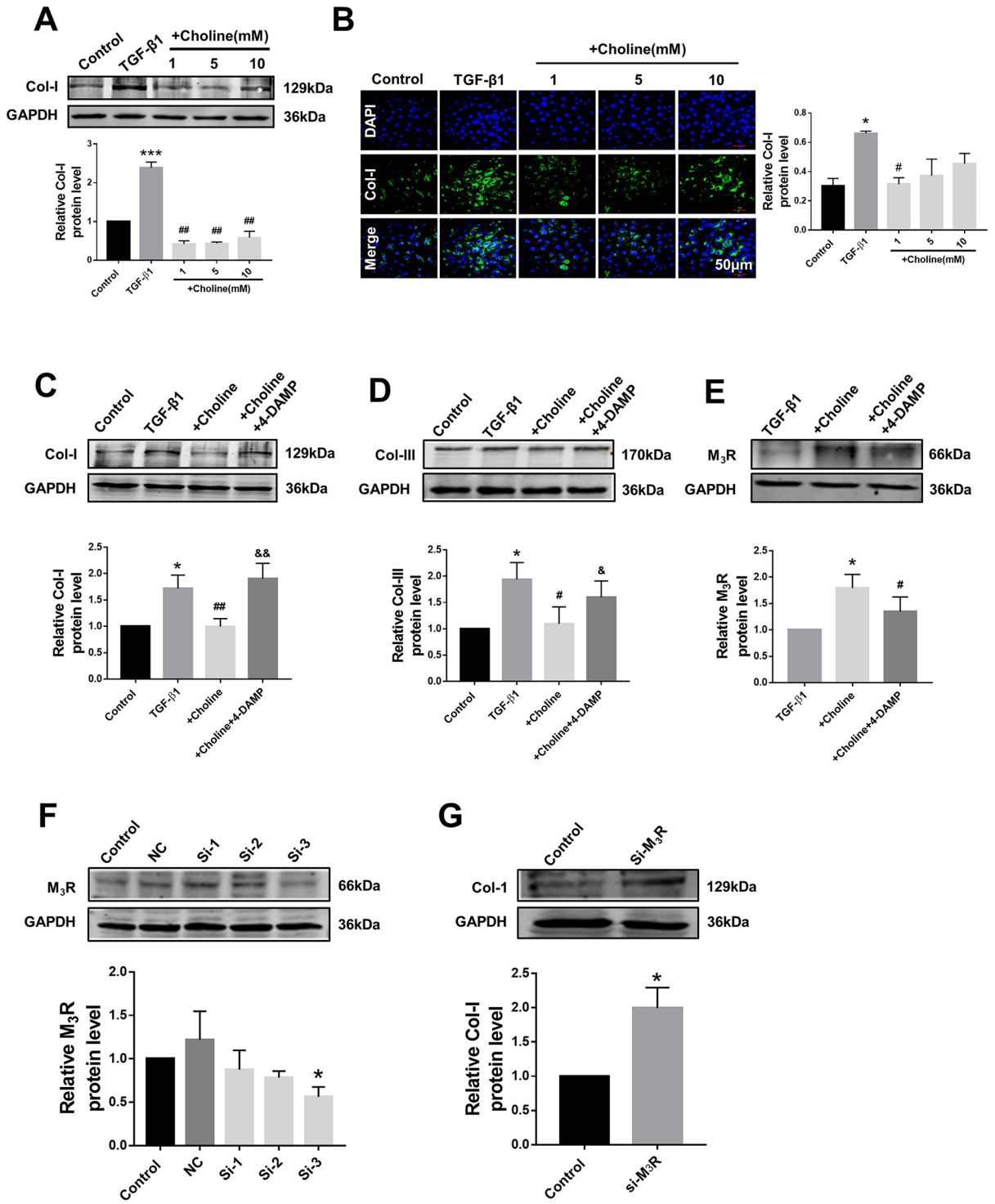

FIGURE 2 | Effects of choline and 4-diphenylacetoxy-*N*-methylpiperidine methiodide (4-DAMP) on transforming growth factor beta 1 (TGF-β1)-induced collagen secretion. **(A)** Effects of different concentrations of choline (1, 5, 10 mM) on protein level of collagen I. $^{***}p < 0.001$ *vs.* Ctrl, $^{\#\#}p < 0.01$ *vs.* TGF-β1, n = 5. **(B)** Immunofluorescence for collagen I in cardiac fibroblasts (CF). Images were obtained using fluorescence microscopy. Blue fluorescence indicates 4′,6-diamidino-2-phenylindole, green fluorescence indicates collagen I, scale bars: 50 μm. $^{*}p < 0.05$ *vs.* Ctrl, $^{\#}p < 0.05$ *vs.* TGF-β1, n = 3. **(C)** Effect of choline on collagen I protein level in the different experimental groups. $^{*}p < 0.05$ *vs.* Ctrl, $^{\#\#}p < 0.01$ *vs.* TGF-β1, $^{\&\&}p < 0.01$ *vs.* choline, n = 7. **(D)** Effect of choline on collagen III protein level in the different experimental groups. $^{*}p < 0.05$ *vs.* Ctrl, $^{\#}p < 0.05$ *vs.* TGF-β1, $^{\&}p < 0.05$ *vs.* choline, n = 6. **(E)** Effects of choline (1 mM) and 4-DAMP (3 nM) on protein level of M_3 muscarinic acetylcholine receptor (M_3R) in TGF-β1-treated CF. $^{*}p < 0.05$ *vs.* Ctrl, $^{\#}p < 0.05$ *vs.* TGF-β1, n = 5. **(F)** Protein level of M_3R after transfecting with three fragments of M_3R-siRNA. $^{*}p < 0.05$ *vs.* Ctrl, n = 4. **(G)** Protein level of collagen I after transfecting M_3R-siRNA-3. $^{*}p < 0.05$ *vs.* Ctrl, n = 5.

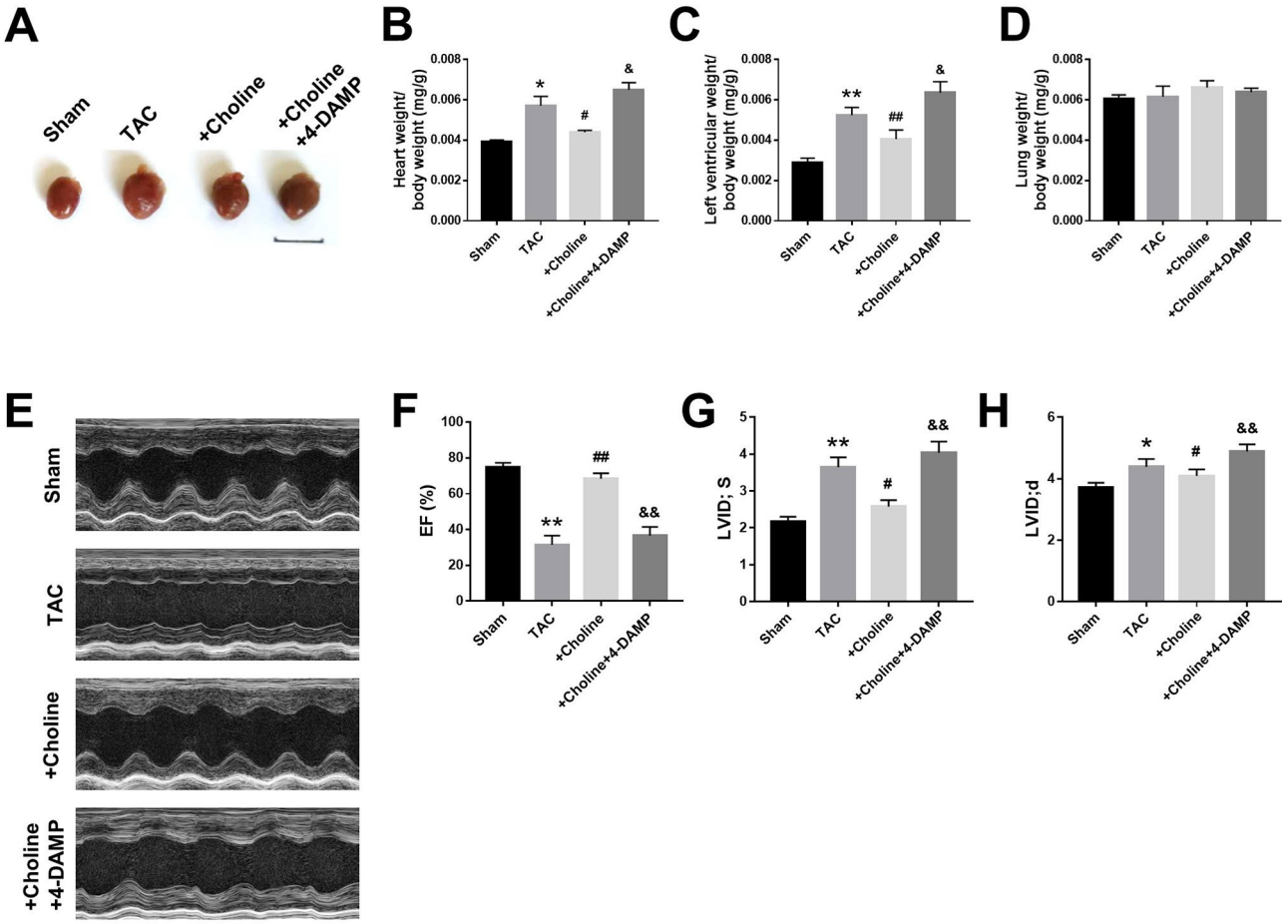

FIGURE 3 | Effects of choline on cardiac function of transverse aortic constriction (TAC) mice model. **(A)** Representative hearts from sham, TAC, and the mice induced by TAC treated with choline (14 mg/kg per day) and 4-DAMP (0.7 μg/kg/day) for 8 weeks. **(B)** The ratio of heart weight/body weight (BW). **(C)** The ratio of left ventricular weight (LVW)/BW. **(D)** The ratio of lung weight/body weight. **(E)** Representative echocardiographic images of mouse hearts in each group. **(F)** Left ventricular ejection fraction (LVEF). **(G)** Systolic left ventricular internal diameter (LVID, s). **(H)** Diastolic left ventricular internal diameter (LVID, d). $^{*}p < 0.05$, $^{**}p < 0.01$ *vs.* sham, $^{\#}p < 0.05$, $^{\#\#}p < 0.01$ *vs.* TAC, $^{\&}p < 0.05$, $^{\&\&}p < 0.01$ *vs.* choline, n = 6.

reversed by 4-DMAP (**Figures 3B**, **C**). No significant difference of the ratio of lung weight/body weight was found (**Figure 3D**). Echocardiographic data revealed that LVEF was increased, while the thickness of the posterior wall of the left ventricle was significantly reduced by choline. These effects were weakened by 4-DAMP pretreatment (**Figures 3F–H**), suggesting that M_3R antagonism accounts at least partially for the cardiac dysfunction in TAC mice and choline improves the impaired cardiac function.

Effects of Choline on Cardiac Interstitial Fibrosis

Masson staining shown in **Figure 4A** revealed that choline treatment decreased the collagen-enriched area and attenuated the inflammatory cell infiltration of myocardial fibrosis induced by TAC, which was reversed by 4-DAMP. Meanwhile, the protein levels of collagens I and collagen III were found significantly higher in the TAC group than in the sham group, and this TAC-induced collagen deposition was essentially inhibited in the choline group (**Figures 4B**, **C**). Meanwhile, protein level of M_3R was increased in TAC mice compared to that in sham mice, and this upregulation was further exaggerated by choline but repressed by 4-DAMP (**Figure 4D**). These results suggest that choline suppresses, whereas M_3R inhibition facilitates cardiac fibrosis.

Suppressive Effects of Choline on the Transforming Growth Factor Beta 1/ Smad Pathway in Cardiac Fibroblasts and Transverse Aortic Constriction Mice

The classical TGF-β1/Smad signaling pathway is a key determinant of cardiac fibrogenesis. Our Western blot results showed that the protein levels of TGF-β1 and Smad2/3 were significantly lower in the choline group than in the TGF-β1 group, 4-DAMP abolished the effects of choline (**Figures 5A**, **B**). Similar results were consistently observed in TAC mice: the protein levels of TGF-β1 and p-Smad2/3 were substantially increased in TAC mice relative to those in sham control group. Moreover, choline mitigated the

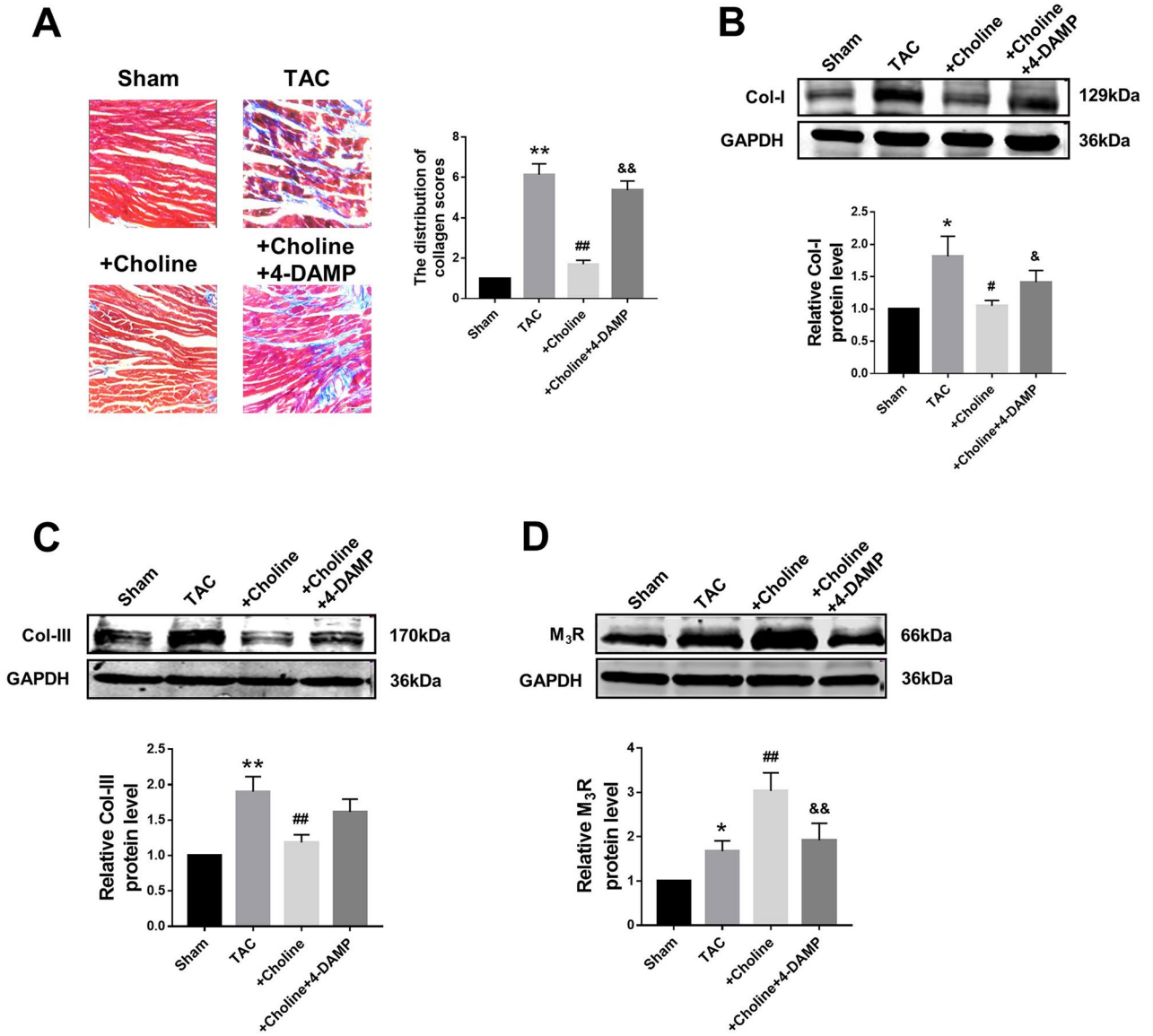

FIGURE 4 | Effects of choline on transverse aortic constriction (TAC)-induced myocardial fibrosis. **(A)** Representative heart section with Masson staining in the experimental groups, scale bar: 100 μm. $^{**}p < 0.01$ *vs.* sham, $^{\#\#}p < 0.01$ *vs.* TAC, $^{\&\&}p < 0.01$ *vs.* choline, n = 5. **(B)** Effects of choline and 4-diphenylacetoxy-*N*-methylpiperidine methiodide (4-DAMP) on the protein level of collagen I. $^{*}p < 0.05$ *vs.* sham, $^{\#}p < 0.05$ *vs.* TAC, $^{\&}p < 0.05$ *vs.* choline, n = 8. **(C)** Effects of choline and 4-DAMP on the protein level of collagen III. $^{**}p < 0.01$ *vs.* sham, $^{\#\#}p < 0.01$ *vs.* TAC, n = 8. **(D)** Cardiac M_3 muscarinic acetylcholine receptor protein level after TAC surgery and choline or 4-DAMP treatment. $^{*}p < 0.05$ *vs.* sham, $^{\#\#}p < 0.01$ *vs.*TAC, $^{\&\&}p < 0.01$ *vs.* choline, n = 8.

TAC-induced upregulation TGF-β1 and p-Smad2/3 levels and addition of 4-DAMP nearly entirely abolished the effects of choline (**Figures 5C**, **D**).

Suppressive Effects of Choline on Mitogen-Activated Protein Kinase Signaling in Cardiac Fibroblasts and Transverse Aortic Constriction Mice

It is well known that the MAPK signaling pathway plays an important role in myocardial ischemia and cardiac hypertrophy. We therefore next explored the potential relationship between M_3R and MAPK signaling. On one hand, the ratio of p-p38/t-p38, and of p-ERK1/2/t-ERK1/2 in the choline group were significantly lower than in the TGF-β1 group, while 4-DAMP eliminated the suppressive effect of choline on p-p38, it failed to affect the effect of choline on p-ERK1/2 (**Figures 6A**, **B**). On the other hand, protein levels of p-p38MAPK and p-ERK were increased in the TAC group compared with the sham group, and choline abrogated such increases while 4-DAMP partially prevented the suppressive effect of choline (**Figures 6C**, **D**). These findings suggesting that M_3R activation inhibits activation of p38 and ERK1/2 thereby MAPK signaling.

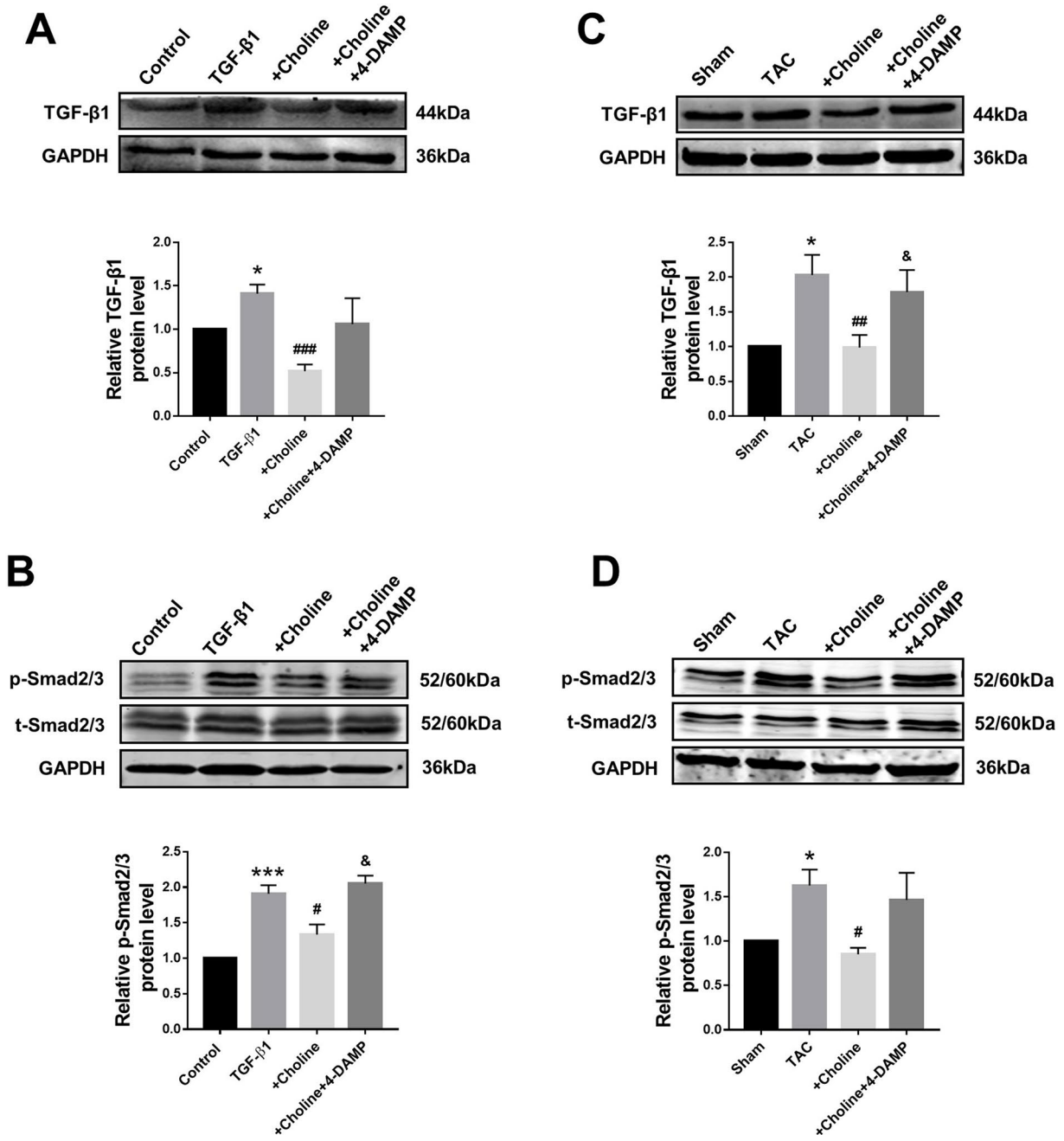

FIGURE 5 | Effects of choline and 4-diphenylacetoxy-*N*-methylpiperidine methiodide (4-DAMP) on protein levels of transforming growth factor beta 1 (TGF-β1)/Smad2/3. **(A)** Effect of choline and 4-DAMP on TGF-β1 protein level in TGF-β1-induced cardiac fibroblasts (CF). $^{*}p < 0.01$ *vs.* Ctrl, $^{\#\#\#}p < 0.001$ *vs.* TGF-β1, n = 5. **(B)** Effect of choline and 4-DAMP on p-Smad2/3 protein level in TGF-β1-induced CF. $^{***}p < 0.001$ *vs.* Ctrl, $^{\#}p < 0.05$ *vs.* TGF-β1, $^{\&}p < 0.05$ *vs.* choline, n = 6. **(C)** Effects of choline and 4-DAMP on the protein level of TGF-β1 in transverse aortic constriction (TAC) mice hearts. $^{*}p < 0.05$ *vs.* sham, $^{\#\#}p < 0.01$ *vs.* TAC, $^{\&}p < 0.05$ *vs.* choline, n = 6. **(D)** Effects of choline and 4-DAMP on the protein level of p-smad2/3 in TAC mice hearts. $^{*}p < 0.5$ *vs.* sham, $^{\#}p < 0.05$ *vs.* TAC, n = 4.

DISCUSSION

Although accumulating evidence has supported that M_3R is expressed in cardiomyocytes of both human and rodents (Gadbut and Galper, 1994; Hellgren et al., 2000; Wang et al., 2001; Stengel et al., 2002; Willmy-Matthes et al., 2003; Wang et al., 2004; Abramochkin et al., 2012), its expression, and function in cardiac fibroblasts remained vaguely understood. To shed light on this issue, we conducted the present study focusing on the possible role M_3R in regulating proliferation and collagen production of rat cardiac fibroblasts *in vitro* and cardiac fibrosis in TAC mice *in vivo*. The results demonstrated for the first time

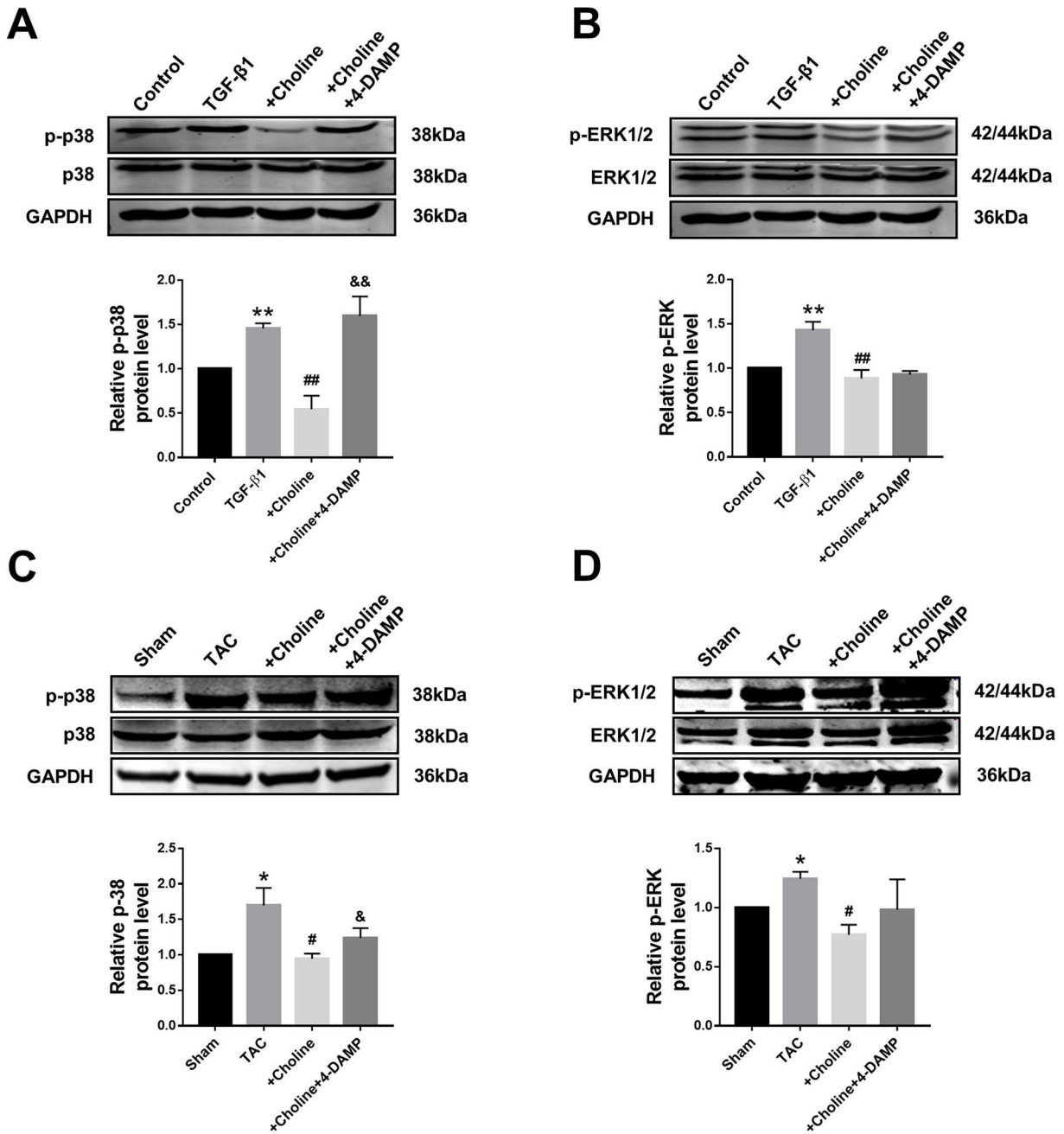

FIGURE 6 | Effect of choline and 4-diphenylacetoxy-*N*-methylpiperidine methiodide (4-DAMP) on protein levels of p38MAPK and ERK1/2. **(A)** Effect of choline and 4-DAMP on p-p38 protein level in transforming growth factor beta 1 (TGF-β1)-induced cardiac fibroblasts (CF). $^{**}p < 0.01$ *vs.* Ctrl, $^{\#\#}p < 0.01$ *vs.* TGF-β1, $^{\&\&}p < 0.01$ *vs.* choline, n = 5. **(B)** Effect of choline and 4-DAMP on p-ERK1/2 protein level in TGF-β1-induced CF. $^{**}p < 0.01$ *vs.* Ctrl, $^{\#\#}p < 0.01$ *vs.* TGF-β1, n = 6. **(C)** Effects of choline and 4-DAMP on the protein level of p-p38 in transverse aortic constriction (TAC) mice hearts. $^{*}p < 0.05$ *vs.* sham, $^{\#}p < 0.05$ *vs.* TAC, $^{\&}p < 0.05$ *vs.* choline, n = 5. **(D)** Effects of choline and 4-DAMP on the protein level of p-ERK in TAC mice hearts. $^{*}p < 0.05$ *vs.* sham, $^{\#}P < 0.05$ *vs.* TAC, n = 4.

that M_3R is expressed in cardiac fibroblasts of rodents, and either pharmacological inhibition or expression silence of M_3R favors, while choline that has the potential to activate M_3R limits cardiac fibrosis by inhibiting p38MAPK signaling.

It has been accepted that M_2R is not the only functional subtype muscarinic and nicotinic acetylcholine receptors (mAChRs) in the heart (Saternos et al., 2018). Numerous studies have reported that M_3R plays an important role in heart diseases (Filatova et al., 2017; Xue et al., 2017). However, these studies primarily focused on cardiomyocytes and no studies have reported the expression and function of M_3R in cardiac fibroblasts, though it has been shown that M_3R is expressed in certain types of non-cardiac fibroblasts. For

example, Pieper et al. demonstrated that M_1, M_2, and M_3 receptors are expressed at the mRNA level in lung fibroblasts. They also found that cholinergic stimuli mediated by muscarinic receptors cause remodeling in chronic airway disease (Pieper et al., 2007). Reina et al. reported that pilocarpine activates muscarinic M_1 and M_3 receptors, which promotes apoptosis in human skin fibroblast cells (Reina et al., 2010). Here, we demonstrate that M_3R proteins are presented in both cardiac fibroblasts and cardiomyocytes with similar abundance. Previous studies by ours and other laboratories suggest that choline produces a protective effect against cardiac hypertrophy by activating M_3R (Wang et al., 2012; Liu et al., 2013; Xu et al., 2019). For example, Xu et al. observed significant attenuation of cardiac fibrosis after choline treatment in cardiac hypertrophy model (Xu et al., 2019). However, the mechanism for the anti-fibrotic effect of choline is unclear. The present study provided direct evidence of the anti-fibrotic effect of choline *via* acting on M_3R. This note was well supported by the data we obtained using M_3R-selective antagonist 4-DAMP and M_3R-specific siRNA. Notably, we found that 1 mM choline produced maximum anti-fibrotic effects and increasing concentrations up to 10 mM did not yield further effects. As already mentioned earlier, two published studies demonstrated that choline promotes cardiac fibrosis in mouse models of TAC and myocardial infarction as well (Organ et al., 2016; Yang et al., 2019), which is in contradiction to the findings presented in the present study. The discrepancy could be explained by the following possibilities. First, in the two published studies, the authors ascribed the results to the microbiome conversion of choline to trimethylamine N-oxide (TMAO) as the animals were fed with choline diet; in other words, the observed enhancement of cardiac fibrosis by choline diet is primarily caused by TMAO. However, such an explanation might not be applied to our case because in our *in vivo* experiments, choline chloride was intraperitoneally injected into mice, and it is unlikely that choline undergoes microbiome conversion to TMAO. Second, in our *in vitro* study, fibroblasts were incubated directly with choline and again it is unlikely for choline to convert to TMAO either. Third, the fact that the beneficial action of choline was efficiently reversed by 4-DAMP suggests that in our models, choline likely acts directly on M_3R without an involvement of TMAO or other factors.

It is well established that the MAPK pathway plays an important role in cardiac fibrosis by modulating the proliferation and differentiation of cardiac fibroblasts (Chang et al., 2018). Cardiac fibroblast-specific p38α MAPK causes cardiac ventricular remodeling and fibrosis promotes cardiac hypertrophy *via* regulating interleukin-6 signaling. Conversely, fibroblast-specific p38α knockout mice exhibits marked protection against myocardial injury and fibrosis (Bageghni et al., 2018). Moreover, a previous study also suggests that activation of M_3R by choline relieves cardiac ischemia and hypertrophy by inhibiting p38MAPK signaling (Wang et al., 2012). The present study shows that the negative impact of M_3R on p38MAPK also exists in cardiac fibroblasts.

In the present study, we used choline as an agonist of M_3R; however, it must be noted that though the ability of choline to activate M_3R has been documented by numerous studies, this compound is not a selective M_3R agonist. Instead, choline has been shown to produce a variety of cellular functions. For instance, it was demonstrated that choline can be uptaken by transporters and then it activates sigma-1 receptors (Sig-1R), a group of integral membrane proteins of endoplasmic reticulum and potentiates Ca^{2+} signals (Brailoiu et al., 2019). Evidence was provided in this study that choline mimics other Sig-1R agonists by potentiating Ca^{2+} signals evoked by the inositol 1,4,5-trisphosphate receptors. The authors conclude that choline is an endogenous agonist of Sig-1Rs linking extracellular stimuli to Ca^{2+} signals. It is also noted that this study reports a choline displacement of Sig-1R specific radioligand binding by [^{3}H](+)-pentazocine with pKi value of around 3.3 mM, which is essentially in the same range of choline for M_3R as reported by Shi et al. (1999). Together these findings, it appears that choline is a non-selective agonist for both M_3R and Sig-1R and maybe for other receptors too. Another study demonstrated that Sig-1R knockout mice have significantly increased cardiac fibrosis and collagen deposition in the hearts, indicating an involvement of Sig-1R in regulating cardiac fibrosis (Abdullah et al., 2018). A most recent report demonstrates that BD1047 (an antagonist of Sig-1R can cause an increase in atrial fibrosis contributing to exacerbating atrial fibrillation (Ye et al., 2019). Due to the present lack of subtype-selective mAChR agonists, we employed choline as a partial agonist of M_3R in the present study. Precaution must therefore be taken in interpreting our results obtained with choline in terms of the mechanism of action; in other words, the present study does not exclude the possibility of choline to interact with Sig-1R and produce the anti-fibrotic action. Nonetheless, it should also be noted that there has not been any evidence for the presence of Sig-1R in cardiac fibroblasts, with which the present study was conducted.

The study reported by Jaiswal et al. in 1989 (Jaiswal et al., 1989) stands the first evidence for functional M_3R in mammalian hearts, which was verified the same group in 1996 in ventricular myocytes of rabbit hearts (Kan et al., 1996). The existence of M_3R in cardiomyocytes has been recognized by several more confirmative studies from multiple research groups with pharmacological, functional, and molecular evidence (Hellgren et al., 2000; Oberhauser et al., 2001; Pönicke et al., 2003; Wang et al., 2004). Nevertheless, whether M_3R also exists in cardiac fibroblasts remained unknown prior to the present study; thus, we present here the first evidence for the expression and function of M_3R in cardiac fibroblasts. Though our study does not provide conclusive evidence, the most rational and objective explanation of our data is the participation of M_3R in cardiac fibrosis.

In addition to M_2R and M_3R, the heart also expressed other subtypes of mAChRs, including M_1R (Colecraft et al., 1998; Hardouin et al., 2002) and M_4R (Colecraft et al., 1998; Shi et al., 2004; Wang et al., 2004). The presence of M_1R and M_2R proteins on the surface membrane of the cultured rat ventricular myocytes was confirmed by immunofluorescence (Colecraft et al., 1998). The study suggests that the positive chronotropic effect of mAChR activation on the contractions is mediated through the M_1R coupled through Gq to phospholipase C-induced phosphoinositide hydrolysis. In contrast, a study suggests the absence of M_1R expression in mouse heart (Hardouin et al., 2002). This conclusion was primarily based on the following two pieces of evidence. First, basal values of heart rate, developed left ventricular pressure, left ventricular dP/dt_{max}, and mean blood

pressure are similar between wild type and M_1R-knockout mice. Second, administration of M_1R-selective agonist McN-A-343 increases hemodynamic function in wild-type mice but fails to cause any changes in M_1R knockout mice.

Regarding the statistical analysis applied to western blots, calculating the average of all data from different batches of experiments represents an appropriate and more powerful analysis. However, in our study, western blot experiments presented too much variability in batches of experiments, so we normalized the data to control in each western blot gel firstly, then analyzed the normalized data from different batches. This might represent a limitation of the study, which should be validated in future study.

In conclusion, our study suggests that choline significantly inhibits cardiac fibroblast proliferation and collagen secretion likely *via* activating M_3R with the functional role of which being associated with the TGF-β1/Smad and p38MAPK pathways.

DATA AVAILABILITY STATEMENT

The raw data supporting the conclusions of this manuscript will be made available by the authors, without undue reservation, to any qualified researcher.

ETHICS STATEMENT

The animal study was reviewed and approved by Ethical Committee of Harbin Medical University.

AUTHOR CONTRIBUTIONS

LZ, TC: acquisition, analysis, and interpretation of data. PH: analysis and interpretation of data, and manuscript writing. JG, WL, YP, JD, YZ: acquisition of data. ZD: conception and design, manuscript revision, and final approval of manuscript.

FUNDING

This work was supported by National Natural Science Foundation of China (No. 81673424 and 81300080).

SUPPLEMENTARY MATERIAL

The Supplementary Material for this article can be found online at: https://www.frontiersin.org/articles/10.3389/fphar.2019.01386/full#supplementary-material

REFERENCES

Abdullah, CS., Alam, S., Aishwarya, R., Miriyala, S., Panchatcharam, M., and Bhuiyan, MAN. (2018). Cardiac dysfunction in the sigma 1 receptor knockout mouse associated with impaired mitochondrial dynamics and bioenergetics. *J Am. Heart Assoc.* 7 (20), e009775. doi: 0.1161/JAHA.118.009775

Abramochkin, D. V., Tapilina, S. V., Sukhova, G. S., Nikolsky, E. E., and Nurullin, L. F. (2012). Functional M3 cholinoreceptors are present in pacemaker and working myocardium of murine heart. *Pflugers Arch.* 463 (4), 523–529. doi: 10.1007/s00424-012-1075-1

Bageghni, S. A., Hemmings, K. E., Zava, N., Denton, C. P., Porter, K. E., and Ainscough, J. F. X. (2018). Cardiac fibroblast-specific p38alpha MAP kinase promotes cardiac hypertrophy *via a* putative paracrine interleukin-6 signaling mechanism. *FASEB J.* 32 (9), 4941–4954. doi: 10.1096/fj.201701455RR

Brailoiu, E., Chakraborty, S., Brailoiu, G. C., Zhao, P., Barr, J. L., Ilies, M. A., et al. (2019). Choline is an intracellular messenger linking extracellular stimuli to IP3-evoked Ca^{2+} signals through sigma-1 receptors. *Cell Rep.* 8, 26(2):330–337. doi: 10.1016/j.celrep.2018.12.051

Brodde, O. E., Bruck, H., Leineweber, K., and Seyfarth, T. (2001). Presence, distribution and physiological function of adrenergic and muscarinic receptor subtypes in the human heart. *Basic Res. Cardiol.* 96 (6), 528–538. doi: 10.1007/s003950170003

Chang, S. L., Hsiao, Y. W., Tsai, Y. N., Lin, S. F., Liu, S. H., and Lin, Y. J. (2018). Interleukin-17 enhances cardiac ventricular remodeling *via* activating MAPK pathway in ischemic heart failure. *J. Mol. Cell Cardiol.* 122, 69–79. doi: 10.1016/j.yjmcc.2018.08.005

Colecraft, H. M., Egamino, J. P., Sharma, V. K., and Sheu, S. S. (1998). Signaling mechanisms underlying muscarinic receptor-mediated increase in contraction rate in cultured heart cells. *J. Biol. Chem.* 273 (48), 32158–32166. doi: 10.1074/jbc.273.48.32158

Filatova, T. S., Naumenko, N., Galenko-Yaroshevsky, P. A., and Abramochkin, D. V. (2017). M3 cholinoreceptors alter electrical activity of rat left atrium *via* suppression of L-type Ca(2+) current without affecting K(+) conductance. *J. Physiol. Biochem.* 73 (2), 167–174. doi: 10.1007/s13105-016-0538-9

Gadbut, A. P., and Galper, J. B. (1994). A novel M3 muscarinic acetylcholine receptor is expressed in chick atrium and ventricle. *J. Biol. Chem.* 269 (41), 25823–25829.

Hang, P. Z., Zhao, J., Wang, Y. P., Sun, L. H., Zhang, Y., and Yang, L. L. (2009). Reciprocal regulation between M3 muscarinic acetylcholine receptor and protein kinase C-epsilon in ventricular myocytes during myocardial ischemia in rats. *Naunyn Schmiedebergs Arch. Pharmacol.* 380 (5), 443–450. doi: 10.1007/s00210-009-0444-6

Hang, P., Zhao, J., Qi, J., Wang, Y., Wu, J., and Du, Z. (2013). Novel insights into the pervasive role of M(3) muscarinic receptor in cardiac diseases. *Curr. Drug Targets* 14 (3), 372–377. doi: 10.2174/13894501380499863

Hardouin, S. N., Richmond, K. N., Zimmerman, A., Hamilton, S. E., Feigl, E. O., and Nathanson, N. M. (2002). Altered cardiovascular responses in mice lacking the M_1 muscarinic acetylcholine receptor. *J. Pharmacol. Exp. Ther.* 301 (1), 129–137. doi: 10.1124/jpet.301.1.129

Hellgren, I., Mustafa, A., Riazi, M., Suliman, I., Sylvén, C., and Adem, A. (2000). Muscarinic M3 receptor subtype gene expression in the human heart. *Cell Mol. Life Sci.* 57 (1), 175–180. doi: 10.1007/s000180050507

Jaiswal, N., Lambrecht, G., Mutschler, E., and Malik, K. U. (1989). Effect of M2 muscarinic receptor antagonist 4-DAMP, on prostaglandin synthesis and mechanical function in the isolated rabbit heart. *Gen. Pharmacol.* 20 (4), 497–502. doi: 10.1016/0306-3623(89)90202-4

Kan, H., Ruan, Y., and Malik, K. U. (1996). Localization and characterization of the subtypes(s) of muscarinic receptor involved in prostacyclin synthesis in rabbit heart. *J. Pharmacol. Exp. Ther.* 276 (3), 934–941.

Khurana, S., Jadeja, R., Twaddell, W., Cheng, K., Rachakonda, V., and Saxena, N. (2013). Effects of modulating M3 muscarinic receptor activity on azoxymethane-induced liver injury in mice. *Biochem. Pharmacol.* 86 (2), 329–338. doi: 10.1016/j.bcp.2013.05.010

Kong, P., Christia, P., and Frangogiannis, N. G. (2014). The pathogenesis of cardiac fibrosis. *Cell Mol. Life Sci.* 71 (4), 549–574. doi: 10.1007/s00018-013-1349-6

Lew, M. (2007). Good statistical practice in pharmacology. Problem 2. *Br. J. Pharmacol.* 152 (3), 299–303. doi: 10.1038/sj.bjp.0707371

Liu, Y., Sun, H. L., Li, D. L., Wang, L. Y., Gao, Y., and Wang, Y. P. (2008). Choline produces antiarrhythmic actions in animal models by cardiac M3 receptors:

improvement of intracellular Ca2+ handling as a common mechanism. *Can. J. Physiol. Pharmacol.* 86 (12), 860–865. doi: 10.1139/Y08-094

Liu, Y., Sun, L., Pan, Z., Bai, Y., Wang, N., and Zhao, J. (2011). Overexpression of M(3) muscarinic receptor is a novel strategy for preventing sudden cardiac death in transgenic mice. *Mol. Med.* 17 (11-12), 1179–1187. doi: 10.2119/molmed.2011.00093

Liu, Y., Wang, S., Wang, C., Song, H., Han, H., and Hang, P. (2013). Upregulation of M(3) muscarinic receptor inhibits cardiac hypertrophy induced by angiotensin II. *J. Transl. Med.* 11, 209. doi: 10.1186/1479-5876-11-209

Liu, L., Lu, Y., Bi, X., Xu, M., Yu, X., and Xue, R. (2017). Choline ameliorates cardiovascular damage by improving vagal activity and inhibiting the inflammatory response in spontaneously hypertensive rats. *Sci. Rep.* 7, 42553. doi: 10.1038/srep42553

Liu, Y., Zhao, D., Qiu, F., Zhang, L. L., Liu, S. K., and Li, Y. Y. (2017). Manipulating PML SUMOylation *via* Silencing UBC9 and RNF4 Regulates Cardiac Fibrosis. *Mol. Ther.* 25 (3), 666–678. doi: 10.1016/j.ymthe.2016.12.021

Oberhauser, V., Schwertfeger, E., Rutz, T., Beyersdorf, F., and Rump, L. C. (2001). Acetylcholine release in human heart atrium: influence of muscarinic autoreceptors, diabetes, and age. *Circulation* 103 (12), 1638–1643. doi: 10.1161/01.CIR.103.12.1638

Organ, C. L., Otsuka, H., Bhushan, S., Wang, Z., Bradley, J., and Trivedi, R. (2016). Choline diet and its gut microbe-derived metabolite, trimethylamine N-oxide, exacerbate pressure overload-induced heart failure. *Circ. Heart Fail* 9 (1), e002314. doi: 10.1161/CIRCHEARTFAILURE.115.002314

Pönicke, K., Heinroth-Hoffmann, I., and Brodde, O. E. (2003). Demonstration of functional M3-muscarinic receptors in ventricular cardiomyocytes of adult rats. *Br. J. Pharmacol.* 138 (1), 156–160. doi: 10.1038/sj.bjp.0704997

Pan, Z., Zhao, W., Zhang, X., Wang, B., Wang, J., and Sun, X. (2011). Scutellarin alleviates interstitial fibrosis and cardiac dysfunction of infarct rats by inhibiting TGFbeta1 expression and activation of p38-MAPK and ERK1/2. *Br. J. Pharmacol.* 162 (3), 688–700. doi: 10.1111/j.1476-5381.2010.01070.x

Pan, Z., Guo, Y., Qi, H., Fan, K., Wang, S., and Zhao, H. (2012). M3 subtype of muscarinic acetylcholine receptor promotes cardioprotection *via the* suppression of miR-376b-5p. *PloS One* 7 (3), e32571. doi: 10.1371/journal.pone.0032571

Pfleger, J., Gresham, K., and Koch, W. J. (2019). G protein-coupled receptor kinases as therapeutic targets in the heart. *Nat. Rev. Cardiol.* 16 (10), 612–622. doi: 10.1038/s41569-019-0220-3

Pieper, M. P., Chaudhary, N. I., and Park, J. E. (2007). Acetylcholine-induced proliferation of fibroblasts and myofibroblasts *in vitro* is inhibited by tiotropium bromide. *Life Sci.* 80 (24-25), 2270–2273. doi: 10.1016/j.lfs.2007.02.034

Reina, S., Sterin-Borda, L., Passafaro, D., and Borda, E. (2010). Muscarinic cholinoceptor activation by pilocarpine triggers apoptosis in human skin fibroblast cells. *J. Cell Physiol.* 222 (3), 640–647. doi: 10.1002/jcp.21981

Saternos, H. C., Almarghalani, D. A., Gibson, H. M., Meqdad, M. A., Antypas, R. B., and Lingireddy, A. (2018). Distribution and function of the muscarinic receptor subtypes in the cardiovascular system. *Physiol. Genomics* 50 (1), 1–9. doi: 10.1152/physiolgenomics.00062.2017

Shi, H., Wang, H., Lu, Y., Yang, B., and Wang, Z. (1999). Choline modulates cardiac membrane repolarization by activating an M3 muscarinic receptor and its coupled K+ channel. *J. Membr. Biol.* 169 (1), 55–64. doi: 10.1007/pl00005901

Shi, H., Wang, H., Li, D., Nattel, S., and Wang Z. (2004). Differential alterations of receptor densities of three muscarinic acetylcholine receptor subtypes and current densities of the corresponding K+ channels in canine atria with atrial fibrillation induced by experimental congestive heart failure. *Cell Physiol Biochem.* 14(1–2), 31–40.

Stengel, P., Yamada, M., Wess, J., and Cohen, M. (2002). M(3)-receptor knockout mice: muscarinic receptor function in atria, stomach fundus, urinary bladder, and trachea. *Am. J. Physiol. Regul. Integr. Comp. Physiol.* 282 (5), R1443–R1449. doi: 10.1152/ajpregu.00486.2001

Wang, H., Han, H., Zhang, L., Shi, H., Schram, G., and Nattel, S. (2001). Expression of multiple subtypes of muscarinic receptors and cellular distribution in the human heart. *Mol. Pharmacol.* 59 (5), 1029–1036. doi: 10.1124/mol.59.5.1029

Wang, Z., Shi, H., and Wang, H. (2004). Functional M3 muscarinic acetylcholine receptors in mammalian hearts. *Br. J. Pharmacol.* 142, 395–408. doi: 10.1038/sj.bjp.0705787

Wang, Y. P., Hang, P. Z., Sun, L. H., Zhang, Y., Zhao, J. L., and Pan, Z. W. (2009). M3 muscarinic acetylcholine receptor is associated with beta-catenin in ventricular myocytes during myocardial infarction in the rat. *Clin. Exp. Pharmacol. Physiol.* 36 (10), 995–1001. doi: 10.1111/j.1440-1681.2009.05176.x

Wang, S., Han, H. M., Pan, Z. W., Hang, P. Z., Sun, L. H., and Jiang, Y. N. (2012). Choline inhibits angiotensin II-induced cardiac hypertrophy by intracellular calcium signal and p38 MAPK pathway. *Naunyn Schmiedebergs Arch. Pharmacol.* 385 (8), 823–831. doi: 10.1007/s00210-012-0740-4

Wang, S., Ding, L., Ji, H., Xu, Z., Liu, Q., and Zheng, Y. (2016). The role of p38 MAPK in the development of diabetic cardiomyopathy. *Int. J. Mol. Sci.* 17 (7), 1037. doi: 10.3390/ijms17071037

Wang, S., Jiang, Y., Chen, J., Dai, C., Liu, D., and Pan, W. (2018). Activation of M3 muscarinic acetylcholine receptors delayed cardiac aging by inhibiting the caspase-1/IL-1beta signaling pathway. *Cell Physiol. Biochem.* 49 (3), 1208–1216. doi: 10.1159/000493332

Willmy-Matthes, P., Leineweber, K., Wangemann, T., Silber, R., and Brodde, O. (2003). Existence of functional M3-muscarinic receptors in the human heart. *Naunyn Schmiedebergs Arch. Pharmacol.* 368 (4), 316–319. doi: 10.1007/s00210-003-0796-2

Xu, M., Xue, R. Q., Lu, Y., Yong, S. Y., Wu, Q., and Cui, Y. L. (2019). Choline ameliorates cardiac hypertrophy by regulating metabolic remodelling and UPRmt through SIRT3-AMPK pathway. *Cardiovasc. Res.* 115 (3), 530–545. doi: 10.1093/cvr/cvy217

Xue, R. Q., Sun, L., Yu, X. J., Li, D. L., and Zang, W. J. (2017). Vagal nerve stimulation improves mitochondrial dynamics *via an* M3 receptor/CaMKKbeta/AMPK pathway in isoproterenol-induced myocardial ischaemia. *J. Cell Mol. Med.* 21 (1), 58–71. doi: 10.1111/jcmm.12938

Yang, B., Lin, H., Xu, C., Liu, Y., Wang, H., and Han, H. (2005). Choline produces cytoprotective effects against ischemic myocardial injuries: evidence for the role of cardiac m3 subtype muscarinic acetylcholine receptors. *Cell Physiol. Biochem.* 16 (4-6), 163–174. doi: 10.1159/000089842

Yang, W., Zhang, S., Zhu, J., Jiang, H., Jia, D., and Ou, T. (2019). Gut microbe-derived metabolite trimethylamine N-oxide accelerates fibroblast-myofibroblast differentiation and induces cardiac fibrosis. *J. Mol. Cell Cardiol.* 134, 119–130. doi: 10.1016/j.yjmcc.2019.07.004

Ye, T., Liu, X., Qu, C., Zhang, C., Fo, Y., and Guo, Y. (2019). Chronic inhibition of the sigma-1 receptor exacerbates atrial fibrillation susceptibility in rats by promoting atrial remodeling. *Life Sci.* 235, 116837. doi: 10.1016/j.lfs.2019.116837

Zhang, M., Pan, X., Zou, Q., Xia, Y., Chen, J., and Hao, Q. (2016). Notch3 ameliorates cardiac fibrosis after myocardial infarction by inhibiting the TGF-beta1/Smad3 pathway. *Cardiovasc. Toxicol.* 16 (4), 316–324. doi: 10.1007/s12012-015-9341-z

Zhao, J., Su, Y., Zhang, Y., Pan, Z., Yang, L., and Chen, X. (2010). Activation of cardiac muscarinic M3 receptors induces delayed cardioprotection by preserving phosphorylated connexin43 and up-regulating cyclooxygenase-2 expression. *Br. J. Pharmacol.* 159 (6), 1217–1225. doi: 10.1111/j.1476-5381.2009.00606.x

Zhao, Y., Wang, C., Wu, J., Wang, Y., Zhu, W., and Zhang, Y. (2013). Choline protects against cardiac hypertrophy induced by increased after-load. *Int. J. Biol. Sci.* 9 (3), 295–302. doi: 10.7150/ijbs.5976

Conflict of Interest: The authors declare that the research was conducted in the absence of any commercial or financial relationships that could be construed as a potential conflict of interest.

frontiers in Physiology

ORIGINAL RESEARCH
published: 12 February 2020
doi: 10.3389/fphys.2020.00076

Elevated β1-Adrenergic Receptor Autoantibody Levels Increase Atrial Fibrillation Susceptibility by Promoting Atrial Fibrosis

Luxiang Shang[1†], Ling Zhang[2†], Mengjiao Shao[1†], Min Feng[1], Jia Shi[1], Zhenyu Dong[1], Qilong Guo[1], Jiasuoer Xiaokereti[1], Ran Xiang[1], Huaxin Sun[1], Xianhui Zhou[1] and Baopeng Tang[1*]*

[1] Department of Pacing and Electrophysiology, The First Affiliated Hospital of Xinjiang Medical University, Urumqi, China, [2] Institute of Clinical Medical Research, The First Affiliated Hospital of Xinjiang Medical University, Urumqi, China

OPEN ACCESS

Edited by:
Markus Wallner,
Medical University of Graz, Austria

Reviewed by:
Martin Manninger,
Medical University of Graz, Austria
Tong Liu,
Tianjin Medical University, China

***Correspondence:**
Xianhui Zhou
zhouxhyf@163.com
Baopeng Tang
tangbaopeng111@163.com

[†] These authors have contributed equally to this work

Specialty section:
This article was submitted to Cardiac Electrophysiology, a section of the journal Frontiers in Physiology

Received: 23 November 2019
Accepted: 23 January 2020
Published: 12 February 2020

Citation:
Shang L, Zhang L, Shao M, Feng M, Shi J, Dong Z, Guo Q, Xiaokereti J, Xiang R, Sun H, Zhou X and Tang B (2020) Elevated β1-Adrenergic Receptor Autoantibody Levels Increase Atrial Fibrillation Susceptibility by Promoting Atrial Fibrosis. Front. Physiol. 11:76. doi: 10.3389/fphys.2020.00076

Objective: Beta 1-adrenergic receptor autoantibodies (β1ARAbs) have been identified as a pathogenic factor in atrial fibrillation (AF), but the underlying pathogenetic mechanism is not well understood. We assessed the hypothesis that elevated β1ARAb levels increase AF susceptibility by promoting atrial fibrosis.

Methods: A total of 70 patients with paroxysmal AF were continuously recruited. The serum levels of β1ARAb and circulating fibrosis biomarkers were analyzed by ELISA. Linear regression was used to examine the correlations of β1ARAb levels with left atrial diameter (LAD) and circulating fibrosis biomarker levels. Furthermore, we established a rabbit β1ARAb overexpression model. We conducted electrophysiological studies and multielectrode array recordings to evaluate the atrial effective refractory period (AERP), AF inducibility and electrical conduction. AF was defined as irregular, rapid atrial beats $>$ 500 bpm for $>$ 1000 ms. Echocardiography, hematoxylin and eosin staining, Masson's trichrome staining, and picrosirius red staining were performed to evaluate changes in atrial structure and detect fibrosis. Western blotting and PCR were used to detect alterations in the protein and mRNA expression of TGF-β1, collagen I and collagen III.

Results: Patients with a LAD $\geq$ 40 mm had higher β1ARAb levels than patients with a smaller LAD (8.87 $\pm$ 3.16 vs. 6.75 $\pm$ 1.34 ng/mL, P = 0.005). β1ARAb levels were positively correlated with LAD and circulating biomarker levels (all $P < 0.05$). Compared with the control group, the rabbits in the immune group showed the following: (1) enhanced heart rate, shortened AERP (70.00 $\pm$ 5.49 vs. 96.46 $\pm$ 3.27 ms, $P < 0.001$), increased AF inducibility (55% vs. 0%, $P < 0.001$), decreased conduction velocity and increased conduction heterogeneity; (2) enlarged LAD and elevated systolic dysfunction; (3) significant fibrosis in the left atrium identified by Masson's trichrome staining (15.17 $\pm$ 3.46 vs. 4.92 $\pm$ 1.72%, $P < 0.001$) and picrosirius red staining

(16.76 ± 6.40 vs. 4.85 ± 0.40%, $P < 0.001$); and (4) increased expression levels of TGF-β1, collagen I and collagen III.

Conclusion: Our clinical and experiential studies showed that β1ARAbs participate in the development of AF and that the potential mechanism is related to the promotion of atrial fibrosis.

Keywords: atrial fibrillation, β1-adrenergic receptor autoantibody, atrial fibrosis, circulating fibrosis biomarker, autoimmune

INTRODUCTION

Atrial fibrillation (AF), the most common clinical cardiac arrhythmia, has high morbidity, disability and mortality and has become a serious public health issue and socioeconomic burden worldwide (Chugh et al., 2014; Ribeiro and Otto, 2018). To date, the pathophysiological mechanisms of AF initiation and progression have not been completely elucidated. Emerging evidence indicates that autoimmunity mechanisms play an important role in the development of AF and might be a direct cause of and contributor to AF in some patients (Stavrakis et al., 2009; Lee et al., 2011; Gollob, 2013).

The beta 1-adrenergic receptor (β1AR) is a type of transmembrane receptor belonging to the cardiovascular G-protein-coupled receptor family. β1AR is the predominant β-adrenoceptor subtype in the human heart, accounting for 60–70% and 70–80% of β-adrenoceptors in the human atrium and ventricle, respectively (Wallukat, 2002). Early studies have confirmed that elevated levels of autoantibodies against β1AR (β1ARAbs) can induce cardiomyopathy and heart failure (Wallukat et al., 1991). Current evidence from both clinical studies and animal-model experiments has revealed that β1ARAb is also of pathogenic importance in AF. Yalcin et al. (2015a) found that serum β1ARAb levels were higher in patients with paroxysmal AF (PAF) than in healthy controls, and β1ARAb levels were an independent predictor of PAF occurrence. Furthermore, Hu et al. (2016) demonstrated an ascending gradient of serum β1ARAb levels from healthy control subjects to PAF patients to patients with persistent AF. Additionally, the area under the curve of β1ARAb concentration predicted AF recurrence after cryoablation in patients with PAF (Yalcin et al., 2015b). Evidence from experiments in a rabbit autoimmune model showed that animals developed high titers of β1ARAbs after immunization with the second extracellular loop (ECL2) peptide of β1AR, and elevated β1ARAbs reduced the atrial effective refractory period (AERP) and facilitated AF induction (Li et al., 2015, 2016). However, the underlying pathogenetic mechanisms of β1ARAb-mediated AF remains unclear.

Atrial fibrosis is one of the fundamental mechanisms of AF (Burstein and Nattel, 2008), and previous studies showed that β1ARAbs could induce cardiomyopathy by promoting ventricular fibrotic structural remodeling (Matsui et al., 1999; Giménez et al., 2005). Thus, we hypothesize that atrial fibrosis might be an important mechanism in β1ARAb-mediated AF. To this end, we measured the levels of β1ARAb in patients with PAF and analyzed their correlation with the presence of atrial fibrosis via non-invasive assessments that included echocardiographic LA diameter and circulating fibrosis biomarkers. Furthermore, we established a rabbit model by passive immunization against β1ARAbs; in this model, we examined whether increased expression of β1ARAbs plays a role in atrial fibrotic remodeling.

MATERIALS AND METHODS

Ethics Committee Approval

The protocol for the clinical study was approved by the Medical Ethics Committee of the First Affiliated Hospital of Xinjiang Medical University (Approval Number: 20170213-02) and conformed to the principles of the Declaration of Helsinki. All participants provided written informed consent for participation. The protocol for the experimental study was approved by the Institutional Animal Care and Use Committee of the First Affiliated Hospital of Xinjiang Medical University (Approval Number: IACUC-20170420-03) and conformed to the principles of the International Association of Veterinary Editors' Consensus Guidelines as well as the Basel Declaration. Anesthesia procedures were performed with pentobarbital sodium (30 mg/kg) via the marginal ear vein, and pentobarbital sodium was given as needed to maintain the depth of anesthesia during surgery. All efforts were made to minimize animal suffering.

Study Population and Data Collection

From July 2017 to March 2018, 70 consecutive patients who were newly diagnosed with PAF and were admitted to the Heart Center of the First Affiliated Hospital of Xinjiang Medical University were recruited. PAF was defined as AF episodes cardioverted within 7 days after onset, as stated by the 2016 European Society of Cardiology AF guidelines (Kirchhof et al., 2016). Patients with autoimmune diseases, heart failure with reduced ejection fraction, history of acute

Abbreviations: AERP, atrial effective refractory period; AF, atrial fibrillation; β1AR, beta 1-adrenergic receptor; β1ARAb, beta 1-adrenergic receptor autoantibody; CV, conduction velocity; ECG, electrocardiogram; ECL2, second extracellular loop; ECM, extracellular matrix; ELISA, enzyme-linked immunosorbent assay; Gal3, galectin-3; H&E, hematoxylin and eosin; LA, left atrial; LAD, left atrial diameter; LVEDD, left ventricular end-diastolic dimension; LVEF, left ventricular ejection fraction; LVESD, left ventricular end-systolic dimension; MEA, multielectrode array; PAF, paroxysmal atrial fibrillation; PIIINP, procollagen type III N-terminal peptide; PICP, procollagen type I C-terminal peptide; RAD, right atrial diameter; RT-PCR, real-time polymerase chain reaction; RVD, right ventricular diameter; TGF-β1, transforming growth factor-β1.

coronary syndrome, severe valvular heart disease, or infectious diseases were excluded from our study. Participants underwent echocardiographic examination by experienced sonographers with a GE Vivid E9 ultrasound instrument (GE Vingmed Ultrasound, Horten, Norway). Information on demographic and clinical characteristics was obtained for all recruited patients.

Enzyme-Linked Immunosorbent Assay (ELISA)

A 5 mL peripheral vein blood sample from each patient was collected in a non-anticoagulant blood-collection tube in the morning after a 12 h fast. The blood was centrifuged at 3000 rpm for 10 min to obtain the serum, which was then stored at -80°C until processing. The serum levels of β1ARAb, procollagen type III N-terminal peptide (PIIINP), procollagen type I C-terminal peptide (PICP), and galectin-3 (Gal3) were measured quantitatively using ELISA kits according to the manufacturer's instructions. PIIINP, PICP and Gal3 were analyzed using kits produced by Elabscience (E-EL-H0183c, E-EL-H0196c, and E-EL-H1470c; Beijing, China), and the kit used to measure β1ARAbs was from Cusabio (CSB-E15079h; Wuhan, China).

Experimental Animals and Design

Sixteen male New Zealand white rabbits (each weighing 3.0–3.5 kg at baseline) were obtained from the Experimental Animal Center of Xinjiang Medical University (Urumqi, China) and were randomly divided into two groups: a control group and an immune group. The generation of the animal model followed the protocols of previous studies (Li et al., 2014, 2015, 2016), and a flow chart of the experimental design is shown in **Figure 1A**. The immune group was initially immunized with 2 mg of the β1AR ECL2 peptide (amino acid sequence: ^{197}HWWRAESDEARRCYNDPKCCDFVTNR^{223}; 98.13% purity, synthesized by Biosynthesis Biotechnology Inc., Beijing, China) in 1 mL of complete Freund's adjuvant (Sigma-Aldrich, St. Louis, MO, United States) at 0 weeks and was boosted with 2 mg of the β1AR ECL2 peptide and incomplete Freund's adjuvant (2 mg in 1 mL; Sigma-Aldrich, St. Louis, MO, United States) three times, spaced 2 week apart. Rabbits in the control group received an equal amount of adjuvant without the β1AR ECL2 peptide at the same time points. Blood samples were collected from both groups every 2 weeks in an awake state before injection, and the serum β1ARAb levels were measures by ELISA and expressed as optical density values based on previous studies (Li et al., 2015). Transthoracic echocardiographic examination was performed at baseline and repeated at 8 weeks after the first immunization. Atrial electrophysiological studies, multielectrode array (MEA) measurement and histological analyses were performed at 8 weeks.

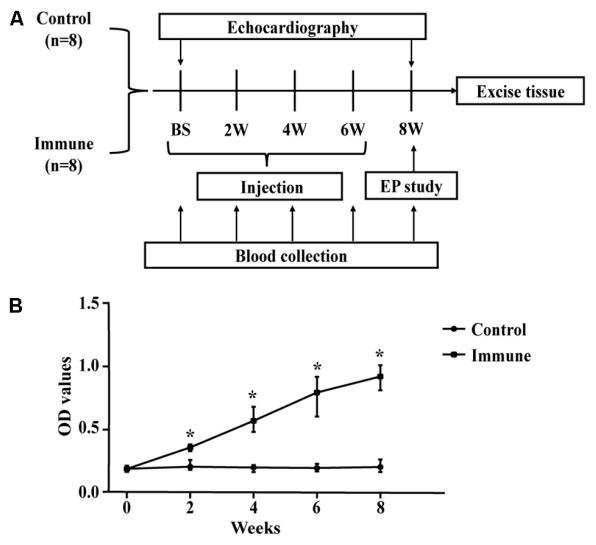

FIGURE 1 | Schematic of the study process. **(A)** study protocol diagram; **(B)** ELISA results (β1ARAb OD values) in the two groups. *$P < 0.05$, control group vs. immune group at the same time point. ELISA, enzyme-linked immunosorbent assay; β1ARAb, beta 1-adrenergic receptor autoantibody; OD, optical density.

Echocardiography

Echocardiographic examinations of all rabbits were performed with a PHILIPS HD11XE transthoracic doppler ultrasound imaging system (Philips Inc., Bothell, WA, United States) with an S12-4 scan probe by an experienced sonographer who was blinded to the nature of the animal experiment. After the rabbits were anesthetized, the hair in the anterior chest area was shaved, the rabbits were placed in the left lateral decubitus position, and the measurements were taken. The left atrial diameter (LAD), right atrial diameter (RAD), left ventricular end-diastolic dimension (LVEDD), left ventricular end-systolic dimension (LVESD), right ventricular diameter (RVD), and left ventricular ejection fraction (LVEF) were measured. Each result was recorded as the average across three consecutive cardiac cycles.

Electrophysiological Measurement

Under anesthesia, surface electrocardiogram (ECG) leads were placed onto the extremities of the animals and connected to a computer-based multichannel physiological laboratory system (LEAD-7000, Jinjiang Electronic Science and Technology Inc., Chengdu, China) to record the heart rate for 5 min. Spontaneous arrhythmia episodes within 5 min were also documented. Then, the neck region was shaved, iodine disinfectant was applied, and an incision was made. The right jugular vein was isolated and intubated with a 4F sheath. The quadripolar electrode catheter entered the right atrium under the control of ECG, and the atrial potential was recorded in combination with surface ECG.

AERP and AF inducibility were measured as described in our previous study (Wang et al., 2017). AERP was conducted with a programmed train of eight basic stimuli (S1-S1 = 260 ms) followed by one extra stimulus (S2) with an initial pacing length of 200 ms and 5 ms decrements until S2 failed to capture the depolarization. The longest S1-S2 interval was defined as the AERP. The AERP was measured three times, and the average value was calculated. The inducibility of AF was assessed by burst pacing to the right atrium (twofold threshold current, cycle length 50 ms, duration 30 s per bout), and this treatment was repeated 5 times for each rabbit. AF inducibility was calculated

as the percentage of successfully recorded AF. AF was defined as irregular, rapid atrial beats > 500 beats per minute (bpm) for more than 1000 ms (Yang et al., 2018). Other types of arrhythmias induced in the rabbit were defined as follows: (1) atrial premature beat: a premature P wave that is morphologically a variant or replica of the P waves of the baseline rhythm; (2) sinus tachycardia: regular, rapid heart rate > 250 bpm with 1:1 atrioventricular conduction arising from the sinus node; and (3) atrial flutter: regular, rapid atrial beats > 250 bpm with distinct P waves between variable QRS cycles (Curtis et al., 2013).

Flexible MEA Recording

MEA measurement was performed at sinus rhythm following electrophysiological study to record the conduction and conduction heterogeneity of the LA appendage epicardial surface *in vivo*. The chest of each rabbit was opened by cutting the center of the sternum, and the heart was exposed. A flexible MEA chip with 36 electrodes (6 × 6 electrodes, interelectrode distance: 300 μm, electrode diameter: 30 μm) was positioned at the surface of the LA appendage (**Supplementary Figure S1**). When the unipolar electrograms of the MEA recording were stable, recordings were taken to generate an activation map and calculate the conduction velocity (CV). The inhomogeneity index was calculated as a variation coefficient of CV (P_{5-95}/P_{50}) (Lammers et al., 1990). Data were collected at 10 kHz per channel and analyzed with Cardio2D + software (Multi Channel Systems, Reutlingen, Germany).

Histological Collection and Processing

The animals were sacrificed with high doses of pentobarbital sodium at the end of the experiment, and the hearts were quickly removed. The left atrial tissues were divided into small pieces, fixed in paraformaldehyde for histological staining, frozen in liquid nitrogen, and stored at −80°C for protein and mRNA analysis.

Atrial tissues were fixed in 4% paraformaldehyde for 24 h and then embedded in paraffin. The atrial tissue was sliced into 5 μm-thick cross-sections to visualize the cell structure. The sections were deparaffinized and subjected to hematoxylin and eosin (H&E) staining, Masson's trichrome staining, and picrosirius red staining for assessment of basic tissue structure and detection of fibrosis following the methods of our previous study (Wang et al., 2017). Digital photographs were taken under a Leica microscope (DM2500, Wetzlar, Germany). The distribution of collagen area was measured by two staining methods (Masson's trichrome staining and picrosirius red staining). The histopathological sections were analyzed using Image-Pro Plus software (version 6.0, Media Cybernetics, United States). The collagen area was calculated as the area of positive collagen staining divided by the entire myocardial area (%).

Western Blotting Analysis

Western blot analysis was performed to detect the expression levels of transforming growth factor-β1 (TGF-β1), collagen I and collagen III; the protocols were as previously described (Wang et al., 2017). Briefly, 40μg of protein was fractionated by 12% SDS-PAGE and then transferred onto PVDF membranes. The membranes were blocked with 5% non-fat milk for 2 h and then incubated with primary antibodies overnight at 4°C. After being washed, the membranes were incubated with horseradish peroxidase-conjugated secondary antibodies for 2 h. Finally, the membranes were visualized with chemiluminescence reagents (EMD Millipore, Billerica, MA, United States). ImageJ 1.41 Software (NIH, Bethesda, MD, United States) was used to analyze the density of the Western blotting bands. The primary antibodies were as follows: anti-TGF-β1 (1:1000; Abcam, Cambridge, MA, United States), anti-collagen I (1:1000; Abcam, Cambridge, MA, United States) and anti-collagen III (1:1000; Bioss, Beijing, China) antibodies. All protein expression levels were normalized to the GAPDH expression level (1:1000; Goodhere Biotech, Hangzhou, China).

Real-Time Polymerase Chain Reaction (RT-PCR)

RT-PCR was used to quantitatively describe the mRNA expression of TGF-β1, collagen I and collagen III. Total RNA was extracted with TRIzol Reagent (Ambion, Austin, TX, United States) according to the manufacturer's instructions. RT-PCR was performed on an ABI QuantStudio 6 Flex RT-PCR System (Applied Biosystems, United States) with the SYBR Green I incorporation method. The relative expression levels of mRNAs were calculated using the $2^{-\Delta\Delta Ct}$ method. GAPDH was used as the internal control. The primers for related genes are listed in **Table 1**.

Statistical Analysis

Data analysis was performed using SPSS software (version 23.0, SPSS Inc., Chicago, IL, United States). Continuous data are presented as the means and standard deviations and were evaluated by Student's *t*-test. Classification data were presented as proportions and evaluated by the chi-squared test or Fisher's exact test. Correlations between β1ARAb levels and other parameters were ascertained by Pearson's correlation coefficient or Spearman's rank correlation coefficient. A two-tailed $P < 0.05$ was considered statistically significant.

RESULTS

Clinical Characteristics of the Study Population

This study enrolled 70 patients with PAF; their baseline clinical characteristics are described in **Table 2**. According to LA anteroposterior diameter, participants were divided into two groups: a group with LA diameter < 40 mm (n = 47) and a group with LA diameter ≥ 40 mm (n = 23). Patients with atrial enlargement had a higher level of β1ARAbs (8.87 ± 3.16 vs. 6.75 ± 1.34 ng/mL, P = 0.005) and a lower LVEF (60.21 ± 4.87 vs. 62.95 ± 5.47%, P = 0.045) than those without atrial enlargement. No differences in age, sex, comorbidity, blood biochemical parameters or fibrosis-related biomarkers were observed between the two groups (all $P > 0.05$).

TABLE 1 | Primer sequences for RT-PCR.

Genes	Forward	Reverse
TGF-β1	5′-AGCTGTACATTGACTTCCGCAAGG-3′	5′-CAGGCAGAAGTTGGCGTGGTAG-3′
Collagen I	5′-AACTTGCCTTCATGCGTCTG-3′	5′-CCTCGGCAACAAGTTCAACA-3′
Collagen III	5′-CGGACTTGCAGGAATTACAGG-3′	5′-TTTCCGTCTCTTCCAGGTTCA-3′
GADPH	5′-CAGGGCTGCTTTTAACTCTGG-3′	5′-TGGAAGATGGTGATGGCCTT-3′

RT-PCR, reverse transcription polymerase chain reaction; TGF-β1, transforming growth factor-beta 1; GAPDH, glyceraldehyde-3-phosphate dehydrogenase.

TABLE 2 | The clinical characteristics of the study population.

Characteristics	Total participants (*n* = 70)	LA anteroposterior diameter		*P*-value
		<40 mm (*n* = 47)	≥40 mm (*n* = 23)	
Age, years	60.57 ± 13.25	60.17 ± 13.47	61.39 ± 13.04	0.720
Male, n (%)	39 (55.7)	27 (57.4)	12 (52.2)	0.677
Hypertension, n (%)	33 (47.1)	21 (44.7)	12 (52.2)	0.555
Diabetes mellitus, n (%)	15 (21.4)	10 (21.3)	5 (21.7)	0.965
Coronary heart disease, n (%)	12 (17.1)	8 (17.0)	4 (17.4)	0.969
History of stroke, n (%)	14 (20.0)	7 (14.9)	7 (30.4)	0.127
CHA_2DS_2-VASc score	2.19 ± 1.84	2.09 ± 1.78	2.39 ± 1.99	0.518
HAS-BLED score	1.01 ± 1.07	0.94 ± 0.99	1.17 ± 1.23	0.386
LVEF, %	62.05 ± 5.40	62.95 ± 5.47	60.21 ± 4.87	0.045
ALT, U/L	20.00 ± 5.46	19.75 ± 5.60	20.52 ± 5.25	0.583
FBG, mmol/L	5.13 ± 0.82	4.97 ± 0.59	5.44 ± 1.12	0.069
TG, mmol/L	1.59 ± 1.01	1.68 ± 1.14	1.39 ± 0.63	0.168
TC, mmol/L	3.76 ± 0.96	3.78 ± 0.88	3.73 ± 1.12	0.855
LDLC, mmol/L	2.35 ± 0.78	2.33 ± 0.76	2.40 ± 0.85	0.745
HDLC, mmol/L	1.11 ± 0.31	1.13 ± 0.33	1.09 ± 0.27	0.602
β1ARAbs, ng/mL	7.45 ± 2.33	6.75 ± 1.34	8.87 ± 3.16	0.005
PIIINP, ng/mL	17.09 ± 6.30	16.17 ± 4.72	18.96 ± 8.51	0.081
PICP, ng/mL	4.10 ± 0.81	4.03 ± 0.61	4.26 ± 1.11	0.254
Gal3, ng/mL	2.02 ± 0.34	1.96 ± 0.29	2.13 ± 0.40	0.058

Values are presented as the mean ± SD, or n (%). LA, left atrial; LVEF, left ventricular ejection fraction; ALT, alanine transferase; FBG, fasting blood glucose; TG, triglyceride; TC, total cholesterol; LDLC, low-density lipoprotein cholesterol; HDLC, high-density lipoprotein cholesterol; β1ARAbs, beta 1-adrenergic receptor autoantibodies; PIIINP, procollagen type β N-terminal peptide; PICP, procollagen type C-terminal peptide; Gal3, galectin-3.

Correlation of β1ARAb Levels With Fibrosis and Clinical Indexes

As demonstrated in **Figure 2**, Pearson's linear correlation analysis showed that the serum β1ARAb levels were positively correlated with LA diameter and circulating biomarkers (LA diameter: $r = 0.272$, $P = 0.023$; PIIINP: $r = 0.694$, $P < 0.001$; PICP: $r = 0.316$, $P = 0.008$; Gal3: $r = 0.545$, $P < 0.001$). β1ARAb levels did not correlate significantly with other clinical indexes, including age, LVEF, hypertension, diabetes mellitus, coronary heart disease, history of stroke, CHA_2DS_2-VASc score and HAS-BLED score (**Table 3**).

Effect of β1ARAbs on Atrial Electrophysiology

All rabbits in both groups survived through the entire research period. From the second week onward, the rabbits in the immune group, immunized with the β1AR ECL2 peptide, developed higher levels of β1ARAb than the control group (**Figure 1B**).

Spontaneous AF episodes were observed in two rabbits in the immune group in the observational period prior to the invasive electrophysiological study, but the rate difference between groups was not statistically significant (2/8 vs. 0/8, $P > 0.05$). Compared with the control group, the immune group showed a significantly increased heart rate (207.13 ± 8.63 vs. 177.13 ± 6.17 bpm, $P < 0.001$), shortened AERP (70.00 ± 5.49 vs. 96.46 ± 3.27 ms, $P < 0.001$), and increased rate of induced AF (55% vs. 0%, $P < 0.001$) 8 weeks after immunization (**Figure 3**).

Figures 4A–C demonstrate the conduction activation maps and CV maps of the LA appendage epicardial surface; a slower CV (34.38 ± 8.48 vs. 61.50 ± 13.40 cm/s, $P < 0.001$, **Figures 4D,E**) and greater conduction inhomogeneity index (2.63 ± 0.40 vs. 1.52 ± 0.25, $P < 0.001$, **Figures 4D,F**) were observed in the immune group than in the control group.

Changes in Echocardiography Parameters

Table 4 and **Figure 5A** show echocardiographic changes. In the immune group, increases in LAD, RAD, LVEDD, and LVESD

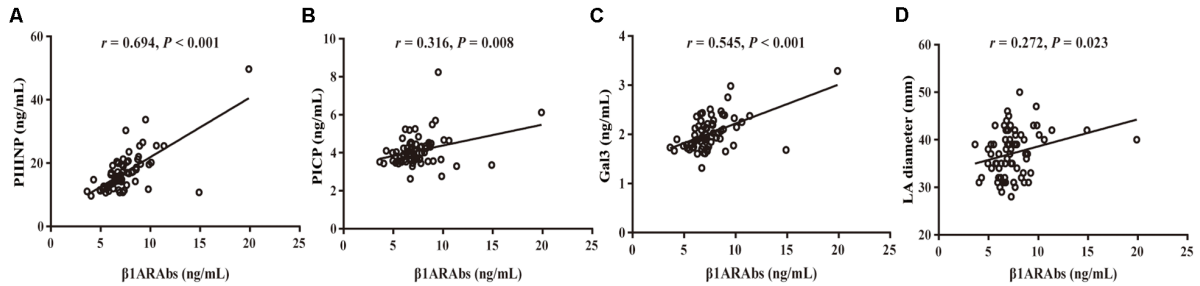

FIGURE 2 | Correlation of serum β1ARAb levels with echocardiographic indexes and fibrosis-related biomarkers (**A**, PIIINP; **B**, PICP; **C**, Gal3; **D**, LA diameter). β1ARAb, beta 1-adrenergic receptor autoantibody; PIIINP, procollagen type III N-terminal peptide; PICP, procollagen type I C-terminal peptide; Gal3, galectin-3; LA, left atrial.

TABLE 3 | Correlation analysis between β1ARAb levels and clinical indexes in patients with PAF.

	r	*P*-value
Age	−0.009	0.939
LVEF	−0.108	0.374
Hypertension	−0.070	0.564
Diabetes mellitus	−0.187	0.121
Coronary heart disease	0.024	0.841
History of stroke	0.140	0.249
CHA_2DS_2-VASc	−0.140	0.248
HAS-BLED	−0.021	0.861

β1ARAb, beta 1-adrenergic receptor autoantibody; LVEF, left ventricular ejection fraction.

and a decrease in LVEF were observed compared with the baseline levels. Compared to the control group, the immune group had significant increases in LAD, LVEDD, and LVESD and a significant decrease in LVEF after 8 weeks. There were no significant differences in LAD, RAD, LVESD, RVD, or LVEF between the baseline and endpoint in the control group, although LVEDD slightly increased after 8 weeks.

Histopathological Changes

In the control group, H&E staining showed that the cardiomyocytes were arranged neatly, and there was a small amount of connective tissue in the extracellular matrix (ECM, **Figure 5B**). However, the interstitial structure was disordered in the immune group, with extensive fibrous tissue hyperplasia accompanied by inflammatory cell infiltration and increased angiogenesis (**Figure 5C**).

Additionally, increased collagen accumulation in the ECM in the immune group was observed by Masson's trichrome staining (15.17 ± 3.46 vs. 4.92 ± 1.72%, immune and control groups, respectively, $P < 0.001$) and picrosirius red staining (16.76 ± 6.40 vs. 4.85 ± 0.40%, immune and control groups, respectively, $P < 0.001$, **Figures 5D,E**). Correlation analysis showed a significant positive correlation between circulating β1ARAb levels at 8 weeks and total fiber area ($r = 0.895$ and 0.786 for Masson's trichrome staining and picrosirius red stain, respectively, both $P < 0.001$, **Figure 5F**).

Fibrosis-Related Protein and Gene Expression

As shown in **Figure 6**, the messenger RNA and protein expression levels of TGF-β1, collagen I and collagen III were significantly upregulated in the immune group compared with the control group.

DISCUSSION

Main Finding

In the present study, we analyzed the relationship between β1ARAbs and non-invasive atrial fibrosis indicators in patients with PAF and examined the effects of atrial structural remodeling in a rabbit model with enhanced β1ARAbs expression. The major findings were as follows: (1) β1ARAb levels were positively correlated with LA anterior-posterior diameter and three circulating fibrosis markers (PIIINP, PICP, Gal3) in PAF patients; (2) excessive expression of β1ARAbs increased LAD and interstitial fibrosis and led to increased inducibility of AF along with shortened AERP, slowed CV and increased conduction heterogeneity.

β1ARAbs in AF Patients

Fibrosis is an important part of atrial remodeling in AF, and an increased LA diameter is a simple indicator of severe atrial structural remodeling and interstitial fibrosis or scarring (Liao et al., 2017). In addition, left atrium enlargement is the pathological basis and a major determinant of AF and its progression. Our study reported for the first time that β1ARAb levels have a positive linear correlation with LA diameter but are not associated with other clinical manifestations or comorbidities, suggesting that β1ARAbs may cause atrial structural remodeling and might be involved in the development of AF. This result supports the previous observation that patients with persistent AF have higher β1ARAb levels than patients with PAF (Hu et al., 2016). At the same time, our finding might also partly explain why elevated β1ARAb levels increased the AF recurrence rate after cryoablation in a previous study (Yalcin et al., 2015b), as enlarged LA size is a well-known, consistent, independent predictor of recurrence following ablation in AF;

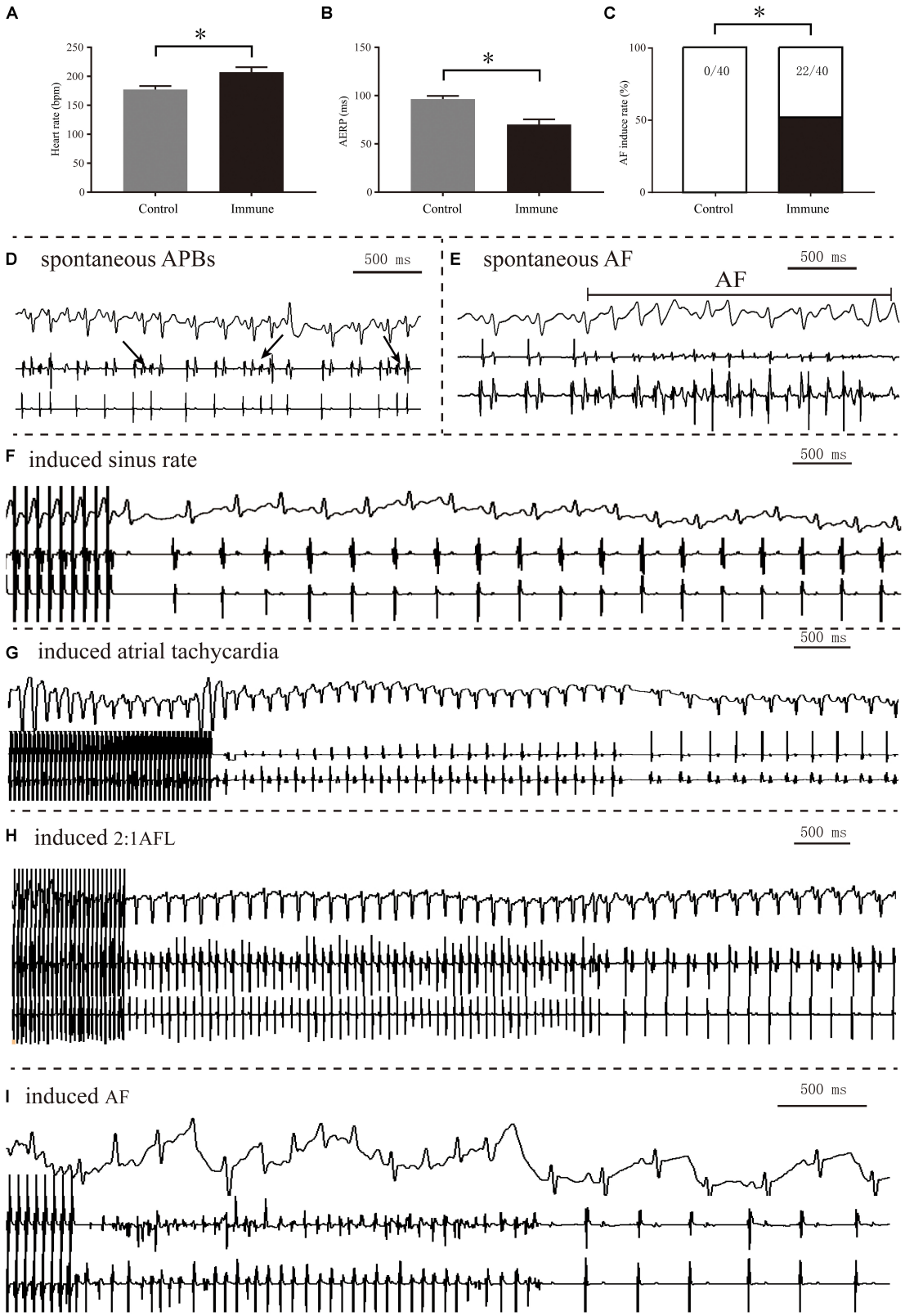

FIGURE 3 | Electrophysiology measurements of the two groups. Comparison of heart rate **(A)**, AERP **(B)**, and AF inducibility **(C)** between the two groups; spontaneous APBs **(D)** and AF **(E)** observed in the immune group; representative sinus rhythm **(F)**, sinus tachycardia **(G)**, AFL episode **(H)** and AF episode **(I)** induced after burst pacing. *$P < 0.05$, control group vs. immune group. AERP, atrial effective refractory period; AF, atrial fibrillation; APB, atrial premature beat; AFL, atrial flutter.

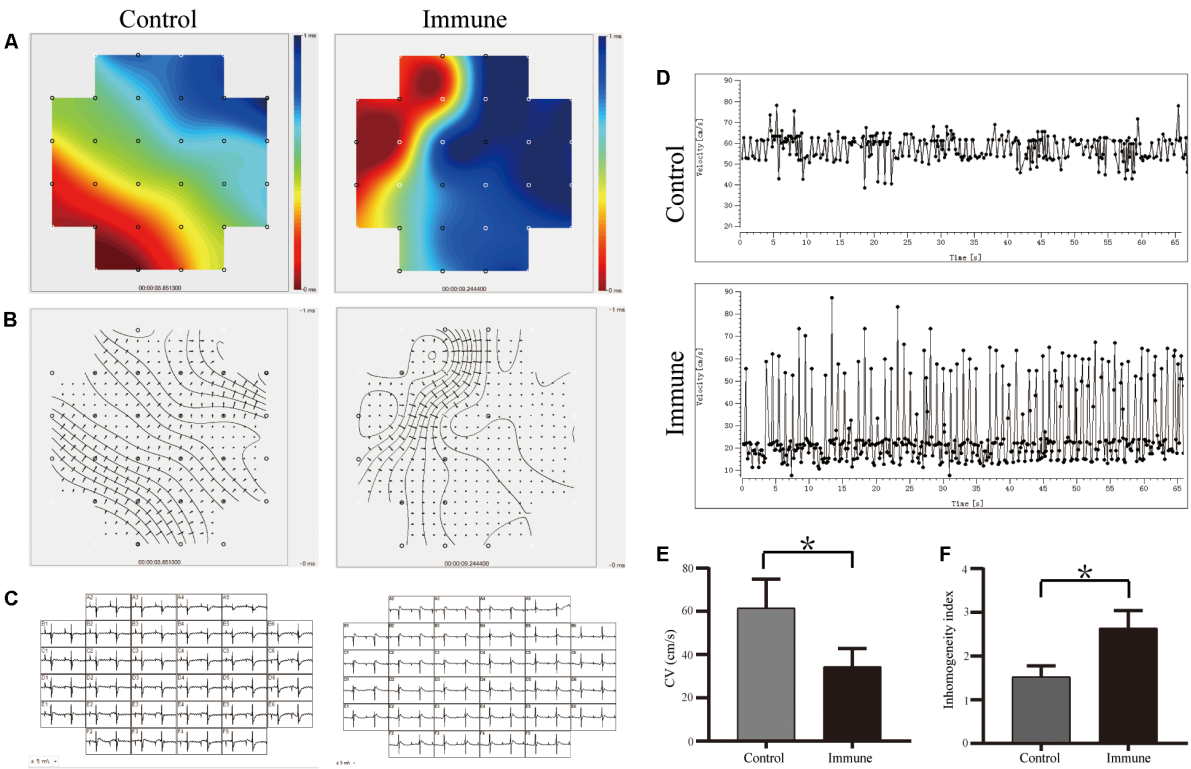

FIGURE 4 | β1ARAbs reduced the LA conduction function. **(A)** Representative color maps of epicardial multielectrode activation in LA appendage; areas of isochronal crowding were found in rabbits of immune group; **(B)** representative examples of conduction heterogeneity map in LA appendage; **(C)** recording propagation map during sinus rhythm; **(D)** conduction maps of activation in LA appendage; β1ARAbs reduced CV **(E)** and increased conduction heterogeneity **(F)**. *$P < 0.05$, control group vs. immune group. β1ARAbs, beta 1-adrenergic receptor autoantibodies; LA, left atrial; CV, conduction velocity.

TABLE 4 | Echocardiographic differences between the two groups.

Parameters	Control group			Immune group		
	Baseline	Endpoint	*P*-value	Baseline	Endpoint	*P*-value
LAD, mm	9.53 ± 0.43	9.77 ± 0.82	0.211	9.13 ± 0.64	10.93 ± 0.99*	0.012
RAD, mm	9.63 ± 0.71	10.53 ± 1.22	0.081	9.40 ± 1.11	11.23 ± 0.96	0.004
LVEDD, mm	15.18 ± 0.83	16.05 ± 0.89	0.047	14.56 ± 0.97	16.89 ± 0.44*	0.001
LVESD, mm	10.67 ± 0.86	11.42 ± 1.08	0.158	9.99 ± 0.97	12.94 ± 1.02*	<0.001
RVD, mm	8.33 ± 0.59	8.55 ± 0.62	0.153	8.16 ± 0.62	8.61 ± 0.34	0.054
LVEF, %	65.12 ± 5.14	63.71 ± 6.82	0.682	67.43 ± 5.77	54.47 ± 9.68*	0.001

$P < 0.05$ compared with the control group at the same time point. LAD, left atrial diameter; RAD, right atrial diameter; LVEDD, left ventricular end-diastolic dimension; LVESD, left ventricular end-systolic dimension; RVD, right ventricular diameter; LVEF, left ventricular ejection fraction.

its predictive ability has been confirmed in large observational studies and meta-analyses (Zhuang et al., 2012; Jin et al., 2018). Furthermore, Duan et al. (2019) found that in hypertrophic cardiomyopathy patients, those with LA diameters ≥ 50 mm had significantly higher levels of β1ARAbs than those with smaller LA diameters [52.78 (46.76, 58.34) vs. 45.03 (36.74, 55.44) ng/mL, $P = 0.042$]. Our result was similar to that of a recently published study investigating the association of another G-protein-coupled receptor autoantibody (against the M2-muscarinic acetylcholine receptor) with atrial fibrosis in AF patients; a positive correlation was found between serum autoantibody levels and collagen volume in LA appendages (Ma et al., 2019).

The main feature of atrial fibrosis is increased collagen deposition in the ECM, and human atrial fibrosis is mainly composed of types I and III collagen (Boldt et al., 2004). In the process of atrial fibrosis development, components for collagen synthesis, secretion, renewal, and deposition, such as PICP and PIIINP, are released into the blood and can be used as circulating biomarkers (Dilaveris et al., 2019). Gal3, a member of the galectin family, is elevated in fibrotic conditions and highly expressed in fibrotic cardiac tissues (Calvier et al., 2013; Clementy et al.,

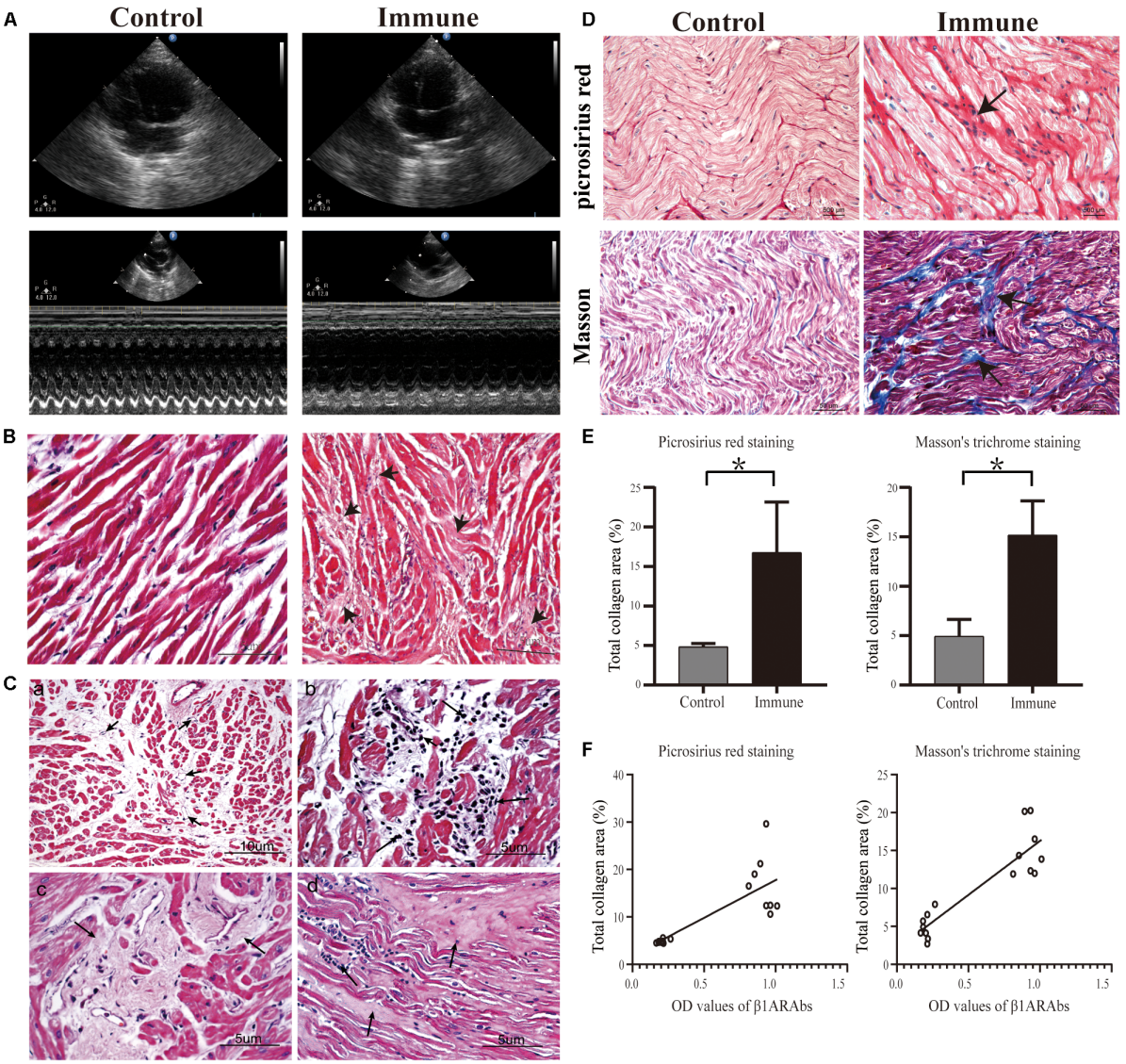

FIGURE 5 | Schematic diagram of echocardiography results and histopathological changes in atrial tissues. **(A)** increased LAD and reduced cardiac function in the immune group; **(B)** representative images of H&E staining (40×); **(C)** angiogenesis (a, 20×), inflammatory cell infiltration (b, 40×), interstitial fibrosis (c, 40×) and increased ECM (d, 40×) in the left atrium of the immune group; **(D)** representative images of picrosirius red staining (40×) and Masson's trichrome staining (20×); **(E)** quantitative assessment of atrial fibrosis between two groups; **(F)** correlation of β1ARAb OD values of 8 weeks with total collagen area. *$P < 0.05$, control group vs. immune group. LAD, left atrial diameter; H&E, hematoxylin and eosin; ECM, extracellular matrix; β1ARAb, beta 1-adrenergic receptor autoantibody; OD, optical density.

2018). In our study, serum β1ARAb levels were correlated with the levels of three fibrosis-related biomarkers. To date, however, there have been conflicting results regarding the predictive value of circulating biomarkers in atrial fibrosis. Data from patients undergoing cardiac surgery demonstrated that serum PICP levels correlated significantly with the percentage of LA fibrosis from atrial biopsy specimens (Swartz et al., 2012). Nevertheless, other studies failed to verify the correlation between these biomarkers and fibrosis as assessed by LA low-voltage area (Begg et al., 2017). A convincing explanation is that the blood levels of fibrosis-related biomarkers are susceptible to non-cardiac fibrosis, and systemic fibrosis masks their peripheral levels (Begg et al., 2018). In our study, we pre-excluded patients with severe heart failure and those with autoimmune or infectious diseases; only patients newly diagnosed with PAF were included. We hoped that, once diseases which could cause non-atrial fibrosis were mainly eliminated, the levels of these biomarkers could indicate the severity of atrial fibrosis. In addition, our results showed only weak to moderate correlations between β1ARAb levels and non-invasive atrial fibrosis indexes, although the correlations were statistically significant. The clinical significance must be interpreted with caution.

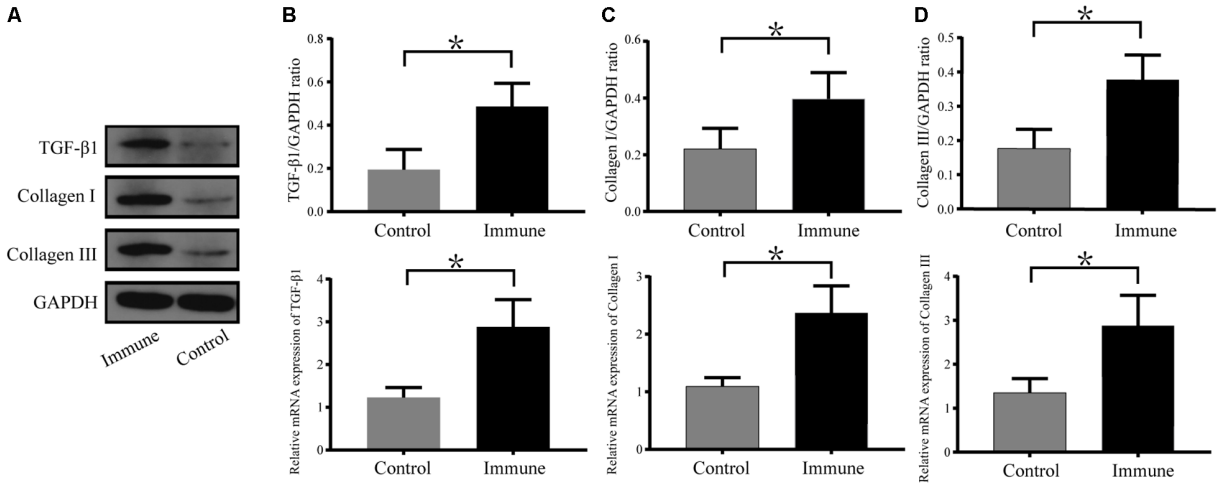

FIGURE 6 | Expression levels of TGF-β1, collagen I and collagen III in atrial tissues. **(A)** Western blotting results for TGF-β1, collagen I and collagen III in the two groups. Relative protein and mRNA expression of TGF-β1 **(B)**, collagen I **(C)**, and collagen III **(D)** are shown, following normalization to GAPDH. *$P < 0.05$, control group vs. immune group. TGF-β1, transforming growth factor-β1; GAPDH, glyceraldehyde-3-phosphate dehydrogenase.

Elevated β1ARAbs Increase AF Susceptibility in an Animal Model

We observed spontaneous AF in two immunized rabbits, although the intergroup difference in proportion was not statistically significant (2/8 vs. 0/8). Nonetheless, this finding suggested that elevated β1ARAbs might be a direct cause of AF. We also evaluated the AF propensity of these animals, and the results showed that the heart rate was enhanced and AERP was shortened after immunization, which was similar to the results of a previous study (Li et al., 2015). However, we observed a much higher rate of induced AF (22/40) than reported in that previous study (1/24), probably because we used a higher dose of injected β1ARAbs and a longer modeling time in our study. These results suggest that β1ARAbs and AF may have a dose-response relationship, as previous studies have also shown a significant negative correlation between β1ARAb levels and AERP (Li et al., 2015).

β1ARAbs Promote Atrial Structural Remodeling and Related Mechanisms

Previous studies have fully demonstrated that the long-term overexpression of β1ARAbs can cause ventricular structural changes and contribute to cardiomyopathy and heart failure progression (Jahns et al., 2004; Zuo et al., 2011). Our results were consistent with those of previous studies and generally corresponded to the expected results, with LVEDD and LVESD being increased and LVEF being decreased in the immune group after 8 weeks. In this present study, we focused on the structural changes in the atrium, and we found that overexpression of β1ARAbs led to atrial structural remodeling, manifested by increased LA diameter, heavy collagen deposition in the ECM, and increased protein and mRNA expression of collagen I and III, indicating that the heart damage caused by β1ARAbs includes both atrial and ventricular damage. This result was also consistent with the reduction in CV and the increase in conduction heterogeneity in the immune group on MEA recording, as extensive atrial fibrosis leads to disturbances in electrical conduction, and fibrous scars impede the normal conduction of atrial myocytes. Previous studies have verified that β1ARAbs specifically bind to β1ARs and exhibit agonistic activity against them, resulting in myocardial damage and cardiac dysfunction (Wang et al., 2019). Since β1AR is one of the predominant adrenergic receptors widely distributed throughout the myocardial tissue, this might explain why β1ARAbs also damage the atrium. Our results were similar to those of a previous study in an autoimmune myocarditis rat model, in which researchers found that the inducibility of AF was dependent on atrial structural remodeling rather than inflammation (Hoyano et al., 2010).

Our study did not delve into the mechanism-based signaling pathways that regulate β1ARAb-mediated atrial fibrosis. However, numerous studies have shown that at the cellular and molecular levels, various cardiac damage and pathogenic factors cause atrial fibrosis through the shared mechanism of fibroproliferative signaling, and TGF-β1 is a key mediator of ECM protein expression and fibrosis (Lijnen et al., 2000). In our models, the protein and mRNA expression levels of TGF-β1 were significantly elevated, indicating that the TGF-β1 signaling pathway is activated in the β1ARAb overexpression model. A previous study found that β1ARAbs activated the β1AR/cAMP/PKA pathway and promoted the proliferation and activation of cardiac fibroblasts (Lv et al., 2016). Activated cardiac fibroblasts are characterized by increased synthesis of collagen I and III and increased deposition of those proteins in the ECM (Cavin et al., 2014). In addition, many cytokines, such as IL-6 and TGF-β1, are secreted by fibroblasts in response to stimulation by pathogenic factors (Fu et al., 2012; Cavin et al., 2014). More interestingly, TGF-β1 can modulate cardiomyocyte survival and activate fibroblasts (Zhang et al., 2018). Therefore,

we speculated that active cardiac fibroblasts and TGF-β1 could promote each other, forming a positive feedback loop that promotes β1ARAb-induced atrial fibrosis and AF propensity, but further verification is needed. In addition, previous research also confirmed that β1ARAb activated the canonical cAMP/PKA signaling pathway in cardiomyocytes, leading to functional alterations in intracellular calcium handling (Jane-wit et al., 2007). Sustained β1ARAb agonism eventually elicited caspase-3 activation and promoted cardiomyocyte apoptosis *in vivo* (Jane-wit et al., 2007).

Therapeutic Implications of β1ARAb-Mediated AF

Evidence from clinical and experimental studies illustrates that immunoadsorption of circulating β1ARAbs improved cardiac function in cardiomyopathy (Matsui et al., 2006; Nagatomo et al., 2017). However, immunoadsorption therapy has the shortcomings of high cost, logistical challenges, and considerable time and labor requirements; oral drug treatment is increasingly coming to the fore (Jahns et al., 2006; Wess et al., 2019). Since β1ARAbs produce downstream effects by stimulating cardiac β1ARs, β-adrenoceptor inhibitors might be an effective treatment for β1ARAb-mediated injury. Evidence from an experimental study showed that nebivolol attenuates TGF-β1 pathways in a renovascular hypertension disease model (Ceron et al., 2013). Further studies are needed to determine whether β-adrenoceptor blockers have beneficial antifibrotic effects in a β1ARAb overexpression model.

Limitations

Our study has several limitations that should be mentioned. First, the cross-sectional study design did not allow us to address the causal relationship between β1ARAb levels and atrial fibrosis in PAF patients, however, we compensated by performing animal experiments. Second, we did not apply more-accurate methods to evaluate the severity of atrial fibrosis, such as cardiac magnetic resonance imaging, electrophysiological mapping, or atrial tissue biopsy. Therefore, further larger-sample cohort studies of healthy controls and different types of AF patients are necessary to demonstrate the clinical significance of β1ARAbs in AF patients. Our experiment did not include groups with different concentrations of β1ARAbs, meaning that it could not address the dose-response relationship between β1ARAbs and AF. Numerous effectors and mechanisms, such as inflammatory reactions and cardiomyocyte apoptosis, are involved in the progression of cardiac fibrosis (Kong et al., 2014); whether these mechanisms are involved in β1ARAb-induced atrial fibrosis remains unclear and needs to be addressed in further research. Additionally, our study lacks pharmacological data; therefore, the results cannot be directly used in clinical practice.

CONCLUSION

In conclusion, β1ARAb levels are positively correlated with LAD and circulating fibrosis-related biomarkers in patients with PAF. β1ARAb overexpression increases AF inducibility by facilitating atrial fibrosis, TGF-β1 signaling activation and collagen accumulation. Our results suggest that reversing atrial fibrosis may be a potential therapeutic target for the upstream prevention of β1ARAb-mediated AF.

DATA AVAILABILITY STATEMENT

The datasets generated for this study are available from the corresponding author on request.

ETHICS STATEMENT

The studies involving human participants were reviewed and approved by the Medical Ethics Committee of the First Affiliated Hospital of Xinjiang Medical University. The patients provided their written informed consent to participate in this study. The animal study was reviewed and approved by the Institutional Animal Care and Use Committee of the First Affiliated Hospital of Xinjiang Medical University.

AUTHOR CONTRIBUTIONS

BT and XZ contributed to the funding acquisition, conception, and design of the study. LS, LZ, MS, MF, JS, ZD, and JX contributed to the animal experiments. QG, RX, and HS contributed to the clinical data collection and processing. LS, LZ, and MS contributed to the statistical analysis and interpretation. All authors contributed to the writing, critical reading, and approval of the manuscript.

FUNDING

This study was supported by the National Natural Science Foundation of China (Nos. 81660053 and 81660055). The funders had no role in study design, data collection and analysis, preparation, interpretation and publish of the manuscript.

ACKNOWLEDGMENTS

We thank all the participants for their cooperation. We also thank all the colleagues in our department and laboratory for their assistance. We are grateful to Lingjie Yang, Ph.D., for her support in echocardiography measurement of experimental animals. We thank AJE (American Journal Experts) for its linguistic assistance during the preparation of this manuscript.

SUPPLEMENTARY MATERIAL

The Supplementary Material for this article can be found online at: https://www.frontiersin.org/articles/10.3389/fphys.2020.00076/full#supplementary-material

FIGURE S1 | Schematic diagram of the flexible microelectrode array experimental setup and data acquisition.

REFERENCES

Begg, G. A., Karim, R., Oesterlein, T., Graham, L. N., Hogarth, A. J., Page, S. P., et al. (2017). Intra-cardiac and peripheral levels of biochemical markers of fibrosis in patients undergoing catheter ablation for atrial fibrillation. *Europace* 19, 1944–1950. doi: 10.1093/europace/euw315

Begg, G. A., Karim, R., Oesterlein, T., Graham, L. N., Hogarth, A. J., Page, S. P., et al. (2018). Left atrial voltage, circulating biomarkers of fibrosis, and atrial fibrillation ablation. *PLoS One* 13:e0189936. doi: 10.1371/journal.pone.0189936

Boldt, A., Wetzel, U., Lauschke, J., Weigl, J., Gummert, J., Hindricks, G., et al. (2004). Fibrosis in left atrial tissue of patients with atrial fibrillation with and without underlying mitral valve disease. *Heart* 90, 400–405. doi: 10.1136/hrt.2003.015347

Burstein, B., and Nattel, S. (2008). Atrial fibrosis: mechanisms and clinical relevance in atrial fibrillation. *J. Am. Coll. Cardiol.* 51, 802–809. doi: 10.1016/j.jacc.2007.09.064

Calvier, L., Miana, M., Reboul, P., Cachofeiro, V., Martinez-Martinez, E., de Boer, R. A., et al. (2013). Galectin-3 mediates aldosterone-induced vascular fibrosis. *Arterioscler. Thromb. Vasc. Biol.* 33, 67–75. doi: 10.1161/atvbaha.112.300569

Cavin, S., Maric, D., and Diviani, D. (2014). A-kinase anchoring protein-Lbc promotes pro-fibrotic signaling in cardiac fibroblasts. *Biochim. Biophys. Acta* 1843, 335–345. doi: 10.1016/j.bbamcr.2013.11.008

Ceron, C. S., Rizzi, E., Guimarães, D. A., Martins-Oliveira, A., Gerlach, R. F., and Tanus-Santos, J. E. (2013). Nebivolol attenuates prooxidant and profibrotic mechanisms involving TGF-β and MMPs, and decreases vascular remodeling in renovascular hypertension. *Free Radic. Biol. Med.* 65, 47–56. doi: 10.1016/j.freeradbiomed.2013.06.033

Chugh, S. S., Havmoeller, R., Narayanan, K., Singh, D., Rienstra, M., Benjamin, E. J., et al. (2014). Worldwide epidemiology of atrial fibrillation: a Global Burden of disease 2010 study. *Circulation* 129, 837–847. doi: 10.1161/circulationaha.113.005119

Clementy, N., Piver, E., Bisson, A., Andre, C., Bernard, A., Pierre, B., et al. (2018). Galectin-3 in atrial fibrillation: mechanisms and therapeutic implications. *Int. J. Mol. Sci.* 19:976. doi: 10.3390/ijms19040976

Curtis, M. J., Hancox, J. C., Farkas, A., Wainwright, C. L., Stables, C. L., Saint, D. A., et al. (2013). The lambeth conventions (II): guidelines for the study of animal and human ventricular and supraventricular arrhythmias. *Pharmacol. Ther.* 139, 213–248. doi: 10.1016/j.pharmthera.2013.04.008

Dilaveris, P., Antoniou, C. K., Manolakou, P., Tsiamis, E., Gatzoulis, K., and Tousoulis, D. (2019). Biomarkers associated with atrial fibrosis and remodeling. *Curr. Med. Chem.* 26, 780–802. doi: 10.2174/0929867324666170918122502

Duan, X., Liu, R., Luo, X., Gao, X., Hu, F., Guo, C., et al. (2019). The relationship between β_1-adrenergic, M_2-muscarinic receptor autoantibody and hypertrophic cardiomyopathy. *Exp. Physiol.* doi: 10.1113/EP088263 [Epub ahead of print].

Fu, Y., Xiao, H., and Zhang, Y. (2012). Beta-adrenoceptor signaling pathways mediate cardiac pathological remodeling. *Front. Biosci. (Elite Ed.)* 4:1625–1637. doi: 10.2741/e484

Giménez, L. E., Hernández, C. C., Mattos, E. C., Brandão, I. T., Olivieri, B., Campelo, R. P., et al. (2005). DNA immunizations with M2 muscarinic and beta1 adrenergic receptor coding plasmids impair cardiac function in mice. *J. Mol. Cell. Cardiol.* 38, 703–714. doi: 10.1016/j.yjmcc.2004.12.009

Gollob, M. H. (2013). Atrial fibrillation as an autoimmune disease? *Heart Rhythm* 10, 442–443. doi: 10.1016/j.hrthm.2013.01.023

Hoyano, M., Ito, M., Kimura, S., Tanaka, K., Okamura, K., Komura, S., et al. (2010). Inducibility of atrial fibrillation depends not on inflammation but on atrial structural remodeling in rat experimental autoimmune myocarditis. *Cardiovasc. Pathol.* 19, e149–e157. doi: 10.1016/j.carpath.2009.07.002

Hu, B., Sun, Y., Li, S., Sun, J., Liu, T., Wu, Z., et al. (2016). Association of β1-adrenergic, M2-muscarinic receptor autoantibody with occurrence and development of nonvalvular atrial fibrillation. *Pacing Clin. Electrophysiol.* 39, 1379–1387. doi: 10.1111/pace.12976

Jahns, R., Boivin, V., Hein, L., Triebel, S., Angermann, C. E., Ertl, G., et al. (2004). Direct evidence for a beta 1-adrenergic receptor-directed autoimmune attack as a cause of idiopathic dilated cardiomyopathy. *J. Clin. Invest.* 113, 1419–1429. doi: 10.1172/jci20149

Jahns, R., Jahns, V., Lohse Martin, J., and Palm, D. (2006). Means for the inhibition of anti-ss1-adrenergic receptor antibodies. Patent No. WO2006EP02977. Würzburg: Julius-Maximilians-Universität. doi: 10.1172/jci200420149

Jane-wit, D., Altuntas, C. Z., Johnson, J. M., Yong, S., Wickley, P. J., Clark, P., et al. (2007). Beta 1-adrenergic receptor autoantibodies mediate dilated cardiomyopathy by agonistically inducing cardiomyocyte apoptosis. *Circulation* 116, 399–410. doi: 10.1161/CIRCULATIONAHA.106.683193

Jin, X., Pan, J., Wu, H., and Xu, D. (2018). Are left ventricular ejection fraction and left atrial diameter related to atrial fibrillation recurrence after catheter ablation? A meta-analysis. *Medicine (Baltimore)* 97:e10822. doi: 10.1097/md.0000000000010822

Kirchhof, P., Benussi, S., Kotecha, D., Ahlsson, A., Atar, D., Casadei, B., et al. (2016). 2016 ESC guidelines for the management of atrial fibrillation developed in collaboration with EACTS. *Europace* 18, 1609–1678.

Kong, P., Christia, P., and Frangogiannis, N. G. (2014). The pathogenesis of cardiac fibrosis. *Cell. Mol. Life Sci.* 71, 549–574. doi: 10.1007/s00018-013-1349-6

Lammers, W. J., Schalij, M. J., Kirchhof, C. J., and Allessie, M. A. (1990). Quantification of spatial inhomogeneity in conduction and initiation of reentrant atrial arrhythmias. *Am. J. Physiol.* 259(4 Pt 2), H1254–H1263.

Lee, H. C., Huang, K. T., Wang, X. L., and Shen, W. K. (2011). Autoantibodies and cardiac arrhythmias. *Heart Rhythm* 8, 1788–1795. doi: 10.1016/j.hrthm.2011.06.032

Li, H., Murphy, T., Zhang, L., Huang, B., Veitla, V., Scherlag, B. J., et al. (2016). β1-adrenergic and M2 muscarinic autoantibodies and thyroid hormone facilitate induction of atrial fibrillation in male rabbits. *Endocrinology* 157, 16–22. doi: 10.1210/en.2015-1655

Li, H., Scherlag, B. J., Kem, D. C., Benbrook, A., Zhang, L., Huang, B., et al. (2014). Atrial tachyarrhythmias induced by the combined effects of β1/2-adrenergic autoantibodies and thyroid hormone in the rabbit. *J. Cardiovasc. Transl. Res.* 7, 581–589. doi: 10.1007/s12265-014-9573-5

Li, H., Zhang, L., Huang, B., Veitla, V., Scherlag, B. J., Cunningham, M. W., et al. (2015). A peptidomimetic inhibitor suppresses the inducibility of β1-adrenergic autoantibody-mediated cardiac arrhythmias in the rabbit. *J. Interv. Card. Electrophysiol.* 44, 205–212. doi: 10.1007/s10840-015-0063-8

Liao, Y. C., Liao, J. N., Lo, L. W., Lin, Y. J., Chang, S. L., Hu, Y. F., et al. (2017). Left atrial size and left ventricular end-systolic dimension predict the progression of paroxysmal atrial fibrillation after catheter ablation. *J. Cardiovasc. Electrophysiol.* 28, 23–30. doi: 10.1111/jce.13115

Lijnen, P. J., Petrov, V. V., and Fagard, R. H. (2000). Induction of cardiac fibrosis by transforming growth factor-beta(1). *Mol. Genet. Metab.* 71, 418–435. doi: 10.1006/mgme.2000.3032

Lv, T., Du, Y., Cao, N., Zhang, S., Gong, Y., Bai, Y., et al. (2016). Proliferation in cardiac fibroblasts induced by β1-adrenoceptor autoantibody and the underlying mechanisms. *Sci. Rep.* 6:32430. doi: 10.1038/srep32430

Ma, G., Wu, X., Zeng, L., Jin, J., Liu, X., Zhang, J., et al. (2019). Association of autoantibodies against M2-muscarinic acetylcholine receptor with atrial fibrosis in atrial fibrillation patients. *Cardiol. Res. Pract.* 2019:8271871. doi: 10.1155/2019/8271871

Matsui, S., Fu, M. L., Hayase, M., Katsuda, S., Yamaguchi, N., Teraoka, K., et al. (1999). Active immunization of combined beta1-adrenoceptor and M2-muscarinic receptor peptides induces cardiac hypertrophy in rabbits. *J. Card. Fail.* 5, 246–254. doi: 10.1016/s1071-9164(99)90009-x

Matsui, S., Larsson, L., Hayase, M., Katsuda, S., Teraoka, K., Kurihara, T., et al. (2006). Specific removal of beta1-adrenoceptor autoantibodies by immunoabsorption in rabbits with autoimmune cardiomyopathy improved cardiac structure and function. *J. Mol. Cell. Cardiol.* 41, 78–85. doi: 10.1016/j.yjmcc.2006.04.016

Nagatomo, Y., McNamara, D. M., Alexis, J. D., Cooper, L. T., Dec, G. W., Pauly, D. F., et al. (2017). Myocardial recovery in patients with systolic heart failure and autoantibodies against β-adrenergic receptors. *J. Am. Coll. Cardiol.* 69, 968–977. doi: 10.1016/j.jacc.2016.11.067

Ribeiro, A. L., and Otto, C. M. (2018). Heartbeat: the worldwide burden of atrial fibrillation. *Heart* 104, 1987–1988. doi: 10.1136/heartjnl-2018-314443

Stavrakis, S., Yu, X., Patterson, E., Huang, S., Hamlett, S. R., Chalmers, L., et al. (2009). Activating autoantibodies to the beta-1 adrenergic and m2 muscarinic receptors facilitate atrial fibrillation in patients with Graves' hyperthyroidism. *J. Am. Coll. Cardiol.* 54, 1309–1316. doi: 10.1016/j.jacc.2009.07.015

Swartz, M. F., Fink, G. W., Sarwar, M. F., Hicks, G. L., Yu, Y., Hu, R., et al. (2012). Elevated pre-operative serum peptides for collagen I and III synthesis result in post-surgical atrial fibrillation. *J. Am. Coll. Cardiol.* 60, 1799–1806. doi: 10.1016/j.jacc.2012.06.048

Wallukat, G. (2002). The beta-adrenergic receptors. *Herz* 27, 683–690. doi: 10.1007/s00059-002-2434-z

Wallukat, G., Morwinski, M., Kowal, K., Förster, A., Boewer, V., and Wollenberger, A. (1991). Autoantibodies against the beta-adrenergic receptor in human myocarditis and dilated cardiomyopathy: beta-adrenergic agonism without desensitization. *Eur. Heart J.* 12(Suppl. D), 178–181. doi: 10.1093/eurheartj/12.suppl_d.178

Wang, H. L., Zhou, X. H., Li, Z. Q., Fan, P., Zhou, Q. N., Li, Y. D., et al. (2017). Prevention of atrial fibrillation by using sarcoplasmic reticulum calcium atpase pump overexpression in a rabbit model of rapid atrial pacing. *Med. Sci. Monit.* 23, 3952–3960. doi: 10.12659/msm.904824

Wang, X., Zhang, Y., Zhang, J., Wang, Y. X., Xu, X. R., Wang, H., et al. (2019). Multiple autoantibodies against cardiovascular receptors as biomarkers in hypertensive heart disease. *Cardiology* 142, 47–55. doi: 10.1159/000497189

Wess, G., Wallukat, G., Fritscher, A., Becker, N. P., Wenzel, K., Müller, J., et al. (2019). Doberman pinschers present autoimmunity associated with functional autoantibodies: a model to study the autoimmune background of human dilated cardiomyopathy. *PLoS One* 14:e0214263. doi: 10.1371/journal.pone.0214263

Yalcin, M. U., Gurses, K. M., Kocyigit, D., Kesikli, S. A., Ates, A. H., Evranos, B., et al. (2015a). Elevated M2-muscarinic and β1-adrenergic receptor autoantibody levels are associated with paroxysmal atrial fibrillation. *Clin. Res. Cardiol.* 104, 226–233. doi: 10.1007/s00392-014-0776-1

Yalcin, M. U., Gurses, K. M., Kocyigit, D., Kesikli, S. A., Dural, M., Evranos, B., et al. (2015b). Cardiac autoantibody levels predict recurrence following cryoballoon-based pulmonary vein isolation in paroxysmal atrial fibrillation patients. *J. Cardiovasc. Electrophysiol.* 26, 615–621. doi: 10.1111/jce.12665

Yang, Y., Zhao, J., Qiu, J., Li, J., Liang, X., Zhang, Z., et al. (2018). Xanthine oxidase inhibitor allopurinol prevents oxidative stress-mediated atrial remodeling in alloxan-induced diabetes mellitus rabbits. *J. Am. Heart Assoc.* 7:e008807. doi: 10.1161/jaha.118.008807

Zhang, Y., Lu, Y., Ong'achwa, M. J., Ge, L., Qian, Y., Chen, L., et al. (2018). Resveratrol inhibits the TGF-1-induced proliferation of cardiac fibroblasts and collagen secretion by downregulating miR-17 in rat. *Biomed. Res. Int.* 2018:8730593. doi: 10.1155/2018/8730593

Zhuang, J., Wang, Y., Tang, K., Li, X., Peng, W., Liang, C., et al. (2012). Association between left atrial size and atrial fibrillation recurrence after single circumferential pulmonary vein isolation: a systematic review and meta-analysis of observational studies. *Europace* 14, 638–645. doi: 10.1093/europace/eur364

Zuo, L., Bao, H., Tian, J., Wang, X., Zhang, S., He, Z., et al. (2011). Long-term active immunization with a synthetic peptide corresponding to the second extracellular loop of β1-adrenoceptor induces both morphological and functional cardiomyopathic changes in rats. *Int. J. Cardiol.* 149, 89–94. doi: 10.1016/j.ijcard.2009.12.023

Conflict of Interest: The authors declare that the research was conducted in the absence of any commercial or financial relationships that could be construed as a potential conflict of interest.

frontiers in Pharmacology

ORIGINAL RESEARCH
published: 19 March 2020
doi: 10.3389/fphar.2020.00256

Icariin Ameliorates Diabetic Cardiomyopathy Through Apelin/Sirt3 Signalling to Improve Mitochondrial Dysfunction

Tingjuan Ni[1], Na Lin[2], Xingxiao Huang[1], Wenqiang Lu[1], Zhenzhu Sun[3], Jie Zhang[3], Hui Lin[3], Jufang Chi[4] and Hangyuan Guo[4]**

[1] Department of Cardiology, Zhejiang University School of Medicine, Hangzhou, China, [2] Department of Cardiology, Zhejiang Chinese Medical University, Hangzhou, China, [3] Department of Cardiology, The First Clinical Medical College, Wenzhou Medical University, Wenzhou, China, [4] Department of Cardiology, Shaoxing people's Hospital (Shaoxing hospital, Zhejiang University School of Medicine), Shaoxing, China

OPEN ACCESS

Edited by:
Claudio de Lucia,
Temple University, United States

Reviewed by:
Xavier Prieur,
INSERM U1087 L'unité de recherche de l'institut du thorax, France
Joachim Neumann,
Institut für Pharmakologie und Toxikologie, Germany

***Correspondence:**
Jufang Chi
jufangc@163.com
Hangyuan Guo
guohangyuan@yeah.net

Specialty section:
This article was submitted to Cardiovascular and Smooth Muscle Pharmacology, a section of the journal Frontiers in Pharmacology

Received: 01 December 2019
Accepted: 24 February 2020
Published: 19 March 2020

Citation:
Ni T, Lin N, Huang X, Lu W, Sun Z, Zhang J, Lin H, Chi J and Guo H (2020) Icariin Ameliorates Diabetic Cardiomyopathy Through Apelin/Sirt3 Signalling to Improve Mitochondrial Dysfunction. Front. Pharmacol. 11:256. doi: 10.3389/fphar.2020.00256

Myocardial contractile dysfunction in diabetic cardiomyocytes is a significant promoter of heart failure. Herein, we investigated the effect of icariin, a flavonoid monomer isolated from *Epimedium*, on diabetic cardiomyopathy (DCM) and explored the mechanisms underlying its unique pharmacological cardioprotective functions. High glucose (HG) conditions were simulated *in vitro* using cardiomyocytes isolated from neonatal C57 mice, while DCM was stimulated *in vivo* in db/db mice. Mice and cardiomyocytes were treated with icariin, with or without overexpression or silencing of Apelin and Sirt3 *via* transfection with adenoviral vectors (Ad-RNA) and specific small hairpin RNAs (Ad-sh-RNA), respectively. Icariin markedly improved mitochondrial function both *in vivo* and *in vitro*, as evidenced by an increased level of mitochondrial-related proteins *via* western blot analysis (PGC-1α, Mfn2, and Cyt-b) and an increased mitochondrial membrane potential, as observed *via* JC-1 staining. Further, icariin treatment decreased cardiac fibrogenesis (Masson staining), and inhibited apoptosis (TUNEL staining). Together, these changes improved cardiac function, according to multiple transthoracic echocardiography parameters, including LVEF, LVSF, LVESD, and LVEDD. Moreover, icariin significantly activated Apelin and Sirt3, which were inhibited by HG and DCM. Importantly, when Ad-sh-Apelin and Ad-sh-Sirt3 were transfected in cardiomyocytes or injected into the heart of db/db mice, the cardioprotective effects of icariin were abolished and mitochondrial homeostasis was disrupted. Further, it was postulated that since Ad-Apelin

Abbreviations: DCM, Diabetic cardiomyopathy; ROS, reactive oxygen species; Cyt-b, cytochrome-b; DHE, dihydroethidium; Ad-EV, Empty adenoviral vectors RNA; Ad-Apelin, recombinant adenoviral vector expressing Apelin; Ad-Sirt3, recombinant adenoviral vector expressing Sirt3; Ad-sh Apelin, recombinant adenoviral vector expressing Apelin-specific small hairpin RNA; Ad-sh-Sirt3, recombinant adenoviral vector expressing Sirt3-specific small hairpin RNA; LVEDD, left ventricular end-diastolic diameter; LVESD, left ventricular end-systolic diameter; LVEF, left ventricular ejection fraction; LVFS, left ventricular fraction shortening; HG, high glucose.

induced different results following increased Sirt3 expression, icariin may have attenuated DCM development by preventing mitochondrial dysfunction through the Apelin/Sirt3 pathway. Hence, protection against mitochondrial dysfunction using icariin may prove to be a promising therapeutic strategy against DCM in diabetes.

Keywords: icariin, diabetic cardiomyopathy, DCM, mitochondrial dysfunction, cardiac dysfunction, Apelin/Sirt3

INTRODUCTION

In the present decade, the prevalence of diabetes and its associated complications have been steadily increasing, particularly within developing countries. In fact, diabetes has been reported by the World Health Organization as the disease requiring the most intervention; its microvascular and macrovascular complications account for the most common causes of death in patients with type 2 diabetes and heart failure (Kosiborod et al., 2018). Despite the introduction of antidiabetic drugs in the United States (US), deaths due to heart failure in diabetic patients have not declined from 1985-2015 (Cheng et al., 2018). Instead, diabetic cardiomyopathy (DCM) has become a proximate cause of heart failure among diabetic patients (Zamora and Villena, 2019), and is one of the primary causes for the reduced functioning of diabetic cardiomyocytes (Dillmann, 2019). To date, however, the mechanism of DCM remains uncharacterized.

Mitochondria are critical organelles for energy production *via* oxidative phosphorylation, a reaction that is conjugated with the production of reactive oxygen species (ROS), which either induces diverse molecular signals or cell persecution and death in cardiomyocytes (Zhou and Tian, 2018). Recent studies have revealed that high glucose (HG) concentrations induce a loss of mitochondrial networks and increased reactive ROS in cardiomyocytes (Evangelista et al., 2019). In addition, increasing evidence demonstrates that mitochondrial dysfunction contributes to the pathogenesis of DCM (Schilling, 2015; Verma et al., 2017; Zhou and Tian, 2018; Mahalakshmi and Kurian, 2019). Alternatively, the overexpression of the mitochondrial protein Mfn2 restores mitochondrial dysfunction and prevents the development of DCM (Hu et al., 2019). The mitochondrion-targeted methylglyoxal- sequestering compound MitoGamide exhibits cardioprotective effects in an experimental model of DCM (Tate et al., 2019), thereby suggesting that the alleviation of mitochondrial dysfunction may provide a novel therapeutic approach for reversing the development of DCM.

Icariin ($C_{33}H_{40}O_{15}$, ICA) is a flavonoid monomer isolated from the herb *Epimedium*, and it has garnered attention for its prospects in pharmacology, including its cardioprotective functions (Zhou et al., 2014; Meng et al., 2015). Icariin protects cardiomyocytes against oxidative stress by activating sirtuin-1 (Wu et al., 2018), thereby alleviating oxidative stress-induced cardiac apoptosis *via* mitochondrial protection (Song et al., 2016), and protects cardiomyocytes from apoptosis induced by hypertrophy *via* inhibition of ROS-dependent JNK (Zhou et al., 2014). However, the protective effect of icariin against DCM has not yet been reported.

Similarly, Apelin contains a G-protein-coupled receptor, APJ, and exhibits positive cardiovascular effects (Japp et al., 2010). Apelin is a gene composed of 77 amino acid proproteins that are readily cleaved into apelin-36, apelin-17, and apelin-13, which are bioactive Apelin fragments (Bertrand et al., 2015). In particular, apelin-13 is a predominant isoform of Apelin found in cardiac tissue (Serpooshan et al., 2015). Apelin is also able to mitigate HG-induced cardiac gap dysfunctions in cardiomyocytes *via* the AMPK pathway (Li et al., 2018). A related study has shown that Apelin gene therapy alleviates DCM through VEGF to increase myocardial vascular density *via* Sirt3 upregulation (Zeng et al., 2014). Sirt3 is a nicotinamide adenine dinucleotide (NAD+)-dependent deacetylase that is highly conserved and localized in the mitochondrial matrix (Hirschey et al., 2010; Heinonen et al., 2019). Further, Sirt3 activates PRDX3 to attenuate mitochondrial oxidative injuries and apoptosis induced by ischaemia-reperfusion injury (Wang et al., 2020). Hence, the upregulation of Sirt3 induced by Apelin gene therapy has been shown to prevent heart failure by increasing autophagy in patients with diabetes (Hou et al., 2015). However, the role Apelin and Sirt3 take in protecting against DCM *via* reducing mitochondrial dysfunction has not yet been elucidated.

In the present study, we sought to define the protective effect of icariin on DCM, while elucidating its underlying mechanism. We hypothesized that icariin would effectively alleviate mitochondrial dysfunction in cardiomyocytes during DCM through Apelin/Sirt3 signalling.

MATERIALS AND METHODS

Reagents

Icariin (purity 98.75%) and JC-1 dye were purchased from MedChem Express (MCE, NJ, USA). The dihydroethidium (DHE) probe and mitochondria isolation kits were obtained from Beyotime Biotechnology (Jiangsu, China). The *in situ* cell death detection kit (Roche) was obtained from Sigma-Aldrich (St. Louis, MO, USA); and the primary antibodies against Sirt3, Sirt1, PGC-1α, Mfn2, Cyt-b, and β-actin, as well as the goat anti-rabbit and goat anti-mouse secondary antibodies were obtained from Abcam Biotechnology (Cambridge, MA, USA). The primary antibody against Apelin was obtained from Signalway Antibody (SAB, USA). Empty adenoviral vectors (Ad-EV) and recombinant adenoviral vectors expressing Apelin (Ad-Apelin),

Sirt3 (Ad-Sirt3) or Apelin-specific small hairpin RNA (Ad-sh-Apelin), as well as Sirt3-specific small hairpin RNA (Ad-sh-Sirt3), were purchased from Hanbio Technology Ltd. (Shanghai, China). The titer of the adenoviruses was approximately 1.2×10^{10} PFU/mL.

Animal Experiments

Male db/db mice and db/+ mice (7 weeks old) were obtained from the Model Animal Research Center of Nanjing University (Nanjing, China). All animals received humanitarian care in adherence with the Institutes of Shaoxing People's Hospital Health Guidelines on the Use of Laboratory Animals. Both db/+ mice and db/db mice were fed a normal diet for four weeks. Thereafter, the adenovirus was injected into their myocardium. Mice were anesthetized with 2.5% isoflurane, and maintained under this condition for the duration of the operation. After the heart was exposed, the adenovirus (using a 50μL needle, Hamilton, 705RN, USA) was injected into the left ventricle free wall (10 μL for each of four sites). Mice (every group n = 10) were then treated with or without the icariin (30mg/kg) for an additional 16 weeks.

Transthoracic Echocardiography Recordings

A Philips iE33 system (Philips Medical, Best, Netherlands) equipped with an s5-1 probe (12-14 MHz) was used to measure the left ventricular end-diastolic diameter (LVEDD) and left ventricular end-systolic diameter (LVESD). A computer algorithm was used to assess the left ventricular ejection fraction (LVEF) and left ventricular fraction shortening (LVFS).

Transmission Electron Microscopy

The left ventricle myocardial tissues were fixed, dehydrated stepwise in an alcohol series, embedded, sectioned into 50-60 mm slices with an LKB-1 ultramicrotome, and double stained with 3% uranyl acetate lead citrate. The morphological mitochondrion changes in the myocardium were visualized with an electron microscope (JEM-2000EX TEM, Tokyo, Japan).

Histological Analysis

The left ventricular myocardial tissues were embedded in paraffin, and sectioned (5-mm thickness). Masson staining was then implemented according to standard procedures to assess cardiac collagen content.

Primary Culture of Neonatal Cardiomyocytes

Primary cardiomyocyte cultures were obtained from the ventricles of newborn (1-day-old) C57 mice according to a previously published protocol (Sreejit et al., 2008). The cardiomyocytes were incubated in a low-glucose medium (5.5 mmol/L glucose) or HG medium (25 mmol/L glucose) and treated with or without 7.5μM, 15μM, or 30μM icariin for 12, 24 or 48 h. Cardiomyocytes were transfected with the adenovirus (10 μL/mL, MOI: 100:1) in serum-free Dulbecco's Modified Eagle Medium (DMEM) for 6-8 h. The cells were then treated with HG or normal medium with or without icariin for an additional 24 h.

Determination of Apoptosis and ROS Production in Cardiac Tissue and Cardiomyocytes

Apoptosis in the myocardial tissue and cardiomyocytes was determined by TUNEL staining using left ventricular myocardial tissue embedded in paraffin according to the manufacture's protocol. Dihydroethidium (DHE) staining was used to detect intracellular levels of superoxide anions in frozen sections of the tissues.

Mitochondrial Membrane Potential Measurement

JC-1 staining and Mito-tracker Red CMXRos staining were used to measure the mitochondrial membrane potential. Cardiomyocytes were stained with 2.5 mmol/L JC-1 dye for 30 min at 37°C in the dark. The images were obtained using fluorescence microscopy (400 ×).

Mitochondria Isolation

Mitochondria were isolated from fresh cardiac tissues and cardiomyocytes using the Mitochondria Isolation Kit (Beyotime, Jiangsu, China) according to the manufacturer's instructions.

Western Blotting Analysis

Protein samples were obtained from cardiac tissues and cardiomyocytes, and their mitochondria were denatured *via* boiling. Western blotting was carried out according to a previously described protocol (Ni et al., 2019). The primary antibodies used were Sirt3, Sirt1, Apelin, Mfn2, PGC-1α, Cyt-b and β-actin.

Statistical Analysis

All experiments were repeated in triplicate. All data are presented as mean ± standard deviation. Multiple groups were compared using one-way ANOVA and the results were qualified by Bonferroni following the event. Unpaired Student's *t* tests were performed on the two groups. P values < 0.05 were considered to be statistically significant.

RESULTS

Icariin Alleviated Cardiac Dysfunction and Rescued Mitochondrial Dysfunction in db/db Mouse Hearts

Icariin significantly increased cardiac function performance, resulting in increased LVEF and LVFS, and decreased LVEDD and LVESD in db/db mice. (**Figures 1A–D**, $P < 0.05$). As demonstrated by Masson staining, collagen deposition was reduced in the myocardium of icariin-treated db/db mice

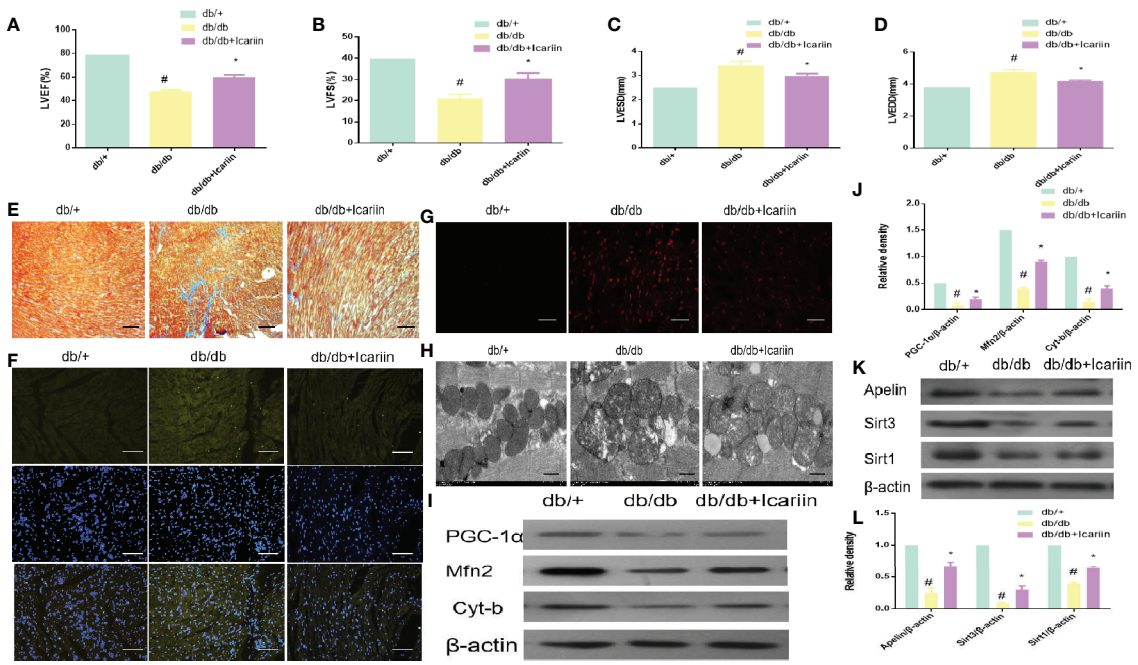

FIGURE 1 | Icariin improves the cardiac function in the diabetic heart, improves mitochondrial dysfunction in diabetic myocardium and increases Apelin expression. Db/db mice (n = 10) were treated with icariin (30 mg/kg), db/+mice (n = 10). **(A)** LVEF (%) recordings; **(B)** LVFS (%) recordings; **(C)** LVESD (mm) recordings; **(D)** LVEDD (mm) recordings; **(E)**, Collagen deposition measured by Masson staining (blue indicates collagen deposition); **(F)** Apoptotic rate of cardiomyocytes measured by TUNEL staining; **(G)** ROS production measured by DHE staining; **(H)**, Mitochondrial morphology measured by TEM; **(I)** Protein expression with representative gel blots of PGC-1α, Mfn2, Cyt-b, and β-actin (loading control); **(J)** Relative levels of PGC-1α, Mfn2, Cyt-b; **(K)**, Protein expression with representative gel blots of Apelin, Sirt1 and Sirt3; **(L)** Relative levels of Apelin, Sirt1 and Sirt3. $^{\#}P < 0.05$ vs db/+and $^{*}P < 0.05$ vs db/db; experiments were performed in triplicate.

(**Figure 1E**). On the other hand, TUNEL staining revealed that icariin treatment rescued the apoptotic rate of cardiomyocytes (**Figure 1F**). Moreover, the myocardial tissue of db/db mice showed a greater production of ROS, which was alleviated by icariin, as shown by DHE staining (**Figure 1G**). TEM revealed that in DCM, the fibrous region of mitochondria had an uneven, more fragmented, and swollen appearance, causing them to lose their recognizable crest; however, these characteristics were significantly mitigated in icariin-treated mice (**Figure 1H**). Further, the mitochondrial dynamics-related protein, Mfn2, mitochondrial biogenesis regulation protein, PGC-1α, and mitochondrial gene, cytochrome-b (Cyt-b), were upregulated in the icariin-treated db/db mice (**Figures 1I, J**, $P < 0.05$). We also observed a downregulation in the expression of the cardiac myocardium gene Apelin and the mitochondrial matrix gene Sirt3 in the hearts of db/db mice following DCM, but their expression increased following icariin treatment. As previously reported, Sirt1 expression was consistent with this change (Saito et al., 2016; Ding et al., 2018) (**Figures 1K, L**, $P < 0.05$). These results indicated the amelioration of excessive mitochondrial damage in DCM following icariin treatment, which exerted cardioprotective effects by reversing mitochondrial dysfunction in DCM and may thus mediate Apelin to exert its positive effect.

Icariin Rescued the Impaired Mitochondria and Reduced Apoptosis in HG-Treated Cardiomyocytes

We next sought to further confirm that mitochondrial dysfunction is required for DCM in hyperglycemia. Firstly, we observed that the number of HG-treated cardiomyocytes was significantly higher following incubation with icariin for 12h, 24h, or 48 h at concentrations of 7.5, 15, or 30 μM, compared to the HG group. For all subsequent experiments, icariin was used at a concentration of 30 μM (**Figure 2A**, $P < 0.05$). Secondly, we found that the expression of mitochondrion-related proteins, including PGC-1α, Mfn2, and Cyt-b, decreased in HG- treated cardiomyocytes, however, the expression of these proteins significantly increased in the HG+ icariin group (**Figures 2B, C**, $P < 0.05$). As shown in **Figure 2E**, icariin increased the mitochondrial membrane potential, as revealed by the transition from red fluorescence to green fluorescence *via* JC-1 staining, Meanwhile, staining the mitochondria with MitoTracker Red (**Figure 2D**) revealed that the loss of mitochondrial membrane potential significantly reduced red fluorescence in the HG group, which was reversed following treatment with icariin. Next, as expected, the level of apoptosis in cardiomyocytes within the icariin + HG group was significantly reduced relative to that of the HG group (**Figure 2F**). Similar to the results obtained in the heart of db/db mice, a marked decrease in the

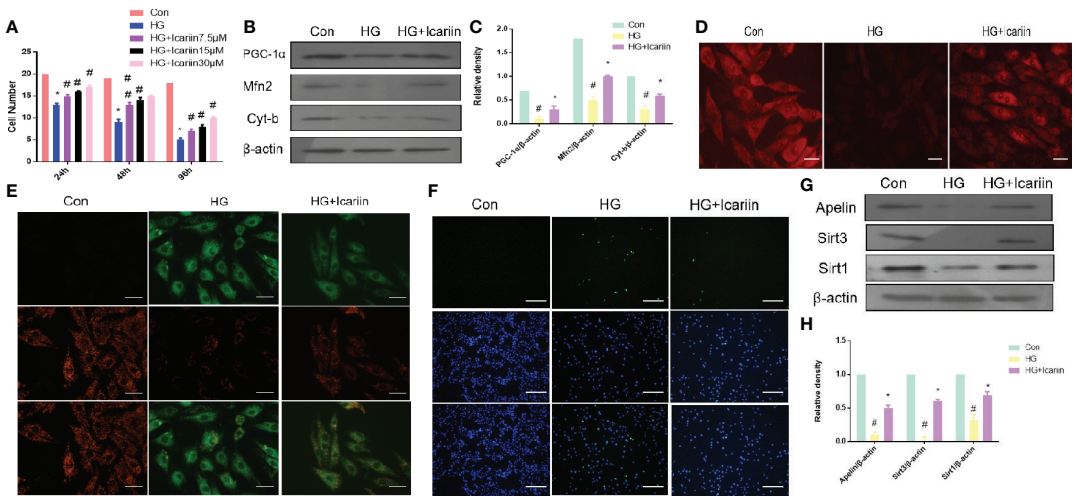

FIGURE 2 | Icariin rescues impaired mitochondria, reduces apoptosis in cardiomyocytes, and increases Apelin expression. **(A)** Cardiomyocytes were treated with 7.5, 15, or 30 μM icariin for 24, 48, and 96 h, followed by DNA quantification to determine cell number/cell proliferation, after treatment with or without 25 mmol/L HG. Cardiomyocytes were then incubated with or without icariin (30μM) under HG (25mmol/L) stimulation. **(B)** Protein expression with representative gel blots of PGC-1α, Mfn2, Cyt-b, and β-actin (loading control); **(C)** Relative levels of PGC-1α, Mfn2, and Cyt-b. **(D)** Mitochondrial membrane potential measured by MitoTracker Red staining; **(E)** Mitochondrial membrane potential measured by JC-1 staining. Magnification ×400; **(F)** Apoptotic rate of cardiomyocytes measured by TUNEL staining. **(G)** Protein expression with representative gel blots of Apelin, Sirt1 and Sirt3, and β-actin (loading control); **(H)** Relative levels of Apelin, Sirt1 and Sirt3. $^{\#}P < 0.05$ vs Con and $^{*}P < 0.05$ vs HG; experiments were performed in triplicate.

expression of Apelin and Sirt3 was observed in the HG group (**Figures 2G, H**, $P < 0.05$), while icariin treatment dramatically alleviated the reduction in Apelin and Sirt3 expression, as previously reported, Sirt1 expression was consistent with this change (Saito and Asai, 2016; Ding and Feng, 2018). Cumulatively, these results confirm that *in vitro* icariin prevents HG-induced mitochondrial dysfunction-mediated cardiac apoptosis and may regulate the expression of Apelin and Sirt3.

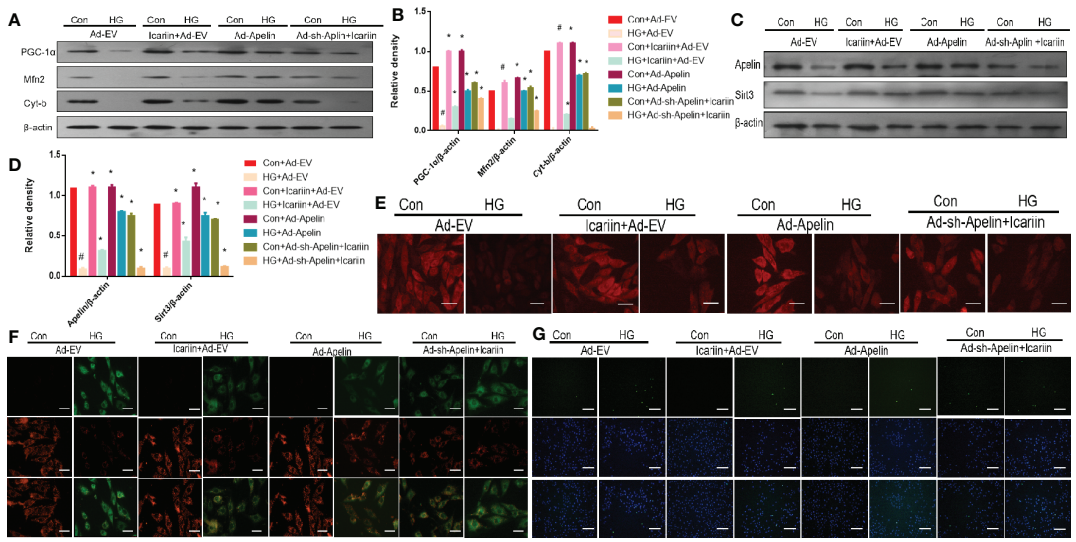

FIGURE 3 | Icariin fails to exert protective effects in cardiomyocytes transfected with Ad-sh-Apelin. Cardiomyocytes were transfected with Ad-EV, Ad-Apelin, and Ad-sh-Apelin (10 μL/mL, MOI: 100:1) for 6-8 hours, and then incubated with or without icariin (30μM) under HG (25mmol/L) stimulation. **(A)** Protein expression with representative gel blots of Apelin, Sirt3 (loading control); **(B)** Relative levels of Apelin and Sirt3; **(C)** Protein expression with representative gel blots of PGC-1α, Mfn2, Cyt-b, and β-actin (loading control); **(D)** Relative levels of PGC-1α, Mfn2 and Cyt-b. **(E)** Mitochondrial membrane potential measured by MitoTracker Red staining. **(F)** Mitochondrial membrane potential measured by JC-1 staining. **(G)** Apoptotic rate of cardiomyocytes measured by TUNEL assay. $^{\#}P < 0.05$ vs Con+Ad-EV and $^{*}P < 0.05$ vs HG+Ad-EV, experiments were performed in triplicate.

Apelin Inhibition Abolished the Cardioprotective Effect of Icariin on Mitochondrial Dysfunction in HG-Treated Cardiomyocytes and Diabetic Mice

We next explored the molecular mechanisms underlying the cardioprotective effects of icariin in HG-treated cardiomyocytes, while also deciphering whether Apelin and Sirt3 are integral components for the cardioprotective effects of icariin. As shown in **Figures 3A, B** ($P < 0.05$), in HG-treated cardiomyocytes without the overexpression of Apelin icariin treatment caused a significant increase in the expression of PGC-1α, Mfn2, and Cyt-b, compared to the HG + Ad-EV group. Moreover, the HG + Ad-Apelin group evidently expressed mitochondrion-related proteins at levels comparable to, or greater than, that of the HG + icariin group. Alternatively, Ad-sh-Apelin administration significantly reversed the effect of icariin, thereby contributing to the offsetting of its cardioprotective function, as demonstrated by a decrease in mitochondrial membrane potential, as detected *via* MitoTracker Red staining (**Figure 3E**) and JC-1 staining (**Figure 3F**). Moreover, cardiomyocyte apoptosis was increased in the HG + icariin + Ad-sh-Apelin group compared to the HG + icariin + Ad-EV group (**Figure 3G**). Interestingly, Apelin significantly directed the expression of Sirt3 in Apelin-overexpressing HG-treated cardiomyocytes and the HG + Ad-sh-Apelin + icariin group (**Figures 3C, D**, $P < 0.05$).

Subsequently, we explored whether icariin administration could restore DCM without overexpression of Apelin in diabetic hearts. As shown in **Figures 4A, D** ($P < 0.05$), Apelin inhibition counteracted the cardioprotective effects of icariin shown by a significant decrease in LVEF and LVFS and an evident increase in LVEDD and LVESD, compared to the HG + icariin + Ad-EV group. Furthermore, the alleviation of mitochondrial dysfunction in DCM by icariin was eliminated following an injection of Ad-sh-Apelin to db/db mice, as indicated by a greater decrease in mitochondrial protein expression (PGC-1α, Mfn2, and Cyt-b) (**Figures 4E, F** $P < 0.05$), and increased production of ROS (**Figure 4I**). The mitochondria were also characterized by a greater loss of cristae, as well as increased swelling and significant distortion (**Figure 4J**). Moreover, increased mitochondrial dysfunction resulted in a greater level of collagen deposition in the heart tissue (**Figure 4K**) and increased cardiomyocyte apoptosis (**Figure 4L**). Although the expression of Sirt3 and Apelin in db/db mice injected with Ad-sh-Apelin was less than that in the db/db + icariin group (**Figures 4G, H**, $P < 0.05$), when Apelin was silenced in db/db mice or cardiomyocytes, icariin treatment failed to improve mitochondrial dysfunction and cardiac dysfunction.

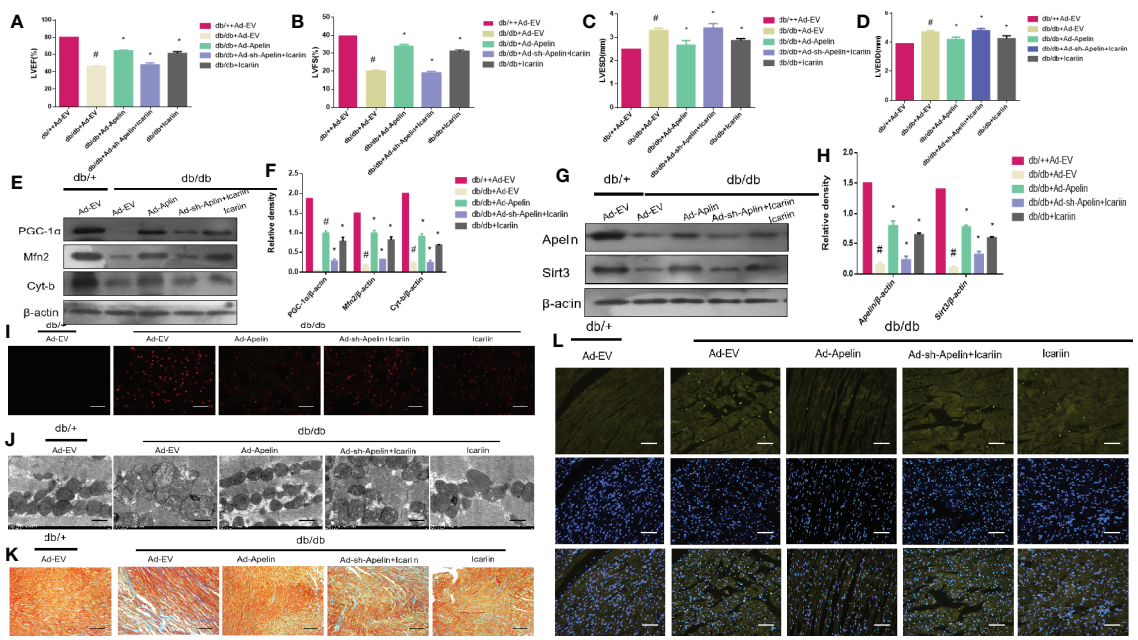

FIGURE 4 | Icariin fails to exert protective effects in diabetic mice injected with Ad-sh-Apelin. Db/+mice (n = 10) and db/db mice (n = 10) fed with or without icariin (30 mg/kg) were injected with Ad-EV, Ad-Apelin, Ad-sh-Apelin (10 μL at each of four sites, 1.2×10^{10} PFU/mL) into the left ventricle free wall. **(A)** LVEF (%) recordings; **(B)** LVFS (%) recordings; **(C)** LVESD (mm) recordings; **(D)** LVEDD (mm) recordings; **(E)** Protein expression with representative gel blots of PGC-1α, Mfn2, Cyt-b, and β-actin (loading control); **(F)** Relative levels of PGC-1α, Mfn2 and Cyt-b; **(G)** Protein expression with representative gel blots of Apelin, Sirt3 and β-actin (loading control); **(H)** Relative levels of Apelin and Sirt3. **(I)** ROS production measured by DHE staining; **(J)** Mitochondrial morphology measured by TEM; **(K)** Collagen deposition measured by Masson staining (blue indicates collagen deposition). **(L)** Apoptotic rate of cardiomyocytes measured by TUNEL staining. $^{\#}P < 0.05$ vs db/+ +Ad-EV and $^{*}P < 0.05$ vs db/db+Ad-EV; experiments were performed in triplicate.

Apelin/Sirt3 signaling Is Involved in Icariin-Mediated Mitigation of Mitochondrial and Cardiac Dysfunction

Our previous results demonstrated that icariin alleviated DCM by increasing the expression of Apelin. In addition, we found that the expression level of Sirt3, a gene located in the mitochondrial matrix, changed with the expression of Apelin. Hence, we next explored the role of Sirt3 in the cardioprotective effect of icariin in HG-treated cardiomyocytes. As shown in **Figures 5A, B** ($P < 0.05$), although Sirt3 overexpression increased the expression of the mitochondrial proteins PGC-1α, Mfn2, and Cyt-b, a significant decrease occurred when Apelin expression was silenced in HG-treated cardiomyocytes (**Figures 5C, D**, $P < 0.05$). This was also demonstrated by the decrease in mitochondrial membrane potential, as assessed by MitoTracker Red staining (**Figure 5E**) and JC-1 staining (**Figure 5F**), as well as the increase in apoptosis of cardiomyocytes (**Figure 5G**).

To further elucidate the role of Sirt3 in the mitochondrion-protective role against DCM following icariin treatment, the hearts of db/db mice were injected with Ad-sh-Sirt3, Ad-Sirt3, Ad-Apelin, or Ad-sh-Apelin. Consistent with previous results, Sirt3 elicited a marked effect when Apelin was not silenced. However, in the db/db + Ad-sh-Apelin + Ad-Sirt3 +icariin group, a significant decrease in LVEF and LVFS (**Figures 6A, B**, $P < 0.05$) as well as an evident increase in LVEDD and LVESD (**Figures 6C, D**, $P < 0.05$) were found relative to the results in the db/db + Ad-Sirt3 + icariin group. In addition, a lower expression of the mitochondrial proteins (**Figures 6E, F**, $P < 0.05$) and greater ROS production were revealed *via* DHE staining (**Figure 6I**). Additionally, the interfibrillar mitochondria displayed less uniformity and more fragmentation as well as a swollen appearance, as seen in the TEM analysis (**Figure 6J**). Lastly, increased apoptosis of the cardiomyocytes was demonstrated *via* TUNEL staining (**Figure 6L**), resulting in more collagen deposition in myocardial tissue, as measured by Masson staining (**Figure 6K**), due to adverse cardiac dysfunction. As expected, Sirt3 expression decreased when Ad-Sirt3 was transfected into the cardiomyocytes under the prerequisite of silent Apelin expression (**Figures 6G, H**, $P < 0.05$). Taken together, these results suggested that Apelin/Sirt3 signaling is directly responsible for the cardioprotective effects of icariin in DCM and under hyperglycemic conditions.

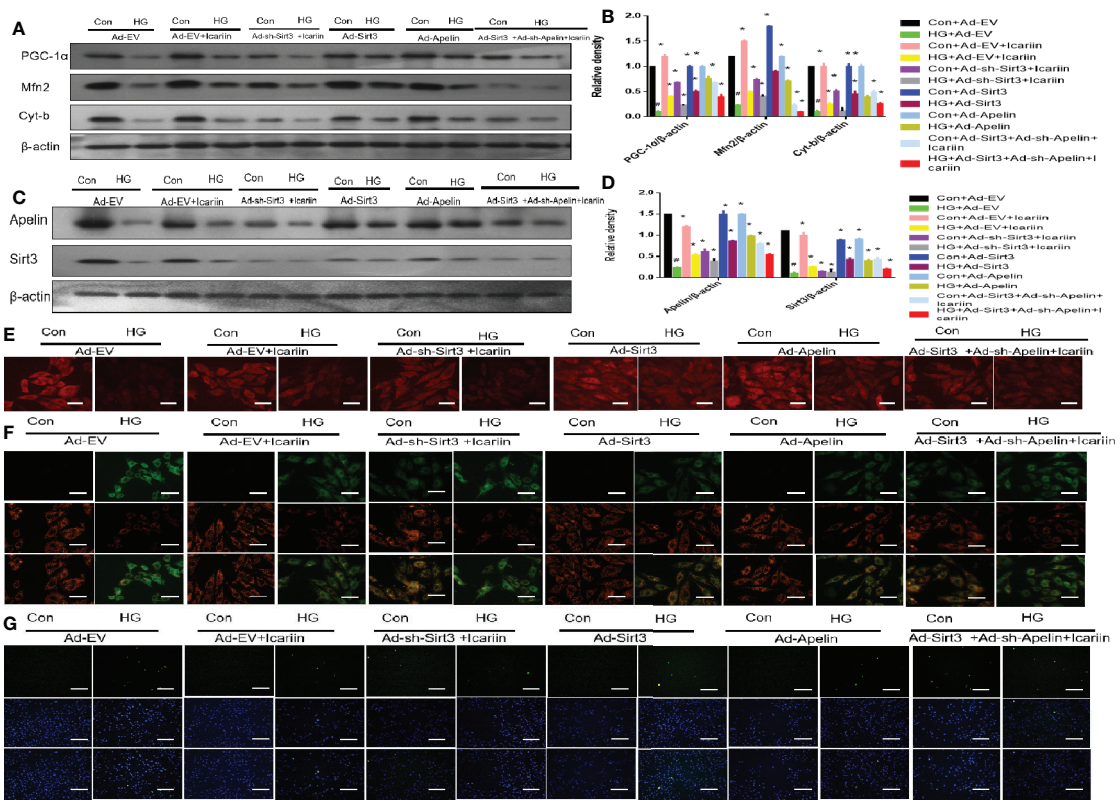

FIGURE 5 | Icariin mitigates mitochondrial dysfunction through the Apelin/Sirt3 pathway. Cardiomyocytes were transfected with Ad-EV, Ad-Apelin, Ad-sh-Apelin, Ad-sh-Sirt3, or Ad-Sirt3 (10 μL/mL, MOI: 100:1) for 6-8 hours, and incubated with or without icariin (30 μM) under HG (25 mmol/L) stimulation. **(A)** Protein expression with representative gel blots of PGC-1α, Mfn2, Cyt-b and β-actin (loading control); **(B)** Relative levels of PGC-1α, Mfn2 and Cyt-b; **(C)** Protein expression with representative gel blots of Apelin, Sirt3, β-actin (loading control); **(D)** Relative levels of Apelin and Sirt3; **(E)** Mitochondrial membrane potential measured by MitoTracker Red staining. **(F)** Mitochondrial membrane potential measured by JC-1 staining; **(G)** Apoptotic rate of cardiomyocytes measured by TUNEL assay. $^{\#}P < 0.05$ vs Con+Ad-EV and $^{*}P < 0.05$ vs HG+Ad-EV; experiments were performed in triplicate.

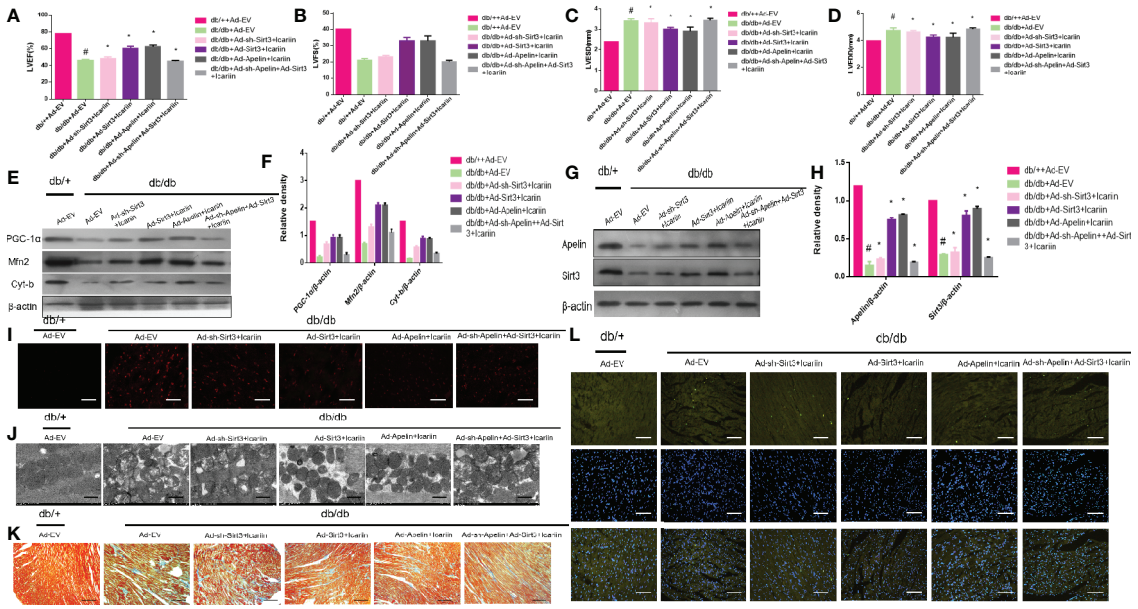

FIGURE 6 | Icariin mitigates adverse cardiac dysfunction through the Apelin/Sirt3 signalling pathway. Db/+mice (n = 10) and db/db mice (n = 10) were injected with Ad-EV, Ad-Apelin, Ad-sh-Apelin,Ad-Sirt3 or Ad-sh-Sirt3 (10 μL at each of four sites, 1.2×10^{10} PFU/mL) into the left ventricle free wall, and treated with or without icariin (30 mg/kg). **(A)** LVEF (%) recordings; **(B)** LVFS (%) recordings; **(C)** LVESD (mm) recordings; **(D)** LVEDD (mm) recordings; **(E)** Protein expression with representative gel blots of PGC-1α, Mfn2, Cyt-b and β-actin(loading control); **(F)** Relative levels of PGC-1α, Mfn2, and Cyt-b; **(G)** Protein expression with representative gel blots of Apelin, Sirt3 and β-actin (loading control); **(H)** Relative levels of Apelin and Sirt3. **(I)** ROS production measured by DHE staining; **(J)** Mitochondrial morphology measured by TEM; **(K)** Collagen deposition measured by Masson staining (blue indicate collagen deposition). **(L)** Apoptotic rate of cardiomyocytes measured by TUNEL staining. $^{\#}P < 0.05$ vs db/++Ad-EV and $^{*}P < 0.05$ vs db/db+Ad-EV; experiments were performed in triplicate.

DISCUSSION

DCM is characterized by cardiac structural and functional abnormalities in diabetic patients without ischaemic or hypertensive heart disease (Jia et al., 2018). The researchers from the Framingham Heart Disease study were the first to report that the risk of heart failure in type 2 diabetes increases by 2-8 times, with 19% of individuals presenting symptoms of heart failure (Kannel et al., 1974). According to the latest report, the economic costs of diabetes and its complications account for an extensive global burden, especially in developing countries (Seuring et al., 2015). However, to date, no specific therapy or western medicine strategy has been shown to cure or alleviate DCM. In addition, a clear molecular mechanism for DCM has not been defined. In the present study, we systematically demonstrated that the cardioprotective effect of icariin against DCM relies on preventing mitochondrial dysfunction through the activation of Apelin/Sirt3 signaling.

Several previous studies have focused on mitochondria as a promising target for the treatment of DCM as mitochondrial dysfunction has been found to be associated with cardiovascular abnormalities in diabetes, which leads to DCM (Ni et al., 2016; Fan et al., 2017; Evangelista et al., 2019; Tang et al., 2019). In our study, mitochondrial dysfunction was apparent in the HG-treated cardiomyocytes and DCM, as demonstrated by the downregulated expression of the mitochondrial dynamic-related protein Mfn2, mitochondrial biogenesis regulation protein PGC-1α, and mitochondrial gene Cyt-b. This was also revealed by the increased production of ROS from the mitochondria as determined by DHE staining, and by the loss of uniform appearance and development of more fragmented swelling within interfibrillar mitochondria, loss of discernible ridges as assessed by TEM, and decreased mitochondrial membrane potential as assessed by JC-1 staining and MitoTracker Red staining (**Figures 1H–J**, **2A–D**). Moreover, the expression of Apelin and Sirt3 was downregulated in HG-treated cardiomyocytes and DCM. Mounting evidence suggests that Apelin acts as an important adipokine against diabetes (Castan-Laurell et al., 2011; Czarzasta et al., 2019). Hence, as expected, the overexpression of Apelin reversed the mitochondrial dysfunction (**Figures 3A–F**). Our findings suggest that the endogenous activation of Apelin may be a potential therapeutic target for DCM.

Many studies have demonstrated that icariin, a polyphenol flavonoid (Meng et al., 2015), protects cardiomyocytes from injury and, therefore, elicits cardioprotective effects (Ke et al., 2015; Zheng et al., 2019). Interestingly, we found that icariin restored the cardiac function in DCM, as demonstrated by the decrease in LVEF and LVFS (**Figures 1A, B**) and the evident increase in LVEDD and LVESD (**Figures 1C, D**). Additionally, icariin alleviated mitochondrial dysfunction in HG-treated cardiomyocytes and the myocardium of db/db mice based on the expression of mitochondrial-related proteins, PGC-1α, Mfn2 and Cyt-b, demonstrated with JC-1 staining, DHE staining, and

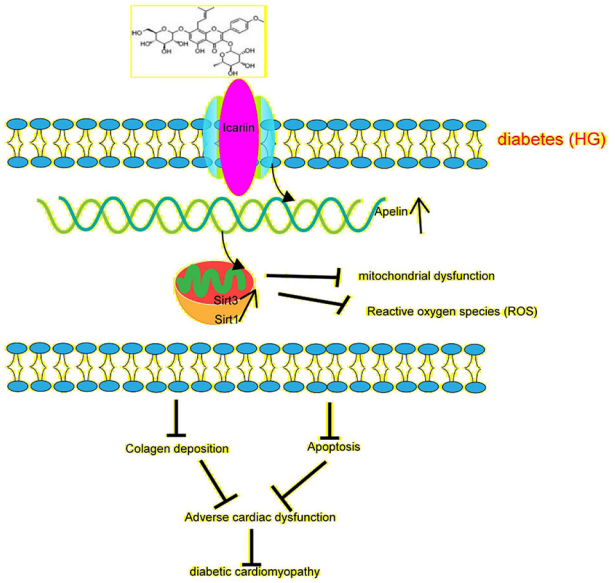

FIGURE 7 | Schematic illustrating icariin's protection against diabetes-induced mitochondrial dysfunction in cardiomyocytes and cardiac dysfunction through Apelin/Sirt3 signaling. represents enhancement represents inhibition.

TEM. (**Figures 1E–I**, **2A–D**). Surprisingly, icariin treatment was found to reduce the expression of Apelin and Sirt3 in HG-treated cardiomyocytes and db/db mice myocardium. (**Figures 1K, L**, **2F, G**).

Emerging studies suggest that sirtuins play a critical role in diabetes (Turkmen, 2014). Sirtuins contain Sirt3 in the mitochondria (Javadipour et al., 2019), which is widely expressed in the heart. Moreover, Sirt3 has been found to prevent the development of DCM in the heart (Sun et al., 2018). In this study, we found that the overexpression of Sirt3 in HG-treated cardiomyocytes alleviated mitochondrial dysfunction (**Figures 5A, B, E, F**), compared to that achieved in the HG + Ad-EV group. More importantly, icariin increased the expression of Sirt3 (**Figures 2F, G**, **3K, L**), however, it did not affect the activity of Sirt3 in Ad-sh-Apelin transfected samples, HG-treated cardiomyocytes (**Figures 3C, D**) or in db/db mice injected with Ad-sh-Apelin (**Figures 4G, H**). Despite the overexpression of Sirt3, icariin had no cardioprotective effect in the presence of Apelin inhibition (**Figures 5A–G**, **6A–L**). Such findings strongly suggest that Apelin/Sirt3 signaling mediates the cardioprotective effects of icariin against the development of DCM (**Figure 7**).

CONCLUSIONS

In the present study, we revealed that icariin can alleviate mitochondrial dysfunction and decrease apoptosis and adverse cardiac dysfunction in DCM. In addition, we found that its mechanisms are associated with Apelin/Sirt3 signaling. Together, the findings of this study demonstrate that icariin may serve as a promising therapeutic agent for the treatment and prevention of DCM.

DATA AVAILABILITY STATEMENT

All datasets generated for this study are included in the article/supplementary material.

ETHICS STATEMENT

The animal study was reviewed and approved by Shaoxing People's Hospital Health Guidelines on the Use of Laboratory Animals.

AUTHOR CONTRIBUTIONS

Conceptualization: JC and HG. Methodology: TN. Software: NL. Validation: TN, HG, JC. Formal analysis: XH. Investigation: WL. Resources: ZS. Data curation: JZ. Writing—original draft preparation: TN. Writing—review and editing: NL. Visualization: HL. Supervision: XH. Project administration: JC. Funding acquisition: HG.

FUNDING

This study was funded by the National Natural Science Foundation of China (81873120) and the Social Development Project of Public Welfare Technology Application in Zhejiang Province (LGF19H020006) and Shaoxing Science and Technology Project (LGD19H110002).

REFERENCES

Bertrand, C., Valet, P., and Castan-Laurell, I. (2015). Apelin and energy metabolism. *Front. Physiol.* 6, 115. doi: 10.3389/fphys.2015.00115

Castan-Laurell, I., Dray, C., Attané, C., Duparc, T., Knauf, C., and Valet, P. (2011). Apelin, diabetes, and obesity. *Endocrine* 40, 1–9. doi: 10.1007/s12020-011-9507-9

Cheng, Y. J., Imperatore, G., and Geiss, L. S. (2018). Trends and Disparities in Cardiovascular Mortality Among U.S. Adults With and Without Self-Reported Diabetes 1988 – 2015. *Diabetes Care* 11, 2306–2315. doi: 10.2337/dc18-0831

Czarzasta, K., Wojno, O., Zera, T., Puchalska, L., Dobruch, J., and Cudnoch-Jedrzejewska, A. (2019). The influence of post-infarct heart failure and high fat diet on the expression of apelin APJ and vasopressin V1a and V1b receptors. *Neuropeptides* 78, 101975. doi: 10.1016/j.npep.2019.101975

Dillmann, W. H. (2019). Diabetic Cardiomyopathy. *Circ. Res.* 124, 1160–1162. doi: 10.1161/CIRCRESAHA.118.314665

Ding, M., Feng, N., Tang, D., Feng, J., Li, Z., Jia, M., et al. (2018). Melatonin prevents Drp1-mediated mitochondrial fission in diabetic hearts through SIRT1-PGC1α pathway. *J. Pineal Res.* 65 (2), e12491. doi: 10.1111/jpi.12491

Evangelista, I., Nuti, R., Picchioni, T., Dotta, F., and Palazzuoli, A. (2019). Molecular Dysfunction and Phenotypic Derangement in Diabetic Cardiomyopathy. *Int. J. Mol. Sci.* 20, 3264. doi: 10.3390/ijms20133264

Fan, F., Zhuang, J., Zhou, P., Liu, X., and Luo, Y. (2017). MicroRNA-34a promotes mitochondrial dysfunction-induced apoptosis in human lens epithelial cells by targeting Notch2. *Oncotarget* 8, 110209. doi: 10.18632/oncotarget.22597

Heinonen, T., Ciarlo, E., Le Roy, D., and Roger, T. (2019). Impact of the Dual Deletion of the Mitochondrial Sirtuins SIRT3 and SIRT5 on Anti-microbial Host Defenses. *Front. Immunol.* 10, 2341. doi: 10.3389/fimmu.2019.02341

Hirschey, M. D., Shimazu, T., Goetzman, E., Jing, E., Schwer, B., Lombard, D. B., et al. (2010). SIRT3 regulates mitochondrial fatty-acid oxidation by reversible enzyme deacetylation. *Nature* 464, 121–125. doi: 10.1038/nature08778

Hou, X., Zeng, H., Tuo, Q., Liao, D., and Chen, J. (2015). Apelin Gene Therapy Increases Autophagy via Activation of Sirtuin 3 in Diabetic Heart. *Diabetes Res. - Open J.* 1, 84–91. doi: 10.17140/DROJ-1-115

Hu, L., Ding, M., Tang, D., Gao, E., Li, C., Wang, K., et al. (2019). Targeting mitochondrial dynamics by regulating Mfn2 for therapeutic intervention in diabetic cardiomyopathy. *Theranostics* 9, 3687–3706. doi: 10.7150/thno.33684

Japp, A. G., Cruden, N. L., Barnes, G., van Gemeren, N., Mathews, J., Adamson, J., et al. (2010). Acute Cardiovascular Effects of Apelin in Humans. *Circulation* 121, 1818–1827. doi: 10.1161/CIRCULATIONAHA.109.911339

Javadipour, M., Rezaei, M., Keshtzar, E., and Khodayar, M. J. (2019). Metformin in contrast to berberine reversed arsenic-induced oxidative stress in mitochondria from rat pancreas probably via Sirt3-dependent pathway. *J. Biochem. Mol. Toxicol.* 33 (9), e22368. doi: 10.1002/jbt.22368

Jia, G., Whaley-Connell, A., and Sowers, J. R. (2018). Diabetic cardiomyopathy: a hyperglycaemia- and insulin-resistance-induced heart disease. *Diabetologia* 61, 21–28. doi: 10.1007/s00125-017-4390-4

Kannel, W. B., Hjortland, M., and Castelli, W. P. (1974). Role of diabetes in congestive heart failure: The Framingham study. *Am. J. Cardiol.* 34, 29–34. doi: 10.1016/0002-9149(74)90089-7

Ke, Z., Liu, J., Xu, P., Gao, A., Wang, L., and Ji, L. (2015). The Cardioprotective Effect of Icariin on Ischemia–Reperfusion Injury in Isolated Rat Heart: Potential Involvement of the PI3K-Akt Signaling Pathway. *Cardiovasc. Ther.* 33, 134–140. doi: 10.1111/1755-5922.12121

Kosiborod, M., Gomes, M. B., Nicolucci, A., Pocock, S., Rathmann, W., Shestakova, M. V., et al. (2018). Vascular complications in patients with type 2 diabetes: prevalence and associated factors in 38 countries (the DISCOVER study program). *Cardiovasc. Diabetol.* 17, 150. doi: 10.1186/s12933-018-0787-8

Li, X., Yu, L., Gao, J., Bi, X., Zhang, J., Xu, S., et al. (2018). Apelin Ameliorates High Glucose-Induced Downregulation of Connexin 43 via AMPK-Dependent Pathway in Neonatal Rat Cardiomyocytes. *Aging Dis.* 9, 66. doi: 10.14336/AD.2017.0426

Mahalakshmi, A., and Kurian, G. A. (2019) Mitochondrial dysfunction plays a key role in the abrogation of cardioprotection by sodium hydrosulfide post-conditioning in diabetic cardiomyopathy rat heart. *Naunyn Schmiedebergs Arch. Pharmacol.* 33(9):e22368. doi: 10.1007/s00210-019-01733-z

Meng, X., Pei, H., and Lan, C. (2015). Icariin Exerts Protective Effect Against Myocardial Ischemia/Reperfusion Injury in Rats. *Cell Biochem. Biophys.* 73, 229–235. doi: 10.1007/s12013-015-0669-6

Ni, R., Zheng, D., Xiong, S., Hill, D. J., Sun, T., Gardiner, R. B., et al. (2016). Mitochondrial Calpain-1 Disrupts ATP Synthase and Induces Superoxide Generation in Type 1 Diabetic Hearts: A Novel Mechanism Contributing to Diabetic Cardiomyopathy. *Diabetes* 65, 255–268. doi: 10.2337/db15-0963

Ni, T., Gao, F., Zhang, J., Lin, H., Luo, H., Chi, J., et al. (2019). Impaired autophagy mediates hyperhomocysteinemia-induced HA-VSMC phenotypic switching. *J. Mol. Histol.* 50, 305–314. doi: 10.1007/s10735-019-09827-x

Saito, T., Asai, K., Sato, S, Hayashi, M., Adachi, A., Sasaki, Y., et al. (2016) Autophagic vacuoles in cardiomyocytes of dilated cardiomyopathy with initially decompensated heart failure predict improved prognosis. *Autophagy*. 12(3): 579–587. doi: 10.1080/15548627.2016.1145326

Schilling, J. D. (2015). The Mitochondria in Diabetic Heart Failure: From Pathogenesis to Therapeutic Promise. *Antioxid. Redox Signaling* 22, 1515–1526. doi: 10.1089/ars.2015.6294

Serpooshan, V., Sivanesan, S., Huang, X., Mahmoudi, M., Malkovskiy, A. V., Zhao, M., et al. (2015). [Pyr1]-Apelin-13 delivery via nano-liposomal encapsulation attenuates pressure overload-induced cardiac dysfunction. *Biomaterials* 37, 289–298. doi: 10.1016/j.biomaterials.2014.08.045

Seuring, T., Archangelidi, O., and Suhrcke, M. (2015). The Economic Costs of Type 2 Diabetes: A Global Systematic Review. *Pharmacoeconomics* 33, 811–831. doi: 10.1007/s40273-015-0268-9

Song, Y.-H., Cai, H., Zhao, Z.-M., and Wu, M. (2016). Icariin attenuated oxidative stress induced-cardiac apoptosis by mitochondria protection and ERK activation. *Biomed. Pharmacother.* 83, 1089–1094. doi: 10.1016/biopha.2016.08.016

Sreejit, P., Kumar, S., and Verma, R. S. (2008). An improved protocol for primary culture of cardiomyocyte from neonatal mice. *In Vitro Cell. Dev. Biol. - Anim.* 44, 45–50. doi: 10.1007/s11626-007-9079-4

Sun, Y., Tian, Z., Liu, N., Zhang, L., Gao, Z., Sun, X., et al. (2018). Exogenous H2S switches cardiac energy substrate metabolism by regulating SIRT3 expression in db/db mice. *J. Mol. Med.* 96, 281–299. doi: 10.1007/s00109-017-1616-3

Tang, M., Huang, Z., Luo, X., Liu, M., Wang, L., Qi, Z., et al. (2019). Ferritinophagy activation and sideroflexin1-dependent mitochondria iron overload is involved in apelin-13-induced cardiomyocytes hypertrophy. *Free Radic. Biol. Med.* 134, 445–457. doi: 10.1016/j.freeradbiomed.2019.01.052

Tate, M., Higgins, G. C., De Blasio, M. J., Lindblom, R., Prakoso, D., Deo, M., et al. (2019). The Mitochondria-Targeted Methylglyoxal Sequestering Compound, MitoGamide, Is Cardioprotective in the Diabetic Heart. *Cardiovasc. Drug Ther.* 33 (6), 669–674. doi: 10.1007/s10557-019-06914-9

Turkmen, K. (2014). Sirtuins as novel players in the pathogenesis of diabetes mellitus. *World J. Diabetes* 5, 894. doi: 10.4239/wjd.v5.i6.894

Verma, S. K., Garikipati, V. N. S., and Kishore, R. (2017). Mitochondrial dysfunction and its impact on diabetic heart. *Biochim. Biophys. Acta Mol. Basis Dis.* 1863, 1098–1105. doi: 10.1016/j.bbadis.2016.08.021

Wang, Z., Sun, R., Wang, G., Chen, Z., Li, Y., Zhao, Y., et al. (2020). SIRT3-mediated deacetylation of PRDX3 alleviates mitochondrial oxidative damage and apoptosis induced by intestinal ischemia/reperfusion injury. *Redox Biol.* 28, 101343. doi: 10.1016/j.redox.2019.101343

Wu, B., Feng, J., Yu, L., Wang, Y., Chen, Y., Wei, Y., et al. (2018). Icariin protects cardiomyocytes against ischaemia/reperfusion injury by attenuating sirtuin 1-dependent mitochondrial oxidative damage. *Br. J. Pharmacol.* 175, 4137–4153. doi: 10.1111/bph.14457

Zamora, M., and Villena, J. A. (2019). Contribution of Impaired Insulin Signaling to the Pathogenesis of Diabetic Cardiomyopathy. *Int. J. Mol. Sci.* 20, 2833. doi: 10.3390/ijms20112833

Zeng, H., He, X., Hou, X., Li, L., and Chen, J. (2014). Apelin gene therapy increases myocardial vascular density and ameliorates diabetic cardiomyopathy via upregulation of sirtuin 3. *Am. J. Physiol. Heart Circ. Physiol.* 306, H585–H597. doi: 10.1152/ajpheart.00821.2013

Zheng, Y., Lu, L., Yan, Z., Jiang, S., Yang, S., Zhang, Y., et al. (2019). mPEG-icariin nanoparticles for treating myocardial ischaemia. *Artif. Cells Nanomed. Biotechnol.* 47, 801–811. doi: 10.1080/21691401.2018.1554579

Zhou, B., and Tian, R. (2018). Mitochondrial dysfunction in pathophysiology of heart failure. *J. Clin. Invest.* 128, 3716–3726. doi: 10.1172/JCI120849

Zhou, H., Yuan, Y., Liu, Y., Deng, W., Zong, J., Bian, Z., et al. (2014). Icariin attenuates angiotensin II-induced hypertrophy and apoptosis in H9c2 cardiomyocytes by inhibiting reactive oxygen species-dependent JNK and p38 pathways. *Exp. Ther. Med.* 7, 1116–1122. doi: 10.3892/etm.2014.1598

Conflict of Interest: The authors declare that the research was conducted in the absence of any commercial or financial relationships that could be construed as a potential conflict of interest.

frontiers in Physiology

ORIGINAL RESEARCH
published: 26 March 2020
doi: 10.3389/fphys.2020.00194

The Role of Membrane Capacitance in Cardiac Impulse Conduction: An Optogenetic Study With Non-excitable Cells Coupled to Cardiomyocytes

Stefano Andrea De Simone[1], Sarah Moyle[1], Andrea Buccarello[2], Christian Dellenbach[1], Jan Pavel Kucera[2†] and Stephan Rohr[1†]*

[1] Laboratory of Cellular Optics II, Department of Physiology, University of Bern, Bern, Switzerland, [2] Integrative Cardiac Bioelectricity Group, Department of Physiology, University of Bern, Bern, Switzerland

OPEN ACCESS

Edited by:
Gianluigi Pironti,
Karolinska Institutet (KI), Sweden

Reviewed by:
Konstantin Agladze,
Moscow Institute of Physics and Technology, Russia
Antoine A. F. De Vries,
Leiden University Medical Center, Netherlands

***Correspondence:**
Stephan Rohr
rohr@pyl.unibe.ch

[†] These authors share last authorship

Specialty section:
This article was submitted to Cardiac Electrophysiology, a section of the journal Frontiers in Physiology

Received: 10 December 2019
Accepted: 20 February 2020
Published: 26 March 2020

Citation:
De Simone SA, Moyle S, Buccarello A, Dellenbach C, Kucera JP and Rohr S (2020) The Role of Membrane Capacitance in Cardiac Impulse Conduction: An Optogenetic Study With Non-excitable Cells Coupled to Cardiomyocytes. Front. Physiol. 11:194. doi: 10.3389/fphys.2020.00194

Non-excitable cells (NECs) such as cardiac myofibroblasts that are electrotonically coupled to cardiomyocytes affect conduction velocity (θ) by representing a capacitive load (CL: increased membrane to be charged) and a resistive load (RL: partial depolarization of coupled cardiomyocytes). In this study, we untangled the relative contributions of both loading modalities to NEC-dependent arrhythmogenic conduction slowing. Discrimination between CL and RL was achieved by reversibly removing the RL component by light activation of the halorhodopsin-based hyperpolarizing membrane voltage actuator eNpHR3.0-eYFP (enhanced yellow fluorescent protein) expressed in communication-competent fibroblast-like NIH3T3 cells ($3T3_{HR}$ cells) that served as a model of coupled NECs. Experiments were conducted with strands of neonatal rat ventricular cardiomyocytes coated at increasing densities with $3T3_{HR}$ cells. Impulse conduction along preparations stimulated at 2.5 Hz was assessed with multielectrode arrays. The relative density of $3T3_{HR}$ cells was determined by dividing the area showing eYFP fluorescence by the area covered with cardiomyocytes [coverage factor (CF)]. Compared to cardiomyocytes, $3T3_{HR}$ cells exhibited a depolarized membrane potential (-34 mV) that was shifted to -104 mV during activation of halorhodopsin. Without illumination, $3T3_{HR}$ cells slowed θ along the preparations from $\sim$330 mm/s (control cardiomyocyte strands) to $\sim$100 mm/s (CF = $\sim$0.6). Illumination of the preparation increased the electrogram amplitudes and induced partial recovery of θ at CF $>$ 0.3. Computer simulations demonstrated that the θ deficit observed during illumination was attributable in full to the CL represented by coupled $3T3_{HR}$ cells with θ showing a power-law relationship to capacitance with an exponent of -0.78 (simulations) and -0.99 (experiments). The relative contribution of CL and RL to conduction slowing changed as a function of CF with CL dominating at CF $\leq$ $\sim$0.3, both mechanisms being equally important at CF = $\sim$0.5, and RL dominating over CL at CF $>$ 0.5.

The finding that RL did not affect θ at CFs ≤ 0.3 is explained by the circumstance that, at the respective moderate levels of cardiomyocyte depolarization, supernormal conduction stabilized propagation. The findings provide experimental estimates for the dependence of θ on membrane capacitance in general and suggest that the myocardium can absorb moderate numbers of electrotonically coupled NECs without showing substantial alterations of θ.

Keywords: heart, fibroblasts, myofibroblasts, conduction velocity, membrane capacitance, optogenetics, computer modeling, arrhythmia

INTRODUCTION

Heart rhythm disorders are frequent complications of cardiac disease. The initiation of reentrant arrhythmias such as flutter and fibrillation results from slow conduction of the cardiac action potential and conduction block (Kleber and Rudy, 2004). Classically, the velocity of conduction is determined primarily by the density and kinetics of voltage-gated channels carrying inward currents, as well as by the level of gap junctional coupling between cardiomyocytes (CMCs) (Shaw and Rudy, 1997; Rohr et al., 1998). More recently, it was shown both *in vitro* and *in vivo* that conduction velocity (θ) can be modulated by non-excitable cells (NECs) such as myofibroblasts and macrophages that are coupled to CMCs by gap junctions (Rohr, 2009; Hulsmans et al., 2017).

Electrotonic coupling of NECs to CMCs slows impulse conduction based on two main mechanisms: (1) NECs like myofibroblasts exhibit a reduced (less negative) membrane potential (V_m) compared to CMCs (Salvarani et al., 2017). Accordingly, they induce partial CMC depolarization upon establishment of heterocellular electrotonic coupling. The extent of CMC depolarization depends on the difference between the membrane potentials of the two cell types (ΔV_m) and the relative magnitudes of the CMC membrane resistance, the NEC membrane resistance, and the gap junctional conductance (Jousset et al., 2016; Kucera et al., 2017). The NEC-dependent reduction of the resting membrane potential (RMP) of coupled CMCs induces sodium channel inactivation and hence reduces θ (Miragoli et al., 2006). The effect of such "resistive loading," that is, the reduction of the RMP of CMCs by coupled, less polarized cells, has been investigated before using bioengineered strands of CMCs that were coated with cardiac myofibroblasts known to establish heterocellular electrotonic coupling. With increasing myofibroblast density, θ was reported to first slightly increase and then monotonically decrease, thereby reproducing the phenomenon of supernormal conduction that characterizes the response of θ to increasing CMC depolarization as induced, for example, by a gradual increasing extracellular potassium concentration (Kagiyama et al., 1982; Shaw and Rudy, 1997; Rohr et al., 1998; Miragoli et al., 2006; Jacquemet and Henriquez, 2008). (2) Even if NECs were to display a V_m similar to the RMP of CMCs, and hence, sodium-channel availability would not be compromised, electrotonic coupling between the two cell types would still be expected to slow conduction because the membrane capacitance of NECs will be charged during activation of coupled CMCs, which results in a reduction of the amount of depolarizing current available for an efficient downstream depolarization of CMCs as shown before in computer simulations (Jacquemet and Henriquez, 2008).

By contrast to the established role of resistive loading of CMCs by coupled NECs in conduction slowing, experimental data that characterize the contribution of capacitive loading to conduction slowing are, to our knowledge, still lacking. In excitable cells, the membrane capacitance (C_m) delays the onset of the action potential upstroke due to a prolongation of the foot potential. This results in slowing of conduction, with θ generally being assumed to show an inverse proportionality to C_m in cardiac tissue (Matsumoto and Tasaki, 1977). The same proportionality is expected to govern conduction in nerve fibers (Hartline and Colman, 2007). For the case of NECs being electrotonically coupled to CMCs, previous *in silico* studies predicted θ to be inversely proportional to the square root of C_m of coupled NECs with the magnitude of the effect on conduction being dependent on the coupling conductance between the two cell types (Plonsey and Barr, 2000; Jacquemet and Henriquez, 2008). However, earlier theoretical work suggests that the relationship between θ and tissue capacitance does not necessarily follow an inverse law or an inverse square root law but more generally a power law with an exponent between −1/2 and −1 and that this power-law relationship depends on the density and kinetic properties of the voltage-gated channels in addition to purely passive electrical properties (Huxley, 1959; Jack et al., 1983).

Whereas the results of previous computer simulations underline the importance of capacitive loading of CMCs by coupled NECs in proarrhythmic slowing of conduction, a lack of appropriate methodologies has precluded a direct experimental assessment of theoretical predictions in the past. This situation has markedly changed with the advent of optogenetics that we use in this study to experimentally untangle the differential contributions of capacitive versus resistive loading to conduction slowing induced by NECs coupled to CMCs. The results show that NEC-dependent capacitive loading slows θ in a $\sim 1/C_m$ fashion. At low NEC densities, this effect is offset by resistive loading that stabilizes θ due to supernormal conduction, whereas at higher NEC densities, both capacitive and resistive loading synergistically reduce θ. Being aware of the complex interactions between the two loading conditions is expected to contribute to the general understanding of the effects that

NECs coupled to CMCs exert on cardiac impulse propagation in health and disease.

MATERIALS AND METHODS

Production of Lentiviral Expression Vectors for the Halorhodopsin Gene eNpHR3.0

The plasmids pLenti-CMV-GFP-Puro-(658-5) (Addgene, ref. #17448) and pLenti-CaMKIIa-eNpHR3.0-EYFP-WPRE (Addgene, ref. #20946) were combined into the customized lentiviral expression vector pLenti-CMV-eNpHR3.0-Puro. This vector induced the expression of the enhanced version of halorhodopsin (HR) (eNpHR3.0) under the CMV (human cytomegalovirus) promoter with the puromycin resistance gene serving to create a 3T3 cell line stably expressing HR. Molecular cloning was performed using classical techniques and by employing the In-Fusion strategy (Takara Bio Europe, Saint-Germain-en-Laye, France).

Lentivirus Production

The lentiviral expression vector was cotransfected in HEK293 cells with the plasmids encoding for the vesicular stomatitis virus G protein (pMD2.G, Addgene ref. #12259) and the Gag and Pol polyproteins and the Tat and Rev proteins of human immunodeficiency virus type 1 (pCMVR8.74, Addgene ref. #22036). HEK293 cells ($3–6 \times 10^7$ cells) were grown and transfected in Dulbecco modified Eagle medium (DMEM) (ThermoFisher, Reinach, Switzerland) supplemented with 10% fetal bovine serum (Bioswisstech Ltd., Schaffhausen, Switzerland) and 0.5 mmol/L sodium pyruvate (Merck, Buchs, Switzerland). Transfection was performed with Transit-LT1 reagent (Mirus Bio LLC, Madison, MI, United States) composed of a mixture of lipids and proteins/polyamines. After transfection, the medium was collected for 2 days and stored at 4°C until the day of ultracentrifugation (74,000 *g* for 2 h at 4°C) to isolate the viral particles. The lentiviral particles were resuspended in an appropriate volume of sterile phosphate-buffered saline and stored at −80°C. Titration was performed by transducing HEK293 cells followed by assessing the transducing units (T.U.), which ranged from 10^8 to 10^{10} T.U./mL. Production, purification, and titration were adapted from Hewinson et al. (2013).

Generation of $3T3_{HR}$ Cells

NIH3T3 cells (mouse embryonic fibroblast cell line) were stably transduced (puromycin selection) with HR-expressing lentiviral particles to generate a cell line that we named $3T3_{HR}$. For this purpose, NIH3T3 cells (Y. Zimmer lab, DBMR, University of Bern, Switzerland) were kept in culture medium consisting of DMEM (ThermoFisher, Reinach, Switzerland) supplemented with 10% fetal bovine serum (Bioswisstech Ltd., Schaffhausen, Switzerland), 10 U/mL penicillin, 10 μg/mL streptomycin (Bioswisstech Ltd., Schaffhausen, Switzerland), and 0.5 mmol/L sodium pyruvate (Merck, Buchs, Switzerland). During transduction, the cell culture medium was replaced by supplemented medium containing polybrene (8 μg/mL; Santa Cruz, Heidelberg, Germany) and lentiviral particles (multiplicity of infection, MOI, ranging between 3 and 8). This medium was replaced after 18 h with normal supplemented DMEM. Cells were cultured at 37°C, 5% CO_2 in culture medium supplemented with puromycin (2 μg/mL; Santa Cruz, Heidelberg, Germany) until reaching confluency after 4 to 7 days. Thereafter, the transduced cells ($3T3_{HR}$ cells) were dissociated, centrifuged (1,000 revolutions per min for 10 min), resuspended in cell culture medium containing 20% fetal bovine serum and 10% dimethyl sulfoxide at 10^6 cells/mL, and finally stored in liquid nitrogen. For use in experiments, $3T3_{HR}$ cells were defrosted and kept in supplemented DMEM medium containing puromycin (2 μg/mL) for 1 week. The cell monolayers were dissociated using trypsin-EDTA solution (Merck, Buchs, Switzerland). The resulting cell suspension was centrifuged, and the cell pellet resuspended in supplemented cell culture medium M199 (for composition cf. below). After determination of the cell count with a hemocytometer, $3T3_{HR}$ cells were seeded at defined densities onto CMC strand preparations (see below) or on glass coverslips (25 cells/mm^2) for patch clamp experiments.

CMC Cell Strands

Neonatal rat ventricular CMC cultures were prepared using established protocols and following Swiss guidelines for animal experimentation under the license BE27/17 of the State Veterinary Department of the Canton of Bern (Rohr et al., 2003). In short, the ventricles of the hearts of 8 to 10 neonatal rats (Wistar, 1 day old) were minced with scissors, and the resulting tissue pieces dissociated in Hanks balanced salt solution (HBSS) (without Ca^{2+} and Mg^{2+}; Bioconcept AG, Allschwil, Switzerland) that contained trypsin (0.1%; Merck, Buchs, Switzerland) and pancreatin (120 μg/mL; Merck, Buchs, Switzerland). After centrifugation, the dissociated cells were resuspended in medium M199 with Hanks salts (Merck, Buchs, Switzerland) that was supplemented with penicillin (20 U/mL; Merck, Buchs, Switzerland), vitamin B_{12} (2 μg/mL; Merck, Buchs, Switzerland), bromodeoxyuridine (100 μmol/L; Merck, Buchs, Switzerland), vitamin C (18 μmol/L; Merck, Buchs, Switzerland), epinephrine (10 μmol/L; Merck, Buchs, Switzerland), L-glutamine (680 μM/L; Merck, Buchs, Switzerland), and 10% neonatal calf serum (NCS; Bioswisstech Ltd., Schaffhausen, Switzerland). The cell suspension underwent differential preplating in cell culture flasks for 120 min in order to separate CMCs from fibroblasts. Cell densities in the supernatant containing predominantly CMCs were determined with a hemocytometer and adjusted by dilution as to result in the required seeding density (5,000 cells/mm^2). Cardiomyocyte cell cultures were kept in the incubator at 36°C in a humidified atmosphere containing 0.8% CO_2. The culture medium was exchanged 24 h after seeding with supplemented medium M199 (cf. above) containing 5% NCS and every other day thereafter. At the time of the initial medium exchange, preparations were inspected by phase contrast microscopy for the presence of non-uniformities in cell density and the presence of holes.

Preparations exhibiting these defects were excluded from further experiments. Experiments were performed 72 to 96 h after seeding of the CMCs.

Patterned Growth Strand Preparations

Cardiomyocyte cell strands measuring 7.45 by 0.4 mm were produced using standard photolithography, with patterns being centered on the rows of electrodes on the multielectrode array (MEA) substrates (Rohr et al., 2003). A schematic illustration of the preparations is presented in **Supplementary Figure S1**.

CMC-3T3$_{HR}$ Cell Strands

3T3$_{HR}$ cells were seeded at densities ranging from 250 to 2500 cells/mm^2 onto the 24-h-old CMC cell strands. Cultures were incubated for 3 h to permit stable adherence of 3T3$_{HR}$ cells to CMCs. Thereafter, the medium was replaced with fresh supplemented cell culture medium lacking bromodeoxyuridine. Preparations were kept in the incubator at 36°C in a humidified atmosphere containing 0.8% CO_2 for a further 48 h before conducting the experiments.

Determination of the Coverage Factor

The coverage factor (CF), that is, the relative cell membrane area of 3T3$_{HR}$ cells in respect to the cell membrane area of CMCs (area 3T3$_{HR}$ cells/area CMCs) of the preparations used in the MEA experiments, was determined by imaging the cell strands on an inverted microscope equipped for epifluorescence (Zeiss Axiovert 200M; excitation 482/35 nm; dichroic 499; emission 536/40 nm). Images were acquired with a cooled CCD camera (Spot RT-KAI2000; Spot Diagnostic Instruments, Sterling Heights, MI, United States). 3T3$_{HR}$ cells were identified based on their eYFP fluorescence. With the objective used (2.5×, 0.075 N.A.), two images covered the entire length of the strands. They were stitched using Image Composite Editor (ICE; Microsoft, Redmond, WA, United States) and segmented with Ilastik (EMBL, Heidelberg, Germany), an interactive software that is trained to distinguish between fluorescent (foreground) and non-fluorescent areas (background). The segmented images were then processed using ImageJ (NIH, Bethesda, MD, United States), and the result, that is, the area covered by 3T3$_{HR}$ cells, was divided by the area of the CMC strand. An example of a preparation is presented in **Supplementary Figure S2**.

Conduction Measurements With Multielectrode Arrays

Impulse propagation characteristics in strands of CMCs (controls) and strands of CMCs coated with 3T3$_{HR}$ cells were determined using a custom-built MEA system. The electrode layout of the MEA substrates was designed to our specification (EPFL, Neuchâtel, Switzerland) and is shown in **Supplementary Figure S1**. It consisted of four rows of recording electrodes that were regularly spaced (interelectrode distance: 0.5 mm) and terminated on either side by a stimulation dipole being positioned at 1 mm from the last recording electrode. Stimulation of the preparations and electrogram recordings were performed with a custom-built stimulation/recording system that provided an internal gain of 1,000. Stimulation dipoles and stimulation parameters (frequency, amplitude, duration) were software selectable. After digitization, data were transferred via a USB link to a PC that permitted following ongoing experiments in real time and was used for storing the data for later offline analysis using custom written software.

Experiments were performed in an incubator (36°C, 0.8% CO_2) with preparations being stimulated by bipolar voltage pulses (±1 V; 4 ms) applied at 2.5 Hz to a stimulation electrode. After a prestimulation period of 50 s that allowed conduction to reach steady state, the recording was started, and the preparations subjected to a dark (20 s)–light (4 s)–dark (25 s) protocol. Preparations were illuminated by a high-brightness LED assembly (Luxeon Star 7 LEDs, SR-02-LO040; 590 nm, Lumileds, San Jose, CA, United States) equipped with a multilens collimating system (Cell Cluster Concentrator Optic # 263; Polymer Optics Ltd., Coventry, United Kingdom) that produced a spatially uniform light beam with a diameter of ∼10 mm that covered the entire preparation. Maximal light intensities reached at the level of the preparations amounted to 10.4 mW/mm^2. To minimize warming of the preparation by the powerful light source, four fans removed the heat from the source. To ensure efficient heat removal, temperature was continuously monitored at the level of the MEA during the experiments.

Conduction velocities were assessed by software-based detection of local activation times defined by the minimum of the first derivative of the electrogram. From these data, conduction velocities were derived from the slope of a linear fit to the distance versus activation time plots.

Whole-Cell Patch Clamp Recordings

For patch clamp experiments, low-density CMC and 3T3$_{HR}$ cell cultures grown on glass coverslips were mounted in an experimental superfusion chamber (Rohr, 1986) and placed on the stage of an inverted microscope (Nikon Eclipse, TE2000-E, Nikon, Egg, Switzerland). Halorhodopsin was activated by a high-power LED (595 nm; Thorlabs, Thorlabs GmbH, Bergkirchen, Germany) that was coupled into the epi-illumination path of the microscope where it passed through an excitation filter (600/43 nm, Semrock, Rochester, NY, United States) followed by a dichroic mirror (570 nm, Semrock, Rochester, NY, United States). Light was projected onto the preparation by a 40× − 0.65 N.A. objective (Nikon). Maximal light power reached with this configuration at the level of the preparation was 8.9 mW/mm^2. Preparations were superfused at 2 to 3 mL/min with HBSS containing 1% NCS at room temperature. Patch pipettes were pulled from borosilicate glass capillaries (GC150F-10, Harvard Apparatus, Holliston, MA, United States) with a horizontal puller (DMZ; Zeitz Instruments, Martinsried, Germany). The patch pipette filling solution contained (in mmol/L) K-aspartate 120, NaCl 10, Mg ATP 3, $CaCl_2$ 1, EGTA 10, and HEPES 5 (pH 7.2; free Ca^{2+} concentration of ∼35 nmol/L). Pipette resistances ranged from 2 to 15 MΩ. Pipettes were positioned with a motorized micromanipulator (MP-225; Sutter Instrument Company, Novato, CA, United States). Pipette

potentials were zeroed before cell contact, and measured potentials were corrected for the liquid junction potential (12.4 mV) as calculated by pCLAMP software (Molecular Devices LLC, San Jose, CA, United States). Analog signals were amplified, filtered (1 kHz), and digitized (2.9 kHz) with a HEKA EPC-10 patch clamp amplifier (HEKA Elektronik GmbH, Lambrecht, Germany). Data were stored on a computer for offline analysis with Patchmaster (V 2.15) and Fitmaster (V 2.53) software (HEKA).

Electrophysiological properties of $3T3_{HR}$ cells were assessed using standard whole-cell patch clamp recording techniques. Seal resistances ranged from 2 to 10 GΩ. After rupture of the membrane, series resistance, membrane capacitance, and the liquid junction potential were compensated. Membrane resistances and cell capacitances were calculated by Patchmaster. Current-to-voltage (I–V) relationships were obtained by applying continuous voltage ramp protocols where, starting from a holding potential of −70 mV, the membrane was clamped to −100 and ramped to 50 mV within 1.2 s (slew rate of 125 mV s^{-1}). In case of $3T3_{HR}$ cells, ramps were performed first in the dark and then in presence of HR-activating light (590 nm). The light intensity used in the experiments (8.9 $mW/mm^{2)}$ has been shown before to cause maximal activation of the optogenetic actuator eNpHR3.0-eYFP (Zhang et al., 2019). In agreement with these data, we found previously in eNpHR3.0-eYFP–transduced cardiac myofibroblasts that photocurrents saturate at light intensities $\geq$3.5 mW/mm^2. Net whole-cell currents were normalized to cell capacitance and are reported as pA/pF. The magnitude of the HR-dependent chloride pump current and its reversal potential were calculated from the difference between the I–V curves measured in the presence of light and in the dark. The time course and size of light-induced hyperpolarizations was measured in current clamp mode (I = 0). Maximal light-induced voltage changes were determined 0.5 s after the start of illumination, which corresponds to ∼5 × the activation time constant (cf. **Supplementary Figure S4**).

Computer Simulations of Conduction

Monodomain computer simulations of action potential propagation were conducted in a fiber containing 100 CMCs, each having a length of 60 μm and a capacitance C_{CMC} of 28.8 pF. Ion currents of CMCs were based on a model that was designed to reproduce findings in strands of neonatal rat ventricular myocytes cocultured with myofibroblasts (Jousset et al., 2016). The lumped gap junctional and myoplasmic conductance between CMCs was adjusted to 0.38 μS to replicate the mean control θ measured in the present study in the absence of $3T3_{HR}$ cells.

Coating of CMC cell strands with $3T3_{HR}$ cells at different CFs was simulated by connecting each CMC laterally to a $3T3_{HR}$ cell having a capacitance $C_{3T3HR} = CF \cdot C_{CMC}$. Ion currents of the $3T3_{HR}$ cells (I_{dark}: total dark current; I_{HR}: HR-induced light-activated current) were modeled based on current–voltage relationships (normalized to cell capacitance) as obtained in patch clamp experiments. Dark conditions were simulated by setting I_{HR} to 0. The absolute membrane current of $3T3_{HR}$ cells was obtained by multiplying it by C_{3T3HR}. In an additional set of simulations, both I_{dark} and I_{HR} were set to 0, which resulted in purely capacitive cells having the same RMP as CMCs.

$3T3_{HR}$ cells were connected to CMCs by a conductance $g_{CMC-3T3HR}$ of 72 nS and scaled by the CF. Scaling both C_{3T3HR} and $g_{CMC-3T3HR}$ by the CF ensured that the time constant determining the passive loading of $3T3_{HR}$ cells ($C_{3T3HR}/g_{CMC-T3HR}$) remained invariant at 0.4 ms, a value based on previous experimental observations in our laboratory (Salvarani et al., 2017). In additional simulations, the effects of a decreased CMC-$3T3_{HR}$ coupling (1.2 nS) on conduction were investigated. $3T3_{HR}$ cells were not connected to each other.

Different CFs were modeled by scaling the capacitance of the $3T3_{HR}$ cells, their ionic currents, and their intercellular coupling conductance to the CMCs. This approach represents a homogenization of the distribution of the $3T3_{HR}$ cells. In a previous study using a detailed cellular structure model, we observed that a random distribution of myofibroblasts on CMCs leads to only minimal spatial variations of the RMP (<0.1 mV) and to equally spaced isochrones at a macroscopic level (Jousset et al., 2016). Thus, the homogenized model is adequate for characterizing macroscopic θ.

Simulations were started with a period of no stimulation (2 s) to allow the CMCs and the $3T3_{HR}$ cells to reach their respective RMPs and to ascertain the absence of spontaneous activity. The fiber was then stimulated by a rectangular current pulse applied to the first CMC. The intensity and duration of the stimulus were adjusted in each simulation to ensure that a propagated action potential was properly initiated without a major stimulation artifact.

Activation time was defined as the time at which the membrane potential of CMCs surpassed –35 mV during depolarization. Conduction velocity was computed by linear regression of activation time versus distance between cell 25 and cell 75 to exclude stimulation artifacts and sealed-end effects. In the CMC model, the Na^+ current (I_{Na}) was represented using a Hodgkin–Huxley formalism with three activation gates (m) and two inactivation gates (h and j) (Luo and Rudy, 1991; Jousset et al., 2016). The availability of I_{Na} was calculated as the product of the steady-state values of h and j at the RMP. Extracellular potentials were reconstructed at a distance of 5 μm from the 50th cell of the fiber using the method of Plonsey and Barr (Plonsey and Barr, 2000) and assuming an extracellular resistivity of 100 Ω cm.

The system of differential equations was integrated numerically using a constant time step of 0.005 ms. Gating variables were integrated using the method of Rush and Larsen (1978) and membrane potentials were determined using the forward Euler method. All simulations were run using MATLAB (The MathWorks, Natick, MA, United States).

Statistical Analysis

Normal distribution of data was assessed using the Shapiro–Wilk test. Data comparison was performed with the Student *t*-test (homoscedastic or heteroscedastic where appropriate). Differences were considered significant at $p < 0.05$.

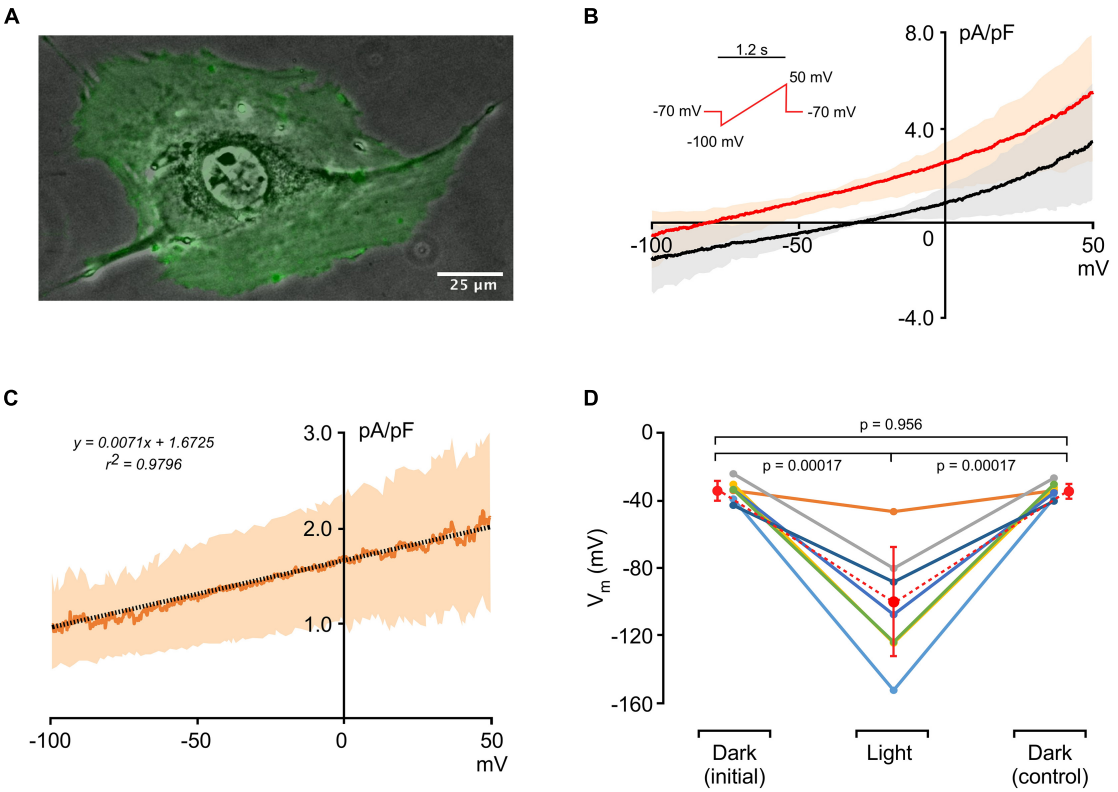

FIGURE 1 | Electrophysiological characterization of 3T3$_{HR}$ cells. **(A)** Fluorescence image of an HR-expressing 3T3 cell (green) overlaid on a phase contrast image. **(B)** Current-to-voltage relationships of 3T3$_{HR}$ cells in the dark (black) and during activation of HR (red) (n = 8; mean ± SD; SD spread indicated by a light-red and gray band; voltage clamp protocol shown in the inset). **(C)** Difference current ($I_{light} - I_{dark}$) induced by activation of HR at saturating light intensities (590 nm; 8.9 mW/mm^2; n = 8; mean ± SD). The linear fit (stippled black line) indicates that the actuator-induced outward current reverses at ∼−235 mV. **(D)** Membrane potentials (V_m) of single 3T3$_{HR}$ cells before, during, and after HR activation (n = 7: 590 nm; 8.9 mW/mm^2).

RESULTS

Electrophysiological Characterization of 3T3$_{HR}$ Cells

An image of an HR-expressing single 3T3 cell (3T3$_{HR}$) is shown in **Figure 1A**. The optogenetic actuator fused to eYFP is uniformly expressed as evidenced by the homogeneous green fluorescence. Currents recorded during application of voltage ramps (-100 to 50 mV within 1.2 s) are shown in **Figure 1B** and indicate slight outward rectification of currents at positive potentials. Membrane potentials of 3T3$_{HR}$ cells in absence of HR activation ranged from -26 to -44 mV (average, 35.0 ± 5.4 mV; n = 7), membrane capacitances from 43 to 78 pF mV (average, 64.7 ± 11.3, n = 7), and input resistances from 0.5 to 1.4 GΩ (0.95 ± 0.33 GΩ, n = 7). During HR activation at saturating light intensities (590 nm; 8.9 mW/mm^2), the current-to-voltage (I–V) curve was shifted upward due to the light-induced Cl^- pump current produced by HR. A linear fit applied to the HR-dependent current indicated a reversal potential at approximately −235 mV (**Figure 1C**). In current clamp mode with I = 0, activation of HR caused a significant hyperpolarization of the membrane potential of 3T3$_{HR}$ cells from −35.0 ± 5.4 mV (dark conditions) to −103.9 ± 31.9 mV (illuminated; n = 7; p = 0.0017), with average membrane potentials before and after HR activation (−35.0 ± 5.4 mV vs. −35.0 ± 4.4 mV) being identical (**Figure 1D**). As shown in **Supplementary Figure S3**, the magnitude of I_{HR} showed a close to linear dependence on the level of expression of the optogenetic reporter, which ranged from 3.0 to 33.3 (a.u.) with I_{HR} measured at a clamp potential of 0 mV increasing from 0.53 pA/pF to 2.58 pA/pF (linear fit: slope 0.06, r^2 = 0.81, n = 5). Time constants of the light-induced hyperpolarizing responses were 94.3 ± 46.4 ms (on-response; n = 18) and 137.7 ± 58.9 ms (off-response; n = 15; **Supplementary Figure S4**). **Supplementary Figure S5** depicts an example of a 3T3$_{HR}$ cell–CMC cell pair with the contact region showing discrete immunofluorescence staining for connexin43.

HR Activation Only Partially Restores θ in 3T3$_{HR}$–CMC Strand Preparations

Impulse conduction along strands of CMCs coated at increasing densities with 3T3$_{HR}$ cells was assessed using a MEA system. Conduction velocities (θ) in strands of CMCs were not significantly altered by illumination (dark: 333 ± 59 mm/s; light-on: 338 ± 54 mm/s; n = 25). Also, electrogram amplitudes (1.5 ± 0.8 mV; n = 25) and downstroke times (time from the maximum to the minimum of the electrogram; 0.29 ± 0.04 ms;

n = 25) remained unchanged. By contrast, CMC strands coated with 3T3$_{HR}$ cells showed a distinct response to HR activation as is illustrated in **Figure 2** for a preparation with a CF of 0.65. The center panel of **Figure 2A** depicts the preparation with green fluorescent 3T3$_{HR}$ cells and the positioning of the stimulation (blue disk) and recording electrodes (red dots). Impulse conduction under control, that is, dark conditions, was uniform and, as expected for heterocellular preparations, slow (108 mm/s; left panel). Uniform illumination of the cell strand (590 nm; 10.4 mW/mm^2) caused, as shown in the right-hand panel, a substantial acceleration of θ to 221 mm/s. The temporal profile of the light-induced change in impulse conduction is shown in **Figure 2B**. θ responded to illumination with an instantaneous increase by over 100% and promptly returned to preillumination values after switching off the light. Apart from accelerating conduction, activation of HR was accompanied by a several-fold increase of the electrogram amplitude as exemplified by the electrogram of electrode #3 in **Figure 2C**. When averaging all electrograms (n = 8) of this preparation, amplitudes increased ~4.4-fold from 0.66 ± 0.13 mV in the dark to 2.88 ± 0.49 mV during HR activation ($p < 2.3 \times 10^{-6}$).

Partial Restoration of Conduction Velocity During HR Activation Depends on 3T3$_{HR}$ Cell Density

Compared to conduction velocities measured in CMC preparations without 3T3$_{HR}$ cells (333 ± 6 mm/s; n = 25),

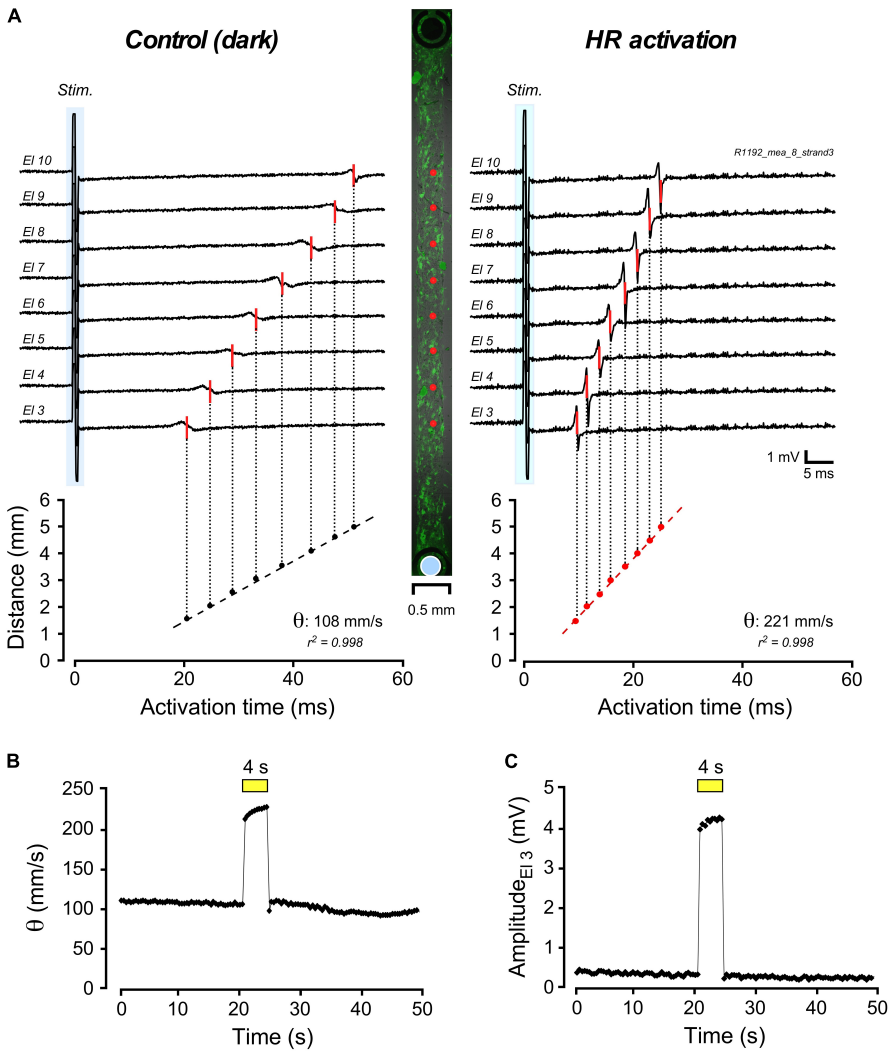

FIGURE 2 | Multielectrode array–based assessment of conduction in heterologous CMC-3T3$_{HR}$ cell strands. **(A)** Electrograms measured along a 400-μm-wide strand of CMCs coated with 3T3$_{HR}$ cells (center panel: fluorescence image of 3T3$_{HR}$ cells with red dots indicating recording sites and the blue disk denoting the stimulation dipole). Compared to the control recordings in the dark (left panel; stimulation artifact marked with blue backdrop), electrical activation of the preparation was accelerated during HR stimulation (right panel). **(B)** Time course of the increase of conduction velocity (θ) during transient light stimulation of HR (yellow bar; 590 nm; 10.4 mW/mm^2). **(C)** Time course of the change of electrogram amplitude as recorded by electrode #3 during light stimulation of HR (yellow bar, same experiment).

strands coated with 3T3$_{HR}$ cells exhibited slow conduction. The degree of conduction slowing was correlated to 3T3$_{HR}$ cell density, and values as low as 100 mm/s were observed at the largest CFs used (**Figure 3A**, black symbols). When removing the depolarizing effect of 3T3$_{HR}$ cells on coupled CMCs by activating HR, θ consistently increased for CFs > 0.3 (**Figure 3A**, red symbols). As shown in **Figure 3B**, the increase of θ was correlated to the density of 3T3$_{HR}$ cells in both absolute and relative terms. At high 3T3$_{HR}$ cell coverage, the light-induced increase of θ relative to initial values in the dark was as high as 160%. Despite this substantial recovery of conduction during light activation of HR, there remained a θ deficit in respect to CMC cell strands that was positively correlated to 3T3$_{HR}$ cell density (**Figure 3C**). At the highest 3T3$_{HR}$ cell densities tested, θ remained depressed by ∼40% (as opposed to ∼70% in absence of HR stimulation), which, as demonstrated by the simulations presented in the following section, reflects capacitive loading of the CMCs by electrotonically coupled 3T3$_{HR}$ cells. Finally, I_{HR} activation by light not only accelerated conduction but, due to the removal of partial inactivation of the sodium current in coupled CMCs, caused a CF-dependent increase in peak-to-peak amplitudes of the electrograms that increased several-fold at large CFs compared to peak-to-peak amplitudes in the dark (**Figure 3D**).

In silico Assessment of Conduction in Heterologous CMC-3T3$_{HR}$ Cell Strands

The plausibility of the argument that activation of HR exposes the capacitive load (CL) of 3T3$_{HR}$ cells exerted on coupled CMCs by removing their depolarizing effect, that is, their resistive load (RL) component, was evaluated by comparing experimental findings to *in silico* models of conduction along strands of CMCs coupled to non-excitable 3T3$_{HR}$ cells.

Ion currents present in CMCs were based on our previously developed model (Jousset et al., 2016). In simulated CMC control strands, intercellular coupling was adjusted as to replicate control conduction velocities observed in CMC strand preparations devoid of 3T3$_{HR}$ cells (experimentally observed velocities: 333 ± 6 mm/s; n = 25; lumped myoplasmic and junctional

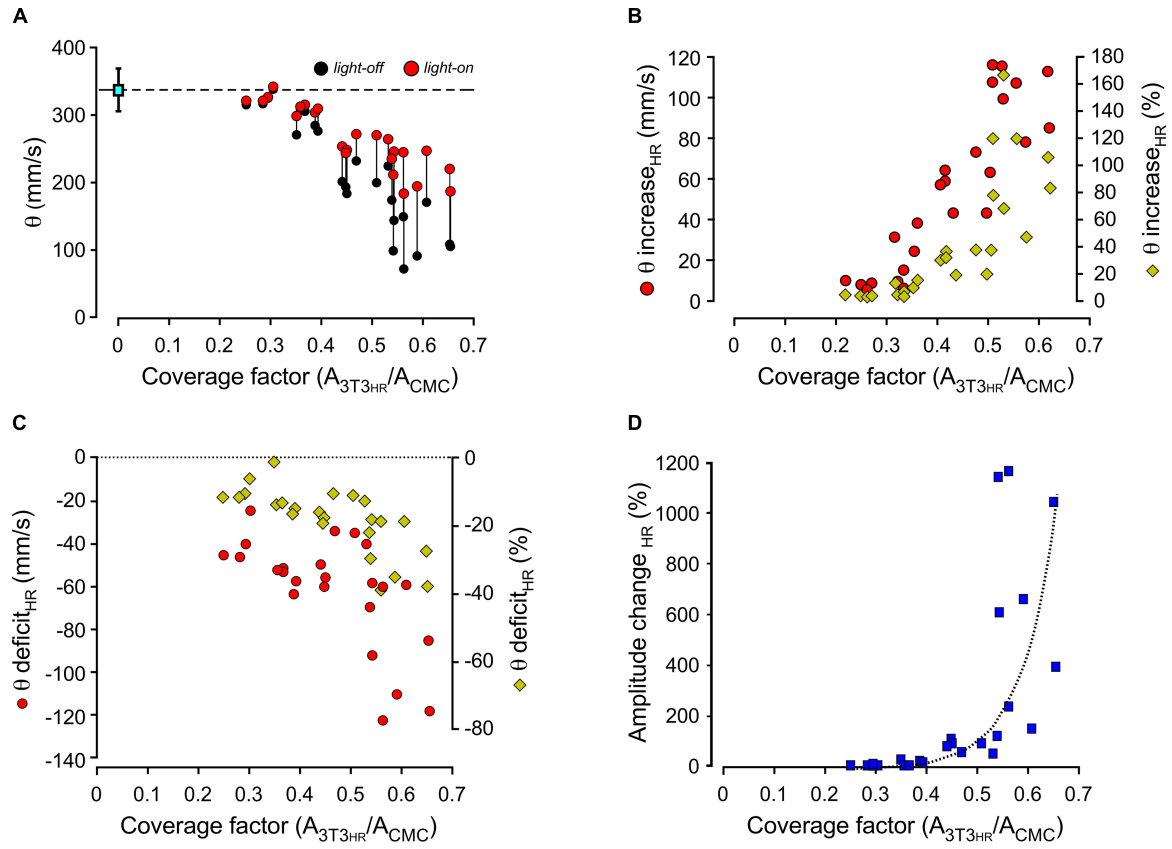

FIGURE 3 | Dependence of conduction velocities and electrogram amplitudes on the coating density of 3T3$_{HR}$ cells. **(A)** Conduction velocities as a function of the CF in the dark (black dots) and during HR activation (red dots; 590 nm; 10.4 mW/mm^2). **(B)** Increase of conduction velocities in CMC-3T3$_{HR}$ cell strands in response to illumination (left ordinate: red symbols, absolute increase in mm/s; right ordinate: yellow diamonds, relative increase in respect to conduction velocities measured in the dark). **(C)** Persistent deficit of conduction velocities during HR activation in CMC-3T3$_{HR}$ cell strands as compared to control CMC strands (left ordinate: red symbols, persistent conduction slowing in absolute values; right ordinate: yellow diamonds, persistent conduction slowing relative to CMC control strands; the stippled line refers to conduction velocities measured in CMC control strands). **(D)** Relative increase of electrogram amplitudes in response to HR activation plotted as a function of 3T3$_{HR}$ cell density.

conductance between myocytes in the model of 0.3817 μS yielded an overall θ of 339 mm/s). The ion currents of 3T3$_{HR}$ cells were modeled as a function of the membrane potential based on the patch clamp experiments presented in **Figure 1**. **Figure 4A** shows the mean total dark current density (I_{dark}, black) and the mean HR-mediated current density (I_{HR}, black) induced by illumination, together with the fitted functions used to represent these currents in the model (red).

The effects of increasing densities of 3T3$_{HR}$ cells on θ and the RMP of CMCs are shown in **Figure 4B**. Simulations were run in the absence of light (black symbols), in the presence of the light-induced I_{HR} (red symbols), and for two different levels of heterocellular gap junctional coupling. The coupling conductance of 72 nS (filled symbols) was based on values found before in pairs of CMCs coupled to non-excitable myofibroblasts (Salvarani et al., 2017). Additionally, we performed simulations at very low levels of intercellular coupling [open symbols; 1.2 nS corresponding to ∼12 connexons when assuming a single connexon conductance of 100 pS (Valiunas et al., 1997)].

At normal levels of CMC-3T3$_{HR}$ coupling and in absence of I_{HR}, increasing the CF led to a prominent conduction slowing (339 mm/s to 67 mm/s) because the moderately polarized 3T3$_{HR}$ cells (V_m of the isolated model 3T3$_{HR}$ cell: −32.3 mV) induced a reduction of the RMP of CMCs from −79.9 mV to −59.9 mV. This depolarization caused partial inactivation of the sodium channels as quantified by I_{Na} availability (bottom panel of **Figure 4B**). For CFs > 0.6, I_{Na} was almost fully inactivated, and slow conduction was essentially supported by the L-type Ca^{2+} current, which is in agreement with previous findings with CMC strands being depolarized by a rise in $[K^+]_o$ or CMC strands coated with myofibroblasts (Rohr et al., 1998; Miragoli et al., 2006). During HR activation, the depolarizing effect of 3T3$_{HR}$ cells on coupled CMCs was entirely suppressed, I_{Na} availability fully restored, and conduction accelerated for CFs > 0.3. Importantly, and in agreement with the experiments (**Figure 3**), θ did not fully return to levels observed in control CMC strands indicating that CMC depolarization, that is, resistive loading, was not the only determinant of 3T3$_{HR}$ cell–induced conduction slowing.

To investigate whether the reduction of θ persisting in the presence of I_{HR} was due to the CL exerted by the 3T3$_{HR}$ cells on coupled CMCs, both I_{dark} and I_{HR} of 3T3$_{HR}$ cells were set to 0,

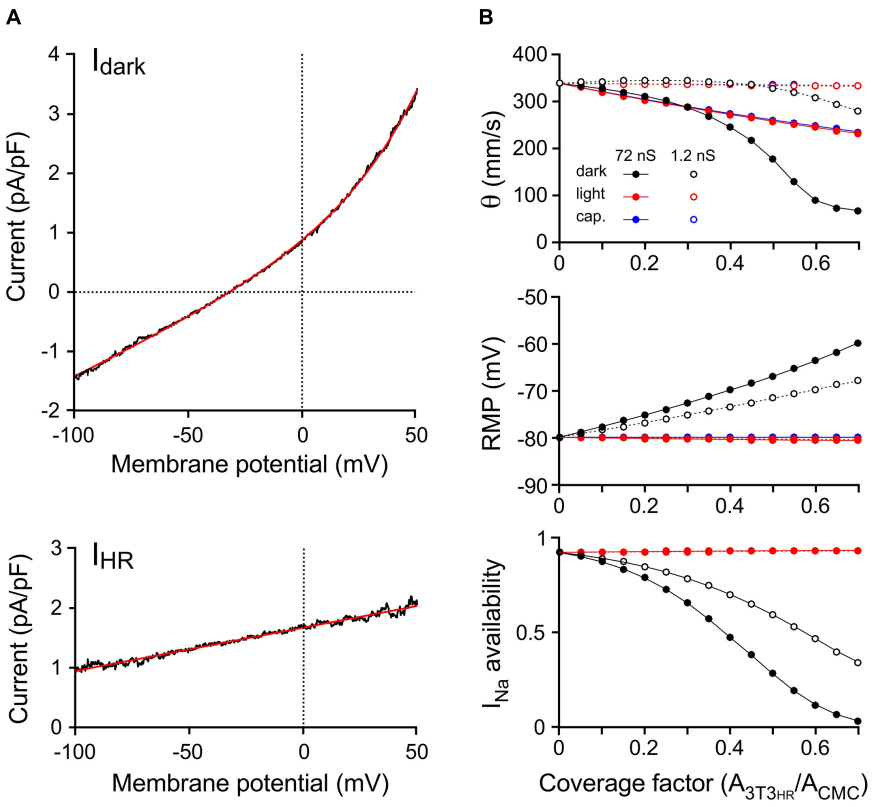

FIGURE 4 | Computer simulations of 3T3$_{HR}$ cell electrophysiology and impulse conduction. **(A)** Mean current-to-voltage relationships of 3T3$_{HR}$ cells during voltage clamp ramps in the absence of light (I_{dark}, top) and during HR activation with light (net light induced HR pump current, I_{HR}, bottom). The black curves denote mean values (n = 8), whereas the red curves represent the fitted functions used in the 3T3$_{HR}$ cell model [I_{dark} = 0.46862·$e^{V/33.751}$ + 0.018636·V + 0.42087; I_{HR} = 0.0072742 · (V + 229.95)]. **(B)** Conduction velocity (top), RMP (middle), and I_{Na} availability (bottom) versus CF for CMC-3T3$_{HR}$ cell strands exhibiting normal (72 ns = 720 connexons; solid lines) and reduced gap junctional coupling (1.2 ns = 12 connexons; stippled lines). Simulations refer to dark conditions (black), light stimulation (red), and to the case of purely capacitive 3T3$_{HR}$ cells (blue). At CFs > 0.7, spontaneous activity occurred in the dark, and θ at a stable RMP could not be determined anymore.

resulting in 3T3$_{HR}$ cells that acted in a purely capacitive manner (**Figure 4B**, blue symbols). While this intervention did not affect the RMP of coupled CMCs, it led to a slowing of conduction that was virtually identical to that observed in the presence of both I_{dark} and I_{HR}. This finding supports the conclusion that the incomplete recovery of θ observed in CMC-3T3$_{HR}$ cell preparations during activation of I_{HR} was primarily caused by the CL imposed by the 3T3$_{HR}$ cells on the coupled CMCs.

At low levels of CMC-3T3$_{HR}$ cell coupling (**Figure 4B**, open symbols), increasing the density of 3T3$_{HR}$ cells first led to a slight increase and then a moderate decrease of conduction velocities to 280 mm/s, which was paralleled by a steady decrease of the RMP of CMCs from −79.9 to −68.0 mV and a reduction of I_{Na} availability to 36.5%. The phenomenon of a transient increase of θ at CFs < 0.3 is reminiscent of supernormal conduction and is explained by the fact that the depolarization caused by the 3T3$_{HR}$ cells brought the RMP of CMCs closer to the threshold of I_{Na} activation. Because I_{Na} inactivation at these low CFs was still moderate, the reduction of the source current necessary to activate I_{Na} prevailed, and hence, θ increased at CF < 0.3.

For the case of weak coupling of 3T3$_{HR}$ cells to CMCs, θ returned to control values during HR activation. This is in contrast to the experimental observations and suggests that the coupling conductance between CMCs and 3T3$_{HR}$ cells in the experimental preparations was closer to 72 nS than 1.2 nS and that robust heterocellular coupling is prerequisite for 3T3$_{HR}$ cells to exert a significant CL on neighboring CMCs.

3T3$_{HR}$ Cell–Induced Electrogram Amplitude Changes: Simulation Versus Experiment

3T3$_{HR}$ cell density-dependent changes in peak-to-peak electrogram amplitude were investigated by computing electrograms at a distance of 5 μm from the middle of the strand (CMC-3T3$_{HR}$ cell coupling conductance of 72 nS). As shown in **Figure 5A**, electrogram amplitudes decreased with increasing 3T3$_{HR}$ cell densities from 9.6 μV (control) to 0.94 μV at a CF of 0.7. This decrease was nearly fully reversed upon HR activation. Specifically, at the highest 3T3$_{HR}$ cell densities, electrogram amplitudes were restored by more than 94% as compared to control conditions (**Figure 5B**, upper panel). The computed relative changes in electrogram amplitudes upon I_{HR} activation (**Figure 5B**, lower panel) were in qualitative agreement with the experimental values, indicating that the parameters chosen for the cell models were adequate. For simulations using a very low coupling conductance (1.2 nS), the effects of resistive loading by coupled 3T3$_{HR}$ cell were, as expected, reduced (9.7 μV to 4.7 μV; **Supplementary Figure S6**).

3T3$_{HR}$ Cell–Induced Conduction Slowing: Simulation Versus Experiment

A direct comparison of experimental and simulated conduction velocities for different 3T3$_{HR}$ cell densities is shown in **Figure 6A**. Within the range of CFs present in experiments (0.25 < CF < 0.65), simulation (solid curves) and experiments (single symbols) showed a high degree of overlap. As hypothesized, the θ deficit persisting during activation of I_{HR} (light-on conditions; red symbols) was closely matched by the simulation data describing capacitive loading (red line). The effects of resistive loading (green symbols) were obtained by subtracting the normalized velocities obtained during I_{HR} activation from the normalized velocities in the dark and adding an offset of 100% to the results. Again, the results closely matched the simulation data of the effect of resistive loading on impulse propagation (green line). The overlay of all signals shown in **Figure 6B** illustrates that resistive loading (sigmoidal) and

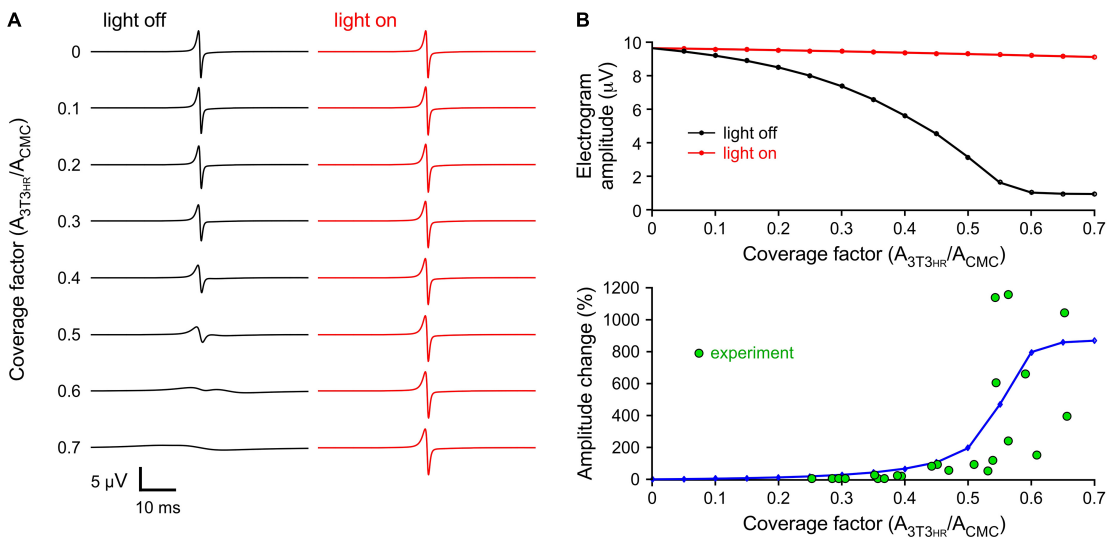

FIGURE 5 | Simulated extracellular electrograms. **(A)** Electrograms under dark conditions (light off, black) and during light stimulation (light on, red) for increasing CFs and a CMC-3T3$_{HR}$ cell coupling conductance of 72 ns. **(B)** Corresponding electrogram amplitudes (top) and relative amplitude changes upon illumination (blue, bottom) versus CF. The green symbols represent the values observed in the experiments.

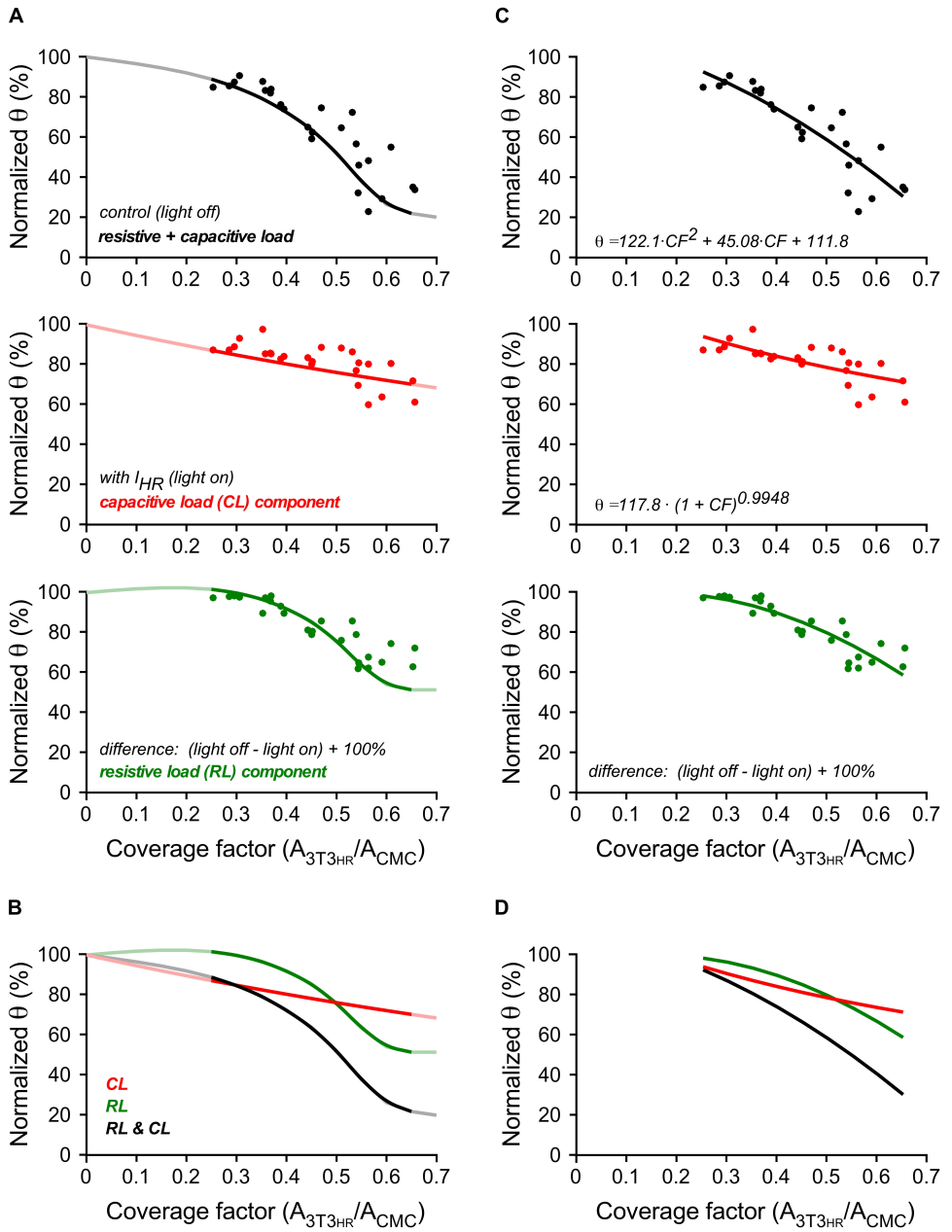

FIGURE 6 | Conduction velocities in $3T3_{HR}$-coated CMC cell strands in experiments and computer simulations. **(A)** Normalized conduction velocities versus CF in experiments (dots) versus simulations (curves). Top panel: light-off conditions (black); middle panel: light-on conditions (red); bottom panel: difference between light-off and light-on conditions corresponding to the effect of resistive loading on θ (green). **(B)** Overlay of the curves shown in panel **(A)**. **(C)** Normalized θ versus CF in experiments (dots, same data and layout as in panel **A**). Black curve: quadratic fit. Red curve: power function fit. Green curve: computed as in panels **A,B** from the fitted functions. **(D)** Overlay of the curves shown in panel **(C)**.

capacitive loading (monotonic) are equally effective in slowing conduction at a CF of ∼0.5. At lower $3T3_{HR}$ cell densities, capacitive loading prevails over resistive loading in slowing conduction and vice versa at CFs > 0.5.

Figures 6C,D illustrate an additional quantification based on curve fitting. Experimental values obtained in the dark were fitted with a polynomial function ($r^2 = 0.78$). The data obtained during illumination representing capacitive loading were fitted by a power function ($r^2 = 0.51$) based on theoretical considerations by Huxley (Huxley, 1959). The power function related θ to the total membrane capacitance present, that is, 1 (for the CMCs) + CF (for the $3T3_{HR}$ cells). From the fitted functions, the expected effect of resistive loading (CMC depolarization) was calculated as described above. Besides confirming that the effect of I_{HR} on

θ is larger for higher $3T3_{HR}$ cell densities, the analysis permitted the estimation of the power law exponent describing the effect of membrane capacitance on θ. For the experimental data presented, a value of −0.99 was obtained (95% confidence interval = −1.42 to −0.57). For the simulations (red curve in **Figure 6A**), the same fitting procedure resulted in an exponent of −0.71 (95% confidence interval = −0.73 to −0.68).

DISCUSSION

The present study was designed with the goal to experimentally determine the relative contributions of resistive versus capacitive loading to conduction slowing as induced in cardiac tissue by electrotonically coupled NECs (Miragoli et al., 2006; Kucera et al., 2017). The results demonstrate that capacitive loading of CMCs by coupled NECs is similarly important for conduction slowing as resistive loading.

Membrane Capacitance and Impulse Propagation: Theoretical Aspects

From a theoretical point of view, it is known for many decades that the membrane capacitance of excitable cells affects propagation. Quantitatively, this problem was addressed by Hodgkin in 1959, as reviewed in Jack et al. (1983). For a homogeneous, infinitely long, and uniform excitable structure (such as a non-myelinated axon), the inverse square law relating θ and axial resistance can be easily derived from cable theory. However, for the same uniform excitable structure, the relation between θ and membrane capacitance cannot be derived analytically. The problem arises from the kinetic behavior, that is, the time dependence of the ion currents underlying the action potential. While membrane capacitance directly influences the speed at which the membrane is charged (and discharged) by ion currents, the time-dependent gating of currents (mainly of I_{Na}, the primary ion current determining θ) exerts a feedback on the rate of rise of the action potential upstroke. Nevertheless, based on the theoretical considerations of Hodgkin, the relation between θ and capacitance is expected to follow a power law behavior with an exponent between −1/2 and −1, depending on the nature of the ion currents. However, the exact exponent can only be determined empirically for a given excitable preparation or mathematical model.

Membrane Capacitance and Impulse Propagation: Existing Experimental Evidence

Membrane capacitance dependent changes in impulse propagation are expected to occur when the membrane area of conducting structures increases while, simultaneously, the total amount of transmembrane currents available to charge the cells to the activation threshold remains unchanged. Such a mechanism has been proposed to underlie, for example, stretch-dependent slowing of conduction in cultured mouse CMCs with unfolding of caveolae being the source of the increased membrane area (Pfeiffer et al., 2014). The same situation is present when NECs or cells exhibiting a reduced excitability compared to CMCs are electrotonically coupled to the latter by either gap junctions or nanotubular structures (Davis and Sowinski, 2008; Quinn et al., 2016). Non-excitable cells that have been shown to establish heterocellular electrotonic coupling to CMCs include cardiac myofibroblasts (Miragoli et al., 2006; Quinn et al., 2016; Salvarani et al., 2017), HeLa cells expressing connexin43 (Gaudesius et al., 2003), macrophages (Hulsmans et al., 2017), and NIH3T3 cells (Haraguchi et al., 2010; Nussinovitch et al., 2014). Because these cell types commonly exhibit a reduced membrane potential compared to CMCs, their net effect on impulse propagation is determined not only by representing an additional capacitance (CL) but also by their depolarizing effect on coupled CMCs (RL). To complicate matters further, the two effects are not simply additive because, in contrast to the theoretically expected gradual slowing of conduction with increasing membrane capacitance, increasing levels of membrane depolarization of CMCs by coupled NECs will result in a biphasic change of conduction due to the phenomenon of supernormal conduction (Kagiyama et al., 1982; Shaw and Rudy, 1997; Rohr et al., 1998; Jacquemet and Henriquez, 2008).

Untangling the Relative Contributions of Resistive and Capacitive Loading to Conduction

In the past, experimental characterizations of the effects of NECs coupled to CMCs on impulse propagation were necessarily limited to descriptions of the combined effect of both resistive and capacitive loading because experimental techniques suitable to differentiate between RL and CL were missing. Ideally, deciphering the individual contributions of RL and CL would consist of reversibly annihilating either the resistive or the capacitive component. Whereas the latter approach is inconceivable, removing the depolarizing effect of NECs on coupled CMCs can be achieved by letting NECs express an optogenetic membrane voltage actuator such as eNpHR3.0 (Gradinaru et al., 2010) that hyperpolarizes NECs during illumination into the range of RMPs of CMCs, thereby removing the RL component and, consequently, unmasking the role of capacitive loading in impulse conduction slowing.

Choice of Experimental NEC Model

Even though the effects of coupled NECs on cardiac impulse propagation have been extensively characterized in the past with primary cardiac myofibroblasts (Gaudesius et al., 2003; Miragoli et al., 2006; Rosker et al., 2011; Salvarani et al., 2017), we resorted to NIH3T3 cells as a model for NECs in this study because pilot experiments had shown that a uniform transduction of cardiac myofibroblasts with eYFP- eNpHR3.0 was difficult to achieve. By contrast, NIH3T3 cells permitted to establish a cell line that stably expressed eYFP-eNpHR3.0 ($3T3_{HR}$ cells). This ascertained that light activation of HR involved all NECs present in the heterologous cell strands, which was a prerequisite for attributing observed effects of HR activation in full to the NECs. As shown in this study, $3T3_{HR}$ cells exhibited I–V relationships and membrane potentials (∼−35 mV) similar to that of

myofibroblasts [∼−27 mV (Salvarani et al., 2017)]. Also, 3T3$_{HR}$ cells reduced θ in heterologous strand preparations by more than 60% at the highest seeding densities used, which matches previous findings with cardiac myofibroblasts (Miragoli et al., 2006). Finally, the small electrogram amplitudes found in slowly conducting preparations indicated that slow conduction, similar to myofibroblasts, was dependent on sodium current inactivation secondary to 3T3$_{HR}$ cell–induced CMC depolarization, that is, resistive loading. Overall, these findings suggested that primary cardiac myofibroblasts can be substituted by 3T3$_{HR}$ cells when probing the relative contributions of CL and RL to conduction slowing in coupled CMCs.

Whereas in the study by Miragoli et al. (2006) myofibroblast density was given as cell count per area, we used a different measure in this study, that is, the CF (CF: area covered by 3T3$_{HR}$ cell divided by area covered by CMCs). The rationale of using this measure relates to the fact that it is ultimately the relative size of the membrane areas of the two cell types and not the cell count that determines the extent of resistive and capacitive loading.

Light Stimulation of 3T3$_{HR}$ Cells: Effects at the Single-Cell Level and in Multicellular Preparations

Light activation of single 3T3$_{HR}$ cells caused their V_m to shift from ∼−35 to ∼−104 mV. While this degree of hyperpolarization eliminates resistive loading of CMCs by coupled 3T3$_{HR}$ cells, the question arises whether light activation may in fact lead to a hyperpolarization of CMCs relevant for conduction (Funken et al., 2019). As reported before (Salvarani et al., 2017), CMC membrane potential changes induced by coupled NECs depend on the relative sizes of the membrane resistance of NECs (∼950 MΩ), the membrane resistance of CMCs [∼290 MΩ, from Salvarani et al. (2017)], and the gap junctional resistance [14 MΩ, from Salvarani et al. (2017)]. Given these resistances, light-activated 3T3$_{HR}$ cells (V_m of −104 mV) would hyperpolarize coupled CMC (RMP of −80 mV) by ∼5 mV for a CF of 1 and by maximally 3 mV for the highest CFs used in this study (0.7), which is in the same range as in the simulations (∼1 mV at a CF of 0.7) and excludes a relevant effect of 3T3$_{HR}$ cells being hyperpolarized by light beyond the RMP of CMCs on conduction.

Illumination of strand preparation coated with 3T3$_{HR}$ cells caused a CF-dependent increase of electrogram amplitudes and an acceleration of impulse conduction. At the highest 3T3$_{HR}$:CMC ratios used, electrogram amplitudes increased ∼10-fold, and θ increased by up to 120 mm/s (absolute) or up to 2.8-fold (relative). Both of these effects are consistent with the concept that light stimulation of 3T3$_{HR}$ cells caused normalization of the RMP of coupled CMCs and hence lead to a recovery of sodium current availability. As hypothesized, this illumination-induced annihilation of resistive loading of CMCs by coupled 3T3$_{HR}$ cells was not sufficient to fully restore θ to values measured in control CMC cell strands. The respective deficit, which likely represented the contribution of capacitive loading to impulse conduction slowing, amounted to ∼30% at the highest 3T3$_{HR}$ CFs investigated.

Effects of Resistive and Capacitive Loading on Conduction: Experiment and Computer Simulation

Because there exists no experimental approach to prove directly that the residual conduction slowing observed during light stimulation of 3T3$_{HR}$ cells reflects the capacitive load component exerted by NECs on coupled CMCs, we tested this hypothesis in computer simulations of fibers of CMCs only and fibers of CMCs coated at increasing densities with 3T3$_{HR}$ cells. The model was based on a previously developed CMC model (Jousset et al., 2016) and a model of 3T3$_{HR}$ cells specifically developed for this study that was based on our patch clamp data. Simulated 3T3$_{HR}$ cells were coupled to CMCs with a conductance of 72 nS as determined before in myofibroblast–CMC cell pairs (Salvarani et al., 2017) and, for comparison purposes, at a reduced coupling conductance of 1.2 nS. The latter assumption of heterocellular coupling strength was inadequate because, unlike experimental findings, θ was largely unaffected at CFs up to 0.5, and at larger CFs, activation of 3T3$_{HR}$ cells led to an almost full recovery of conduction. By contrast, results from simulations using a heterocellular coupling conductance of 72 nS closely reflected the experimental findings.

Starting from control conduction velocities as determined in CMC strands, non-stimulated 3T3$_{HR}$ cells reduced θ in a CF-dependent manner from ∼340 mm/s to less than 100 mm/s, thereby closely mimicking experimental observations made before with myofibroblasts. The CF-dependent decrease of θ showed multiple phases with a slow initial decline (CF $<$ 0.3) being followed by a steep decrease that leveled off at CFs $>$ 0.6. When removing the RL component by simulating 3T3$_{HR}$ cell activation, the moderate decay of θ at CFs $<$ 0.3 remained largely unchanged. On close inspection, conduction velocities during simulated illumination were in fact slightly lower than those obtained in dark conditions, which can be explained by the loss of the support by supernormal conduction that is afforded, in the dark, by the depolarizing influence of 3T3$_{HR}$ cells on coupled CMCs. The steep decline of conduction velocities at 0.3 $<$ CF $<$ 0.6 was explained by the equally steep decline of sodium current availability due to resistive loading of the CMCs by coupled 3T3$_{HR}$ cells. Upon illumination, sodium current availability was fully restored, as were the simulated electrogram amplitudes. By contrast and in agreement with experiments, θ was only partially restored with the deficit being likely due to the continued presence of capacitive loading. That this was indeed the correct explanation was demonstrated by the finding that coupling of cells acting as pure capacitances slowed conduction in a manner indistinguishable from light-activated 3T3$_{HR}$ cells. The isolation of the effect of resistive loading on propagation by subtracting the results obtained under light-on conditions (CL) from those obtained during light-off conditions (RL + CL) showed a slight acceleration of θ in the range 0 $<$ CF $<$ 0.3 reminiscent of NEC-induced supernormal conduction (Miragoli et al., 2006).

At maximal CFs tested, RL contributed ∼50% and CL ∼30% to overall conduction slowing (−80%). Differences in the CF dependence of the two components (monophasic for CL, multiphasic for RL) caused the two components to crossover at a CF of ∼0.5. Below this value, conduction slowing was dominated by CL, whereas above, RL became increasingly important.

The comparison of experimental and simulation results showed convergence for all parameters investigated including changes in electrogram amplitudes and the dependence of conduction velocities on CFs in the presence and absence of resistive loading. Of particular interest for this study, fitting the CL-dependent conduction slowing to a power function unveiled θ to be inversely proportional to $C_m{}^{-0.99}$ (experimental data; 95% confidence interval = $C_m{}^{-1.42}$ to $C_m{}^{-0.57}$) and $C_m{}^{-0.71}$ (simulation: 95% confidence interval = $C_m{}^{-0.73}$ to $C_m{}^{-0.68}$). These experimental results, even though displaying a broad confidence interval because of data scattering, provide for the first time a "wet" verification of the longstanding theoretical prediction that membrane capacitance determines cardiac θ according to a power law with an exponent between −1/2 and −1.

To test whether findings obtained with 3T3$_{HR}$ cells are relevant for other types of NECs as well, results were compared to HR-transduced cardiac myofibroblasts (MFB$_{HR}$). The comparison showed that, at equal levels of depression of conduction in the dark, light activation of HR caused similar increases of θ with the resistive and capacitive loading components of 3T3$_{HR}$ cells matching those of MFB$_{HR}$ cells (**Supplementary Figure S7**). This suggests that the conclusions drawn from 3T3$_{HR}$ cell experiments in the present study are likely valid for other NECs that exhibit a depolarized phenotype and establish heterocellular electrotonic coupling with CMCs.

LIMITATIONS OF THE STUDY

The main limitation of this study in respect to describing the dependence of θ on membrane capacitance refers to the problem of obtaining exact values of the cell membrane areas of CMCs and 3T3$_{HR}$ cells. Whereas the CMC strands were formed by continuous cell monolayer, taking the area of these strands as a measure of CMC capacitance likely represented an underestimate because CMCs forming these monolayers are known to overlap to a certain extent. Similarly, the determination of the cell area covered by 3T3$_{HR}$ cell based on their eYFP fluorescence was likely underestimating the true area because eYFP fluorescence tends to escape detection in fine and flat extensions of the fibroblastic cells. While obtaining the ratio of the two parameters as used in the study likely alleviated this problem to some extent, the power law coefficient describing the dependence of conduction on membrane capacitance is subject to some uncertainty as illustrated also by the wide confidence interval.

Linked to the problem of an exact determination of the membrane area of 3T3$_{HR}$ cells is the presence of endogenous myofibroblasts that, similar to 3T3$_{HR}$ cells, induce slow conduction in a cell density–dependent manner (Miragoli et al., 2006). Underlying mechanisms are identical; that is, myofibroblasts display, compared to CMCs, a depolarized phenotype and, once electrotonically coupled to the latter, represent a capacitive and resistive load. In the context of our study, myofibroblasts will add membrane capacitance to the system, and their RL will persist during illumination as they are devoid of the optogenetic actuator. In previous works, the baseline myofibroblast content of our cell cultures was estimated to be less than 10% (Rohr et al., 1991; Miragoli et al., 2006). To investigate the contribution of these non-actuated cells to conduction slowing in the presence of 3T3$_{HR}$ cells, we performed additional simulations (**Supplementary Figure S8**) in which we added 10% of non-excitable and non-actuated cells to the 3T3$_{HR}$-CMC strands. The simulations showed that the presence of these myofibroblast surrogates essentially shifts the relationship between θ and the coverage by 3T3$_{HR}$ cells by 0.1 CF unit to the left. Important to note in the context of this study is that the shift did not substantially modify the effect of capacitive loading and its power-law relationship to θ.

CONCLUSION

This study experimentally untangles the relative contributions of resistive loading (aka depolarization) and capacitive loading to conduction slowing induced by NECs that are electrotonically coupled to CMCs. At low numbers of NECs, conduction slowing is exclusively related to capacitive loading. At moderate numbers of NECs, the rate of conduction slowing increases based on the combined effects of resistive loading causing sodium current inactivation and the further increase of capacitive loading. Both effects are balanced when the total membrane area of coupled NECs reaches ∼50% of the membrane area of CMCs. Beyond this value, resistive loading becomes the prominent factor in conduction slowing. Unveiling this cell density–dependent change of mechanisms dominating NEC-induced conduction slowing contributes to the general understanding of the biophysical mechanism underlying NEC-dependent modulation of conduction. Appreciating the importance of both mechanisms is likely relevant, for example, for cardiac stem cell therapies with communication-competent cells that may act proarrhythmic (Almeida et al., 2015) not only because of constituting an RL (Smit and Coronel, 2014) but also, as demonstrated in this study, by inducing slow conduction based on capacitive loading. Finally, the study provides for the first time experimental data describing the dependence of cardiac impulse conduction on membrane capacitance. Experimental data are in line with the theoretical prediction that cell membrane capacitance affects θ in cardiac tissue according to a power law with an exponent ranging from −1/2 to −1.

DATA AVAILABILITY STATEMENT

The datasets generated for this study are available by request to the corresponding author.

ETHICS STATEMENT

The animal study was reviewed and approved by the State Veterinary Department of the Canton Bern, licence BE27/17.

AUTHOR CONTRIBUTIONS

SR conceived the study. SD designed and performed the 3T3 cell experiments, analyzed and interpreted the data, and wrote part of the methods section. AB performed the simulations and wrote part of the methods section. SM developed the optogenetically modified cardiac myofibroblasts and conducted the respective experiments. CD developed the MEA system. Computational and experimental work was supervised by JK and SR who also wrote the manuscript. All authors read and approved the submitted version of the manuscript.

FUNDING

The study was supported by the Swiss National Science Foundation (310030_169234 to SR and 310030_184707 to JK).

ACKNOWLEDGMENTS

We greatly acknowledge the excellent cell culture work performed by Regula Flückiger-Labrada.

SUPPLEMENTARY MATERIAL

The Supplementary Material for this article can be found online at: https://www.frontiersin.org/articles/10.3389/fphys.2020.00194/full#supplementary-material

REFERENCES

Almeida, S. O., Skelton, R. J., Adigopula, S., and Ardehali, R. (2015). Arrhythmia in stem cell transplantation. *Card. Electrophysiol. Clin.* 7, 357–370. doi: 10.1016/j.ccep.2015.03.012

Davis, D. M., and Sowinski, S. (2008). Membrane nanotubes: dynamic long-distance connections between animal cells. *Nat. Rev. Mol. Cell Biol.* 9, 431–436. doi: 10.1038/nrm2399

Funken, M., Malan, D., Sasse, P., and Bruegmann, T. (2019). Optogenetic hyperpolarization of cardiomyocytes terminates ventricular arrhythmia. *Front. Physiol.* 10:498. doi: 10.3389/fphys.2019.00498

Gaudesius, G., Miragoli, M., Thomas, S. P., and Rohr, S. (2003). Coupling of cardiac electrical activity over extended distances by fibroblasts of cardiac origin. *Circ. Res.* 93, 421–428. doi: 10.1161/01.res.0000089258.40661.0c

Gradinaru, V., Zhang, F., Ramakrishnan, C., Mattis, J., Prakash, R., Diester, I., et al. (2010). Molecular and cellular approaches for diversifying and extending optogenetics. *Cell* 141, 154–165. doi: 10.1016/j.cell.2010.02.037

Haraguchi, Y., Shimizu, T., Yamato, M., and Okano, T. (2010). Electrical interaction between cardiomyocyte sheets separated by non-cardiomyocyte sheets in heterogeneous tissues. *J. Tissue Eng. Regen. Med.* 4, 291–299. doi: 10.1002/term.241

Hartline, D. K., and Colman, D. R. (2007). Rapid conduction and the evolution of giant axons and myelinated fibers. *Curr. Biol.* 17, R29–R35.

Hewinson, J., Paton, J. F., and Kasparov, S. (2013). Viral gene delivery: optimized protocol for production of high titer lentiviral vectors. *Methods Mol. Biol.* 998, 65–75. doi: 10.1007/978-1-62703-351-0_5

Hulsmans, M., Clauss, S., Xiao, L., Aguirre, A. D., King, K. R., Hanley, A., et al. (2017). Macrophages facilitate electrical conduction in the heart. *Cell* 169, 510.e20–522.e20.

Huxley, A. F. (1959). Ion movements during nerve activity. *Ann. N. Y. Acad. Sci.* 81, 221–246. doi: 10.1111/j.1749-6632.1959.tb49311.x

Jack, J. B., Noble, D., and Tsien, R. W. (1983). *Electric Current Flow in Excitable Cells*. Oxford: Oxford University Press.

Jacquemet, V., and Henriquez, C. S. (2008). Loading effect of fibroblast-myocyte coupling on resting potential, impulse propagation, and repolarization: insights from a microstructure model. *Am. J. Physiol. Heart Circ. Physiol.* 294, H2040–H2052. doi: 10.1152/ajpheart.01298.2007

Jousset, F., Maguy, A., Rohr, S., and Kucera, J. P. (2016). Myofibroblasts electrotonically coupled to cardiomyocytes alter conduction: insights at the cellular level from a detailed in silico tissue structure model. *Front. Physiol.* 7:496. doi: 10.3389/fphys.2016.00496

Kagiyama, Y., Hill, J. L., and Gettes, L. S. (1982). Interaction of acidosis and increased extracellular potassium on action potential characteristics and conduction in guinea pig ventricular muscle. *Circ. Res.* 51, 614–623. doi: 10.1161/01.res.51.5.614

Kleber, A. G., and Rudy, Y. (2004). Basic mechanisms of cardiac impulse propagation and associated arrhythmias. *Physiol. Rev.* 84, 431–488. doi: 10.1152/physrev.00025.2003

Kucera, J. P., Rohr, S., and Kleber, A. G. (2017). Microstructure, cell-to-cell coupling, and ion currents as determinants of electrical propagation and arrhythmogenesis. *Circ. Arrhythm. Electrophysiol.* 10:e004665.

Luo, C. H., and Rudy, Y. (1991). A model of the ventricular cardiac action potential. depolarization, repolarization, and their interaction. *Circ. Res.* 68, 1501–1526. doi: 10.1161/01.res.68.6.1501

Matsumoto, G., and Tasaki, I. (1977). Study of conduction-velocity in non-myelinated nerve-fibers. *Biophys. J.* 20, 1–13.

Miragoli, M., Gaudesius, G., and Rohr, S. (2006). Electrotonic modulation of cardiac impulse conduction by myofibroblasts. *Circ. Res.* 98, 801–810. doi: 10.1161/01.res.0000214537.44195.a3

Nussinovitch, U., Shinnawi, R., and Gepstein, L. (2014). Modulation of cardiac tissue electrophysiological properties with light-sensitive proteins. *Cardiovasc. Res.* 102, 176–187. doi: 10.1093/cvr/cvu037

Pfeiffer, E. R., Wright, A. T., Edwards, A. G., Stowe, J. C., Mcnall, K., Tan, J., et al. (2014). Caveolae in ventricular myocytes are required for stretch-dependent conduction slowing. *J. Mol. Cell. Cardiol.* 76, 265–274. doi: 10.1016/j.yjmcc.2014.09.014

Plonsey, R., and Barr, R. C. (2000). *Bioelectricity : A Quantitative Approach*. New York, NY: Kluwer Academic/Plenum Publishers.

Quinn, T. A., Camelliti, P., Rog-Zielinska, E. A., Siedlecka, U., Poggioli, T., O'toole, E. T., et al. (2016). Electrotonic coupling of excitable and nonexcitable cells in the heart revealed by optogenetics. *Proc. Natl. Acad. Sci. U.S.A.* 113, 14852–14857. doi: 10.1073/pnas.1611184114

Rohr, S. (1986). Temperature-controlled perfusion chamber suited for mounting on microscope stages. *J. Physiol. (Lond.)* 378:90.

Rohr, S. (2009). Myofibroblasts in diseased hearts: new players in cardiac arrhythmias? *Heart Rhythm* 6, 848–856. doi: 10.1016/j.hrthm.2009.02.038

Rohr, S., Fluckiger-Labrada, R., and Kucera, J. P. (2003). Photolithographically defined deposition of attachment factors as a versatile method for patterning the growth of different cell types in culture. *Pflugers Arch.* 446, 125–132. doi: 10.1007/s00424-002-1000-0

Rohr, S., Kucera, J. P., and Kleber, A. G. (1998). Slow conduction in cardiac tissue, I: effects of a reduction of excitability versus a reduction of electrical coupling on microconduction. *Circ. Res.* 83, 781–794. doi: 10.1161/01.res.83.8.781

Rohr, S., Scholly, D. M., and Kleber, A. G. (1991). Patterned growth of neonatal rat heart cells in culture. Morphological and electrophysiological characterization. *Circ. Res.* 68, 114–130. doi: 10.1161/01.res.68.1.114

Rosker, C., Salvarani, N., Schmutz, S., Grand, T., and Rohr, S. (2011). Abolishing myofibroblast arrhythmogeneicity by pharmacological ablation of alpha-smooth muscle actin containing stress fibers. *Circ. Res.* 109, 1120–1131. doi: 10.1161/CIRCRESAHA.111.244798

Rush, S., and Larsen, H. (1978). A practical algorithm for solving dynamic membrane equations. *IEEE Trans. Biomed. Eng.* 25, 389–392. doi: 10.1109/tbme.1978.326270

Salvarani, N., Maguy, A., De Simone, S. A., Miragoli, M., Jousset, F., and Rohr, S. (2017). TGF-beta1 (Transforming Growth Factor-beta1) plays a pivotal role in cardiac myofibroblast arrhythmogenicity. *Circ. Arrhythm. Electrophysiol.* 10:e004567. doi: 10.1161/CIRCEP.116.004567

Shaw, R. M., and Rudy, Y. (1997). Electrophysiologic effects of acute myocardial ischemia. A mechanistic investigation of action potential conduction and conduction failure. *Circ. Res.* 80, 124–138. doi: 10.1161/01.res.80.1.124

Smit, N. W., and Coronel, R. (2014). Stem cells can form gap junctions with cardiac myocytes and exert pro-arrhythmic effects. *Front. Physiol.* 5:419. doi: 10.3389/fphys.2014.00419

Valiunas, V., Bukauskas, F. F., and Weingart, R. (1997). Conductances and selective permeability of connexin43 gap junction channels examined in neonatal rat heart cells. *Circ. Res.* 80, 708–719. doi: 10.1161/01.res.80.5.708

Zhang, C., Yang, S., Flossmann, T., Gao, S., Witte, O. W., Nagel, G., et al. (2019). Optimized photo-stimulation of halorhodopsin for long-term neuronal inhibition. *BMC Biol.* 17:95. doi: 10.1186/s12915-019-0717-6

Conflict of Interest: The authors declare that the research was conducted in the absence of any commercial or financial relationships that could be construed as a potential conflict of interest.

frontiers in Physiology

REVIEW
published: 08 April 2020
doi: 10.3389/fphys.2020.00301

Leukocyte-Dependent Regulation of Cardiac Fibrosis

*Ama Dedo Okyere and Douglas G. Tilley**

Center for Translational Medicine, Lewis Katz School of Medicine, Temple University, Philadelphia, PA, United States

Cardiac fibrosis begins as an intrinsic response to injury or ageing that functions to preserve the tissue from further damage. Fibrosis results from activated cardiac myofibroblasts, which secrete extracellular matrix (ECM) proteins in an effort to replace damaged tissue; however, excessive ECM deposition leads to pathological fibrotic remodeling. At this extent, fibrosis gravely disturbs myocardial compliance, and ultimately leads to adverse outcomes like heart failure with heightened mortality. As such, understanding the complexity behind fibrotic remodeling has been a focal point of cardiac research in recent years. Resident cardiac fibroblasts and activated myofibroblasts have been proven integral to the fibrotic response; however, several findings point to additional cell types that may contribute to the development of pathological fibrosis. For one, leukocytes expand in number after injury and exhibit high plasticity, thus their distinct role(s) in cardiac fibrosis is an ongoing and controversial field of study. This review summarizes current findings, focusing on both direct and indirect leukocyte-mediated mechanisms of fibrosis, which may provide novel targeted strategies against fibrotic remodeling.

Keywords: cardiac fibrosis, neutrophil, monocyte macrophage, mast cells, lymphocytes, dendritic cells, eosinophils, inflammation

OPEN ACCESS

Edited by:
Domenico Corradi,
University of Parma, Italy

Reviewed by:
Nikolaos G. Frangogiannis,
Albert Einstein College of Medicine, United States
Paolo Fiorina,
University of Milan, Italy

***Correspondence:**
Douglas G. Tilley
douglas.tilley@temple.edu

Specialty section:
This article was submitted to Integrative Physiology, a section of the journal Frontiers in Physiology

Received: *25 November 2019*
Accepted: *17 March 2020*
Published: *08 April 2020*

Citation:
Okyere AD and Tilley DG (2020) Leukocyte-Dependent Regulation of Cardiac Fibrosis. Front. Physiol. 11:301. doi: 10.3389/fphys.2020.00301

CARDIAC FIBROSIS

The healthy heart is supported by a distinct network of extracellular matrix (ECM) proteins, which function in part to preserve chamber structure and aid in cardiac cell communication (Lu et al., 2011; Frangogiannis, 2017). Fibroblasts resident to the heart are primarily responsible for maintaining the ECM, which typically consists of roughly 80 percent type I collagens, 10 percent type III collagens, and a combination of proteoglycans, glycoproteins, and glycosaminoglycans (Kong et al., 2014). The cardiac ECM is highly dynamic, and it's homeostasis is preserved through a few mechanisms: a strict balance between protein synthesis and degradation, as well as protein reorganization within the network (Lu et al., 2011). However, virtually any injury to the heart will activate fibrosis, or a dysregulated and enhanced growth of the ECM milieu, since the adult heart holds limited capacity for regeneration (Humeres and Frangogiannis, 2019). For instance, following a myocardial infarction (MI), the severe loss of cardiomyocytes triggers increased matrix production in an effort to replace lost and damaged tissue (Frangogiannis, 2019a). Further, other pathologies like pressure overload due to hypertension, volume overload, diabetes, obesity, and even aging can stress any chamber of the heart, therefore leading to fibrotic growth around the vasculature and within the interstitium (Aguiar et al., 2019; Frangogiannis, 2019a). Although this matrix growth initially serves as a form of repair, it can quickly become detrimental (Frangogiannis, 2019a). An exaggerated production of collagens can result in myocardial stiffening, which disrupts cardiac compliance and ultimately decreases systolic and diastolic function (Kong et al., 2014; Tallquist and Molkentin, 2017). Importantly, it has recently been shown that severe cardiac fibrosis,

especially when accompanied by heart failure (HF) is associated with increased mortality in patients (Aoki et al., 2011; Gyongyosi et al., 2017). While there are currently treatment options that help in managing the symptoms of heart disease, there are no effective therapies targeted at controlling pathological fibrosis. Therefore, an in-depth discussion, focusing on the mechanisms that contribute to the genesis of fibrosis is extremely necessary (Gyongyosi et al., 2017; Tallquist and Molkentin, 2017; Aghajanian et al., 2019; Humeres and Frangogiannis, 2019).

In past years, numerous rigorous studies have identified the resident cardiac fibroblast as a crucial cell effector of pathological fibrosis (Davis and Molkentin, 2014; Kanisicak et al., 2016; Tallquist and Molkentin, 2017; Fu et al., 2018; Ivey et al., 2018). Due to injury, resident fibroblasts proliferate, and differentiate into mature cardiac myofibroblasts, which, through *de novo* expression of α smooth muscle actin (αSMA) can contract to support wound healing (Davis and Molkentin, 2014). Activated myofibroblasts also contribute to fibrosis by secreting copious amounts of matrix protein, which then overwhelms the ECM (Davis and Molkentin, 2014; Stempien-Otero et al., 2016; Tallquist and Molkentin, 2017). Due to the hearts cellular complexity, additional sources, including vascular and bone marrow derived cells have been considered for their contribution to myofibroblast differentiation and fibrosis (Kanisicak et al., 2016; Travers et al., 2016; Tallquist and Molkentin, 2017; Fu et al., 2018). This review will focus on the leukocyte dependent regulation of fibrosis since it has been well reported that the activation of resident fibroblasts into myofibroblasts is heavily influenced by changes in the myocardial environment (Davis and Molkentin, 2014; Stempien-Otero et al., 2016). This is important to note, as injury results in damaged cardiomyocytes which incite inflammation and promote a large expansion and infiltration of leukocytes (Swirski and Nahrendorf, 2013; Grisanti et al., 2016a,b; Swirski and Nahrendorf, 2018). These infiltrating leukocytes occupy spaces near sites of injury, and function through cytokines and growth factors secretions, which contribute to changes in myocardial environment (Swirski and Nahrendorf, 2013, 2018). As such, the role of leukocytes in cardiac fibrosis has been a longstanding research focus. Since leukocytes drastically expand in number following injury, and exhibit high cellular plasticity, earlier studies sought to determine if, and to what extent, leukocytes serve as additional cell sources for myofibroblast transdifferentiation (van Amerongen et al., 2008; Alex and Frangogiannis, 2018). More recent studies have focused on both the direct and indirect roles of distinct leukocyte subsets in cardiac fibrosis. Below, we will examine the current understanding of leukocytes in cardiac biology, focusing on how they may regulate cardiac fibrosis, and examining if they can be targeted to control fibrosis.

LEUKOCYTES IN CARDIAC PHYSIOLOGY AND PATHOLOGY

Any tissue injury leads to inflammation, which engages a collective of white blood cells termed leukocytes (Geissmann et al., 2010; Kondo, 2010). The primary function of leukocytes is to sense and respond to pathogens or damage in order to suppress any additional danger (Kondo, 2010). Leukocytes exist in various subsets, and can be classified as being of either lymphoid or myeloid origin (Kondo, 2010). Their origin and subsequent gene expression profiles are key to their function (Geissmann et al., 2010; Kondo, 2010). All leukocytes initially derive from hematopoietic stem cells, which differentiate into either lymphoid or myeloid progenitors (Kondo, 2010). Lymphoid progenitors give rise to B and T lymphocytes, natural killer cells, and some subsets of dendritic cells (Kondo, 2010). Myeloid progenitors are precursors for megakaryocytes, erythrocytes, granulocytes, and monocytes (Kondo, 2010). Seminal studies in recent years have provided ample evidence for the roles and origins of leukocytes both in the steady-state and injured heart (Epelman et al., 2014; Swirski and Nahrendorf, 2018).

Through flow cytometry and single cell RNA sequencing technologies, researchers have established the presence of many leukocyte subsets in the injured and healthy heart, with most of them being macrophages (Epelman et al., 2014; Swirski and Nahrendorf, 2018; Aguiar et al., 2019; Dick et al., 2019). Further studies using adult mouse hearts have allowed us to gain greater appreciation for the existence and diversity of these cardiac macrophage populations (Swirski and Nahrendorf, 2018). A minority of cardiac macrophages, expressing chemokine receptor 2 (CCR2), stem from circulating monocyte precursors (Epelman et al., 2014; Bajpai et al., 2018). However, additional cardiac macrophage subsets have been shown to inhabit the heart early, and persist throughout adulthood via proliferation (Epelman et al., 2014; Bajpai et al., 2018; Dick et al., 2019). Functionally, cardiac macrophages are thought to act as pathogen sensors, but they may also take more active part in myocardial electrical conduction (Ma et al., 2018; Swirski and Nahrendorf, 2018). Interestingly, recent findings suggest an abundance of connexin 43-expressing macrophages in the atrioventricular (AV) node, which exhibit an ability to couple to cardiomyocytes and alter their membrane potential (Hulsmans et al., 2017). Other leukocyte populations in the steady-state heart include lymphocytes, dendritic and mast cells (Choi et al., 2009; Swirski and Nahrendorf, 2018). The complete function of these cells is still not entirely understood, however, mast cells have been shown to be stores of preformed cytokines, which may prove beneficial at the onset of injury (Frangogiannis et al., 1998).

Cardiac fibrosis is a typical feature of ageing and injury, both of which are known to trigger leukocyte expansion and inflammation within the heart (Epelman et al., 2015; Lu et al., 2017; Suetomi et al., 2018; Aguiar et al., 2019). For instance, a plethora of studies have revealed the rapid and continuous innate immune response that follows acute ischemic injuries. Neutrophils and inflammatory monocytes/macrophages infiltrate the myocardium in response to endogenous damage-associated molecular patterns (DAMPs) where they can effectively clear dying cells and regulate inflammation through cytokines, chemokines, and reactive oxygen species (Forte et al., 2018). Following this pro-inflammatory phase, additional monocyte subsets (Ly6C^{lo}) are recruited to promote transition to injury repair through secretion of pro-repair factors (Nahrendorf et al., 2007; Forte et al., 2018). Cluster of differentiation

(CD) $11b^+/CD11c^+$ dendritic cells have also been shown to accumulate in the border zone post-myocardial infarction (MI), peaking around 7 days post-injury (Gallego-Colon et al., 2015). Dendritic cells are thought to aid in preserving left ventricle (LV) function activate T lymphocyte subsets through antigen presenting functions (Forte et al., 2018). The role of adaptive immunity in response to ischemic injury is still being uncovered, however, recent studies suggest the involvement of both B and T lymphocytes in cardiac remodeling post-MI (Forte et al., 2018). For instance, $CD4^+$ T cells have been shown to invade the heart by 7 days post-MI, where they are presumed to modulate LV function (Hofmann et al., 2012). Similarly, B cell volumes expand following MI, reaching a peak around 5–7 days post-injury (Yan et al., 2013; Zouggari et al., 2013). Functionally, B cells may contribute to the regulation of inflammatory gene expression post-ischemic injury (Zouggari et al., 2013). The innate and adaptive immune response have also been characterized in ageing and injuries of non-ischemic etiology. For instance, mouse models of advanced ageing, and hypertension through high salt, unilateral nephrectomy, and aldosterone infusion, reveal increased neutrophil and macrophage populations within the heart (Hulsmans et al., 2018). The presence of these immune cells is associated with enhanced diastolic dysfunction. Further, pressure overload induced pathology due to transverse aortic constriction (TAC) has also been shown to result in an increased infiltration of leukocytes, both $CCR2^+$ macrophages and $CD4^+$ T cells (Laroumanie et al., 2014; Patel et al., 2018). The rise in leukocytes to the heart following these pathophysiological changes has prompted many researchers to question the link between inflammation and fibrosis.

LEUKOCYTE INVOLVEMENT IN CARDIAC FIBROSIS

Fibrosis and inflammation are essential physiological processes that follow essentially all cardiac pathologies (Swirski and Nahrendorf, 2018). During inflammation, leukocytes function to resolve injury and defend the host through several eloquent mechanisms (Kondo, 2010; Bajpai and Tilley, 2018). The existing literature suggests several connections between leukocyte driven inflammation and cardiac fibrosis. Below, we consider the evidence supporting leukocyte dependent regulation of fibrosis with the ultimate goal of highlighting novel targets in the quest for combating detrimental fibrotic remodeling (**Table 1** and **Figure 1**).

Neutrophils

Neutrophils are polymorphous nuclear leukocytes that are often recognized as the first responders to injury (Amulic et al., 2012). Neutrophils mature in the bone marrow, and their release is strictly regulated by shifting chemokine gradients; however, it's important to recognize that neutrophils may alter their phenotypes upon exposure to distinct tissue environments (Amulic et al., 2012; Deniset and Kubes, 2018). Circulating neutrophils begin injury resolution in the heart by extravasating the activated endothelium, releasing their noxious granular contents, employing their phagocytic capacity, and forming extracellular chromatin traps rich in inflammatory enzymes (Amulic et al., 2012; Horckmans et al., 2017; Martinod et al., 2017). The content within neutrophil granules can vary, as they are shaped by the transcriptional program present during formation; however, they typically encompass agents like myeloperoxidase, cathepsins, and neutrophil gelatinase-associated lipocalin (NGAL) which help to repress injury through oxidative and proteolytic actions (Amulic et al., 2012). Release of neutrophil granules can occur very rapidly after activation, but neutrophil extracellular traps (NETs) are more insidious. NETs result from slow cell death (NETosis) or non-lytic secretions (Papayannopoulos, 2018). Essentially, released granular proteases like neutrophil elastase (NE) degrade actin polymers, and disrupt chromatin structure; as neutrophil membranes rupture, these intracellular contents expand to the extracellular space (Metzler et al., 2014; Papayannopoulos, 2018). Altogether, these actions make neutrophils very inflammatory, so consequently, as a benefit to the host, they are very short lived cells (Amulic et al., 2012).

Neutrophils have gained traction in the field of cardiac fibrosis given their early prevalence in injuries like MI and myocarditis (Horckmans et al., 2017; Weckbach et al., 2019). Following MI, neutrophils invade the heart in response to necrosing tissue, and they accumulate in the infarct border zone (Askari et al., 2003; Prabhu and Frangogiannis, 2016). They release inflammatory mediators and proteolytic enzymes in order to assist in clearing dead cells and matrix debris (Prabhu and Frangogiannis, 2016). Neutrophils have mostly been regarded as highly inflammatory cells; earlier studies even suggest that their persistence in sterile inflammation may cause further damage to viable cardiomyocytes (Entman et al., 1992; Prabhu and Frangogiannis, 2016). Therefore, recent studies have sought to understand how neutrophil depletion may impact post-MI healing (Horckmans et al., 2017). Interestingly, 1 week following MI, neutralization of neutrophils has been shown to result in worsened cardiac function that is accompanied by enhanced fibroblast activation and excessive collagen deposition (Horckmans et al., 2017). These data suggest that the neutrophil function and secretome may actually be important for mitigating the onset of fibrotic remodeling in a time- and context-dependent manner post-MI. For instance, neutrophils have been shown to persist in post-MI injury due to constant cytokine and DAMP production; these later stage neutrophils function to promote resolution of inflammation (Ma et al., 2016). They express archetypal anti-inflammatory genes and release distinct lipid mediators, which are critical in dampening further pro-inflammatory responses (Serhan et al., 1995; Ma et al., 2016; Prabhu and Frangogiannis, 2016). Through gene expression analysis, further studies have provided evidence to support that neutrophils exist along a phenotypic continuum post-MI; they express pro-inflammatory genes early after injury, but participate in ECM reorganization during post-MI repair (Ma et al., 2016; Daseke et al., 2019). Interestingly, the deletion of an enzyme that catalyzes inflammatory metabolites (12/15 lipoxygenase) promotes anti-inflammatory neutrophil phenotypes post-MI, which also correlates with decreased

TABLE 1 | This table lists evidence in support of how each leukocyte class may regulate cardiac fibrosis in distinct pathological contexts.

Leukocyte class	Pathological context	Contribution to fibrosis
Neutrophils	Ischemia	5 day post MI, increase in **CD206** and or **Arg-1** expressing neutrophils is associated with decreased myofibroblast transdifferentiation (Kain et al., 2018) 7 days post MI, neutrophils express **Fibronectin**, **Gal-3**, **Fibrinogen** which contributes to ECM reorganization (Daseke et al., 2019) 21 days post MI, loss of **MPO** reduces fibrosis (Mollenhauer et al., 2017) Post MI, loss of **NGAL** expressing neutrophils may affect dead myocyte phagocytosis and contribute to fibrosis (Horckmans et al., 2017)
	Myocarditis/DCM; Ageing	In chronic myocarditis and ageing decreased neutrophil infiltration and **NETosis**/**NET** formation is associated with reduced fibrosis (Martinod et al., 2017; Weckbach et al., 2019)
Monocytes/Macrophages	Ischemia	1–6 weeks post MI, macrophages may transition to fibroblast-like cells, capable of secreting collagen (Haider et al., 2019) **IL-10** and **TGFβ** secreting macrophages promote myofibroblasts transdifferentiation (O'Rourke et al., 2019) 1 week post ischemia/reperfusion, loss of **MCP-1** is associated with decreased macrophage infiltration and interstitial fibrosis (Frangogiannis et al., 2007) 4 weeks post MI, **Gata6** expressing pericardial macrophages limit cardiac fibrosis (Deniset et al., 2019)
	Pressure Overload	Macrophage associated **Gal-3** correlates with increased cardiac fibrosis in hypertensive rats (de Boer et al., 2009) 8 weeks following uninephrectomy and salty drinking water, loss of macrophage expressed **mineralocorticoid receptor** reduces cardiac collagen content (Rickard et al., 2009)
Mast Cells	Pressure Overload	Mast cells contribute to **PDGF-A** expression and fibrosis in the heart following TAC (Liao et al., 2010)
	DCM	Mast cells are a large source of **FGF-2**, and found within fibrotic sections of cardiac tissue (Bradding and Pejler, 2018)
Eosinophils	Myocarditis/DCM	Eosinophil depletion post myocarditis is associated with decreased levels of **MMP-2** and **TIMP-2** (Diny et al., 2017)
Dendritic Cells	Ischemia	Ablation of dendritic cells results in increased **MMP-9** and **MMP-2** activity 3–28 days post MI (Anzai et al., 2012)
	Pressure Overload	Dendritic cell ablation following TAC is associated with decreased **IL-1β** and **TGFβ** and less fibrosis (Wang et al., 2017)
	Myocarditis/DCM	**BATF3** dependent dendritic cells limit cardiac fibrosis following viral infection (Clemente-Casares et al., 2017)
B and T Cells	Ischemia	Depletion of **TNFα** T regulatory cells improves fibrosis post MI (Bansal et al., 2019)
	Pressure Overload	B cell depletion results in decreased fibrosis following TAC (Ma et al., 2019) **IFNγ** T cells promote myofibroblast trans differentiation and cardiac fibrosis (Nevers et al., 2017) CD73 expressing T cells attenuate fibrosis following TAC (Quast et al., 2017)
	Myocarditis/DCM	**TNFα** secreting B cells correlate with greater fibrosis in DCM patients (Yu et al., 2013)

MI, myocardial infarction; CD, cluster of differentiation; Arg-1, arginase 1; GAL3, galectin-3; MPO, myeloperoxidase; NGAL, neutrophil gelatinase-associated lipocalin; NETosis, neutrophil extracellular trap formation; IL-10, interleukin 10; TGFβ, transforming growth factor beta; MCP-1, monocyte chemoattractant protein 1; Gata6, GATA binding protein 6; PDGF, platelet derived growth factor; FGF, fibroblast growth factor; MMP, matrix metallopeptidase; TIMP, tissue inhibitor of metalloproteinases; IL-1β, interleukin 1 beta; TGFβ, transforming growth factor beta; BATF3, basic leucine zipper transcription factor ATF-like 3; IFNγ, interferon gamma; TNFα, tumor necrosis factor alpha.

fibroblast activation and collagen deposition by 5 days post-MI injury (Kain et al., 2018).

Additional studies have characterized the neutrophil-dependent regulation of fibrosis focusing on other pathological states. For instance, neutrophils have been examined for their contribution to fibrosis and ultimately, atrial fibrillation (Friedrichs et al., 2014). After 2 weeks of angiotensin II infusion and deletion of macrophage integrin Mac-1, attenuating the neutrophil infiltration and accumulation within the atrium leads to decreased atrial fibrosis and fibrillation episodes (Friedrichs et al., 2014). Recent studies have also focused on how neutrophil processes like NETosis may impact ventricular fibrotic remodeling after injury. Sustained inflammation, even after pathogen clearance makes myocarditis a major risk factor for developing inflammatory dilated cardiomyopathy (DCM) (Weckbach et al., 2019). NETs have been detected in human cases of myocarditis, which can be replicated in mice using experimental models of myocarditis (Weckbach et al., 2019). Following experimental myocarditis, an increase in NETs corresponds to an increase in collagen deposition, which is alleviated upon neutralizing a cytokine essential to neutrophil recruitment and NET formation (Weckbach et al., 2019). The correlation between NETs and fibrosis is further supported in the context of ageing. Ageing is known to trigger the expansion of neutrophils and NETs; disrupting NET formation in aged mice has been shown to improve cardiac function and decrease ageing related interstitial fibrosis (Martinod et al., 2017). Taken together, neutrophils may serve to regulate fibrosis; however, their actions are clearly context-dependent.

Monocytes and Macrophages

Since their early discovery, we have come to appreciate the complexity of monocyte and macrophage biology. These leukocytes primarily function as key defenders of the innate immune system by sensing for pathogens, digesting debris, and releasing inflammatory mediators (Hulsmans et al., 2016). However, years of intense scrutiny has revealed numerous other roles for monocytes and macrophages in organ homeostasis and injury, even in the heart (Lavine et al., 2018; Skelly et al., 2018; Williams et al., 2018). Macrophages that are

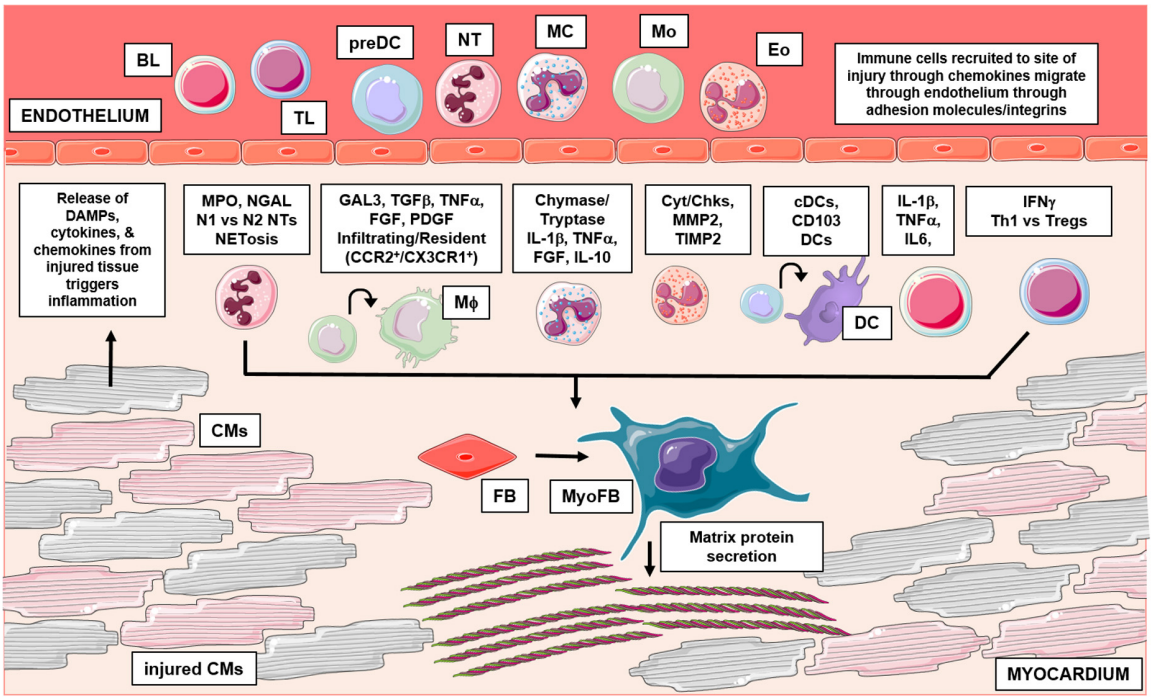

FIGURE 1 | This graphical abstract summarizes the role of leukocytes in cardiac fibrosis. Following injury, damaged cardiac tissue (inclusive of all resident cell types) can release inflammatory mediators like DAMPs, which trigger an influx of leukocytes to the site of injury. Activated leukocytes then function through numerous mechanisms to regulate pathological cardiac fibrosis. Briefly, granulocytes (mast cells, eosinophils, neutrophils) have been shown to influence fibrosis in part, through their ability to secrete fibrotic mediators, regulate expression of MMPs/TIMPs and form inflammatory extracellular traps, respectively. Additionally, recent studies have identified varying subsets of macrophages and dendritic cells which differentially regulate fibrosis outcomes; cells of monocytic origin have also been examined for their direct contribution in myofibroblast differentiation. Lastly, numerous findings also implicate lymphocytes in cardiac fibrosis, these adaptive immune cells have been shown to influence remodeling outcomes through many mechanisms. BL, b lymphocyte; TL, t lymphocyte; preDC, precursor dendritic cell; NT, neutrophil; MC, mast cell; Mo, monocyte; Eo, eosinophil; Mϕ, macrophage; DC, dendritic cell; CM, cardiomyocyte; FB, fibroblast; MyoFB, myofibroblast; DAMP, damage associated molecular pattern; MPO, myeloperoxidase; NGAL, neutrophil gelatinase-associated lipocalin; N1, inflammatory NT; N2, antiinflammatory NT; NETosis, NT extracellular trap formation; GAL3, galectin-3; TGFβ, transforming growth factor beta; TNFα, tumor necrosis factor alpha; FGF, fibroblast growth factor; PDGF, platelet derived growth factor; CCR2, C-C chemokine receptor 2; CX3CR1, CX3C chemokine receptor 1; IL-1β, interleukin 1 beta; IL-10, interleukin 10; Cyt, cytokines; Chk, chemokines; MMP2, matrix metallopeptidase 2; TIMP 2, tissue inhibitor of metalloproteinases 2; cDC, conventional DC; CD, cluster of differentiation; IL-6, interleukin 6; IFNγ, interferon gamma; Th1, t helper type 1; Treg, regulatory t cells. Graphics were created using Servier Medical Art templates, which are licensed under a Creative Commons Attribution 3.0 Uniported License; https://smart.servier.com.

innate to the heart stem mainly from embryonic precursors, with some input from circulating monocytes (Ma et al., 2018; Williams et al., 2018; Dick et al., 2019). These resident cardiac macrophages exhibit distinct gene expression profiles, and have the capacity for self-renewal through adulthood (Skelly et al., 2018; Williams et al., 2018). In the case of injury, circulating monocytes infiltrate and differentiate in the heart; these monocyte/macrophage populations have long been evaluated for their contribution in the fibrotic response. Owing to their remarkable plasticity and heterogeneity, monocytes and macrophages have been assessed for their ability to impart both pro- or anti-fibrotic effects in the myocardium (Wynn and Barron, 2010). For instance, studies have sought to characterize subsets of monocytes/macrophages which may act as additional cells capable of myofibroblast transdifferentiation. Further, numerous studies have also questioned monocytes/macrophages ability to initiate fibroblast activation or aid in resolution of fibrosis through debris clearance mechanisms (Kong et al., 2014). Below, we consider findings of these studies, which suggest subset dependent roles for macrophages and monocytes in cardiac fibrosis.

Until recently, the origin of cardiac myofibroblasts was not entirely clear; however, their induction in response to injury was widely documented (van Amerongen et al., 2008). Earlier findings revealed potential roles for leukocytes in heart regeneration post-MI, and posited leukocytes as cell sources of myofibroblast populations in other organs (Orlic et al., 2001; Forbes et al., 2004). This led cardiac researchers to hypothesize the same phenomena in the context of ischemic injury. To test the leukocyte contribution to myofibroblast transdifferentiation, studies took advantage of bone marrow transplantation with fluorescent-labeled cells (Mollmann et al., 2006; van Amerongen et al., 2008). Following ischemic injury, researchers were able to identify GFP and F4/80 (monocytes/macrophages marker) double positive cells in the infarct, which also co-localized with αSMA (Mollmann et al., 2006; van Amerongen et al., 2008). Importantly, the lack of CD31 co-localization suggested these cells were independent of the vasculature (Mollmann et al., 2006).

Further analyses of these bone marrow derived myofibroblasts even suggested that they partake in collagen production (van Amerongen et al., 2008). Indeed, a recent study using myeloid-specific cre reporter mice ($LysM^{Cre/+}$; ROSA26-eYFP) mice has suggested that macrophages can indeed transition toward fibroblast-like cells in the heart following MI with respect to their expression profile of fibroblast markers over time (Haider et al., 2019). However, additional genetic lineage tracing studies using similar reporter mice ($LysM^{Cre/+}$; Rosa26-eGFP) showed negligible contribution of monocytes and macrophages to myofibroblasts post-MI, which suggest that myofibroblasts derive largely from proliferating and transdifferentiating resident cardiac fibroblasts (Kanisicak et al., 2016).

In the injured heart, infiltrating monocytes differentiate into macrophages near spaces rich with collagen producing myofibroblasts; these macrophages can then influence the surrounding cells and ECM through numerous mechanisms (Pappritz et al., 2018; O'Rourke et al., 2019). For instance, activated macrophages within the injured myocardium have been shown to contribute to fibroblast activation, proliferation and myofibroblast transformation via secretion of pro-fibrotic factors, including transforming growth factor-beta (TGFβ) and galectin-3 (Gal3) (de Boer et al., 2009; Hundae and McCullough, 2014). Additionally, macrophage phagocytosis can often be a trigger in regulating fibrosis (Kim et al., 2017), where macrophage ingestion of dead cells and debris leads to the release of pro-fibrotic mediators including TGFβ (Nacu et al., 2008). However, macrophage phagocytic activity may also contribute to resolution of fibrosis; their ability to take up myofibroblasts and matrix debris may function to reduce the level of fibrotic stimuli (Wynn and Barron, 2010; Kong et al., 2014). Macrophages also function to secrete inflammatory mediators, which regulate fibroblast activation or ECM remodeling. In detail, activated macrophages can secrete cytokines and factors like interleukin (IL)-1β, tumor necrosis factor α (TNFα), fibroblast growth factor (FGF) and platelet derived growth factor (PDGF) which directly activate fibroblast transdifferentiation, or contribute to increased production of matrix metalloproteinases (MMPs) (Kaikita et al., 2004; Kong et al., 2014; O'Rourke et al., 2019). Increased production of MMPs leads to excessive matrix remodeling which disrupts fibrotic remodeling (Yan et al., 2006; Halade et al., 2013; Aghajanian et al., 2019). Additional associative studies, particularly focusing on epicardial adipose tissue (EAT) and its role in atrial fibrillation have hinted macrophages involvement in fibrosis (Abe et al., 2018). Specifically, an increase in macrophage density in EAT is positively associated with severe EAT fibrosis, which correlates with enhanced atrial fibrosis (Abe et al., 2018). Importantly, patients with atrial fibrillation exhibited greater severity of fibrosis (Abe et al., 2018). Altogether, these findings provide evidence for the opposing fibrogenic actions of macrophages and its secretome, which suggests the need for careful context dependent analysis when targeting macrophage function in the fibrotic response.

In recent years, much attention has been focused upon tissue resident monocyte/macrophage populations, which function uniquely in the post-injury repair process. For instance, studies have identified distinct peritoneal Gata6 macrophage subsets that are critical for the resolution of inflammation (Rosas et al., 2014). Gata6 is thought to be essential to these macrophages phenotype, and is key to their ability to self-renew and persist through homeostasis and inflammation (Rosas et al., 2014). Notably, Gata6 macrophages have been identified in the pericardial cavity of both mice and humans, and they have been shown to regulate cardiac fibrosis following cardiac injury (Deniset et al., 2019). Four weeks following MI, myeloid-specific deletion of Gata6 resulted in enhanced fibrosis especially in the remote myocardium (Deniset et al., 2019). These findings suggest the benefits of pericardial macrophages, namely in preventing adverse fibrotic remodeling in viable tissue. Further studies have sought to characterize how resident macrophage subsets influence fibrosis in cardiac injury. For instance, depletion of $CCR2^{+}$ resident macrophages prior to a model of ischemia/reperfusion resulted in decreased fibrosis (Bajpai et al., 2018), while depletion of $CX3CR1^{+}$ resident macrophages led to worsening fibrosis, remodeling and functional outcomes (Dick et al., 2019). Considering these findings, it is clear that resident macrophages exert important effects on post-injury cardiac remodeling outcomes, potentially through the regulation of fibrotic responses.

Mast Cells

Mast cells (MC) are most recognized for their function in regulating allergic responses; however, years of thorough investigation has revealed their much more considerable and widespread involvement in the immune system (Rao and Brown, 2008; da Silva et al., 2014). These secretory leukocytes are characterized by their abundant and diverse granules, which contain a combination of preformed cytokines, growth factors, and proteases (da Silva et al., 2014). In the absence of injury, MCs reside in low density in tissues like the heart; they originate from bone marrow derived precursors that migrate and subsequently mature into phenotypes dependent on their microenvironments (Levick and Widiapradja, 2018). Injury triggers additional MC precursors to infiltrate the myocardium (Ngkelo et al., 2016). For instance, numerous reports have shown increased mast cell counts in DCM patient hearts and animal models of cardiac injury like hypertension and MI (Sperr et al., 1994; Engels et al., 1995; Patella et al., 1997; Shiota et al., 2003; Janicki et al., 2015). This increase in mast cells following injury has led many researchers to question their involvement in cardiac fibrotic remodeling.

To date, a plethora of compelling results suggest roles for MCs in cardiac fibrosis (Legere et al., 2019). For one, in injury, the presence of DAMPs can trigger MC degranulation, which results in the release of inflammatory mediators like tryptase, chymase, IL-1β, and TNFα (Legere et al., 2019). Studies have shown that both tryptase and chymase activate TGFβ, a potent fibrogenic mediator known to promote myofibroblast differentiation and collagen production (Lindstedt et al., 2001; Tatler et al., 2008; Legere et al., 2019). Similarly, inflammatory cytokines including TNFα have been implicated in the development of cardiac fibrosis during hypertension (Mayr et al., 2016). MC are also direct sources of fibrogenic mediators. For one, MC have been implicated in atrial fibrosis and fibrillation through

enhanced production of the pro-proliferative and fibrotic factor PDGF-A (Liao et al., 2010). MC granules have also been shown to contain fibroblast growth factor-2 (FGF2), which has been shown to positively regulate fibroblast proliferation and collagen production (Hamada et al., 2000; Virag et al., 2007; Wernersson and Pejler, 2014). As degranulation products have been shown to induce fibrosis, recent studies have assessed the impact of inhibiting this inflammatory release. Interestingly, treatment with MC stabilizers has been shown to reduce collagen deposition, and collagen gene expression (Wang et al., 2016). Further, recent studies focusing on pressure overload induced injury have also identified an association between increasing mast cell volume and fibrosis (Luitel et al., 2017). These results imply that MCs function to promote adverse fibrotic remodeling; however, arriving at that conclusion may not be accurately reflective. Mice lacking mast cells exhibit only marginally decreased fibrosis 2 weeks after MI (Ngkelo et al., 2016). These finding suggest insignificant roles for mast cells in fibrosis, however, interestingly, there is also evidence, which proposes mast cells as anti-fibrotic mediators. Following induction of cardiac dysfunction, mast cell deficient mice show increased perivascular fibrosis (Joseph et al., 2005). Further, MCs have been shown to produce anti-inflammatory agents including IL-10 which act against fibrosis (Lin and Befus, 1997). Specifically, IL-10 has been repeatedly noted for its ability to oppose fibrosis through reducing collagen gene expression and fibrotic scarring after injury (Krishnamurthy et al., 2009; Verma et al., 2017). In sum, the current understanding of the role of mast cells in fibrosis is not entirely clear, which necessitates further studies to address the inconsistencies seen throughout the literature.

Eosinophils

Eosinophils are a subset of circulating leukocytes that contribute to the clearance of injury primarily through their hydrolase rich granules (Seguela et al., 2015). Recent focus has been placed on this leukocyte subset as patients exhibiting high levels of eosinophils (eosinophilia) can be at risk for cardiac complications (Diny et al., 2017; Prows et al., 2019). This clinical phenomenon is supported by recent animal studies that characterize cardiac remodeling in eosinophilia, and see a large response featuring replacement fibrosis (Prows et al., 2019). Specifically, mice that develop eosinophilia experience a large influx of eosinophils to the heart, along with enhanced chemokines and cytokines which may function to promote fibrosis (Prows et al., 2019). Beyond these findings, additional studies have shown a correlation between enhanced eosinophil accumulation and cardiac fibrosis. Following experimental myocarditis, the depletion of natural killer (NK) cells leads to an accumulation of eosinophils with a concomitant rise in fibrosis (Ong et al., 2015). These findings suggest that eosinophils contribute to cardiac fibrosis through cytokine secretion and cellular cross talk; however, more evidence is required in order to understand the exact contribution of eosinophils to cardiac fibrosis. Some studies have begun to address these needs through eosinophil depletion studies. In a model of myocarditis, a lack of eosinophils prevents against the development of inflammatory DCM (DCMi) (Diny et al., 2017). While there are no significant changes in total ventricle fibrosis, eosinophil depletion post-myocarditis leads to decreased expression of MMP2 and tissue inhibitor of metalloproteinases 2 (TIMP2) (Diny et al., 2017). These reports highlight the need for definitive assessment of the mechanisms by which eosinophils may trigger cardiac fibrosis.

Dendritic Cells

Dendritic cells (DC) are key immune regulators that function to initiate adaptive responses through antigen processing and presentation (Durai and Murphy, 2016). They can be characterized as being classical or non-classical, both of which exist in numerous subsets (Mildner and Jung, 2014). DCs are highly abundant in barrier tissues like the skin, however, many reports have shown their presence in heart tissue (Van der Borght and Lambrecht, 2018). Specifically, recent studies have suggested at least two types of classical or conventional DCs (cDC) in the healthy heart (Van der Borght et al., 2017). These cDCs have been shown to mediate tolerance to self-antigens (Van der Borght et al., 2017). DCs become of even greater relevance as the heart experiences injury (Clemente-Casares et al., 2017; Van der Borght et al., 2017; Wang et al., 2017). Their specific roles in pathology, especially in relation to cardiac fibrosis, is distinct; we consider them below.

A few studies have highlighted an influx of $CD11c^+$ cDCs to the heart following ischemic injury that increase starting 1 day post-MI that peak around 5–7 days post-MI (Anzai et al., 2012; Van der Borght et al., 2017). This early rise in DCs has led researchers to hypothesize additional roles for DCs in repair and remodeling post-injury. Accordingly, models of $CD11c^+$ depletion have been applied, and following MI, a lack of bone marrow derived $CD11c^+$ cells results in decreased survival rates and significantly enhanced fibrosis (Anzai et al., 2012). Although this model relies on the non-specific loss of all $CD11c^+$ cells, these findings provided evidence for DCs as being somewhat protective after infarction. Interestingly, this protective DC theory can be further supported by studies analyzing DC densities in humans post-MI or in DCM (Pistulli et al., 2013; Nagai et al., 2014). For instance, patients with DCM have decreased DCs compared to controls, and experience enhanced fibrosis and worsened cardiac function (Pistulli et al., 2013). There are also additional studies, focused on myocarditis, which suggest protective DC roles following injury (Clemente-Casares et al., 2017). A specific deletion of cardiac $CD103^+$ DCs results in significantly enhanced fibrosis following viral myocarditis, which suggests the role of DCs in blunting the transition to HF following injury (Clemente-Casares et al., 2017).

Beyond these findings, however, it is also important to note the wealth of literature that hints at an opposing role for DCs following injury. With $CD11c^+$ cell depletion, 24 weeks after TAC, mice exhibit reduced LV fibrosis and decreased expression of fibroblast activating genes (Wang et al., 2017). These studies are met with similar critiques regarding lack of DC specificity, however, studies using a more specific model of cDC ablation also show decreased LV fibrosis 3 weeks post-MI (Lee et al., 2018). These findings are further supported by earlier studies which show cardiac and splenic DC activation and expansion 8 weeks post-MI (Ismahil et al., 2014). Interestingly, transfer

of splenocytes from these HF mice into naïve mice results in the development of HF accompanied with significant fibrosis (Ismahil et al., 2014). Taken together, these studies provide evidence for DCs in post-injury remodeling, however, there is limited insight into how DCs may influence fibrosis. Overall, consideration of findings from each of these studies suggests a continued need for further DC characterization in the heart, focusing on how unique and specific populations of DCs may act to govern the fibrotic response.

B and T – Lymphocytes

An abundance of literature suggests an involvement of both B and T– Lymphocytes (B and T cells) in cardiac fibrosis. These adaptive immune cells are found in small numbers in the steady state heart, but are known to rise post-injury (Zouggari et al., 2013; Wang et al., 2019). The functional relevance of these lymphocytes in the steady state heart is still becoming understood, however, following injury, several reports have documented their ability to influence long-term remodeling outcomes (Yu et al., 2013; Zouggari et al., 2013; Horckmans et al., 2018). For instance, B cells have been shown to be associated with enhanced fibrosis; their depletion results in reduced collagen deposition following TAC, MI, and the development of non-ischemic cardiomyopathy (Cordero-Reyes et al., 2016; Horckmans et al., 2018; Ma et al., 2019). B cells are thought to promote fibrosis through inflammatory cytokines like IL-1β, IL6, and TNFα, all of which have been linked to increased fibrosis (Cordero-Reyes et al., 2016). Interestingly, these findings are supported by other studies that identify increased B cell densities and cardiac fibrosis in DCM patients when compared to healthy controls (Yu et al., 2013). B cells isolated from these DCM patients secrete larger quantities of pro-fibrotic factors including TNFα; these findings provide additional evidence to support the pro-fibrotic actions of B cells in injury (Yu et al., 2013). In moving forward, much remains to be understood in the field of cardiac B cell biology, including the explicit role that B cells play in the uninjured heart, as well as the mechanisms by which they elicit pathological fibrotic remodeling.

Similar to B cells, T cells have been shown to infiltrate the injured myocardium where they greatly influence remodeling outcomes (Blanton et al., 2019). T cells come in many subsets, some of which have divergent functions in cardiac fibrosis. For one, $CD4^+$ T cells accumulate in the heart post-MI and -TAC, and are associated with enhanced cardiac fibrosis (Laroumanie et al., 2014; Nevers et al., 2015, 2017; Bansal et al., 2017, 2019; Borg et al., 2017; Quast et al., 2017). Studies have shown increased Th1 polarization following injury, leading to the production of pro-inflammatory and -fibrotic cytokines like interferon γ (IFNγ) (Laroumanie et al., 2014; Nevers et al., 2017). As these subsets of T cells are implicated in worsening fibrosis, many reports have sought to characterize their direct involvement in the remodeling response. The depletion or dampening of T cell infiltration post-injury has been shown to result in a significant reduction of fibrosis and fibrosis associated gene expression (Laroumanie et al., 2014; Nevers et al., 2015; Salvador et al., 2016). Recent studies have also shown a direct increase in cardiac fibrosis following adoptive transfer of HF splenic $CD4^+$ T cells into naïve mice (Bansal et al., 2017). Mechanistically, a few targets have been investigated in their role for inducing pro-fibrotic T cell actions. Namely, studies have determined an involvement of CD73 and adenosine generation, as T cell-specific CD73 knockout mice show enhanced fibrosis (Borg et al., 2017; Quast et al., 2017). These studies suggest that adenosine functions in an autocrine manner to reduce the production of pro- inflammatory and -fibrotic cytokines (Borg et al., 2017). Further, signaling through the mineralocorticoid receptor (MR) has been shown to enhance pro-fibrotic T cell actions, as the loss of T cell MR has been shown to decrease T cell activation and fibrotic cytokine production (Li et al., 2017). Interestingly, all of these findings seem to be associated with $CD4^+$ T cells, as similar assessments have revealed no significant role for $CD8^+$ T cells in cardiac fibrosis (Groschel et al., 2018).

Studies have also examined the role of T regulatory (Treg) subsets in fibrosis, and have mainly shown their role in protecting against fibrosis (Kvakan et al., 2009; Kanellakis et al., 2011; Tang et al., 2012). Early studies have shown decreased collagen content and lower expression of pro-fibrotic mediators following Treg introduction into hypertensive injury models (Kvakan et al., 2009; Kanellakis et al., 2011). Additionally, the introduction of Tregs post-MI has also been shown to reduce border zone fibrosis, further suggesting a protective mechanism through which Tregs influence remodeling (Tang et al., 2012). However, recent studies have shown alternative Treg functions post-injury, wherein an increase in a pro-inflammatory $CD4^+$ Treg subset has been shown to lead to the production of fibrotic cytokines like TNFα (Bansal et al., 2019). Additional studies directed toward the characterization of the impact of specific T cell subsets on cardiac fibrosis at distinct timepoints after injury will be helpful to illuminate potential targets against pathological cardiac fibrosis.

CONCLUDING REMARKS

Fibrotic remodeling is a normal physiological response to injury in the heart, however, when it becomes excessive, fibrosis leaves the heart at a great detriment in that it leads to tissue stiffness and dysfunction (Hinderer and Schenke-Layland, 2019). As such, the prevention or reversal of pathological fibrotic remodeling has been a research target for numerous years and has led to a wealth of studies aimed in uncovering the mechanistic basis for cardiac fibrosis. Recently, studies using isolated myofibroblasts from HF patients have suggested the possibility of reversing fibrosis by inhibition of TGFβ receptor signaling (Frangogiannis, 2019b; Nagaraju et al., 2019). These findings provide support to reason the idea of myofibroblasts returning to quiescent fibroblast states (Nagaraju et al., 2019). However, translating these findings *in vivo* will require consideration of numerous other factors which influence cardiac fibrosis. For one, several leukocyte subsets are implicated in the development of fibrosis. Currently, their explicit contribution to cardiac fibrosis, which appears context-dependent, is still being unraveled, as is the practicality of targeting specific subtypes at particular phases of post-injury remodeling of HF development. For instance, the presence of

dendritic cells may be beneficial toward stable scar formation in MI patients, however, their exact role in the regulation of fibrotic remodeling and how to support their activity will need to be understood to effectively translate this knowledge toward therapeutic application (Nagai et al., 2014). Further, patients with non-ischemic HF have been shown to exhibit higher numbers of activated $CD3^+$ T cells; given the number of animal studies showcasing their association with fibrosis, antagonizing these lymphocytes could serve as a feasible therapeutic avenue against pathological fibrosis during HF (Nevers et al., 2015). To conclude, a growing body of evidence suggests multifaceted roles for leukocytes in cardiac injury: both innate and adaptive leukocytes influence pathological fibrotic remodeling, presenting an exciting trajectory for the development of novel therapeutic strategies that modulate their recruitment, secretions and phenotypes to prevent the progression of both ischemic and non-ischemic forms of HF.

AUTHOR CONTRIBUTIONS

AO and DT wrote the manuscript.

FUNDING

This work was supported by the NIH grant R01 HL139522 (to DT).

REFERENCES

Abe, I., Teshima, Y., Kondo, H., Kaku, H., Kira, S., Ikebe, Y., et al. (2018). Association of fibrotic remodeling and cytokines/chemokines content in epicardial adipose tissue with atrial myocardial fibrosis in patients with atrial fibrillation. *Heart Rhythm.* 15, 1717–1727. doi: 10.1016/j.hrthm.2018.06.025

Aghajanian, H., Kimura, T., Rurik, J. G., Hancock, A. S., Leibowitz, M. S., Li, L., et al. (2019). Targeting cardiac fibrosis with engineered T cells. *Nature* 573, 430–433. doi: 10.1038/s41586-019-1546-z

Aguiar, C. M., Gawdat, K., Legere, S., Marshall, J., Hassan, A., Kienesberger, P. C., et al. (2019). Fibrosis independent atrial fibrillation in older patients is driven by substrate leukocyte infiltration: diagnostic and prognostic implications to patients undergoing cardiac surgery. *J. Transl. Med.* 17:413. doi: 10.1186/s12967-019-02162-5

Alex, L., and Frangogiannis, N. G. (2018). The cellular origin of activated fibroblasts in the infarcted and remodeling myocardium. *Circ. Res.* 122, 540–542. doi: 10.1161/CIRCRESAHA.118.312654

Amulic, B., Cazalet, C., Hayes, G. L., Metzler, K. D., and Zychlinsky, A. (2012). Neutrophil function: from mechanisms to disease. *Annu. Rev. Immunol.* 30, 459–489. doi: 10.1146/annurev-immunol-020711-074942

Anzai, A., Anzai, T., Nagai, S., Maekawa, Y., Naito, K., Kaneko, H., et al. (2012). Regulatory role of dendritic cells in postinfarction healing and left ventricular remodeling. *Circulation* 125, 1234–1245. doi: 10.1161/CIRCULATIONAHA.111.052126

Aoki, T., Fukumoto, Y., SugimurA, K., Oikawa, M., Satoh, K., and Nakano, M. (2011). Prognostic impact of myocardial interstitial fibrosis in non-ischemic heart failure. -Comparison between preserved and reduced ejection fraction heart failure. *Circ. J.* 75, 2605–2613.

Askari, A. T., Brennan, M. L., Zhou, X., Drinko, J., Morehead, A., Thomas, J. D., et al. (2003). Myeloperoxidase and plasminogen activator inhibitor 1 play a central role in ventricular remodeling after myocardial infarction. *J. Exp. Med.* 197, 615–624. doi: 10.1084/jem.20021426

Bajpai, A., and Tilley, D. G. (2018). The role of leukocytes in diabetic cardiomyopathy. *Front. Physiol.* 9:1547. doi: 10.3389/fphys.2018.01547

Bajpai, G., Schneider, C., Wong, N., Bredemeyer, A., Hulsmans, M., Nahrendorf, M., et al. (2018). The human heart contains distinct macrophage subsets with divergent origins and functions. *Nat. Med.* 24, 1234–1245. doi: 10.1038/s41591-018-0059-x

Bansal, S. S., Ismahil, M. A., Goel, M., Patel, B., Hamid, T., Rokosh, G., et al. (2017). Activated T lymphocytes are essential drivers of pathological remodeling in ischemic heart failure. *Circ. Heart Fail.* 10:e003688. doi: 10.1161/CIRCHEARTFAILURE.116.003688

Bansal, S. S., Ismahil, M. A., Goel, M., Zhou, G., Rokosh, G., Hamid, T., et al. (2019). Dysfunctional and proinflammatory regulatory T-Lymphocytes are essential for adverse cardiac remodeling in ischemic cardiomyopathy. *Circulation* 139, 206–221. doi: 10.1161/CIRCULATIONAHA.118.036065

Blanton, R. M., Carrillo-Salinas, F. J., and Alcaide, P. (2019). T-cell recruitment to the heart: friendly guests or unwelcome visitors? *Am. J. Physiol. Heart Circ. Physiol.* 317, H124–H140. doi: 10.1152/ajpheart.00028.2019

Borg, N., Alter, C., Gorldt, N., Jacoby, C., Ding, Z., Steckel, B., et al. (2017). CD73 on T cells orchestrates cardiac wound healing after myocardial infarction by purinergic metabolic reprogramming. *Circulation* 136, 297–313. doi: 10.1161/CIRCULATIONAHA.116.023365

Bradding, P., and Pejler, G. (2018). The controversial role of mast cells in fibrosis. *Immunol. Rev.* 282, 198–231. doi: 10.1111/imr.12626

Choi, J. H., Do, Y., Cheong, C., Koh, H., Boscardin, S. B., Oh, Y. S., et al. (2009). Identification of antigen-presenting dendritic cells in mouse aorta and cardiac valves. *J. Exp. Med.* 206, 497–505. doi: 10.1084/jem.20082129

Clemente-Casares, X., Hosseinzadeh, S., Barbu, I., Dick, S. A., Macklin, J. A., Wang, Y., et al. (2017). A CD103(+) conventional dendritic cell surveillance system prevents development of overt heart failure during subclinical viral myocarditis. *Immunity* 47, 974.e8–989.e8. doi: 10.1016/j.immuni.2017.10.011

Cordero-Reyes, A. M., Youker, K. A., Trevino, A. R., Celis, R., Hamilton, D. J., Flores-Arredondo, J. H., et al. (2016). Full expression of cardiomyopathy is partly dependent on b-cells: a pathway that involves cytokine activation, immunoglobulin deposition, and activation of apoptosis. *J. Am. Heart Assoc.* 5: e002484. doi: 10.1161/JAHA.115.002484

da Silva, E. Z., Jamur, M. C., and Oliver, C. (2014). Mast cell function: a new vision of an old cell. *J. Histochem. Cytochem.* 62, 698–738. doi: 10.1369/0022155414545334

Daseke, M. J. II, Valerio, F. M., Kalusche, W. J., Ma, Y., DeLeon-Pennell, K. Y., and Lindsey, M. L. (2019). Neutrophil proteome shifts over the myocardial infarction time continuum. *Basic Res. Cardiol.* 114:37. doi: 10.1007/s00395-019-0746-x

Davis, J., and Molkentin, J. D. (2014). Myofibroblasts: trust your heart and let fate decide. *J. Mol. Cell Cardiol.* 70, 9–18. doi: 10.1016/j.yjmcc.2013.10.019

de Boer, R. A., Voors, A. A., Muntendam, P., van Gilst, W. H., and van Veldhuisen, D. J. (2009). Galectin-3: a novel mediator of heart failure development and progression. *Eur. J. Heart Fail.* 11, 811–817. doi: 10.1093/eurjhf/hfp097

Deniset, J. F., Belke, D., Lee, W. Y., Jorch, S. K., Deppermann, C., Hassanabad, A. F., et al. (2019). Gata6(+) pericardial cavity macrophages relocate to the injured heart and prevent cardiac fibrosis. *Immunity* 51, 31.e5–140.e5 doi: 10.1016/j.immuni.2019.06.010

Deniset, J. F., and Kubes, P. (2018). Neutrophil heterogeneity: bona fide subsets or polarization states? *J. Leukoc Biol.* 103, 829–838. doi: 10.1002/JLB.3RI0917-361R

Dick, S. A., Macklin, J. A., Nejat, S., Momen, A., Clemente-Casares, X., Althagafi, M. G., et al. (2019). Self-renewing resident cardiac macrophages limit adverse remodeling following myocardial infarction. *Nat. Immunol.* 20, 29–39. doi: 10.1038/s41590-018-0272-2

Diny, N. L., Baldeviano, G. C., Talor, M. V., Barin, J. G., Ong, S., Bedja, D., et al. (2017). Eosinophil-derived IL-4 drives progression of myocarditis to inflammatory dilated cardiomyopathy. *J. Exp. Med.* 214, 943–957. doi: 10.1084/jem.20161702

Durai, V., and Murphy, K. M. (2016). Functions of murine dendritic cells. *Immunity* 45, 719–736. doi: 10.1016/j.immuni.2016.10.010

Engels, W., Reiters, P. H., Daemen, M. J., Smits, J. F., and van der Vusse, G. J. (1995). Transmural changes in mast cell density in rat heart after infarct induction in vivo. *J. Pathol.* 177, 423–429. doi: 10.1002/path.1711770414

Entman, M. L., Youker, K., Shoji, T., Kukielka, G., Shappell, S. B., Taylor, A. A., et al. (1992). Neutrophil induced oxidative injury of cardiac myocytes. A compartmented system requiring CD11b/CD18-ICAM-1 adherence. *J. Clin. Invest.* 90, 1335–1345. doi: 10.1172/JCI115999

Epelman, S., Lavine, K. J., Beaudin, A. E., Sojka, D. K., Carrero, J. A., Calderon, B., et al. (2014). Embryonic and adult-derived resident cardiac macrophages are maintained through distinct mechanisms at steady state and during inflammation. *Immunity* 40, 91–104. doi: 10.1016/j.immuni.2013.11.019

Epelman, S., Liu, P. P., and Mann, D. L. (2015). Role of innate and adaptive immune mechanisms in cardiac injury and repair. *Nat. Rev. Immunol.* 15, 117–129. doi: 10.1038/nri3800

Forbes, S. J., Russo, F. P., Rey, V., Burra, P., Rugge, M., Wright, N. A., et al. (2004). A significant proportion of myofibroblasts are of bone marrow origin in human liver fibrosis. *Gastroenterology* 126, 955–963. doi: 10.1053/j.gastro.2004.02.025

Forte, E., Furtado, M. B., and Rosenthal, N. (2018). The interstitium in cardiac repair: role of the immune-stromal cell interplay. *Nat. Rev. Cardiol.* 15, 601–616. doi: 10.1038/s41569-018-0077-x

Frangogiannis, N. G. (2017). The extracellular matrix in myocardial injury, repair, and remodeling. *J. Clin. Invest.* 127, 1600–1612. doi: 10.1172/JCI87491

Frangogiannis, N. G. (2019a). Cardiac fibrosis: cell biological mechanisms, molecular pathways and therapeutic opportunities. *Mol. Asp. Med.* 65, 70–99. doi: 10.1016/j.mam.2018.07.001

Frangogiannis, N. G. (2019b). Can Myocardial fibrosis be reversed? *J. Am. Coll Cardiol.* 73, 2283–2285. doi: 10.1016/j.jacc.2018.10.094

Frangogiannis, N. G., Dewald, O., Xia, Y., Ren, G., Haudek, S., Leucker, T., et al. (2007). Critical role of monocyte chemoattractant protein-1/CC chemokine ligand 2 in the pathogenesis of ischemic cardiomyopathy. *Circulation* 115, 584–592. doi: 10.1161/CIRCULATIONAHA.106.646091

Frangogiannis, N. G., Lindsey, M. L., Michael, L. H., Youker, K. A., Bressler, R. B., Mendoza, L. H., et al. (1998). Resident cardiac mast cells degranulate and release preformed TNF-alpha, initiating the cytokine cascade in experimental canine myocardial ischemia/reperfusion. *Circulation* 98, 699–710. doi: 10.1161/01.cir.98.7.699

Friedrichs, K., Adam, M., Remane, L., Mollenhauer, M., Rudolph, V., Rudolph, T. K., et al. (2014). Induction of atrial fibrillation by neutrophils critically depends on CD11b/CD18 integrins. *PLoS One* 9:e89307. doi: 10.1371/journal.pone.0089307

Fu, X., Khalil, H., Kanisicak, O., Boyer, J. G., Vagnozzi, R. J., Maliken, B. D., et al. (2018). Specialized fibroblast differentiated states underlie scar formation in the infarcted mouse heart. *J. Clin. Invest.* 128, 2127–2143. doi: 10.1172/JCI98215

Gallego-Colon, E., Sampson, R. D., Sattler, S., Schneider, M. D., Rosenthal, N., and Tonkin, J. (2015). Cardiac-restricted IGF-1Ea overexpression reduces the early accumulation of inflammatory myeloid cells and mediates expression of extracellular matrix remodelling genes after myocardial infarction. *Mediators Inflamm.* 2015:484357. doi: 10.1155/2015/484357

Geissmann, F., Manz, M. G., Jung, S., Sieweke, M. H., Merad, M., and Ley, K. (2010). Development of monocytes, macrophages, and dendritic cells. *Science* 327, 656–661. doi: 10.1126/science.1178331

Grisanti, L. A., Gumpert, A. M., Traynham, C. J., Gorsky, J. E., Repas, A. A., Gao, E., et al. (2016a). Leukocyte-expressed beta2-adrenergic receptors are essential for survival after acute myocardial injury. *Circulation* 134, 153–167. doi: 10.1161/CIRCULATIONAHA.116.022304

Grisanti, L. A., Traynham, C. J., Repas, A. A., Gao, E., Koch, W. J., and Tilley, D. G. (2016b). Beta2-Adrenergic receptor-dependent chemokine receptor 2 expression regulates leukocyte recruitment to the heart following acute injury. *Proc. Natl. Acad. Sci. U.S.A.* 113, 15126–15131. doi: 10.1073/pnas.1611023114

Groschel, C., Sasse, A., Monecke, S., Rohrborn, C., Elsner, L., Didie, M., et al. (2018). CD8(+)-T cells with specificity for a model antigen in cardiomyocytes can become activated after transverse aortic constriction but do not accelerate progression to heart failure. *Front. Immunol.* 9:2665. doi: 10.3389/fimmu.2018.02665

Gyongyosi, M., Winkler, J., Ramos, I., Do, Q. T., Firat, H., McDonald, K., et al. (2017). Myocardial fibrosis: biomedical research from bench to bedside. *Eur. J. Heart Fail.* 19, 177–191. doi: 10.1002/ejhf.696

Haider, N., Bosca, L., Zandbergen, H. R., Kovacic, J. C., Narula, N., Gonzaelz-Ramos, S., et al. (2019). Transition to macrophages to fibroblast-like cells in healing myocardial infarction. *J. Am. Coll. Cardiol.* 74, 3124–3135. doi: 10.1016/j.jacc.2019.10.036

Halade, G. V., Jin, Y. F., and Lindsey, M. L. (2013). Matrix metalloproteinase (MMP)-9: a proximal biomarker for cardiac remodeling and a distal biomarker for inflammation. *Pharmacol. Ther.* 139, 32–40. doi: 10.1016/j.pharmthera.2013.03.009

Hamada, H., Vallyathan, V., Cool, C. D., Barker, E., Inoue, Y., and Newman, L. S. (2000). Mast cell basic fibroblast growth factor in silicosis. *Am. J. Respir. Crit. Care Med.* 161, 2026–2034. doi: 10.1164/ajrccm.161.6.9812132

Hinderer, S., and Schenke-Layland, K. (2019). Cardiac fibrosis - A short review of causes and therapeutic strategies. *Adv. Drug Deliv. Rev* 146, 77–82. doi: 10.1016/j.addr.2019.05.011

Hofmann, U., Beyersdorf, N., Weirather, J., Podolskaya, A., Bauersachs, J., Ertl, G., et al. (2012). Activation of CD4+ T lymphocytes improves wound healing and survival after experimental myocardial infarction in mice. *Circulation* 125, 1652–1663. doi: 10.1161/CIRCULATIONAHA.111.044164

Horckmans, M., Bianchini, M., Santovito, D., Megens, R. T. A., Springael, J. Y., Negri, I., et al. (2018). Pericardial adipose tissue regulates granulopoiesis, fibrosis, and cardiac function after myocardial infarction. *Circulation* 137, 948–960. doi: 10.1161/CIRCULATIONAHA.117.028833

Horckmans, M., Ring, L., Duchene, J., Santovito, D., Schloss, M. J., Drechsler, M., et al. (2017). Neutrophils orchestrate post-myocardial infarction healing by polarizing macrophages towards a reparative phenotype. *Eur. Heart J.* 38, 187–197. doi: 10.1093/eurheartj/ehw002

Hulsmans, M., Clauss, S., Xiao, L., Aguirre, A. D., King, K. R., Hanley, A., et al. (2017). Macrophages facilitate electrical conduction in the heart. *Cell* 169, 10.e20–522.e20. doi: 10.1016/j.cell.2017.03.050

Hulsmans, M., Sager, H. B., Roh, J. D., Valero-Munoz, M., Houstis, N. E., Iwamoto, Y., et al. (2018). Cardiac macrophages promote diastolic dysfunction. *J. Exp. Med.* 215, 423–440. doi: 10.1084/jem.20171274

Hulsmans, M., Sam, F., and Nahrendorf, M. (2016). Monocyte and macrophage contributions to cardiac remodeling. *J. Mol. Cell Cardiol.* 93, 149–155. doi: 10.1016/j.yjmcc.2015.11.015

Humeres, C., and Frangogiannis, N. G. (2019). Fibroblasts in the infarcted, remodeling, and failing heart. *JACC Basic Transl. Sci.* 4, 449–467. doi: 10.1016/j.jacbts.2019.02.006

Hundae, A., and McCullough, P. A. (2014). Cardiac and renal fibrosis in chronic cardiorenal syndromes. *Nephron Clin. Pract.* 127, 106–112. doi: 10.1159/000363705

Ismahil, M. A., Hamid, T., Bansal, S. S., Patel, B., Kingery, J. R., and Prabhu, S. D. (2014). Remodeling of the mononuclear phagocyte network underlies chronic inflammation and disease progression in heart failure: critical importance of the cardiosplenic axis. *Circ. Res.* 114, 266–282. doi: 10.1161/CIRCRESAHA.113.301720

Ivey, M. J., Kuwabara, J. T., Pai, J. T., Moore, R. E., Sun, Z., and Tallquist, M. D. (2018). Resident fibroblast expansion during cardiac growth and remodeling. *J. Mol. Cell Cardiol.* 114, 161–174. doi: 10.1016/j.yjmcc.2017.11.012

Janicki, J. S., Brower, G. L., and Levick, S. P. (2015). The emerging prominence of the cardiac mast cell as a potent mediator of adverse myocardial remodeling. *Methods Mol. Biol.* 1220, 121–139. doi: 10.1007/978-1-4939-1568-2_8

Joseph, J., Kennedy, R. H., Devi, S., Wang, J., Joseph, L., and Hauer-Jensen, M. (2005). Protective role of mast cells in homocysteine-induced cardiac remodeling. *Am. J. Physiol. Heart Circ. Physiol.* 288, H2541–H2545. doi: 10.1152/ajpheart.00806.2004

Kaikita, K., Hayasaki, T., Okuma, T., Kuziel, W. A., Ogawa, H., and Takeya, M. (2004). Targeted deletion of CC chemokine receptor 2 attenuates left ventricular

remodeling after experimental myocardial infarction. *Am. J. Pathol.* 165, 439–447. doi: 10.1016/s0002-9440(10)63309-3

Kain, V., Ingle, K. A., Kabarowski, J., Barnes, S., Limdi, N. A., Prabhu, S. D., et al. (2018). Genetic deletion of 12/15 lipoxygenase promotes effective resolution of inflammation following myocardial infarction. *J. Mol. Cell Cardiol.* 118, 70–80. doi: 10.1016/j.yjmcc.2018.03.004

Kanellakis, P., Dinh, T. N., Agrotis, A., and Bobik, A. (2011). CD4(+)CD25(+)Foxp3(+) regulatory T cells suppress cardiac fibrosis in the hypertensive heart. *J. Hypertens* 29, 1820–1828. doi: 10.1097/HJH.0b013e328349c62d

Kanisicak, O., Khalil, H., Ivey, M. J., Karch, J., Maliken, B. D., Correll, R. N., et al. (2016). Genetic lineage tracing defines myofibroblast origin and function in the injured heart. *Nat. Commun.* 7:12260. doi: 10.1038/ncomms12260

Kim, Y. B., Yoon, Y. S., Choi, Y. H., Park, E. M., and Kang, J. L. (2017). Interaction of macrophages with apoptotic cells inhibits transdifferentiation and invasion of lung fibroblasts. *Oncotarget* 8, 112297–112312. doi: 10.18632/oncotarget.22737

Kondo, M. (2010). Lymphoid and myeloid lineage commitment in multipotent hematopoietic progenitors. *Immunol. Rev.* 238, 37–46. doi: 10.1111/j.1600-065X.2010.00963.x

Kong, P., Christia, P., and Frangogiannis, N. G. (2014). The pathogenesis of cardiac fibrosis. *Cell Mol. Life. Sci.* 71, 549–574.

Krishnamurthy, P., Rajasingh, J., Lambers, E., Qin, G., Losordo, D. W., and Kishore, R. (2009). IL-10 inhibits inflammation and attenuates left ventricular remodeling after myocardial infarction via activation of STAT3 and suppression of HuR. *Circ. Res.* 104, e9–e18. doi: 10.1161/CIRCRESAHA.108.188243

Kvakan, H., Kleinewietfeld, M., Qadri, F., Park, J. K., Fischer, R., Schwarz, I., et al. (2009). Regulatory T cells ameliorate angiotensin II-induced cardiac damage. *Circulation* 119, 2904–2912. doi: 10.1161/CIRCULATIONAHA.108.832782

Laroumanie, F., Douin-Echinard, V., Pozzo, J., Lairez, O., Tortosa, F., Vinel, C., et al. (2014). CD4+ T cells promote the transition from hypertrophy to heart failure during chronic pressure overload. *Circulation* 129, 2111–2124. doi: 10.1161/CIRCULATIONAHA.113.007101

Lavine, K. J., Pinto, A. R., Epelman, S., Kopecky, B. J., Clemente-Casares, X., Godwin, J., et al. (2018). The macrophage in cardiac homeostasis and disease: JACC macrophage in CVD series (Part 4). *J. Am. Coll. Cardiol.* 72, 2213–2230. doi: 10.1016/j.jacc.2018.08.2149

Lee, J. S., Jeong, S. J., Kim, S., Chalifour, L., Yun, T. J., Miah, M. A., et al. (2018). Conventional dendritic cells impair recovery after myocardial infarction. *J. Immunol.* 201, 1784–1798. doi: 10.4049/jimmunol.1800322

Legere, S. A., Haidl, I. D., Legare, J. F., and Marshall, J. S. (2019). Mast cells in cardiac fibrosis: new insights suggest opportunities for intervention. *Front. Immunol.* 10:580. doi: 10.3389/fimmu.2019.00580

Levick, S. P., and Widiapradja, A. (2018). Mast cells: key contributors to cardiac fibrosis. *Int. J. Mol. Sci.* 19:E231 doi: 10.3390/ijms19010231

Li, C., Sun, X. N., Zeng, M. R., Zheng, X. J., Zhang, Y. Y., Wan, Q., et al. (2017). Mineralocorticoid receptor deficiency in T cells attenuates pressure overload-induced cardiac hypertrophy and dysfunction through modulating T-Cell activation. *Hypertension* 70, 137–147. doi: 10.1161/HYPERTENSIONAHA.117.09070

Liao, C. H., Akazawa, H., Tamagawa, M., Ito, K., Yasuda, N., Kudo, Y., et al. (2010). Cardiac mast cells cause atrial fibrillation through PDGF-A-mediated fibrosis in pressure-overloaded mouse hearts. *J. Clin. Invest.* 120, 242–253. doi: 10.1172/JCI39942

Lin, T. J., and Befus, A. D. (1997). Differential regulation of mast cell function by IL-10 and stem cell factor. *J. Immunol.* 159, 4015–4023.

Lindstedt, K. A., Wang, Y., Shiota, N., Saarinen, J., Hyytiainen, M., Kokkonen, J. O., et al. (2001). Activation of paracrine TGF-beta1 signaling upon stimulation and degranulation of rat serosal mast cells: a novel function for chymase. *FASEB J.* 15, 1377–1388. doi: 10.1096/fj.00-0273com

Lu, L., Guo, J., Hua, Y., Huang, K., Magaye, R., Cornell, J., et al. (2017). Cardiac fibrosis in the ageing heart: contributors and mechanisms. *Clin. Exp. Pharmacol. Physiol.* 44(Suppl. 1), 55–63. doi: 10.1111/1440-1681.12753

Lu, P., Takai, K., Weaver, V. M., and Werb, Z. (2011). Extracellular matrix degradation and remodeling in development and disease. *Cold Spring Harb. Perspect. Biol.* 3: a005058. doi: 10.1101/cshperspect.a005058

Luitel, H., Sydykov, A., Schymura, Y., Mamazhakypov, A., Janssen, W., Pradhan, K., et al. (2017). Pressure overload leads to an increased accumulation and activity of mast cells in the right ventricle. *Physiol. Rep.* 5:e13146. doi: 10.14814/phy2.13146

Ma, X. L., Lin, Q. Y., Wang, L., Xie, X., Zhang, Y. L., and Li, H. H. (2019). Rituximab prevents and reverses cardiac remodeling by depressing B cell function in mice. *Biomed. Pharmacother.* 114:108804. doi: 10.1016/j.biopha.2019.108804

Ma, Y., Mouton, A. J., and Lindsey, M. L. (2018). Cardiac macrophage biology in the steady-state heart, the aging heart, and following myocardial infarction. *Transl. Res.* 191, 15–28. doi: 10.1016/j.trsl.2017.10.001

Ma, Y., Yabluchanskiy, A., Iyer, R. P., Cannon, P. L., Flynn, E. R., Jung, M., et al. (2016). Temporal neutrophil polarization following myocardial infarction. *Cardiovasc. Res.* 110, 51–61. doi: 10.1093/cvr/cvw024

Martinod, K., Witsch, T., Erpenbeck, L., Savchenko, A., Hayashi, H., Cherpokova, D., et al. (2017). Peptidylarginine deiminase 4 promotes age-related organ fibrosis. *J. Exp. Med.* 214, 439–458. doi: 10.1084/jem.20160530

Mayr, M., Duerrschmid, C., Medrano, G., Taffet, G. E., Wang, Y., Entman, M. L., et al. (2016). TNF/Ang-II synergy is obligate for fibroinflammatory pathology, but not for changes in cardiorenal function. *Physiol. Rep.* 4:e12765. doi: 10.14814/phy2.12765

Metzler, K. D., Goosmann, C., Lubojemska, A., Zychlinsky, A., and Papayannopoulos, V. (2014). A myeloperoxidase-containing complex regulates neutrophil elastase release and actin dynamics during NETosis. *Cell Rep.* 8, 883–896. doi: 10.1016/j.celrep.2014.06.044

Mildner, A., and Jung, S. (2014). Development and function of dendritic cell subsets. *Immunity* 40, 642–656. doi: 10.1016/j.immuni.2014.04.016

Mollenhauer, M., Friedrichs, K., Lange, M., Gesenberg, J., Remane, L., Kerkenpab, C., et al. (2017). Myeloperoxidase mediates postischemic arrhythmogenic ventricular remodeling. *Circ. Res.* 121, 56–70. doi: 10.1161/CIRCRESAHA.117.310870

Mollmann, H., Nef, H. M., Kostin, S., von Kalle, C., Pilz, I., Weber, M., et al. (2006). Bone marrow-derived cells contribute to infarct remodelling. *Cardiovasc. Res.* 71, 661–671. doi: 10.1016/j.cardiores.2006.06.013

Nacu, N., Luzina, I. G., Highsmith, K., Lockatell, V., Pochetuhen, K., Cooper, Z. A., et al. (2008). Macrophages produce TGF-beta-induced (beta-ig-h3) following ingestion of apoptotic cells and regulate MMP14 levels and collagen turnover in fibroblasts. *J. Immunol.* 180, 5036–5044. doi: 10.4049/jimmunol.180.7.5036

Nagai, T., Honda, S., Sugano, Y., Matsuyama, T. A., Ohta-Ogo, K., Asaumi, Y., et al. (2014). Decreased myocardial dendritic cells is associated with impaired reparative fibrosis and development of cardiac rupture after myocardial infarction in humans. *J. Am. Heart Assoc.* 3, e000839. doi: 10.1161/JAHA.114.000839

Nagaraju, C. K., Robinson, E. L., Abdesselem, M., Trenson, S., Dries, E., Gilbert, G., et al. (2019). Myofibroblast phenotype and reversibility of fibrosis in patients with end-stage heart failure. *J. Am. Coll. Cardiol.* 73, 2267–2282. doi: 10.1016/j.jacc.2019.02.049

Nahrendorf, M., Swirski, F. K., Aikawa, E., Stangenberg, L., Wurdinger, T., Figueiredo, J. L., et al. (2007). The healing myocardium sequentially mobilizes two monocyte subsets with divergent and complementary functions. *J. Exp. Med.* 204, 3037–3047. doi: 10.1084/jem.20070885

Nevers, T., Salvador, A. M., Grodecki-Pena, A., Knapp, A., Velazquez, F., Aronovitz, M., et al. (2015). Left ventricular T-Cell recruitment contributes to the pathogenesis of heart failure. *Circ. Heart Fail* 8, 776–787. doi: 10.1161/CIRCHEARTFAILURE.115.002225

Nevers, T., Salvador, A. M., Velazquez, F., Ngwenyama, N., Carrillo-Salinas, F. J., Aronovitz, M., et al. (2017). Th1 effector T cells selectively orchestrate cardiac fibrosis in nonischemic heart failure. *J. Exp. Med.* 214, 3311–3329. doi: 10.1084/jem.20161791

Ngkelo, A., Richart, A., Kirk, J. A., Bonnin, P., Vilar, J., Lemitre, M., et al. (2016). Mast cells regulate myofilament calcium sensitization and heart function after myocardial infarction. *J. Exp. Med.* 213, 1353–1374. doi: 10.1084/jem.20160081

Ong, S., Ligons, D. L., Barin, J. G., Wu, L., Talor, M. V., Diny, N., et al. (2015). Natural killer cells limit cardiac inflammation and fibrosis by halting eosinophil infiltration. *Am. J. Pathol.* 185, 847–861. doi: 10.1016/j.ajpath.2014.11.023

Orlic, D., Kajstura, J., Chimenti, S., Jakoniuk, I., Anderson, S. M., Li, B., et al. (2001). Bone marrow cells regenerate infarcted myocardium. *Nature* 410, 701–705. doi: 10.1038/35070587

O'Rourke, S. A., Dunne, A., and Monaghan, M. G. (2019). The role of macrophages in the infarcted myocardium: orchestrators of ECM remodeling. *Front. Cardiovasc. Med.* 6:101. doi: 10.3389/fcvm.2019.00101

Papayannopoulos, V. (2018). Neutrophil extracellular traps in immunity and disease. *Nat. Rev. Immunol.* 18, 134–147. doi: 10.1038/nri.2017.105

Pappritz, K., Savvatis, K., Koschel, A., Miteva, K., Tschope, C., and Van Linthout, S. (2018). Cardiac (myo)fibroblasts modulate the migration of monocyte subsets. *Sci. Rep.* 8:5575.

Patel, B., Bansal, S. S., Ismahil, M. A., Hamid, T., Rokosh, G., Mack, M., et al. (2018). CCR2(+) monocyte-derived infiltrating macrophages are required for adverse cardiac remodeling during pressure overload. *JACC Basic Transl. Sci.* 3, 230–244. doi: 10.1016/j.jacbts.2017.12.006

Patella, V., de Crescenzo, G., Lamparter-Schummert, B., De Rosa, G., Adt, M., and Marone, G. (1997). Increased cardiac mast cell density and mediator release in patients with dilated cardiomyopathy. *Inflamm. Res.* 46(Suppl. 1), S31–S32.

Pistulli, R., Konig, S., Drobnik, S., Kretzschmar, D., Rohm, I., Lichtenauer, M., et al. (2013). Decrease in dendritic cells in endomyocardial biopsies of human dilated cardiomyopathy. *Eur. J. Heart Fail.* 15, 974–985. doi: 10.1093/eurjhf/hft054

Prabhu, S. D., and Frangogiannis, N. G. (2016). The biological basis for cardiac repair after myocardial infarction: from inflammation to fibrosis. *Circ. Res.* 119, 91–112. doi: 10.1161/CIRCRESAHA.116.303577

Prows, D. R., Klingler, A., Gibbons, W. J. Jr., Homan, S. M., and Zimmermann, N. (2019). Characterization of a mouse model of hypereosinophilia-associated heart disease. *Am. J. Physiol. Heart Circ. Physiol.* 317, H405–H414. doi: 10.1152/ajpheart.00133.2019

Quast, C., Alter, C., Ding, Z., Borg, N., and Schrader, J. (2017). Adenosine formed by CD73 on T Cells inhibits cardiac inflammation and fibrosis and preserves contractile function in transverse aortic constriction-induced heart failure. *Circ. Heart Fail.* 10:e003346. doi: 10.1161/CIRCHEARTFAILURE.116.003346

Rao, K. N., and Brown, M. A. (2008). Mast cells: multifaceted immune cells with diverse roles in health and disease. *Ann. N. Y. Acad. Sci.* 1143, 83–104. doi: 10.1196/annals.1443.023

Rickard, A. J., Morgan, J., Tesch, G., Funder, J. W., Fuller, P. J., and Young, M. J. (2009). Deletion of mineralocorticoid receptors from macrophages protect against deoxycorticosterone/salt-induced cardiac fibrosis and increased blood pressure. *Hypertension* 54, 537–543. doi: 10.1161/HYPERTENSIONAHA.109.131110

Rosas, M., Davies, L. C., Giles, P. J., Liao, C. T., Kharfan, B., Stone, T. C., et al. (2014). The transcription factor Gata6 links tissue macrophage phenotype and proliferative renewal. *Science* 344, 645–648. doi: 10.1126/science.1251414

Salvador, A. M., Nevers, T., Velazquez, F., Aronovitz, M., Wang, B., Abadia Molina, A., et al. (2016). Intercellular adhesion molecule 1 regulates left ventricular leukocyte infiltration. Cardiac remodeling, and function in pressure overload-induced heart failure. *J. Am. Heart Assoc.* 5:e003126. doi: 10.1161/JAHA.115.003126

Seguela, P. E., Iriart, X., Acar, P., Montaudon, M., Roudaut, R., and Thambo, J. B. (2015). Eosinophilic cardiac disease: molecular, clinical and imaging aspects. *Arch. Cardiovasc. Dis.* 108, 258–268. doi: 10.1016/j.acvd.2015.01.006

Serhan, C. N., Maddox, J. F., Petasis, N. A., Akritopoulou-Zanze, I., Papayianni, A., Brady, H. R., et al. (1995). Design of lipoxin A4 stable analogs that block transmigration and adhesion of human neutrophils. *Biochemistry* 34, 14609–14615. doi: 10.1021/bi00044a041

Shiota, N., Rysa, J., Kovanen, P. T., Ruskoaho, H., Kokkonen, J. O., and Lindstedt, K. A. (2003). A role for cardiac mast cells in the pathogenesis of hypertensive heart disease. *J. Hypertens* 21, 1935–1944. doi: 10.1097/00004872-200310000-00022

Skelly, D. A., Squiers, G. T., McLellan, M. A., Bolisetty, M. T., Robson, P., Rosenthal, N. A., et al. (2018). Single-Cell transcriptional profiling reveals cellular diversity and intercommunication in the mouse heart. *Cell Rep.* 22, 600–610. doi: 10.1016/j.celrep.2017.12.072

Sperr, W. R., Bankl, H. C., Mundigler, G., Klappacher, G., Grossschmidt, K., Agis, H., et al. (1994). The human cardiac mast cell: localization, isolation, phenotype, and functional characterization. *Blood* 84, 3876–3884. doi: 10.1182/blood.v84.11.3876.bloodjournal84113876

Stempien-Otero, A., Kim, D. H., and Davis, J. (2016). Molecular networks underlying myofibroblast fate and fibrosis. *J. Mol. Cell Cardiol.* 97, 153–161. doi: 10.1016/j.yjmcc.2016.05.002

Suetomi, T., Willeford, A., Brand, C. S., Cho, Y., Ross, R. S., Miyamoto, S., et al. (2018). Inflammation and NLRP3 inflammasome activation initiated in response to pressure overload by Ca(2+)/Calmodulin-Dependent protein kinase II delta signaling in cardiomyocytes are essential for adverse cardiac remodeling. *Circulation* 138, 2530–2544. doi: 10.1161/CIRCULATIONAHA.118.034621

Swirski, F. K., and Nahrendorf, M. (2013). Leukocyte behavior in atherosclerosis, myocardial infarction, and heart failure. *Science* 339, 161–166. doi: 10.1126/science.1230719

Swirski, F. K., and Nahrendorf, M. (2018). Cardioimmunology: the immune system in cardiac homeostasis and disease. *Nat. Rev. Immunol.* 18, 733–744. doi: 10.1038/s41577-018-0065-8

Tallquist, M. D., and Molkentin, J. D. (2017). Redefining the identity of cardiac fibroblasts. *Nat. Rev. Cardiol.* 14, 484–491. doi: 10.1038/nrcardio.2017.57

Tang, T. T., Yuan, J., Zhu, Z. F., Zhang, W. C., Xiao, H., Xia, N., et al. (2012). Regulatory T cells ameliorate cardiac remodeling after myocardial infarction. *Basic Res. Cardiol.* 107, 232.

Tatler, A. L., Porte, J., Knox, A., Jenkins, G., and Pang, L. (2008). Tryptase activates TGFbeta in human airway smooth muscle cells via direct proteolysis. *Biochem. Biophys. Res. Commun.* 370, 239–242. doi: 10.1016/j.bbrc.2008.03.064

Travers, J. G., Kamal, F. A., Robbins, J., Yutzey, K. E., and Blaxall, B. C. (2016). Cardiac fibrosis: the fibroblast awakens. *Circ. Res.* 118, 1021–1040. doi: 10.1161/CIRCRESAHA.115.306565

van Amerongen, M. J., Bou-Gharios, G., Popa, E., van Ark, J., Petersen, A. H., van Dam, G. M., et al. (2008). Bone marrow-derived myofibroblasts contribute functionally to scar formation after myocardial infarction. *J. Pathol.* 214, 377–386. doi: 10.1002/path.2281

Van der Borght, K., and Lambrecht, B. N. (2018). Heart macrophages and dendritic cells in sickness and in health: a tale of a complicated marriage. *Cell Immunol.* 330, 105–113. doi: 10.1016/j.cellimm.2018.03.011

Van der Borght, K., Scott, C. L., Nindl, V., Bouche, A., Martens, L., Sichien, D., et al. (2017). Myocardial infarction primes autoreactive T Cells through activation of dendritic cells. *Cell Rep.* 18, 3005–3017. doi: 10.1016/j.celrep.2017.02.079

Verma, S. K., Garikipati, V. N. S., Krishnamurthy, P., Schumacher, S. M., Grisanti, L. A., Cimini, M., et al. (2017). Interleukin-10 inhibits bone marrow fibroblast progenitor cell-mediated cardiac fibrosis in pressure-overloaded myocardium. *Circulation* 136, 940–953. doi: 10.1161/CIRCULATIONAHA.117.027889

Virag, J. A., Rolle, M. L., Reece, J., Hardouin, S., Feigl, E. O., and Murry, C. E. (2007). Fibroblast growth factor-2 regulates myocardial infarct repair: effects on cell proliferation, scar contraction, and ventricular function. *Am. J. Pathol.* 171, 1431–1440. doi: 10.2353/ajpath.2007.070003

Wang, H., da Silva, J., Alencar, A., Zapata-Sudo, G., Lin, M. R., Sun, X., et al. (2016). Mast cell inhibition attenuates cardiac remodeling and diastolic dysfunction in middle-aged. ovariectomized fischer 344 x brown norway rats. *J. Cardiovasc. Pharmacol.* 68, 49–57. doi: 10.1097/FJC.0000000000000385

Wang, H., Kwak, D., Fassett, J., Liu, X., Yao, W., Weng, X., et al. (2017). Role of bone marrow-derived CD11c(+) dendritic cells in systolic overload-induced left ventricular inflammation, fibrosis and hypertrophy. *Basic Res. Cardiol.* 112,

Wang, J., Duan, Y., Sluijter, J. P., and Xiao, J. (2019). Lymphocytic subsets play distinct roles in heart diseases. *Theranostics* 9, 4030–4046. doi: 10.7150/thno.33112

Weckbach, L. T., Grabmaier, U., Uhl, A., Gess, S., Boehm, F., Zehrer, A., et al. (2019). Midkine drives cardiac inflammation by promoting neutrophil trafficking and NETosis in myocarditis. *J. Exp. Med.* 216, 350–368. doi: 10.1084/jem.20181102

Wernersson, S., and Pejler, G. (2014). Mast cell secretory granules: armed for battle. *Nat. Rev. Immunol.* 14, 478–494. doi: 10.1038/nri3690

Williams, J. W., Giannarelli, C., Rahman, A., Randolph, G. J., and Kovacic, J. C. (2018). Macrophage biology, classification, and phenotype in cardiovascular disease: JACC macrophage in CVD series (Part 1). *J. Am. Coll. Cardiol.* 72, 2166–2180. doi: 10.1016/j.jacc.2018.08.2148

Wynn, T. A., and Barron, L. (2010). Macrophages: master regulators of inflammation and fibrosis. *Semin. Liver Dis.* 30, 245–257. doi: 10.1055/s-0030-1255354

Yan, A. T., Yan, R. T., Spinale, F. G., Afzal, R., Gunasinghe, H. R., Arnold, M., et al. (2006). Plasma matrix metalloproteinase-9 level is correlated with left ventricular volumes and ejection fraction in patients with heart failure. *J. Card. Fail.* 12, 514–519. doi: 10.1016/j.cardfail.2006.05.012

Yan, X., Anzai, A., Katsumata, Y., Matsuhashi, T., Ito, K., Endo, J., et al. (2013). Temporal dynamics of cardiac immune cell accumulation following acute myocardial infarction. *J. Mol. Cell Cardiol.* 62, 24–35. doi: 10.1016/j.yjmcc.2013.04.023

Yu, M., Wen, S., Wang, M., Liang, W., Li, H. H., Long, Q., et al. (2013). TNF-alpha-secreting B cells contribute to myocardial fibrosis in dilated cardiomyopathy. *J. Clin. Immunol.* 33, 1002–1008. doi: 10.1007/s10875-013-9889-y

Zouggari, Y., Ait-Oufella, H., Bonnin, P., Simon, T., Sage, A. P., Guerin, C., et al. (2013). B lymphocytes trigger monocyte mobilization and impair heart function after acute myocardial infarction. *Nat. Med.* 19, 1273–1280. doi: 10.1038/nm.3284

Conflict of Interest: The authors declare that the research was conducted in the absence of any commercial or financial relationships that could be construed as a potential conflict of interest.

frontiers in Pharmacology

ORIGINAL RESEARCH
published: 15 April 2020
doi: 10.3389/fphar.2020.00493

Isoproterenol Increases Left Atrial Fibrosis and Susceptibility to Atrial Fibrillation by Inducing Atrial Ischemic Infarction in Rats

Shiyu Ma[1†], *Jin Ma*[1†], *Qingqiang Tu*[2], *Chaoyang Zheng*[1], *Qiuxiong Chen*[1*] *and Weihui Lv*[1*]

[1] The Second Affiliated Hospital of Guangzhou University of Chinese Medicine, Guangdong Provincial Hospital of Chinese Medicine, Guangzhou, China, [2] Zhongshan School of Medicine, Sun Yat-sen University, Guangzhou, China

OPEN ACCESS

Edited by:
Markus Wallner,
Medical University of Graz, Austria

Reviewed by:
Roberta d'Emmanuele di Villa Bianca,
University of Naples Federico II, Italy
Donna Jayne Sellers,
Bond University, Australia
Jae-Sun Uhm,
Severance Hospital, South Korea

***Correspondence:**
Qiuxiong Chen
drchenqx@126.com
Weihui Lv
drlvwh@126.com

†These authors have contributed equally to this work

Specialty section:
This article was submitted to Cardiovascular and Smooth Muscle Pharmacology, a section of the journal Frontiers in Pharmacology

Received: 03 January 2020
Accepted: 30 March 2020
Published: 15 April 2020

Citation:
Ma S, Ma J, Tu Q, Zheng C, Chen Q and Lv W (2020) Isoproterenol Increases Left Atrial Fibrosis and Susceptibility to Atrial Fibrillation by Inducing Atrial Ischemic Infarction in Rats. Front. Pharmacol. 11:493. doi: 10.3389/fphar.2020.00493

Left atrial (LA) fibrosis is a major arrhythmogenic substrate for atrial fibrillation (AF). The purpose of this study was to assess whether isoproterenol (ISO) induces LA fibrosis and increases susceptibility to AF, exploring the underlying mechanisms. Male Sprague-Dawley rats were subcutaneously injected ISO once per day for 2 days. Five weeks after injection, the ISO group had higher susceptibility AF and prolonged AF duration compared with the control group. ISO decreased LA conduction velocity (CV) and increased LA conduction heterogeneity. ISO increased fibrosise areas and the protein levels of collagen types I and III in the left atrium. Antifibrosis drug pirfenidone decreased AF occurrence and reduced LA fibrosis in ISO treated rats. ISO injection induced atrial ischemia infarction by increasing heart rate and decreasing diastolic and systolic blood pressures. These findings demonstrated that ISO increases susceptibility to AF by increasing LA fibrosis and LA conduction abnormalities 5 weeks after injection. ISO injection induces atrial ischemic injury is the main cause of fibrosis. Rats with ISO-induced LA fibrosis may be used in further AF research.

Keywords: atrial fibrillation, fibrosis, myocardial ischemia, isoproterenol, atrium

INTRODUCTION

Atrial fibrillation (AF) is the most common tachyarrhythmia; its incidence increases due to widespread population aging. AF is the final common endpoint of atrial remodeling caused by a variety of cardiac diseases and conditions, and promotes important remodeling that contributes to the progressive nature of arrhythmia (Tan and Zimetbaum, 2011). Left atrial (LA) fibrosis is considered the key element of atrial remodeling in patients with structural heart disease and persistent AF (Velagapudi et al., 2013). Experimental studies have provided convincing evidence that fibrotic transformation of the left atrium results in the deterioration of atrial conduction, increasing impulse propagation anisotropy and building boundaries that promote re-entry in the atrial wall, which may be directly relevant for the mechanisms responsible for AF maintenance (Heijman et al., 2014; Krul et al., 2015).

Catecholamines increase the contractile force and beating rate of the heart, resulting in markedly increased cardiac pumping output and oxygen consumption (Nichtova et al., 2012). Excess of catecholamines in circulation is responsible for myocardial tissue damage in clinical conditions such as ischemia, angina, infarction, cardiac arrhythmias and sudden cardiac death. Increased administration of exogenous catecholamines leads to remodeling of myocardium and cardiomyocytes at the subcellular level. Isoproterenol (ISO) is a synthetic catecholamine and nonselective β-adrenoceptor agonist. Single or repeated doses of ISO administered to experimental animals induce fibrosis (Ma et al., 2017), cardiac hypertrophy, and myocardial damage in the left ventricle. ISO models contribute effectively to the understanding of pathologies in signal transduction, energetic, excitability, and contractility, which may contribute concomitantly to cardiac dysfunction and heart failure (Nichtova et al., 2012). The aim of this study was to assess whether ISO could induce LA fibrosis and increase susceptibility to AF and exploring the underlying mechanisms.

MATERIALS AND METHODS

Animals

All animal experiments were performed in accordance with the National Institutes of Health Guidelines for the Care and Use of Laboratory Animals, and the National Standard of the People's Republic of China for Laboratory animal Guidelines for ethical review of animal welfare. Male Sprague-Dawley rats (9-10 weeks, SPF, Guangdong Medical Experimental Animal Center) were housed at 20 ± 3°C and 55% ± 10% humidity, under a 12-h–12-h light/dark cycle. ISO hydrochloride (Sigma-Aldrich, St. Louis, MO, USA) was dissolved and injected subcutaneously at different doses once daily for two days. Choose the best dose for the animal study. The rats were divided into three groups, including control (CTL), ISO injection (ISO), and ISO injection with pirfenidone (PFD) treatment (ISO+PFD) groups. PFD is a broad-spectrum antifibrotic drug that has shown potential in numbers of animal models of fibrosis and clinical trials (Lopez-de La Mora et al., 2015). One week after injection, PFD (Sigma-Aldrich, St. Louis, MO, USA) was dissolved in water and gavaged for 4 weeks at a dose of 300 mg/kg in the ISO+PFD group. Meanwhile, equal volume of water was gavaged to the control and ISO groups for 4 weeks.

2, 3, 5-Triphenylteyltetrazolium Chloride Staining

The heart was removed and cooled in a −20°C freezer. After freezing, heart sections at 2 mm thickness were obtained. Atria were then incubated with 2% 2, 3, 5-triphenylteyltetrazolium chloride (TTC) (Sigma-Aldrich, St. Louis, MO) in a 37°C bath for 20 min to visualize the unstained infarcted region. After TTC staining, viable myocardium stained brick red while the infarct appeared pale white. TTC-stained tissue sections were photographed using a digital scanner.

Echocardiogram

After the induction of general anesthesia by 2% sevoflurane.The probe (Vevo 2100 system and MS-250 transducer, VisualSonics Inc, Canada) was placed on the chest and collected data along the short and long axes of the heart in all groups. Signals from M-mode echocardiography were recorded. Parameters obtained from the echocardiogram including left ventricular internal dimensions during systole (LVIDs) and diastole (LVIDd), the ejection fraction (EF), and fractional shortening (FS) were measured according to the leading-edge method. Each echocardiographic variable was determined in at least four separate images taken from the same heart.

Programmed Electrical Stimulation and Induction of AF

AF was defined as irregular, rapid atrial activation with varying electrogram morphology lasting ≥2 s, as we described previously (Ma et al., 2018a; Ma et al., 2018b). Rats were anesthetized with urethane and instrumented with subcutaneous electrodes for ECG recordings (Power Lab 16/35, AD Instruments, Castle Hill, NSW, Australia). The rat was tracheotomized and ventilated (Harvard Apparatus, Holliston Co) with room air supplemented with oxygen at 65 breaths/min. For atrial stimulation, a 4-French quadripolar catheter was advanced through the esophagus and placed at the site with the lowest threshold for atrial capture. Atrial pacing was performed at twice the diastolic threshold using two poles on the pacing catheter. Inducibility of AF was tested by applying 35-s bursts. The burst had a cycle length of 20 ms and pulse width of 5 ms. This series of bursts was repeated once. All rats were allowed 5 min of recovery in the sinus rhythm between stimulations for respiratory and circulatory recovery. If one or more bursts in the two series of bursts evoked an AF episode, AF was inducible in that rat. Otherwise, AF was noninducible. The duration and probability of inducible AF episodes were analyzed. The longest record time was 30 min after the burst pacing.

Multielectrodes Arrays Measurements

Multielectrode arrays (MEA) measurements were performed, as we described previously (Ma et al., 2018a; Ma et al., 2018b). The heart was removed rapidly, and the left atrium from the isolated heart was dissected and then immersed in Tyrode's solution. For MEA mapping, the epicardial LA surface rested on the MEA (Multi Channel Systems, Reutlingen, Germany) culture dish containing 120 tipped platinum recording electrodes of diameter 30 μm with an interelectrode spacing of 100 μm, and continuously superfused at a flow rate of 3 ml/min with oxygenated Tyrode's solution with at 37°C. During recordings, contractility was blocked with 15 mM butadione monoxime (BDM). The electrode arrays were mounted onto a printed circuit board and then fitted into the MEASystem interface. Electrical stimulation (bipolar pulses, 1–7 V, 1,000-μs duration) was applied *via* one of the MEA microelectrodes. Data were sampled at 10 kHz per channel with simultaneous data acquisition using the Cardio 2D software (Multi Channel Systems), and five fields were recorded in each atrium. All the data were analyzed to generate activation maps and measure CV.

Masson Trichrome Staining

For the quantification of atrial fibrosis, Masson's trichrome staining of coronalplane slices prepared from paraformaldehyde fixed samples was performed as previously described (Ma et al., 2017). Slices (5 μm) were stained with Masson's trichrome, and photographed using a digital camera under a BX53 microscope (Olympus, Tokyo, Japan). Images were quantified by the CellSens Dimension 1.16 software. Fibrotic areas were expressed as a percentage of blue-positive stained area to the total tissue area.

Western Blot

Protein from samples was separated by SDS-PAGE. Separated protein was transferred on a polyvinylidene difluoride membrane that was blocked at room temperature for 1 h in Tris-buffered saline with 0.2% Tween 20 containing 5% skim milk and probed with primary antibodies overnight at 4°C. Protein bands on Western blot were visualized using ECL Plus (Millipore, Billerica, MA, USA). Relative band densities of proteins were normalized against GAPDH.

Implantation of Telemetry Transmitter

Seven days prior to the test, a telemetry transmitter (Millar Instruments, Houston, TX, USA) was implanted and secured in the abdominal cavity, with the leads tunneled under the skin. The rats were housed in individual cages placed on a receiver that continuously captured signals, independent of animal activity. The signals were recorded with the LabChart 8 software and stored for analysis.

Cardiac Marker Enzyme Levels in the Serum

Two hours after the second injection of ISO, collected serum samples were assesssed for the cardiac marker enzyme creatinine kinase-MB (CK-MB). Analysis was performed with commercially available standard enzymatic kits.

Data Analysis and Statistics

Data were expressed as mean ± SD except for AF duration, which was expressed as median and interquartile range (25%–75%). The Fisher exact test was applied to compare AF inducibility. Normally distributed variables were tested using one-way analysis of variance (ANOVA). Differences between nonnormally distributed variables were examined by Mann-Whitney U test. All data analysis was performed using SPSS statistical software (SPSS, IL, USA). Statistical significance was defined as $P < 0.05$.

RESULTS

ISO Injection Causes LA Ischemia and Fibrosis

Representative illustrations of myocardial injury after TTC staining are shown in **Figure 1A**. CTL rats exhibited major portions stained positively, indicating tissue viability. There was little or zero percent of infract, however, the ISO group showed some unstained areas in the atrium. It is concentration-dependent increased in ISO group. The infarct size was significantly larger in 120 mg/kg group (25.4% ± 3.1%) than two lower dose groups. Masson's trichrome staining of heart sections confirmed that ISO injection with 120 mg/kg (ISO group) resulted in increased fibrosis in the left atrium 5 weeks later (**Figure 1B**). The fibrotic area was overtly decreased in the ISO+PFD group compared with the ISO group (**Figure 1C**). Type I and III collagen was detected by western blot to further assess fibrosis (**Figures 1D, E**). ISO administration resulted in increased deposition of type I ($P< 0.05$, **Figure 1D**) and III ($P < 0.05$, **Figure 1E**) collagen in the left atrium. Antifibrosis drug PFD treatment significantly reduced such deposition ($P < 0.05$).

ISO Increases Susceptibility to AF Five Weeks After Injection

In the 7 days after ISO subcutaneous injection, total mortality (10/50, 20%) was higher than in CTL rats (no death). Spontaneous episodes of AF were not observed throughout the induced episodes. **Figures 2A**, B show representative examples of non-AF and AF ECG. **Figure 2B** shows a representative example of induced AF electrocardiogram. AF occurred after induction termination by transesophageal programmed electrical stimulation (**Figure 2B II**). After seconds, the AF episode spontaneously stopped, and the sinus rhythm resumed. Susceptibility to AF in ISO treated rats (15/20, 75%) was significantly higher than that of CTL rats (3/20, 15%, **Figure 2C**). Treatment with PFD resulted in significantly decreased inducibility to 45% (9/20, $P < 0.01$). The mean AF episode duration was obviously longer in ISO treated rats compared with CTL animals ($P < 0.01$, **Figure 2D**). PFD treatment significantly decreased AF duration ($P < 0.05$, **Figure 2D**).

Electrocardiographic Findings

Three-lead electrocardiograms were recorded in anesthetized rats 5 weeks after injection. **Figure 3** depicts representative examples of ECGs. Surface ECG parameters were summarized in **Figure 3D**. P duration, RR interval, PQ interval, QRS, and QT durations were not significantly different among the three groups ($P > 0.05$).

ISO Decreases Cardiac Function

Five weeks after injection, echocardiography showed clear anterior wall motion abnormality (**Figure 4A**). As shown in **Figures 4B, C**, the ISO group had reduced EF (76.5% ± 4.9% vs. 38% ± 4.1%, $P < 0.05$) and FS (47.8% ± 3.6% vs. 21.1% ± 4.7%, $P < 0.05$) compared with the CTL group. Both FS and EF in the PFD group were increased compared with values obtained for the ISO group ($P < 0.05$). Both LVIDs ($P < 0.01$, **Figure 4D**) and LVIDd ($P < 0.01$, **Figure 4E**) were elevated in the ISO group, but decreased after PFD treatment (both $P < 0.05$).

ISO Increases LA Conduction Heterogeneity

LA surface conduction was measured using a 120-electrode MEA. Isochronal maps clearly showed a large zone of conduction blockage, which could block wave propagation in

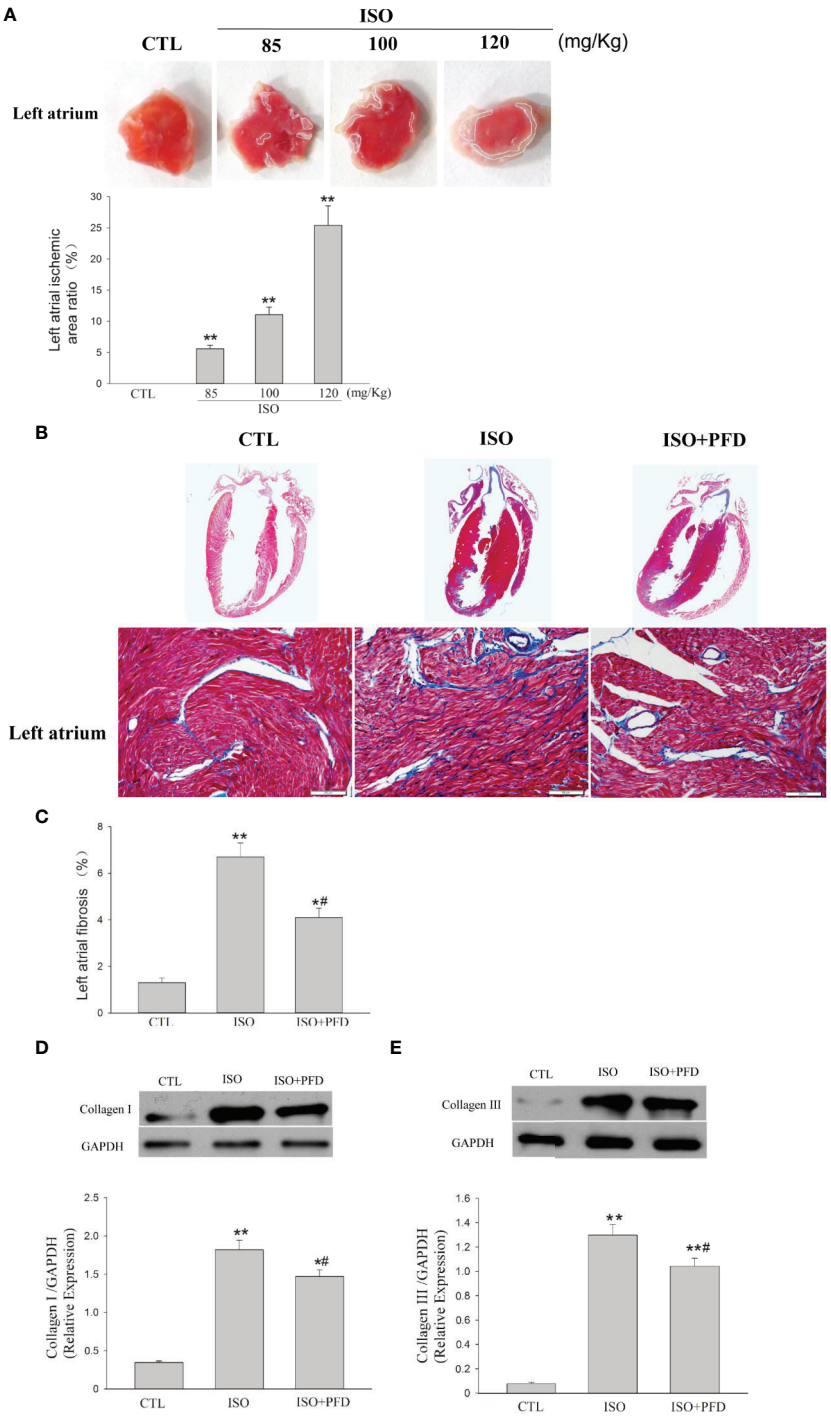

FIGURE 1 | Isoproterenol (ISO) causes left atrial ischemia and fibrosis in rats. **(A)** Representative images of left atrium by 2, 3, 5-triphenylteyltetrazolium chloride (TTC) staining. Red-colored regions in the TTC stained sections indicate nonischemic areas; pale-colored regions indicate ischemic portions of the heart. Quantification of ischemic area/total area in the left atrium (n = 5 rats/group). **(B)** Representative images for myocardial fibrosis of the whole heart (Masson's trichrome staining, which stains fibrosis blue and viable muscle red; scale bar: 100 μm). **(C)** Quantitation of left atrial fibrosis; ISO increased fibrosis-positive areas in the left atrium. **(D)** Western blot analysis of collagen I protein expression. ISO increased the protein levels of collagen I in the left atrium (n=5 rats/group). **(E)** Western blot analysis of collagen I protein amounts. ISO increased the protein levels of collagen III in the left atrium (n=5 rats/group). $^{*}P < 0.05$, $^{**}P < 0.01$ versus control (CTL) group; $^{\#}P < 0.05$ versus ISO group.

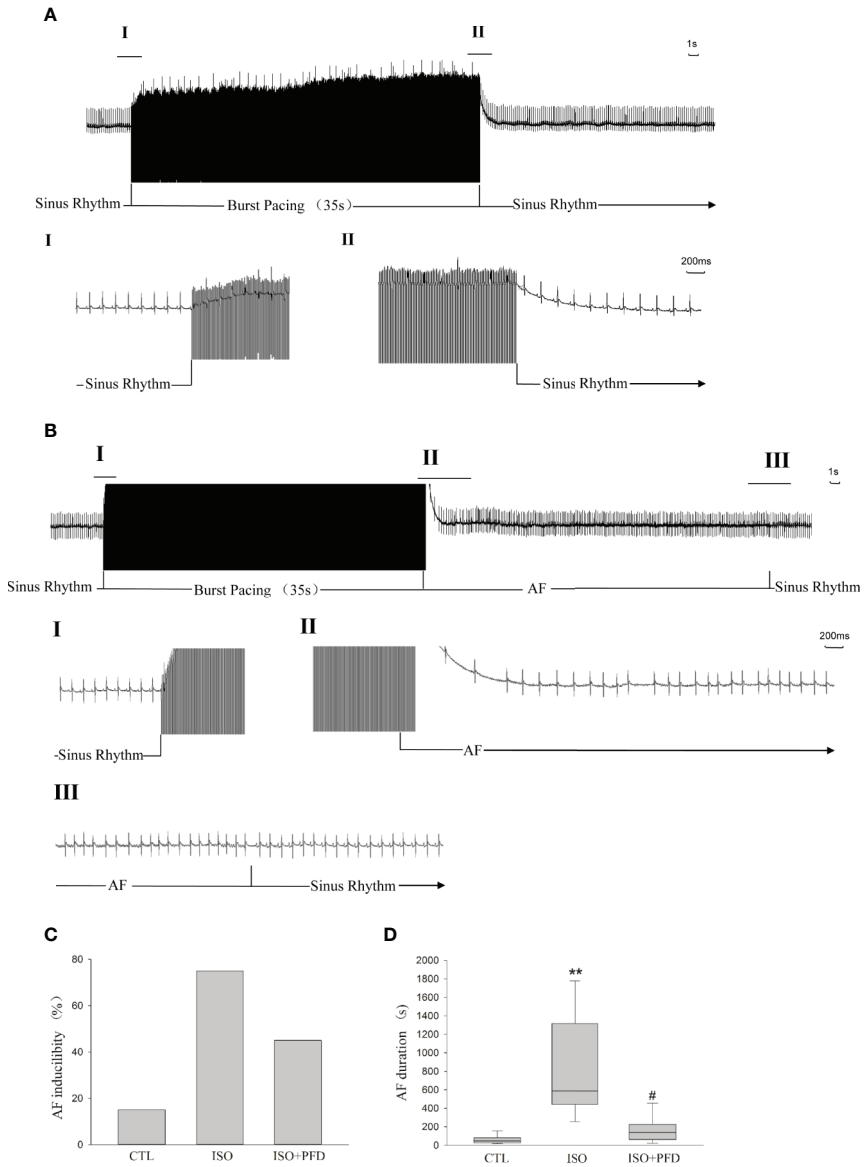

FIGURE 2 | Isoproterenol (ISO) increases atrial fibrillation (AF) inducibility and duration in rats 5 weeks after injection. **(A)** Representative noninduced AF episode. After termination of the burst, the rat also displayed sinus rhythm (II). **(B)** Representative induced AF episode. Before the burst (I), the rat was in the sinus rhythm. After termination of the burst (II), the rat displayed an irregular atrial rhythm with an irregular ventricular response. After seconds (III), the AF episode stopped spontaneously and the sinus rhythm resumed. **(C)** ISO increases AF inducibility in rats (n=20 rats/group). **(D)** ISO increases AF duration (n=20 rats/group). $^{**}P < 0.01$ versus control (CTL) group; $^{\#}P < 0.05$ versus ISO group.

the ISO group (**Figure 5A**). The activation located distally propagated to the block zone. There was no or limited conduction block zone in the CTL and PFD-treatment groups. Compared with the CTL and PFD-treatment groups, the ISO group showed more heterogeneous conduction. CV in the ISO group was significantly lower than that of the CTL group (**Figure 5B**, $P < 0.01$). Compared with the ISO group, PFD administration increased the LA CV ($P < 0.05$). PFD improved the LA CV and homogeneity.

ISO Induces Myofibroblast Differentiation

To assess the effects of ISO on fibroblast differentiation into myofibroblasts, immunohistochemistry was performed to detect α-SMA levels (**Figure 6A**). The results showed that ISO induced α-SMA expression in the left atrium ($P < 0.05$, **Figure 6B**). This effect was further validated by α-SMA protein expression levels. Compared with CTL rats, ISO treatment resulted in increased α-SMA protein levels ($P < 0.05$, **Figure 6C**). PFD reduced α-SMA-positive areas and protein amounts.

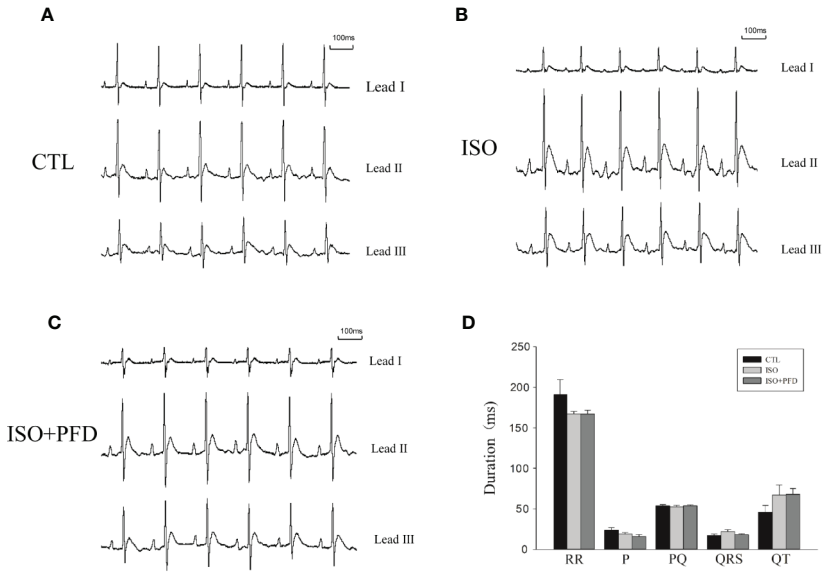

FIGURE 3 | Surface ECGs in rats 5 weeks after injection. **(A)** Representative ECG in the control (CTL) group. Einthoven Leads: Leads I, II, and III. **(B)** Representative ECG in the isoproterenol (ISO) group. **(C)** Representative ECG in the ISO+ pirfenidone (PFD) group. **(D)** Bar graph indicates ECG intervals and durations. There were no significant differences in ECG parameters in rats 5 weeks after ISO injection (n=20 rats/group).

ISO Induces Atrial Ischemic Infarction by Increasing the Heart Rate and Reduces Blood Pressure

Figure 7A telemetry transmitter recording showed that ISO injection resulted in at least 6–7 h increase in temperature. The heart rate was also increased substantially after treatment with ISO (**Figure 7B**). However, injection of 0.9% saline had not obviously changes in CTL rats. Heart rates before ISO injection were similar in both groups. The maximum heart rate change was from 395.2 ± 21.5 to 486.6 ± 2.9 bpm 1 h after first ISO injection, which increased oxygen consumption. **Figures 7C, D** show mean blood pressures 48 h after injection. Abdominal aortic arterial pressure decreased from 121.4 ± 4.3 to 84.6 ± 2.8 mmHg and 85 ± 6.7 to 55.7 ± 2 mmHg for systolic and diastolic blood pressures 1 h after first ISO injection. The blood pressure reduction continued for about 20 h. Before the second injection, arterial pressure in ISO treated rats was close to that of CTL rats. The second ISO injection caused further decrease in arterial pressure in rats. Two injections of 0.9% saline in CTL rats had no obvious effects on arterial pressure. ISO treatment resulted in significantly elevated ST-segment (**Figure 7E**) and increased CK-MB levels ($P < 0.01$, **Figure 7F**). These data indicate that ISO caused myocardial ischemic infarction by increasing heart rate, and decreasing diastolic and systolic blood pressures.

DISCUSSION

Cardiac fibrosis in the left atrium is an important arrhythmogenic substrate for AF. This study showed that: (1) ISO increased AF inducibility and extended its duration in rats 5 weeks after injection; (2) ISO increased LA fibrosis and LA conduction heterogeneity in rats 5 weeks after injection; (3) ISO injection induced atrial ischemic infarction by increasing the heart rate and decreasing coronary flow due to a significant drop in blood pressure; (4) Antifibrosis drug PFD decreased AF occurrence in rats 5 weeks after ISO injection by reducing LA fibrosis. Taken together, these results suggested that ISO could increase LA fibrosis and AF susceptibility 5 weeks after injection by inducing atrial ischemic injury. Rats with ISO-induced LA fibrosis may be used as a model in AF research.

Myocardial ischemia refers to the pathological state of reduced oxygen supply and residual metabolites caused by decreased blood perfusion, and reflects an imbalance between myocardial oxygen supply and demand (Heusch, 2016). In many circumstances, myocardial ischemia results from the combined effects of increased oxygen demand and reduced amounts of oxygen. ISO, a systemic β-adrenergic receptor agonist, is associated with marked ventricular myocardial ischemia (Patel et al., 2016; Song et al., 2016), hypertrophy (Zhang et al., 2015) and fibrosis (Ma et al., 2017). Merino reported that ISO increases both atrial frequency and contractility (Merino et al., 2015), suggesting that ISO may affect the atrium. In the present study, high doses of ISO injected at an interval of 24 h induced a variety of myocardial ischemic injury phenomena, such as ST-segment elevation and increased plasma CK-MB, by increasing the heart rate and decreasing diastolic and systolic blood pressures (also accompanied by a decrease in coronary flow) for hours. TTC staining showed large areas of ischemia zone in the atrium after injection. Masson's trichrome staining also showed large fibrotic areas in the left atrium 5 weeks after injection. These results strongly suggested that ISO injection induces atrial ischemic infarction by promoting imbalance between increased

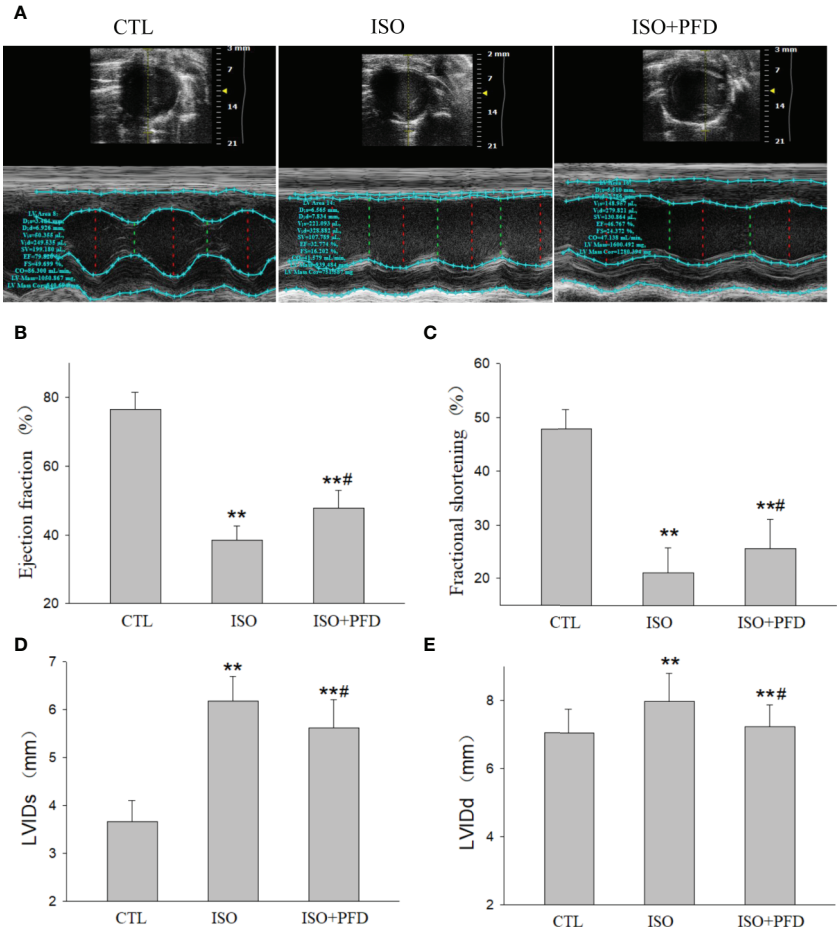

FIGURE 4 | Isoproterenol (ISO) decreases cardiac function. **(A)** Representative M-mode echocardiogram in rats 5 weeks after ISO injection. **(B)** Bar graph indicates EF (*n*=20 rats/group). **(C)** Bar graph indicates FS (*n* = 20 rats/group). **(D)** Bar graph indicates left ventricular internal dimensions during systole (LVIDs) (*n* = 20 rats/group). **(E)** Bar graph indicates left ventricular internal dimensions during diastole LVIDd (*n*=20 rats/group). $^{**}P < 0.01$ versus control (CTL) group, $^{\#}P < 0.05$ versus ISO group.

myocardial oxygen demand and reduced coronary blood supply. In clinic, atrial infarction is rarely diagnosed before death because of its characteristic subtle and nonspecific electrocardiographic findings (Lu et al., 2016). Atrial infarction has been observed in 17% of MI patients in a large postmortem study. In addition, increased risk of atrial tachyarrhythmia has been observed in patients with atrial infarction. Studies on atrial ischemic infarction in animal models (dogs, sheep, and pigs) by left circumflex coronary artery ligation also suggested that experimental atrial ischemia could create a substrate for AF maintenance (Aguero et al., 2017a).

High doses of ISO stimulate myocardial ischemia, hypoxia, necrosis, and fibroblastic hyperplasia, which are strongly similar to local myocardial damage and acute myocardial infarction (Qu et al., 2020). After myocardial injury, various peptide growth factors stimulate fibroblasts to migrate into the wound site and proliferate to reconstitute various connective tissue components (Dobaczewski et al., 2012; Lajiness and Conway, 2014). Otherwise, ISO could directly induce cardiac fibroblast proliferation and collagen synthesis *in vivo* (Sun et al., 2015). A critical event in the process is fibroblast differentiation into active-phenotype myofibroblasts (Honda et al., 2013; Mack and Yanagita, 2015). This results in functional changes, including increased proliferation, altered release of signaling molecules, and extracellular matrix deposition (Vasquez et al., 2011). In wound healing these cells provide additional extracellular collagen fiber deposition, which strengthens the injured tissue. However, when myofibroblasts persist in injured areas and continue to function, this helpful response becomes harmful, leading to progressive fibrosis (Davis and Molkentin, 2014). The present data showed that heart myofibroblasts persisted in atrial infarct scars, which induced large atrial fibrosis areas 5 weeks after ISO injection. The present findings corroborated Aguero *et al.*, who assessed atrial fibrosis changes in dogs with atrial infarction by left circumflex coronary artery ligation (Aguero et al., 2017b).

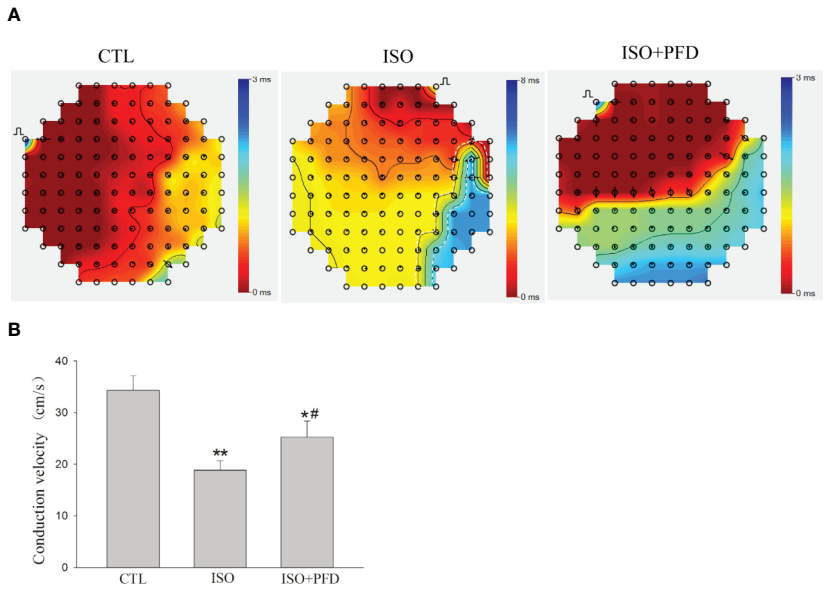

FIGURE 5 | Isoproterenol (ISO) increases left atrial conduction heterogeneity in rats. **(A)** Representative isochronous maps in the left atrium as obtained by multielectrode array (MEA) recording. Areas of isochronal crowding were found in the ISO group. The degree of crowding decreased in pirfenidone (PFD)-treated rats. Conduction was more heterogeneous in the ISO group compared with the control (CTL) group. **(B)** Bar graph indicates CV (n=5 rats/group). $^{*}P < 0.05$, $^{**}P < 0.01$versus CTL group; $^{\#}P < 0.05$ versus ISO group.

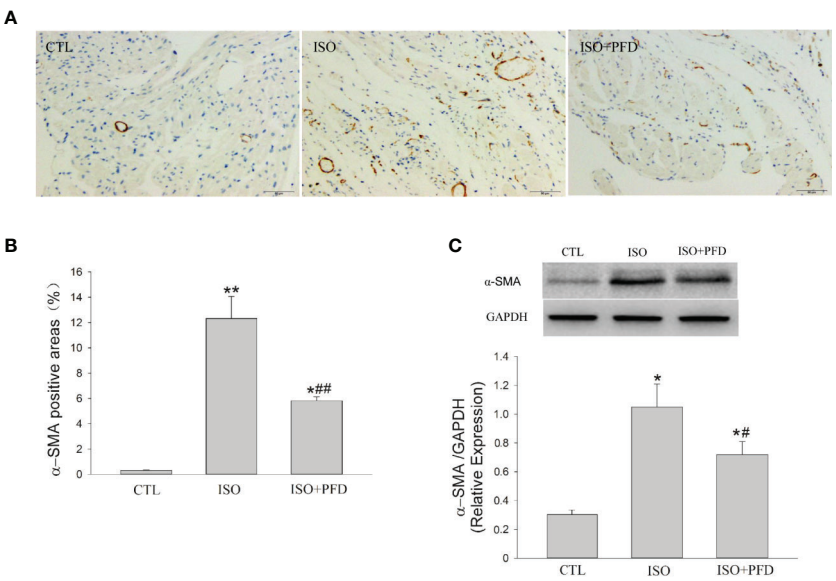

FIGURE 6 | Isoproterenol (ISO) induces myofibroblast differentiation in rats. **A**. Representative images showing the expression and distribution of the myofibroblast-specific marker α-SMA (Immunochemistry, scale bar: 50 μm) in the left atrium. **(B)** Quantitation of α-SMA positive areas. ISO increased α-SMA positive area (n=5 rats/group). **(C)** Western blot analysis of α-SMA protein expression. ISO increased the protein levels of α-SMA (n=5 rats/group). $^{*}P < 0.05$, $^{**}P < 0.01$ versus control (CTL) group, $^{\#}P < 0.05$, $^{\#\#}P < 0.01$ versus ISO group.

Cardiac fibrosis refers to a variety of quantitative and qualitative changes in the interstitial myocardial collagen network, and occurs in response to cardiac ischemic insults, systemic diseases, drugs, or other harmful stimuli; it alters myocardial architecture, promoting the development of cardiac dysfunction and arrhythmias, and influencing the clinical course and outcome of related-diseases. With the development of noninvasive methods, such as the late gadolinium–enhanced

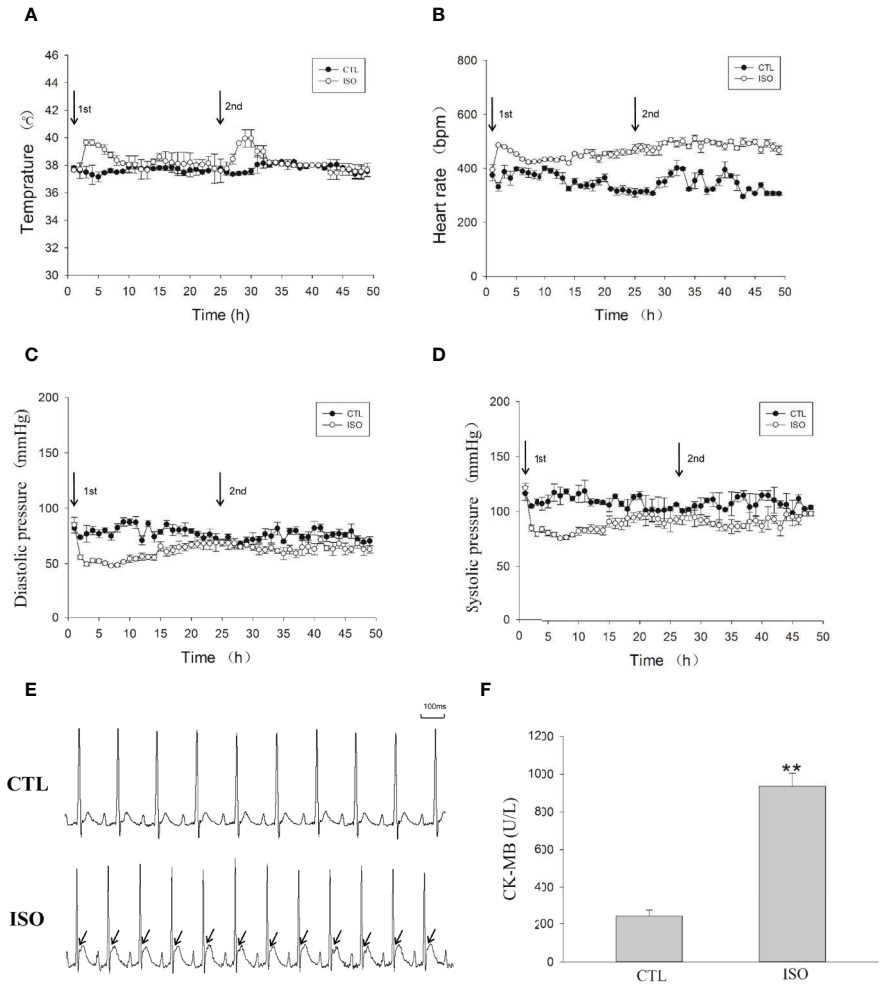

FIGURE 7 | Isoproterenol (ISO) induces left atrial ischemia by increasing the heart rate and reducing blood pressure. An implantable telemetry transmitter was used for the continuous monitoring of temperature, ECG, and blood pressure. **(A)** Temperature analysis during the 48-h following ISO injection. **(B)** Heart rate during the 48-h following ISO injection. **(C)** Diastolic pressure during the 48-h following ISO injection. **(D)** Systolic pressure during the 48-h following ISO injection. **(E)** Representative ECG after injection of ISO. **(F)** Bar graph indicates creatinine kinase-MB (CK-MB) changes after ISO injection. $^{**}P < 0.01$ versus CTL group.

cardiac magnetic resonance (LGE-CMR) imaging technology, LA fibrosis is considered the hallmark of structural remodeling in AF and the substrate for AF maintenance (Azadani et al., 2017). Experimental studies have provided convincing evidence that fibrotic transformation of the atrium results in altered atrial conduction, increasing impulse propagation anisotropy. Heterogeneous atrial tissue is more susceptible to reentry, leading to conduction blockage in regions with high conduction anisotropy. In LA appendages from patients undergoing antiarrhythmic surgery for AF, the optical mapping technology found conduction abnormalities with different longitudinal conduction velocities in different regions (Arroja et al., 2016). In the present study, conduction abnormalities were also found in the left atrium, with elevated AF inducibility 5 weeks after ISO injection in rats. The mean CV in the ISO group was significantly lower than that of CTL rats. These results suggested that ISO increases susceptibility to AF by enhancing LA fibrosis and conduction heterogeneity 5 weeks after injection.

In recent years, several animal models with increased atrial interstitial fibrosis have been described with high vulnerability to AF. Spontaneously hypertensive rats develop a substrate for AF *via* increased LA interstitial fibrosis (Lau et al., 2013). Left coronary artery ligation in rats leads to heart failure, with atrial dilatation, atrial fibrosis and AF promotion (Cardin et al., 2012; Ma et al., 2018a; Ma et al., 2018b). A transgenic mouse with TGF-β1 overexpression and selective atrial fibrosis has increased AF inducibility. These animal models are widely used in studies exploring mechanisms and pharmacological therapeutics for AF (Zhang et al., 2013; Zhang et al., 2014; Ma et al., 2018a). In the present study, ISO increased susceptibility to AF by enhancing LA fibrosis and conduction heterogeneity 5 weeks after injection.

PFD is one of two approved therapies for the treatment of idiopathic pulmonary fibrosis. Basic and clinical evidence suggests PFD may slow or inhibit the progressive fibrosis after tissue injuries. In vitro studies have shown that PFD can attenuate the proliferation and activation of fibroblasts and the expression of profibrotic factors (Shi et al., 2011). PFD significantly reduced arrhythmogenic atrial fibrosis and AF vulnerability in congestive heart failure canines (Lee et al., 2006). In this study, we used PFD (300 mg/kg, the usual dose) as a positive control drug to test the ISO model. Pirfenidone was given 1 week after ISO injection for 4 weeks to avoid impairing early repairs, according to the Nguyen study (Nguyen et al., 2010). After four weeks of administration, PFD decreased AF inducibility (45% in the ISO+PFD group vs. 75% in the ISO group) and LA fibrosis area caused by ISO ($P < 0.05$), close to the effects of PFD or other antifibrotic drugs in the myocardial infarction model induced by ligation of the left anterior descending coronary artery (Ma et al., 2018c; Qiu et al., 2018). PFD also improved the cardiac function, CV and reduced myofibroblasts differentiation. The effects of PFD in this ISO model were close to other antifibrosis drugs in other animal models (Wang et al., 2013; Beiert et al., 2017; Ma et al., 2018c). These results indicate that ISO-induced LA fibrosis rats may be used as a model in AF research. Compared with other animal models, the ISO model has the advantages of low cost, easy operation and good repeatability (Allawadhi et al., 2018). The effects of ISO on other vulnerable substrates for AF apart from fibrosis are unclear and need further investigation.

CONCLUSIONS

The present study showed that high-dose ISO induces atrial ischemic infarction in rats. Five weeks after injection, ISO increased LA fibrosis and LA conduction heterogeneity, ultimately leading to increased susceptibility to AF in rats. Rats with ISO-induced LA fibrosis may be used as a model in AF research.

DATA AVAILABILITY STATEMENT

All datasets generated for this study are included in the article/supplementary material.

ETHICS STATEMENT

The animal study was reviewed and approved by Animal Care Commitee of Guangdong Provincial Hospital of Chinese Medicine.

AUTHOR CONTRIBUTIONS

SM and JM conceived the study, designed, performed, and analyzed the experiments, carried out the data collection and wrote the paper. QT and CZ carried out the data collection. QC and WL coordinated the study and revised the paper. All authors reviewed the results and approved the final version of the manuscript.

FUNDING

This work was supported by grant from Guangdong Basic and Applied Basic Research Foundation (No.2019A1515010808), Natural Science Foundation of Guangdong Province (No.2017A030313888, No.2016A030313634), TCM Science and Technology Foundation of Guangdong Provincial Hospital of Chinese Medicine (No.YN2018MJ02), and Guangzhou science and Technology Foundation (No.201607010364).

REFERENCES

Aguero, J., Galan-Arriola, C., Fernandez-Jimenez, R., Sanchez-Gonzalez, J., Ajmone, N., Delgado, V., et al. (2017a). Atrial Infarction and Ischemic Mitral Regurgitation Contribute to Post-MI Remodeling of the Left Atrium. *J. Am. Coll. Cardiol.* 70, 2878–2889. doi: 10.1016/j.jacc.2017.10.013

Aguero, J., Galan-Arriola, C., Fernandez-Jimenez, R., Sanchez-Gonzalez, J., Ajmone, N., Delgado, V., et al. (2017b). Atrial Infarction and Ischemic Mitral Regurgitation Contribute to Post-MI Remodeling of the Left Atrium. *J. Am. Coll. Cardiol.* 70, 2878–2889. doi: 10.1016/j.jacc.2017.10.013

Allawadhi, P., Khurana, A., Sayed, N., Kumari, P., and Godugu, C. (2018). Isoproterenol-induced cardiac ischemia and fibrosis: Plant-based approaches for intervention. *Phytother Res.* 3, 1908–1932. doi: 10.1002/ptr.6152

Arroja, J. D., Burri, H., Park, C. I., Giraudet, P., and Zimmermann, M. (2016). Electrophysiological abnormalities in patients with paroxysmal atrial fibrillation in the absence of overt structural heart disease. *Indian Pacing Electrophysiol. J.* 16, 152–156. doi: 10.1016/j.ipej.2016.11.002

Azadani, P. N., King, J. B., Kheirkhahan, M., Chang, L., Marrouche, N. F., and Wilson, B. D. (2017). Left atrial fibrosis is associated with new-onset heart failure in patients with atrial fibrillation. *Int. J. Cardiol.* 248, 161–165. doi: 10.1016/j.ijcard.2017.07.007

Beiert, T., Tiyerili, V., Knappe, V., Effelsberg, V., Linhart, M., Stockigt, F., et al. (2017). Relaxin reduces susceptibility to post-infarct atrial fibrillation in mice due to anti-fibrotic and anti-inflammatory properties. *Biochem. Bioph. Res. Co.* 490, 643–649. doi: 10.1016/j.bbrc.2017.06.091

Cardin, S., Guasch, E., Luo, X., Naud, P., Le Quang, K., Shi, Y., et al. (2012). Role for MicroRNA-21 in atrial profibrillatory fibrotic remodeling associated with experimental postinfarction heart failure. *Circ. Arrhythm Electrophysiol.* 5, 1027–1035. doi: 10.1161/CIRCEP.112.973214

Davis, J., and Molkentin, J. D. (2014). Myofibroblasts: trust your heart and let fate decide. *J. Mol. Cell Cardiol.* 70, 9–18. doi: 10.1016/j.yjmcc.2013.10.019

Dobaczewski, M., de Haan, J. J., and Frangogiannis, N. G. (2012). The extracellular matrix modulates fibroblast phenotype and function in the infarcted myocardium. *J. Cardiovasc. Transl. Res.* 5, 837–847. doi: 10.1007/s12265-012-9406-3

Heijman, J., Voigt, N., Nattel, S., and Dobrev, D. (2014). Cellular and molecular electrophysiology of atrial fibrillation initiation, maintenance, and progression. *Circ. Res.* 114, 1483–1499. doi: 10.1161/CIRCRESAHA.114.302226

Heusch, G. (2016). Myocardial Ischemia: Lack of Coronary Blood Flow or Myocardial Oxygen Supply/Demand Imbalance? *Circ. Res.* 119, 194–196. doi: 10.1161/CIRCRESAHA.116.308925

Honda, E., Park, A. M., Yoshida, K., Tabuchi, M., and Munakata, H. (2013). Myofibroblasts: Biochemical and proteomic approaches to fibrosis. *Tohoku J. Exp. Med.* 230, 67–73. doi: 10.1620/tjem.230.67

Krul, S. P., Berger, W. R., Smit, N. W., van Amersfoorth, S. C., Driessen, A. H., van Boven, W. J., et al. (2015). Atrial fibrosis and conduction slowing in the left atrial appendage of patients undergoing thoracoscopic surgical pulmonary vein isolation for atrial fibrillation. *Circ. Arrhythm Electrophysiol.* 8, 288–295. doi: 10.1161/CIRCEP.114.001752

Lajiness, J. D., and Conway, S. J. (2014). Origin, development, and differentiation of cardiac fibroblasts. *J. Mol. Cell Cardiol.* 70, 2–8. doi: 10.1016/j.yjmcc.2013.11.003

Lau, D. H., Shipp, N. J., Kelly, D. J., Thanigaimani, S., Neo, M., Kuklik, P., et al. (2013). Atrial arrhythmia in ageing spontaneously hypertensive rats: unraveling the substrate in hypertension and ageing. *PloS One* 8, e72416. doi: 10.1371/journal.pone.0072416

Lee, K. W., Everett, T. H., Rahmutula, D., Guerra, J. M., Wilson, E., Ding, C. H., et al. (2006). Pirfenidone prevents the development of a vulnerable substrate for atrial fibrillation in a canine model of heart failure. *Circulation* 114, 1703–1712. doi: 10.1161/CIRCULATIONAHA.106.624320

Lopez-de La Mora, D. A., Sanchez-Roque, C., Montoya-Buelna, M., Sanchez-Enriquez, S., Lucano-Landeros, S., Macias-Barragan, J., et al. (2015). Role and New Insights of Pirfenidone in Fibrotic Diseases. *Int. J. Med. Sci.* 12, 840–847. doi: 10.7150/ijms.11579

Lu, M. L., De Venecia, T., Patnaik, S., and Figueredo, V. M. (2016). Atrial myocardial infarction: A tale of the forgotten chamber. *Int. J. Cardiol.* 202, 904–909. doi: 10.1016/j.ijcard.2015.10.070

Ma, J., Ma, S. Y., and Ding, C. H. (2017). Curcumin reduces cardiac fibrosis by inhibiting myofibroblast differentiation and decreasing transforming growth factor beta1 and matrix metalloproteinase 9/tissue inhibitor of metalloproteinase 1. *Chin. J. Integr. Med.* 23, 362–369. doi: 10.1007/s11655-015-2159-5

Ma, J., Ma, S., Yin, C., and Wu, H. (2018a). Matrine reduces susceptibility to post-infarct atrial fibrillation in rats due to anti-fibrotic properties. *J. Cardiovasc. Electrophysiol.* 29, 616–627. doi: 10.1111/jce.13448

Ma, J., Ma, S., Yin, C., and Wu, H. (2018b). Shengmai San-derived herbal prevents the development of a vulnerable substrate for atrial fibrillation in a rat model of ischemic heart failure. *Biomed. Pharmacother.* 100, 156–167. doi: 10.1016/j.biopha.2018.02.013

Ma, J., Ma, S. Y., Yin, C. X., and Wu, H. L. (2018c). Matrine reduces susceptibility to postinfarct atrial fibrillation in rats due to antifibrotic properties. *J. Cardiovasc. Electr.* 29, 616–627. doi: 10.1111/jce.13448

Mack, M., and Yanagita, M. (2015). Origin of myofibroblasts and cellular events triggering fibrosis. *Kidney Int.* 87, 297–307. doi: 10.1038/ki.2014.287

Merino, B., Quesada, I., and Hernandez-Cascales, J. (2015). Glucagon Increases Beating Rate but Not Contractility in Rat Right Atrium. Comparison with Isoproterenol. *PloS One* 10, e0132884. doi: 10.1371/journal.pone.0132884

Nguyen, D. T., Ding, C., Wilson, E., Marcus, G. M., and Olgin, J. E. (2010). Pirfenidone mitigates left ventricular fibrosis and dysfunction after myocardial infarction and reduces arrhythmias. *Heart Rhythm.* 7, 1438–1445. doi: 10.1016/j.hrthm.2010.04.030

Nichtova, Z., Novotova, M., Kralova, E., and Stankovicova, T. (2012). Morphological and functional characteristics of models of experimental myocardial injury induced by isoproterenol. *Gen. Physiol. Biophys.* 31, 141–151. doi: 10.4149/gpb_2012_015

Patel, P., Parikh, M., Shah, H., and Gandhi, T. (2016). Inhibition of RhoA/Rho kinase by ibuprofen exerts cardioprotective effect on isoproterenol induced myocardial infarction in rats. *Eur. J. Pharmacol.* 791, 91–98. doi: 10.1016/j.ejphar.2016.08.015

Qiu, H. L., Liu, W., Lan, T. H., Pan, W. J., Chen, X. L., Wu, H. L., et al. (2018). Salvianolate reduces atrial fibrillation through suppressing atrial interstitial fibrosis by inhibiting TGF-beta 1/Smad2/3 and TXNIP/NLRP3 inflammasome signaling pathways in post-MI rats. *Phytomedicine* 51, 255–265. doi: 10.1016/j.phymed.2018.09.238

Qu, C., Xu, D. Q., Yue, S. J., Shen, L. F., Zhou, G. S., Chen, Y. Y., et al (2020). Pharmacodynamics and pharmacokinetics of Danshen in isoproterenol-induced acute myocardial ischemic injury combined with Honghua. *J. Ethnopharmacol.* 247, 112–284. doi: 10.1016/j.jep.2019.112284

Shi, Q., Liu, X. Y., Bai, Y. Y., Cui, C. J., Li, J., Li, Y. S., et al. (2011). In Vitro Effects of Pirfenidone on Cardiac Fibroblasts: Proliferation, Myofibroblast Differentiation, Migration and Cytokine Secretion. *PloS One* 6, e28134. doi: 10.1371/journal.pone.0028134

Song, Q., Chu, X., Zhang, X., Bao, Y., Zhang, Y., Guo, H., et al. (2016). Mechanisms underlying the cardioprotective effect of Salvianic acid A against isoproterenol-induced myocardial ischemia injury in rats: Possible involvement of L-type calcium channels and myocardial contractility. *J. Ethnopharmacol.* 189, 157–164. doi: 10.1016/j.jep.2016.05.038

Sun, M., Yu, H., Zhang, Y., Li, Z., and Gao, W. (2015). MicroRNA-214 Mediates Isoproterenol-induced Proliferation and Collagen Synthesis in Cardiac Fibroblasts. *Sci. Rep.* 5, 18351. doi: 10.1038/srep18351

Tan, A. Y., and Zimetbaum, P. (2011). Atrial fibrillation and atrial fibrosis. *J. Cardiovasc. Pharmacol.* 57, 625–629. doi: 10.1097/FJC.0b013e3182073c78

Vasquez, C., Benamer, N., and Morley, G. E. (2011). The cardiac fibroblast: functional and electrophysiological considerations in healthy and diseased hearts. *J. Cardiovasc. Pharmacol.* 57, 380–388. doi: 10.1097/FJC.0b013e31820cda19

Velagapudi, P., Turagam, M. K., Leal, M. A., and Kocheril, A. G. (2013). Atrial fibrosis: a risk stratifier for atrial fibrillation. *Expert Rev. Cardiovasc. Ther.* 11, 155–160. doi: 10.1586/erc.12.174

Wang, Y. L., Wu, Y. Q., Chen, J. W., Zhao, S. M., and Li, H. W. (2013). Pirfenidone Attenuates Cardiac Fibrosis in a Mouse Model of TAC-Induced Left Ventricular Remodeling by Suppressing NLRP3 Inflammasome Formation. *Cardiology* 126, 1–11. doi: 10.1159/000351179

Zhang, Y., Dedkov, E. I., Teplitsky, D., Weltman, N. Y., Pol, C. J., Rajagopalan, V., et al. (2013). Both hypothyroidism and hyperthyroidism increase atrial fibrillation inducibility in rats. *Circ. Arrhythm Electrophysiol.* 6, 952–959. doi: 10.1161/CIRCEP.113.000502

Zhang, Y., Dedkov, E. I., Lee, B.3rd, Li, Y., Pun, K., and Gerdes, A. M. (2014). Thyroid hormone replacement therapy attenuates atrial remodeling and reduces atrial fibrillation inducibility in a rat myocardial infarction-heart failure model. *J. Card Fail* 20, 1012–1019. doi: 10.1016/j.cardfail.2014.10.003

Zhang, S., Tang, F., Yang, Y., Lu, M., Luan, A., Zhang, J., et al. (2015). Astragaloside IV protects against isoproterenol-induced cardiac hypertrophy by regulating NF-kappaB/PGC-1alpha signaling mediated energy biosynthesis. *PloS One* 10, e0118759. doi: 10.1371/journal.pone.0118759

Conflict of Interest: The authors declare that the research was conducted in the absence of any commercial or financial relationships that could be construed as a potential conflict of interest.

frontiers in Physiology

METHODS
published: 22 April 2020
doi: 10.3389/fphys.2020.00346

Minimal Invasive Pericardial Perfusion Model in Swine: A Translational Model for Cardiac Remodeling After Ischemia/Reperfusion Injury

*Stefanie Marek-Iannucci, Amandine Thomas and Roberta A. Gottlieb**

Cedars-Sinai Medical Center, Smidt Heart Institute, Los Angeles, CA, United States

Rationale: Adverse remodeling leads to heart failure after myocardial infarction (MI), with important impact on morbidity and mortality. New therapeutic approaches are needed to further improve and broaden heart failure therapy. We established a minimally invasive, reproducible pericardial irrigation model in swine, as a translational model to study the impact of temperature on adverse cardiac remodeling and its molecular mechanisms after MI.

Objective: Chronic heart failure remains a leading cause of death in western industrialized countries, with a tremendous economic impact on the health care system. Previously, many studies have investigated mechanisms to reduce infarct size after ischemia/reperfusion injury, including therapeutic hypothermia. Nonetheless, the molecular mechanisms of adverse remodeling after MI remain poorly understood. By deciphering the latter, new therapeutic strategies can be developed to not only reduce rehospitalization of heart failure patients but also reduce or prevent adverse remodeling in the first place.

Methods and Results: After 90 min of MI, a 12Fr dual lumen dialysis catheter was place into the pericardium via minimal invasive, sub-xiphoidal percutaneous puncture. We performed pericardial irrigation with cold or warm saline for 60 min in 25 female farm pigs after ischemia and reperfusion. After one week of survival the heart was harvested for further studies. After cold pericardial irrigation we observed a significant decrease of systemic body temperature measured with a rectal probe in the cold group, reflecting that the heart was chilled throughout its entire thickness. The temperature remained stable in the control group during the procedure. We did not see any difference in arrhythmia or hemodynamic stability between both groups.

Conclusion: We established a minimally invasive, reproducible and translational model of pericardial irrigation in swine. This method enables the investigation of mechanisms involved in myocardial adverse remodeling after ischemia/reperfusion injury in the future.

Keywords: myocardial remodeling, ischemia-reperfusion injury, therapeutic hypothermia, heart failure, pericardial irrigation

OPEN ACCESS

Edited by:
Claudio de Lucia,
Temple University, United States

Reviewed by:
Cesario Bianchi,
University of Mogi das Cruzes, Brazil
Ilias P. Doulamis,
Boston Children's Hospital, Harvard Medical School, United States

****Correspondence:***
Roberta A. Gottlieb
Roberta.Gottlieb@cshs.org

Specialty section:
This article was submitted to Clinical and Translational Physiology, a section of the journal Frontiers in Physiology

Received: *08 January 2020*
Accepted: *26 March 2020*
Published: *22 April 2020*

Citation:
Marek-Iannucci S, Thomas A and Gottlieb RA (2020) Minimal Invasive Pericardial Perfusion Model in Swine: A Translational Model for Cardiac Remodeling After Ischemia/Reperfusion Injury. Front. Physiol. 11:346. doi: 10.3389/fphys.2020.00346

INTRODUCTION

We recently reported beneficial effects of hypothermia in a novel swine ischemia-reperfusion model (Marek-Iannucci et al., 2019). Because of repeatedly expressed interest in the model, we here present details of the methodology, the aim of this manuscript being to demonstrate the safety and reproducibility of this novel technique, in order to make it accessible to other research groups interested in studying molecular mechanisms of adverse myocardial remodeling after ischemia-reperfusion injury. Despite percutaneous coronary angioplasty, about one third of the patients with myocardial infarction (MI), will not achieve a thrombolysis in myocardial infarction (TIMI) flow grade 3, which can partially explain the increased incidence of chronic heart failure despite early intervention (Rochitte, 2008; Kaul, 2014; Bouleti et al., 2015; Dai et al., 2017). This phenomenon, known as no-reflow, is thought to represent microvascular damage caused by extended ischemia, leading to tissue loss and non-regeneration of the myocardium (Kloner et al., 1974; Rochitte, 2008; Kloner, 2011; Rezkalla et al., 2017; Shi et al., 2017). No-reflow increases adverse remodeling of the left ventricle after MI, leading to increased dilation, congestive heart failure and mortality with an overall worse outcome (Kloner et al., 1974; Rochitte, 2008; Dai et al., 2017). Furthermore, it amplifies myocardial stunning, reperfusion arrhythmia, microvascular obstruction and cardiomyocyte death and is held responsible for about half of the eventual infarction size (Hausenloy, 2012). Therapeutic hypothermia (TH) has been applied in various forms in animal studies, showing a reduction in no-reflow area and MI size (Erlinge et al., 2013; Erlinge et al., 2014; Dai et al., 2015; Dai et al., 2017; Rezkalla et al., 2017). Even components of inflammation have shown to be attenuated after TH application (Mohammad et al., 2017; Shi et al., 2017). Various hypotheses have been proposed to explain adverse remodeling after MI, yet the exact molecular mechanisms behind it remain poorly understood (Rochitte, 2008; Kloner, 2011; Schirone et al., 2017). One approach has been to study the influence of TH on the myocardium after MI. Although studies in small animals have yielded promising results, clinical trials were not as successful and human findings remain controversial (Erlinge et al., 2014; Herring et al., 2014; Erlinge et al., 2015). Possibly the models used in successful animal studies are not feasible in the clinical setting and the correct translational model has not been described yet. Systemic TH has been used in the clinical setting after resuscitation for decades, focusing primarily on neurologic outcome after cardiac arrest (Spiel et al., 2009; Haugk et al., 2011). More recent research focused on the direct effect of TH on the myocardium, but multicenter trials such as CHILL-MI and RAPID-MI-ICE failed to show significant reduction in infarction size (Erlinge et al., 2014, 2015; Mohammad et al., 2017). Nonetheless those trials showed a decreased incidence in heart failure. Methods used in the clinical setting include retrograde cold perfusion through the coronary sinus, endovascular cooling with special catheters, intraperitoneal cooling systems, cold saline infusions and topical cooling with cooling pads or blankets (Erlinge et al., 2014; Herring et al., 2014; Nichol et al., 2015; Kloner et al., 2017). This leads us in two possible directions regarding future studies: First, the right technique regarding TH application, implementable in the clinical setting has not been found yet (Herring et al., 2014). Second, it might be necessary to study the exact mechanism by which TH improves myocardial remodeling in animal models to design specific therapies targeting these pathways independently of the use of TH in the clinical field. Therefore, we designed a minimally invasive large animal model in swine, utilizing pericardial perfusion with cold saline after MI. The focus of our study is to investigate the influence of TH on myocardial remodeling on a molecular basis, with the goal of inhibiting the adverse effects of remodeling after MI and preventing chronic heart failure. Importantly, this model can be used for various other studies requiring direct application of substances or stimulation of the myocardium.

MATERIALS AND METHODS

Animal Procurement

All procedures and protocols were approved by the Institutional Animal Care and Use Committee (IACUC) and were performed according to the National Institutes of Health (NIH) Guidelines for the Care and Use of Laboratory Animals. For the entire project, using a novel minimal invasive pericardial perfusion model in swine, 25 female farm pigs (35–40 kg) were ordered at S&S Farms (Ramona, CA, United States). The animals had a one-week acclimatization period prior to the procedure. They received food (Lab Diet-Porcine lab grower) twice a day and water *ad libitum*. Among all the 25 pigs, 6 animals died due to refractory arrhythmia within the first 45 min of MI, resulting in a survival rate of 76%. None of the animals died during the pericardial perfusion treatment or within the observation period until euthanasia, making the cause of death a common complication of ischemic injury of the myocardium, with no difference between the groups. Most of the data acquired with this model has recently been published by our group (Marek-Iannucci et al., 2019). The data in this manuscript consists in additional hemodynamic studies, supplementary to our prior publication, in order to demonstrate the reproducibility and safety of this method, the final goal being to make this novel method accessible to many other laboratories interested in studying molecular mechanisms of adverse myocardial remodeling after MI in a large animal model.

Anesthesia

On the day of procedure, the pigs received sedating premedication with Ketamine (20 mg/kg IM), Acepromazine (0.25 mg/kg IM), Atropine (0.05 mg/kg IM), and Propofol (2.0 mg/kg IM). Two intravenous cannulas were placed and the animals were intubated. Continuous general anesthesia was maintained with Isoflurane 1–3%.

Medication

Amiodarone 10 mg/kg was given continuously intravenous over 30 min in 250 ml of 5% Dextrose prior to intervention. 2% Lidocaine was given as continuous infusion (2 mg/kg/h)

throughout the whole procedure to reduce the risk of arrhythmia. To prevent blood clotting in the catheters we administered two boli of intravenous heparin (100 IU/kg) once prior to intervention and once after pericardial catheter placement. We used intravenous Amiodarone (Bolus dose of 10 mg/kg given in a 1:10 dilution of 5% Dextrose) and Lidocaine (bolus dose 40–60 mg) to terminate arrhythmia if necessary. Phenylephrine 1 mg/ml was used in boli of 1 ml as needed in case of systolic blood pressure drops below 40 mmHg.

Angiography and Myocardial Infarction

We performed one procedure per day, at the same time each day, to minimize possible differences due to circadian rhythm. At first, basal left ventricular function (LVF) was measured with echocardiography (GE, vivid 7, and M-mode long axis). Mean LVF was 88% and mean end-diastolic volume 58 ml. Vital signs were measured continuously throughout the procedure. Heart rate and rhythm were monitored with defibrillator patches and conventional electrocardiogram. Peripheral oxygen saturation was measured with pulse oximetry and blood pressure with a sphygmomanometer prior to intervention. We performed a left sided surgical cutdown of the neck, to access the left common carotid artery and the left common jugular vein. An 8-Fr and 7-Fr sheath were placed into the carotid artery and jugular vein respectively. The central venous access was used for continuous intravenous fluid infusion, blood collection and administration of medication. After successful placement of the arterial sheath, blood pressure was measured invasively. A coronary guide catheter was used for angiography. A 3.00 or 3.50 mm balloon (depending on the size of the coronaries, visualized in the angiogram) was then advanced into the left anterior descending artery and placed just distal of the first diagonal branch. The balloon was inflated until complete occlusion of the vessel and the pigs underwent 90 min of MI. All animals had to be shocked at least once with 200 Joules due to ventricular fibrillation but were otherwise stable throughout the MI. After 90 min the balloon was completely deflated and extracted under fluoroscopic control, followed by a 30 min period of reperfusion (see **Table 1** for required material).

TABLE 1 | List of the material required for the procedure.

List of material	
Description	**Amount**
12Fr dual lumen dialysis catheter set (Mahurkar-Elite, Medtronic®, Dublin, Ireland) includes all necessary tools for pericardial puncture	1/animal
Perisafe® Weiss Epidural Needle (Becton Dickinson, Franklin Lakes, New Jersey)	Optional
7Fr and sheath for coronary angiography	1 (reusable)
8Fr and sheath for coronary angiography	1 (reusable)
3.0–3.5 mm angioplasty balloon	1 (reusable)
i.v. line perfusion set	2 (inflow and outflow)/animal
Sterile container to collect fluid	1/animal
Thermo-bag for infusion sets	1 (reusable)
Sterile saline for infusion	1–2 L/animal, depending of infusion rate

Pericardial Puncture

During the first 30 min of reperfusion, we performed a sub-xiphoidal, and percutaneous pericardial puncture. We filled a 10 cc syringe with 5 cc sterile saline and attached it to the puncture needle provided in the catheter set. To reduce the risk of ventricular perforation it is possible to use a Perisafe™ Weiss Epidural Needle (Becton Dickinson, Franklin Lakes, NJ, United States) instead. Under fluoroscopic imaging we performed a midline, percutaneous, sub-xiphoidal puncture, and 1–2 cm below the xiphoid. Under fluoroscopic imaging the needle was inserted in a 45 degrees angle and advanced for about 1 cm. After that the angle was reduced to 15–20 degrees and the needle was advanced directing toward the midline of the right clavicle of the animal (when performed from the left side of the animal). There was a small resistance when penetrating the diaphragm. Under continuous vision with fluoroscopy and while maintaining suction on the syringe, the pericardium was punctured. While doing so one can feel a loss of resistance and loose forward movement of the needle. This crucial moment can be visualized via fluoroscopy when observed carefully. It is important to aspirate after puncture to ensure correct positioning. Aspirating blood suggests ventricle puncture (bright red for the left and dark red for the right ventricle). In case of correct positioning of the needle, nothing or a minimal amount of clear fluid (pericardial fluid) can be aspirated. There can also appear a small air bubble in the syringe, suggesting correct positioning in the pericardium. After that the syringe is detached and a guidewire (supplied with the puncture set) is advanced through the needle. Keep the needle secured with one hand at all time to avoid displacement. While inserting the guide wire under fluoroscopic control you can observe the wire encircle the heart. Always insert the guide wire generously to avoid displacement (**Supplementary Figure S1**). After that, we removed the puncture needle while the wire remains in place. We then performed a 3–4 mm incision with a sterile disposable scalpel at the entry site of the guide wire. A 12Fr dilator (supplied with the puncture set) was inserted over the guide wire and advanced to the incision site. It is important never to insert a catheter or dilator into the tissue without having the end of the guide wire reaching out at the end of the latter and secured with one hand. The dilator is then inserted under simultaneous and cautious retraction of the wire into the pericardium. It is crucial that a sufficient length of guide wire always remains inside the pericardium to avoid displacement (about 10 cm on imaging screen). After that, the dilator is removed and the guidewire gently advanced more deeply. We then performed the same maneuver once again using a 12-Fr dual lumen dialysis catheter (Mahurkar-Elite, Medtronic®, Dublin, Ireland) (**Supplementary Figure S2**). Once the catheter is in place, one lumen of the latter can be opened and a 10 cc syringe filled with 5 cc sterile saline and 5 cc dye can be injected to confirm correct placement under fluoroscopy (**Supplementary Figure S3**). If positioned correctly, the catheter will lie in a crescent form at the border of the heart

shadow. It is important that the catheter is inserted neither too low nor too deep, to avoid occlusion. The dye should spread widely over the whole surface of the ventricle (**Supplementary Figure S3**). Finally, the guide wire can be removed, and the catheter secured with one or two single sutures.

Pericardial Perfusion

The catheter was connected to a closed tube system filled with sterile saline. One port was used as inlet and the other one as outlet. The inlet port was attached to a standard intravenous fluid administration set with sterile saline. The outflow was collected in a sterile collection bottle. We performed one hour of pericardial irrigation with an average infusion rate of 1250 ml/h (20.8 ml/min). The animals were overall stable throughout the entire pericardial irrigation period, meaning that the infusion rate can be increased if desired. In the first couple of minutes the outflow may appear pink, tinged with blood, although it should not be deep red or viscous, which would suggest active bleeding into the pericardium. Infusion rate can be controlled with a pump or a flow metering system. After one hour the pericardial irrigation was ended. The inlet port was closed first and the outlet port only after complete arrest of fluid outflow. Suction at the end of the procedure on the outlet port can minimize the amount of remaining fluid in the pericardium. During the whole perfusion period it is important to monitor heart rate and blood pressure continuously via the arterial sheath. A reduction in blood pressure can indicate cardiac tamponade. To avoid the latter, the flow rate should be increased gradually over the first 2 min. Finally, the catheter was cautiously removed after opening the sutures. There should not occur any bleeding after removal of the catheter.

End of Procedure

The sub-xiphoidal incision site was cleaned and betadine ointment was used to avoid infection. Sutures were not necessary, due to the minimal size of incision. If necessary one steri-strip can be used to close the incision. Following the intervention, the venous and arterial sheath were removed and both vessels were ligated. The skin was closed using 4-0 absorbable Vicryl* sutures intracutaneously.

Optimization of the Technique

We lost 3 pigs due to ventricular fibrillation refractory to defibrillation therapy which eventually ended in electro-mechanic dissociation (EMD), most likely due to tamponade. As a matter of fact, placing the 12F dialysis catheter inside the pericardium prior to MI was not well tolerated by the animals. After changing strategy and placing the dialysis catheter after 90 min of MI and during coronary reperfusion we had no more animal losses. Furthermore, we tried to add a temperature probe into the pericardium for continuous measurements during pericardial irrigation. Unfortunately, the measurements were extremely dependent of the position of the dialysis catheter and the probe itself, making the data not entirely reliable (**Supplementary Figure S4**). We therefore decided to measure left ventricular temperature with a specific thermocouple probe (ThermoWorks, American Fork, UT, United States), inserted under fluoroscopic control into the left anterolateral ventricular wall percutaneously (**Supplementary Figure S5**).

Statistical Analysis

For all experiments with a single comparison, we applied a 2-tailed unpaired Student's *t*-test. For multiple comparisons we performed a one-way ANOVA including a Tukey's *post hoc* analysis. Results are represented by the mean and standard error for the mean (SEM). A *p*-value of less than 0.05 war regarded as significant. All data acquired with echocardiography and Swan-Ganz pressure measurements have been repeated 3 times per animal and the mean has been used for further analysis. Regarding the temperature and blood pressure measurements, these consist in continuous monitoring throughout the procedures and have been there for performed only once per animal for each given timepoint.

RESULTS

We used this pericardial irrigation model on 25 female farm pigs (35–40 kg) to cool the myocardium locally and study its influence on myocardial remodeling after MI. The data presented here is acquired from 6 out of the 25 animals and consists in additional information to previously published data (Marek-Iannucci et al., 2019) on this novel technique, in order to demonstrate its safety and make it accessible to other laboratories interested in studying molecular mechanisms of adverse myocardial remodeling after MI in a large animal model.

The saline was either cooled in the fridge (8°C) or warmed in the heating cabinet (37°C) for 3 days. To keep the temperature of the saline bag constant we used a specific thermo-bag for infusion sets. In case of cold saline, we added a consistent amount of cool packs into the latter. In the control group, pigs underwent pericardial perfusion with 37°C sterile saline for 60 min and remained at a stable systemic temperature, measured by a rectal temperature probe, and throughout the procedure. After the complete procedure of 3 h, their mean body temperature was 37.4°C (SEM = 0.17), with a mean temperature variation (ΔT) of 0.1°C (SEM = 0.07) from beginning to end. The infusion temperature was measured at 37°C and the mean outflow of the pericardium was at 28.7°C. In the cold group, the pigs had a mean systemic temperature of 36.1°C (SEM = 0.35) with a mean drop of 1.7°C (SEM = 0.26) compared to the control group after one hour of cold pericardial irrigation. The mean inflow temperature was 11.5°C and the mean outflow 20.8°C. This can be optimized by adjusting the pericardial perfusion flow rate. The difference in mean systemic body temperature and ΔT were both statistically significant ($p = 0.011$ and $p = 0.002$ respectively) as shown in **Figures 1**, **2** respectively. We only needed to use phenylephrine in one animal with a blood pressure drop. During pericardial irrigation we did not encounter malignant arrhythmias. Overall, we did not encounter any differences in vital parameters or heart rhythm in the 2 groups (**Table 2**). The animals adapted well and we did not have any loss after the intervention. After one week the pigs were euthanized and the heart was harvested.

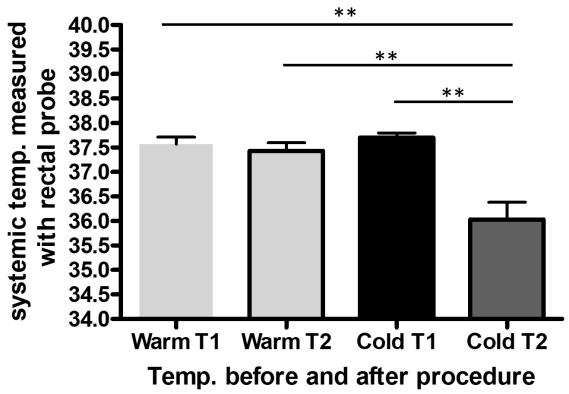

FIGURE 1 | Average systemic body temperature (SBT) measured with a rectal probe throughout the procedure in the control (n = 3) and cold (n = 3) group. The data represents the systemic temperature before (T1) and after (T2) the entire procedure in the warm compared to the cold group. We performed one-way ANOVA, with $^{**}p < 0.01$.

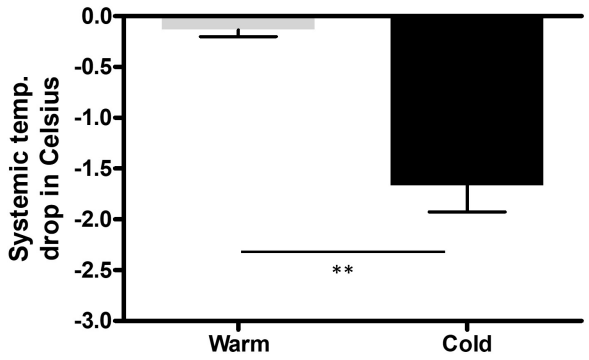

FIGURE 2 | Change (ΔT) in systemic body temperature (SBT) measured with a rectal probe throughout the procedure in the control (n = 3) and cold (n = 3) group from beginning to end of procedure. We performed an unpaired, two tailed t-test, with $^{**}p = 0.0047$.

Prior to euthanasia the pigs were anesthetized, and we performed echocardiography as well as ventriculography to assess LVF. We did not detect a significant difference in ejection fraction (EF) one week post MI (**Figure 3**). This is consistent with previously published data, where significant improvement of EF could be detected only beginning 4 weeks post MI (Marek-Iannucci et al., 2019). These beneficial effects of local hypothermia on EF were accompanied by a strong correlation

TABLE 2 | Vital parameter measurements throughout the procedure.

		pre procedure NIBP	Incision NIBP	Sheath placement NIBP	Angiogram NIBP	Balloon inflation PB	Balloon deflation PB	Beginn irrigation PB	End irrigation PB	End procedure NIBP
17P49 Warm 1	HR	76	67	69	70	70	87	78	80	83
	RR syst	79	78	73	88	50	53	50	50	83
	RR diast	33	27	26	34	35	32	3i	32	30
	Sp02	98	100	99	98	98	100	100	100	100
17P54 Warm 2	HR	110	95	104	95	92	92	93	93	90
	RR syst	80	90	83	77	66	57	51	59	81
	RR diast	31	36	30	23	39	45	37	46	24
	Sp02	98	99	94	100	94	95	99	97	96
17P67 Warm 3	HR	82	75	73	54	65	68	66	68	73
	RR syst	62	80	72	69	54	60	53	60	79
	RR diast	20	37	31	31	36	42	38	22	22
	Sp02	97	96	95	96	96	100	100	100	100
17P62 Cold 1	HR	85	74	75	70	69	65	68	63	78
	RR syst	92	93	90	94	59	51	50	52	78
	RR diast	31	31	28	26	33	35	27	40	22
	Sp02	100	100	100	100	100	100	95	100	100
17P53 Cold 2	HR	92	77	76	74	73	68	68	66	72
	RR syst	86	97	101	54	59	50	51	45	87
	RR diast	17	24	24	33	38	32	33	28	16
	Sp02	98	99	98	98	33	98	98	96	98
17P66 Cold 3	HR	93	69	66	62	64	57	56	55	53
	RR syst	73	63	62	53	63	52	59	74	89
	RR diast	18	38	21	21	47	25	35	50	66
	Sp02	98	100	100	99	99	99	99	99	99

Regarding blood pressure measurements, NIBP represent non-invasive blood pressure measurements on the extremities, whereas PB represents invasive pressure measurement in the ascending aorta throughout the procedure with the catheter. PB measurements are preferred, because more accurate, but not available throughout the entire time.

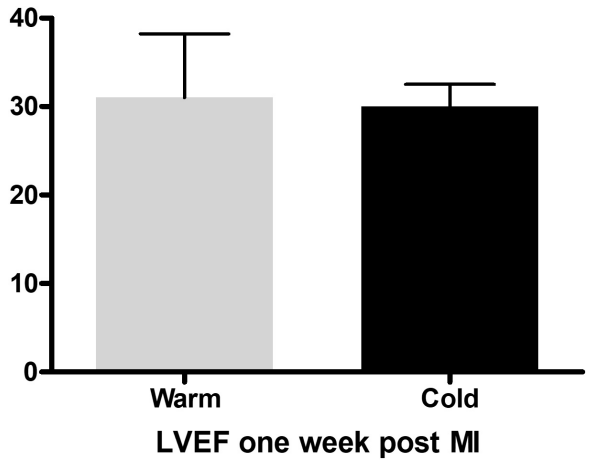

FIGURE 3 | Ejection fraction measured with the Teichholz method in *M*-Mode one week after myocardial infarction in the control (n = 3) and cold (n = 3) group, with no difference between the groups, measured with an unpaired, two-tailed *t*-test.

between EF and effective cooling of the left ventricle as previously published (Marek-Iannucci et al., 2019). Furthermore, by using echocardiography our group published a significant increase in E′, a reduced E/E′ and left atrial pressure (LAP) in the cold group compared to the warm, suggesting improved diastolic function, when using this technique (Marek-Iannucci et al., 2019). With this method we were also able to demonstrate a significant reduction in Troponin I levels in the blood one week after MI in the cold compared to the warm group, as well as a reduction of neutral lipid droplets in the myocardium measured by electron microscopy, both reflecting a reduction in ischemic tissue injury as previously reported (Marek-Iannucci et al., 2019).

Blood analysis 3 h post MI showed a significant reduction of cardiac troponin I ($p < 0.05$); consistent with that, creatinine kinase and lactate dehydrogenase also trended lower in the cold (**Figures 2E–G**). Lastly, EM images of LV septal biopsies 3 h post MI showed a significant reduction of neutral lipid droplets ($p < 0.05$) correlating with tissue injury.

All animals had a minimal pericardial effusion with a maximal width of 1 mm without impairment of cardiac function. Furthermore, pressure measurements with a Swan-Ganz-catheter one week after survival were within the normal range in all animals (**Table 3**).

TABLE 3 | Right heart catheter (Swan-Ganz-catheter) measurements one week after MI and prior to euthanizing the animals for tissue harvest.

	Syst *P*		Diast *P*	
	mean	***SEM***	***mean***	***SEM***
Warm (*n* = 3)				
RA	6.67	*0.33*	2.67	*1.33*
RV	22.33	*1.20*	5.33	*1.20*
Ao	63.00	*1.73*	37.67	*0.67*
Cold (*n* = 3)				
RA	6.33	*0.88*	3.00	*0.00*
RV	22.00	*1.53*	5.67	*0.67*
Ao	63.33	*1.76*	37.00	*5.51*

The values represent pressure measurements in the right atrium (RA), right ventricle (RV), and the ascending aorta (Ao) in mmHg.

DISCUSSION

To our knowledge this is the first local pericardial cooling model in a large animal. Dave et al. (1998) described a similar method in rabbits in 1998, with the disadvantage of requiring a specifically designed catheter for implementation. Furthermore, their group focused on myocardial infarct size reduction, without seeking to investigate the molecular mechanisms implicated in adverse remodeling after ischemia/reperfusion injury. Additionally, in their study the pericardium was perfused 30 min prior to infarction, making it a preconditioning model, which is not translatable to the clinical setting. Most prior studies have focused on treatment with hypothermia prior to, or few minutes after occlusion, and Hale et al. suggested that hypothermic treatment should be started prior to reperfusion to be effective (Hale and Kloner, 2011). TH has been studied in animals for decades and various models have been implemented. Kloner et al. developed a whole-body cooling method (Thermosuit®), with the capability of reducing the core body temperature to moderate hypothermia (Dai et al., 2015; Rezkalla et al., 2017; Shi et al., 2017). Other non-invasive models include cooling blankets, tested in rabbits, as well as convective immersion therapy (Herring et al., 2014). On the other hand, many invasive models have been established. Topical regional hypothermia was obtained with bags of iced saline, directly applied onto the outer surface of the heart in an open chest model in rabbits (Herring et al., 2014). Similarly, Dai et al. used a circuit to pump cold fluid directly into the thoracic cavity of rodents (Dai et al., 2017). Furthermore, studies showed the efficacy of retrograde blood cardioplegia and endovascular cooling, with a heat exchange balloon placed in the inferior vena cava in rodents (Kamlot et al., 1997; Herring et al., 2014). Other invasive approaches have been total liquid ventilation in Rabbits undergoing open chest surgery, as well as cold sterile saline infusion in swine (Herring et al., 2014), the latter being the only large animal model used for TH so far. From these studies we know that the time, temperature, and duration of TH application are crucial for the effects on the myocardium (Erlinge et al., 2013; Erlinge et al., 2014).

Our study is the first to prove that hypothermic treatment after coronary reperfusion is as effective as preconditioning or cold irrigation during ischemia, making this a clinically translatable model. This is demonstrated by the significant reduction of systemic temperature after the procedure, ensuring that the myocardium was affected in its entire thickness. The efficacy of this model can be underlined by a significant reduction of the temperature of the left ventricle, directly measured with a temperature probe inserted into the ventricle, as previously published (Marek-Iannucci et al., 2019). Furthermore, our previous study using this novel technique, demonstrated

that Corrected TIMI frame count (CTFC), was significantly reduced after MI combined with pericardial irrigation in the cold compared to the warm group, with a strong correlation between ventricular cooling and CTFC, reflecting improved coronary reflow after MI (Marek-Iannucci et al., 2019). This is consistent with other studies demonstrating a beneficial effect of TH on the endothelium (Stamler et al., 1996). The fact that we cannot detect a difference in EF one week after MI is consistent with our previously published paper, as well as other studies, demonstrating that to detect substantial differences in ventricular function due to remodeling after MI, a longer follow-up (beginning at 4 weeks post MI) is required (Pokorney et al., 2012; Marek-Iannucci et al., 2019). In fact, by using this newly established large animal model, we showed significant beneficial effects on EF with local TH treatment four weeks after MI (Marek-Iannucci et al., 2019). Furthermore, by using this technique, were able to detect a significant reduction in local inflammation and fibrosis of the myocardium in the cold compared to the warm group, measured by immunohistochemistry with iNos, Arginase-1 and Picrosirius red staining respectively. Additionally, we observed a reduction in apoptotic cells in the myocardium of the cold group compared to the warm, as previously reported (Marek-Iannucci et al., 2019). Also, we previously demonstrated that this technique leads to a significant reduction of tissue stress markers in the myocardium, such as GRP78, HSP90, and HSP70, in the cold compared to the warm group, measured by western blotting (Marek-Iannucci et al., 2019). More importantly our previously published data demonstrates a significant increase in autophagic flux in the myocardium after cold pericardial irrigation, compared to the warm group, as well as a significant increase in spare respiratory capacity of the mitochondria, measured by respirometry. This suggests a more efficient cell renewal and more oxidative phosphorylation machinery per mitochondrion respectfully (Marek-Iannucci et al., 2019).

Furthermore, all pressure measurements, performed with a Swan-Ganz-catheter one week post MI, were within the normal range, demonstrating that the minimal amount of pericardial effusion remaining post procedure does not compromise contractile function, which was also confirmed by echocardiography (Kearns and Walley, 2018). Even if TH might not be directly implementable into the clinical setting with the existing animal models, it still remains an important tool to further study the underlying mechanisms of adverse remodeling after ischemia/reperfusion injury. The focus is to decipher possible new targets which can be therapeutically manipulated to reduce adverse remodeling and prevent progressive heart failure. The latter is known to be an independent prognostic factor for hospitalization and mortality, with an important socioeconomic burden for the health care system and remains a leading cause of death (Cohn et al., 2000; Wang et al., 2018). The introduction of Neprilysin-inhibitors is the first new substance group added to a well-established but stagnating therapeutic strategy for decades (McMurray et al., 2014). This underlines the necessity of further studies focusing on the molecular mechanisms behind adverse remodeling after ischemia/reperfusion injury, to broaden the therapeutic possibilities and eventually prevent progressive chronic heart failure.

To conclude, not only is our model very cost effective, with standard materials easily acquirable, it is also the first model in swine making it an important clinically translational model. It is well known that the physiology and coronary anatomy of swine very much resemble human. Furthermore, it is the first model that applied hypothermia to the heart after reperfusion with a long term survival. This model can be used for further studies on TH and its effects on myocardial adverse remodeling, as well as direct application of drugs or other agents influencing the latter.

DATA AVAILABILITY STATEMENT

All datasets generated for this study are included in the article/**Supplementary Material**.

ETHICS STATEMENT

Animal studies were conducted under a protocol approved by the Cedars-Sinai Medical Center Institutional Animal Care and Use Committee (IACUC).

AUTHOR CONTRIBUTIONS

SM-I developed the model and performed the experiments. AT helped with the experiments and design of this manuscript. RG was the main PI and mentor of this project.

FUNDING

Funding was a program project grant (P01-HL112730) awarded by the National Institutes of Health: Mitochondrial Quality in Cardioprotection: Overcoming Co-Morbidities to principal investigator RG.

ACKNOWLEDGMENTS

The authors acknowledge the Dorothy and E. Phillip Lyon Endowed Chair in Molecular Cardiology (to RG).

SUPPLEMENTARY MATERIAL

The Supplementary Material for this article can be found online at: https://www.frontiersin.org/articles/10.3389/fphys.2020.00346/full#supplementary-material

FIGURE S1 | Visualization of the guide wire used for pericardial puncture (provided with the dialysis catheter set).

FIGURE S2 | Insertion on the dual lumen dialysis catheter (Mahurkar-Elite, Medtronic®, Dublin, Ireland), under continuous fluoroscopic control and consecutive injection of minimal amount of dye.

FIGURE S3 | Injection of dye into the dual lumen dialysis catheter (Mahurkar-Elite, Medtronic®, Dublin, Ireland), under continuous fluoroscopic control to ensure correct placement.

FIGURE S4 | Visualization of the dual lumen dialysis catheter (Mahurkar-Elite, Medtronic®, Dublin, Ireland), and the temperature probe inside the pericardium under continuous fluoroscopic control to ensure correct placement.

FIGURE S5 | Visualization of the temperature probe, inserted percutaneously under fluoroscopic control into the left ventricle wall, allowing continuous temperature measurement.

REFERENCES

Bouleti, C., Mewton, N., and Germain, S. (2015). The no-reflow phenomenon: state of the art. *Arch. Cardiovasc. Dis.* 108, 661–674. doi: 10.1016/j.acvd.2015.09.006

Cohn, J. N., Ferrari, R., and Sharpe, N. (2000). Cardiac remodeling–concepts and clinical implications: a consensus paper from an international forum on cardiac remodeling. Behalf of an International Forum on Cardiac Remodeling. *J. Am. Coll. Cardiol.* 35, 569–582.

Dai, W., Hale, S., and Kloner, R. A. (2017). Delayed therapeutic hypothermia protects against the myocardial no-reflow phenomenon independently of myocardial infarct size in a rat ischemia/reperfusion model. *Int. J. Cardiol.* 236, 400–404. doi: 10.1016/j.ijcard.2017.01.079

Dai, W., Herring, M. J., Hale, S. L., and Kloner, R. A. (2015). Rapid surface cooling by thermosuit system dramatically reduces scar size, prevents post-infarction adverse left ventricular remodeling, and improves cardiac function in rats. *J. Am. Heart Assoc.* 4:e002265. doi: 10.1161/JAHA.115.002265

Dave, R. H., Hale, S. L., and Kloner, R. A. (1998). Hypothermic, closed circuit pericardioperfusion: a potential cardioprotective technique in acute regional ischemia. *J. Am. Coll. Cardiol.* 31, 1667–1671.

Erlinge, D., Götberg, M., Grines, C., Dixon, S., Baran, K., Kandzari, D., et al. (2013). A pooled analysis of the effect of endovascular cooling on infarct size in patients with ST-elevation myocardial infarction. *Eurointervention* 8, 1435–1440. doi: 10.4244/EIJV8I12A217

Erlinge, D., Götberg, M., Lang, I., Holzer, M., Noc, M., Clemmensen, P., et al. (2014). Rapid endovascular catheter core cooling combined with cold saline as an adjunct to percutaneous coronary intervention for the treatment of acute myocardial infarction. The CHILL-MI trial: a randomized controlled study of the use of central venous catheter core cooling combined with cold saline as an adjunct to percutaneous coronary intervention for the treatment of acute myocardial infarction. *J. Am. Coll. Cardiol.* 63, 1857–1865. doi: 10.1016/j.jacc.2013.12.027

Erlinge, D., Götberg, M., Noc, M., Lang, I., Holzer, M., Clemmensen, P., et al. (2015). Therapeutic hypothermia for the treatment of acute myocardial infarction-combined analysis of the RAPID MI-ICE and the CHILL-MI trials. *Ther. Hypothermia Temp. Manag.* 5, 77–84.

Hale, S. L., and Kloner, R. A. (2011). Mild hypothermia as a cardioprotective approach for acute myocardial infarction: laboratory to clinical application. *J. Cardiovasc. Pharmacol. Ther.* 16, 131–139. doi: 10.1177/1074248410387280

Haugk, M., Testori, C., Sterz, F., Uranitsch, M., Holzer, M., Behringer, W., et al. (2011). Relationship between time to target temperature and outcome in patients treated with therapeutic hypothermia after cardiac arrest. *Crit. Care* 15:R101.

Hausenloy, D. J. (2012). Magnitude and relevance of reperfusion injury. *Heart Metab.* 54, 5–8.

Herring, M. J., Hale, S. L., Dai, W., Oskui, P. M., and Kloner, R. A. (2014). Hypothermia in the setting of experimental acute myocardial infarction: a comprehensive review. *Ther. Hypothermia Temp. Manag.* 4, 159–167. doi: 10.1089/ther.2014.0016

Kamlot, A., Bellows, S. D., Simkhovich, B. Z., Hale, S. L., Aoki, A., Kloner, R. A., et al. (1997). Is warm retrograde blood cardioplegia better than cold for myocardial protection? *Ann. Thorac. Surg.* 63, 98–104.

Kaul, S. (2014). The "no reflow" phenomenon following acute myocardial infarction: mechanisms and treatment options. *J. Cardiol.* 64, 77–85. doi: 10.1016/j.jjcc.2014.03.008

Kearns, M. J., and Walley, K. R. (2018). Tamponade: hemodynamic and echocardiographic diagnosis. *Chest* 153, 1266–1275. doi: 10.1016/j.chest.2017.11.003

Kloner, R. A. (2011). No-reflow phenomenon: maintaining vascular integrity. *J. Cardiovasc. Pharmacol. Ther.* 16, 244–250. doi: 10.1177/1074248411405990

Kloner, R. A., Ganote, C. E., and Jennings, R. B. (1974). The "no-reflow" phenomenon after temporary coronary occlusion in the dog. *J. Clin. Invest.* 54, 1496–1508.

Kloner, R. A., Hale, S. L., Dai, W., and Shi, J. (2017). Cardioprotection: where to from here? *Cardiovasc. Drugs Ther.* 31, 53–61.

Marek-Iannucci, S., Thomas, A., Hou, J., Crupi, A. N., Sin, J., Esmailian, F., et al. (2019). Myocardial hypothermia increases autophagic flux, mitochondrial mass and myocardial function after ischemia-reperfusion injury. *Sci. Rep.* 9:10001. doi: 10.1038/s41598-019-46452-w

McMurray, J. J., Packer, M., Desai, A. S., Gong, J., Lefkowitz, M. P., Rizkala, A. R., et al. (2014). Angiotensin-neprilysin inhibition versus enalapril in heart failure. *N. Engl. J. Med.* 371, 993–1004.

Mohammad, M. A., Noc, M., Lang, I., Holzer, M., Clemmensen, P., Jensen, U., et al. (2017). Proteomics in hypothermia as adjunctive therapy in patients with ST-segment elevation myocardial infarction: a CHILL-MI substudy. *Ther. Hypothermia Temp. Manag.* 7, 152–161. doi: 10.1089/ther.2016.0041

Nichol, G., Strickland, W., Shavelle, D., Maehara, A., Ben-Yehuda, O., Genereux, P., et al. (2015). Prospective, multicenter, randomized, controlled pilot trial of peritoneal hypothermia in patients with ST-segment-elevation myocardial infarction. *Circ. Cardiovasc. Interv.* 8:e001965. doi: 10.1161/CIRCINTERVENTIONS.114.001965

Pokorney, S. D., Rodriguez, J. F., Ortiz, J. T., Lee, D. C., Bonow, R. O., and Wu, E. (2012). Infarct healing is a dynamic process following acute myocardial infarction. *J. Cardiovasc. Magn. Reson.* 14:62. doi: 10.1186/1532-429X-14-62

Rezkalla, S. H., Stankowski, R. V., Hanna, J., and Kloner, R. A. (2017). Management of no-reflow phenomenon in the catheterization laboratory. *JACC Cardiovasc. Interv.* 10, 215–223.

Rochitte, C. E. (2008). Microvascular obstruction the final frontier for a complete myocardial reperfusion. *J. Am. Coll. Cardiol.* 51, 2239–2240.

Schirone, L., Forte, M., Palmerio, S., Yee, D., Nocella, C., Angelini, F., et al. (2017). A review of the molecular mechanisms underlying the development and progression of cardiac remodeling. *Oxid. Med. Cell Longev.* 2017:3920195. doi: 10.1155/2017/3920195

Shi, J., Dai, W., and Kloner, R. A. (2017). Therapeutic hypothermia reduces the inflammatory response following ischemia/reperfusion injury in rat hearts. *Ther. Hypothermia Temp. Manag.* 7, 162–170. doi: 10.1089/ther.2016.0042

Spiel, A. O., Kliegel, A., Janata, A., Uray, T., Mayr, F. B., Laggner, A. N., et al. (2009). Hemostasis in cardiac arrest patients treated with mild hypothermia initiated by cold fluids. *Resuscitation* 80, 762–765. doi: 10.1016/j.resuscitation.2009.03.026

Stamler, A., Wang, S. Y., Li, J., Thurer, R. L., Schoen, F. J., and Sellke, F. W. (1996). Moderate hypothermia reduces cardiopulmonary bypass-induced impairment of cerebrovascular responses to platelet products. *Ann. Thorac. Surg.* 62, 191–198.

Wang, B., Nie, J., Wu, L., Hu, Y., Wen, Z., Dong, L., et al. (2018). AMPKalpha2 protects against the development of heart failure by enhancing mitophagy via PINK1 phosphorylation. *Circ. Res.* 122, 712–729. doi: 10.1161/CIRCRESAHA.117.312317

Conflict of Interest: The authors declare that the research was conducted in the absence of any commercial or financial relationships that could be construed as a potential conflict of interest.

frontiers in Physiology

REVIEW
published: 06 May 2020
doi: 10.3389/fphys.2020.00416

Cardiac Fibrosis and Cardiac Fibroblast Lineage-Tracing: Recent Advances

Xing Fu, Qianglin Liu, Chaoyang Li, Yuxia Li and Leshan Wang*

School of Animal Sciences, Louisiana State University Agricultural Center, Baton Rouge, LA, United States

Cardiac fibrosis is a common pathological change associated with cardiac injuries and diseases. Even though the accumulation of collagens and other extracellular matrix (ECM) proteins may have some protective effects in certain situations, prolonged fibrosis usually negatively affects cardiac function and often leads to deleterious consequences. While the development of cardiac fibrosis involves several cell types, the major source of ECM proteins is cardiac fibroblast. The high plasticity of cardiac fibroblasts enables them to quickly change their behaviors in response to injury and transition between several differentiation states. However, the study of cardiac fibroblasts *in vivo* was very difficult due to the lack of specific research tools. The development of cardiac fibroblast lineage-tracing mouse lines has greatly promoted cardiac fibrosis research. In this article, we review the recent cardiac fibroblast lineage-tracing studies exploring the origin of cardiac fibroblasts and their complicated roles in cardiac fibrosis, and briefly discuss the translational potential of basic cardiac fibroblast researches.

Keywords: cardiac fibroblast, lineage-tracing, fibrosis, heart, cardiac disease

OPEN ACCESS

Edited by:
Gianluigi Pironti,
Karolinska Institutet, Sweden

Reviewed by:
Yaoliang Tang,
Augusta University, United States
Daniel G. Donner,
Baker Heart and Diabetes Institute, Australia

****Correspondence:***
Xing Fu
xfu1@agcenter.lsu.edu

Specialty section:
This article was submitted to Integrative Physiology, a section of the journal Frontiers in Physiology

Received: *20 December 2019*
Accepted: *06 April 2020*
Published: *06 May 2020*

Citation:
Fu X, Liu Q, Li C, Li Y and Wang L (2020) Cardiac Fibrosis and Cardiac Fibroblast Lineage-Tracing: Recent Advances. Front. Physiol. 11:416. doi: 10.3389/fphys.2020.00416

INTRODUCTION

Cardiac fibrosis is commonly associated with cardiovascular diseases (CVDs), the leading cause of death in western countries. In the United States, the direct health expenditures and lost productivity associated with CVDs in 2010 was estimated to be $315.4 billion (Go et al., 2014). Cardiac fibrosis is mainly present in two forms which are replacement fibrosis and interstitial fibrosis. Replacement fibrosis is characterized by the formation of collagenous scar tissue replacing the dead cardiomyocytes, which is often observed after myocardial infarction (MI) (Segura et al., 2014). Interstitial fibrosis, in contrast, usually does not involve massive cardiomyocyte death and is characterized by the accumulation of ECM proteins in the interstitial space between cardiomyocytes, which may be caused by pressure overload and infection (Fenoglio et al., 1983; Creemers and Pinto, 2010). In both forms of cardiac fibrosis, the activation of cardiac fibroblasts is involved (Ivey et al., 2018). The mechanical stress and inflammation stimulate cardiac fibroblast proliferation and promote their differentiation into myofibroblasts with elevated expression of ECM proteins (Ivey and Tallquist, 2016; Tallquist and Molkentin, 2017). Besides the accumulated ECM which stiffens the heart, the fibrotic tissue and activated fibroblasts also affect the contraction of adjacent cardiomyocytes, leading to the reduction of cardiac function (Kong et al., 2014). However, despite the deleterious effects of fibrosis on cardiac function, the accumulated ECM and myofibroblasts filled with stress fibers may play an important role in maintaining tissue integrity especially when a substantial death of cardiomyocytes occurs (Talman and Ruskoaho, 2016).

In addition, cardiac fibroblasts may also regulate cardiac function through cross-talking with other cell types residing in the heart such as cardiomyocytes (Zhang et al., 2012) and immune cells (Van Linthout et al., 2014). Due to the complicated role of cardiac fibroblasts in the diseased heart, manipulation of cardiac fibroblast activities to promote their beneficial effects and limit their deleterious effects is needed, which requires a complete understanding of the regulation of cardiac fibroblast activities. The development of cardiac fibroblast lineage-tracing mouse lines promoted researches addressing many fundamental questions about cardiac fibroblast. This review summarizes the recent advances in cardiac fibroblast lineage-tracing and the findings resulted from researches utilizing these tools. The clinical implication of cardiac fibroblast lineage-tracing studies is also briefly discussed.

CARDIAC FIBROBLAST MARKERS

By definition, fibroblasts are a group of cells secreting collagen and other ECM proteins. They reside in the interstitial spaces between tissue parenchymal cells. Under basal conditions, these cells stay mostly quiescent and likely play important roles in maintaining the interstitial connective tissue and mediating the communication between surrounding cells (Ivey and Tallquist, 2016; Tallquist and Molkentin, 2017). Under stressed conditions, their production of ECM proteins significantly increases, which is responsible for the formation of fibrotic tissue (Souders et al., 2009; Ivey and Tallquist, 2016; Tallquist and Molkentin, 2017). Thus, many identified fibroblast markers are ECM proteins. Some ECM proteins highly expressed by fibroblasts are fibrillar collagens such as collagen I and collagen III and fibronectin (Carver et al., 1991; Philips et al., 1994). The expression of these ECM proteins significantly increases after the differentiation of cardiac fibroblasts into myofibroblasts (Baum and Duffy, 2011). In addition, myofibroblasts express some unique ECM proteins such as periostin (Conway and Molkentin, 2008; Shimazaki et al., 2008), and ECM remodeling enzymes such as matrix metalloproteases (MMPs), tissue inhibitors of metalloproteinases (TIMPs), and lysyl oxidase (LOX) (Polyakova et al., 2004; Brown et al., 2007; Fan et al., 2012; Lindner et al., 2012; El Hajj et al., 2017). Similar to other types of cells, a cytoskeletal network is present in fibroblasts. While many components in this network are common proteins also expressed in other cell types, some of them have been used as fibroblast markers due to their unique expression in fibroblasts. Vimentin, an intermediate filament protein, is abundant in both quiescent fibroblasts and myofibroblasts (Wang et al., 2003; Baum and Duffy, 2011). In contrast, smooth muscle α-actin (αSMA, encoded by *Acta2*) is exclusively expressed after myofibroblast differentiation (Leslie et al., 1991). Another group of fibroblast markers are transcription factors that are specifically expressed in fibroblasts. Transcription factors that have been used as cardiac fibroblast markers include Tcf21, WT1, Tbx18, and Tie2 (Quaggin et al., 1999; Cai et al., 2008; Zeisberg and Kalluri, 2010; Zhou and Pu, 2012; Moore-Morris et al., 2014). Developmentally, epicardial fibroblast progenitors express Tcf21, WT1, and Tbx18, while Tie2 expression has only been identified in endocardial cardiac fibroblast progenitors. Studies have also reported cell surface markers of fibroblasts, which are important due to their potential use in cell sorting (Smith et al., 2011; Asli et al., 2019). Among these identified cell surface markers, platelet-derived growth factor receptor alpha (PDGFRα) is the most widely used that is abundantly expressed in fibroblasts found in various tissues (Smith et al., 2011; Asli et al., 2019). Other cell surface markers that have been reported to be expressed by fibroblasts include NG2 and PDGFRβ which, however, are primarily expressed in pericytes which are fibroblast-like cells associated with blood vessels (Chen et al., 2016).

CARDIAC FIBROBLAST LINEAGE-TRACING SYSTEMS AND TOOLS

The definition of lineage-tracing is the identification of all progeny of a single cell or cell population. The principle of lineage-tracing is that the expression of reporter genes under the control of the *cis*-regulatory elements of a gene that is specifically expressed in a cell type permits the identification of this cell population and its descendants. Thus, the identification of fibroblast markers has facilitated the development of some fibroblast lineage-tracing tools. However, not all previously identified fibroblast markers are suitable for fibroblast lineage-tracing because most of those markers are not exclusive to cardiac fibroblasts. The currently widely used lineage-tracing systems can be classified into two categories. The first category utilizes a reporter gene, such as GFP, directly controlled by a tissue-specific promoter or locus, which is referred to as direct lineage-tracing in this article. The reporter gene can be introduced into the genome as a transgene together with a tissue-specific promoter or inserted into a tissue-specific locus (knock-in) (Hamilton et al., 2003; LeBleu et al., 2013). The other category employs the Cre-loxP recombination system (Sauer, 1998) which includes two components, a Cre recombinase (Cre) gene driven by a tissue-specific promoter/locus and a reporter gene downstream of a stop codon flanked by two loxP sites (Soriano, 1999). The expression of Cre induces the deletion of the stop codon between the two loxP sites, leading to the expression of the reporter gene, which is thus referred to as indirect lineage-tracing. Similarly, Cre can be introduced into the genome together with a tissue-specific promoter as a transgene or knocked into a specific tissue-specific locus. In the Cre-loxP system, the reporter gene is usually inserted into the ROSA26 locus and under the control of a strong promoter (Madisen et al., 2010). Multiple Cre isoforms have been developed by different researchers. While the original Cre becomes active once being expressed (Soriano, 1999), the Cre mutants fused to one (CreERT and CreERT2) or two (MerCreMer) mutated murine estrogen-binding domains are only active when bound to 4-hydroxy-tamoxifen (Metzger et al., 1995; Zhang et al., 1996; Indra et al., 1999). CreERT2 is the second generation of tamoxifen-inducible Cre developed based on CreERT and is

more sensitive to 4-hydroxy-tamoxifen as compared to CreERT (Indra et al., 1999). The MerCreMer mediates more stringent recombination likely because each MerCreMer requires two, rather than one, 4-hydroxy-tamoxifen molecules for activation (Verrou et al., 1999).

The major advantage of the direct control of the report gene expression by a tissue-specific promoter/locus is that the expression level of the reporter usually reflects the promoter activity, which enables the tracking of the expression of the tissue-specific gene. However, when the activity of the tissue-specific promoter is low, the expression of the reporter may not be strong enough for certain experiments. In addition, the activity of some promoters or loci may totally disappear or start in a particular developmental or disease stage. Thus, the reporter-labeled cells identified at a time point may not be the same population of cells observed at an earlier time point or their descendants. Examples of this system include α*SMA-RFP* mice (Magness et al., 2004), *Col1a1-GFP* mice (Kalajzic et al., 2002; Yata et al., 2003), *Tcf21-lacZ* (Quaggin et al., 1999), *Pdgfra-GFP* (Hamilton et al., 2003), and *Postn-lacZ* (Snider et al., 2008). In contrast to the direct lineage-tracing system, one common advantage of the indirect lineage-tracing system is that the expression of the reporter in a cell and all its descendants is permanent once the recombination has taken place regardless of the change in the activity of the promoter driving the Cre, which is favored in some studies. Lineage-tracing mouse lines of this category that have been used in cardiac fibroblast studies include *Acta2-CreERT2* (Wendling et al., 2009), *Col1a2-CreERT* (Ubil et al., 2014), *Col1a1-CreERT2* (Biswas, 2016), *Postn-CreERT2* (Kaur et al., 2016), *Tbx18-Cre* (Cai et al., 2008), *Tbx18-CreERT2* (Moore-Morris et al., 2014), *Tcf21-Cre* (Acharya et al., 2011), *Tcf21-MerCreMer* (Acharya et al., 2011), *Tie2-Cre* (Kisanuki et al., 2001), *Sox9-CreER* (He et al., 2017), *WT1-Cre* (Moore-Morris et al., 2014), and *WT1-CreERT2* (Ali et al., 2014; Moore-Morris et al., 2014). The choice between a non-inducible Cre and an inducible Cre depends on the goal of the study. A unique feature of the lineage-tracing system using non-inducible Cre is that the reporter expression starts once the promoter driving the Cre becomes active. This can be an advantage in some developmental studies focusing on the fate of cells derived from an embryonic lineage. However, such a feature can be a problem in some studies aimed at lineage-tracing cells expressing a certain gene at a particular time point as some of the lineage-traced cells observed in non-inducible Cre lines may be a result of a previous recombination and may no longer express the gene whose promoter drives the Cre, which may lead to a false conclusion. The inducible Cre, on the other hand, allows the timely control of recombination. A drawback of the inducible Cre is the lower recombination efficiency as compared with non-inducible Cre. Repeated or continuous tamoxifen treatment is required to induce sufficient recombination. However, some side effects associated with tamoxifen have been reported and may affect the experimental result. In particular, tamoxifen often induces dystocia when applied to pregnant female mice (Narver, 2012). The retrieval of the pups requires cesarean sections which are very labor-intense. Moreover, it has been shown that tamoxifen can induce physiological changes such as the browning of adipose tissue in female mice (Zhao et al., 2019), likely due to its anti-estrogenic activity, which may affect the experimental results.

As mentioned previously in this article, both the reporter gene in the direct lineage-tracing system and the Cre in the indirect lineage-tracing system can be introduced into the animal together with the promoter as a transgene randomly inserted into the genome or specifically knocked into a locus that is only active in certain cell type. Some examples of the mouse lines generated using the transgene strategy are α*SMA-RFP* (Magness et al., 2004), *Col1a1-GFP* (Kalajzic et al., 2002; Yata et al., 2003), *Col1a2-CreERT* (Ubil et al., 2014), *Col1a1-CreERT2* (Biswas, 2016), *Tie2-Cre* (Kisanuki et al., 2001), and α*SMA-CreERT2* (Wendling et al., 2009). The major advantage of the transgene strategy is that it is relatively simple to generate a lineage-tracing mouse line in this way. However, the efficiency and reliability of these lines vary significantly. The reason is that the included promoter may lack certain regulatory elements. For example, among the 3 *Col1a1-GFP* mouse lines, only the one containing the collagen gene promoter (−3122 to +111) and upstream DNase I-hypersensitive sites has been shown to specifically and efficiently label cardiac fibroblasts (Yata et al., 2003), while GFP expression was absent in the heart of the other *Col1a1-GFP* mouse lines (Kalajzic et al., 2002). Moreover, α*SMA-CreERT2* efficiently induced reporter expression in cardiac myofibroblast after MI (Fu et al., 2018), however, the α*SMA-RFP* mouse line failed to do so (personal experience). In addition, the random insertion of the transgene may disrupt endogenous gene expression causing unintended mutation. In contrast, the knock-in strategy usually allows the precise control of the reporter or Cre expression by the endogenous tissue-specific locus, which is desired in most lineage-tracing studies. Examples of cardiac fibroblast lineage-tracing mouse lines created using this strategy include *Postn-CreERT2* (Kaur et al., 2016), *Tbx18-Cre* (Cai et al., 2008), *Tbx18-CreERT2* (Moore-Morris et al., 2014), *Tcf21-Cre* (Acharya et al., 2011), *Tcf21-MerCreMer* (Acharya et al., 2011), *Postn-MerCreMer* (Kanisicak et al., 2016), *WT1-Cre* (Moore-Morris et al., 2014), and *WT1-CreERT2* (Ali et al., 2014; Moore-Morris et al., 2014). However, the knock-in of the Cre also abolishes the expression of the endogenous gene expression from the disrupted allele. Even though homozygous knockout can be avoided through genotyping, the heterozygous knockout may also have a milder effect.

Recently, the Dre-rox, a system similar to Cre-loxP (Anastassiadis et al., 2009), has been applied in lineage-tracing studies of cardiac fibroblasts and other cell types (He et al., 2017; Pu et al., 2018). The expression of Dre induces the recombination of rox sites, resulting in the expression or knockout of a gene. In addition to the original Dre allele, Dre fused to murine estrogen-binding domains has also being generated, which enables tamoxifen-dependent Dre activity (He et al., 2017). More important, due to the high specificity of Cre-loxP and Dre-rox systems, the dual lineage-tracing combining these two systems is a recent trend in lineage-tracing studies. Mice carrying both Cre-loxP and Dre-rox permit the simultaneous tracing of two distinct or related cell types (Liu et al., 2019). These mice

may be particularly useful in the study of cardiac fibroblast differentiation and transdifferentiation when the precursor cells and their descendants express different marker genes.

Besides the use of cardiac fibroblast lineage-tracing mouse lines to understand the origin of cardiac fibroblasts and their cell fate changes in response to cardiac injuries, an equally, if not more, important application of these tools is the study of mechanisms regulating cardiac fibroblast activities after injuries and their therapeutic potentials. When cross-bred with a mouse line carrying a gene with its essential exon(s) flanked by *loxP* sites or a Cre-dependent gene overexpression cassette containing a 5′ *loxP*-flanked stop sequence, cardiac fibroblast-specific knockout or overexpression of the gene can be achieved *in vivo*. Importantly, even though many of the aforementioned Cre lines have been utilized to study the cardiac fibroblast-specific functions of genes, they do have different advantages and limitations largely due to the variation in the activities of promoters driving Cre expression. For example. *Tcf21-MerCreMer* mouse line has been successfully employed to lineage-trace cardiac fibroblasts during development and in normal hearts and study cardiac fibroblast differentiation after cardiac injuries (Acharya et al., 2011; Kanisicak et al., 2016; Khalil et al., 2017; Ivey et al., 2018). However, the ability of this line to specifically induce gene knockout or overexpression in myofibroblasts may be limited as the expression of *Tcf21* in cardiac fibroblasts dramatically decreases during myofibroblast differentiation (Fu et al., 2018). As a result, pre-injury tamoxifen treatment to mouse lines carrying *Tcf21-MerCreMer* is usually required for successful and efficient recombination (Khalil et al., 2017; Xiang et al., 2017). However, the myofibroblast-specific expression of the target genes may render pre-injury tamoxifen treatment less efficient in these lines, as the condensed chromatin may reduce the accessibility of Cre to *loxP* sites in the genes that are not being actively expressed. In contrast, mouse lines such as *Postn-MerCreMer* and *Col1a2-CreERT2* are likely more efficient in inducing gene knockout and overexpression in myofibroblasts due to their high level of expression in these cells (Fu et al., 2018). And combining two Cre lines, such as *Tcf21-MerCreMer* and *Postn-MerCreMer* may grant more efficient and complete recombination in cardiac fibroblasts of different states.

THE DEVELOPMENTAL ORIGIN OF CARDIAC FIBROBLASTS

One of the most important fundamental questions about cardiac fibroblasts is their developmental origin. Studies utilizing *Tcf21* (*Tcf21-MerCreMer*), *Wt1* (*Wt1-Cre*), and *Tbx18* (*Tbx18-Cre*) *cis*-regulatory elements-controlled lineage-tracing mouse lines have shown that epicardial progenitors give rise to both cardiac fibroblasts and vascular smooth muscle cells developmentally (Cai et al., 2008; Zhou et al., 2008; Smith et al., 2011; Acharya et al., 2012; Moore-Morris et al., 2014), which is consistent with earlier experiments conducted using chick embryos (Mikawa and Gourdie, 1996). In mice, these epicardial cardiac fibroblast progenitors express PDGFRα and start the epithelial-to-mesenchymal transition (EMT) around embryonic day 14.5 (E14.5). Disruption of PDGFRα, Wt1, or Tcf21 signaling caused significantly defects in this process (Moore et al., 1999; Smith et al., 2011; Acharya et al., 2012). The requirement of Tbx18 in this process, however, has not been revealed. Using the *Tie2-Cre* lineage-tracing mouse line, it was shown that some cardiac fibroblasts were derived from endocardium through the endothelial-to-mesenchymal transition (EndoMT) (Kisanuki et al., 2001; Ali et al., 2014). In mouse heart, the EndoMT process of *Tie2* lineage-traced endocardial cells first starts around E11.5 day in the outflow septum (Kisanuki et al., 2001). It was estimated that around 85% of cardiac fibroblasts are derived from epicardial cells, while the other ∼15% are derived from endothelial cells (Moore-Morris et al., 2014). Moreover, a difference in the spatial distribution of these two cardiac fibroblast subpopulations has been noticed. While endocardium-derived cardiac fibroblasts are more prevalent in the interventricular septum, the ones derived from epicardium are more dominant in the left ventricular free wall (Moore-Morris et al., 2014). It is worth noting that the *Wt1-Cre* mice and *Tie2-Cre* mice used in this study also labeled cardiomyocytes and endothelial cells, respectively. Moreover, experiments treating adult *Tcf21-MerCreMer*, *WT1-CreERT2*, and *Tbx18-CreERT2* mice with tamoxifen showed that only *Tcf21* was still expressed in adult cardiac fibroblast while the lineage-traced cells in *WT1-CreERT2* and *Tbx18-CreERT2* mice were primarily epicardial cells (Moore-Morris et al., 2014), indicating the limitations of some of these lines.

CARDIAC FIBROBLAST ORIGIN IN THE DISEASED HEART

Many heart diseases trigger cardiac fibrosis. Both interstitial fibrosis and replacement fibrosis involves the activation of cardiac fibroblasts and their differentiation into myofibroblasts. As the major fibroblast lineages in the normal heart, it is not a surprise that endocardium and epicardium-derived resident cardiac fibroblasts are also the major contributors to the cardiac myofibroblast population in the injured heart (Ali et al., 2014; Moore-Morris et al., 2014; Kanisicak et al., 2016; Fu et al., 2018). Dramatic changes in cellular composition happen in the diseased heart. A question asked by many researchers is whether epicardial and endocardial cells in the adult heart still have the ability to transdifferentiate into cardiac fibroblasts in response to injury. While earlier studies suggested the existence of EMT in the adult heart (van Tuyn et al., 2007; Russell et al., 2011; Zhou and Pu, 2011; Duan et al., 2012), careful lineage-tracing studies using *WT1-CreERT2* and *Tbx18-CreERT2* mouse lines found that the adult epicardial cells do not give rise to cardiac fibroblasts after cardiac injury (Ali et al., 2014; Moore-Morris et al., 2014). In contrast, the study of the EndoMT of *Tie2* lineage-traced cells in the injured adult heart is still missing. This is largely due to the limitation of the *Tie2-Cre* mouse line (Kisanuki et al., 2001; Ali et al., 2014). Interestingly, in contrast to *Tcf21* lineage-traced cardiac fibroblasts which all differentiated into myofibroblasts expressing *Postn* in response to injury (Kanisicak et al., 2016;

Fu et al., 2018), a study using another endothelial/endocardial lineage-tracing mouse line, *Cdh5-Cre*, found that less than 1% of *Cdh5* lineage-traced cells (including both endothelial cells and endothelium-derived cardiac fibroblasts) expressed *Postn* after MI (Kanisicak et al., 2016), suggesting a difference in the transcriptomic regulation of cardiac fibroblasts of different origins. It is possible that the EndoMT taken place in some of the endothelial/endocardial cells during development is actually a partial EndoMT, causing an incomplete cell fate change (Li et al., 2018). However, a definitive answer about EndMT in the adult heart requires inducible endothelial lineage-tracing mouse lines such as *Tie2-CreERT2* and *Cdh5-CreERT* mice, both of which are available now (Wang et al., 2010; Maliken et al., 2018). The hematopoietic cell is another cell type that has been reported to transdifferentiate into cardiac fibroblasts in response to ischemic injury. Bone marrow transplantation experiments showed that bone marrow-derived cells positive for collagen I and αSMA were present in the infarct (Haudek et al., 2006; Möllmann et al., 2006; van Amerongen et al., 2008; Verma et al., 2017). However, studies using hematopoietic cell lineage-tracing mouse lines found that these cells minimally contributed to the cardiac fibroblast population (Ali et al., 2014; Moore-Morris et al., 2014; Kanisicak et al., 2016), suggesting that this transdifferentiation is a rather rare event. It is possible that the bone marrow-derived fibroblasts identified in the recipient mice in bone marrow transplantation experiments were actually derived from transplanted bone marrow mesenchymal progenitor cells instead of hematopoietic cells as myofibroblast differentiation of bone marrow mesenchymal progenitor cells has been reported (Quante et al., 2011). Thus, further lineage-tracing studies of bone marrow mesenchymal progenitor cells is required to answer this question.

CARDIAC FIBROBLAST PLASTICITY

In general, the fibroblast is a very plastic cell type. The differentiation of cardiac fibroblasts into myofibroblast has been verified by many groups using multiple cardiac fibroblast lineage-tracing lines (Ali et al., 2014; Moore-Morris et al., 2014; Kanisicak et al., 2016; Khalil et al., 2017; Fu et al., 2018). The transcriptional regulation of myofibroblast differentiation is very complicated as many signaling pathways including TGFβ and novel mechanisms have been revealed (see section "Targeting Cardiac Fibroblasts to Treat Heart Diseases" for more detailed discussion). It was once believed that myofibroblasts were terminal-differentiated and were cleared by apoptosis once the infarct scar was stabilized, which was evidenced by the disappearance of αSMA^{+} myofibroblasts (Takemura et al., 1998). However, our recent lineage-tracing study showed that *Tcf21* lineage-traced cardiac fibroblasts persisted in infarct scar beyond 8 weeks after MI (Fu et al., 2018). Myofibroblasts in stabilized infarct scar further differentiated into matrifibrocytes which did not express αSMA and only expressed low levels of typical myocardial ECM proteins such as collagen 1 and collagen 3 (Fu et al., 2018). Instead, matrifibrocytes expressed a high level of cartilage ECM proteins, suggesting a partial transcriptomic switch to chondrocyte (Fu et al., 2018). Removal of matrifibrocytes from infarct scar by cryoinjury caused a reduction in cardiac function and exacerbation of dilation, suggesting an important function of matrifibrocytes in maintaining the infarct stability (Fu et al., 2018). However, mechanisms responsible for matrifibrocyte differentiation are still not clear. Another study found that in mouse lines susceptible to injury-induced myocardial calcification, *Col1a2* lineage-traced cardiac fibroblasts differentiated into a calcium-depositing cell type similar to osteoblast, a process believed to be mediated by Runx2, an osteogenic transcription factor (Pillai et al., 2017). Moreover, it was recently shown that *Tcf21* lineage-traced cardiac fibroblasts differentiated into adipocytes in response to a high-fat diet (HFD), which is normally inhibited by cardiomyocyte-secreted prokineticin-2 (Qureshi et al., 2017), further suggesting the plasticity of these cells. The transdifferentiation of cardiac fibroblasts into endothelial cells upon MI has also been investigated. It was reported that ∼35% of *Col1a2* lineage-traced cardiac fibroblasts expressed endothelial markers such as VECAD and contributed to the neovascularization in injured hearts (Ubil et al., 2014), suggesting a novel therapeutic role of cardiac fibroblasts. However, the study conducted by another group using multiple cardiac fibroblast lineage-tracing lines including the same *Col1a2-CreERT* mouse line showed that the neovascularization process was mainly mediated by the expansion of pre-existing endothelial cells but not cardiac fibroblasts (He et al., 2017). The contradictory results of the two studies may be partially due to the difference in the markers and antibodies used for endothelial cell identification. A study using a dual lineage-tracing system may help clarify this contradiction.

TARGETING CARDIAC FIBROBLASTS TO TREAT HEART DISEASES

An ultimate goal of cardiac fibroblast lineage-tracing is to treat heart diseases through manipulating cardiac fibroblast activities. This requires the understanding of the functions of genes expressed in cardiac fibroblasts and their roles in disease development. These studies have been greatly promoted by Cre-loxP-mediated cardiac fibroblast lineage-tracing mouse lines, which allows specific knockout and overexpression of genes in cardiac fibroblasts *in vivo* without affecting other tissues/cell types (see **Table 1** for a summary of recent relevant studies).

Targeting TGFβ and Related Signaling

The correlation between TGFβ signaling and cardiac fibrosis has long been noticed (Casscells et al., 1990). Only recently, with the help of cardiac fibroblast lineage-tracing and specific gene knockout, many details in this process have been revealed *in vivo*. Using *Tcf21-MerCreMer* and *Postn-MerCreMer*-mediated cardiac fibroblast-specific knockout of *Tgfbr1/2 Smad2* and *Smad3*, which are important components of canonical TGFβ signaling, we found that in cardiac fibroblast canonical TGFβ signaling played an important role in activating cardiac

TABLE 1 | Summarization of recent findings by employing Cre-loxP-mediated cardiac fibroblast-specific gene deletion or overexpression mouse lines.

Cre lines used	Genes deleted or overexpressed	Injury model	Changes in cardiac fibroblasts	Impact on cardiac function and phenotype	References
Tcf21-MerCreMer; Postn-MerCreMer	*Tgfbr1/2* double deletion; *Smad2/3* single and double deletion	TAC	Reduced myofibroblast proliferation, differentiation, contraction, and ECM protein expression	Improved function (Tgfbr1/2 deletion only); reduced fibrosis (all except Smad2 deletion)	Khalil et al., 2017
Tcf21-MerCreMer; *Postn-MerCreMer*	*Ctnnb1* deletion	TAC	Increased ECM gene expression	Improved function; reduced fibrosis	Xiang et al., 2017
Tcf21-MerCreMer	*Pkr1* deletion	HFD	Increased adipogenesis	Reduced function	Qureshi et al., 2017
Tcf21-MerCreMer	*Fn1* deletion	I/R	Reduced myofibroblast number	Improved function; reduced fibrosis and cardiomyocyte hypertrophy	Valiente-Alandi et al., 2018
Tcf21-MerCreMer	*Loxl2* deletion	TAC	Reduced TGF-β2 production and myofibroblast differentiation	Improved function; reduced fibrosis	Yang et al., 2016
Tcf21-MerCreMer	*Lats1/2* double deletion	None	Spontaneous myofibroblast differentiation	Reduced function; increased fibrosis	Xiao et al., 2019
Postn-MerCreMer	*Tgfbr2* deletion	Mouse model of proteotoxic cardiac disease	Reduced myofibroblast number	Improved function and survival rate; reduced cardiomyocyte hypertrophy	Bhandary et al., 2018
Postn-MerCreMer	*Tgfbr2* deletion	Mouse model of cardiac myosin binding protein c-induced cardiomyopathy	Reduced myofibroblast number	Improved function and survival rate; reduced fibrosis	Meng et al., 2018
Postn-MerCreMer	*Mapk14* deletion	MI; I/R	Reduced myofibroblast differentiation and expansion	Improved function; reduced fibrosis	Molkentin et al., 2017
Postn-MerCreMer	*Ccn2* deletion	Ang II infusion	Attenuated TGFβ-induced myofibroblast differentiation	Reduced fibrosis	Dorn et al., 2018
Postn-MerCreMer	*Hsp47* deletion	TAC; MI	Reduced collagen production	Improved function (TAC); reduced fibrosis (TAC and MI); increased rupture (MI); reduced function (MI)	Khalil et al., 2019
Postn-MerCreMer	*Grk2* deletion	I/R	Reduced myofibroblast differentiation	Improved function; reduced fibrosis	Travers et al., 2017
Postn-Cre	*Smad2* and *Smad3* deletion	MI; I/R	Enhanced proliferation; disorganized stress fibers (Smad3 deletion)	Temporary improved of function (Smad2 deletion); exacerbated long-term function and enchanced ECM maladaptive remodeling (Smad3 deletion)	Kong et al., 2018; Huang et al., 2019

(Continued)

TABLE 1 | Continued

Cre lines used	Genes deleted or overexpressed	Injury model	Changes in cardiac fibroblasts	Impact on cardiac function and phenotype	References
Postn-Cre	*Rock2* deletion; *Rock2* overexpression	Ang II infusion	Reduced myofibroblast phenotype (Rock 2 deletion vs. overexpression)	Improved function and reduced fibrosis (Rock 2 deletion vs. overexpression)	Shimizu et al., 2017
Postn-Cre	*Pkd1* deletion	I/R; MI	Attenuated TGFβ-induced myofibroblast differentiation	Reduced scar size; increased cardiomyocyte hypertrophy	Villalobos et al., 2019
Postn-Cre	*Il17ra* deletion	MI	Reduced granulocyte macrophage colony-stimulating factor^{+} (GM-CSF^{+}) fibroblast	Increased survival rate; reduced infarct size	Chen et al., 2018
Postn-Cre	*Klf5* deletion	TAC	Reduced IGF-1 secretion	Improved function; reduced cardiomyocyte hypertrophy	Takeda et al., 2010
Postn-Cre	*Sox9* deletion	MI	Reduced myofibroblast phenotype	Improved function; reduced dilation and scar size	Scharf et al., 2019
Postn-Cre	*miR-33* deletion	TAC	Reduced proliferation and lipid raft content	Reduced fibrosis	Nishiga et al., 2017; Dorn et al., 2018
Col1a2-CreERT	*Atf3* overexpression	Ang II infusion	Reduced p38 activation	Improved function; reduced fibrosis	Li et al., 2017
Col1a2-CreERT	*Il1r1* deletion	MI	Reduced IL-1α–induced Il6, Mmp3, and Mmp9 expression	Improved function; reduced fibrosis	Bageghni et al., 2019
Col1a2-CreERT	*Il11* overexpression	None	Increased myofibroblast differentiation	Reduced function; increased fibrosis	Schafer et al., 2017
Col1a2-CreERT	*Grk2* deletion	I/R	Reduced TNFα secretion	Improved function; reduced fibrosis and inflammation	Woodall et al., 2016
Col1a2-CreERT	*Mcu* deletion	MI; Ang II infusion	Increased myofibroblast differentiation	Reduced function; increased fibrosis	Lombardi et al., 2019

Studies were grouped based on Cre mouse lines used.

fibroblasts, which was mainly mediated by Smad3 but not Smad2 (Khalil et al., 2017). Interestingly, even though both cardiac fibroblast-specific deletion of *Tgfbr1/2* and *Smad2/3* significantly reduced cardiac fibrosis induced by transverse aortic constriction (TAC), only the deletion of *Tgfbr1/2* in cardiac fibroblasts ameliorated cardiac hypertrophy and resulted in a functional improvement at 4 and 12 weeks after TAC (Khalil et al., 2017). Similarly, myofibroblast-specific *Tgfbr2* deletion led to improved cardiac function in mouse models of proteotoxic cardiac disease and cardiac myosin binding protein C-induced cardiomyopathy (Bhandary et al., 2018; Meng et al., 2018). Studies conducted by another group using *Postn-Cre*-mediated myofibroblast-specific deletion of *Smad3* and *Smad2* found that while deletion of *Smad2* temporarily improved cardiac function around 7 days after myocardial infarct (MI) in mice, deletion of *Smad3* caused a reduction in cardiac function 28 days after MI (Kong et al., 2018; Huang et al., 2019). The identified difference between *Smad2* and *Smad3* deletion was likely because of the differential regulation of myofibroblast and collagen matrix organization by Smad2 and Smad3 (Kong et al., 2018; Huang et al., 2019; Russo et al., 2019). The limited controversies in the effect of Smad gene deletion on cardiac function reported in these studies were possibly due to the different injury models used in which the expression of Smad2/3 in cardiac fibroblasts may have different effects on cardiac function. Moreover, the phenotypic and functional differences between mice with cardiac fibroblast-specific deletion of *Tgfbr1/2* and *Smad2/3* suggest that non-canonical TGFβ signaling also plays an important role in cardiac fibroblast-mediated post-injury remodeling (Khalil et al., 2017). Indeed, using the same cardiac fibroblast-specific Cre lines, the role of TGFβ-MAPK kinase 6 (MKK6)-p38 signaling in myofibroblast differentiation of cardiac fibroblasts was revealed (Molkentin et al., 2017). Cardiac fibroblast-specific deletion of *Mapk14* (the gene encoding p38) significantly reduced myofibroblast expansion and cardiac fibrosis and improved cardiac function after ischemia/reperfusion (I/R) in mice (Molkentin et al., 2017). A similar protective effect was observed in mice with cardiac fibroblast-specific deletion of *Atf3*, a transcription factor that activates the expression of *Map2k3*, a p38 kinase (Li et al., 2017). Besides, the TGFβ-RhoA-Rock pathway has also been found to play an important role in the actin stress fiber formation, which is essential for myofibroblast differentiation (Bhowmick et al., 2001; Shi and Massagué, 2003; Costanza et al., 2017). A study found that in angiotensin II (Ang II) infusion-induced cardiomyopathy, the myofibroblast-specific deletion of *Rock2* significantly reduced αSMA expression in these cells, together with reduced connective tissue growth factor (CTGF) and FGF2 expression in cardiac fibroblasts, and improved cardiac function and fibrosis (Shimizu et al., 2017). However, how the disrupted stress fiber formation led to reduced cytokine production is still not clear.

Besides the direct regulatory roles of canonical and non-canonical TGFβ signaling in the myofibroblast differentiation of cardiac fibroblasts and cardiac fibrosis, the cross-talk between TGFβ signaling and other signaling pathways has also been studied using fibroblast-specific Cre mouse lines. CTGF is an important mediator in TGFβ-induced myofibroblast differentiation (Mori et al., 1999; Shi-wen et al., 2006). Interestingly, despite the fact that cardiomyocyte is the major source of CTGF in the heart, the deletion of *Ccn2* (the gene encoding CTGF) in cardiomyocytes failed to protect the heart from pressure overload-induced cardiomyopathy (Accornero et al., 2015). A later study found that CTGF functioned as an autocrine factor in cardiac fibroblasts and cardiac fibroblast-specific deletion of *Ccn2* significantly improved cardiac function after Ang II infusion (Dorn et al., 2018). It was demonstrated that Wnt signaling and TGFβ signaling also cross-talk during myofibroblast differentiation (Chen et al., 2011; Akhmetshina et al., 2012). The elevated level of TGFβ in injured myocardium activated Wnt signaling which led to cardiac fibrosis in experimental autoimmune myocarditis (Blyszczuk et al., 2016). In a recent study specifically deleting *Ctnnb1* (the gene encoding β-catenin) in cardiac fibroblasts, the cardiac function and fibrosis were found to be improved, which was primarily due to reduced ECM protein secretion by cardiac fibroblasts (Xiang et al., 2017). Moreover, it was recently found that canonical TGFβ signaling during myofibroblast differentiation of cardiac fibroblasts required functional primary cilia in cardiac fibroblasts. When primary cilium is disrupted in cardiac fibroblasts due to cardiac fibroblast-specific *Pkd1* deletion, the TGFβ-Smad3 signaling-induced ECM protein production and myofibroblast differentiation of cardiac fibroblasts were impaired, leading to insufficient scar formation and increased cardiomyocyte hypertrophy after MI (Villalobos et al., 2019). Interleukin (IL) is an important group of inflammatory cytokines. Multiple IL receptors are expressed in cardiac fibroblasts, which regulates myofibroblast activities (Shinde and Frangogiannis, 2014; Turner, 2014; Francis Stuart et al., 2016). Using cardiac fibroblast-specific Cre lines, it was found that blocking the effects of proinflammatory ILs on cardiac fibroblasts through cardiac fibroblast-specific deletion of IL receptors, *Il1r1* (Bageghni et al., 2019) or *Il17ra* (Chen et al., 2018), both alleviated injury-induced cardiac fibrosis and cardiac function reduction. Interestingly, in both studies, cardiac fibroblast-specific deletion of IL receptor genes reduced the infiltration/activity of immune cells in the injured heart, suggesting that cardiac fibroblasts play an important role in the regulation of post-injury inflammation, which is mediated by IL signaling. In contrast, overexpressing *Il11*, whose expression in fibroblasts is activated by TGFβ, in cardiac fibroblasts caused spontaneous cardiac fibrosis without injury (Schafer et al., 2017).

Direct Targeting ECM

Being one of the most important characteristics of the fibroblast, the direct regulation of collagen secretion and ECM remodeling in fibroblast is also an important research target. Collagen is first secreted from cells in the form of procollagen. *In vitro* studies identified that the secretion of procollagen required HSP47, a stress-inducible chaperone protein (Nagata et al., 1988; Satoh et al., 1996; Ishida et al., 2006). As expected, the deletion of *Hsp47* in cardiac fibroblasts specifically reduced collagen production but not the general paracrine secretory activity (Khalil et al., 2019). Cardiac fibroblast-specific *Hsp47* deletion significantly reduced

cardiac fibrosis and improved heart diastolic function after TAC. However, the reduced collagen accumulation in these mice led to an increase in lethality after MI, owing to the insufficient scar formation (Khalil et al., 2019). This study strongly suggests that the effect of cardiac fibroblast-mediated fibrotic response after cardiac injury can vary significantly among different injury types. While the beneficial effect of fibrotic tissue may outweigh its deleterious effect after an acute injury that causes massive cardiomyocyte death, the effect of interstitial fibrosis in chronic cardiomyopathy may be largely detrimental. Fibronectin is another abundant ECM protein in the heart. Its level in the heart increases significantly after injuries (Heling et al., 2000; Dobaczewski et al., 2006; van Dijk et al., 2008). Cardiac fibroblast-specific *Fn1* deletion led to improved cardiac function, reduced cardiac fibroblast activity, and attenuated cardiac fibrosis and hypertrophy after I/R (Valiente-Alandi et al., 2018), which was likely related to the function of fibronectin in collagen assembly (Sottile et al., 2007). The post-injury ECM remodeling involves collagen crosslinking, which is primarily mediated by isoforms of lysyl oxidases (LOXs). Yang et al. (2016) identified a specific increase in lysyl oxidase-like 2 (LOXL2) level after TAC. Cardiac fibroblast-specific deletion of *Loxl2* significantly improved TAC-induced cardiac function (Yang et al., 2016). Interestingly, besides the expected reduction in fibrosis, the production of TGFβ2 was also reduced in cardiac fibroblasts lacking *Loxl2*, which was found to be mediated by PI3K/AKT signaling (Yang et al., 2016).

A Re-look at Cardiomyocyte-Expressed Genes

Previous research focusing on cardiomyocytes revealed the cardiomyocyte-specific functions of many genes. The development of cardiac fibroblast-specific gene deletion and overexpression strategies has recently permitted the study of these genes in cardiac fibroblasts. The function of G protein-coupled receptors (GPCRs) in the pathological changes of cardiomyocytes after injuries has been studied extensively (Koch et al., 1995; Raake et al., 2008; Schumacher et al., 2015). However, the role of GPCRs in cardiac fibroblast-mediated fibrosis was only revealed recently. It was reported that cardiac fibroblast-specific deletion of *Grk2* (G protein-coupled receptor kinase 2) reduced the secretion of TNFα by cardiac fibroblasts and cardiac fibrosis after I/R, together with improved cardiac function (Woodall et al., 2016; Travers et al., 2017). Moreover, the function of Hippo pathway, which is known for its inhibitory effect on cardiomyocyte proliferation (Halder and Johnson, 2011; Leach et al., 2017), in cardiac fibroblasts was studied (Xiao et al., 2019). It was found that cardiac fibroblast-specific deletion of Hippo pathway kinases, *Lats1* and *Lats2*, caused spontaneous myofibroblast differentiation (Xiao et al., 2019). This mechanistic study identified that Yap directly activated myofibroblast genes, which was blocked by the phosphorylation of Yap by Lats1/2.

Novel Transcription Factors

Using cardiac fibroblast-specific Cre lines, novel transcription factors regulating cardiac fibroblast activities have also been identified. Krüppel-like factor 5 (Klf5) is a transcription factor regulating cell differentiation and animal development (Dang et al., 2000; Bieker, 2001; Black et al., 2001). The Nagai group recently reported that the global heterozygous knockout of *Klf5* reduced cardiac hypertrophy and fibrosis induced by Ang II infusion (Shindo et al., 2002). A later study conducted by the same group found that cardiac fibroblast-specific *Klf5* deletion ameliorated cardiac hypertrophy induced by moderate-intensity pressure overload, which, however, was not observed in cardiomyocyte-specific *Klf5* knockout mice (Takeda et al., 2010). It was found that KLF5 activated IGF-1 secretion from cardiac fibroblasts, which then served as the mediator in the crosstalk between cardiac fibroblasts and cardiomyocytes (Takeda et al., 2010). Another recent study combining TOMO-seq and transcription factor binding site analysis identified SOX9 as a potential novel transcription factor activating the expression of fibrotic genes in the heart (Lacraz et al., 2017), which might explain the amelioration in MI-induced cardiac dysfunction, fibrosis, and dilation in mice with cardiac fibroblast-specific deletion of *Sox9* (Scharf et al., 2019).

Epigenetic Regulation

The study of epigenetic regulation of myofibroblast differentiation and cardiac fibrosis has also benefited from cardiac fibroblast-specific Cre lines. It was recently found that a metabolic switch to glycolysis during myofibroblast differentiation due to the shutdown of mitochondrial calcium uniporter complex increased the production of α-ketoglutarate which then enabled histone demethylation at myofibroblast gene loci, promoting myofibroblast differentiation (Lombardi et al., 2019). Deletion of mitochondrial calcium uniporter (*Mcu*) in fibroblasts, blocked mitochondria calcium influx, and therefore promoted the metabolic switch. As a result, cardiac fibroblast-specific deletion of *Mcu* attenuated myofibroblast differentiation and improved cardiac function after cardiac injury (Lombardi et al., 2019). Moreover, another study found that microRNA, miR-33 regulated cholesterol metabolic gene expression in cardiac fibroblasts, which was important for cardiac fibroblast proliferation. Cardiac fibroblasts lacking *miR-33* had reduced proliferation due to altered lipid raft cholesterol content. *Postn-Cre*-induced deletion of *miR-33* in mice led to decreased cardiac fibrosis (Nishiga et al., 2017).

THE CLINICAL IMPLICATION OF CARDIAC FIBROBLAST LINEAGE-TRACING

Studies have shown that simply depleting cardiac fibroblasts from the heart after an injury usually causes detrimental effects (Kanisicak et al., 2016; Fu et al., 2018). More and more evidence generated using cardiac fibroblast lineage-tracing tools and cardiac fibroblast-specific Cre lines have suggested an increasing number of cardiac fibroblast-expressed genes as potential targets for treating cardiac diseases. Thus, manipulation of the cardiac fibroblast gene expression profile may be a feasible approach. Systemic delivery of traditional medication that regulates the

expression of certain genes or the activity of relevant signaling pathways has been tested in clinical trials for cardiac fibrosis treatment, which, however, usually indiscriminately targets all the cells in the body and has unintended targets, often leading to severe side effects. For instance, animal studies have shown the anti-cardiac fibrosis effects of TGFβ inhibitors such as pirfenidone and tranilast (Edgley et al., 2012). However, a hepatic adverse effect was identified in a clinical trial testing the therapeutic effect of tranilast in restenosis caused by percutaneous coronary intervention (Holmes et al., 2002). The development of gene therapies, especially the adeno-associated virus (AAV)-mediated gene therapy (Finer and Glorioso, 2017), has now made it possible to specifically manipulate gene expression in certain cell types. Dependent on the transgene selected, gene therapy allows both direct overexpression and knockdown of a certain gene in the cell (Eaton et al., 2002; Chadderton et al., 2009; Samulski and Muzyczka, 2014). Over the years, different AAV serotypes that specifically target different organs have been reported (Wu et al., 2006). A greater specificity has been achieved using cell type-specific promoters to drive the expression of transgenes (Peel et al., 1997; Dashkoff et al., 2016; Hanlon et al., 2017). Using this approach, multiple groups have reported successful specific expression of transgenes in cardiomyocytes (Aikawa et al., 2002; Pleger et al., 2007; Pacak et al., 2008). Recently, AAV carrying a *Postn* promoter-driven transgene has also been used to specifically induce transgene expression in myofibroblasts in the heart (Piras et al., 2016), strongly suggesting a bright future of this treatment strategy.

CONCLUSION

The great plasticity of cardiac fibroblasts allows them to quickly respond to the injury/disease signal and then contribute to the alteration and remodeling of the myocardial environment. Being the most abundant cell type in the heart, it is undoubted that the cardiac fibroblast is an excellent target for treating cardiac diseases. The development of cardiac fibroblast lineage-tracing mouse lines has led to a huge acceleration in cardiac fibroblast research. Using these tools, researchers have been able to reveal the developmental origin of cardiac fibroblasts and their differentiation pathways in injuries and diseases. Even though an increasing number of signaling pathways have been suggested to play a role in the regulation of cardiac fibroblast activities and differentiation, more studies are still required to reveal the details of these regulations, such as how these signaling pathways specifically regulate the beneficial and deleterious effects of cardiac fibroblasts and how they crosstalk with each other. Moreover, due to difference in the effect of fibrosis on cardiac tissue healing and function after different cardiac injuries indicated in recent studies (Khalil et al., 2019), more work comparing the effects of the cardiac fibroblast-specific knockout and overexpression of the same genes in different disease/injury models are also needed. These studies are particularly important for the selection of appropriate treatment target. In addition, the current mechanistic understanding of the plasticity of cardiac fibroblasts is largely limited to myofibroblast differentiation. Signaling pathways regulating other differentiation potentials of cardiac fibroblasts may also deserve more attention because of the increased evidences of these differentiations in diseased hearts. In addition, even though many of the cardiac fibroblast lineage-tracing tools have shown high fibroblast-specificity in the heart, most of the promoters/loci used in these cardiac fibroblast lineage-tracing tools are also active in fibroblasts and similar cell types residing in other organs (Quaggin et al., 1999; Kanisicak et al., 2016). Thus, further studies are required to engineer those promoters/loci to achieve absolute cardiac fibroblast-specificity, which is required for the specific regulation of target genes in cardiac fibroblasts in gene therapy. However, considering the relatively short history of the modern lineage-tracing system, it is expected that the progress of this research area will further accelerate. In summary, the advances in cardiac fibroblast lineage-tracing studies and their potential application in gene therapy may shed light on novel treatment approaches for cardiac diseases.

AUTHOR CONTRIBUTIONS

XF was the primary author who is responsible for the design and writing of the manuscript. QL, CL, YL, and LW assisted with the writing of the manuscript.

FUNDING

This research was supported by Louisianan Board of Regents R&D, Research Competitiveness Subprogram (RCS) BOR.Fu.LEQSF (2019-22)-RD-A-01 and National Institutes of Health (NIH) 1R15DK122383-01.

ACKNOWLEDGMENTS

We would like to acknowledge all authors involved in this study and the support by LSU AgCenter and School of Animal Sciences.

REFERENCES

Accornero, F., van Berlo, J. H., Correll, R. N., Elrod, J. W., Sargent, M. A., York, A., et al. (2015). Genetic analysis of connective tissue growth factor as an effector of transforming growth factor β signaling and cardiac remodeling. *Mol. Cell. Biol.* 35, 2154–2164. doi: 10.1128/mcb.00199-15

Acharya, A., Baek, S. T., Banfi, S., Eskiocak, B., and Tallquist, M. D. (2011). Efficient inducible Cre-mediated recombination in Tcf21cell lineages in the heart and kidney. *Genesis* 49, 870–877. doi: 10.1002/dvg.20750

Acharya, A., Baek, S. T., Huang, G., Eskiocak, B., Goetsch, S., Sung, C. Y., et al. (2012). The bHLH transcription factor Tcf21 is required for lineage-specific EMT of cardiac fibroblast progenitors. *Development* 139, 2139–2149. doi: 10.1242/dev.079970

Aikawa, R., Huggins, G. S., and Snyder, R. O. (2002). Cardiomyocyte-specific gene expression following recombinant adeno-associated viral vector transduction. *J. Biol. Chem.* 277, 18979–18985. doi: 10.1074/jbc.M201257200

Akhmetshina, A., Palumbo, K., Dees, C., Bergmann, C., Venalis, P., Zerr, P., et al. (2012). Activation of canonical Wnt signalling is required for TGF-β-mediated fibrosis. *Nat. Commun.* 3:735. doi: 10.1038/ncomms1734

Ali, S. R., Ranjbarvaziri, S., Talkhabi, M., Zhao, P., Subat, A., Hojjat, A., et al. (2014). Developmental heterogeneity of cardiac fibroblasts does not predict pathological proliferation and activation. *Circ. Res.* 115, 625–635. doi: 10.1161/circresaha.115.303794

Anastassiadis, K., Fu, J., Patsch, C., Hu, S., Weidlich, S., Duerschke, K., et al. (2009). Dre recombinase, like Cre, is a highly efficient site-specific recombinase in *E. coli*, mammalian cells and mice. *Dis. Models Mech.* 2, 508–515. doi: 10.1242/dmm.003087

Asli, N. S., Xaymardan, M., Patrick, R., Farbehi, N., Cornwell, J., Forte, E., et al. (2019). PDGFRα signaling in cardiac fibroblasts modulates quiescence, metabolism and self-renewal, and promotes anatomical and functional repair. *bioRxiv* [Preprint] doi: 10.1101/225979

Bageghni, S. A., Hemmings, K. E., Yuldasheva, N. Y., Maqbool, A., Gamboa-Esteves, F. O., Humphreys, N. E., et al. (2019). Fibroblast-specific deletion of IL-1 receptor-1 reduces adverse cardiac remodeling following myocardial infarction. *JCI Insight* 4, e125074. doi: 10.1172/jci.insight.125074

Baum, J., and Duffy, H. S. (2011). Fibroblasts and myofibroblasts: what are we talking about? *J. Cardiovasc. Pharmacol.* 57, 376–379. doi: 10.1097/FJC.0b013e3182116e39

Bhandary, B., Meng, Q., James, J., Osinska, H., Gulick, J., Valiente-Alandi, I., et al. (2018). Cardiac fibrosis in proteotoxic cardiac disease is dependent upon Myofibroblast TGF-β signaling. *J. Am. Heart Assoc.* 7:e010013. doi: 10.1161/JAHA.118.010013

Bhowmick, N. A., Ghiassi, M., Bakin, A., Aakre, M., Lundquist, C. A., Engel, M. E., et al. (2001). Transforming growth factor-β1 mediates epithelial to mesenchymal transdifferentiation through a RhoA-dependent mechanism. *Mol. Biol. Cell* 12, 27–36. doi: 10.1091/mbc.12.1.27

Bieker, J. J. (2001). Kruppel-like factors: three fingers in many pies. *J. Biol. Chem.* 276, 34355–34358. doi: 10.1074/jbc.R100043200

Biswas, H. (2016). Action of SNAIL1 protein is critical for fibrosis. *Arts Sci. Electr. Theses Dissert.* 831.

Black, A. R., Black, J. D., and Azizkhan-Clifford, J. (2001). Sp1 and krüppel-like factor family of transcription factors in cell growth regulation and cancer. *J. Cell. Physiol.* 188, 143–160. doi: 10.1002/jcp.1111

Blyszczuk, P., Müller-Edenborn, B., Valenta, T., Osto, E., Stellato, M., Behnke, S., et al. (2016). Transforming growth factor-β-dependent Wnt secretion controls myofibroblast formation and myocardial fibrosis progression in experimental autoimmune myocarditis. *Eur. Heart J.* 38, 1413–1425. doi: 10.1093/eurheartj/ehw116

Brown, R. D., Jones, G. M., Laird, R. E., Hudson, P., and Long, C. S. (2007). Cytokines regulate matrix metalloproteinases and migration in cardiac fibroblasts. *Biochem. Biophys. Res. Commun.* 362, 200–205. doi: 10.1016/j.bbrc.2007.08.003

Cai, C.-L., Martin, J. C., Sun, Y., Cui, L., Wang, L., Ouyang, K., et al. (2008). A myocardial lineage derives from Tbx18 epicardial cells. *Nature* 454, 104–108. doi: 10.1038/nature06969

Carver, W., Nagpal, M. L., Nachtigal, M., Borg, T. K., and Terracio, L. (1991). Collagen expression in mechanically stimulated cardiac fibroblasts. *Circ. Res.* 69, 116–122. doi: 10.1161/01.RES.69.1.116

Casscells, W., Bazoberry, F., Speir, E., Thompson, N., Flanders, K., Kondaiah, P., et al. (1990). Transforming growth factor-beta 1 in normal heart and in myocardial infarction. *Ann. N. Y. Acad. Sci.* 593, 148–160. doi: 10.1111/j.1749-6632.1990.tb16107.x

Chadderton, N., Millington-Ward, S., Palfi, A., O'Reilly, M., Tuohy, G., Humphries, M. M., et al. (2009). Improved Retinal Function in a Mouse Model of Dominant Retinitis Pigmentosa Following AAV-delivered Gene Therapy. *Mol. Ther.* 17, 593–599. doi: 10.1038/mt.2008.301

Chen, G., Bracamonte-Baran, W., Diny, N. L., Hou, X., Talor, M. V., Fu, K., et al. (2018). Sca-1+ cardiac fibroblasts promote development of heart failure. *Eur. J. Immunol.* 48, 1522–1538. doi: 10.1002/eji.201847583

Chen, J.-H., Chen, W. L. K., Sider, K. L., Yip, C. Y. Y., and Simmons, C. A. (2011). β-Catenin mediates mechanically regulated, transforming growth Factor-β1-Induced Myofibroblast differentiation of aortic valve interstitial cells. *Arterioscler. Thromb. Vasc. Biol.* 31, 590–597. doi: 10.1161/ATVBAHA.110.220061

Chen, Q., Zhang, H., Liu, Y., Adams, S., Eilken, H., Stehling, M., et al. (2016). Endothelial cells are progenitors of cardiac pericytes and vascular smooth muscle cells. *Nat. Commun.* 7:12422. doi: 10.1038/ncomms12422

Conway, S. J., and Molkentin, J. D. (2008). Periostin as a heterofunctional regulator of cardiac development and disease. *Curr. Genom.* 9, 548–555. doi: 10.2174/138920208786847917

Costanza, B., Umelo, I. A., Bellier, J., Castronovo, V., and Turtoi, A. (2017). Stromal modulators of TGF-β in cancer. *J. Clin. Med.* 6:7. doi: 10.3390/jcm6010007

Creemers, E. E., and Pinto, Y. M. (2010). Molecular mechanisms that control interstitial fibrosis in the pressure-overloaded heart. *Cardiovasc. Res.* 89, 265–272. doi: 10.1093/cvr/cvq308

Dang, D. T., Pevsner, J., and Yang, V. W. (2000). The biology of the mammalian Krüppel-like family of transcription factors. *Int. J. Biochem. Cell Biol.* 32, 1103–1121. doi: 10.1016/S1357-2725(00)00059-5

Dashkoff, J., Lerner, E. P., Truong, N., Klickstein, J. A., Fan, Z., Mu, D., et al. (2016). Tailored transgene expression to specific cell types in the central nervous system after peripheral injection with AAV9. *Mol. Ther Methods Clin. Dev.* 3:16081. doi: 10.1038/mtm.2016.81

Dobaczewski, M., Bujak, M., Zymek, P., Ren, G., Entman, M. L., and Frangogiannis, N. G. (2006). Extracellular matrix remodeling in canine and mouse myocardial infarcts. *Cell Tissue Res.* 324, 475–488. doi: 10.1007/s00441-005-0144-6

Dorn, L. E., Petrosino, J. M., Wright, P., and Accornero, F. (2018). CTGF/CCN2 is an autocrine regulator of cardiac fibrosis. *J. Mol. Cell Cardiol.* 121, 205–211. doi: 10.1016/j.yjmcc.2018.07.130

Duan, J., Gherghe, C., Liu, D., Hamlett, E., Srikantha, L., Rodgers, L., et al. (2012). Wnt1/βcatenin injury response activates the epicardium and cardiac fibroblasts to promote cardiac repair. *EMBO J.* 31, 429–442. doi: 10.1038/emboj.2011.418

Eaton, M., Blits, B., Ruitenberg, M. J., Verhaagen, J., and Oudega, M. (2002). Amelioration of chronic neuropathic pain after partial nerve injury by adeno-associated viral (AAV) vector-mediated over-expression of BDNF in the rat spinal cord. *Gene Ther.* 9:1387. doi: 10.1038/sj.gt.3301814

Edgley, A. J., Krum, H., and Kelly, D. J. (2012). Targeting fibrosis for the treatment of heart failure: a role for transforming growth factor-β. *Cardiovasc. Ther.* 30, e30–e40. doi: 10.1111/j.1755-5922.2010.00228.x

El Hajj, E. C., El Hajj, M. C., Ninh, V. K., Bradley, J. M., Claudino, M. A., and Gardner, J. D. (2017). Detrimental role of lysyl oxidase in cardiac remodeling. *J. Mol. Cell Cardiol.* 109, 17–26. doi: 10.1016/j.yjmcc.2017.06.013

Fan, D., Takawale, A., Lee, J., and Kassiri, Z. (2012). Cardiac fibroblasts, fibrosis and extracellular matrix remodeling in heart disease. *Fibrogenesis Tissue Repair* 5:15. doi: 10.1186/1755-1536-5-15

Fenoglio, J. J., Ursell, P. C., Kellogg, C. F., Drusin, R. E., and Weiss, M. B. (1983). Diagnosis and classification of myocarditis by endomyocardial biopsy. *N. Eng. J. Med.* 308, 12–18. doi: 10.1056/nejm198301063080103

Finer, M., and Glorioso, J. (2017). A brief account of viral vectors and their promise for gene therapy. *Gene Ther.* 24, 1–2. doi: 10.1038/gt.2016.71

Francis Stuart, S. D., De Jesus, N. M., Lindsey, M. L., and Ripplinger, C. M. (2016). The crossroads of inflammation, fibrosis, and arrhythmia following myocardial infarction. *J. Mol. Cell Cardiol.* 91, 114–122. doi: 10.1016/j.yjmcc.2015.12.024

Fu, X., Khalil, H., Kanisicak, O., Boyer, J. G., Vagnozzi, R. J., Maliken, B. D., et al. (2018). Specialized fibroblast differentiated states underlie scar formation in the infarcted mouse heart. *J. Clin. Invest.* 128, 2127–2143. doi: 10.1172/JCI98215

Go, A. S., Mozaffarian, D., Roger, V. L., Benjamin, E. J., Berry, J. D., Blaha, M. J., et al. (2014). Heart disease and stroke statistics—2014 update: a report from the American Heart Association. *Circulation* 129:e28. doi: 10.1161/01.cir.0000441139.02102.80

Halder, G., and Johnson, R. L. (2011). Hippo signaling: growth control and beyond. *Development* 138, 9–22. doi: 10.1242/dev.045500

Hamilton, T. G., Klinghoffer, R. A., Corrin, P. D., and Soriano, P. (2003). Evolutionary divergence of platelet-derived growth factor alpha receptor signaling mechanisms. *Mol. Cell. Biol.* 23, 4013–4025. doi: 10.1128/mcb.23.11.4013-4025.2003

Hanlon, K. S., Chadderton, N., Palfi, A., Blanco Fernandez, A., Humphries, P., Kenna, P. F., et al. (2017). A novel retinal ganglion cell promoter for utility in AAV vectors. *Front. Neurosci.* 11:521. doi: 10.3389/fnins.2017.00521

Haudek, S. B., Xia, Y., Huebener, P., Lee, J. M., Carlson, S., Crawford, J. R., et al. (2006). Bone marrow-derived fibroblast precursors mediate ischemic cardiomyopathy in mice. *Proc. Natl. Acad. Sci. U.S.A.* 103, 18284–18289. doi: 10.1073/pnas.0608799103

He, L., Huang, X., Kanisicak, O., Li, Y., Wang, Y., Li, Y., et al. (2017). Preexisting endothelial cells mediate cardiac neovascularization after injury. *J. Clin. Invest.* 127, 2968–2981. doi: 10.1172/JCI93868

Heling, A., Zimmermann, R., Kostin, S., Maeno, Y., Hein, S., Devaux, B., et al. (2000). Increased expression of cytoskeletal, linkage, and extracellular proteins in failing human Myocardium. *Circ. Res.* 86, 846–853. doi: 10.1161/01.RES.86.8.846

Holmes, D. R., Savage, M., LaBlanche, J.-M., Grip, L., Serruys, P. W., Fitzgerald, P., et al. (2002). Results of prevention of REStenosis with tranilast and its outcomes (PRESTO) Trial. *Circulation* 106, 1243–1250. doi: 10.1161/01.CIR.0000028335.31300.DA

Huang, S., Chen, B., Su, Y., Alex, L., Humeres, C., Shinde, A. V., et al. (2019). Distinct roles of myofibroblast-specific Smad2 and Smad3 signaling in repair and remodeling of the infarcted heart. *J. Mol. Cell Cardiol.* 132, 84–97. doi: 10.1016/j.yjmcc.2019.05.006

Indra, A. K., Warot, X., Brocard, J., Bornert, J.-M., Xiao, J.-H., Chambon, P., et al. (1999). Temporally-controlled site-specific mutagenesis in the basal layer of the epidermis: comparison of the recombinase activity of the tamoxifen-inducible Cre-ERT and Cre-ERT2 recombinases. *Nucleic Acids Res.* 27, 4324–4327. doi: 10.1093/nar/27.22.4324

Ishida, Y., Kubota, H., Yamamoto, A., Kitamura, A., Bächinger, H. P., and Nagata, K. (2006). Type I Collagen in Hsp47-null cells is aggregated in endoplasmic reticulum and deficient in N-Propeptide processing and fibrillogenesis. *Mol. Biol. Cell* 17, 2346–2355. doi: 10.1091/mbc.e05-11-1065

Ivey, M. J., Kuwabara, J. T., Pai, J. T., Moore, R. E., Sun, Z., and Tallquist, M. D. (2018). Resident fibroblast expansion during cardiac growth and remodeling. *J. Mol. Cell Cardiol.* 114, 161–174. doi: 10.1016/j.yjmcc.2017.11.012

Ivey, M. J., and Tallquist, M. D. (2016). Defining the cardiac fibroblast. *Circ. J.* 80, 2269–2276. doi: 10.1253/circj.CJ-16-1003

Kalajzic, I., Kalajzic, Z., Kaliterna, M., Gronowicz, G., Clark, S. H., Lichtler, A. C., et al. (2002). Use of Type I collagen green fluorescent protein transgenes to identify subpopulations of cells at different stages of the osteoblast lineage. *J. Bone Mineral Res.* 17, 15–25. doi: 10.1359/jbmr.2002.17.1.15

Kanisicak, O., Khalil, H., Ivey, M. J., Karch, J., Maliken, B. D., Correll, R. N., et al. (2016). Genetic lineage tracing defines myofibroblast origin and function in the injured heart. *Nat. Commun.* 7:12260. doi: 10.1038/ncomms12260

Kaur, H., Takefuji, M., Ngai, C. Y., Carvalho, J., Bayer, J., Wietelmann, A., et al. (2016). Targeted ablation of periostin-expressing activated fibroblasts prevents adverse cardiac remodeling in mice. *Circ. Res.* 118, 1906–1917. doi: 10.1161/CIRCRESAHA.116.308643

Khalil, H., Kanisicak, O., Prasad, V., Correll, R. N., Fu, X., Schips, T., et al. (2017). Fibroblast-specific TGF-β-Smad2/3 signaling underlies cardiac fibrosis. *J. Clin. Invest.* 127, 3770–3783. doi: 10.1172/JCI94753

Khalil, H., Kanisicak, O., Vagnozzi, R. J., Johansen, A. K., Maliken, B. D., Prasad, V., et al. (2019). Cell-specific ablation of Hsp47 defines the collagen-producing cells in the injured heart. *JCI Insight* 4:e128722. doi: 10.1172/jci.insight.128722

Kisanuki, Y. Y., Hammer, R. E., Miyazaki, J.-I., Williams, S. C., Richardson, J. A., and Yanagisawa, M. (2001). Tie2-Cre transgenic mice: a new model for endothelial cell-lineage analysis in vivo. *Dev. Biol.* 230, 230–242. doi: 10.1006/dbio.2000.0106

Koch, W., Rockman, H., Samama, P., Hamilton, R., Bond, R., Milano, C., et al. (1995). Cardiac function in mice overexpressing the beta-adrenergic receptor kinase or a beta ARK inhibitor. *Science* 268, 1350–1353. doi: 10.1126/science.7761854

Kong, P., Christia, P., and Frangogiannis, N. G. (2014). The pathogenesis of cardiac fibrosis. *Cell. Mol. Life Sci.* 71, 549–574. doi: 10.1007/s00018-013-1349-6

Kong, P., Shinde, A. V., Su, Y., Russo, I., Chen, B., Saxena, A., et al. (2018). Opposing actions of fibroblast and Cardiomyocyte Smad3 signaling in the infarcted Myocardium. *Circulation* 137, 707–724. doi: 10.1161/CIRCULATIONAHA.117.029622

Lacraz, G. P. A., Junker, J. P., Gladka, M. M., Molenaar, B., Scholman, K. T., Vigil-Garcia, M., et al. (2017). Tomo-Seq Identifies SOX9 as a key regulator of cardiac fibrosis during ischemic injury. *Circulation* 136, 1396–1409. doi: 10.1161/CIRCULATIONAHA.117.027832

Leach, J. P., Heallen, T., Zhang, M., Rahmani, M., Morikawa, Y., Hill, M. C., et al. (2017). Hippo pathway deficiency reverses systolic heart failure after infarction. *Nature* 550, 260–264. doi: 10.1038/nature24045

LeBleu, V. S., Teng, Y., O'Connell, J. T., Charytan, D., Müller, G. A., Müller, C. A., et al. (2013). Identification of human epididymis protein-4 as a fibroblast-derived mediator of fibrosis. *Nat. Med.* 19, 227–231. doi: 10.1038/nm.2989

Leslie, K. O., Taatjes, D. J., Schwarz, J., vonTurkovich, M., and Low, R. B. (1991). Cardiac myofibroblasts express alpha smooth muscle actin during right ventricular pressure overload in the rabbit. *Am. J. Pathol.* 139, 207–216.

Li, Y., Li, Z., Zhang, C., Li, P., Wu, Y., Wang, C., et al. (2017). Cardiac Fibroblast–specific activating transcription factor 3 protects against heart failure by suppressing MAP2K3-p38 signaling. *Circulation* 135, 2041–2057. doi: 10.1161/CIRCULATIONAHA.116.024599

Li, Y., Lui, K. O., and Zhou, B. (2018). Reassessing endothelial-to-mesenchymal transition in cardiovascular diseases. *Nat. Rev. Cardiol.* 15, 445–456. doi: 10.1038/s41569-018-0023-y

Lindner, D., Zietsch, C., Becher, P. M., Schulze, K., Schultheiss, H.-P., Tschöpe, C., et al. (2012). Differential expression of matrix metalloproteases in human fibroblasts with different origins. *Biochem. Res. Int.* 2012:10. doi: 10.1155/2012/875742

Liu, K., Tang, M., Jin, H., Liu, Q., He, L., Zhu, H., et al. (2019). Triple-cell lineage tracing by a dual reporter on a single allele. *J. Biol. Chem.* 295, 690–700. doi: 10.1074/jbc.RA119.011349

Lombardi, A. A., Gibb, A. A., Arif, E., Kolmetzky, D. W., Tomar, D., Luongo, T. S., et al. (2019). Mitochondrial calcium exchange links metabolism with the epigenome to control cellular differentiation. *Nat. Commun.* 10:4509. doi: 10.1038/s41467-019-12103-x

Madisen, L., Zwingman, T. A., Sunkin, S. M., Oh, S. W., Zariwala, H. A., Gu, H., et al. (2010). A robust and high-throughput Cre reporting and characterization system for the whole mouse brain. *Nat. Neurosci.* 13, 133–140. doi: 10.1038/nn.2467

Magness, S. T., Bataller, R., Yang, L., and Brenner, D. A. (2004). A dual reporter gene transgenic mouse demonstrates heterogeneity in hepatic fibrogenic cell populations. *Hepatology* 40, 1151–1159. doi: 10.1002/hep.20427

Maliken, B. D., Kanisicak, O., Karch, J., Khalil, H., Fu, X., Boyer, J. G., et al. (2018). Gata4-Dependent Differentiation of c-Kit^{+}–derived endothelial cells underlies artefactual cardiomyocyte regeneration in the Heart. *Circulation* 138, 1012–1024. doi: 10.1161/CIRCULATIONAHA.118.033703

Meng, Q., Bhandary, B., Bhuiyan, M. S., James, J., Osinska, H., Valiente-Alandi, I., et al. (2018). Myofibroblast-Specific TGFβ Receptor II signaling in the fibrotic response to cardiac myosin binding protein C-induced cardiomyopathy. *Circ. Res.* 123, 1285–1297. doi: 10.1161/CIRCRESAHA.118.313089

Metzger, D., Clifford, J., Chiba, H., and Chambon, P. (1995). Conditional site-specific recombination in mammalian cells using a ligand-dependent chimeric Cre recombinase. *Proc. Natl. Acad. Sci. U.S.A.* 92, 6991–6995. doi: 10.1073/pnas.92.15.6991

Mikawa, T., and Gourdie, R. G. (1996). Pericardial mesoderm generates a population of coronary smooth muscle cells migrating into the heart along with ingrowth of the epicardial organ. *Dev. Biol.* 174, 221–232. doi: 10.1006/dbio.1996.0068

Molkentin, J. D., Bugg, D., Ghearing, N., Dorn, L. E., Kim, P., Sargent, M. A., et al. (2017). Fibroblast-specific genetic manipulation of p38 Mitogen-activated protein kinase in vivo reveals its central regulatory role in Fibrosis. *Circulation* 136, 549–561. doi: 10.1161/CIRCULATIONAHA.116.026238

Möllmann, H., Nef, H. M., Kostin, S., von Kalle, C., Pilz, I., Weber, M., et al. (2006). Bone marrow-derived cells contribute to infarct remodelling. *Cardiovasc. Res.* 71, 661–671. doi: 10.1016/j.cardiores.2006.06.013

Moore, A. W., McInnes, L., Kreidberg, J., Hastie, N. D., and Schedl, A. (1999). YAC complementation shows a requirement for Wt1 in the development of epicardium, adrenal gland and throughout nephrogenesis. *Development* 126, 1845–1857.

Moore-Morris, T., Guimarães-Camboa, N., Banerjee, I., Zambon, A. C., Kisseleva, T., Velayoudon, A., et al. (2014). Resident fibroblast lineages mediate pressure overload–induced cardiac fibrosis. *J. Clin. Invest.* 124, 2921–2934. doi: 10.1172/JCI74783

Mori, T., Kawara, S., Shinozaki, M., Hayashi, N., Kakinuma, T., Igarashi, A., et al. (1999). Role and interaction of connective tissue growth factor with transforming growth factor-beta in persistent fibrosis: a mouse fibrosis model. *J. Cell. Physiol.* 181, 153–159. doi: 10.1002/(SICI)1097-4652(199910)181:1<153::AID-JCP16>3.0.CO;2-K

Nagata, K., Saga, S., and Yamada, K. M. (1988). Characterization of a novel transformation-sensitive heat-shock protein (HSP47) that binds to collagen. *Biochem. Biophys. Res. Commun.* 153, 428–434. doi: 10.1016/S0006-291X(88)81242-7

Narver, H. L. (2012). Oxytocin in the treatment of dystocia in mice. *JAALAS* 51, 10–17.

Nishiga, M., Horie, T., Kuwabara, Y., Nagao, K., Baba, O., Nakao, T., et al. (2017). MicroRNA-33 Controls Adaptive Fibrotic response in the remodeling heart by preserving lipid raft cholesterol. *Circ. Res.* 120, 835–847. doi: 10.1161/CIRCRESAHA.116.309528

Pacak, C. A., Sakai, Y., Thattaliyath, B. D., Mah, C. S., and Byrne, B. J. (2008). Tissue specific promoters improve specificity of AAV9 mediated transgene expression following intra-vascular gene delivery in neonatal mice. *Genet. Vaccines Ther.* 6:13. doi: 10.1186/1479-0556-6-13

Peel, A. L., Zolotukhin, S., Schrimsher, G. W., Muzyczka, N., and Reier, P. J. (1997). Efficient transduction of green fluorescent protein in spinal cord neurons using adeno-associated virus vectors containing cell type-specific promoters. *Gene Ther.* 4, 16–24. doi: 10.1038/sj.gt.3300358

Philips, N., Bashey, R. I., and Jimenez, S. A. (1994). Collagen and fibronectin expression in cardiac fibroblasts from hypertensive rats. *Cardiovasc. Res.* 28, 1342–1347. doi: 10.1093/cvr/28.9.1342

Pillai, I. C. L., Li, S., Romay, M., Lam, L., Lu, Y., Huang, J., et al. (2017). Cardiac Fibroblasts adopt Osteogenic fates and can be targeted to attenuate pathological heart calcification. *Cell Stem Cell* 20:218-232.e215. doi: 10.1016/j.stem.2016.10.005

Piras, B. A., Tian, Y., Xu, Y., Thomas, N. A., O'Connor, D. M., and French, B. A. (2016). Systemic injection of AAV9 carrying a periostin promoter targets gene expression to a myofibroblast-like lineage in mouse hearts after reperfused myocardial infarction. *Gene Ther.* 23, 469–478. doi: 10.1038/gt.2016.20

Pleger, S. T., Most, P., Boucher, M., Soltys, S., Chuprun, J. K., Pleger, W., et al. (2007). Stable Myocardial-Specific AAV6-S100A1 gene therapy results in chronic functional heart failure rescue. *Circulation* 115, 2506–2515. doi: 10.1161/CIRCULATIONAHA.106.671701

Polyakova, V., Hein, S., Kostin, S., Ziegelhoeffer, T., and Schaper, J. (2004). Matrix metalloproteinases and their tissue inhibitors in pressure-overloaded human myocardium during heart failure progression. *J. Am. Coll. Cardiol.* 44, 1609–1618. doi: 10.1016/j.jacc.2004.07.023

Pu, W., He, L., Han, X., Tian, X., Li, Y., Zhang, H., et al. (2018). Genetic targeting of organ-specific blood vessels. *Circ. Res.* 123, 86–99. doi: 10.1161/CIRCRESAHA.118.312981

Quaggin, S. E., Schwartz, L., Cui, S., Igarashi, P., Deimling, J., Post, M., et al. (1999). The basic-helix-loop-helix protein pod1 is critically important for kidney and lung organogenesis. *Development* 126, 5771–5783.

Quante, M., Tu, S. P., Tomita, H., Gonda, T., Wang, S. S. W., Takashi, S., et al. (2011). Bone Marrow-Derived Myofibroblasts contribute to the mesenchymal stem cell niche and promote tumor growth. *Cancer Cell* 19, 257–272. doi: 10.1016/j.ccr.2011.01.020

Qureshi, R., Kindo, M., Arora, H., Boulberdaa, M., Steenman, M., and Nebigil, C. G. (2017). Prokineticin receptor-1-dependent paracrine and autocrine pathways control cardiac tcf21+ fibroblast progenitor cell transformation into adipocytes and vascular cells. *Sci. Rep.* 7:12804. doi: 10.1038/s41598-017-13198-2

Raake, P. W., Vinge, L. E., Gao, E., Boucher, M., Rengo, G., Chen, X., et al. (2008). G Protein–Coupled Receptor Kinase 2 ablation in cardiac myocytes before or after myocardial infarction prevents heart failure. *Circ. Res.* 103, 413–422. doi: 10.1161/CIRCRESAHA.107.168336

Russell, J. L., Goetsch, S. C., Gaiano, N. R., Hill, J. A., Olson, E. N., and Schneider, J. W. (2011). A dynamic notch injury response activates epicardium and contributes to fibrosis repair. *Circ. Res.* 108, 51–59. doi: 10.1161/circresaha.110.233262

Russo, I., Cavalera, M., Huang, S., Su, Y., Hanna, A., Chen, B., et al. (2019). Protective effects of activated Myofibroblasts in the pressure-overloaded Myocardium are mediated through Smad-dependent activation of a matrix-preserving program. *Circ. Res.* 124, 1214–1227. doi: 10.1161/CIRCRESAHA.118.314438

Samulski, R. J., and Muzyczka, N. (2014). AAV-Mediated gene therapy for research and therapeutic purposes. *Ann. Rev. Virol.* 1, 427–451. doi: 10.1146/annurev-virology-031413-085355

Satoh, M., Hirayoshi, K., Yokota, S., Hosokawa, N., and Nagata, K. (1996). Intracellular interaction of collagen-specific stress protein HSP47 with newly synthesized procollagen. *J. Cell Biol.* 133, 469–483. doi: 10.1083/jcb.133.2.469

Sauer, B. (1998). Inducible Gene Targeting in Mice Using the Cre/loxSystem. *Methods* 14, 381–392. doi: 10.1006/meth.1998.0593

Schafer, S., Viswanathan, S., Widjaja, A. A., Lim, W.-W., Moreno-Moral, A., DeLaughter, D. M., et al. (2017). IL-11 is a crucial determinant of cardiovascular fibrosis. *Nature* 552, 110–115. doi: 10.1038/nature24676

Scharf, G. M., Kilian, K., Cordero, J., Wang, Y., Grund, A., Hofmann, M., et al. (2019). Inactivation of Sox9 in fibroblasts reduces cardiac fibrosis and inflammation. *JCI Insight* 4:e126721. doi: 10.1172/jci.insight.126721

Schumacher, S. M., Gao, E., Zhu, W., Chen, X., Chuprun, J. K., Feldman, A. M., et al. (2015). Paroxetine-mediated GRK2 inhibition reverses cardiac dysfunction and remodeling after myocardial infarction. *Sci. Transl. Med.* 7:277ra231. doi: 10.1126/scitranslmed.aaa0154

Segura, A. M., Frazier, O. H., and Buja, L. M. (2014). Fibrosis and heart failure. *Heart Fail. Rev.* 19, 173–185. doi: 10.1007/s10741-012-9365-4

Shi, Y., and Massagué, J. (2003). Mechanisms of TGF-β signaling from cell membrane to the nucleus. *Cell* 113, 685–700. doi: 10.1016/S0092-8674(03)00432-X

Shimazaki, M., Nakamura, K., Kii, I., Kashima, T., Amizuka, N., Li, M., et al. (2008). Periostin is essential for cardiac healingafter acute myocardial infarction. *J. Exp. Med.* 205, 295–303. doi: 10.1084/jem.20071297

Shimizu, T., Narang, N., Chen, P., Yu, B., Knapp, M., Janardanan, J., et al. (2017). Fibroblast deletion of ROCK2 attenuates cardiac hypertrophy, fibrosis, and diastolic dysfunction. *JCI Insight* 2:e93187. doi: 10.1172/jci.insight.93187

Shinde, A. V., and Frangogiannis, N. G. (2014). Fibroblasts in myocardial infarction: a role in inflammation and repair. *J. Mol. Cell Cardiol.* 70, 74–82. doi: 10.1016/j.yjmcc.2013.11.015

Shindo, T., Manabe, I., Fukushima, Y., Tobe, K., Aizawa, K., Miyamoto, S., et al. (2002). Krüppel-like zinc-finger transcription factor KLF5/BTEB2 is a target for angiotensin II signaling and an essential regulator of cardiovascular remodeling. *Nat. Med.* 8, 856–863. doi: 10.1038/nm738

Shi-wen, X., Stanton, L. A., Kennedy, L., Pala, D., Chen, Y., Howat, S. L., et al. (2006). CCN2 is necessary for adhesive responses to transforming growth factor-beta1 in embryonic fibroblasts. *J. Biol. Chem.* 281, 10715–10726. doi: 10.1074/jbc.M511343200

Smith, C. L., Baek, S. T., Sung, C. Y., and Tallquist, M. D. (2011). Epicardial-derived cell epithelial-to-mesenchymal transition and fate specification require PDGF receptor signaling. *Circ. Res.* 108, e15–e26. doi: 10.1161/circresaha.110.235531

Snider, P., Hinton, R. B., Moreno-Rodriguez, R. A., Wang, J., Rogers, R., Lindsley, A., et al. (2008). Periostin is required for maturation and extracellular matrix stabilization of noncardiomyocyte lineages of the heart. *Circ. Res.* 102, 752–760. doi: 10.1161/CIRCRESAHA.107.159517

Soriano, P. (1999). Generalized lacZ expression with the ROSA26 Cre reporter strain. *Nat. Genet.* 21, 70–71. doi: 10.1038/5007

Sottile, J., Shi, F., Rublyevska, I., Chiang, H.-Y., Lust, J., and Chandler, J. (2007). Fibronectin-dependent collagen I deposition modulates the cell response to fibronectin. *Am. J. Physiol. Cell Physiol.* 293, C1934–C1946. doi: 10.1152/ajpcell.00130.2007

Souders, C. A., Bowers, S. L. K., and Baudino, T. A. (2009). Cardiac Fibroblast. *Circ. Res.* 105, 1164–1176. doi: 10.1161/CIRCRESAHA.109.209809

Takeda, N., Manabe, I., Uchino, Y., Eguchi, K., Matsumoto, S., Nishimura, S., et al. (2010). Cardiac fibroblasts are essential for the adaptive response of the murine heart to pressure overload. *J. Clin. Invest.* 120, 254–265. doi: 10.1172/JCI40295

Takemura, G., Ohno, M., Hayakawa, Y., Misao, J., Kanoh, M., Ohno, A., et al. (1998). Role of apoptosis in the disappearance of infiltrated and proliferated interstitial cells after myocardial infarction. *Circ. Res.* 82, 1130–1138. doi: 10.1161/01.RES.82.11.1130

Tallquist, M. D., and Molkentin, J. D. (2017). Redefining the identity of cardiac fibroblasts. *Nat. Rev. Cardiol.* 14, 484–491. doi: 10.1038/nrcardio.2017.57

Talman, V., and Ruskoaho, H. (2016). Cardiac fibrosis in myocardial infarction—from repair and remodeling to regeneration. *Cell Tissue Res.* 365, 563–581. doi: 10.1007/s00441-016-2431-9

Travers, J. G., Kamal, F. A., Valiente-Alandi, I., Nieman, M. L., Sargent, M. A., Lorenz, J. N., et al. (2017). Pharmacological and Activated Fibroblast Targeting of Gβγ-GRK2 After Myocardial Ischemia Attenuates Heart Failure Progression. *J. Am. Coll. Cardiol.* 70, 958–971. doi: 10.1016/j.jacc.2017.06.049

Turner, N. A. (2014). Effects of interleukin-1 on cardiac fibroblast function: relevance to post-myocardial infarction remodelling. *Vasc. Pharmacol.* 60, 1–7. doi: 10.1016/j.vph.2013.06.002

Ubil, E., Duan, J., Pillai, I. C. L., Rosa-Garrido, M., Wu, Y., Bargiacchi, F., et al. (2014). Mesenchymal–endothelial transition contributes to cardiac neovascularization. *Nature* 514, 585–590. doi: 10.1038/nature13839

Valiente-Alandi, I., Potter, S. J., Salvador, A. M., Schafer, A. E., Schips, T., Carrillo-Salinas, F., et al. (2018). Inhibiting Fibronectin attenuates fibrosis and improves cardiac function in a model of heart failure. *Circulation* 138, 1236–1252. doi: 10.1161/CIRCULATIONAHA.118.034609

van Amerongen, M., Bou-Gharios, G., Popa, E., van Ark, J., Petersen, A., van Dam, G., et al. (2008). Bone marrow-derived myofibroblasts contribute functionally to scar formation after myocardial infarction. *J. Pathol.* 214, 377–386. doi: 10.1002/path.2281

van Dijk, A., Niessen, H. W. M., Ursem, W., Twisk, J. W. R., Visser, F. C., and van Milligen, F. J. (2008). Accumulation of fibronectin in the heart after myocardial infarction: a putative stimulator of adhesion and proliferation of adipose-derived stem cells. *Cell Tissue Res.* 332, 289–298. doi: 10.1007/s00441-008-0573-0

Van Linthout, S., Miteva, K., and Tschöpe, C. (2014). Crosstalk between fibroblasts and inflammatory cells. *Cardiovasc. Res.* 102, 258–269. doi: 10.1093/cvr/cvu062

van Tuyn, J., Atsma, D. E., Winter, E. M., van der Velde-van Dijke, I., Pijnappels, D. A., Bax, N. A. M., et al. (2007). Epicardial cells of human adults can undergo an Epithelial-to-Mesenchymal transition and obtain characteristics of smooth muscle cells in vitro. *Stem Cells* 25, 271–278. doi: 10.1634/stemcells.2006-0366

Verma, S. K., Garikipati, V. N. S., Krishnamurthy, P., Schumacher, S. M., Grisanti, L. A., Cimini, M., et al. (2017). Interleukin-10 inhibits bone marrow fibroblast progenitor cell–mediated cardiac fibrosis in pressure-overloaded myocardium. *Circulation* 136, 940–953. doi: 10.1161/CIRCULATIONAHA.117.027889

Verrou, C., Zhang, Y., Zurn, C., Schamel, W. W., and Reth, M. (1999). Comparison of the tamoxifen regulated chimeric Cre recombinases MerCreMer and CreMer. *Biol. Chem.* 380, 1435–1438. doi: 10.1515/bc.1999.184

Villalobos, E., Criollo, A., Schiattarella, G. G., Altamirano, F., French, K. M., May, H. I., et al. (2019). Fibroblast Primary Cilia are required for cardiac Fibrosis. *Circulation* 139, 2342–2357. doi: 10.1161/circulationaha.117.028752

Wang, J., Chen, H., Seth, A., and McCulloch, C. A. (2003). Mechanical force regulation of myofibroblast differentiation in cardiac fibroblasts. *Am. J. Physiol. Heart Circ. Physiol.* 285, H1871–H1881. doi: 10.1152/ajpheart.00387.2003

Wang, Y., Nakayama, M., Pitulescu, M. E., Schmidt, T. S., Bochenek, M. L., Sakakibara, A., et al. (2010). Ephrin-B2 controls VEGF-induced angiogenesis and lymphangiogenesis. *Nature* 465, 483–486. doi: 10.1038/nature09002

Wendling, O., Bornert, J.-M., Chambon, P., and Metzger, D. (2009). Efficient temporally-controlled targeted mutagenesis in smooth muscle cells of the adult mouse. *Genesis* 47, 14–18. doi: 10.1002/dvg.20448

Woodall, M. C., Woodall, B. P., Gao, E., Yuan, A., and Koch, W. J. (2016). Cardiac Fibroblast GRK2 deletion enhances contractility and remodeling following ischemia/reperfusion injury. *Circ. Res.* 119, 1116–1127. doi: 10.1161/CIRCRESAHA.116.309538

Wu, Z., Asokan, A., and Samulski, R. J. (2006). Adeno-associated virus serotypes: vector toolkit for human gene therapy. *Mol. Ther.* 14, 316–327. doi: 10.1016/j.ymthe.2006.05.009

Xiang, F.-L., Fang, M., and Yutzey, K. E. (2017). Loss of β-catenin in resident cardiac fibroblasts attenuates fibrosis induced by pressure overload in mice. *Nat. Commun.* 8:712. doi: 10.1038/s41467-017-00840-w

Xiao, Y., Hill, M. C., Li, L., Deshmukh, V., Martin, T. J., Wang, J., et al. (2019). Hippo pathway deletion in adult resting cardiac fibroblasts initiates a cell state transition with spontaneous and self-sustaining fibrosis. *Genes Dev.* 33, 1491–1505. doi: 10.1101/gad.329763.119

Yang, J., Savvatis, K., Kang, J. S., Fan, P., Zhong, H., Schwartz, K., et al. (2016). Targeting LOXL2 for cardiac interstitial fibrosis and heart failure treatment. *Nat. Commun.* 7:13710. doi: 10.1038/ncomms13710

Yata, Y., Scanga, A., Gillan, A., Yang, L., Reif, S., Breindl, M., et al. (2003). DNase I–hypersensitive sites enhance α1(I) collagen gene expression in hepatic stellate cells. *Hepatology* 37, 267–276. doi: 10.1053/jhep.2003.50067

Zeisberg, E. M., and Kalluri, R. (2010). Origins of cardiac fibroblasts. *Circ. Res.* 107, 1304–1312. doi: 10.1161/CIRCRESAHA.110.231910

Zhang, P., Su, J., and Mende, U. (2012). Cross talk between cardiac myocytes and fibroblasts: from multiscale investigative approaches to mechanisms and functional consequences. *Am. J. Physiol. Heart Circ. Physiol.* 303, H1385–H1396. doi: 10.1152/ajpheart.01167.2011

Zhang, Y., Riesterer, C., Ayrall, A.-M., Sablitzky, F., Littlewood, T. D., and Reth, M. (1996). Inducible Site-directed recombination in mouse embryonic stem cells. *Nucleic Acids Res.* 24, 543–548. doi: 10.1093/nar/24.4.543

Zhao, L., Wang, B., Gomez, N. A., de Avila, J. M., Zhu, M.-J., and Du, M. (2019). Even a low dose of tamoxifen profoundly induces adipose tissue browning in female mice. *Int. J. Obes.* 44, 226–234. doi: 10.1038/s41366-019-0330-3

Zhou, B., Ma, Q., Rajagopal, S., Wu, S. M., Domian, I., Rivera-Feliciano, J., et al. (2008). Epicardial progenitors contribute to the cardiomyocyte lineage in the developing heart. *Nature* 454, 109–113. doi: 10.1038/nature07060

Zhou, B., and Pu, W. T. (2011). Epicardial epithelial-to-mesenchymal transition in injured heart. *J. Cell Mol. Med.* 15, 2781–2783. doi: 10.1111/j.1582-4934.2011.01450.x

Zhou, B., and Pu, W. T. (2012). Genetic Cre-loxP Assessment of Epicardial Cell Fate Using Wt1-Driven Cre Alleles. *Circ. Res.* 111, e276–e280. doi: 10.1161/CIRCRESAHA.112.275784

Conflict of Interest: The authors declare that the research was conducted in the absence of any commercial or financial relationships that could be construed as a potential conflict of interest.

frontiers in Physiology

ORIGINAL RESEARCH
published: 19 May 2020
doi: 10.3389/fphys.2020.00403

PTX3 Predicts Myocardial Damage and Fibrosis in Duchenne Muscular Dystrophy

*Andrea Farini[1], Chiara Villa[1], Dario Di Silvestre[2], Pamela Bella[1], Luana Tripodi[1], Rossana Rossi[2], Clementina Sitzia[3], Stefano Gatti[4], Pierluigi Mauri[2] and Yvan Torrente[1]**

[1] Stem Cell Laboratory, Department of Pathophysiology and Transplantation, Università degli Studi di Milano, Unit of Neurology, Fondazione IRCCS Ca' Granda Ospedale Maggiore Policlinico, Centro Dino Ferrari, Milan, Italy, [2] Institute of Technologies in Biomedicine, National Research Council (ITB-CNR), Milan, Italy, [3] Residency Program in Clinical Pathology and Clinical Biochemistry, Università degli Studi di Milano, Milan, Italy, [4] Center for Surgical Research, Fondazione IRCCS Cà Granda, Ospedale Maggiore Policlinico, Milan, Italy

Pentraxin 3 (PTX3) is a main component of the innate immune system by inducing complement pathway activation, acting as an inflammatory mediator, coordinating the functions of macrophages/dendritic cells and promoting apoptosis/necrosis. Additionally, it has been found in fibrotic regions co-localizing with collagen. In this work, we wanted to investigate the predictive role of PTX3 in myocardial damage and fibrosis of Duchenne muscular dystrophy (DMD). DMD is an X-linked recessive disease caused by mutations of the dystrophin gene that affects muscular functions and strength and accompanying dilated cardiomyopathy. Here, we expound the correlation of PTX3 cardiac expression with age and Toll-like receptors (TLRs)/interleukin-1 receptor (IL-1R)-MyD88 inflammatory markers and its modulation by the so-called alarmins IL-33, high-mobility group box 1 (HMGB1), and S100β. These findings suggest that cardiac levels of PTX3 might have prognostic value and potential in guiding therapy for DMD cardiomyopathy.

Keywords: Duchenne muscular dystrophy (DMD), muscular dystrophy, cardiomyopathy, pentraxin 3 (PTX3), alarmins

OPEN ACCESS

Edited by:
Claudio de Lucia,
Temple University, United States

Reviewed by:
Alessandra Ferlini,
University of Ferrara, Italy
Bjorn Cools,
University Hospital Leuven, Belgium

****Correspondence:***
Yvan Torrente
yvan.torrente@unimi.it

Specialty section:
This article was submitted to Integrative Physiology, a section of the journal Frontiers in Physiology

Received: *20 December 2019*
Accepted: *03 April 2020*
Published: *19 May 2020*

Citation:
Farini A, Villa C, Di Silvestre D, Bella P, Tripodi L, Rossi R, Sitzia C, Gatti S, Mauri P and Torrente Y (2020) PTX3 Predicts Myocardial Damage and Fibrosis in Duchenne Muscular Dystrophy. Front. Physiol. 11:403. doi: 10.3389/fphys.2020.00403

INTRODUCTION

Pentraxins (PTXs) are a superfamily of proteins containing the highly conserved C-terminal PTX domain. According to the primary structure of the promoter, they are divided into two distinct groups: short and long (Deban et al., 2011). Among the longer subfamily, the Pentraxin 3 (PTX3) is an inflammatory mediator, mainly produced during the first phase of the inflammatory processes by phagocytes, neutrophils, fibroblasts, endothelial cells, following the secretion of inflammatory cytokines (Doni et al., 2008). PTX3 is a fundamental component of humoral innate immunity and – in synergy with other proteins as the PTX C-reactive protein (CRP) and serum amyloid P-component (SAP) – mediates the innate resistance to pathogens, allows the activation of complement pathway, coordinates the functions of macrophages/dendritic cells (DCs), and

fosters apoptosis/necrosis (Garlanda et al., 2005; Liu et al., 2014). PTX3 plays a role in vessel repair and remodeling (Presta et al., 2007; Deban et al., 2010), and it has been documented synthesized by endothelial and smooth muscle cells as well as granulocytes at sites of active vasculitis (Fazzini et al., 2001; Presta et al., 2007; Castellano et al., 2010; Cieslik and Hrycek, 2015). Moreover, PTX3 participates in the regulation of inflammation as well as in extracellular matrix formation promoting fibrocyte differentiation (Pilling et al., 2015). However, in acute myocardial infarction as well as in myocarditis, increased PTX3 expression of both macrophages and endothelial cells was found (Nebuloni et al., 2011). In the heart, PTX3 can be induced by MyD88, which is a canonical adaptor for inflammatory signaling pathways downstream of members of the Toll-like receptor (TLR) and interleukin-1 (IL-1) receptor families. The TLRs/IL-1R-MyD88 signaling can lead to distinct outputs depending on the context: pro-inflammatory by the activation of transcription factor NF-κB (Kunes et al., 2012) or anti-inflammatory *via* type I interferon production or complement binding (Salio et al., 2008). Inflammatory signals might also participate in PTX3 expression by the catalytic activity of the induced form of the proteasome [the immunoproteasome (IP)] together with the mitogen-activated protein (MAP)-kinases p38 and extracellular signal-regulated kinase (ERK)1/2 (Paeschke et al., 2016). According to its dual role, the cardioprotective function of PTX3 has been demonstrated in acute myocardial infarction (Salio et al., 2008; Casula et al., 2017). Interestingly, Liu et al. (2018) demonstrated that PTX3 was able to modulate the expression of several cardiac genes and enhanced the transformation of mouse embryonic stem cells into cardiomyocytes. Among inflammatory signals, the IL-33 and its receptor sST2 have been associated with the overexpression of PTX3 following cardiac infarction (Ristagno et al., 2015). IL-33 is a member of the IL-1 family of cytokines produced by primarily non-hematopoietic cells in response to mechanical stress and injury. IL-1/IL-33 and other proteins as HMGB1, S100β are the so-called alarmins that are released by both resident immune cells and necrotic cells that underwent damage. These alarmins are then recognized by specific receptors [e.g., the receptor for advanced glycation end-products (RAGE) and TLRs] of various immune cells that initiate inflammatory and repair responses.

More interestingly, the IL-33/ST2 system emerged as a novel fibroblast–cardiomyocyte communication system that regulates the accumulation of anti-inflammatory T regulatory lymphocytes (Tregs) and was proposed as a biomarker for cardiomyopathy in Duchenne muscular dystrophy (DMD) (Kuswanto et al., 2016). DMD cardiomyopathy is the major cause of mortality for DMD patients, and it is characterized by unresolved cardiac inflammation and fibrosis. Recently, Frohlich et al. (2016) confirmed high expression of PTX3 in DMD dystrophic animal models. Taking into account the critical role of PTX3 in the inflammatory/fibrotic pathways and the absence of predictor markers of cardiomyopathy in DMD patients, we argued to investigate the role of PTX3 in myocardial damage and fibrosis of the *mdx* mouse model for DMD. Dystrophic cardiac expression of PTX3 correlated positively with age and inflammatory/fibrotic pathways, suggesting that cardiac levels of PTX3 have prognostic value and potential in guiding therapy for cardiomyopathy of DMD.

MATERIALS AND METHODS

Animal Statement

All procedures involving living animals were performed in accordance with Italian law (D.L.vo 116/92 and subsequent additions), which conforms to the European Union guidelines. The use of animals in this study was authorized by the National Ministry of Health (protocol number 10/13–2014/2015). Ten weeks (10w), 3 months (3m), 5m, and 7m C57Bl and 11 days (11dy), 10w, 3m, 9m, 14m, and 18m mdx (*C57BL6*/10ScSn-DMD*mdx*/J) mice were provided by Charles River. All animals were housed in a controlled ambient environment (12 h light/dark cycle) at a temperature between 21 and 23°C. Cage population was limited to a maximum of four animals each to ensure the health and welfare of animals. The mice had free access to clean water and food. Systemic intraperitoneal injection of the IP inhibitor ONX-0914 (Clini Sciences, 6 mg/kg) was performed in 10w and 9m mdx mice for 5 weeks (two injections/week, $n = 10$). Untreated aged-matched mdx mice were used as controls. After 1 month of treatment, mice were deeply anesthetized with 2% avertin (0.015 ml/kg), then sacrificed by cervical dislocation.

RT-qPCR Experiments

Total RNA was extracted from cardiac tissues obtained from 11dy, 10w, 3m, 9m, and 18m mdx mice. cDNA was generated using the Reverse Transcriptase Kit (Thermo Fisher Scientific) followed by the SYBR-Green reaction to quantify the expression of the genes in **Table 1**. All the cDNA samples were tested in duplicate, and the threshold cycles (Ct) of target genes were normalized against a housekeeping gene, the glyceraldehyde 3-phosphate dehydrogenase (GAPDH). Relative transcript levels were calculated from the Ct values as $X = 2^{-\Delta\ \Delta\ ct}$ where X is the fold difference in the amount of target gene versus GAPDH and $\Delta Ct = Ct_{target} - Ct_{GAPDH}$.

Network-Based Prediction of Protein Interactions

A protein–protein interaction (PPI) network (30 nodes and 70 edges) was built by matching differentially expressed proteins

TABLE 1 | Sequence of primers used in RT-qPCR.

	Forward (5′→3′)	Reverse (5′→3′)
C1s	tgaaggaagagggaaagacaag	gattttggaggtaaagggcagt
C1r	acttccgctacatcaccacaa	ctctccttcctcttcattcttcc
C3	acaaactcacacagagcaaga	atccatgaagacaccagcatag
C5	cagcaaggaggagtcaacat	tccacaagagcccgtaaatc
FH	tctcaggctcgtggtcagaa	ccagggcggcatttgtag
C4	tctcacaaacccctcgacat	agcatcctggaacacctgaa

and *Mus musculus* PPI data retrieved from STRING (Szklarczyk et al., 2019)[1]; only Experimental and Database annotated interactions (Score > 0.15) were considered (Doncheva et al., 2019). Protein expression data were further processed by Pearson's correlation (Score > | 0.6|, $p < 0.05$), and significant correlations were visualized as a network (27 nodes and 99 edges) using Cytoscape software (Vella et al., 2017). Reconstructed network was analyzed at the topological level, and Cytoscape's plugin CentiScaPe was used to calculate centrality indices of each node (Scardoni et al., 2009); specifically, nodes with Betweenness, Bridging, and Degree above the network average were retained and considered hubs as previously reported (Sereni et al., 2019).

Western Blot Analysis

Total proteins from skeletal muscles and cardiac biopsies isolated from normal and dystrophic mice were extracted as in Farini et al. (2019). Samples were resolved on polyacrylamide gels (ranging from 10% to 14%) and transferred to nitrocellulose membranes (Bio-Rad Laboratories). Filters were incubated overnight with the following antibodies: vinculin (1:600, MA5-11690, Invitrogen); PTX3 (C-10 1:600, sc-373951, Santa Cruz Biotechnology); phospho-p38 (Thr180) (1:500, E-AB-20949, Elabscience); p38 (1:500, E-AB-32460, Elabscience); ERK1/2 (1:500, E-AB-31374, Elabscience); phospho-ERK1/2 (Thr202) (1:500, E-AB-20868, Elabscience); PSMB5 (1:500, ab3330, Abcam); PSMB8 (1:500, Proteasome 20S LMP7, ab3329, Abcam); PSMB9 [1:500, Proteasome 20S LMP2 (EPR13785) ab184172, Abcam]; RAGE (1:500, NBP2-03950, Novusbio); S-100β chain (C-3) (1:500, sc-393919, Santa Cruz Biotechnology); monocyte chemoattractant protein (MCP)-1 (ECE.2) (1:500, sc-52701, Santa Cruz Biotechnology); Foxp3 (FJK-16s) (1:500, 14-5773-82, eBioscience); IL-33 (1:500, AF3626, R&D Systems); collagen VI (1:500, ab6588, Abcam); phospho-SMAD2/3 (Thr8) (1:500, E-AB-21040, Elabscience); TLR9 (26C593) (1:500, sc-52966, Santa Cruz Biotechnology); matrix metalloproteinase (MMP)-9 (E-11) (1:500, sc-393859, Santa Cruz Biotechnology); TLR4 (25) (1:500, sc-293072, Santa Cruz Biotechnology); TRAF6 (D-10) (1:500, sc-8409, Santa Cruz Biotechnology); SMAD3 (1:500, E-AB-32921, Elabscience); TLR2 (1:500, orb229137, Biorbyt); TLR5 (19D759.2) (1:500, sc-57461, Santa Cruz Biotechnology); NF-κB p65 (A-12) (1:500, sc-514451, Santa Cruz Biotechnology); RelB (D-4) (1:500, sc-48366, Santa Cruz Biotechnology); MYD88 (1:500, 23230-1-AP, Proteintech); transforming growth factor (TGF)β1 (1:500, E-AB-33090, Elabscience); IL-6 (10E5) (1:500, sc-57315, Santa Cruz Biotechnology); tumor necrosis factor (TNF)α (1:500, E-AB-40015, Elabscience); poly(ADP-ribose) polymerase (PPAR)γ (1:600, ab-59256, Abcam); autophagy-related (ATG)7 (1:600, SAB4200304, Sigma Aldrich); p62 (1:600, P0067, Sigma Aldrich); LC3B (1:500, L7543, Sigma Aldrich); HMGB1 (HAP46.5) (1:600, sc-56698, Santa Cruz Biotechnology); actin (1:600, A2066, Sigma Aldrich); GAPDH (0411) (1:600, sc-47724, Santa Cruz Biotechnology). Membranes were incubated with primary antibodies ON at 4°C, followed by washing, detection with horseradish peroxidase (HRP)-conjugated secondary antibodies (DakoCytomation, United States), and developed by enhanced chemiluminescence (ECL) (Amersham Biosciences, United States). Bands were visualized using an Odyssey Infrared Imaging System (Li-COR Biosciences, United States). Densitometric analysis was performed using ImageJ software[2].

Immunofluorescence and Immunohistochemistry Analysis

Cardiac biopsies were collected from 10w C57Bl and 10w, 9m, and 18m mdx mice, frozen in liquid nitrogen-cooled isopentane, and then sectioned on a cryostat (LEICA CM 1850). Serial sections (8 μm thick) were stained with Azan Mallory. Densitometric analyses and manual or automatic counting (Threshold color Plug-in) were performed using ImageJ software[2] in 20 sections/muscle.

For immunofluorescence staining, sections were fixed in 4% paraformaldehyde (PFA) methanol-free (28908, Thermo Fisher Scientific) and permeabilized with phosphate-buffered saline (PBS) 1 × + 0.1% Triton X-100 (T9284, Sigma Aldrich) for 20 min at room temperature (RT). Sections were then incubated with PBS 1× + 10% donkey serum (blocking solution) for 1 h at RT. Primary antibodies anti-PTX3 (C-10, sc-373951, Santa Cruz Biotechnology), anti-CD31 (MEC 13.3, 5550274, BD Pharmingen), and anti-NG2 (AB5320, Merck Millipore) were diluted 1:100 in blocking solution and added to slides overnight at 4°C. Alexa Fluor-conjugated secondary antibodies against mouse (A32766, Thermo Fisher Scientific, for PTX3), rat (A21209, Thermo Fisher Scientific, for CD31), and rabbit (A31573, Thermo Fisher Scientific, for NG2) were diluted 1:200 in PBS and applied onto slides for 1 h at RT. Phycoerythrin (PE)-conjugated CD206 antibody (1:50, 141705, BioLegend) and fluorescein isothiocyanate (FITC)-conjugated α-smooth muscle actin (1:150, 1A4, Sigma Aldrich) were directly diluted in PBS and incubated for 2 h. Nuclei were counterstained with 4',6-diamidino-2-phenylindole (DAPI), and slides were mounted with Fluoromount-G mounting medium (00-4958-02, Thermo Fisher Scientific). Images were captured using the epifluorescence microscopy DMi8 (Leica, Germany).

Immunohistochemistry of PTX3 and PMSB8 (1:100, ab3329, Abcam) was performed by blocking endogenous peroxidase activity in 0.3% alcoholic hydrogen peroxide for 30 min. Antigen retrieval was then performed in 0.01 M sodium citrate buffer at pH 6 for 30 min at 100°C. Sections were blocked with 5% horse and 5% fetal bovine serum for 30 min at RT and incubated overnight at 4°C with either anti-PTX3 or anti-PMSB8, diluted 1:100 in blocking solution. Cardiac tissues were then incubated with appropriate biotinylated immunoglobulin antibodies for 30 min at RT, followed by peroxidase–avidin–biotin complex (Vectastain ABC Elite kit; Vector Labs, Burlingame, CA, United States) incubation for 30 min. 3,3′-Diaminobenzidine (DAB) was used as the chromogen.

[1]https://string-db.org/

[2]http://rsbweb.nih.gov/ij/

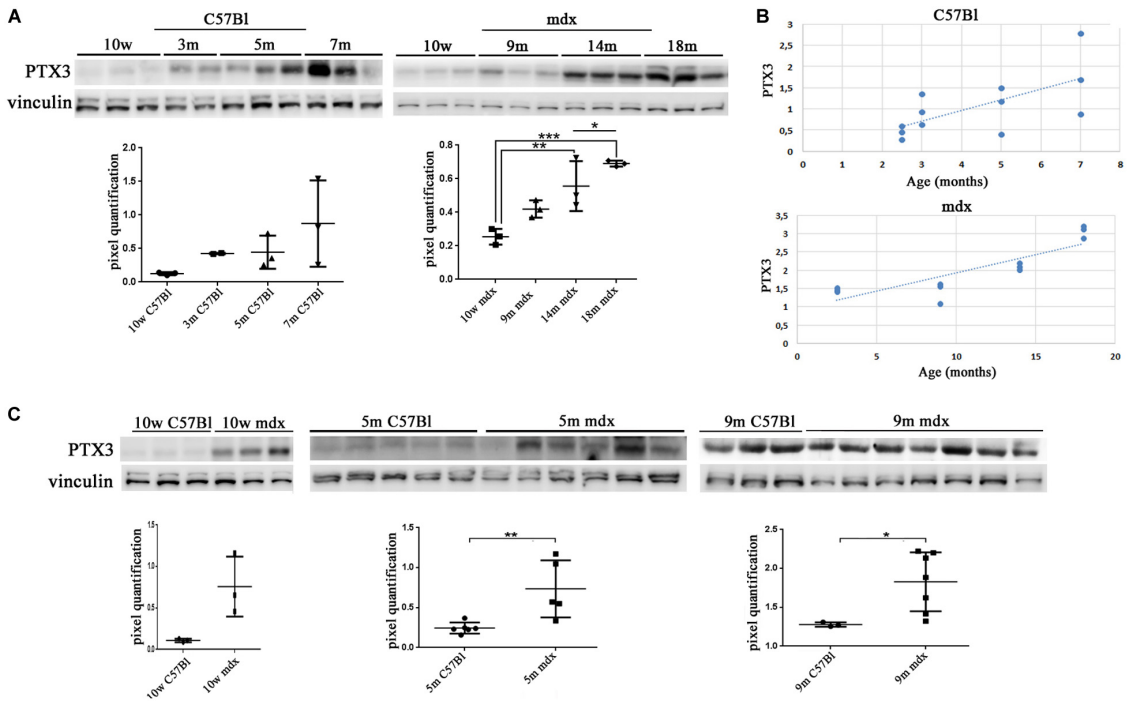

FIGURE 1 | Pentraxin (PTX)3 expression in skeletal muscle biopsies of mdx mice at different ages. Representative Western blot (WB) of PTX3 in TAs of 10 weeks (10w), 3 months (3m), 5m, 7m C57Bl mice and in TAs of 10w, 9m, 14m, and 18m mdx mice. Data from densitometric analysis are expressed as PTX3/vinculin ratio in arbitrary units in the lower panels. One-way ANOVA with Tukey's multiple comparisons test: $^{*}p < 0.05$; $^{**}p < 0.01$; $^{***}p < 0.001$ **(A)**. In the lateral panels, the scheme representing PTX3 expression, in C57Bl and mdx mice, according to ages **(B)**. Representative WB of PTX3 in TA of 10w, 5m, and 9m C57Bl mice and age-matched mdx mice. Data from densitometric analysis are expressed as the ratio of PTX3/vinculin in arbitrary units in the lateral panels. Student's *t*-test: $^{*}p < 0.05$; $^{**}p < 0.01$ **(C)**. Each experiment was performed in triplicate wells. All values are expressed as the mean ± SD.

Availability of Data

The raw data supporting the conclusions of this manuscript will be made available by the authors, without undue reservation, to any qualified researcher.

Statistics

Data were analyzed by GraphPad Prism™ and expressed as mean ± SD or mean ± SEM. To compare multiple group means, one-way ANOVA followed by Tukey's multiple comparison test was used to determine significance ($^{*}p < 0.05$, $^{**}p < 0.01$, $^{***}p < 0.001$; $^{****}p < 0.0001$). To compare two groups, Student's *t*-test was applied assuming equal variances: difference was considered significant at $^{*}p < 0.05$. To correlate protein's expression, linear regression and multivariate regression analyses were performed.

RESULTS

Pentraxin 3 Expression in Skeletal Muscle of Mdx Mice Is Strictly Upregulated and Dependent on Age

We firstly evaluated the expression of PTX3 in muscular biopsies of normal and dystrophic mice. In C57Bl, we determined a non-significant increase of PTX3 expression with age (**Figure 1A**). Conversely, we found a PTX3 downregulation in 10w C57Bl mice compared to mdx mice in the 10 weeks–18 months age range (C57Bl versus 14m mdx, $p = 0.0044$; C57Bl versus 18m mdx, $p = 0.0005$). Moreover, the dystrophic mice displayed an age-related upregulation of PTX3, particularly significant considering the older mdx (10w mdx versus 14m mdx, $p = 0.0071$; 10w mdx versus 18m mdx, $p = 0.0005$; 9m mdx versus 18m mdx, $p = 0.0139$) (**Figure 1A**). Statistical analysis through Pearson's correlation coefficient also showed that PTX3 amount was dramatically dependent on the age (Pearson $r = 0.8533$; 95% confidence interval: 0.5475–0.9581 with $p = 0.0004$) (**Figure 1B**). We thus compared the amount of PTX3 in aged-matched muscular biopsies (10w, 5 m, 9 m), and we found a significant upregulation of PTX3 in 10w ($p = 0.0365$), 5m ($p = 0.0089$), and 9m ($p = 0.0415$) mdx related to C57Bl mice (**Figure 1C**).

Pentraxin 3 Is Upregulated in Cardiac Muscles of Mdx Mice in Age-Dependent Manner

We then aimed at determining the PTX3 role in the cardiac muscle, by assessing its amount in 10w and 5m C57Bl and mdx mouse hearts. We found a PTX3 expression increasing with ages in control mice (10w C57Bl versus 5m C57Bl, $p = 0.0318$), while both in younger and older dystrophic hearts, PTX3 was upregulated compared to 10w C57Bl (with $p = 0.0140$ and

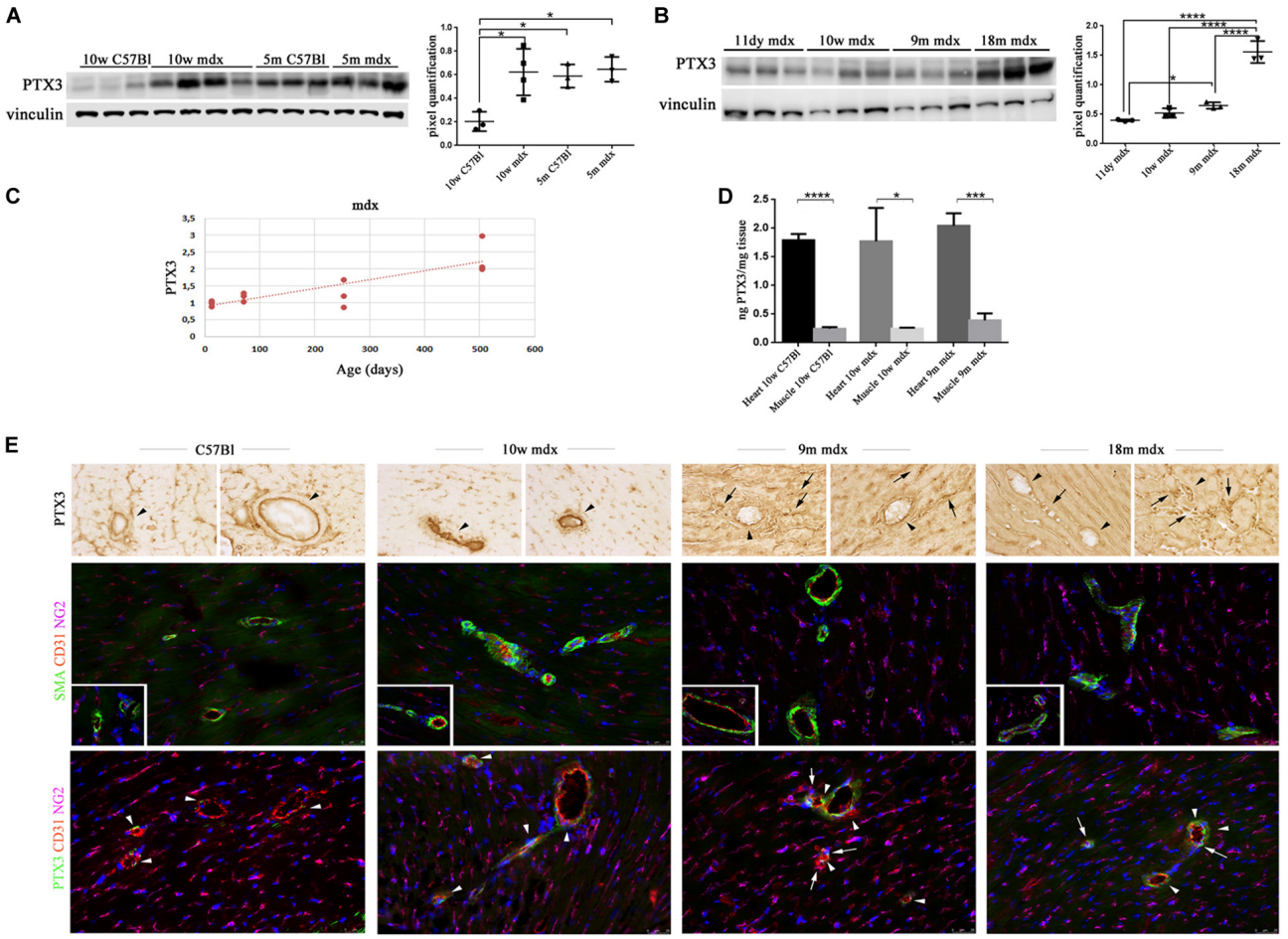

FIGURE 2 | Pentraxin (PTX)3 expression in skeletal cardiac tissues of mdx mice at different ages. Representative Western blot (WB) of PTX3 in cardiac tissues of 10 weeks (10w) and 5 months (5m) C57Bl mice and age-matched mdx mice. Data from densitometric analysis are expressed as the ratio of PTX3/vinculin in arbitrary units in lateral panels. One-way ANOVA with Tukey's multiple comparisons test: $^{*}p < 0.05$ **(A)**. Representative WB of PTX3 in cardiac tissues of 11 days (11dy), 10w, 9m, and 18m mdx mice. Data from densitometric analysis are expressed as PTX3/vinculin ratio in arbitrary units in the lateral panel. One-way ANOVA with Tukey's multiple comparisons test: $^{*}p < 0.05$; $^{****}p < 0.0001$ **(B)**. The line graph represents the dependence of PTX3 expression according to the age in mdx cardiac tissues **(C)**. ELISA quantification of PTX3 in cardiac muscles of 10w C57Bl and 10w and 9m mdx mice related to skeletal muscles of age-matched mice. Student's *t*-test: $^{*}p < 0.05$; $^{***}p < 0.001$; $^{****}p < 0.0001$ **(D)**. **(E)** Representative images of hearts from 10w C57Bl and 10w, 9m, and 18m mdx mice ($n = 5$ each) showing PTX3 and vascular staining. Representative images of PTX3 immunohistochemistry staining of endothelial (arrowheads) and mural cells (pericytes) (arrows) within coronary vessel wall from C57Bl and mdx (first row). Representative images of coronary vessels expressing smooth muscle actin (SMA) (green) and CD31 (red) showing increased expression of NG2 (magenta) and altered morphology of NG2-expressing pericytes around and between cardiac vessels in 9m and 10m mdx hearts compared to C57Bl (second row). Magnification in the second row inserts indicates the presence of NG2 + pericyte processes covering C57Bl cardiac vessels, while mdx pericyte processes are spread out along the cardiac vessels. Representative images of PTX3 (green), CD31 (red), and NG2 (magenta) staining in hearts indicate PTX3-expressing endothelial CD31 + cells (arrowheads) and PTX3-expressing NG2 + pericytes (arrows) between vessels. These latter cells displayed a rounder morphology in mdx than in C57Bl hearts, and the lack of a complete covering of a large portion of cardiac vessels by NG2 + pericyte processes (third row). Nuclei were counterstained with 4′,6-diamidino-2-phenylindole (DAPI) (blue). Scale bar: 25 mm. Each experiment was performed in triplicate wells. All values are expressed as the mean ± SD.

$p = 0.0152$ related to mdx 10w and mdx 5m, respectively) (**Figure 2A**). In line with the experiments involving skeletal muscles, we evaluated PTX3 expression in mdx mice at different ages—11dy, 10w, 9m, 18m. This time, we showed that PTX3 was only slightly upregulated in 9m related to 11dy mdx ($p = 0.0458$) (**Figure 2B**), but presenting a dramatic increase toward 18 months of age (with $p < 0.0001$ related to all the other mdx mice). We suggested that this condition was correlated to mdx cardiomyopathy onset, becoming evident from 8 months of age and worsening later than in skeletal muscles. Interestingly, the expression of PTX3 was age-dependent (Pearson $r = 0.8342$; 95% confidence interval: 0.4993–0.9522 with $p = 0.0007$) (**Figure 2C**). ELISA quantification showed that the amount of PTX3 was fivefold higher in cardiac muscles of C57Bl and 10w and 9m mdx mice related to skeletal muscles of age-matched mice (with $p < 0.0001$, $p = 0.0106$, $p = 0.0003$, respectively) (**Figure 2D**). We also investigated the expression of PTX3 by immunohistochemistry and immunofluorescence staining in

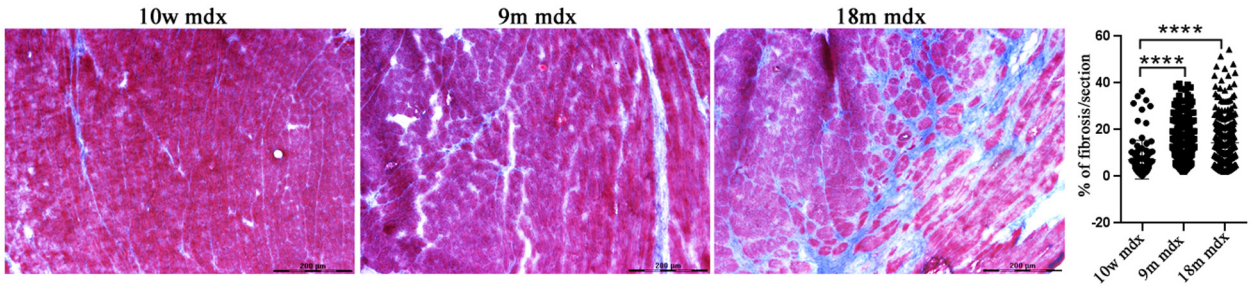

FIGURE 3 | Evaluation of fibrosis in cardiac tissues of mdx mice at different ages. Representative Azan Mallory images of cardiac tissues of 10 weeks (10w), 9 months (9m), and 18m mdx mice ($n = 5$ each). Histogram represents the percentage of fibrotic area per cardiac section of mdx mice. Scale bar: 200 mm. One-way ANOVA with Tukey's multiple comparisons test: ****$p < 0.0001$.

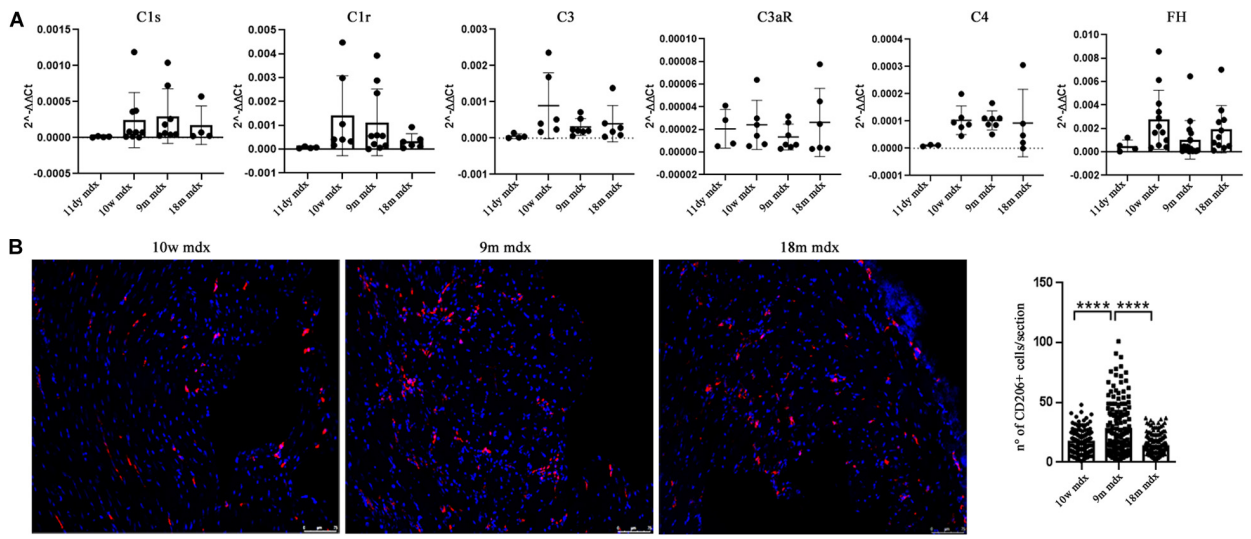

FIGURE 4 | RT-qPCR of complement and evaluation of CD206 + cells in cardiac tissues of mdx mice at different ages. **(A)** RT-qPCR expression of genes involved in complement activation pathway in 11 days (11dy), 10 weeks (10w), 9 months (9m), and 18m mdx mice. **(B)** Immunofluorescence analysis of CD206 (red) in cardiac tissues of 10w, 9m, and 18m mdx mice ($n = 5$ each). Nuclei were counterstained with 4',6-diamidino-2-phenylindole (DAPI) (blue) Scale bar: 75 mm. One-way ANOVA with Tukey's multiple comparisons test: ****$p < 0.0001$. Each experiment was performed in triplicate wells. All values are expressed as the mean ± SD.

cardiac tissues of C57Bl and mdx mice. Interestingly, we noted an increased signal for proteoglycan neural/glial2 (NG2) and an altered morphology of NG2-expressing pericytes in 9m and 18m mdx compared with 10w C57Bl and 10m mdx hearts (**Figure 2E**). Moreover, a lessened fluorescent PTX3 signal was found in CD31 + endothelial cells of both younger C57Bl and mdx hearts, whereas PTX3 staining become increased in CD31 + endothelial cells of 9m and 18m mdx hearts (**Figure 2E**). On the other hand, PTX3-expressing NG2 + pericytes between cardiac vessels with a rounder morphology were present only in 9m and 18m mdx (**Figure 2E**).

Pentraxin 3 in Dystrophic Cardiac Remodeling: Complement Activation and M2 Macrophages

Considering the established involvement of PTX3 in fibrotic and inflammatory pathways, we aimed at discovering the effects of PTX3 upregulation and of the associated proteins in regulating the rising of pathological signs in dystrophic cardiac tissues. Azan Mallory staining of cardiac muscles showed a marked upregulation of fibrosis (calculated as a percentage of fibrosis per single image) in older mdx hearts (9m mdx and 18m mdx) related to 10w mdx mice (with $p < 0.0001$ for both). In line with previous results published by Van Erp et al. (2010), we demonstrated that the 18m mdx mice did not display a significant upregulation of fibrosis compared to 9m mice (**Figure 3**). Regulation of complement activation by PTX3 seems to be involved in tissue damage through a complex scheme. In brief, PTX3 can bind the C1q protein to activate the classical component cascade, allowing the deposition of C3 and C4 (Kunes et al., 2012). Alternatively, PTX3 can bind to the Factor H (FH) and limit the activation of the alternative pathway of complement (Ristagno et al., 2019). In this sense, we verified whether the elevated expression of PTX3 correlated to dysfunction of the complement signaling cascade in older 18m mdx mice. However, we did

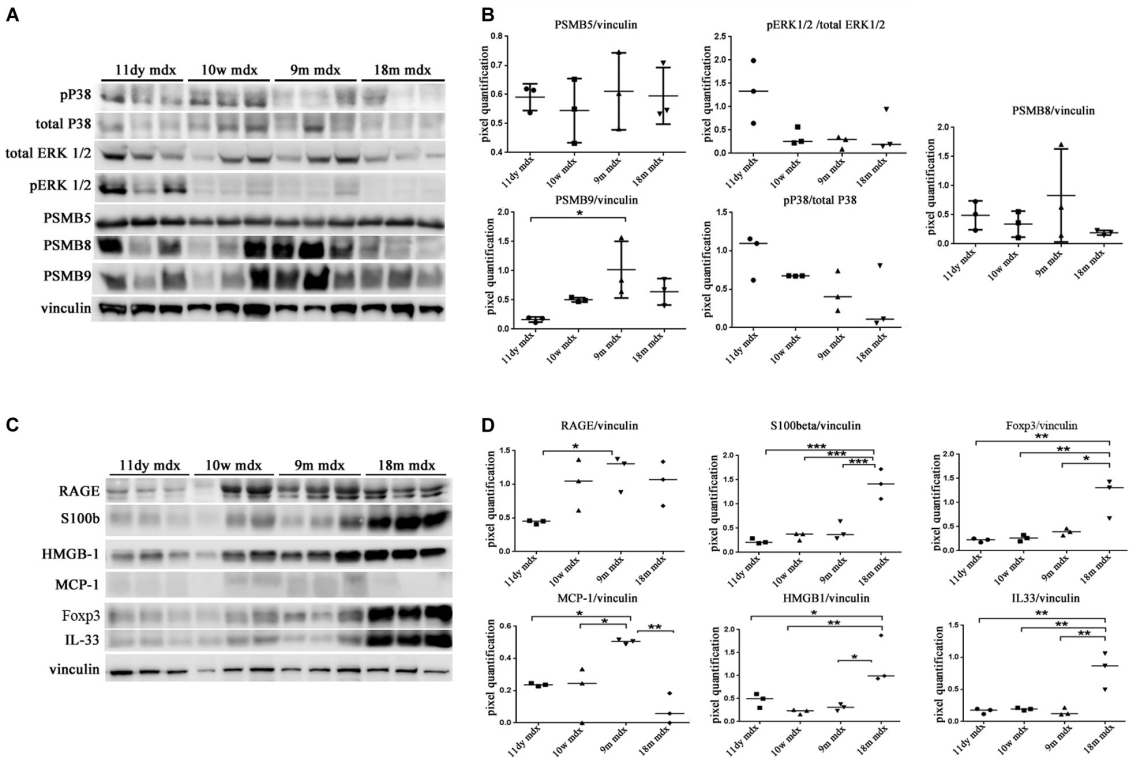

FIGURE 5 | Western blot (WB) analysis of immunoproteasome (IP) subunits and alarmins in cardiac tissues of mdx mice at different ages. Representative WB of PSMB5, PSMB8, PSMB9, pERK/total ERK, and p38/total p38 in cardiac tissues of 11 days (11dy), 10 weeks (10w), 9 months (9m), and 18m mdx mice **(A)**. In the lateral panel, densitometric analysis of data, expressed as the ratio of different proteins versus vinculin in arbitrary units. One-way ANOVA with Tukey's multiple comparisons test: $^{*}p < 0.05$ **(B)**. Representative WB of receptor for advanced glycation end-products (RAGE), S100β, Foxp3, monocyte chemoattractant protein (MCP)-1, high-mobility group box (HMGB)1, and interleukin (IL)-33 in cardiac tissues of 11dy, 10w, 9m, and 18m mdx mice **(C)**. Data from densitometric analysis are expressed as the ratio of different proteins versus vinculin in arbitrary units in the lateral panel **(D)**. One-way ANOVA with Tukey's multiple comparisons test: $^{*}p < 0.05$; $^{**}p < 0.01$; $^{***}p < 0.001$. Each experiment was performed in triplicate wells. All values are expressed as the mean ± SD.

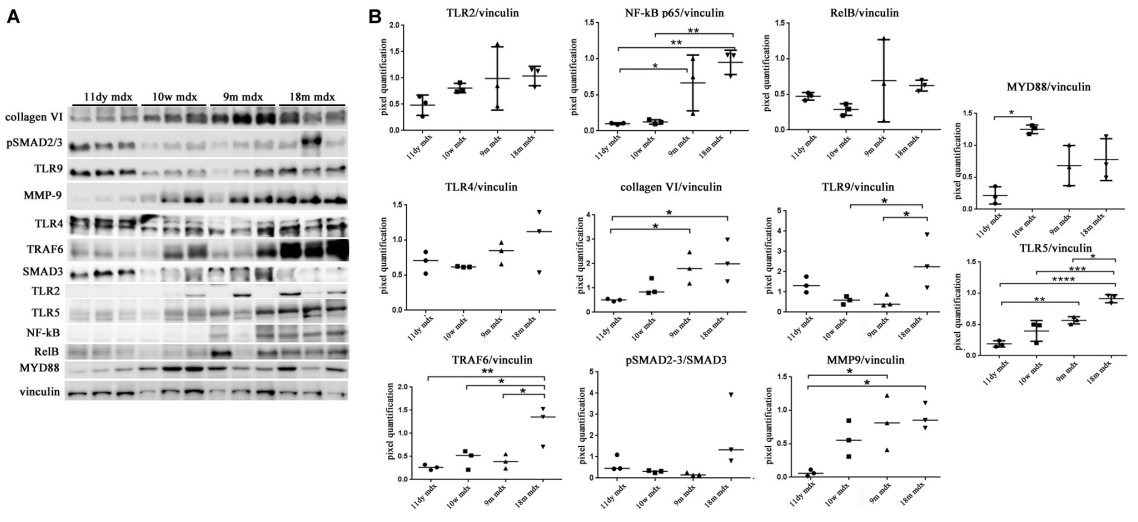

FIGURE 6 | Evaluation of proteins involved in inflammation and fibrosis in cardiac tissues of mdx mice at different ages. Representative Western blot (WB) of several inflammatory and fibrotic mediators in cardiac tissues of 11 days (11dy), 10 weeks (10w), 9 months (9m), and 18m mdx mice **(A)**. Data from densitometric analysis are expressed as the ratio of different proteins versus vinculin in arbitrary units in the lateral panel. One-way ANOVA with Tukey's multiple comparisons test: $^{*}p < 0.05$; $^{**}p < 0.01$; $^{***}p < 0.001$; $^{****}p < 0.0001$ **(B)**. Each experiment was performed in triplicate wells. All values are expressed as the mean ± SD.

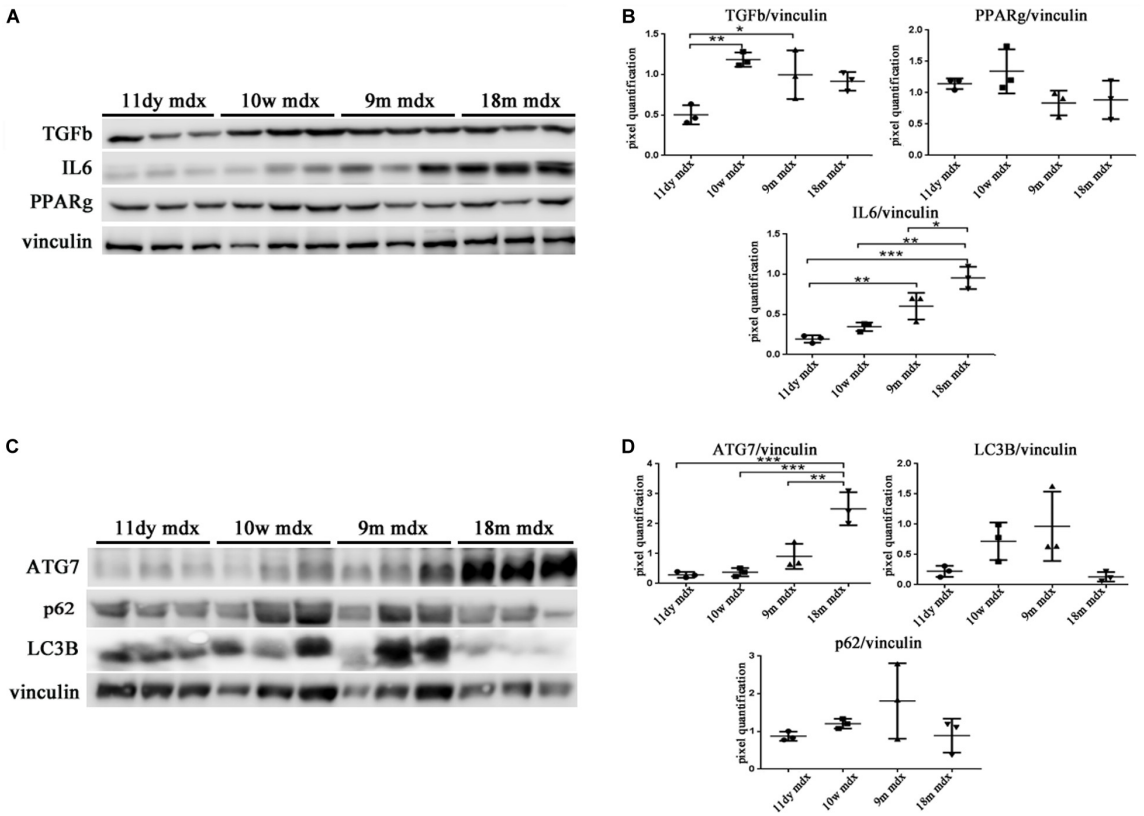

FIGURE 7 | Evaluation of inflammatory cytokines and autophagic mediators in cardiac tissues of mdx mice at different ages. Representative Western blot (WB) of transforming growth factor (TGF)-b, poly(ADP-ribose) polymerase (PPAR)g, interleukin (IL)-6, and tumor necrosis factor (TNF)-a in cardiac tissues of 11 days (11dy), 10 weeks (10w), 9 months (9m), and 18m mdx mice **(A)**. Data from densitometric analysis are expressed as the ratio of different proteins versus vinculin in arbitrary units in the lateral panel. One-way ANOVA with Tukey's multiple comparisons test: $*p < 0.05$; $**p < 0.01$; $***p < 0.001$ **(B)**. Representative WB of ATG-7, LC3B, and p62 in cardiac tissues of 11dy, 10w, 9m, and 18m mdx mice **(C)**. Data from densitometric analysis are expressed as the ratio of different proteins versus vinculin in arbitrary units in the lateral panels. One-way ANOVA with Tukey's multiple comparisons test: $**p < 0.01$; $***p < 0.001$ **(D)**. Each experiment was performed in triplicate wells. All values are expressed as the mean ± SD.

not find any significant variation in the expression of several components of complement cascade (**Figure 4A**). We then considered the infiltration of M1 and M2 F4/80 + macrophages (Van Erp et al., 2010) into mdx cardiac muscles and its age-related augment. Since PTX3 can coordinate the functions of macrophages, and macrophages themselves represent a source of PTX3, we counted the anti-inflammatory CD206 + M2 macrophages, finding a significant increase only in 9m mdx mice compared to 10w and 18m (with $p < 0.0001$ for both), ruling out a correlation between M2 macrophages and PTX3 expression (**Figure 4B**).

Pentraxin 3-Dependent Pro-Inflammatory and Fibrotic Signaling: Immunoproteasomes, Alarmins, and Autophagic Markers

We moved to investigate other pathways whose activity could foster PTX3 upregulation and modulate the inflammatory and dystrophic cues. Among these pathways, we considered PTX3 expression dependency on the IP and ERK1/2–p38MAPK activity, as already demonstrated in myocardial inflammation (Paeschke et al., 2016). However, in mdx mice, we did not see any difference except for a slightly higher expression of PSMB9 in 9m mice (9m mdx versus 11dy mdx, $p = 0.0193$) (**Figures 5A,B**). Therefore, we looked into alarmins that are recognized by specific receptors such as RAGE and TLRs: alarmins are activated through their ligand binding by different signaling cascades (as those dependent on IL-1R/MYD88 and MAPKs) leading to NF-κB and inflammatory cytokines release which might influence PTX3 expression and fibrosis development. In this case, we discovered that the amount of inflammatory and fibrotic proteins increases in mdx 18m cardiac muscles, likely explaining a more jeopardized pathological phenotype. Among alarmins, the S100β (18m mdx versus 9m mdx, $p = 0.0009$; versus 10w mdx, $p = 0.0005$; versus 11dy mdx, $p = 0.0002$), HMGB1 (18m mdx versus 9m mdx, $p = 0.0447$; versus 10w mdx, $p = 0.0047$; versus 11dy mdx, $p = 0.0017$), and IL-33 (18m mdx versus 9m mdx, $p = 0.0027$; versus 10w mdx, $p = 0.0042$; versus 11dy mdx, $p = 0.0031$) have been found significantly increased according to the age. Instead, RAGE expression was not dependent on the age, but its expression was elevated in mdx 9m hearts related to 11dy

TABLE 2 | Statistical analysis of pentraxin (PTX)3 expression.

Correlation Ptx3	r	*P*-value
Age	0.898#	<0.0001
MMP9	0.571#	0.0524
HMGB1	0.866#	0.0003
S100β	0.959#	<0.0001
IL-6	0.871#	0.0002
NF-κB	0.727#	0.0074
TLR5	0.871#	0.0002
Foxp3	0.825*	0.001
IL-33	0.545*	0.0666
TRAF6	0.797*	0.0019
ATG7	0.839*	0.0006
TLR9	0.154*	0.6331

*r Pearson, r Spearman, and p-value confirmed the positive correlation between the expression of PTX3 and high-mobility group box (HMGB)1, S100β, and Foxp3 (**A**); Toll-like receptor (TLR)5 and TRAF-6 (**B**); autophagy-related (ATG)-7 (**C**). # r Pearson. * r Spearman. The bold values are statistically significant according to the value of p.*

mdx mice ($p = 0.0494$). Furthermore, we envisaged a role of Treg cells in the dystrophic framework, in line with previous literature describing how the phenotype and the specialization of Tregs were determined by IL-33/ST2 (Pastille et al., 2019) and IL-1/IL-33 (Alvarez et al., 2019) pathway, respectively. Since it is known that Tregs are abundant in mdx necrotic muscles (Burzyn et al., 2013), we were not surprised to find that Foxp3 amount was more abundant in older mdx mice compared to the younger (18m mdx versus 9m mdx, $p = 0.0107$; 18m mdx versus 10w mdx, $p = 0.0041$; 18m mdx versus 11dy mdx, $p = 0.0031$). MCP-1 protein, involved in fibrosis and inflammatory events, was also upregulated in mdx mice at 9 months related to the other ages (9m mdx versus 18m mdx, $p = 0.0035$; 9m mdx versus 10w mdx, $p = 0.0205$; 9m mdx versus 11dy mdx, $p = 0.0433$) (**Figures 5C,D**). It was described that cardiac HMGB1 overexpression can mediate a pro-inflammatory immune response independently from RAGE (Bangert et al., 2016). Accordingly, in mdx cardiac muscles, we demonstrated an upregulation of other alarmin receptor expression, according to the age: TLR4 and TLR5 (18m mdx versus 9m mdx, $p = 0.0101$; 18m mdx versus 10w mdx, $p = 0.0008$; 18m mdx versus 11dy mdx, $p < 0.0001$; 9m mdx versus 11dy mdx, $p = 0.0062$) and TLR9 (18m mdx versus 9m mdx, $p = 0.0465$; 18m mdx versus 10w mdx, $p = 0.0470$). This condition further promoted the overexpression of NF-κB-p65 (18m mdx versus 10w mdx, $p = 0.0060$; 18m mdx versus 11dy mdx, $p = 0.0051$; 9m mdx versus 11dy mdx, $p = 0.0457$) and TRAF6 (18m mdx versus 9m mdx, $p = 0.0198$; 18m mdx versus 10w mdx, $p = 0.0287$; 18m mdx versus 11dy mdx, $p = 0.0088$) in older mdx mice. In turn, alarmins/TLRs/TRAF6-NF-κB pathway allowed the overexpression of PTX3 and the promotion of fibrosis, as highlighted by the upregulation of collagen VI (18m mdx versus 11dy mdx, $p = 0.0367$; 9m mdx versus 11dy mdx, $p = 0.0418$) and MMP9 (18m mdx versus 11dy mdx, $p = 0.0192$; 9m mdx versus 11dy mdx, $p = 0.0331$) (**Figures 6A,B**).

Within this environment, we determined the amount of IL-6 pro-inflammatory cytokine, finding a significant augment in older compared to younger mdx mice (18m mdx versus 9m mdx, $p = 0.0225$; 18m mdx versus 10w mdx, $p = 0.0008$; 18m mdx versus 11dy mdx, $p = 0.0002$; 9m mdx versus 11dy mdx, $p = 0.0100$). Moreover, we established that even though the TGF-β extent was higher in 10w mdx mice and lower in 9m mdx related to younger animals (9m mdx versus 11dy mdx, $p = 0.0366$; 10w mdx versus 11dy mdx, $p = 0.0066$), its expression did not vary significantly with the age, as described in Van Erp et al. (2010) (**Figures 7A,B**). PTX3 has been shown to regulate mitochondrial membrane potential and apoptosis (Lee et al., 2018) and, *vice versa*, its expression can be controlled by ATG7 (Qiang et al., 2017). Thus, we investigated the expression of autophagy markers ATG7, p62, and LC3B, and we found an increased ATG7 expression at 18 months of age (18m mdx versus 9m mdx, $p = 0.0026$; 18m mdx versus 10w mdx, $p = 0.0004$; 18m mdx versus 11dy mdx, $p = 0.0003$), confirming a dependency on the age (**Figures 7C,D**). Following these results, we performed a statistical test to determine whether there was a significant correlation between the expression of PTX3 and the proteins whose amount was significantly modified in mdx cardiac tissues at different ages. Interestingly, we found that there was a positive significant correlation dependent on the age between PTX3 and inflammatory and fibrotic players such as S100β and HMGB1, TLR5, IL-6, MMP9, and TRAF6 (**Table 2A**). Thus, the expression of other proteins (Foxp3, TRAF6, ATG7) was correlated with PTX3 independently from the age (**Table 2B**). In addition, we performed a multiple regression analysis, and we obtained a model of PTX3 considering S100β, HMGB1, TLR5, and TLR9 (corrected $r^2 = 0.91$), suggesting their involvement in a common pathway.

ONX-0914 Modulates Pentraxin 3 Expression in Cardiac Tissues of 9m Mdx Mice

We have determined that PTX3 could be an important target to modulate the inflammatory/fibrotic pathways in dystrophic cardiac tissues. Upregulation of PTX3 in cardiomyocytes is dependent on IP, whose inhibition has been shown to be effective in downregulating PTX3 expression and other NF-κB-dependent pathways (Voigt, personal communication). We have also demonstrated that dystrophic murine hearts treated with IP inhibitor ONX-0914 witness a downregulation of the expression of fibrotic mediators such as STAT3, STAT1, OPN, and ERK1/2 (Farini et al., 2019). We firstly confirmed the occurrence and the increase of IP subunits PSMB8 and PSMB9 in mdx hearts of different ages (**Figure 5A**). Interestingly, both PTX3 and PSMB8 signals were clearly detectable by immunohistochemistry in tight correlation with endothelial cells of cardiac vessels in 9m and 18m mdx mice (**Figure 8A**). To strengthen the possibility that IP played a role in controlling inflammatory/fibrotic pathways leading to PTX3 expression, a selective inhibition of the IP subunit PSMB8 by ONX-0914 supplementation was performed on mdx mice. In the cardiac tissues of 10w mdx mice, we demonstrated that the ONX-0914 did not vary significantly the expression of autophagic, fibrotic, and inflammatory markers (**Supplementary Figure S1**). In older mdx mice, we found

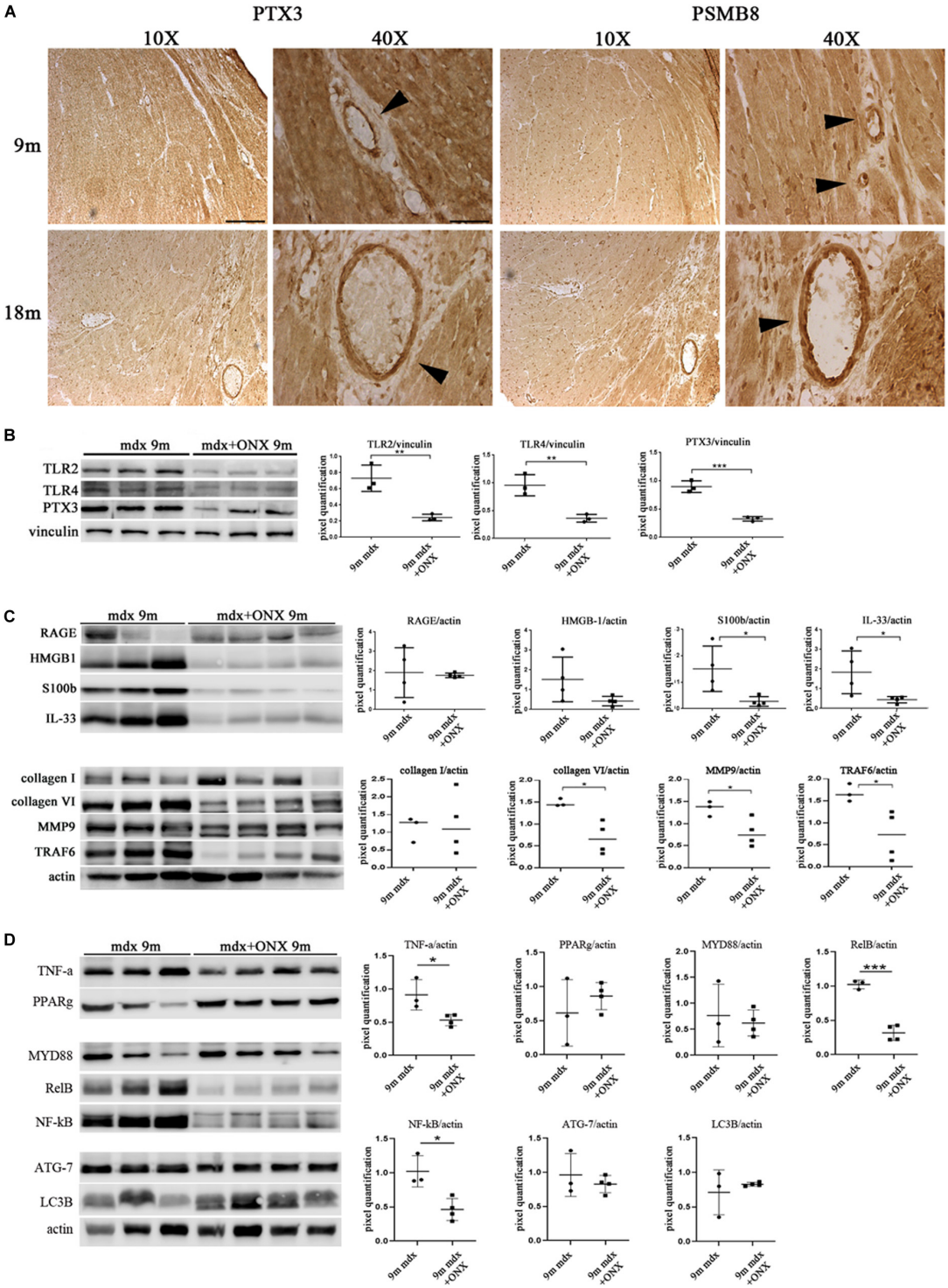

FIGURE 8 | Modulation of proteins in cardiac tissues of mdx mice at different ages following ONX-0914 treatment. Representative images of pentraxin (PTX)3 and PMSB8 immunohistochemistry staining of cardiac tissues showing PTX3- and PSMB8-positive endothelial cells (arrowheads) in cardiac tissues from 9 months (9m) and 18m mdx mice. Image magnifications: 10 × (scale bar: 200 mm) and 40 × (scale bar: 50 mm) **(A)**. Representative Western blot (WB) in cardiac tissues of untreated and ONX-0914-treated 9m mdx mice for Toll-like receptor (TLR)2, TLR4, PTX3 **(B)**; receptor for advanced glycation end-products (RAGE), high-mobility group box (HMGB)1, S100β, and interleukin (IL)-33; collagen I, collagen VI, matrix metalloproteinase (MMP)9, and TRAF-6 **(C)**; tumor necrosis factor (TNF)-a, poly(ADP-ribose) polymerase (PPAR)g, MYD88, RelB, nuclear factor (NF)-κB, ATG-7, and LC3B **(D)**. Data from densitometric analysis are expressed as the ratio of different proteins versus vinculin **(B)** and actin **(C,D)** in arbitrary units in the lateral panels. Student's *t*-test: $^{**}p < 0.01$; $^{***}p < 0.001$ **(B)**; $^{*}p < 0.05$ **(C)**; $^{*}p < 0.05$; $^{***}p < 0.001$ **(D)**. Each experiment was performed in triplicate wells. All values are expressed as the mean ± SD.

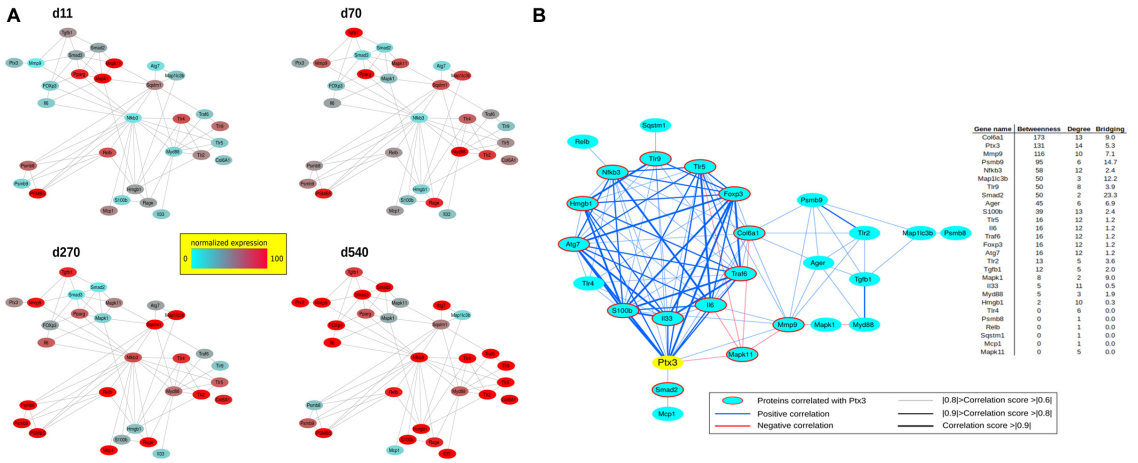

FIGURE 9 | Protein–protein interaction (PPI) and co-expression network of proteins differentially expressed at days (d)11, d70, d270, and d540. PPIs were retrieved by STRING Cytoscape's App; only Experimental and Database annotated interactions, with a score > 0.15, were considered. Protein expression normalized in range 0–100 (%) **(A)**. Betweenness, Degree, and Bridging centralities calculated by Centiscape Cytoscape's App. In red and bold centrality values above the average calculated on whole network; nodes with Betweenness, Degree, and Bridging above the average were considered hubs (genes in red) **(B)**.

instead that there was a significant downregulation of PTX3 ($p = 0.0008$) and TLR2 ($p = 0.0074$) and TLR4 ($p = 0.0072$), whose activities are fundamental for PTX3 activation (**Figure 8B**). We confirmed that ONX-0914 treatment was effective in reducing significantly the amount of IL-33 ($p = 0.0441$) and alarmins HMGB1 and S100β ($p = 0.0306$), while the expression of RAGE did not vary (**Figure 8C**). Furthermore, in line with our previous work (Farini et al., 2019), we found that different proteins involved in fibrotic development—whose activity could be dependent on PTX3 expression – were downregulated in ONX-0914-treated mice (collagen VI, $p = 0.0148$; MMP9, $p = 0.0400$; TRAF6, $p = 0.0377$) (**Figure 8C**). Importantly, we determined a significant downregulation of key mediators of fibrosis as TNF-a ($p = 0.0258$), RelB ($p = 0.0002$), and NF-κB ($p = 0.0123$), whose importance in PTX3 modulation had been previously demonstrated (Li et al., 2020; **Figure 8D**). However, the expression of autophagy markers such as ATG7 and LC3B was not modified by ONX-0914 treatment (**Figure 8D**).

Network-Based Prediction of Cardiac Tissues of Mdx Recapitulates the Pentraxin 3 Protein Interactions Involving Inflammatory/Fibrotic Pathways

To investigate the correlation of PTX3 expression with inflammatory/fibrotic pathways of mdx cardiac tissues, we reconstructed the PPIs retrieved from bioinformatic STRING analysis of the differentially expressed proteins of cardiac tissues in mdx mice at different ages (11, 70, 270, and 540 days old). In these analyses, we counted 30 nodes and 70 edges. During aging, inflammatory mediators, such as alarmins, NF-κB, RAGE, TLRs, and RelB, increased earlier and progressively peaked in cardiac tissues of 540 days old mdx (**Figure 9A**). In addition to these inflammatory proteins, we found cardiac increase of IP subunits throughout the life of the mdx mice (**Figure 9A**). On the other hand, the fibrotic remodeling of mdx hearts begins from 70 days old and peaks at 540 days old according to the increase of TGFβ1, MMP9, and collagen VI proteins (**Figure 9A**). The critical role of PTX3 in promoting the inflammatory pathway was confirmed by its early expression in cardiac tissues of 11dy mdx mice. Moreover, cardiac PTX3 upregulation was observed after activation of TLR4/MMP9 pathway in 270 and 540 days old mdx (**Figure 9A**). The results collectively suggested that PTX3 and IP might be both the targets of similar inflammatory/fibrotic pathways. By evaluating the structure of PPI networks, Nfkb3 (STAT3) could be considered as a protein hub due to its number of interactions as well as its central role in connecting different clusters of nodes (**Figures 9**, **10**). Similarly, PTX3, collagen VI (Col61a1), MMP9, and PSMB9 resulted hubs in the protein co-expression network showing centrality values above the average calculated on the whole network (**Figure 9B**). Moreover, PTX3 resulted in the most correlated protein in the observed inflammatory/fibrotic pathway (Degree = 14) (**Figure 9B**) with higher correlation (score > 0.9) to Foxp3, ATG7, and S100β (**Supplementary Figure S1**). Most PTX3 correlations resulted positive, while a single negative correlation was found between PTX3 and MAPK11 (**Supplementary Figure S1**). Besides, at 270 days in age, the mdx heart is affected by a cardiomyopathy (Quinlan et al., 2004, p. 491). Especially striking was the decrease of PTX3 expression and inflammatory/fibrotic pathway downregulation following treatment with ONX-0914 in hearts of 270 days old mdx (**Figure 10**).

DISCUSSION

Pentraxins are key components of the humoral innate immune system: the long pentraxin PTX3 is highly expressed during tissue-damaging events and, in turn, coordinates inflammation and vascular remodeling (Manfredi et al., 2008). Despite a

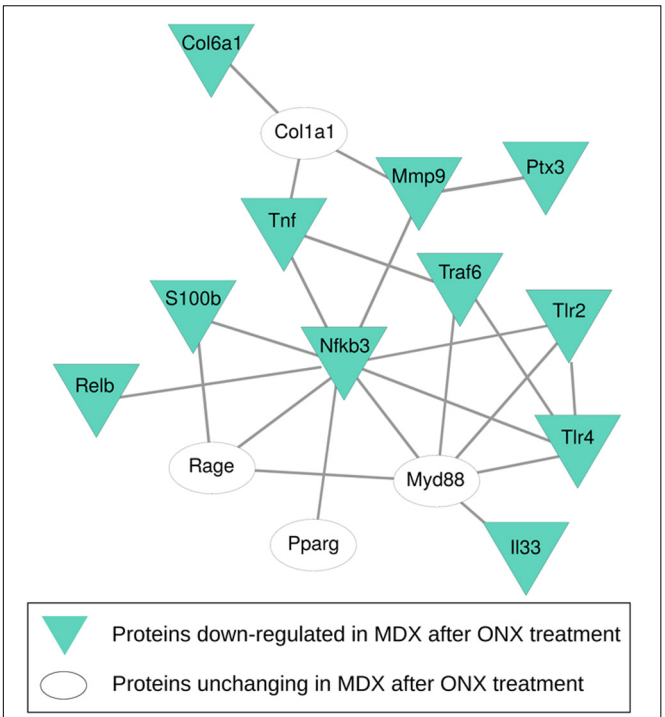

FIGURE 10 | Protein–protein interaction (PPI) network of proteins differentially expressed after ONX-0914 treatment. PPIs were retrieved by STRING Cytoscape's App; only Experimental and Database annotated interactions, with a score > 0.15, were considered. Blue triangles indicate proteins downregulated after ONX-0914 treatment.

recent interest in the measurement of pentraxins in ischemic heart disorders (Peri et al., 2000; Salio et al., 2008; Paeschke et al., 2016), there is no evidence as to their actual role in the pathogenesis of dystrophic cardiomyopathy. In this study, we demonstrated that dystrophic cardiac expression of PTX3 correlated positively with age and inflammatory/fibrotic pathways. Expression of PTX3 in the heart had already been observed at later stages of inflammation (Nebuloni et al., 2011). Accordingly, Pucci et al. (2014) demonstrated the fundamental role of M2 macrophages in determining the higher amount of PTX3 in arteriosclerotic plaque development. Moreover, PTX3 can interact with endothelial cells and, through the binding with P-selectin, can modulate the recruitment of monocytes and macrophages at the inflammatory sites (Deban et al., 2010). Interestingly, the IP modulates PTX3 expression through a complex mechanism involving TLRs, NF-κB, MAP kinases (Paeschke et al., 2016). According to these premises, we found co-expression of the IP subunit PSMB8 and PTX3 in mdx hearts and reduced expression of PTX3 after IP inhibition. Thus, local dystrophic cardiac expression of PTX3 might extend the well-known role of circulating PTX3 as a biomarker (Salio et al., 2008). In fact, we found aging-associated upregulation of PTX3 in muscles and hearts of mdx mice with predominant localization in fibrotic areas and, more interestingly, in vessels and perivascular areas. Interestingly, we found no correlation between PTX3 expression and M2 macrophages of mdx hearts, suggesting a specific role of dystrophic endothelial cells in the release or expression of PTX3. These evidences are in accordance with data provided from several labs describing PTX3 as a biomarker of endothelial dysfunctions, regulating nitric oxide, P-selectin, and fibroblast growth factor-2 production (Kotooka et al., 2008; Yasunaga et al., 2014; Carrizzo et al., 2015). Strong evidences suggest that complement components amplify tissue damages recruiting leukocytes: in the present study, we found that PTX3 expression was not influenced by complement components; conversely, alarmins facilitate inflammatory reactions and consequent fibrosis participating to the PTX3 secretion (Tsoporis et al., 2012; Bangert et al., 2016). Among alarmins' receptors, the TLR5 is commonly expressed in cardiomyocytes and endothelial cells (Hayashi et al., 2001) and enhances cardiac innate immune responses (Rolli et al., 2010). Recently, it was shown that TLR5 inhibition ameliorates cardiac fibrosis by modulating inflammation and tissues' remodeling (Liu et al., 2015). Other studies determined that HMGB1 blockade alleviates myocardial fibrosis (Wang et al., 2014), possibly interfering with the TLR2-HMGB1 ligand and cardiac autophagy (Wu et al., 2018; Liu et al., 2019). Consistent with these evidences, we demonstrated that mdx cardiac dysfunctions could be partly due to an inflammatory signaling pathway in which PTX3 is involved together with S100β, HMGB1, TLR5, and TLR9, with consequent increment of collagen deposition and fibrosis. Since PTX3 has been shown to regulate apoptosis (Lee et al., 2018) and its expression can be controlled by ATG7 (Qiang et al., 2017), we investigated the expression of autophagy markers ATG7, p62, and LC3B, and we found an increased ATG7 expression in older cardiac mdx. However, expression of PTX3 in cardiomyocytes is dependent on IP activity (Paeschke et al., 2016), and we have already demonstrated that IP inhibitor ONX-0914 had a fundamental role in modulating the pathological phenotype in skeletal (Farini et al., 2016) and cardiac (Farini et al., 2019) muscles of mdx mice. Since we found that PTX3 and IP were co-expressed in the fibrotic/inflammatory areas in cardiac tissues, we explored the effects of ONX-0914 in mediating PTX3-dependent pathways, confirming a downregulation of expression levels of alarmins-, collagen-, and NF-κB-dependent proteins. While critical for antigen presentation, the IP of endothelial cells may be a key link between inflammatory factors and vascular cell remodeling and thus may be an important factor in myocardial damage of mdx, as previously described in myocardial infarction (Yang et al., 2009). Interestingly, we noted PTX3 and PSMB8 co-expression in dystrophic mdx cardiac vessels. Moreover, we found that myocardial damage of older mdx triggered expansion of NG2 + pericyte population with altered morphology. In adult mouse hearts, endothelial cells and pericytes are the most abundant non-cardiac muscle cells (Nees et al., 2012; Pinto et al., 2016). Considering their abundance, phenotypic plasticity, and functional diversity, endothelial cells and pericytes may be critically involved in regulating inflammatory, fibrotic, angiogenic, and reparative responses in dystrophic hearts of mdx mice. Meanwhile, the network-based prediction analysis of changed inflammatory/fibrotic proteins raised the possibility of Nfkb3 (STAT3) as an important hub node. Importantly, endothelial cell-released STAT3 has a key

role in inflammation that underlies cardiovascular disease, and conversely, cardiomyocyte STAT3 is important for maintaining endothelial cell functions and the capillary integrity (Zouein et al., 2019). Furthermore, PTX3 resulted the most correlated protein in the inflammatory/fibrotic pathway with higher correlation to Foxp3, ATG7, and S100β proteins that have been linked to endothelial cell functions (Kreisel et al., 2004; Krupnick et al., 2005; Pober and Sessa, 2007; Tsoporis et al., 2010; Singh et al., 2015; Vion et al., 2017). Overall, these results provide the first stringent correlation between PTX3 cardiac expression and inflammatory/fibrotic pathways in an animal model of DMD. So far, data available propose a role for PTX3 as a predictive marker of fibrosis in dystrophic cardiac tissues. In general, PTX3 levels in dystrophic cardiac tissues rise first, reflecting the inflammatory response affecting myocardial damage and subsequently modulating the fibrotic response. However, PTX3 may have different kinetics of production and different patterns of recognized ligands between inflammatory and fibrotic pathways. On this regard, high PTX3 levels were associated with dystrophic cardiac vessels. The evidence for a regulatory role in the pathogenesis of dystrophic cardiomyopathy provides further incentive to the assessment of the clinical relevance of PTX3 measurement in prognostic value and in guiding therapy for cardiomyopathy of DMD.

DATA AVAILABILITY STATEMENT

All datasets generated for this study are included in the article/**Supplementary Material**.

ETHICS STATEMENT

The animal study was reviewed and approved by all procedures involving living animals were performed in accordance with Italian law (D.L.vo 116/92 and subsequent additions), which conforms to the European Union guidelines. The use of animals in this study was authorized by the National Ministry of Health (protocol number 10/13–2014/2015).

AUTHOR CONTRIBUTIONS

YT, AF, CS, and PM conceived and designed the experiments. AF, YT, and CV wrote the manuscript. PB, LT, CS, DD, and RR interpreted and analyzed the data. AF, PB, LT, CV, and SG performed the experiments and acquired the data. All authors stated were involved in the critical revision of the manuscript and approved the final version of the manuscript, including the authorship list. YT had full access to all the data in the study and had final responsibility for the decision to submit for publication.

FUNDING

This study was supported by the Associazione Centro Dino Ferrari and the French Telethon AFM grant (No. 21104). Funders of the study had no role in the study design, data analysis, data interpretation, or writing of the report.

SUPPLEMENTARY MATERIAL

The Supplementary Material for this article can be found online at: https://www.frontiersin.org/articles/10.3389/fphys.2020.00403/full#supplementary-material

FIGURE S1 | PTX3 correlation network. Proteins correlated with PTX3 and their expression values at day (d)11, d70, d270, and d540. Protein expression was normalized in range 0–100 (%).

REFERENCES

Alvarez, F., Istomine, R., Shourian, M., Pavey, N., Al-Aubodah, T. A., Qureshi, S., et al. (2019). The alarmins IL-1 and IL-33 differentially regulate the functional specialisation of Foxp3(+) regulatory T cells during mucosal inflammation. *Mucosal Immunol.* 12, 746–760. doi: 10.1038/s41385-019-0153-155

Bangert, A., Andrassy, M., Muller, A. M., Bockstahler, M., Fischer, A., Volz, C. H., et al. (2016). Critical role of RAGE and HMGB1 in inflammatory heart disease. *Proc. Natl. Acad. Sci. U.S.A.* 113, E155–E164. doi: 10.1073/pnas.1522288113

Burzyn, D., Kuswanto, W., Kolodin, D., Shadrach, J. L., Cerletti, M., Jang, Y., et al. (2013). A special population of regulatory T cells potentiates muscle repair. *Cell* 155, 1282–1295. doi: 10.1016/j.cell.2013.10.054

Carrizzo, A., Lenzi, P., Procaccini, C., Damato, A., Biagioni, F., Ambrosio, M., et al. (2015). Pentraxin 3 induces vascular endothelial dysfunction through a P-selectin/matrix metalloproteinase-1 pathway. *Circulation* 131, 1495–1505; discussion 1505. doi: 10.1161/CIRCULATIONAHA.114.014822

Castellano, G., Di Vittorio, A., Dalfino, G., Loverre, A., Marrone, D., Simone, S., et al. (2010). Pentraxin 3 and complement cascade activation in the failure of arteriovenous fistula. *Atherosclerosis* 209, 241–247. doi: 10.1016/j.atherosclerosis.2009.08.044

Casula, M., Montecucco, F., Bonaventura, A., Liberale, L., Vecchie, A., Dallegri, F., et al. (2017). Update on the role of Pentraxin 3 in atherosclerosis and cardiovascular diseases. *Vascul. Pharmacol.* 99, 1–12. doi: 10.1016/j.vph.2017.10.003

Cieslik, P., and Hrycek, A. (2015). Pentraxin 3 as a biomarker of local inflammatory response to vascular injury in systemic lupus erythematosus. *Autoimmunity* 48, 242–250. doi: 10.3109/08916934.2014.983264

Deban, L., Jaillon, S., Garlanda, C., Bottazzi, B., and Mantovani, A. (2011). Pentraxins in innate immunity: lessons from PTX3. *Cell Tissue Res.* 343, 237–249. doi: 10.1007/s00441-010-1018-1010

Deban, L., Russo, R. C., Sironi, M., Moalli, F., Scanziani, M., Zambelli, V., et al. (2010). Regulation of leukocyte recruitment by the long pentraxin PTX3. *Nat. Immunol.* 11, 328–334. doi: 10.1038/ni.1854

Doncheva, N. T., Morris, J. H., Gorodkin, J., and Jensen, L. J. (2019). Cytoscape StringApp: network analysis and visualization of proteomics data. *J. Proteome Res.* 18, 623–632. doi: 10.1021/acs.jproteome.8b00702

Doni, A., Mantovani, G., Porta, C., Tuckermann, J., Reichardt, H. M., Kleiman, A., et al. (2008). Cell-specific regulation of PTX3 by glucocorticoid hormones in hematopoietic and nonhematopoietic cells. *J. Biol. Chem.* 283, 29983–29992. doi: 10.1074/jbc.M805631200

Farini, A., Gowran, A., Bella, P., Sitzia, C., Scopece, A., Castiglioni, E., et al. (2019). Fibrosis rescue improves cardiac function in dystrophin-deficient mice and duchenne patient-specific cardiomyocytes by immunoproteasome modulation. *Am. J. Pathol.* 189, 339–353. doi: 10.1016/j.ajpath.2018.10.010

Farini, A., Sitzia, C., Cassani, B., Cassinelli, L., Rigoni, R., Colleoni, F., et al. (2016). Therapeutic potential of immunoproteasome inhibition in duchenne muscular dystrophy. *Mol. Ther.* 24, 1898–1912. doi: 10.1038/mt.2016.162

Fazzini, F., Peri, G., Doni, A., Dell'Antonio, G., Dal Cin, E., Bozzolo, E., et al. (2001). PTX3 in small-vessel vasculitides: an independent indicator of disease activity produced at sites of inflammation. *Arthritis Rheum.* 44, 2841–2850. doi: 10.1002/1529-0131(200112)44:12<2841:aid-art472<3.0.co;2-6

Frohlich, T., Kemter, E., Flenkenthaler, F., Klymiuk, N., Otte, K. A., Blutke, A., et al. (2016). Progressive muscle proteome changes in a clinically relevant pig model of Duchenne muscular dystrophy. *Sci. Rep.* 6:33362. doi: 10.1038/srep33362

Garlanda, C., Bottazzi, B., Bastone, A., and Mantovani, A. (2005). Pentraxins at the crossroads between innate immunity, inflammation, matrix deposition, and female fertility. *Annu. Rev. Immunol.* 23, 337–366. doi: 10.1146/annurev.immunol.23.021704.115756

Hayashi, F., Smith, K. D., Ozinsky, A., Hawn, T. R., Yi, E. C., Goodlett, D. R., et al. (2001). The innate immune response to bacterial flagellin is mediated by Toll-like receptor 5. *Nature* 410, 1099–1103. doi: 10.1038/35074106

Kotooka, N., Inoue, T., Fujimatsu, D., Morooka, T., Hashimoto, S., Hikichi, Y., et al. (2008). Pentraxin3 is a novel marker for stent-induced inflammation and neointimal thickening. *Atherosclerosis* 197, 368–374. doi: 10.1016/j.atherosclerosis.2007.05.031

Kreisel, D., Krasinskas, A. M., Krupnick, A. S., Gelman, A. E., Balsara, K. R., Popma, S. H., et al. (2004). Vascular endothelium does not activate CD4+ direct allorecognition in graft rejection. *J. Immunol.* 173, 3027–3034. doi: 10.4049/jimmunol.173.5.3027

Krupnick, A. S., Gelman, A. E., Barchet, W., Richardson, S., Kreisel, F. H., Turka, L. A., et al. (2005). Murine vascular endothelium activates and induces the generation of allogeneic CD4+25+Foxp3+ regulatory T cells. *J. Immunol.* 175, 6265–6270. doi: 10.4049/jimmunol.175.10.6265

Kunes, P., Holubcova, Z., Kolackova, M., and Krejsek, J. (2012). Pentraxin 3(PTX 3): an endogenous modulator of the inflammatory response. *Mediators Inflamm.* 2012:920517. doi: 10.1155/2012/920517

Kuswanto, W., Burzyn, D., Panduro, M., Wang, K. K., Jang, Y. C., Wagers, A. J., et al. (2016). Poor repair of skeletal muscle in aging mice reflects a defect in local, Interleukin-33-Dependent accumulation of regulatory T cells. *Immunity* 44, 355–367. doi: 10.1016/j.immuni.2016.01.009

Lee, H. H., Kim, S. Y., Na, J. C., Yoon, Y. E., and Han, W. K. (2018). Exogenous pentraxin-3 inhibits the reactive oxygen species-mitochondrial and apoptosis pathway in acute kidney injury. *PLoS One* 13:e0195758. doi: 10.1371/journal.pone.0195758

Li, Y., Ma, L., Gu, S., Tian, J., Cao, Y., Jin, Z., et al. (2020). UBE3A alleviates isoproterenol-induced cardiac hypertrophy through the inhibition of the TLR4/MMP-9 signaling pathway. *Acta Biochim. Biophys. Sin.* 52, 58–63. doi: 10.1093/abbs/gmz119

Liu, F. Y., Fan, D., Yang, Z., Tang, N., Guo, Z., Ma, S. Q., et al. (2019). TLR9 is essential for HMGB1-mediated post-myocardial infarction tissue repair through affecting apoptosis, cardiac healing, and angiogenesis. *Cell Death Dis.* 10:480. doi: 10.1038/s41419-019-1718-1717

Liu, H., Jiang, Q., Ju, Z., Guan, S., and He, B. (2018). Pentraxin 3 promotes cardiac differentiation of mouse embryonic stem cells through JNK signaling pathway. *Cell Biol. Int.* 42, 1556–1563. doi: 10.1002/cbin.11049

Liu, S., Qu, X., Liu, F., and Wang, C. (2014). Pentraxin 3 as a prognostic biomarker in patients with systemic inflammation or infection. *Mediators Inflamm.* 2014:421429. doi: 10.1155/2014/421429

Liu, Y., Hu, Z. F., Liao, H. H., Liu, W., Liu, J., Ma, Z. G., et al. (2015). Toll-like receptor 5 deficiency attenuates interstitial cardiac fibrosis and dysfunction induced by pressure overload by inhibiting inflammation and the endothelial-mesenchymal transition. *Biochim. Biophys. Acta* 1852, 2456–2466. doi: 10.1016/j.bbadis.2015.08.013

Manfredi, A. A., Rovere-Querini, P., Bottazzi, B., Garlanda, C., and Mantovani, A. (2008). Pentraxins, humoral innate immunity and tissue injury. *Curr. Opin. Immunol.* 20, 538–544. doi: 10.1016/j.coi.2008.05.004

Nebuloni, M., Pasqualini, F., Zerbi, P., Lauri, E., Mantovani, A., Vago, L., et al. (2011). PTX3 expression in the heart tissues of patients with myocardial infarction and infectious myocarditis. *Cardiovasc. Pathol.* 20, e27–e35. doi: 10.1016/j.carpath.2010.02.005

Nees, S., Weiss, D. R., Senftl, A., Knott, M., Förch, S., Schnurr, M., et al. (2012). Isolation, bulk cultivation, and characterization of coronary microvascular pericytes: the second most frequent myocardial cell type in vitro. *Am. J. Physiol. Heart Circ. Physiol.* 302, H69–H84. doi: 10.1152/ajpheart.00359.2011

Paeschke, A., Possehl, A., Klingel, K., Voss, M., Voss, K., Kespohl, M., et al. (2016). The immunoproteasome controls the availability of the cardioprotective pattern recognition molecule Pentraxin3. *Eur. J. Immunol.* 46, 619–633. doi: 10.1002/eji.201545892

Pastille, E., Wasmer, M. H., Adamczyk, A., Vu, V. P., Mager, L. F., Phuong, N. N. T., et al. (2019). The IL-33/ST2 pathway shapes the regulatory T cell phenotype to promote intestinal cancer. *Mucosal Immunol.* 12, 990–1003. doi: 10.1038/s41385-019-0176-y

Peri, G., Introna, M., Corradi, D., Iacuitti, G., Signorini, S., Avanzini, F., et al. (2000). PTX3, A prototypical long pentraxin, is an early indicator of acute myocardial infarction in humans. *Circulation* 102, 636–641. doi: 10.1161/01.cir.102.6.636

Pilling, D., Cox, N., Vakil, V., Verbeek, J. S., and Gomer, R. H. (2015). The long pentraxin PTX3 promotes fibrocyte differentiation. *PLoS One* 10:e0119709. doi: 10.1371/journal.pone.0119709

Pinto, A., Jahn, A., Immohr, M. B., Jenke, A., Döhrn, L., Kornfeld, M., et al. (2016). Modulation of immunologic response by preventive everolimus application in a rat CPB model. *Inflammation* 39, 1771–17782. doi: 10.1007/s10753-016-0412-415

Pober, J. S., and Sessa, W. C. (2007). Evolving functions of endothelial cells in inflammation. *Nat. Rev. Immunol.* 7, 803–815. doi: 10.1038/nri2171

Presta, M., Camozzi, M., Salvatori, G., and Rusnati, M. (2007). Role of the soluble pattern recognition receptor PTX3 in vascular biology. *J. Cell Mol. Med.* 11, 723–738. doi: 10.1111/j.1582-4934.2007.00061.x

Pucci, S., Fisco, T., Zonetti, M. J., Bonanno, E., Mazzarelli, P., and Mauriello, A. (2014). PTX3: a modulator of human coronary plaque vulnerability acting by macrophages type 2. *Int. J. Cardiol.* 176, 710–717. doi: 10.1016/j.ijcard.2014.07.109

Qiang, L., Sample, A., Shea, C. R., Soltani, K., Macleod, K. F., and He, Y. Y. (2017). Autophagy gene ATG7 regulates ultraviolet radiation-induced inflammation and skin tumorigenesis. *Autophagy* 13, 2086–2103. doi: 10.1080/15548627.2017.1380757

Quinlan, J. G., Hahn, H. S., Wong, B. L., Lorenz, J. N., Wenisch, A. S., and Levin, L. S. (2004). Evolution of the mdx mouse cardiomyopathy: physiological and morphological findings. *Neuromuscul. Disord.* 14, 491–496. doi: 10.1016/j.nmd.2004.04.007

Ristagno, G., Fumagalli, F., Bottazzi, B., Mantovani, A., Olivari, D., Novelli, D., et al. (2019). Pentraxin 3 in cardiovascular disease. *Front. Immunol.* 10:823. doi: 10.3389/fimmu.2019.00823

Ristagno, G., Varpula, T., Masson, S., Greco, M., Bottazzi, B., Milani, V., et al. (2015). Elevations of inflammatory markers PTX3 and sST2 after resuscitation from cardiac arrest are associated with multiple organ dysfunction syndrome and early death. *Clin. Chem. Lab. Med.* 53, 1847–1857. doi: 10.1515/cclm-2014-1271

Rolli, J., Rosenblatt-Velin, N., Li, J., Loukili, N., Levrand, S., Pacher, P., et al. (2010). Bacterial flagellin triggers cardiac innate immune responses and acute contractile dysfunction. *PLoS One* 5:e12687. doi: 10.1371/journal.pone.0012687

Salio, M., Chimenti, S., De Angelis, N., Molla, F., Maina, V., Nebuloni, M., et al. (2008). Cardioprotective function of the long pentraxin PTX3 in acute myocardial infarction. *Circulation* 117, 1055–1064. doi: 10.1161/CIRCULATIONAHA.107.749234

Scardoni, G., Petterlini, M., and Laudanna, C. (2009). Analyzing biological network parameters with CentiScaPe. *Bioinformatics* 25, 2857–2859. doi: 10.1093/bioinformatics/btp517

Sereni, L., Castiello, M. C., Di Silvestre, D., Della Valle, P., Brombin, C., Ferrua, F., et al. (2019). Lentiviral gene therapy corrects platelet phenotype and function in patients with Wiskott-Aldrich syndrome. *J. Allergy Clin. Immunol.* 144, 825–838. doi: 10.1016/j.jaci.2019.03.012

Singh, K. K., Lovren, F., Pan, Y., Quan, A., Ramadan, A., Matkar, P. N., et al. (2015). The essential autophagy gene ATG7 modulates organ fibrosis via regulation of endothelial-to-mesenchymal transition. *J. Biol. Chem.* 290, 2547–2559. doi: 10.1074/jbc.M114.604603

Szklarczyk, D., Gable, A. L., Lyon, D., Junge, A., Wyder, S., Huerta-Cepas, J., et al. (2019). STRING v11: protein-protein association networks with increased coverage, supporting functional discovery in genome-wide experimental datasets. *Nucleic Acids Res.* 47, D607–D613. doi: 10.1093/nar/gky1131

Tsoporis, J. N., Izhar, S., Proteau, G., Slaughter, G., and Parker, T. G. (2012). S100B-RAGE dependent VEGF secretion by cardiac myocytes induces myofibroblast proliferation. *J. Mol. Cell Cardiol.* 52, 464–473. doi: 10.1016/j.yjmcc.2011.08.015

Tsoporis, J. N., Mohammadzadeh, F., and Parker, T. G. (2010). Intracellular and extracellular effects of S100B in the cardiovascular response to disease. *Cardiovasc. Psychiatry Neurol.* 2011:206073. doi: 10.1155/2010/206073

Van Erp, C., Loch, D., Laws, N., Trebbin, A., and Hoey, A. J. (2010). Timeline of cardiac dystrophy in 3-18-month-old MDX mice. *Muscle Nerve* 42, 504–513. doi: 10.1002/mus.21716

Vella, D., Zoppis, I., Mauri, G., Mauri, P., and Di Silvestre, D. (2017). From protein-protein interactions to protein co-expression networks: a new perspective to evaluate large-scale proteomic data. *EURASIP J. Bioinform. Syst. Biol.* 2017:6. doi: 10.1186/s13637-017-0059-z

Vion, A. C., Kheloufi, M., Hammoutene, A., Poisson, J., Lasselin, J., Devue, C., et al. (2017). Autophagy is required for endothelial cell alignment and atheroprotection under physiological blood flow. *Proc. Natl. Acad. Sci. U.S.A.* 114, E8675–E8684. doi: 10.1073/pnas.1702223114

Wang, W. K., Wang, B., Lu, Q. H., Zhang, W., Qin, W. D., Liu, X. J., et al. (2014). Inhibition of high-mobility group box 1 improves myocardial fibrosis and dysfunction in diabetic cardiomyopathy. *Int. J. Cardiol.* 172, 202–212. doi: 10.1016/j.ijcard.2014.01.011

Wu, R. N., Yu, T. Y., Zhou, J. C., Li, M., Gao, H. K., Zhao, C., et al. (2018). Targeting HMGB1 ameliorates cardiac fibrosis through restoring TLR2-mediated autophagy suppression in myocardial fibroblasts. *Int. J. Cardiol.* 267, 156–162. doi: 10.1016/j.ijcard.2018.04.103

Yang, Z., Gagarin, D., St Laurent, G. III, Hammell, N., Toma, I., Hu, C. A., et al. (2009). Cardiovascular inflammation and lesion cell apoptosis: a novel connection via the interferon-inducible immunoproteasome. *Arterioscler. Thromb. Vasc. Biol.* 29, 1213–1219. doi: 10.1161/ATVBAHA.109.189407

Yasunaga, T., Ikeda, S., Koga, S., Nakata, T., Yoshida, T., Masuda, N., et al. (2014). Plasma pentraxin 3 is a more potent predictor of endothelial dysfunction than high-sensitive C-reactive protein. *Int. Heart J.* 55, 160–164. doi: 10.1536/ihj.13-253

Zouein, F. A., Booz, G. W., and Altara, R. (2019). STAT3 and endothelial cell-cardiomyocyte dialog in cardiac remodeling. *Front. Cardiovasc. Med.* 24:50. doi: 10.3389/fcvm.2019.00050

Conflict of Interest: The authors declare that the research was conducted in the absence of any commercial or financial relationships that could be construed as a potential conflict of interest.

frontiers in Physiology

REVIEW
published: 21 May 2020
doi: 10.3389/fphys.2020.00479

Extracellular Vesicles as Therapeutic Agents for Cardiac Fibrosis

Russell G. Rogers, Alessandra Ciullo, Eduardo Marbán and Ahmed G. Ibrahim*

Smidt Heart Institute, Cedars-Sinai Medical Center, Los Angeles, CA, United States

Heart disease remains an increasing major public health challenge in the United States and worldwide. A common end-organ feature in diseased hearts is myocardial fibrosis, which stiffens the heart and interferes with normal pump function, leading to pump failure. The development of cells for regenerative therapy has been met with many pitfalls on its path to clinical translation. Recognizing that regenerative cells secrete therapeutically bioactive vesicles has paved the way to circumvent many failures of cell therapy. In this review, we provide an overview of extracellular vesicles (EVs), with a focus on their utility as therapeutic agents for cardiac regeneration. We also highlight the engineering potential of EVs to enhance their therapeutic application.

Keywords: bioengineering, cardiac fibrosis, extracellular vesicles, progenitor cells, next generation therapeutics

OPEN ACCESS

Edited by:
Claudio de Lucia,
Temple University, United States

Reviewed by:
Alexander E. Berezin,
Zaporizhia State Medical University, Ukraine
Rainer Schulz,
University of Giessen, Germany
Ian Dixon,
University of Manitoba, Canada

****Correspondence:***
Eduardo Marbán
Eduardo.Marban@csmc.edu

Specialty section:
This article was submitted to Clinical and Translational Physiology, a section of the journal Frontiers in Physiology

Received: *11 March 2020*
Accepted: *20 April 2020*
Published: *21 May 2020*

Citation:
Rogers RG, Ciullo A, Marbán E and Ibrahim AG (2020) Extracellular Vesicles as Therapeutic Agents for Cardiac Fibrosis. Front. Physiol. 11:479. doi: 10.3389/fphys.2020.00479

INTRODUCTION

Despite significant advances in science and medicine, heart disease remains an increasing public health concern, and is a leading cause of morbidity and mortality worldwide (Roth et al., 2017). In adult mammals, the default response to cardiac insults or disease is scar formation which lowers myocardial compliance, decreases ventricular filling, interferes with electrical coupling, and ultimately leads to depressed cardiac performance (Sharma and Kass, 2014). Conventional therapies such as β-blockers are beneficial in patients with myocardial fibrosis; however, they do not directly treat the underlying causes of fibrosis (Jameel and Zhang, 2009; Members et al., 2012). There is ample evidence for the efficacy of cardiac cell therapy to treat myocardial fibrosis in preclinical models (Zwetsloot et al., 2016) and, to a lesser extent, in patients (Nigro et al., 2018). However, cells are fragile, living entities which can be difficult to manufacture and to handle (Dodson and Levine, 2015).

In recent years, the emphasis has shifted away from cell therapy toward a cell-free therapeutic paradigm. Although extracellular vesicles (EVs) have long been known to be produced by eukaryotic cells, only recently were EVs implicated as mediators of the paracrine benefits of cell therapy. Extensive evidence now supports the concept that EVs are vital for the benefits of numerous therapeutic cells such as neural progenitors (Marzesco et al., 2005), mesenchymal stem cells (Lai et al., 2010), CD34+ cells (Sahoo et al., 2011), and cardiosphere-derived cells (CDCs; Ibrahim et al., 2014). Importantly, EVs offer the potential to overcome key limitations of cell therapy. For example, advantages may include product stability (Akers et al., 2016), immune tolerability (Gallet et al., 2017; Aminzadeh et al., 2018), flexibility of dosing (not limited by microvascular plugging or loss of transplanted cell viability; Ibrahim and Marbán, 2016), and the potential for engineering to enhance efficacy (Conlan et al., 2017). In this review, we summarize EV biology, cellular and molecular players in myocardial fibrosis, the utility of EVs as therapeutic agents, and conclude with the promise of engineered EVs as next-generation therapeutic candidates.

EXTRACELLULAR VESICLES DEFINED

Conserved through evolution, cellular release of EVs occurs in bacteria, fungi, plants, and animals (Barile et al., 2017). Based on studies of sheep reticulocytes, EV secretion was originally postulated to be a mechanism for elimination of cell waste including non-essential proteins (Johnstone et al., 1987). More recently, EVs have come to be viewed as key mediators of intercellular communication. EVs can deliver and exchange bioactive components from donor to recipient cells, regulating gene expression and altering cellular function (Stahl and Raposo, 2018). Several lines of evidence implicate EVs as important signaling mediators that carry proteins, lipids, and nucleic acids in physiological and pathophysiological conditions (Ibrahim et al., 2014; Ibrahim and Marbán, 2016).

Classification of Extracellular Vesicles

In the classical sense, the term EVs refers to all cell-secreted membrane vesicles. Based on their size, biogenesis, and secretory pathway, EVs can be broadly classified into three major classes: exosomes, microvesicles, and apoptotic bodies (**Figure 1**). The primary focus here will be on the first two classes of EVs.

Exosomes are secreted and taken up by all eukaryotic cells and have been found abundantly in nearly all biological fluids. Exosomes are lipid-bilayer vesicles of endosomal origin that arise from inward budding of multivesicular bodies, and range in size from 30 to ∼100 nm in diameter. Multivesicular bodies can fuse with the plasma membrane to release their contents into the extracellular space, or can be trafficked to lysosomes for degradation (Colombo et al., 2014). Exosomal cargo contains non-random assortments of protein, RNA, and lipids, differing substantially from the cytoplasmic contents of the parent cells, but nevertheless reflecting the parent cell type and its metabolic state. According to ExoCarta[1], at least 9,769 proteins, 4,946 mRNAs, 2,838 miRNAs, and 1,116 lipids have been identified in exosomes from various cell types. Though the diversity of exosomal cargo is vast, exosomes share common molecular markers including tetraspanins (CD9, CD63, and CD81). However, diversity exists among the expression of these tetraspanins – although the biological significance is currently unclear (Bobrie et al., 2012).

In contrast to exosomes, *microvesicles* are generally larger and range in size (100–1000 nm in diameter). The mechanism of microvesicle biogenesis is not well understood; however, it is thought to require cytoskeletal components such as actin and microtubules (along with the respective molecular motors), and fusion machinery (SNAREs and tethering proteins) (Cai et al., 2007). Microvesicles arise by direct budding from the plasma membrane and enter the extracellular space (He et al., 2018). Accordingly, microvesicle contents closely resemble the composition of the cytosol of the parent cell (Mohammadi et al., 2019).

We next consider the biology of cardiac fibrosis, then return to EVs as therapeutic candidates to offset fibrosis. For a detailed review of cardiac regeneration and EV biology, the reader is referred to recently published reviews (Balbi et al., 2020; Tikhomirov et al., 2020).

[1]http://www.exocarta.org

ORIGIN OF CARDIAC FIBROSIS

The deposition of collagen occurs in three forms: replacement, interstitial, and perivascular (**Figure 2**). As a result of cardiomyocyte loss, replacement fibrosis ensues to fill devoid space within the myocardium (Rogers and Otis, 2017). Dominating in acute myocardial infarction (MI), replacement fibrosis is critical to protecting the myocardium from rupture and dilative remodeling by preserving structural integrity and normalizing myocardial wall stress. Interstitial and perivascular fibrosis develop as excess collagen deposits in the myocardial interstitium and surrounding the peri-adventitia, respectively (Frangogiannis, 2019). The latter two are the unfortunate consequences of a number of insults, including myocardial inflammation, which lead to chronic heart disease. The extent of interstitial and perivascular fibrosis is closely associated with adverse clinical outcomes (Berk et al., 2007; Kong et al., 2014). As such, the development of therapeutic interventions to combat myocardial fibrosis remain a major focus of current research.

Cellular and Molecular Players in Cardiac Fibrosis

The hallmark of any cardiac insult remains the universal activation of the innate and adaptive immune system. For example, following acute myocardial infarction, dead cardiomyocytes release DNA (Roers et al., 2016) and cellular proteins (Scaffidi et al., 2002; Panayi et al., 2004) into the extracellular space which serve as damage-associated molecular patterns (Rubartelli and Lotze, 2007). These signals are sensed by leukocytes (Tang et al., 2012) and activate nuclear factor kappa-light-chain-enhancer of activated B cells (NFκB)-mediated transcription of pro-inflammatory cytokines, chemokines, and other mediators of the inflammatory response (Legrand et al., 2019). Mounting evidence suggests infiltrating macrophages are key mediators of the pro-fibrotic response to injury (Frangogiannis, 2019). In animal models of pressure overload-induced heart failure, recruited M1 macrophages communicate with $CD4^+$ T lymphocytes and perpetuate the pro-inflammatory wave leading to fibrosis, cardiac dysfunction, and heart failure (Nevers et al., 2015; Patel et al., 2018). Moreover, macrophages can activate resident stromal cells which contribute directly to collagen deposition. For example, in response to angiotensin-induced hypertrophic cardiomyopathy, macrophages stimulate cardiac fibroblasts to produce IL-6 leading to TGFβ1 production and subsequent development of cardiac fibrosis (Ma et al., 2012).

Perhaps the most widely known macrophage-secreted cytokine to drive fibrosis is TGFβ, which binds to its cognate receptors on cardiac tissue (TGFβR2, ALK, and others) and mobilizes Smad2 and Smad3 transcription factors to initiate myofibroblast differentiation (Khalil et al., 2017; Pardali et al., 2017). The principal source of myofibroblasts in the heart are resident fibroblasts, and to a lesser degree, endothelial cells. However, not all macrophages are created equal. M2c

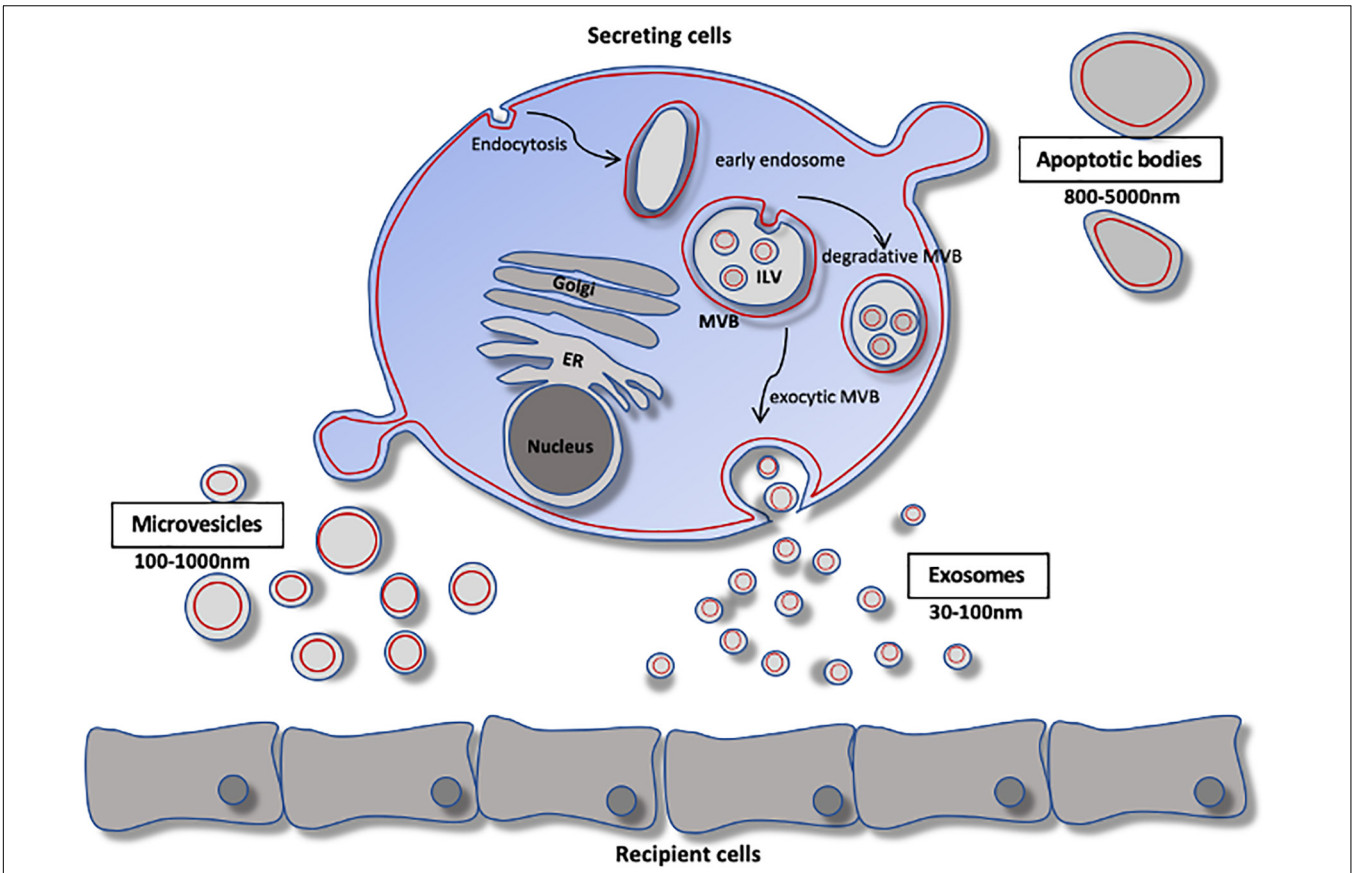

FIGURE 1 | Extracellular vesicle biology. Schematic of extracellular vesicle biogenesis. Exosomes arise from the fusion of inward budding of multivesicular bodies. The resulting vesicles are either degraded by lysosomes or secreted as exsomes. Microvesicles arise by direct budding from the plasma membrane and enter the extracellular space. Apoptotic bodies arise from membrane protrusions fragmentation of an apoptotic cell. ER, endoplasmic reticulum; ILV, intraluminal vesicle; MVB, multivesicular body.

macrophages, for example, phagocytose dead cells and debris and secrete matrix metalloproteinases, which can reabsorb collagen deposits and contribute to remodeling of the extracellular matrix (Cheng et al., 2018; Krzyszczyk et al., 2018). The interplay among macrophages, fibroblasts, and endothelial cells is now understood to be a major driving force of myocardial fibrosis. Thus, in the context of anti-fibrogenesis, EVs can intervene by direct stimulation of pro-inflammatory M1 macrophages to differentiate into an M2-like phenotype (Silva et al., 2017). This step is important for the resolution of inflammation and subsequent anti-fibrotic actions. We will next discuss, in more detail, immunomodulatory actions of EVs.

EXTRACELLULAR VESICLES AS THERAPEUTIC AGENTS

Recently, EVs (and exosomes in particular) are attracting much interest – not only in physiological and pathological cell–cell communication, but also as a platform for therapeutic development (Sluijter et al., 2018). The recognition that progenitor cells secrete EVs that are bioactive ushered in the concept of EVs as cell-free therapeutic candidates (**Figure 3**). As the holy grail of regenerative medicine, restoring both cardiac structure and function are fundamental goals of any therapeutic candidate. Indeed, EVs harvested from cardiac stem/progenitor cells, mesenchymal stem/stromal cells (MSCs), embryonic stem cells (ESCs), induced pluripotent stem cells (iPSCs), and non-stem cell sources have demonstrated benefits in cardiac regeneration (Alibhai et al., 2018; **Figure 4**). By supplanting cell transplantation with administration of EVs, many concerns and limitations regarding safety and feasibility from cell therapy can be attenuated.

Production of EVs for Therapeutic Applications

Therapeutic exosomes are of great potential interest, but it should be noted that there are no FDA-approved EV products. Nevertheless, some scholarship on the topic of isolating such exosomes has appeared (for example, Marbán, 2018b). Briefly, we start by culturing therapeutically potent cells *in vitro* in serum-free media (to exclude contaminating exosomes naturally found in serum), and allowing the cells to condition the media. The conditioning phase is variable and can be as brief as 24 h or as

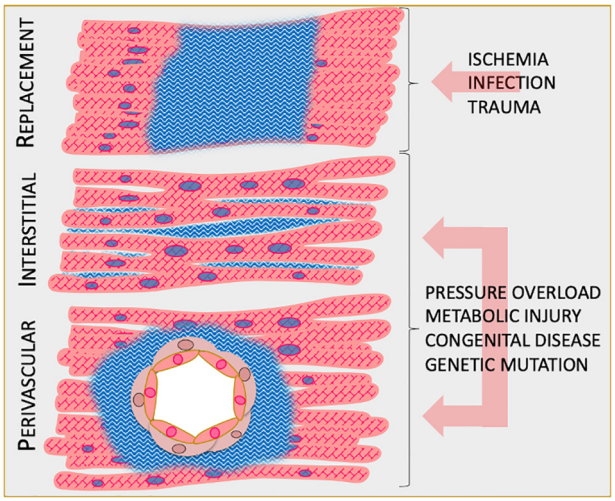

FIGURE 2 | Manifestations of cardiac fibrosis. Schematic of the three main types of cardiac fibrosis. Replacement fibrosis develops to fill necrotic lesions within the myocardium as a result of ischemia, infection, or trauma. Interstitial fibrosis develops in the interstitial space of the myocardium as a result of non-ischemic cardiomyopathies. Perivascular fibrosis develops in the peri-adventitial space as a result of non-ischemic cardiomyopathies.

long as 15 days under normoxic or hypoxic conditions. Varying conditioning phase parameters can influence cargo loading into exosomes, which may impact their disease-modifying bioactivity. Conditioned media contains not only exosomes but also other EVs, proteins, and products of metabolism. To remove non-EV components, further processing by laboratory personnel typically involves ultrafiltration (i.e., by molecular weight exclusion). In order to separate exosomes from larger EVs such as microvesicles or apoptosomes, ultracentrifugation or size exclusion chromatography may be used (Baranyai et al., 2015). Finally, the purified product is aliquoted into dosage-defined units and packaged into vials for later use.

Cardiosphere-Derived Cell EVs

Cardiosphere-derived cells (CDCs) are stromal cells of intrinsic cardiac origin (White et al., 2013), and are multipotent and clonogenic (but not self-renewing; Davis et al., 2009). CDCs uniformly express CD105 and are negative for CD45 and other hematogenous markers. Since the isolation of CDCs was first reported in 2007 (Smith et al., 2007), >200 papers have been published using this cell type from >55 independent labs worldwide. CDCs secrete EVs (CDC-EVs) which transfer payloads into target cells, inducing epigenomic, transcriptomic, and phenotypic changes that underlie the benefits of CDC therapy (Marbán, 2018b). Indeed, therapeutic bioactivity by CDC-EVs has been demonstrated in several animal studies such as acute MI (Ibrahim et al., 2014; De Couto et al., 2017; Gallet et al., 2017), non-ischemic cardiomyopathy (Aminzadeh et al., 2015), and Duchenne muscular dystrophy (DMD)-related cardiomyopathy (Aminzadeh et al., 2018; Rogers et al., 2019b). In preclinical studies, CDC-EVs induce cardiomyogenesis and angiogenesis, reduce fibrosis, modulate the immune response, and generally improve cardiac function (Marbán, 2018b). The mechanism of benefit appears to hinge on their cargo, particularly non-coding ribonucleic acids (ncRNA). Of the numerous RNA species, microRNAs (miRs) are the best-described class of small ncRNA.

Several CDC-EV associated miRs impact on inflammation and fibrosis including miR-146a (Barile et al., 2014; Ibrahim et al., 2014), miR-210 (Barile et al., 2014), miR-181b (De Couto et al., 2017), miR-148a (Aminzadeh et al., 2018), and miR-92a (Ibrahim et al., 2019). miR-146a targets multiple pathways active in cardiac disease including inflammation and fibrosis. Indeed, miR-146a regulates NFκB (Saba et al., 2014) and TGFβ signaling (Geraldo et al., 2012). Specifically, miR-146a inhibits Smad4-mediated myofibroblast differentiation to attenuate myocardial fibrosis (Liu et al., 2012). Delivery of a miR-146a mimic in infarcted mouse hearts reproduced some, but not all the benefits observed with CDC-EV treatment, suggesting cooperative effects of other CDC-EV cargo in the overall benefits. Moreover, it is unclear if other CDC-EV miRs share overlapping or synergistic bioactivity. For example, miR-181b blunts pro-inflammatory cytokine production by targeting protein kinase Cδ in a rat model of acute MI (De Couto et al., 2017), while miR-148a attenuates NFκB phosphorylation in the *mdx* mouse model of DMD (Aminzadeh et al., 2018; Rogers et al., 2019b). We have recently demonstrated CDC-EVs modulate the *mdx* mouse macrophage toward a pro-regenerative phenotype with prominent secretion of tissue inhibitor of matrixmetalloproteinase 2 (TIMP-2; Rogers et al., 2019a). We speculate that enhanced TIMP-2 secretion may contribute to the anti-fibrotic effect of CDC-EVs. In TIMP-2 null mice, MI led to greater ventricular dilation and infarct expansion (Kandalam et al., 2010). In contrast, TIMP-2 overexpression reduced ventricular dilation and infarct expansion post-MI (Ramani et al., 2011), and TIMP-2 inhibits human fibroblast activation at high concentrations (Ngu et al., 2014).

In addition to miRs, other less described ncRNAs, such as Y-RNAs, have been shown to influence the transcriptome in cardiac tissue. Y-RNAs are components of the Ro60 ribonucleoproteins and play a key role in DNA replication by interacting with chromatin and replication initiation proteins (Christov et al., 2006; Zhang et al., 2011). EV-YF1, a Y-RNA fragment found abundantly in CDC-EVs, skews macrophage polarization toward a pro-regenerative phenotype, which provides cardioprotection against ischemia/reperfusion injury in rats (Cambier et al., 2017). Moreover, in a mouse model of angiotensin-induced hypertrophic cardiomyopathy, EV-YF1 treatment attenuated myocardial hypertrophy, inflammation, and fibrosis, which were mediated by IL-10 (Cambier et al., 2018). While much work has focused on well-known ncRNAs such as miRs, it is clear that other RNA species contained within EVs are therapeutically bioactive. Further work will be required to better understand the role other lesser-known ncRNAs play in the mechanistic basis of EV-based therapeutics.

Mesenchymal Stem Cell-Derived EVs

MSCs are multipotent stem/stromal cells found in loose connective tissue (e.g., areolar, reticular, and adipose), bone marrow, and lymph tissue (Bianco et al., 2008; Choi et al., 2019).

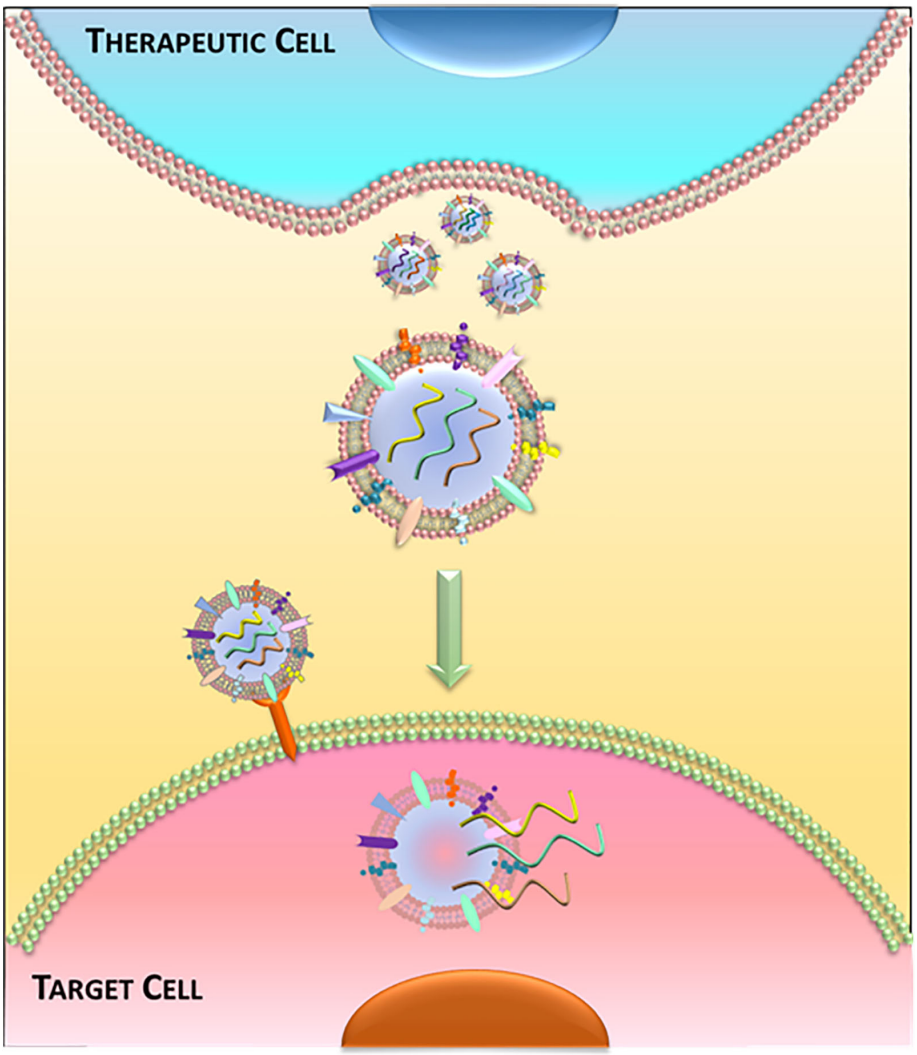

FIGURE 3 | Extracellular vesicle-mediated communication. Schematic of release and uptake of extracellular vesicles. Therapeutic cells secrete bioactive extracellular vesicles, which are taken up by diseased cells to alter cell function.

While initial enthusiasm regarding MSCs originated from their capacity to differentiate into various cell types, it is now widely accepted that their engraftment and differentiation are negligible, and do not account for the therapeutic effects of MSC infusions (Iso et al., 2007; Leiker et al., 2008; Keating, 2012; Tokita et al., 2016). In congruency with CDCs (though a distinctly different cell type), MSCs mediate their disease-modifying bioactivity through the secretion of paracrine factors including EVs (MSC-EVs). Moreover, like CDC-EVs, MSC-EVs contain a plethora of RNA species, including miRs. For example, MSC-EVs from bone marrow-derived MSCs are enriched with miR-22, which confers anti-apoptotic and anti-fibrotic properties in a mouse model of acute MI (Feng et al., 2014). Further, cardioprotective miRs miR-19a and miR-221 are commonly found in MSC-EVs (Yu et al., 2013; Yu et al., 2015; Shi et al., 2018). Unlike MSCs, MSC-EVs are said to have no risk of tumorigenicity or extraosseous calcification, and a lower possibility of immune rejection following *in vivo* allogeneic administration (Stoltz et al., 2015). These features further support the notion of EVs as next-generation therapeutic candidates.

Embryonic Stem Cell- and Induced Pluripotent Stem Cell-Derived EVs

Embryonic stem cells (ESCs) and induced pluripotent stem cells (iPSCs), like CDCs and MSCs, secrete bioactive EVs against cardiac injury and fibrosis, although they are traditionally believed to work by engraftment and differentiation rather than by paracrine mechanisms (Marbán, 2018a). ESC-EVs are enriched in the miR-290/295 cluster; one member, miR-294, promotes cardiomyocyte survival and attenuates fibrosis in MI (Khan et al., 2015). Similarly, iPSC-EVs have also demonstrated cardioprotective properties, mediated in part by miR-21 and miR-210 (Wang et al., 2015).

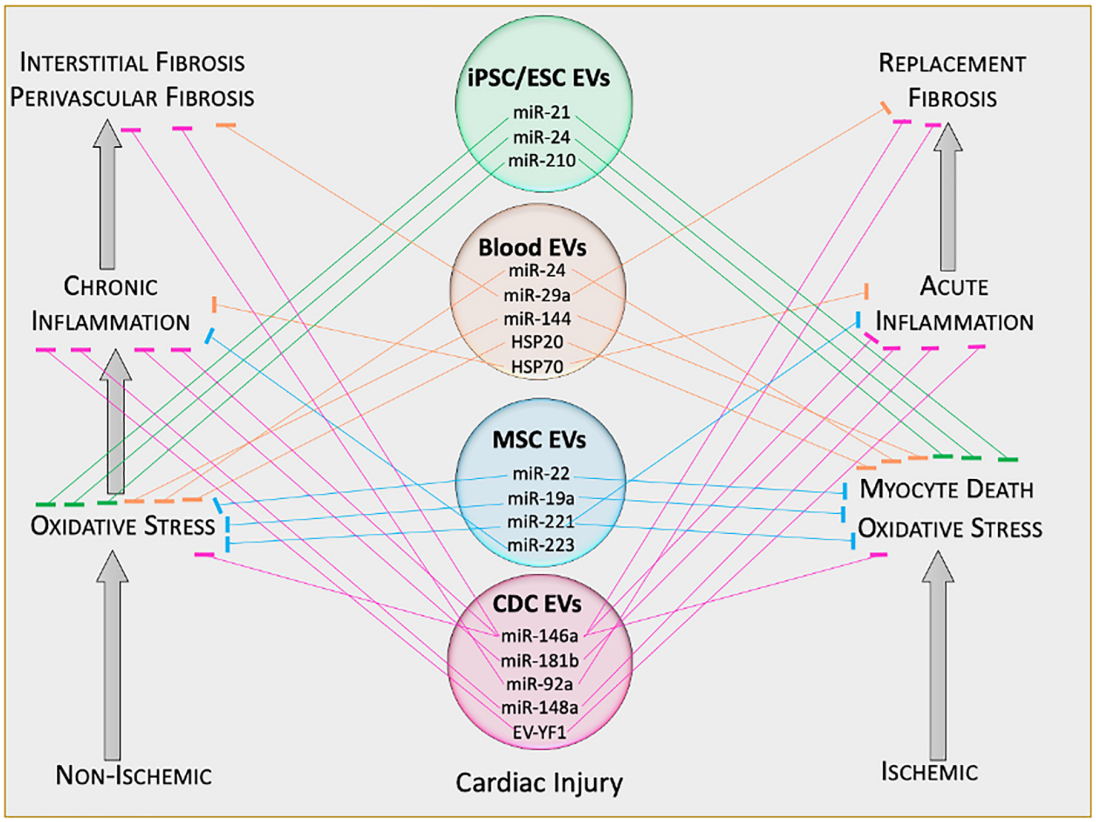

FIGURE 4 | Therapeutic functions of extracellular vesicle cargo. Schematic of therapeutically active cargo found inside extracellular vesicles. Defined molecules exert specific biological functions in target tissues. EV, extracellular vesicle; ESC, embryonic stem cell; iPSC, induced pluripotent stem cell; miR, microRNA; EV-YF1, extracellular vesicle Y-RNA fragment.

Peripheral Blood-Derived EVs

Secreted mostly by platelets and the vascular endothelium, peripheral blood-derived EVs (PB-EVs) exhibit tissue-protective bioactivity. PB-EVs from healthy humans or rodents exert anti-oxidant (Vicencio et al., 2015), anti-apoptotic (Minghua et al., 2018), and anti-fibrotic (Yamaguchi et al., 2015) effects in animal models of MI. These therapeutic benefits appear to be, in part, mediated by miRs. The anti-fibrotic effects appear to be largely driven by miR-29, which has been validated to target col1a1, col1a2, col3a1, fbn1, and eln1 transcripts (Van Rooij et al., 2008). Moreover, PB-EVs were demonstrated to attenuate fibrosis and cardiac dysfunction in a streptozotocin-induced diabetic cardiomyopathy model, which was mediated, in part, by HSP20 (Wang et al., 2016).

THE PROMISE OF EXTRACELLULAR VESICLE ENGINEERING FOR NEXT-GENERATION THERAPEUTICS

The nature and the physiological state of the EV-secreting cell affects the tropism and therapeutic bioactivity of the produced vesicles (Wiklander et al., 2015; Lai et al., 2016). In the circulation, the balance between EV production and clearance reflects the steady-state level. Upon systemic delivery, the detection window of labeled EVs is typically very short (Yáñez-Mó et al., 2015). Generally speaking, EVs are distributed to many body tissues including the liver, bone, skin, muscle, spleen, kidney, and lung. EV-specific expression of selective adhesion molecules may influence biodistribution. For example, CD169-expressing macrophages in the spleen and lymph nodes capture B cell-derived EVs. In contrast, EV trafficking to the lymphoid system is dysregulated in CD169 knockout mice (Saunderson et al., 2014). Other insights into cell-specific EV uptake indicate the potential influence of saccharides. In the presence of D-mannose or D-glucosamine, EV uptake by dendritic cells was blunted, suggesting an EV uptake mechanism based on C-type lectin interaction (Hao et al., 2007). However, other studies have demonstrated sugars do not seem to play a significant role in EV-cell interaction and uptake (Escrevente et al., 2011), suggesting cell- or condition-specific difference in EV uptake mechanisms.

Given the identification of EV-derived biomolecules that mediate many of the therapeutic benefits associated with EV therapy, selectively loading EVs with defined biomolecules is one goal which can be achieved using various approaches reviewed elsewhere (Kenari et al., 2020). Briefly, a non-invasive method for loading therapeutic molecules into EVs is

via co-incubation (Zhuang et al., 2011). This method allows hydrophobic biomolecules to enter the EV lumen through passive diffusion without disrupting the lipid membrane. Other methods include, but not limited to, electroporation or sonication (Tian et al., 2014; Kim et al., 2016). Although these methods have been successfully used to load exogenous biomolecules into EVs, they disrupt the lipid membrane and may result in EV damage or lysis. Further research will be required to determine if these are viable methods to produce clinical-grade therapeutic EVs. In addition to loading defined molecules into EVs, engineering their delivery to specific target tissues would be a significant enhancement to such a therapeutic. As such, we have recently developed a platform using membrane cloaking and surface display technology to direct EVs to target tissues. Cloaking lends itself to utilizing any biotinylated antibody – to which countless are commercially available for testing. For example, we previously demonstrated that CDC-EV uptake by cardiac fibroblasts, which is ordinarily minimal, could be augmented *in vitro* by ligating a DDR2 antibody (Antes et al., 2018). Addition of an ischemic targeting peptide to the surface of CDC-EV conferred enhanced *in vivo* targeting to the myocardium. Such an advent may provide significant therapeutic value to target a major cell source contributing to the development of myocardial fibrosis.

CONCLUSION

Extracellular vesicles represent a mode of intercellular communication near and far. These tiny vesicles carry messages in the form of biomolecules to inform recipient cells of the current (patho)physiological state and direct the cell to respond appropriately. The recognition that EVs secreted from stem/progenitor cells are therapeutically bioactive when given to animals with heart disease represents a paradigm shift away from cell therapy toward a cell-free platform. Such a paradigm shift overcomes many key concerns and limitations of cell therapy, while conferring the amendable ability to modify vesicle cargo and tissue targeting. Indeed, we and others have demonstrated that payload RNAs, notably miRs, long non-coding RNAs, Y-RNAs, and piRNA, produce transcriptomic and epigenomic modifications that impart lasting effects on recipient cells. By targeting key cellular and molecular players in cardiac fibrosis, these defined molecules contained within therapeutically potent EVs provide insight into avenues for bioengineering. Time will certainly tell if EV-based therapeutics live up to their promise.

AUTHOR CONTRIBUTIONS

RR drafted the manuscript. AI and AC generated the figures. EM approved the final version. All authors helped to write the manuscript.

FUNDING

Support for this research program was provided by NHLBI/NIH and the U.S. Department of Defense. EM holds the Mark S. Siegel Family Distinguished Chair of the Cedars-Sinai Medical Center.

REFERENCES

Akers, J. C., Ramakrishnan, V., Yang, I., Hua, W., Mao, Y., Carter, B. S., et al. (2016). Optimizing preservation of extracellular vesicular miRNAs derived from clinical cerebrospinal fluid. *Cancer Biomark.* 17, 125–132. doi: 10.3233/CBM-160609

Alibhai, F. J., Tobin, S. W., Yeganeh, A., Weisel, R. D., and Li, R.-K. (2018). Emerging roles of extracellular vesicles in cardiac repair and rejuvenation. *Am. J. Physiol. Heart Circul. Physiol.* 315, H733–H744. doi: 10.1152/ajpheart.00100.2018

Aminzadeh, M. A., Rogers, R. G., Fournier, M., Tobin, R. E., Guan, X., Childers, M. K., et al. (2018). Exosome-mediated benefits of cell therapy in mouse and human models of duchenne muscular dystrophy. *Stem Cell Rep.* 10, 942–955. doi: 10.1016/j.stemcr.2018.01.023

Aminzadeh, M. A., Tseliou, E., Sun, B., Cheng, K., Malliaras, K., Makkar, R. R., et al. (2015). Therapeutic efficacy of cardiosphere-derived cells in a transgenic mouse model of non-ischaemic dilated cardiomyopathy. *Eur. Heart J.* 36, 751–762. doi: 10.1093/eurheartj/ehu196

Antes, T. J., Middleton, R. C., Luther, K. M., Ijichi, T., Peck, K. A., Liu, W. J., et al. (2018). Targeting extracellular vesicles to injured tissue using membrane cloaking and surface display. *J. Nanobiotechnol.* 16, 1–15. doi: 10.1186/s12951-018-0388-4

Balbi, C., Costa, A., Barile, L., and Bollini, S. (2020). Message in a bottle: upgrading cardiac repair into rejuvenation. *Cells* 9:724. doi: 10.3390/cells9030724

Baranyai, T., Herczeg, K., Onódi, Z., Voszka, I., Módos, K., Marton, N., et al. (2015). Isolation of exosomes from blood plasma: qualitative and quantitative comparison of ultracentrifugation and size exclusion chromatography methods. *PLoS One* 10:e0145686. doi: 10.1371/journal.pone.0145686

Barile, L., Lionetti, V., Cervio, E., Matteucci, M., Gherghiceanu, M., Popescu, L. M., et al. (2014). Extracellular vesicles from human cardiac progenitor cells inhibit cardiomyocyte apoptosis and improve cardiac function after myocardial infarction. *Cardiovasc. Res.* 103, 530–541. doi: 10.1093/cvr/cvu167

Barile, L., Moccetti, T., Marbán, E., and Vassalli, G. (2017). Roles of exosomes in cardioprotection. *Eur. Heart J.* 38, 1372–1379.

Berk, B. C., Fujiwara, K., and Lehoux, S. (2007). ECM remodeling in hypertensive heart disease. *J. Clin. Invest.* 117, 568–575.

Bianco, P., Robey, P. G., and Simmons, P. J. (2008). Mesenchymal stem cells: revisiting history, concepts, and assays. *Cell Stem Cell* 2, 313–319. doi: 10.1016/j.stem.2008.03.002

Bobrie, A., Colombo, M., Krumeich, S., Raposo, G., and Théry, C. (2012). Diverse subpopulations of vesicles secreted by different intracellular mechanisms are present in exosome preparations obtained by differential ultracentrifugation. *J. Extracell. Ves.* 1:18397. doi: 10.3402/jev.v1i0.18397

Cai, H., Reinisch, K., and Ferro-Novick, S. (2007). Coats, tethers, Rabs, and SNAREs work together to mediate the intracellular destination of a transport vesicle. *Dev. Cell* 12, 671–682. doi: 10.1016/j.devcel.2007.04.005

Cambier, L., De Couto, G., Ibrahim, A., Echavez, A. K., Valle, J., Liu, W., et al. (2017). Y RNA fragment in extracellular vesicles confers cardioprotection via modulation of IL-10 expression and secretion. *EMBO Mol. Med.* 9, 337–352. doi: 10.15252/emmm.201606924

Cambier, L., Giani, J. F., Liu, W., Ijichi, T., Echavez, A. K., Valle, J., et al. (2018). Angiotensin II-induced end-organ damage in mice is attenuated by human exosomes and by an exosomal Y RNA fragment. *Hypertension* 72, 370–380. doi: 10.1161/HYPERTENSIONAHA.118.11239

Cheng, Z., Zhou, Y. Z., Wu, Y., Wu, Q. Y., Liao, X. B., Fu, X. M., et al. (2018). Diverse roles of macrophage polarization in aortic aneurysm: destruction and repair. *J. Transl. Med.* 16:354. doi: 10.1186/s12967-018-1731-0

Choi, Y. J., Koo, J. B., Kim, H. Y., Seo, J. W., Lee, E. J., Kim, W. R., et al. (2019). Umbilical cord/placenta-derived mesenchymal stem cells inhibit fibrogenic

activation in human intestinal myofibroblasts via inhibition of myocardin-related transcription factor A. *Stem Cell Res. Ther.* 10, 1–16. doi: 10.1186/s13287-019-1385-8

Christov, C. P., Gardiner, T. J., Szuts, D., and Krude, T. (2006). Functional requirement of noncoding Y RNAs for human chromosomal DNA replication. *Mol. Cell. Biol.* 26, 6993–7004. doi: 10.1128/MCB.01060-06

Colombo, M., Raposo, G., and Théry, C. (2014). Biogenesis, secretion, and intercellular interactions of exosomes and other extracellular vesicles. *Annu. Rev. Cell Dev. Biol.* 30, 255–289. doi: 10.1146/annurev-cellbio-101512-122326

Conlan, R. S., Pisano, S., Oliveira, M. I., Ferrari, M., and Pinto, I. M. (2017). Exosomes as reconfigurable therapeutic systems. *Trends Mol. Med.* 23, 636–650. doi: 10.1016/j.molmed.2017.05.003

Davis, D. R., Zhang, Y., Smith, R. R., Cheng, K., Terrovitis, J., Malliaras, K., et al. (2009). Validation of the cardiosphere method to culture cardiac progenitor cells from myocardial tissue. *PLoS One* 4:e7195. doi: 10.1371/journal.pone.07195

De Couto, G., Gallet, R., Cambier, L., Jaghatspanyan, E., Makkar, N., Dawkins, J. F., et al. (2017). Exosomal MicroRNA transfer into macrophages mediates cellular postconditioning. *Circulation* 136, 200–214. doi: 10.1161/CIRCULATIONAHA.117.031555

Dodson, B. P., and Levine, A. D. (2015). Challenges in the translation and commercialization of cell therapies. *BMC Biotechnol.* 15:70. doi: 10.1186/s12896-015-0190-4

Escrevente, C., Keller, S., Altevogt, P., and Costa, J. (2011). Interaction and uptake of exosomes by ovarian cancer cells. *BMC Cancer* 11:108. doi: 10.1186/1471-2407-11-108

Feng, Y., Huang, W., Wani, M., Yu, X., and Ashraf, M. (2014). Ischemic preconditioning potentiates the protective effect of stem cells through secretion of exosomes by targeting Mecp2 via miR-22. *PLoS One* 9:e88685. doi: 10.1371/journal.pone.088685

Frangogiannis, N. G. (2019). Cardiac fibrosis: cell biological mechanisms, molecular pathways and therapeutic opportunities. *Mol. Aspects Med.* 65, 70–99. doi: 10.1016/j.mam.2018.07.001

Gallet, R., Dawkins, J., Valle, J., Simsolo, E., De Couto, G., Middleton, R., et al. (2017). Exosomes secreted by cardiosphere-derived cells reduce scarring, attenuate adverse remodelling, and improve function in acute and chronic porcine myocardial infarction. *Eur. Heart J.* 38, 201–211. doi: 10.1093/eurheartj/ehw240

Geraldo, M. V., Yamashita, A. S., and Kimura, E. T. (2012). MicroRNA miR-146b-5p regulates signal transduction of TGF-beta by repressing SMAD4 in thyroid cancer. *Oncogene* 31, 1910–1922. doi: 10.1038/onc.2011.381

Hao, S., Bai, O., Li, F., Yuan, J., Laferte, S., and Xiang, J. (2007). Mature dendritic cells pulsed with exosomes stimulate efficient cytotoxic T-lymphocyte responses and antitumour immunity. *Immunology* 120, 90–102. doi: 10.1111/j.1365-2567.2006.02483.x

He, C., Zheng, S., Luo, Y., and Wang, B. (2018). Exosome theranostics: biology and translational medicine. *Theranostics* 8:237. doi: 10.7150/thno.21945

Ibrahim, A., and Marbán, E. (2016). Exosomes: fundamental biology and roles in cardiovascular physiology. *Annu. Rev. Physiol.* 78, 67–83. doi: 10.1146/annurev-physiol-021115-104929

Ibrahim, A. G., Cheng, K., and Marban, E. (2014). Exosomes as critical agents of cardiac regeneration triggered by cell therapy. *Stem Cell Rep.* 2, 606–619. doi: 10.1016/j.stemcr.2014.04.006

Ibrahim, A. G. E., Li, C., Rogers, R., Fournier, M., Li, L., Vaturi, S. D., et al. (2019). Augmenting canonical Wnt signalling in therapeutically inert cells converts them into therapeutically potent exosome factories. *Nat. Biomed. Eng.* 3, 695–705. doi: 10.1038/s41551-019-0448-6

Iso, Y., Spees, J. L., Serrano, C., Bakondi, B., Pochampally, R., Song, Y.-H., et al. (2007). Multipotent human stromal cells improve cardiac function after myocardial infarction in mice without long-term engraftment. *Biochem. Biophys. Res. Commun.* 354, 700–706. doi: 10.1016/j.bbrc.2007.01.045

Jameel, M. N., and Zhang, J. (2009). Heart failure management: the present and the future. *Antioxid. Redox Signal.* 11, 1989–2010.

Johnstone, R. M., Adam, M., Hammond, J., Orr, L., and Turbide, C. (1987). Vesicle formation during reticulocyte maturation. Association of plasma membrane activities with released vesicles (exosomes). *J. Biol. Chem.* 262, 9412–9420.

Kandalam, V., Basu, R., Abraham, T., Wang, X., Soloway, P. D., Jaworski, D. M., et al. (2010). TIMP2 deficiency accelerates adverse post-myocardial infarction remodeling because of enhanced MT1-MMP activity despite lack of MMP2 activation. *Circ. Res.* 106:796. doi: 10.1161/CIRCRESAHA.109.209189

Keating, A. (2012). Mesenchymal stromal cells: new directions. *Cell Stem Cell* 10, 709–716. doi: 10.1016/j.stem.2012.05.015

Kenari, A. N., Cheng, L., and Hill, A. F. (2020). Methods for loading therapeutics into extracellular vesicles and generating extracellular vesicles mimetic-nanovesicles. *Methods* 177, 103–113.

Khalil, H., Kanisicak, O., Prasad, V., Correll, R. N., Fu, X., Schips, T., et al. (2017). Fibroblast-specific TGF-beta-Smad2/3 signaling underlies cardiac fibrosis. *J. Clin. Invest.* 127, 3770–3783. doi: 10.1172/JCI94753

Khan, M., Nickoloff, E., Abramova, T., Johnson, J., Verma, S. K., Krishnamurthy, P., et al. (2015). Embryonic stem cell-derived exosomes promote endogenous repair mechanisms and enhance cardiac function following myocardial infarction. *Circ. Res.* 117, 52–64. doi: 10.1161/CIRCRESAHA.117.305990

Kim, M. S., Haney, M. J., Zhao, Y., Mahajan, V., Deygen, I., Klyachko, N. L., et al. (2016). Development of exosome-encapsulated paclitaxel to overcome MDR in cancer cells. *Nanomedicine* 12, 655–664. doi: 10.1016/j.nano.2015.10.012

Kong, P., Christia, P., and Frangogiannis, N. G. (2014). The pathogenesis of cardiac fibrosis. *Cell Mol. Life. Sci.* 71, 549–574.

Krzyszczyk, P., Schloss, R., Palmer, A., and Berthiaume, F. (2018). The role of macrophages in acute and chronic wound healing and interventions to promote pro-wound healing phenotypes. *Front. Physiol.* 9:419. doi: 10.3389/fphys.2018.00419

Lai, R. C., Arslan, F., Lee, M. M., Sze, N. S. K., Choo, A., Chen, T. S., et al. (2010). Exosome secreted by MSC reduces myocardial ischemia/reperfusion injury. *Stem Cell Res.* 4, 214–222. doi: 10.1016/j.scr.2009.12.003

Lai, R. C., Tan, S. S., Yeo, R. W. Y., Choo, A. B. H., Reiner, A. T., Su, Y., et al. (2016). MSC secretes at least 3 EV types each with a unique permutation of membrane lipid, protein and RNA. *J. Extracell. Ves.* 5:29828. doi: 10.3402/jev.v5.29828

Legrand, A. J., Konstantinou, M., Goode, E. F., and Meier, P. (2019). The diversification of cell death and immunity: memento mori. *Mol. Cell.* 76, 232–242. doi: 10.1016/j.molcel.2019.09.006

Leiker, M., Suzuki, G., Iyer, V. S., John, M., and Lee, T. (2008). Assessment of a nuclear affinity labeling method for tracking implanted mesenchymal stem cells. *Cell Transpl.* 17, 911–922. doi: 10.3727/096368908786576444

Liu, Z., Lu, C.-L., Cui, L.-P., Hu, Y.-L., Yu, Q., Jiang, Y., et al. (2012). MicroRNA-146a modulates TGF-β1-induced phenotypic differentiation in human dermal fibroblasts by targeting SMAD4. *Arch. Dermatol. Res.* 304, 195–202. doi: 10.1007/s00403-011-1178-0

Ma, F., Li, Y., Jia, L., Han, Y., Cheng, J., Li, H., et al. (2012). Macrophage-stimulated cardiac fibroblast production of IL-6 is essential for TGF β/Smad activation and cardiac fibrosis induced by angiotensin II. *PLoS One* 7:e35144. doi: 10.1371/journal.pone.0035144

Marbán, E. (2018a). A mechanistic roadmap for the clinical application of cardiac cell therapies. *Nat. Biomed. Eng.* 2, 353–361. doi: 10.1038/s41551-018-0216-z

Marbán, E. (2018b). The secret life of exosomes: what bees can teach us about next-generation therapeutics. *J. Am. Coll. Cardiol.* 71, 193–200. doi: 10.1016/j.jacc.2017.11.013

Marzesco, A.-M., Janich, P., Wilsch-Bräuninger, M., Dubreuil, V., Langenfeld, K., Corbeil, D., et al. (2005). Release of extracellular membrane particles carrying the stem cell marker prominin-1 (CD133) from neural progenitors and other epithelial cells. *J. Cell Sci.* 118, 2849–2858. doi: 10.1242/jcs.02439

Members, A. T. F., Mcmurray, J. J., Adamopoulos, S., Anker, S. D., Auricchio, A., Böhm, M., et al. (2012). ESC guidelines for the diagnosis and treatment of acute and chronic heart failure 2012: the task force for the diagnosis and treatment of acute and chronic heart failure 2012 of the european society of cardiology. developed in collaboration with the heart failure association (HFA) of the ESC. *Eur. J. Heart Fail.* 14, 803–869. doi: 10.1093/eurjhf/hfs105

Minghua, W., Zhijian, G., Chahua, H., Qiang, L., Minxuan, X., Luqiao, W., et al. (2018). Plasma exosomes induced by remote ischaemic preconditioning attenuate myocardial ischaemia/reperfusion injury by transferring miR-24. *Cell Death Dis.* 9:320. doi: 10.1038/s41419-018-0274-x

Mohammadi, M. R., Riazifar, M., Pone, E. J., Yeri, A., Van Keuren-Jensen, K., Lässer, C., et al. (2019). Isolation and characterization of microvesicles from mesenchymal stem cells. *Methods* 177, 50–57. doi: 10.1016/j.ymeth.2019.10.010

Nevers, T., Salvador, A. M., Grodecki-Pena, A., Knapp, A., Velazquez, F., Aronovitz, M., et al. (2015). Left ventricular T-cell recruitment contributes to

the pathogenesis of heart failure. *Circ. Heart Fail.* 8, 776–787. doi: 10.1161/CIRCHEARTFAILURE.115.002225

Ngu, J. M., Teng, G., Meijndert, H. C., Mewhort, H. E., Turnbull, J. D., Stetler-Stevenson, W. G., et al. (2014). Human cardiac fibroblast extracellular matrix remodeling: dual effects of tissue inhibitor of metalloproteinase-2. *Cardiovasc. Pathol.* 23, 335–343. doi: 10.1016/j.carpath.2014.06.003

Nigro, P., Bassetti, B., Cavallotti, L., Catto, V., Carbucicchio, C., and Pompilio, G. (2018). Cell therapy for heart disease after 15 years: unmet expectations. *Pharmacol. Res.* 127, 77–91. doi: 10.1016/j.phrs.2017.02.015

Panayi, G. S., Corrigall, V. M., and Henderson, B. (2004). Stress cytokines: pivotal proteins in immune regulatory networks. *Opinion. Curr. Opin. Immunol.* 16, 531–534. doi: 10.1016/j.coi.2004.05.017

Pardali, E., Sanchez-Duffhues, G., Gomez-Puerto, M. C., and Ten Dijke, P. (2017). TGF-beta-induced endothelial-mesenchymal transition in fibrotic diseases. *Int. J. Mol. Sci.* 18:2157. doi: 10.3390/ijms18102157

Patel, B., Bansal, S. S., Ismahil, M. A., Hamid, T., Rokosh, G., Mack, M., et al. (2018). CCR2(+) monocyte-derived infiltrating macrophages are required for adverse cardiac remodeling during pressure overload. *JACC Basic Transl. Sci.* 3, 230–244. doi: 10.1016/j.jacbts.2017.12.006

Ramani, R., Nilles, K., Gibson, G., Burkhead, B., Mathier, M., Mcnamara, D., et al. (2011). Tissue inhibitor of metalloproteinase-2 gene delivery ameliorates postinfarction cardiac remodeling. *Clin. Transl. Sci.* 4, 24–31. doi: 10.1111/j.1752-8062.2010.00252.x

Roers, A., Hiller, B., and Hornung, V. (2016). Recognition of endogenous nucleic acids by the innate immune system. *Immunity* 44, 739–754. doi: 10.1016/j.immuni.2016.04.002

Rogers, R. G., De Couto, G., Liu, W., Sanchez, L., and Marban, E. (2019a). Cardiosphere-derived cell exosomes modulate mdx macrophage phenotype and alter their secretome. *FASEB J.* 33, lb611–lb611.

Rogers, R. G., Fournier, M., Sanchez, L., Ibrahim, A. G., Aminzadeh, M. A., Lewis, M. I., et al. (2019b). Disease-modifying bioactivity of intravenous cardiosphere-derived cells and exosomes in mdx mice. *JCI Insight* 4:e130202. doi: 10.1172/jci.insight.130202

Rogers, R. G., and Otis, J. S. (2017). Resveratrol-mediated expression of KLF15 in the ischemic myocardium is associated with an improved cardiac phenotype. *Cardiovasc. Drugs. Ther.* 31, 29–38. doi: 10.1007/s10557-016-6707-9

Roth, G. A., Johnson, C., Abajobir, A., Abd-Allah, F., Abera, S. F., Abyu, G., et al. (2017). Global, regional, and national burden of cardiovascular diseases for 10 causes, 1990 to 2015. *J. Am. Coll. Cardiol.* 70, 1–25. doi: 10.1016/j.jacc.2017.04.052

Rubartelli, A., and Lotze, M. T. (2007). Inside, outside, upside down: damage-associated molecular-pattern molecules (DAMPs) and redox. *Trends Immunol.* 28, 429–436. doi: 10.1016/j.it.2007.08.004

Saba, R., Sorensen, D. L., and Booth, S. A. (2014). MicroRNA-146a: a dominant, negative regulator of the innate immune response. *Front. Immunol.* 5:578. doi: 10.3389/fimmu.2014.00578

Sahoo, S., Klychko, E., Thorne, T., Misener, S., Schultz, K. M., Millay, M., et al. (2011). Exosomes from human CD34+ stem cells mediate their proangiogenic paracrine activity. *Circ. Res.* 109, 724–728. doi: 10.1161/CIRCRESAHA.111.253286

Saunderson, S. C., Dunn, A. C., Crocker, P. R., and Mclellan, A. D. (2014). CD169 mediates the capture of exosomes in spleen and lymph node. *Blood J. Am. Soc. Hematol.* 123, 208–216. doi: 10.1182/blood-2013-03-489732

Scaffidi, P., Misteli, T., and Bianchi, M. E. (2002). Release of chromatin protein HMGB1 by necrotic cells triggers inflammation. *Nature* 418, 191–195. doi: 10.1038/nature00858

Sharma, K., and Kass, D. A. (2014). Heart failure with preserved ejection fraction: mechanisms, clinical features, and therapies. *Circ. Res.* 115, 79–96. doi: 10.1161/CIRCRESAHA.115.302922

Shi, B., Wang, Y., Zhao, R., Long, X., Deng, W., and Wang, Z. (2018). Bone marrow mesenchymal stem cell-derived exosomal miR-21 protects C-kit+ cardiac stem cells from oxidative injury through the PTEN/PI3K/Akt axis. *PLoS One* 13:e0191616. doi: 10.1371/journal.pone.0191616

Silva, A. M., Teixeira, J. H., Almeida, M. I., Goncalves, R. M., Barbosa, M. A., and Santos, S. G. (2017). Extracellular vesicles: immunomodulatory messengers in the context of tissue repair/regeneration. *Eur. J. Pharm. Sci.* 98, 86–95. doi: 10.1016/j.ejps.2016.09.017

Sluijter, J. P. G., Davidson, S. M., Boulanger, C. M., Buzas, E. I., De Kleijn, D. P. V., Engel, F. B., et al. (2018). Extracellular vesicles in diagnostics and therapy of the ischaemic heart: position paper from the working group on cellular biology of the heart of the european society of cardiology. *Cardiovasc. Res.* 114, 19–34. doi: 10.1093/cvr/cvx211

Smith, R. R., Barile, L., Cho, H. C., Leppo, M. K., Hare, J. M., Messina, E., et al. (2007). Regenerative potential of cardiosphere-derived cells expanded from percutaneous endomyocardial biopsy specimens. *Circulation* 115, 896–908. doi: 10.1161/CIRCULATIONAHA.106.655209

Stahl, P. D., and Raposo, G. (2018). Exosomes and extracellular vesicles: the path forward. *Essays Biochem.* 62, 119–124. doi: 10.1042/EBC20170088

Stoltz, J.-F., De Isla, N., Li, Y., Bensoussan, D., Zhang, L., Huselstein, C., et al. (2015). Stem cells and regenerative medicine: myth or reality of the 21th century. *Stem Cells Intern.* 2015:734731. doi: 10.1155/2015/734731

Tang, D., Kang, R., Coyne, C. B., Zeh, H. J., and Lotze, M. T. (2012). PAMPs and DAMPs: signal 0s that spur autophagy and immunity. *Immunol. Rev.* 249, 158–175. doi: 10.1111/j.1600-065X.2012.01146.x

Tian, Y., Li, S., Song, J., Ji, T., Zhu, M., Anderson, G. J., et al. (2014). A doxorubicin delivery platform using engineered natural membrane vesicle exosomes for targeted tumor therapy. *Biomaterials* 35, 2383–2390. doi: 10.1016/j.biomaterials.2013.11.083

Tikhomirov, R., Donnell, B. R.-O., Catapano, F., Faggian, G., Gorelik, J., Martelli, F., et al. (2020). Exosomes: from potential culprits to new therapeutic promise in the setting of cardiac fibrosis. *Cells* 9:592. doi: 10.3390/cells9030592

Tokita, Y., Tang, X.-L., Li, Q., Wysoczynski, M., Hong, K. U., Nakamura, S., et al. (2016). Repeated administrations of cardiac progenitor cells are markedly more effective than a single administration: a new paradigm in cell therapy. *Circ. Res.* 119, 635–651. doi: 10.1161/CIRCRESAHA.116.308937

Van Rooij, E., Sutherland, L. B., Thatcher, J. E., Dimaio, J. M., Naseem, R. H., Marshall, W. S., et al. (2008). Dysregulation of microRNAs after myocardial infarction reveals a role of miR-29 in cardiac fibrosis. *Proc. Natl. Acad. Sci. U.S.A.* 105, 13027–13032. doi: 10.1073/pnas.0805038105

Vicencio, J. M., Yellon, D. M., Sivaraman, V., Das, D., Boi-Doku, C., Arjun, S., et al. (2015). Plasma exosomes protect the myocardium from ischemia-reperfusion injury. *J. Am. Coll. Cardiol.* 65, 1525–1536. doi: 10.1016/j.jacc.2015.02.026

Wang, X., Gu, H., Huang, W., Peng, J., Li, Y., Yang, L., et al. (2016). Hsp20-mediated activation of exosome biogenesis in cardiomyocytes improves cardiac function and angiogenesis in diabetic mice. *Diabetes Metab. Res. Rev.* 65, 3111–3128. doi: 10.2337/db15-1563

Wang, Y., Zhang, L., Li, Y., Chen, L., Wang, X., Guo, W., et al. (2015). Exosomes/microvesicles from induced pluripotent stem cells deliver cardioprotective miRNAs and prevent cardiomyocyte apoptosis in the ischemic myocardium. *Int. J. Cardiol.* 192, 61–69. doi: 10.1016/j.ijcard.2015.05.020

White, A. J., Smith, R. R., Matsushita, S., Chakravarty, T., Czer, L. S., Burton, K., et al. (2013). Intrinsic cardiac origin of human cardiosphere-derived cells. *Eur. Heart J.* 34, 68–75. doi: 10.1093/eurheartj/ehr172

Wiklander, O. P., Nordin, J. Z., O'loughlin, A., Gustafsson, Y., Corso, G., Mäger, I., et al. (2015). Extracellular vesicle in vivo biodistribution is determined by cell source, route of administration and targeting. *J. Extracell. Ves.* 4:26316. doi: 10.3402/jev.v4.26316

Yamaguchi, T., Izumi, Y., Nakamura, Y., Yamazaki, T., Shiota, M., Sano, S., et al. (2015). Repeated remote ischemic conditioning attenuates left ventricular remodeling via exosome-mediated intercellular communication on chronic heart failure after myocardial infarction. *Int. J. Cardiol.* 178, 239–246. doi: 10.1016/j.ijcard.2014.10.144

Yáñez-Mó, M., Siljander, P. R.-M., Andreu, Z., Bedina Zavec, A., Borràs, F. E., Buzas, E. I., et al. (2015). Biological properties of extracellular vesicles and their physiological functions. *J. Extracell. Ves.* 4:27066. doi: 10.3402/jev.v4.27066

Yu, B., Gong, M., Wang, Y., Millard, R. W., Pasha, Z., Yang, Y., et al. (2013). Cardiomyocyte protection by GATA-4 gene engineered mesenchymal stem cells is partially mediated by translocation of miR-221 in microvesicles. *PLoS One* 8:e73304. doi: 10.1371/journal.pone.073304

Yu, B., Kim, H. W., Gong, M., Wang, J., Millard, R. W., Wang, Y., et al. (2015). Exosomes secreted from GATA-4 overexpressing mesenchymal stem cells serve as a reservoir of anti-apoptotic microRNAs for cardioprotection. *Int. J. Cardiol.* 182, 349–360. doi: 10.1016/j.ijcard.2014.12.043

Zhang, A. T., Langley, A. R., Christov, C. P., Kheir, E., Shafee, T., Gardiner, T. J., et al. (2011). Dynamic interaction of Y RNAs with chromatin and initiation proteins during human DNA replication. *J. Cell Sci.* 124, 2058–2069. doi: 10.1242/jcs.086561

Zhuang, X., Xiang, X., Grizzle, W., Sun, D., Zhang, S., Axtell, R. C., et al. (2011). Treatment of brain inflammatory diseases by delivering exosome encapsulated anti-inflammatory drugs from the nasal region to the brain. *Mol. Ther.* 19, 1769–1779. doi: 10.1038/mt.2011.222

Zwetsloot, P. P., Végh, A. M. D., Lorkeers, S. J., Van Hout, G. P., Currie, G. L., Sena, E. S., et al. (2016). Cardiac stem cell treatment in myocardial infarction: a systematic review and meta-analysis of preclinical studies. *Circ. Res.* 118, 1223–1232. doi: 10.1161/CIRCRESAHA.115.307676

Conflict of Interest: EM is a founding equity share-holder of Capricor Therapeutics.

The remaining authors declare that the research was conducted in the absence of any commercial or financial relationships that could be construed as a potential conflict of interest.

frontiers in Physiology

ORIGINAL RESEARCH
published: 30 June 2020
doi: 10.3389/fphys.2020.00669

Notch3 Modulates Cardiac Fibroblast Proliferation, Apoptosis, and Fibroblast to Myofibroblast Transition via Negative Regulation of the RhoA/ROCK/Hif1α Axis

Jianli Shi[1†], Peilin Xiao[1†], Xiaoli Liu[1], Yunlin Chen[1], Yanping Xu[1], Jinqi Fan[1,2] and Yuehui Yin[1]*

[1] Department of Cardiology, The Second Affiliated Hospital of Chongqing Medical University, Chongqing, China,
[2] Department of Biomedical Engineering and Pediatrics, Emory University, Atlanta, GA, United States

OPEN ACCESS

Edited by:
Claudio de Lucia,
Temple University, United States

Reviewed by:
JoAnn Trial,
Baylor College of Medicine, United States
Susanne Lutz,
University of Göttingen, Germany
Maria Pelullo,
Center for Life Nano Science (IIT), Italy

***Correspondence:**
Yuehui Yin
yinyh@hospital.cqmu.edu.cn

[†] These authors have contributed equally to this work and share first authorship

Specialty section:
This article was submitted to Integrative Physiology, a section of the journal Frontiers in Physiology

Received: 29 November 2019
Accepted: 25 May 2020
Published: 30 June 2020

Citation:
Shi J, Xiao P, Liu X, Chen Y, Xu Y, Fan J and Yin Y (2020) Notch3 Modulates Cardiac Fibroblast Proliferation, Apoptosis, and Fibroblast to Myofibroblast Transition via Negative Regulation of the RhoA/ROCK/Hif1α Axis. Front. Physiol. 11:669. doi: 10.3389/fphys.2020.00669

Cardiac fibrosis is a common pathological process in multiple cardiovascular diseases, including myocardial infarction (MI). Abnormal cardiac fibroblast (CF) activity is a key event in cardiac fibrosis. Although the Notch signaling pathway has been reported to play a vital role in protection from cardiac fibrosis, the exact mechanisms underlying cardiac fibrosis and protection from it have not yet been elucidated. Similarly, Hif1α and the RhoA/ROCK signaling pathway have been shown to participate in cardiac fibrosis. The RhoA/ROCK signaling pathway has been reported to be an upstream pathway of Hif1α in several pathophysiological processes. In the present study, we aimed to determine the effects of notch3 on CF activity and its relationship with the RhoA/ROCK/Hif1α signaling pathway. Using *in vitro* experiments, we demonstrated that notch3 inhibited CF proliferation and fibroblast to myofibroblast transition (FMT) and promoted CF apoptosis. A knockdown of notch3 using siRNAs had the exact opposite effect. Next, we found that notch3 regulated CF activity by negative regulation of the RhoA/ROCK/Hif1α signaling pathway. Extending CF-based studies to an *in vivo* rat MI model, we showed that overexpression of notch3 by the Ad-N3ICD injection attenuated the increase of RhoA, ROCK1, ROCK2, and Hif1α levels following MI and further prevented MI-induced cardiac fibrosis. On the basis of these results, we conclude that notch3 is involved in the regulation of several aspects of CF activity, including proliferation, FMT, and apoptosis, by inhibiting the RhoA/ROCK/Hif1α signaling pathway. These findings are significant to further our understanding of the pathogenesis of cardiac fibrosis and to ultimately identify new therapeutic targets for cardiac fibrosis, potentially based on the RhoA/ROCK/Hif1α signaling pathway.

Keywords: notch, cardiac fibroblast, cardiac fibrosis, myocardial infarction, extracellular matrix

INTRODUCTION

Heart failure (HF), secondary to ischemic or non-ischemic cardiomyopathy, is a serious health issue with high rates of associated morbidity and mortality. The progression of HF is in part caused by cardiac fibrosis, which is characterized by the deposition of extracellular matrix (ECM) and the activation of cardiac fibroblasts (CFs). Cardiac fibrosis is a common pathological process during the development of HF in multiple cardiovascular diseases (Li K. et al., 2019; Wang et al., 2019). Excessive cardiac fibrosis is furthermore a predictor of sudden cardiac death and overall mortality for cardiomyopathy (Gulati et al., 2013).

The myocardium consists of cardiomyocytes, CFs, and endothelial cells. CFs are predominantly involved in the maintenance of the ECM, which plays an important role in myocardial fibrosis (Prabhu and Frangogiannis, 2016). During myocardial fibrosis, CFs have a proliferative and migratory phenotype and exhibit enhanced secretion of ECM. This alteration in CF activity is a key regulatory event in cardiac fibrosis. Several proinflammatory and profibrotic factors are involved in the regulation of CF activity in cardiac fibrosis, such as NF-κB, bone morphogenetic protein, and TGF-β1 (Sun et al., 2013; Fix et al., 2019; Li A.Y. et al., 2019). These factors have been shown to be involved in similar pathological processes for several different etiologies (Harvey and Leinwand, 2011).

The Notch signaling pathway is a highly conserved signaling system involved in cellular differentiation, proliferation, apoptosis, and epithelial-to-mesenchymal transformation (EMT) (Hu and Phan, 2016; MacGrogan et al., 2018). Previous studies have demonstrated that the notch signaling pathway is able to protect the myocardium from ischemia (Zhou et al., 2019). However, the molecular mechanisms of notch3 in alleviating cardiac fibrosis are not fully elucidated, and further research is required.

Hif1 is part of the family of basic-helix-loop-helix/Per-ARNT-Sim (bHLH/PAS) DNA binding transcription factors (Greer et al., 2012) and is a major regulator of the hypoxic response. Hif1α is unstable and rapidly degraded by the ubiquitin–proteasome system. The role of Hif1α in cardiovascular diseases is controversial (Kido et al., 2005; Shyu et al., 2005a,b; Natarajan et al., 2008). In a review of previous studies, Xiong and Liu (2017) suggested that Hif1α may contribute to excessive ECM deposition and vascular remodeling and thus constitutes a vital therapeutic target for fibrotic diseases. The majority of previous studies investigating Hif1α was looking at the hypoxia pathway, but Hif1α is involved in a variety of other pathways. For example, angiotensin II (Ang II) has been shown to increase Hif1α levels in vascular smooth muscle cells independent of the oxygen environment (Richard et al., 2000). Furthermore, the RhoA/ROCK signaling pathway has been found to act as an upstream pathway of Hif1α in several pathophysiological processes, constituting a molecular switch in regulating cellular adherence, proliferation, and apoptosis (Sarrabayrouse et al., 2007; Jing et al., 2015; Rao et al., 2017). There is mounting evidence suggesting that RhoA/ROCK participates in the regulation of fibrosis by interacting with other signaling pathways or regulators (Bei et al., 2016; Tang et al., 2018; Zhou et al., 2018; Lai et al., 2019). However, no studies have so far clearly demonstrated the mechanisms underlying the regulation of CF activity via interaction of the notch signaling pathway with Hif1α and RhoA/ROCK. To explore these signaling events in cardiac fibrosis, we investigated the effects of Hif1α–RhoA/ROCK interaction on the modulation of notch-dependent fibrotic events under normoxia. Our results showed that notch3 regulated CF activity *in vitro* and cardiac fibrosis *in vivo*. Besides, we confirmed the involvement of the RhoA/ROCK/Hif1α signaling pathway in these processes.

MATERIALS AND METHODS

Animal Care and Procedures

Six- to eight-week-old male Sprague–Dawley rats (weighing 250 ± 20 g) were obtained from the Animal Research Center of Chongqing Medical University (Chongqing, China) and housed in a temperature-controlled environment on a 12-h/12-h light/dark cycle. All experimental procedures were approved by the Institutional Ethics Committee of Chongqing Medical University. The rats were anesthetized using sodium pentobarbital (60 mg/kg, i.p.), and thoracotomy was performed. We injected N3ICD (notch3 intracellular domain)-expressing adenovirus (Ad-N3ICD) and GFP-expressing adenovirus (Ad-GFP) [purchased from Genechem (Shanghai, China)] into the free anterior wall of the left ventricle at five different sites (2×10^9 pfu/ml, 5 μl per injection). Two days later, we introduced a myocardial infarction (MI) model as previously published (Qian et al., 2019). Briefly, ligation was accomplished at the proximal third of the left anterior descending (LAD) artery, and then the anterior wall of the left ventricle turned pale. Two months after thoracotomy, the rats were sacrificed, and the ventricular myocardium from the ischemic or region bordering the scar was harvested for further experiments.

Echocardiography

Transthoracic echocardiography was performed using Toshiba Aplio 500 ultrasound system equipped with a linear transducer probe (PLT-1204BT) at 2 months after thoracotomy. Two-dimensional and M-mode echocardiography was obtained both in parasternal short- and long-axis views. Left ventricular end-diastolic diameter (LVEDD) and calculated left ventricular ejection fraction (LVEF) were acquired on heart rates ranging between 400 and 500 beats per minute. All measurements were averaged across 10 consecutive cardiac cycles.

Masson Staining

The ischemic or bordering scar region of the left ventricle myocardium were isolated, fixed in 4% paraformaldehyde, and embedded in paraffin. The paraffin sections were sliced at 5 μm and stained with hematoxylin staining solution for 3 min following deparaffinization. Next, the sections were stained with Masson Ponceau acid fuchsin solution for 5–10 min, followed by differentiation with 1% phosphomolybdic acid aqueous solution for 3 min, and stained with aniline blue solution for 5 min.

Lastly, the sections were blocked with neutral gum and observed under the microscope (Nikon TE2000-U microscope, Japan). The area of myocardial fibrosis was quantified using Image J (v1.8.0, National Institutes of Health, United States). Myocardial tissues were stained with red; collagenous fibers were presented in blue. Vasculature and scar regions with a high abundance of collagen were excluded from quantification.

Cardiac Fibroblast Isolation, Culture, and Cell Transfection

Cardiac fibroblasts were obtained by digesting the ventricles of 1- to 2-day-old Sprague–Dawley rats with 0.08% collagenase II (Sigma, United States) and 0.1% trypsin (Beyotime, Shanghai) as previously reported (Tao et al., 2014) and cultured in Dulbecco's modified Eagle's medium (DMEM) (high glucose, Gibco) containing 10% fetal bovine serum (FBS) (Gibco, Gaithersburg, United States), 100 U/ml of penicillin, and 100 μg/ml of streptomycin (Beyotime, Shanghai) in 5% CO_2 at 37°C. The CFs were passaged upon 80–90% confluency. Fibroblasts were only passaged once before conducting further experiments.

Notch3-specific small interfering ribonucleic acid (si notch3) and scrambled siRNA (sc notch3) were synthesized by Genepharm Biotech (Shanghai, China). The siRNA sequences were as follows:

siRNA1: 5′-GCAUCUGCCAUGGAGGAUATT-3′;
siRNA2: 5′-CCUGCAACCCGGUUUAUAATT-3′;
siRNA3: 5′-CCGUGUGGCCUCUUUCUAUTT-3′; and
scramble siRNA: 5′-UUCUCCGAACGUGUCACGUTT-3′.

The N3ICD cDNA was cloned into an expression vector (GV314) and coupled to a Flag tag. Recombinant expression of the pFlag-N3ICD plasmid was confirmed by DNA sequencing (Genechem, Shanghai China). When the CFs reached 60% confluency, si notch3, sc notch3, notch3 overexpression plasmid (ov-N3ICD), or the empty vector plasmid (vector) was transfected into CFs using the Lipofectamine 3000 transfection reagent (Invitrogen). The transfection efficiency was quantified using RT-qPCR and western blotting 48 h after transfection.

To investigate the role of Hif1α and the RhoA/ROCK signaling pathway in the regulation of notch3-dependent effects on CF activity, 2-ME (an inhibitor of Hif1α, MedChemExpress, United States, 10 μmol), DMOG (an inhibitor of Hif-1α prolyl hydroxylase, MedChemExpress, United States, 100 μmol), and Y-27632 (an inhibitor of the RhoA/ROCK pathway, MedChemExpress, United States, 30 μmol) were applied with a 2-h preincubation prior to transfection.

Real-Time qPCR

Total RNA from CFs and myocardial tissue was extracted using TRIzol (Takara, Japan). Reverse transcription was carried out with the PrimeScript RT reagent Kit with gDNA Eraser (Takara, Japan). The qPCR primers were obtained from Invitrogen (Carlsbad, CA, United States). The primer sequences were as follows:

Notch3 forward primer: 5′-GCACGAACTGACCGAACTGG-3′;
Notch3 reverse primer: 5′-TGATGAGAATCTGGAAGACACCC-3′;
GAPDH forward primer: 5′-AAGTTCAACGGCACAGTCAAGG-3′; and
GAPDH reverse primer: 5′-ACGCCAGTAGACTCCACGACAT-3′.

Notch3 gene expression was quantified by PCR Amplification Kit (Takara, Japan). Briefly, the PCR included the following steps: denaturation of cDNA at 95°C for 30 s, followed by 40 cycles of 95°C for 5 s (denaturation) and 60°C for 30 s (annealing and elongation). GAPDH was used as a loading reference. Differential expression values were calculated using the ΔΔCT method.

Western Blot Analysis

Protein was extracted from isolated CFs and ventricular tissue using radioimmunoprecipitation assay (RIPA) buffer (Beyotime, China) containing protease and a phosphatase inhibitor cocktail (MCE). To separate cytosolic and membrane fractions, we used a membrane and cytosol protein extraction kit (Beyotime, Haimen, China) according to the manufacturer"s instructions. Protein concentrations were quantified with the bicinchoninic acid (BCA) assay (Beyotime, China). Proteins were separated on an 8–12% sodium dodecyl sulfate–polyacrylamide gel electrophoresis (SDS-PAGE) and transferred to polyvinylidene difluoride (PVDF) membranes (Roche Applied Science, Germany). After being blocked with 5% milk for 1 h, the membranes were incubated with primary antibodies at 4°C overnight. We used the following antibodies: notch3 (1:1,000), α-SMA (1:2,000), total caspase3 (1:1,000), GAPDH (1:1,000), Pan cadherin (1:1,000), and β-actin (1:1,000), all from Proteintech (Rosemont, United States); Col I (1:1,000), Hif1α (1:1,000), Col III (1:1,000), and Bcl2 (1:1,000) from GeneTex (Irvine, CA, United States); and RhoA (1:1,000), ROCK1 (1:1,000), and ROCK2 (1:1,000) from Abcam (Cambridge, United States). The membranes were washed with TBST three times and then incubated with horseradish peroxidase (HRP)-conjugated secondary antibodies (Proteintech, Rosemont, United States) at room temperature for 1 h. Images were acquired with the ChemiDoc Imager (Bio-Rad, Hercules, CA, United States).

Cell Counting Kit-8 Assay

Cell viability was evaluated with Cell Counting Kit-8 (CCK8; MedChemExpress, United States) according to the manufacturer's instructions. Briefly, CFs were seeded in 96-well culture plates at a density of 5×10^3 cells/well and cultured at 5% CO_2 at 37°C. After transfection for 48 h, we added 10 μl of CCK8 solution, incubated at 37°C for 1–4 h, and then detected optical density of each well at 450 nm with a microplate reader (Molecular Devices).

EdU Proliferation Assay

Cardiac fibroblast proliferation was evaluated using an EdU cell proliferation assay kit (Ribobil^{TM}, China). The CFs were seeded in 24-well plate, transfected with si notch3 or ov-N3ICD plasmid for 48 h, and incubated with 10 μm EdU for 24 h. We then fixed the cells with 4% paraformaldehyde, permeabilized

them with 0.5% Triton-X 100 in phosphate-buffered saline (PBS), stained with EdU, and then counterstained with DAPI (Boster, China). Images were acquired using a Nikon TE2000-U microscope (Tokyo, Japan). The percentage of EdU-positive cells was calculated from six random fields over three wells.

Immunofluorescence

After transfection with si notch3 or ov-N3ICD plasmid for 12 h, CFs were fixed with 4% paraformaldehyde for 20 min, incubated with 0.1% Triton-X 100 in PBS for 15 min, blocked in 10% goat serum for 30 min, and then incubated with an anti-Hif1α primary antibody (GeneTex, United States, 1:200) overnight at 4°C. After three PBS washing steps, CFs were incubated with DyLight 594-conjugated goat anti-rabbit IgG (red) (EarthOx, Millbrae, United States) at room temperature for 1 h protected from light. The nuclei were counterstained using DAPI (Boster, China) for 5 min. We acquired confocal images at 600 × magnification on a LEICA TCS SP2 confocal microscope. Fluorescence intensities were quantified using Image J (v1.8.0, National Institutes of Health, United States).

Flow Cytometry

After transfection for 48 h, CFs were digested with 0.25% trypsin and washed three times with PBS. CFs were resuspended in 500 μl of PBS, labeled with Annexin V-APC and propidium iodide (PI), and incubated for 15 min in the dark. Apoptotic cells were detected by flow cytometry sorting of Annexin V and PI double-stained cells (FACS Vantage SE, BD, United States). The apoptotic index was calculated as follows: (number of apoptotic cells/total number of cells tested) × 100%.

Statistical Analyses

We employed GraphPad Prism 5.0 (GraphPad Software Inc., San Diego, CA, United States) for data analysis. Continuous variables were presented as the mean ± SD. Statistical comparisons were performed by Student's *t*-test or one-way analysis of variance (ANOVA). All experiments were repeated at least three times. Statistical significance was defined as $P < 0.05$.

RESULTS

Notch3 Inhibits the Proliferation of Cardiac Fibroblasts

To examine the effect of notch3 on CF proliferation, we transfected cells with either overexpression plasmid (ov-N3ICD) or siRNA duplexes (si notch3). After the transfection of the ov-N3ICD plasmid, the mRNA and protein expression levels of notch3 were significantly higher than in the control vector group (**Figures 1A,B**). For silencing notch3, we constructed three siRNA duplexes (si notch3 1, si notch3 2, and si notch3 3). RT-qPCR confirmed that both si notch3 1 and si notch3 3 effectively knocked down notch3 (**Figure 1C**). Similarly, western blotting analysis showed that both si notch3 1 and si notch3 3 effectively reduced protein expression of notch3 (**Figure 1D**). Therefore, we used these two constructs for the following experiments.

To measure the proliferative capacity of CFs after notch3 overexpression or silencing, we carried out EdU and CCK8 staining assays. As shown in **Figures 2A,B**, CFs in the ov-N3ICD group exhibited a significantly lower proliferation rate than in the vector control group. Conversely, we found that CFs had a higher proliferation rate after siRNA notch3 knockdown than CFs in the scrambled notch3 control group (**Figures 2C,D**). Therefore, our experiments suggested that notch3 has an inhibitory effect on CF proliferation.

Notch3 Promotes Cardiac Fibroblast Apoptosis

The caspase family plays an important role in the execution of cellular apoptosis. Caspase3, in particular cleaved caspase 3—the active form of caspase3—is widely considered as an apoptotic marker (Zheng et al., 1998; Langford et al., 2011). It is well known that Bcl2 protects many cell lines from apoptosis (Lessene et al., 2008). To further detect anti-apoptotic proteins, we also measured Bcl2 expression. Western blot analysis showed that notch3 overexpression resulted in a significant increase in the ratio of cleaved caspase3 to total caspase3 as well as a significantly lower Bcl2 level as compared with controls (**Figure 3A**). In contrast, notch3 knockdown exerted an opposite effect on the cleaved caspase3 to total caspase3 ratio and expression levels of Bcl2 (**Figure 3B**).

Next, we determined the CF apoptosis by flow cytometry with Annexin V and PI double staining. In line with our previous experiments, we found that notch3 overexpression significantly elevated CF apoptosis (**Figure 3C**), whereas knockdown of notch3 inhibited it (**Figure 3D**). In summary, these findings suggest that notch3 may promote apoptosis of CFs by increasing the ratio of cleaved caspase3 to total caspase3 and decreasing Bcl2 expression levels.

Notch3 Inhibits Cardiac Fibroblast to Myofibroblast Transition and Extracellular Matrix Production

Previous studies have demonstrated that fibroblast to myofibroblast transition (FMT) and ECM production (Col I and Col III) are key steps in cardiac fibrosis. We therefore quantified α-SMA (a biomarker of myofibroblasts), Col I, and Col III protein levels by western blot. The expression of α-SMA, Col I, and Col III was lower in ov-N3ICD-transfected CFs than in the vector control group (**Figure 4A**). On the other hand, protein expression of α-SMA, Col I, and Col III increased significantly after notch3 downregulation (**Figure 4B**). Taken together, these results suggested that notch3 inhibits both the differentiation of CFs into myofibroblasts and ECM production.

Notch3 Alters the Expression of Hif1α and RhoA/ROCK in Cardiac Fibroblasts

To investigate the effects of notch3 on Hif1α, we quantified Hif1α levels after notch3 overexpression or knockdown, respectively. Immunofluorescence of CFs showed that the nuclear expression of Hif1α was significantly lower after notch3

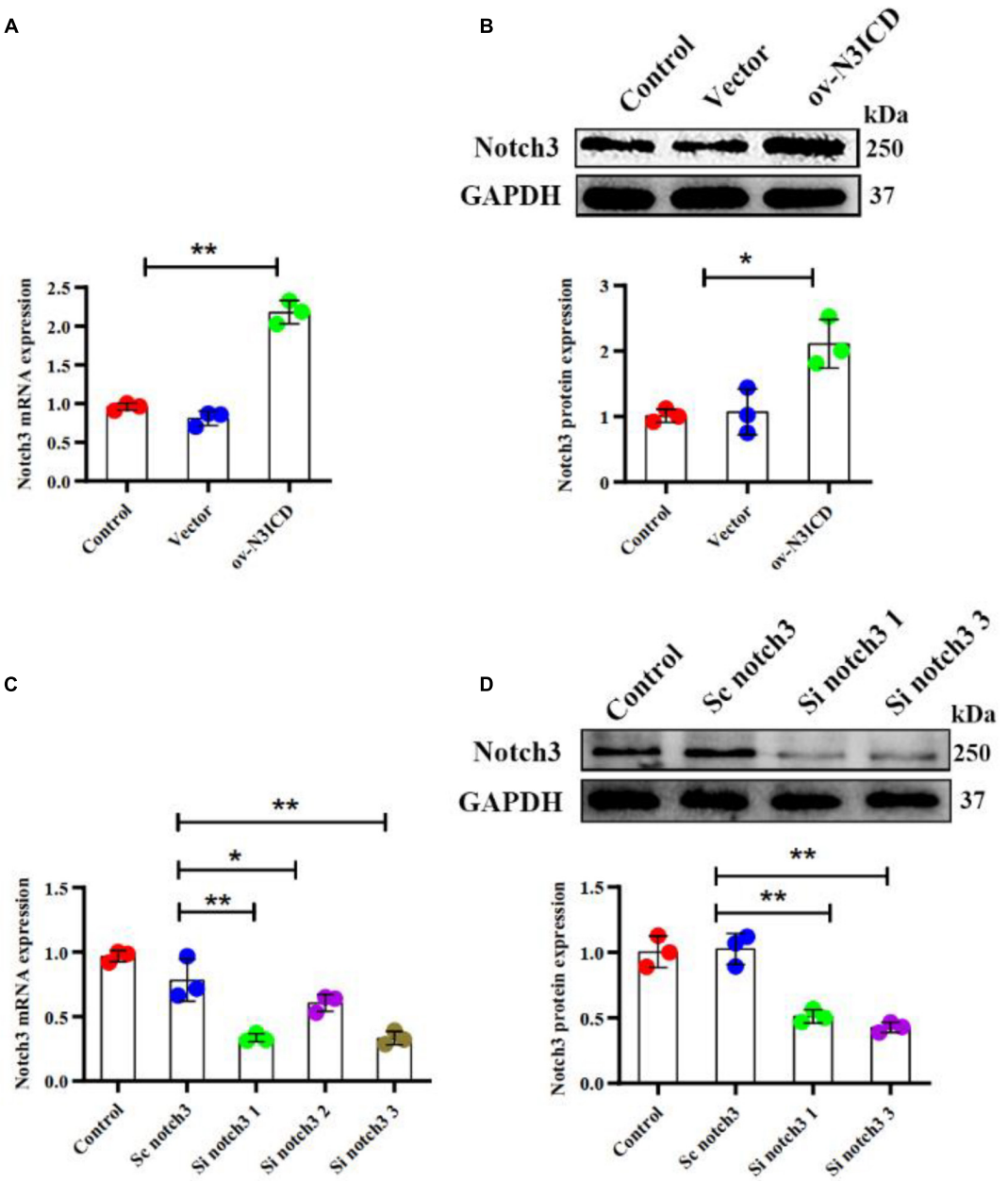

FIGURE 1 | Notch3 was overexpressed and knocked down successfully in cardiac fibroblasts (CFs). **(A,B)** Rat CFs were transfected with ov-N3ICD plasmid or vector. Notch3 expression was detected by RT-qPCR and western blotting analysis (n = 3). **(C)** CFs were treated with small interfering RNA constructs (sc notch3, si notch3 1, si notch3 2, or si notch3 3), and mRNA expression of notch3 was quantified by RT-qPCR (n = 3). **(D)** Western blot analysis of notch3 expression after notch3 knockdown (n = 3). Values represent the mean ± SD. $^{*}P < 0.05$, $^{**}P < 0.01$.

overexpression (**Figure 5A**), whereas notch3 knockdown induced Hif1α expression in the nucleus (**Figure 5D**). The western blotting analysis demonstrated that notch3 overexpression reduced the expression of Hif1α, RhoA, ROCK1, and ROCK2 (**Figure 5B**). To further evaluate the function of the RhoA/ROCK signaling pathway in CFs, we also measured the activity levels of RhoA. Previous studies suggested that membrane-associated RhoA GTP is the active form of RhoA (Somlyo and Somlyo, 2000) and showed that RhoA activity is correlated with membrane-associated RhoA protein levels (Tamma et al., 2003). Western blot analysis showed that pan cadherin (membrane marker) was strongly expressed whereas β-actin was extremely low in the membrane fractions. However, β-actin was present at a very high concentration, whereas pan cadherin was hardly detected in the cytosolic fractions. These results suggest that the membrane fractions and the cytosolic fractions were separated adequately. We also found that notch3 overexpression reduced the ratio

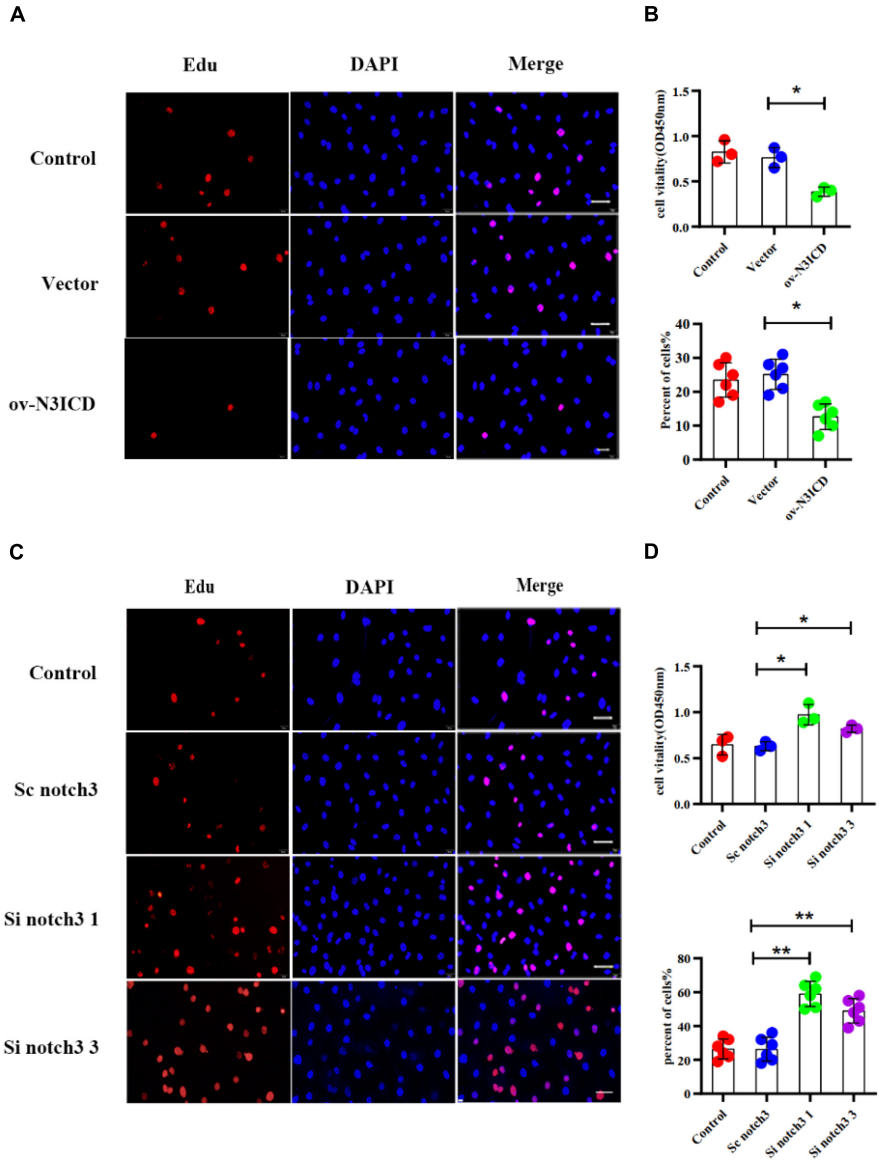

FIGURE 2 | Notch3 inhibits the proliferation of rat cardiac fibroblasts (CFs). **(A,C)** We used the EdU assay to measure CF proliferation after notch3 overexpression or knockdown (n = 6). Scale bars = 200 μm. **(B,D)** We next used the Cell Counting Kit-8 (CCK8) assay to determine CF proliferation (above, n = 3). Quantification of the CF proliferation determined by EdU assay (below, n = 6) and CCK8 assay (above, n = 3) in different groups, as indicated. Values represent the mean ± SD. $^{*}P < 0.05$, $^{**}P < 0.01$.

of membrane-associated RhoA to total RhoA (**Figure 5C**). Conversely, notch3 knockdown changed the expression levels of Hif1α, RhoA, ROCK1, ROCK2, and membrane-bound RhoA (**Figures 5E,F**).

Notch3 Regulates Cardiac Fibroblast Proliferation, Apoptosis, and Fibroblast to Myofibroblast Transition via the RhoA/ROCK/Hif1α Pathway

Among the two effective siRNA duplexes (si notch3 1 and si notch3 3), si notch3 1 exhibited better interference and was therefore used for the following experiment. To clarify the role of Hif1α in regulation of CF proliferation via notch3, CFs were pretreated with Hif1α inhibitor, 2-ME, for 2 h and then transfected with si notch3 1 for 48 h. The EdU assay and CCK8 staining demonstrated that 2-ME reversed the notch3 knockdown-induced positive regulation on CF proliferation (**Figures 6A,B**) and resulted in attenuated CF proliferation. Similarly, 2-ME pretreatment could effectively weaken the rise of α-SMA, Col I, and Col III caused by notch3 knockdown (**Figure 6E**).

We next used DMOG, a potent Hif1α prolyl hydroxylase inhibitor and therefore Hif1α activator, to investigate the

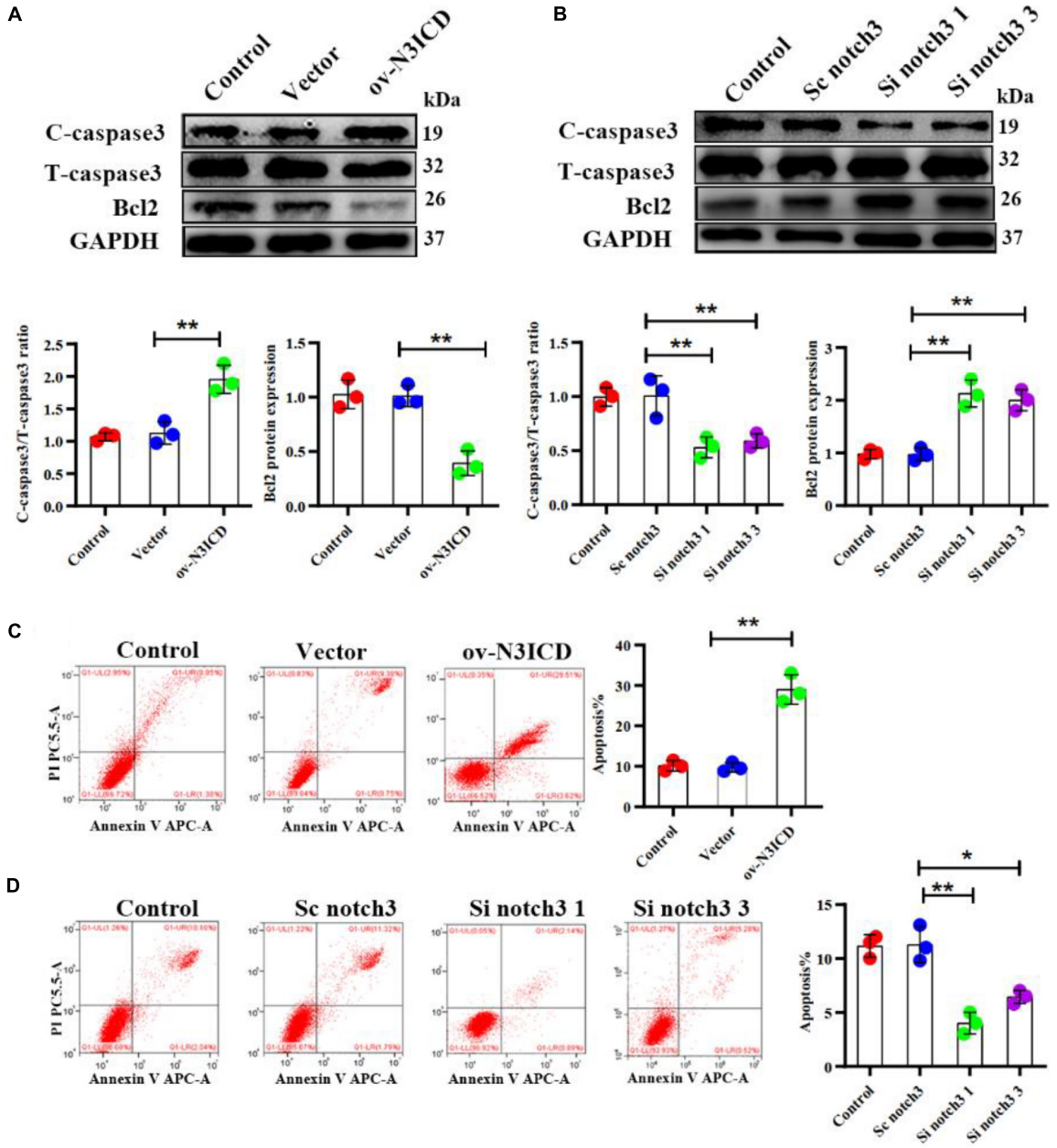

FIGURE 3 | Notch3 promotes the apoptosis of rat cardiac fibroblasts (CFs). **(A,B)** Representative western blot and quantitative data of cleaved caspase3, total caspase3, and Bcl2 after notch3 overexpression or knockdown ($n = 3$). **(C,D)** The CF apoptotic rate after notch3 overexpression or knockdown, detected by flow cytometry. Q1-UR and Q1-LR were used to analyze the change of apoptotic rate in different experimental groups ($n = 3$). Values represent the mean ± SD. $^{*}P < 0.05$, $^{**}P < 0.01$. C-caspase3, cleaved caspase3; T-caspase3, total caspase3.

interaction between Hif1α and notch3 in the regulation of CF apoptosis. The ratio of cleaved caspase 3 to total caspase 3 and Bcl2 levels were restored when CFs were pretreated with DMOG before ov-N3ICD plasmid transfection (**Figure 6C**). Meanwhile, we had previously shown by flow cytometry that overexpression of notch3 increases apoptosis; this effect was abolished by DMOG pretreatment (**Figure 6D**).

Therefore, our results suggested that Hif1α is involved in the notch3-dependent regulation of CFs. To further explore the relationship between the RhoA/ROCK pathway and Hif1α, we applied Y-27632, an inhibitor of RhoA/ROCK pathway, to CFs before notch3 overexpression and knockdown. We found that Y-27632 pretreatment was able to abolish the increase in Hif1α protein expression induced by notch3 knockdown (**Figures 6F,G**). These results indicated that

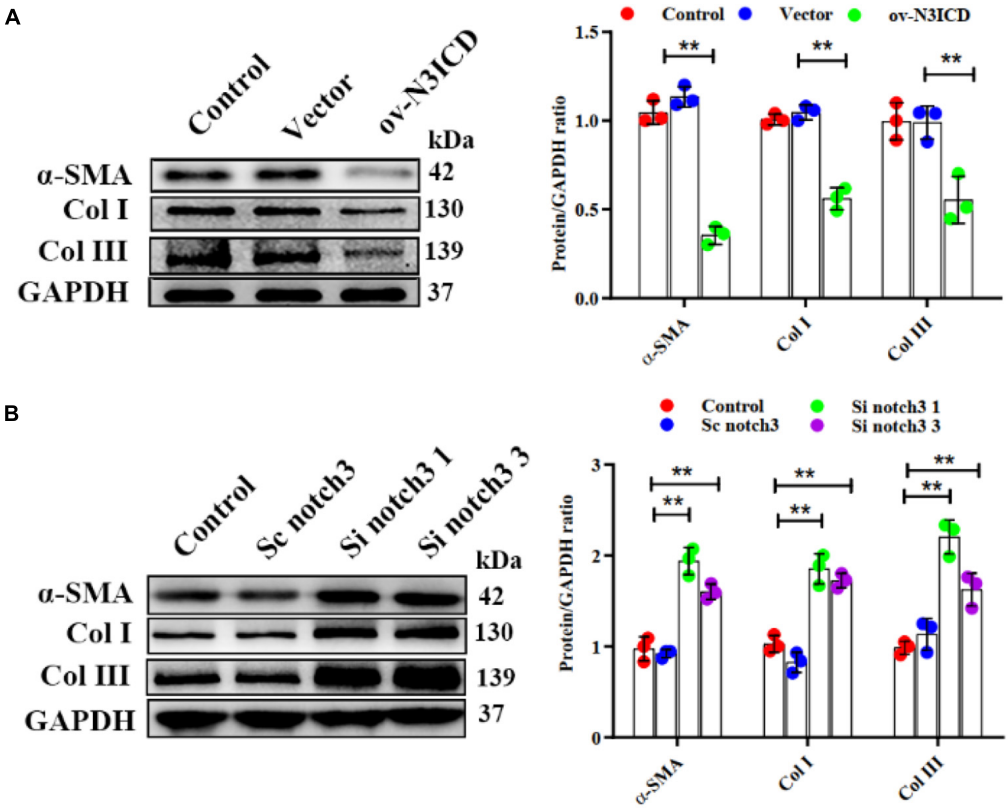

FIGURE 4 | Notch3 inhibits cardiac fibroblast to myofibroblast transition. **(A,B)** Western blots measuring α-SMA, Col I, and Col III after notch3 overexpression or knockdown. The quantification of the protein bands is shown on the right ($n = 3$). Values represent the mean ± SD. *$P < 0.05$, **$P < 0.01$.

Hif1α might be a downstream molecule of the RhoA/ROCK signaling pathway in CFs.

Overall, our results therefore indicate that the RhoA/ROCK/Hif1α signaling pathway is associated with the proliferation, apoptosis, and FMT of CFs *in vitro*.

Notch3 Alleviates Cardiac Fibrosis After Myocardial Infarction via the RhoA/ROCK/Hif1α Pathway

Next, we went on to confirm our findings *in vivo*. We therefore injected an N3ICD-overexpressing adenovirus into myocardium 48 h before LAD ligation to investigate the effects of notch3 on cardiac fibrosis and its underlying mechanism. Both RT-qPCR and western blotting analysis confirmed that notch3 was successfully overexpressed in the myocardium after adenovirus injection (**Figures 7A,B**). Two months after ligation, echocardiography revealed that Ad-N3ICD + MI animals had a higher LVEF (**Figure 7C**, 54.60 ± 4.93% vs. 38.40 ± 3.65%, $P = 0.004$) and lower LVEDD (**Figure 7C**, 6.68 ± 0.43 vs. 5.30 ± 0.51 mm, $P = 0.017$) than the control group (Ad-GFP + MI). Masson staining revealed that myocardial fibrosis area in the Ad-GFP + MI group increased significantly compared with that in the sham group (**Figure 7D**, 3.54 ± 1.31% vs. 38.58 ± 6.68%, respectively; $P < 0.001$). However, the Ad-N3ICD injection alleviated myocardial fibrosis induced by MI (**Figure 7D**, 38.58 ± 6.68% vs. 14.62 ± 6.21%, respectively; $P < 0.001$).

Using western blotting, we confirmed that the expression of α-SMA, Hif1α, RhoA, ROCK1, and ROCK2 increased after MI, whereas notch3 overexpression in myocardium can ameliorate these protein expressions induced by MI (**Figure 7E**). The expression of membrane-bound RhoA increased after MI. However, this effect can be abolished by notch3 overexpression (**Figure 7F**). Therefore, we conclude that notch3 may alleviate MI-induced cardiac fibrosis via the RhoA/ROCK/Hif1α signaling pathway *in vivo*.

DISCUSSION

Cardiac fibrosis is a pathological process present in most heart diseases accompanied by loss of myocardium and fibrous tissue replacement, thereby affecting the compliance and function of the ventricle (Kong et al., 2014). CFs predominantly regulate ECM protein synthesis and degradation, and therefore an aberrant and persistent stimulation of CFs has been suggested to be a

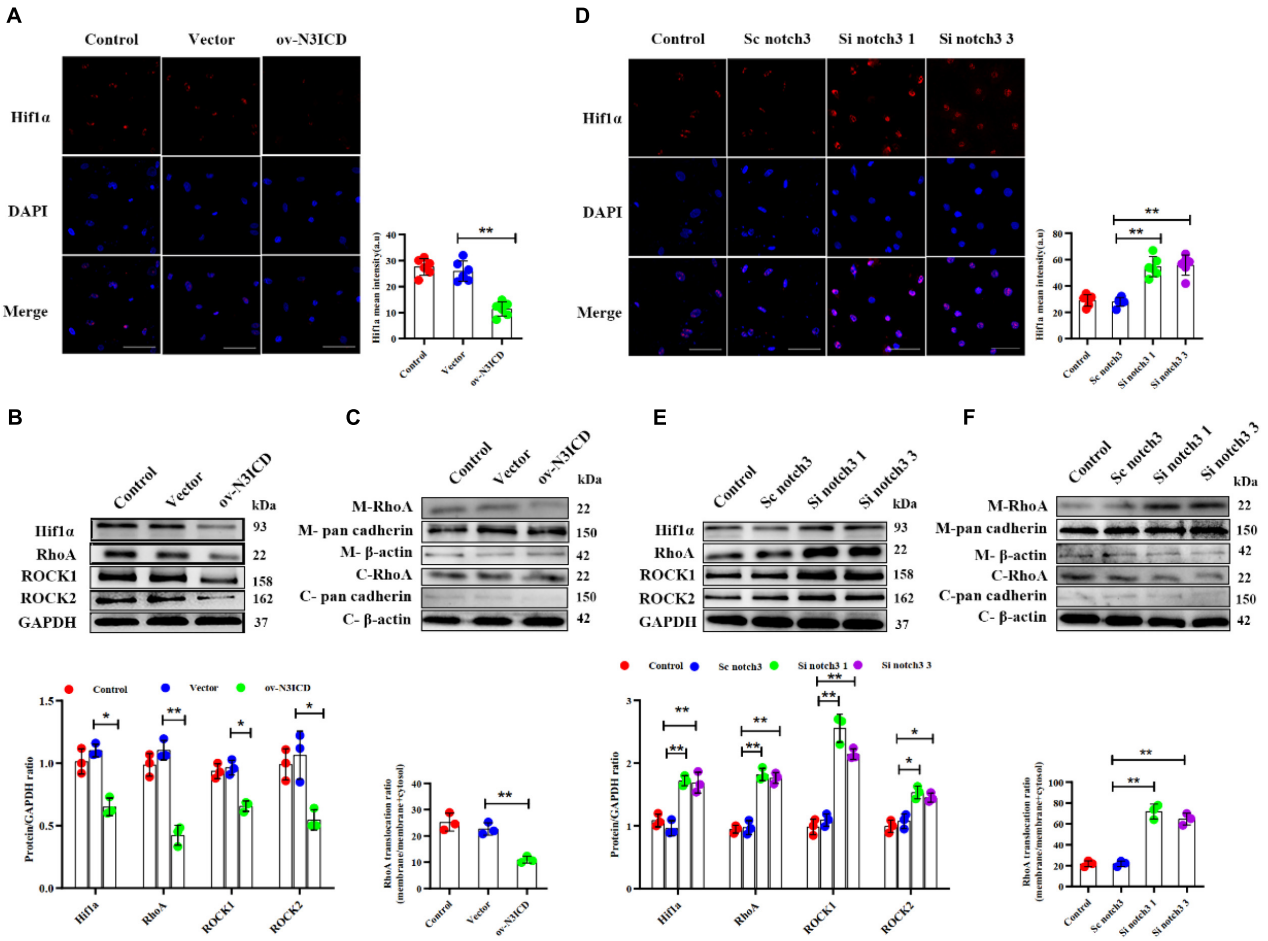

FIGURE 5 | The effects of notch3 on Hif1α, RhoA, ROCK1, and ROCK2 in rat cardiac fibroblasts (CFs) with different treatments. **(A)** Representative immunofluorescence images and quantitative data of Hif1α (red) in neonatal rat cardiac fibroblasts after notch3 overexpression (n = 6). Nuclei were detected with DAPI (blue). Scale bars = 200 μm. **(B)** The protein expression of Hif1α, RhoA, ROCK1, and ROCK2 was determined by western blot after notch3 overexpression (n = 3). **(C)** Western blots of RhoA in the membrane and cytosol after notch3 overexpression (n = 3). **(D)** Hif1α (red) in neonatal rat cardiac fibroblasts after notch3 knockdown was detected by immunofluorescence and statistical analysis of mean intensity (n = 6). Nuclei were detected with DAPI (blue). Scale bars = 200 μm. (E) Hif1α, RhoA, ROCK1, and ROCK2 were detected by western blot after notch3 silencing (n = 3). **(F)** Western blots of RhoA and cadherins in the membrane and cytosol after notch3 silencing (n = 3). Values represent the mean ± SD. $^*P < 0.05$, $^{**}P < 0.01$. M-RhoA, membrane RhoA; C-RhoA, cytosolic RhoA; M-pan cadherin, membrane pan cadherin; C-pan cadherin, cytosolic pan cadherin; M-β-actin, membrane β-actin; C-β-actin, cytosolic β-actin.

decisive cause of cardiac fibrosis (Krenning et al., 2010; Travers et al., 2016).

Notch in Cardiac Fibroblast Proliferation, Apoptosis, and Fibroblast to Myofibroblast Transition

Several studies have confirmed that the notch signaling pathway regulates organ development and fibrosis. However, the exact functions of notch receptors depend on different cellular and physiological pathological conditions. Accumulated evidence shows that notch1 is a protective factor during myocardial fibrosis (Zhou et al., 2015), whereas few researches were reported on notch2, notch3, and notch4. Luxan et al. (2013) reported that inactivation of the notch pathway causes left ventricular non-compaction cardiomyopathy. Urbanek et al. (2010) found that inhibition of notch1-dependent cardiomyogenesis results in cardiomyopathy of the neonatal heart (Urbanek et al., 2010). In addition, Yu and Song (2014) identified that notch1 inhibits cardiomyocyte apoptosis after myocardial ischemia. Besides, notch3 has been suggested to be a protective factor for prevention of post-MI myocardial fibrosis (Zhang et al., 2016), but the underlying molecular mechanism remained unclear. Owing to the crucial role of CFs in myocardial fibrosis, the effects of notch3 on CF activity required further investigation. Therefore, we evaluated CF activity upon both notch3 overexpression and knockdown. Our results revealed that notch3 overexpression inhibits CF proliferation and promotes CF apoptosis. Activated CFs, labeled with the contractile protein α-SMA, secrete large amounts of collagen, which determines myocardial stiffness and compliance. In our study, we found that notch3 overexpression inhibits FMT and decreases

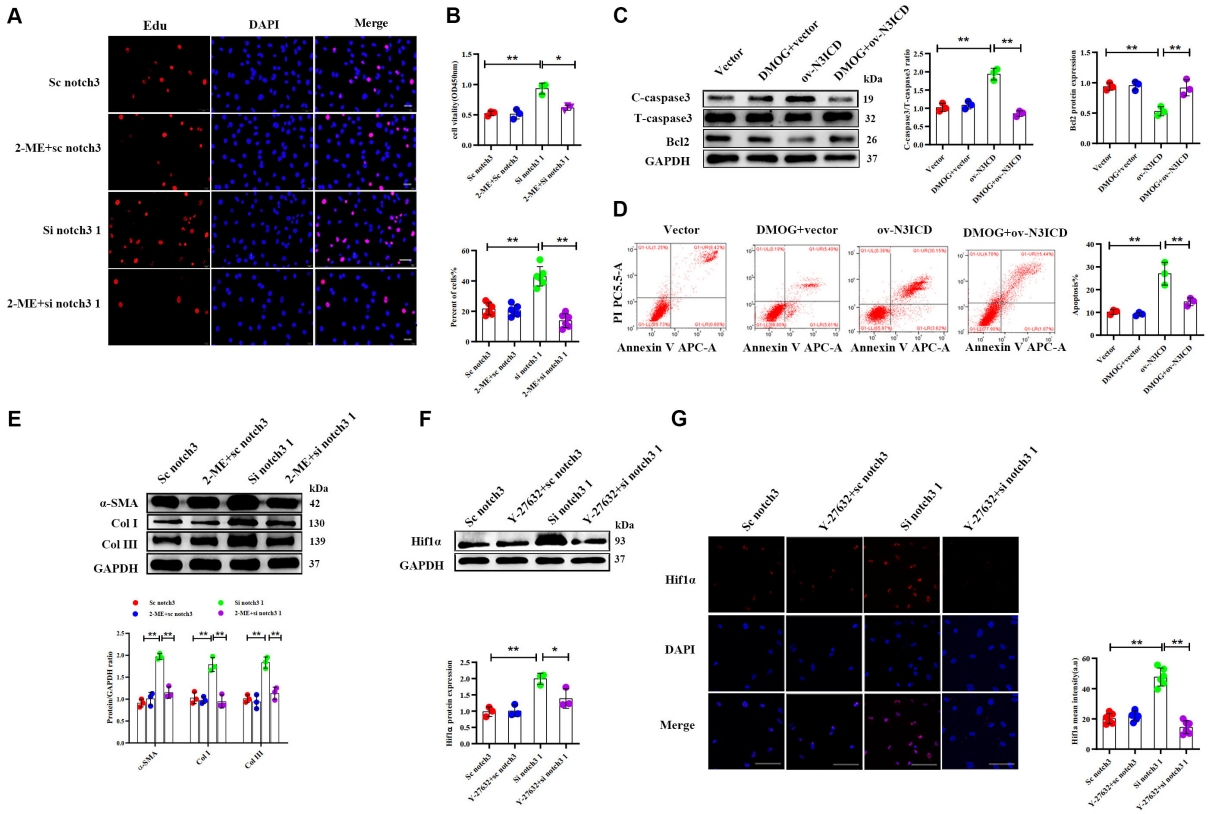

FIGURE 6 | Notch3 regulates cardiac fibroblast (CF) function via the RhoA/ROCK/Hif1α pathway. **(A)** CFs were pretreated with 2-ME for 2 h before notch3 knockdown. CF proliferation was quantified using the EdU assay ($n = 6$). Scale bars = 200 μm. **(B)** The Cell Counting Kit-8 (CCK8) assay was also used to determine CF proliferation (above, $n = 3$). Quantification of CF proliferation determined by EdU assay (below, $n = 6$). **(C)** Western blot analysis of cleaved caspase-3, total caspase3, and Bcl2 in different groups. The quantification of the protein bands is shown on the right ($n = 3$). **(D)** CFs were pretreated with DMOG for 2 h before notch3 overexpression. Flow cytometry quantified the percentage of apoptosis in each group ($n = 3$). **(E)** Western blot analysis of α-SMA, Col I, and Col III in CFs pretreated with 2-ME for 2 h before notch3 knockdown. The quantification of the protein bands is shown below ($n = 3$). **(F)** Representative Western blot and quantification of Hif1α in CFs pretreated with Y-27632 for 2 h before notch3 knockdown ($n = 3$). **(G)** Representative immunofluorescence images and quantification of Hif1α (red) in CFs pretreated with Y-27632 for 2 h before notch3 knockdown ($n = 6$). Nuclei were detected with DAPI (blue). Scale bars = 200 μm. Values represent the mean ± SD. $^*P < 0.05$, $^{**}P < 0.01$.

protein levels of α-SMA, Col I, and Col III, whereas notch3 downregulation shows inverse effects. Several pathways are involved in ECM maintenance. Here, we investigated one line of notch signaling; however, as ECM deposition is a key regulatory event in fibrosis, other involved molecules, such as matrix metalloproteinases (MMPs), should also be investigated. Future research should therefore address the pathophysiological mechanisms of MMPs in modulating the Notch-dependent fibrosis.

Notch and the RhoA/ROCK/Hif1α Pathway

Hif1 is ubiquitously expressed in nearly all mammalian cells and is an essential regulator under hypoxia. Hif1 contains two subunits, Hif1α and Hif1β (Imtiyaz and Simon, 2010; Masoud and Li, 2015). Hif1α has been shown to be closely associated with organ fibrosis: Han et al. (2019) suggested Hif1α promotes liver fibrosis by action on the PTEN/p65 pathway in non-alcoholic fatty liver disease. Ichihara et al. (2019) found that Hif1α was elevated in Ang II-induced cardiac fibrosis. In addition, Hif1α has been shown to participate in the activation of the notch signaling pathway in both odontogenic keratocysts (Miranda da Costa et al., 2019) and neurogenesis during acute epilepsy (Li et al., 2018). Moreover, notch signaling can enhance the expression of Hif1α in human adipose-derived mesenchymal stromal cells (Moriyama et al., 2018). Even so, the direct effects of Hif1α on CF activity and its interaction with the notch signaling pathway in CFs remained incompletely understood. Our results showed that Hif1α can be detected in CFs and is downregulated by notch3 overexpression but upregulated by notch3 knockdown.

Hif1α is a central component of the oxygen sensing system. Normoxia provokes ubiquitin–proteasome system, thereby promoting Hif1α degradation (Huang et al., 1998; Kaelin and Ratcliffe, 2008). Therefore, the expression of Hif1α is very low under normoxia and even at an undetectable level. Besides hypoxia, Hif1α can be also induced by inflammatory cytokines, growth factors, and hormones under normoxic conditions (Zhou and Brüne, 2006). McMahon et al. (2006) have demonstrated

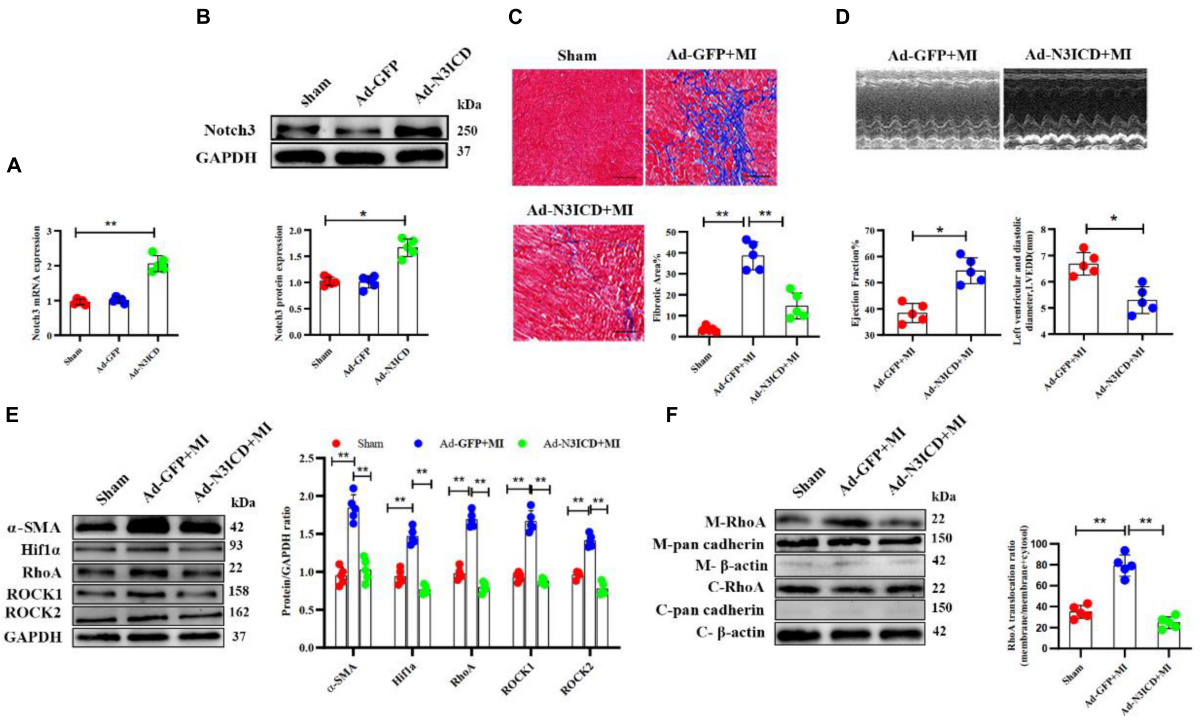

FIGURE 7 | Notch3 alleviates cardiac fibrosis after myocardial infarction via the RhoA/ROCK/Hif1α pathway. **(A,B)** Notch3 overexpression in the myocardium after Ad-N3ICD injection was confirmed by RT-qPCR and western blot ($n = 5$). **(C)** Measurements of cardiac function indices of rats in each group 2 months after myocardial infarction (MI) injury ($n = 5$). **(D)** Masson staining of the rat heart tissues. The positively stained area (blue) represents fibrosis ($n = 5$). **(E)** Western blot analysis and quantitative results of α-SMA, RhoA, ROCK1, ROCK2, and Hif1α ($n = 5$). **(F)** Western blot analysis of membrane-bound RhoA and cadherins in rat hearts from different treatments. Values represent the mean ± SD. $^{*}P < 0.05$, $^{**}P < 0.01$. M-RhoA, membrane RhoA; C-RhoA, cytosolic RhoA; M-pan cadherin, membrane pan cadherin; C-pan cadherin, cytosolic pan cadherin; M-β-actin, membrane β-actin; C-β-actin, cytosolic β-actin.

TGF-β1 enhances Hif1α protein stability by inhibiting PHD2 expression in hepatoma cells. Our present research found that Hif1α could be detected and is regulated by the notch signaling pathway under normoxic conditions. Taken together, these results suggest that Hif1α can be activated by both hypoxia-dependent and hypoxia-independent pathways. To clarify the relationship between Hif1α and notch signaling pathway in a normoxic environment, CFs were pretreated with 2-ME (Hif1α inhibitor) or DMOG (Hif1α enhancer) before transfection with notch3 overexpressing or silencing constructs. We found that 2-ME weakened the positive regulation of notch3 interference on α-SMA, Col I, Col III, and CF proliferation, whereas DMOG abolished the effect of notch3 on CF apoptosis. To our knowledge, our results describe for the first time that notch3 is capable of inhibiting the expression of Hif1α in CFs and regulates CF activity by Hif1α inactivation.

We further investigated how notch3 regulates Hif1α levels in CFs. We found that the RhoA/ROCK signaling pathway potentially acts as a molecular bridge, connecting notch and Hif1α in the regulation of CF activity. The RhoA/ROCK signaling pathway has been shown to be involved in cardiac protection (Lee et al., 2014; Lai et al., 2017), but the effects of the notch on the RhoA/ROCK signaling pathway vary in different pathological processes. In the ischemic liver, the RhoA/ROCK pathway is activated by Notch1 deficiency (Lu et al., 2018). On the other hand, notch activates the RhoA/ROCK pathway in endothelial barrier dysfunction (Venkatesh et al., 2011). Takata et al. (2008) reported that a Rho-kinase inhibitor, fasudil, prevents Hif1α expression under hypoxia in endothelial cells. Our results suggest that notch3 regulates CF activity via suppression of the RhoA/ROCK pathway. We used Y-27632, RhoA/ROCK pathway inhibitor, to confirm the relationship between the RhoA/ROCK pathway and Hif1α in CFs, and we found that inhibition of the RhoA/ROCK pathway attenuated a notch3-knockdown-induced increase in Hif1α levels. These results provide evidence for a role of notch3 in modulating CF activity by negative regulation of the RhoA/ROCK/Hif1α axis *in vitro*.

Previous studies have confirmed that notch overexpression in rat heart is capable of preventing cardiac fibrosis after MI (Rodriguez et al., 2019; Zhou et al., 2019). Similarly, we confirmed our findings with an *in vivo* rat MI model. Consistent with previous studies, Masson staining and α-SMA expression levels showed that notch3 overexpression could alleviate MI-induced myocardial fibrosis. We furthermore found that notch3 overexpression inhibited the protein expression of RhoA, ROCK1, and ROCK2. Therefore, it is plausible that notch3 interacts with the RhoA/ROCK/Hif1α pathway to inhibit pathologic CF activity and further prevent MI-related cardiac fibrosis in the rat hearts.

A key limitation of our research is that we did not measure the local oxygen concentration in CFs and were therefore unable to determine whether CFs experience intrinsic hypoxia and whether notch3 affects intracellular oxygen balance or not. So far, our results only confirm that notch3 regulates CF activity by inhibiting the RhoA/ROCK/Hif1α axis in a normoxic environment.

CONCLUSION

Our study demonstrates, for the first time, that notch3 inhibits both CF proliferation and cardiac FMT and promotes apoptosis via inhibition of the RhoA/ROCK/Hif1α signaling pathway to ultimately attenuate MI-induced myocardial fibrosis. These findings are significant for the further understanding of cardiac fibrosis pathogenesis and provide new therapeutic avenues for future treatment of cardiac fibrosis.

ETHICS STATEMENT

The animal study was reviewed and approved by the Institutional Ethics Committee of Chongqing Medical University.

AUTHOR CONTRIBUTIONS

All authors listed have made a substantial, direct and intellectual contribution to the work, and approved it for publication.

FUNDING

This work was supported by the National Natural Science Foundation of China (No. 81600215 to PX) and the Kuanren Talents Program of the Second Affiliated Hospital of Chongqing Medical University to PX.

REFERENCES

Bei, Y., Hua-Huy, T., Nicco, C., Duong-Quy, S., Le-Dong, N. N., Tiev, K. P., et al. (2016). RhoA/Rho-kinase activation promotes lung fibrosis in an animal model of systemic sclerosis. *Exp. Lung Res.* 42, 44–55. doi: 10.3109/01902148.2016.1141263

Fix, C., Carver-Molina, A., Chakrabarti, M., Azhar, M., and Carver, W. (2019). Effects of the isothiocyanate sulforaphane on TGF-beta1-induced rat cardiac fibroblast activation and extracellular matrix interactions. *J. Cell. Physiol.* 234, 13931–13941. doi: 10.1002/jcp.28075

Greer, S. N., Metcalf, J. L., Wang, Y., and Ohh, M. (2012). The updated biology of hypoxia-inducible factor. *EMBO J.* 31, 2448–2460. doi: 10.1038/emboj.2012.125

Gulati, A., Jabbour, A., Ismail, T. F., Guha, K., Khwaja, J., Raza, S., et al. (2013). Association of fibrosis with mortality and sudden cardiac death in patients with nonischemic dilated cardiomyopathy. *JAMA* 309, 896–908.

Han, J., He, Y., Zhao, H., and Xu, X. (2019). Hypoxia inducible factor-1 promotes liver fibrosis in nonalcoholic fatty liver disease by activating PTEN/p65 signaling pathway. *J. Cell. Biochem.* 120, 14735–14744. doi: 10.1002/jcb.28734

Harvey, P. A., and Leinwand, L. A. (2011). The cell biology of disease: cellular mechanisms of cardiomyopathy. *J. Cell Biol.* 194, 355–365. doi: 10.1083/jcb.201101100

Hu, B., and Phan, S. H. (2016). Notch in fibrosis and as a target of anti-fibrotic therapy. *Pharmacol. Res.* 108, 57–64. doi: 10.1016/j.phrs.2016.04.010

Huang, L. E., Gu, J., Schau, M., and Bunn, H. F. (1998). Regulation of hypoxia-inducible factor 1alpha is mediated by an O2-dependent degradation domain via the ubiquitin-proteasome pathway. *Proc. Natl. Acad. Sci. U.S.A.* 95, 7987–7992. doi: 10.1073/pnas.95.14.7987

Ichihara, S., Li, P., Mise, N., Suzuki, Y., Izuoka, K., Nakajima, T., et al. (2019). Ablation of aryl hydrocarbon receptor promotes angiotensin II-induced cardiac fibrosis through enhanced c-Jun/HIF-1alpha signaling. *Arch. Toxicol.* 93, 1543–1553. doi: 10.1007/s00204-019-02446-1

Imtiyaz, H. Z., and Simon, M. C. (2010). Hypoxia-inducible factors as essential regulators of inflammation. *Curr. Top. Microbiol. Immunol.* 345, 105–120. doi: 10.1007/82_2010_74

Jing, J., Chen, L., Fu, H. Y., Fan, K., Yao, Q., Ge, Y. F., et al. (2015). Annexin V-induced rat Leydig cell proliferation involves Ect2 via RhoA/ROCK signaling pathway. *Sci. Rep.* 5:9437.

Kaelin, W. G. Jr., and Ratcliffe, P. J. (2008). Oxygen sensing by metazoans: the central role of the HIF hydroxylase pathway. *Mol. Cell* 30, 393–402. doi: 10.1016/j.molcel.2008.04.009

Kido, M., Du, L., Sullivan, C. C., Li, X., Deutsch, R., Jamieson, S. W., et al. (2005). Hypoxia-inducible factor 1-alpha reduces infarction and attenuates progression of cardiac dysfunction after myocardial infarction in the mouse. *J. Am. Coll. Cardiol.* 46, 2116–2124. doi: 10.1016/j.jacc.2005.08.045

Kong, P., Christia, P., and Frangogiannis, N. G. (2014). The pathogenesis of cardiac fibrosis. *Cell. Mol. Life Sci.* 71, 549–574.

Krenning, G., Zeisberg, E. M., and Kalluri, R. (2010). The origin of fibroblasts and mechanism of cardiac fibrosis. *J. Cell. Physiol.* 225, 631–637. doi: 10.1002/jcp.22322

Lai, D., Gao, J., Bi, X., He, H., Shi, X., Weng, S., et al. (2017). The Rho kinase inhibitor, fasudil, ameliorates diabetes-induced cardiac dysfunction by improving calcium clearance and actin remodeling. *J. Mol. Med.* 95, 155–165. doi: 10.1007/s00109-016-1469-1

Lai, S. S., Fu, X., Cheng, Q., Yu, Z. H., Jiang, E. Z., Zhao, D. D., et al. (2019). HSC-specific knockdown of GGPPS alleviated CCl4-induced chronic liver fibrosis through mediating RhoA/Rock pathway. *Am. J. Transl. Res.* 11, 2382–2392.

Langford, M. P., McGee, D. J., Ta, K. H., Redens, T. B., and Texada, D. E. (2011). Multiple caspases mediate acute renal cell apoptosis induced by bacterial cell wall components. *Renal Fail.* 33, 192–206. doi: 10.3109/0886022x.2011.553304

Lee, T. M., Lin, S. Z., and Chang, N. C. (2014). Membrane ERalpha attenuates myocardial fibrosis via RhoA/ROCK-mediated actin remodeling in ovariectomized female infarcted rats. *J. Mol. Med.* 92, 43–51. doi: 10.1007/s00109-013-1103-4

Lessene, G., Czabotar, P. E., and Colman, P. M. (2008). BCL-2 family antagonists for cancer therapy. *Nat. Rev. Drug Discov.* 7, 989–1000. doi: 10.1038/nrd2658

Li, A. Y., Wang, J. J., Yang, S. C., Zhao, Y. S., Li, J. R., Liu, Y., et al. (2019). Protective role of Gentianella acuta on isoprenaline induced myocardial fibrosis in rats via inhibition of NF-kappaB pathway. *Biomed. Pharmacother.* 110, 733–741. doi: 10.1016/j.biopha.2018.12.029

Li, K., Zhai, M., Jiang, L., Song, F., Zhang, B., Li, J., et al. (2019). Tetrahydrocurcumin ameliorates diabetic cardiomyopathy by attenuating high glucose-induced oxidative stress and fibrosis via activating the SIRT1 pathway. *Oxidat. Med. Cell. Longev.* 2019:6746907.

Li, Y., Wu, L., Yu, M., Yang, F., Wu, B., Lu, S., et al. (2018). HIF-1alpha is critical for the activation of notch signaling in neurogenesis during acute epilepsy. *Neuroscience* 394, 206–219. doi: 10.1016/j.neuroscience.2018.10.037

Lu, L., Yue, S., Jiang, L., Li, C., Zhu, Q., Ke, M., et al. (2018). Myeloid Notch1 deficiency activates the RhoA/ROCK pathway and aggravates hepatocellular damage in mouse ischemic livers. *Hepatology* 67, 1041–1055. doi: 10.1002/hep.29593

Luxan, G., Casanova, J. C., Martinez-Poveda, B., Prados, B., D'Amato, G., MacGrogan, D., et al. (2013). Mutations in the NOTCH pathway regulator MIB1 cause left ventricular noncompaction cardiomyopathy. *Nat. Med.* 19, 193–201. doi: 10.1038/nm.3046

MacGrogan, D., Munch, J., and de la Pompa, J. L. (2018). Notch and interacting signalling pathways in cardiac development, disease, and regeneration. *Nat. Rev. Cardiol.* 15, 685–704. doi: 10.1038/s41569-018-0100-2

Masoud, G. N., and Li, W. (2015). HIF-1alpha pathway: role, regulation and intervention for cancer therapy. *Acta Pharma. Sin. B* 5, 378–389. doi: 10.1016/j.apsb.2015.05.007

McMahon, S., Charbonneau, M., Grandmont, S., Richard, D. E., and Dubois, C. M. (2006). Transforming growth factor beta1 induces hypoxia-inducible factor-1 stabilization through selective inhibition of PHD2 expression. *J. Biol. Chem.* 281, 24171–24181. doi: 10.1074/jbc.m604507200

Miranda da Costa, N. M., Abe, C. T. S., Mitre, G. P., Mesquita, R. A., da Silva Kataoka, M. S., Ribeiro, A. L. R., et al. (2019). HIF-1alpha is overexpressed in odontogenic keratocyst suggesting activation of HIF-1alpha and NOTCH1 signaling pathways. *Cells* 8:731. doi: 10.3390/cells8070731

Moriyama, H., Moriyama, M., Ozawa, T., Tsuruta, D., Iguchi, T., Tamada, S., et al. (2018). Notch signaling enhances stemness by regulating metabolic pathways through modifying p53, NF-kappaB, and HIF-1alpha. *Stem Cells Dev.* 27, 935–947. doi: 10.1089/scd.2017.0260

Natarajan, R., Salloum, F. N., Fisher, B. J., Kukreja, R. C., and Fowler, A. A. III (2008). Hypoxia inducible factor-1 upregulates adiponectin in diabetic mouse hearts and attenuates post-ischemic injury. *J. Cardiovasc. Pharm.* 51, 178–187. doi: 10.1097/fjc.0b013e31815f248d

Prabhu, S. D., and Frangogiannis, N. G. (2016). The biological basis for cardiac repair after myocardial infarction: from inflammation to fibrosis. *Circ. Res.* 119, 91–112. doi: 10.1161/circresaha.116.303577

Qian, L., Pan, S., Shi, L., Zhou, Y., Sun, L., Wan, Z., et al. (2019). Downregulation of microRNA-218 is cardioprotective against cardiac fibrosis and cardiac function impairment in myocardial infarction by binding to MITF. *Aging* 11, 5368–5388.

Rao, J., Ye, Z., Tang, H., Wang, C., Peng, H., Lai, W., et al. (2017). The RhoA/ROCK pathway ameliorates adhesion and inflammatory infiltration induced by AGEs in glomerular endothelial cells. *Sci. Rep.* 7:39727.

Richard, D. E., Berra, E., and Pouyssegur, J. (2000). Nonhypoxic pathway mediates the induction of hypoxia-inducible factor 1alpha in vascular smooth muscle cells. *J. Biol. Chem.* 275, 26765–26771.

Rodriguez, P., Sassi, Y., Troncone, L., Benard, L., Ishikawa, K., Gordon, R. E., et al. (2019). Deletion of delta-like 1 homologue accelerates fibroblast-myofibroblast differentiation and induces myocardial fibrosis. *Eur. Heart J.* 40, 967–978. doi: 10.1093/eurheartj/ehy188

Sarrabayrouse, G., Synaeve, C., Leveque, K., Favre, G., and Tilkin-Mariame, A. F. (2007). Statins stimulate in vitro membrane FasL expression and lymphocyte apoptosis through RhoA/ROCK pathway in murine melanoma cells. *Neoplasia* 9, 1078–1090. doi: 10.1593/neo.07727

Shyu, K.-G., Liou, J.-Y., Wang, B.-W., Fang, W.-J., and Chang, H. (2005a). Carvedilol prevents cardiac hypertrophy and overexpression of hypoxia-inducible factor-1α and vascular endothelial growth factor in pressure-overloaded rat heart. *J. Biomed. Sci.* 12, 409–420. doi: 10.1007/s11373-005-3008-x

Shyu, K. G., Lu, M. J., Chang, H., Sun, H. Y., Wang, B. W., and Kuan, P. (2005b). Carvedilol modulates the expression of hypoxia-inducible factor-1alpha and vascular endothelial growth factor in a rat model of volume-overload heart failure. *J. Cardiac Fail.* 11, 152–159. doi: 10.1016/j.cardfail.2004.06.433

Somlyo, A. P., and Somlyo, A. V. (2000). Signal transduction by G-proteins, rho-kinase and protein phosphatase to smooth muscle and non-muscle myosin II. *J. Physiol.* 522(Pt 2), 177–185. doi: 10.1111/j.1469-7793.2000.t01-2-00177.x

Sun, B., Huo, R., Sheng, Y., Li, Y., Xie, X., Chen, C., et al. (2013). Bone morphogenetic protein-4 mediates cardiac hypertrophy, apoptosis, and fibrosis in experimentally pathological cardiac hypertrophy. *Hypertension* 61, 352–360. doi: 10.1161/hypertensionaha.111.00562

Takata, K., Morishige, K., Takahashi, T., Hashimoto, K., Tsutsumi, S., Yin, L., et al. (2008). Fasudil-induced hypoxia-inducible factor-1alpha degradation disrupts a hypoxia-driven vascular endothelial growth factor autocrine mechanism in endothelial cells. *Mol. Cancer Ther.* 7, 1551–1561. doi: 10.1158/1535-7163.mct-07-0428

Tamma, G., Klussmann, E., Procino, G., Svelto, M., Rosenthal, W., and Valenti, G. (2003). cAMP-induced AQP2 translocation is associated with RhoA inhibition through RhoA phosphorylation and interaction with RhoGDI. *J. Cell Sci.* 116(Pt 8), 1519–1525. doi: 10.1242/jcs.00355

Tang, L., Dai, F., Liu, Y., Yu, X., Huang, C., Wang, Y., et al. (2018). RhoA/ROCK signaling regulates smooth muscle phenotypic modulation and vascular remodeling via the JNK pathway and vimentin cytoskeleton. *Pharm. Res.* 133, 201–212. doi: 10.1016/j.phrs.2018.05.011

Tao, X., Fan, J., Kao, G., Zhang, X., Su, L., Yin, Y., et al. (2014). Angiotensin-(1-7) attenuates angiotensin II-induced signalling associated with activation of a tyrosine phosphatase in Sprague-Dawley rats cardiac fibroblasts. *Biol. Cell* 106, 182–192. doi: 10.1111/boc.201400015

Travers, J. G., Kamal, F. A., Robbins, J., Yutzey, K. E., and Blaxall, B. C. (2016). Cardiac fibrosis: the fibroblast awakens. *Circ. Res.* 118, 1021–1040. doi: 10.1161/circresaha.115.306565

Urbanek, K., Cabral-da-Silva, M. C., Ide-Iwata, N., Maestroni, S., Delucchi, F., Zheng, H., et al. (2010). Inhibition of notch1-dependent cardiomyogenesis leads to a dilated myopathy in the neonatal heart. *Circ. Res.* 107, 429–441. doi: 10.1161/circresaha.110.218487

Venkatesh, D., Fredette, N., Rostama, B., Tang, Y., Vary, C. P. H., Liaw, L., et al. (2011). RhoA-mediated signaling in Notch-induced senescence-like growth arrest and endothelial barrier dysfunction. *Arterioscler. Thromb. Vasc. Biol.* 31, 876–882. doi: 10.1161/atvbaha.110.221945

Wang, Q., Qu, X., Zheng, L., and Wang, H. (2019). Thymic stromal lymphopoietin alleviates fibrosis after myocardial infarction through regulating STAT3. *Panminerva Med.* doi: 10.23736/S0031-0808.19.03683-8

Xiong, A., and Liu, Y. (2017). Targeting hypoxia inducible factors-1alpha as a novel therapy in fibrosis. *Front. Pharmacol.* 8:326. doi: 10.3389/fphar.2017.00326

Yu, B., and Song, B. (2014). Notch 1 signalling inhibits cardiomyocyte apoptosis in ischaemic postconditioning. *Heart Lung Circ.* 23, 152–158. doi: 10.1016/j.hlc.2013.07.004

Zhang, M., Pan, X., Zou, Q., Xia, Y., Chen, J., Hao, Q., et al. (2016). Notch3 ameliorates cardiac fibrosis after myocardial infarction by inhibiting the TGF-beta1/Smad3 pathway. *Cardiovasc. Toxicol.* 16, 316–324. doi: 10.1007/s12012-015-9341-z

Zheng, T. S., Schlosser, S. F., Dao, T., Hingorani, R., Crispe, I. N., Boyer, J. L., et al. (1998). Caspase-3 controls both cytoplasmic and nuclear events associated with Fas-mediated apoptosis in vivo. *Proc. Natl. Acad. Sci. U.S.A.* 95, 13618–13623. doi: 10.1073/pnas.95.23.13618

Zhou, H., Sun, Y., Zhang, L., Kang, W., Li, N., and Li, Y. (2018). The RhoA/ROCK pathway mediates high glucose-induced cardiomyocyte apoptosis via oxidative stress, JNK, and p38MAPK pathways. *Diab. Metab. Res. Rev.* 34:e3022. doi: 10.1002/dmrr.3022

Zhou, J., and Brüne, B. (2006). Cytokines and hormones in the regulation of hypoxia inducible factor-1alpha (HIF-1alpha). *Cardiovasc. Hematol. Agents Med. Chem.* 4, 189–197.

Zhou, X., Chen, X., Cai, J. J., Chen, L. Z., Gong, Y. S., Wang, L. X., et al. (2015). Relaxin inhibits cardiac fibrosis and endothelial-mesenchymal transition via the Notch pathway. *Drug Design Dev. Ther.* 9, 4599–4611.

Zhou, X. L., Fang, Y. H., Wan, L., Xu, Q. R., Huang, H., Zhu, R. R., et al. (2019). Notch signaling inhibits cardiac fibroblast to myofibroblast transformation by antagonizing TGF-β1/Smad3 signaling. *J. Cell. Physiol.* 234, 8834–8845. doi: 10.1002/jcp.27543

Conflict of Interest: The authors declare that the research was conducted in the absence of any commercial or financial relationships that could be construed as a potential conflict of interest.

frontiers in Physiology

REVIEW
published: 15 September 2020
doi: 10.3389/fphys.2020.529075

The Dynamic Interplay Between Cardiac Inflammation and Fibrosis

*Toby P. Thomas and Laurel A. Grisanti**

Department of Biomedical Sciences, College of Veterinary Medicine, University of Missouri, Columbia, MO, United States

Heart failure is a leading cause of death worldwide. While there are multiple etiologies contributing to the development of heart failure, all cause result in impairments in cardiac function that is characterized by changes in cardiac remodeling and compliance. Fibrosis is associated with nearly all forms of heart failure and is an important contributor to disease pathogenesis. Inflammation also plays a critical role in the heart and there is a large degree of interconnectedness between the inflammatory and fibrotic response. This review discusses the cellular and molecular mechanisms contributing to inflammation and fibrosis and the interplay between the two.

Keywords: cardiac, fibrosis, fibroblast, inflammation, leukocyte, cytokine

INTRODUCTION

Cardiovascular disease is the leading cause of death worldwide and represents an immense health and economic burden (Benjamin et al., 2019). It is comprised of a group of conditions affecting the blood vessels and heart, culminating in impaired cardiovascular performance. Heart failure, the clinical manifestation of cardiovascular disease, is characterized by fibrosis, chamber remodeling and a reduction in ventricular compliance. Cardiomyocytes have limited capacity for regeneration thus, injury to the heart, leading to death of cardiomyocytes, results in clearing of dead cardiomyocytes and repair through fibrotic scar tissue replacement. This helps maintain the structural and functional integrity of the heart, but results in impairments in contractility and cardiac function when excessive. Ischemic heart disease is the leading type of cardiovascular disease and results in a fibrotic scar, however, fibrosis is a major contributor to many forms of heart disease and is recognized as a pathological hallmark in the heart (Travers et al., 2016).

Inflammation is a major regulator of the reparative response after cardiac injury. Following injury, there is an acute, intense inflammatory response that is important for initiating healing (Prabhu and Frangogiannis, 2016). Later immune responses promote repair. Proper timing and magnitude of inflammatory responses is critical for normal healing. Persistent inflammation can promote further tissue destruction while insufficient responses prolong the injurious stimuli. Inflammation regulates all aspects of cardiovascular health including cardiac fibrosis. There is a high degree of interconnectedness between immune cells and fibroblasts with each regulating the other's function. While recently these responses have been increasingly studied, inflammatory events that occur in the heart continue to not be fully understood. This further need to understand the mechanisms of cardiac repair is exemplified by the fact that no large-scale immunomodulatory or anti-inflammatory therapeutic strategies have been successfully translated into clinical practice.

CARDIAC FIBROSIS

Cardiac fibrosis is the process of pathological extracellular matrix (ECM) remodeling resulting in abnormal matrix composition leading to impairments in cardiac contractility and function.

OPEN ACCESS

Edited by:
Markus Wallner,
Medical University of Graz, Austria

Reviewed by:
Bing Hui Wang,
Monash University, Australia
Thomas Langenickel,
Ethris GmbH, Germany

***Correspondence:**
Laurel A. Grisanti
grisantil@missouri.edu

Specialty section:
This article was submitted to Integrative Physiology, a section of the journal Frontiers in Physiology

Received: *22 January 2020*
Accepted: *14 August 2020*
Published: *15 September 2020*

Citation:
Thomas TP and Grisanti LA (2020) The Dynamic Interplay Between Cardiac Inflammation and Fibrosis. Front. Physiol. 11:529075. doi: 10.3389/fphys.2020.529075

Fibrosis is involved in nearly all types of heart disease including various ischemic and non-ischemic etiologies (Liu et al., 2017). Initially, ECM deposition is protective and important for wound healing, but excessive or prolonged deposition can lead to impairments in tissue function. Fibrosis leads to a stiffer and less compliant heart, ultimately contributing to the progression of heart failure.

In the mammalian adult heart, cardiomyocytes are organized in a network of parenchymal cells, which includes a large number of fibroblasts, and ECM proteins. The ECM is composed predominantly of fibrillary collagens with type I collagen being the predominant form and type III collagen representing a smaller fraction along with other proteins such as fibronectin and elastin (Rienks et al., 2014). The ECM serves as a scaffold for cells and is also important in transmission of contractile forces in the normal myocardium.

Cardiac fibroblasts are the predominant cell type involved in cardiac fibrosis. They reside in the interstitium, epicardial and perivascular regions of the heart. Studies assessing fibroblast numbers have varied depending on species, technique and markers used, but regardless, it is appreciated that there is an abundant fibroblast population in the heart (Nag, 1980; Banerjee et al., 2007). Due to a lack of fibroblast specific markers, studies involving fibroblast have been difficult and likely represent a heterogeneous population of cells and numbers likely vary depending on the species studied, age and gender (Nag, 1980; Camelliti et al., 2005; Banerjee et al., 2007).

While fibroblasts are plentiful in the non-pathological heart, their function remains poorly understood. Resident fibroblasts originate from the embryonic epicardium (Gittenberger-de Groot et al., 1998). Under normal conditions, fibroblasts contribute to the homeostasis of the heart through the contribution of ECM, which serves as a structural scaffold for cardiomyocytes, distributes mechanical forces and mediates electrical conduction (Travers et al., 2016). Fibroblasts also contribute to matrix remodeling through the production of ECM regulatory proteins including the matrix metalloproteinases (MMPs) and TIMPs. Fibroblasts also have the ability to rapidly respond to alterations in their microenvironment. They are networked into the interstitial and perivascular matrix putting them in a strategic location for serving as sentinel cells to sense injury and trigger reparative responses (Kawaguchi et al., 2011; Diaz-Araya et al., 2015).

In the healthy heart, resident fibroblasts remain in the quiescent state, however, during pathological conditions, these resident fibroblasts and other precursor cells become activated and transdifferentiate into myofibroblasts. The origin of activated cardiac myofibroblasts is less clear with potential sources include resident fibroblasts, vascular endothelium, epicardium, perivascular cells and hematopoietic bone marrow-derived progenitor cells. There is substantial evidence that resident fibroblasts proliferate and activate in response to pathological stimuli (Fredj et al., 2005; Teekakirikul et al., 2010; Ali et al., 2014; Moore-Morris et al., 2014) however, these studies do not discount the possibility of other sources of activated fibroblasts. With the advent of transgenic mouse models, lineage tracing studies are beginning to be used to address this question. Endothelial, epicardial and perivascular cells have been proposed to undergo an endothelial-mesenchymal transition to acquire a fibroblast, pro-fibrotic phenotype. Lineage tracing studies have been performed to identify the contribution of these cell populations to the fibroblast population after injury however, many of the markers used such as Tie2 and vascular endothelial cadherin are not specific to the cell population being studied and immune cells express many of these same markers (Kisanuki et al., 2001; Monvoisin et al., 2006; Zeisberg et al., 2007; Russell et al., 2011; Ali et al., 2014; Kramann et al., 2015). Similarly, hematopoietic bone marrow-derived progenitor cells have also been proposed as a potential source of fibroblasts during pathology. This is due to initial studies using GFP-labeled bone marrow transplants where a large number of GFP-positive cells were located in fibrotic regions after pressure overload and myocardial ischemia (Haudek et al., 2006; Zeisberg et al., 2007; van Amerongen et al., 2008). However, these findings may be due to the presence of inflammatory cells in the fibrotic region and not a transition of these cell populations into myofibroblasts (Yano et al., 2005; van Amerongen et al., 2007). Regardless, CD45-positive cells including monocytes can express myofibroblast markers (Haudek et al., 2006) and it is known that inhibition of monocyte recruitment diminishes the cardiac fibroblast population (van Amerongen et al., 2007). Whether this is due to the importance of early immune responses in the recruitment and activation of fibroblast populations is unknown. However, lineage tracing experiments using the Vav-Cre and other lines suggest minimal contribution of hematopoietic cells to the cardiac fibroblast population (Ali et al., 2014; Moore-Morris et al., 2014, 2018).

The identification of fibrocytes in the circulation has renewed the interest of cells of hematopoietic origin as potential fibroblast contributors (Bucala et al., 1994). Fibrocytes are a unique fibroblast progenitor population that expresses fibroblast markers such as pro-collagen I and vimentin as well as hematopoietic markers (Abe et al., 2001). They originate from hematopoietic stem cells and have been shown to contribute to cardiac fibrosis in several injury models (Mollmann et al., 2006; Zeisberg et al., 2007; Xu et al., 2011).

Regardless of their origin, myofibroblasts appear shortly after injury and have a fibroblast-smooth muscle cell phenotype, with the acquisition of α-smooth muscle actin, contractile functions and enhanced secretion of collagens and other ECM components to promote scar formation. In accordance with their hypothesized sentinel cell function, following insult or injury, there is an upregulation of pro-inflammatory and pro-fibrotic factors in cardiac fibroblasts, which culminates in increases in fibroblast proliferation and the transition to a myofibroblast phenotype.

Myofibroblasts are the major cell type responsible for ECM and secretion. They are characterized by the development of stress fibers and expression of contractile proteins such as α-smooth muscle actin (Frangogiannis et al., 2000b; Santiago et al., 2010). Myofibroblasts secrete collagen and other ECM proteins to preserve the structural integrity of the heart. Failure of the heart to adapt and meet the pressure-generating capacity results in myocardial dysfunction and rupture. After

ECM deposition, the tensile strength increases at the site of injury leading to mature scar formation. While these processes are initially adaptive, they can lead to the development of adverse changes in compliance and structure, worsening the progression of heart failure over time. Pathological remodeling is characterized by fibroblast accumulation and excessive ECM deposition. This leads to alterations in the heart's architecture and has additional consequences on cardiac function. Fibrosis damages cardiac function due to the increased stiffness in the ventricle, producing contractile impairments. ECM and fibroblasts can disrupt the mechano-electric coupling of cardiomyocytes, diminishing cardiac contraction and increasing the risk of arrhythmia. Paracrine signaling from fibroblasts can induce hypertrophy and further cardiac dysfunction. Additionally, apoptosis resistant myofibroblasts can reside in mature scars perpetuating these responses.

Cardiac fibrosis presents itself in three forms: perivascular, reactive interstitial, and replacement fibrosis (Anderson et al., 1979), which are exemplified in **Figure 1**. Reactive interstitial fibrosis is adaptive to preserve cardiac structure and function whereas replacement fibrosis fills areas cause by cardiomyocyte death. Perivascular fibrosis, often occurring with other forms of fibrosis, is characterized by increased collagen deposition around vessels and microvasculature which function to provide oxygen and nutrients to cardiac tissue (Ytrehus et al., 2018). Perivascular fibrosis is heavily involved in hypertension and leads to impaired blood flow hampering the delivery of oxygen and nutrients to potentiate a pathogenic response (Kai et al., 2006). Pressure overload models, such as transaortic constriction, have a period of reactive interstitial fibrosis while the heart adapts to the hemodynamic changes followed by replacement fibrosis upon cardiomyocyte death. During myocardial infarction or ischemia/reperfusion injury, where there is an acute, extensive cardiomyocyte death, replacement fibrosis occurs, which fills the region devoid of cardiomyocytes and prevent cardiac rupture.

Fibrosis is also an essential aspect of cardiac repair. Initially it is a protective process and acts to preserve the architecture of the heart through the deposition of connective tissue. However, fibrosis can become pathological when progressive and excessive, leading to aberrant scarring, further organ damage and impairments in cardiac function. Ischemic diseases, hypertension, valvular disorders, and primary/secondary cardiomyopathies all include at least one of the three types of fibrosis and ECM remodeling (Burt et al., 2014). As the heart adopts a pathologic state, ECM remodeling and excessive fibrosis in turn lead to changes in chamber dimension and in some cases cardiomyocyte hypertrophy. As the injured healing heart adjusts to meet the demands of the rest of the body the myocardium around the fibrotic scar dilates. The progressive increased load on the heart causes a further dilation of the left ventricle, thereby increasing ventricular cavity size. Due to the naturally quiescent non-proliferative state of cardiomyocytes, existing viable cardiomyocytes undergo hypertrophy to account for an increased volume load. These changes lead to progressive ECM remodeling and interstitial fibrosis resulting in decompensated heart failure.

INFLAMMATION IN THE HEART

Inflammation is an important defense mechanism that acts to remove harmful stimuli and promote recovery. While some wound healing and fibrotic processes can occur in the absence of cellular immunity, inflammation is an important contributor to cardiac health both in the normal and diseased state. Inflammation of the appropriate timing, duration and magnitude is critical for normal healing. Failure to activate sufficient inflammatory responses can lead to persistence of the injurious stimuli whereas failure to resolve inflammation can further tissue destruction.

Under non-pathological conditions, cardiac macrophages and other resident immune populations help regulate homeostasis. While the role of immune responses in cardiac homeostasis has been an understudied area, it is known that the heart has resident populations of mast cells and macrophages that play an important role in homeostasis and following injury (Sperr et al., 1994; Frangogiannis et al., 1999). There are also small populations of B and T cells present in the healthy myocardium (Pinto et al., 2016). Under steady-state conditions, resident immune cells are believed to play a sentinel role in surveilling against invading pathogens, similar to what is observed in other tissues (Franken et al., 2016). Mast cells are located in the perivascular areas and contain stores of inflammatory mediators such as tumor necrosis factor (TNF), histamine and tryptase, which can be quickly released following injury and represent an important contributor to triggering inflammatory responses (Frangogiannis et al., 1998a; Somasundaram et al., 2005).

The heart also contains resident macrophage populations that are comprised primarily of CCR2- cells of embryonically derived cells that originate from yolk sac macrophages and fetal monocytes (Pinto et al., 2012; Epelman et al., 2014; Heidt et al., 2014; Mylonas et al., 2015). There is also a small population derived from CCR2+ monocytes. Some studies suggest that resident cardiac macrophages die following injury and are replaced by monocyte-derived CCR2-expressing populations that are highly pro-inflammatory (Heidt et al., 2014). Outside of pathogen surveillance, resident immune populations are hypothesized to facilitate physiological turnover of cells and ECM, debris clearance after changes in metabolic load, and also play a role in the conduction system (Swirski et al., 2009). Gene expression profiling has identified distinct profiles of CCR2- macrophages in human myocardium compared to CCR2+ populations with enhanced expression of pathways involved in cell growth and ECM formation (Bajpai et al., 2018). While functional outcomes of these differences of these gene expression differences is not well characterized, these findings are consistent with the role of resident macrophage populations in other tissues (Franken et al., 2016). Outside of the classic role of tissue macrophages, cardiac macrophages have also been recognized as having organ-specific functions. Resident cardiac macrophages are enriched in the conduction system of the heart and depletion disrupts electrical conduction in the heart (Hulsmans et al., 2017). These studies have identified a relationship between cardiomyocytes and macrophages through the formation of

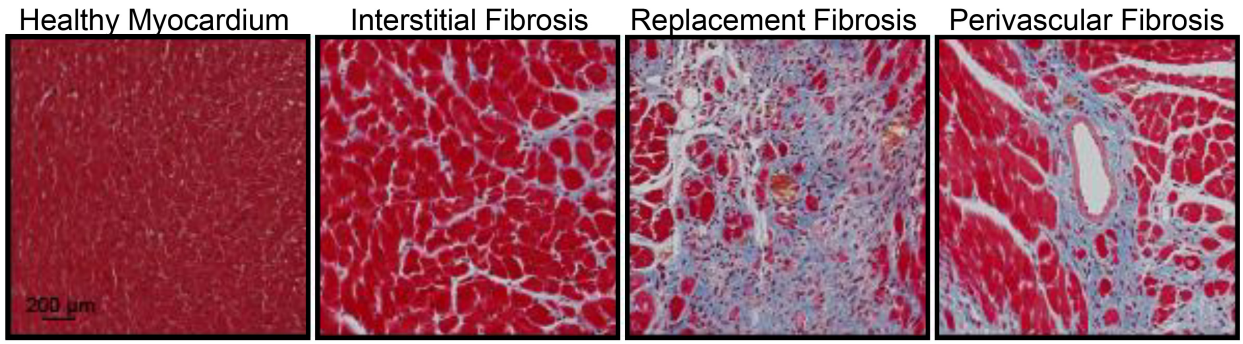

FIGURE 1 | Masson's trichrome staining of the mouse heart demonstrating fibrosis (blue) in the healthy myocardium, interstitial fibrosis following isoproterenol administration (30 mg/kg/d for 2 weeks), replacement fibrosis after myocardial infarction (4 weeks) or perivascular fibrosis following isoproterenol infusion (30 mg/kg/d for 2 weeks). Red represents the cytoplasm and black represent nuclei. Animal procedures were performed in house with approval by the Institutional Animal Care and Use Committee at the University of Missouri and in accordance to the National Institutes of Health *Guidelines on the Use of Laboratory Animals*.

gap junctions that enable cardiac macrophages to contribute to steady-state electrical conduction.

Pathologically, inflammation regulates virtually all aspects of cardiovascular health including cardiomyocyte contractility and cardiac fibrosis and represents an important regulatory mechanism. Following injury, acute inflammatory responses occur that help remove dead or damaged cardiomyocytes, ECM debris and initiate healing. Cardiac repair after injury is a finely tuned and regulated series of events that is critical for adequate healing (**Figure 2**). With the exception of myocarditis, other forms of cardiac injury are considered sterile inflammation and follow a similar series of events. This progression of events has been well defined for myocardial infarction and include the inflammatory, proliferative and maturation phases (Prabhu and Frangogiannis, 2016). While these responses may not be identical in timing, duration and magnitude between heart failure etiologies, they are thought to be broadly applicable to other forms of sterile cardiac damage (Fildes et al., 2009). Following insult or injury, there is an acute inflammatory phase characterized by infiltration of pro-inflammatory immune cell populations that digest and clear damaged cells and ECM tissue. This is followed by a reparative phase with the resolution of pro-inflammatory responses and activation of reparative responses such as myofibroblast accumulation, ECM deposition and neovascularization. Appropriate magnitude and duration of each event is critical for optimal repair. Early inflammatory activation is needed for the transition to a reparative response whereas an excessive inflammatory phase can further tissue damage and lead to improper healing.

THE INFLAMMATORY PHASE

The inflammatory phase is characterized by the recruitment of inflammatory cells to the site of damage (Prabhu and Frangogiannis, 2016). Cardiomyocytes are more susceptible to ischemic injury or damage than non-cardiomyocytes. Injury or death of cardiomyocytes causes the release of danger-associated molecular patterns (DAMPs) that bind to a cognate pattern recognition receptor (PRR) on neighboring cells to initiate inflammatory responses (**Figure 3**). A number of factors released from damaged or dying cardiomyocytes have been identified as DAMPs including mitochondrial DNA (Bliksoen et al., 2016), the chromatin protein high mobility group box 1 (HMGB1) (Lotze and Tracey, 2005), purine metabolites (Kono et al., 2010; McDonald et al., 2010), sarcomeric protein fragments (Lipps et al., 2016), and S100 proteins (Rohde et al., 2014). Additionally, fragments of the ECM that arise from damage including biglycan (Schaefer et al., 2005), decorin (Merline et al., 2011), hyaluronan (Scheibner et al., 2006) and fibronectin (Gondokaryono et al., 2007; Lefebvre et al., 2011; Sofat et al., 2012) have been shown to activate PRRs to contribute to inflammatory responses.

DAMP activation of PRRs induces the production of a cascade of inflammatory mediators including cytokines, chemokines and cell adhesion molecules (Mann, 2011). PRRs are present on cells of the innate immune system but can also act on surviving resident cell populations including cardiomyocytes (Kukielka et al., 1993; Frantz et al., 1999; Tarzami et al., 2002), fibroblasts (Zhang et al., 2015; Turner, 2016) and endothelial cells (Kumar et al., 1997) to potentiate the inflammatory cascade (Frantz et al., 1999). The best characterized family of PRRs are the Toll-like receptors (TLR) but others include nucleotide-binding oligomerization domain-like receptors (NLRs) and receptor for advanced glycation end-products (RAGE). Signal transduction by PRRs has been extensively delineated and converges on the activation of mitogen-activated protein kinases (MAPKs) and nuclear factor (NF)-κB to regulate the expression of a large panel of pro-inflammatory genes including cytokines, chemokines and adhesion receptors (Akira and Takeda, 2004). These factors enhance leukocyte recruitment to amplify the inflammatory response, promote efferocytosis of dying cells and augment tissue digestion by proteases and oxidases.

Due to their close proximity, wide distribution in the myocardium, ability to rapidly respond to stimuli and potential as a source of inflammatory mediators, fibroblasts have been proposed to serve as sentinel cells in the heart. Within days of tissue damage, cardiac fibroblasts acquire a

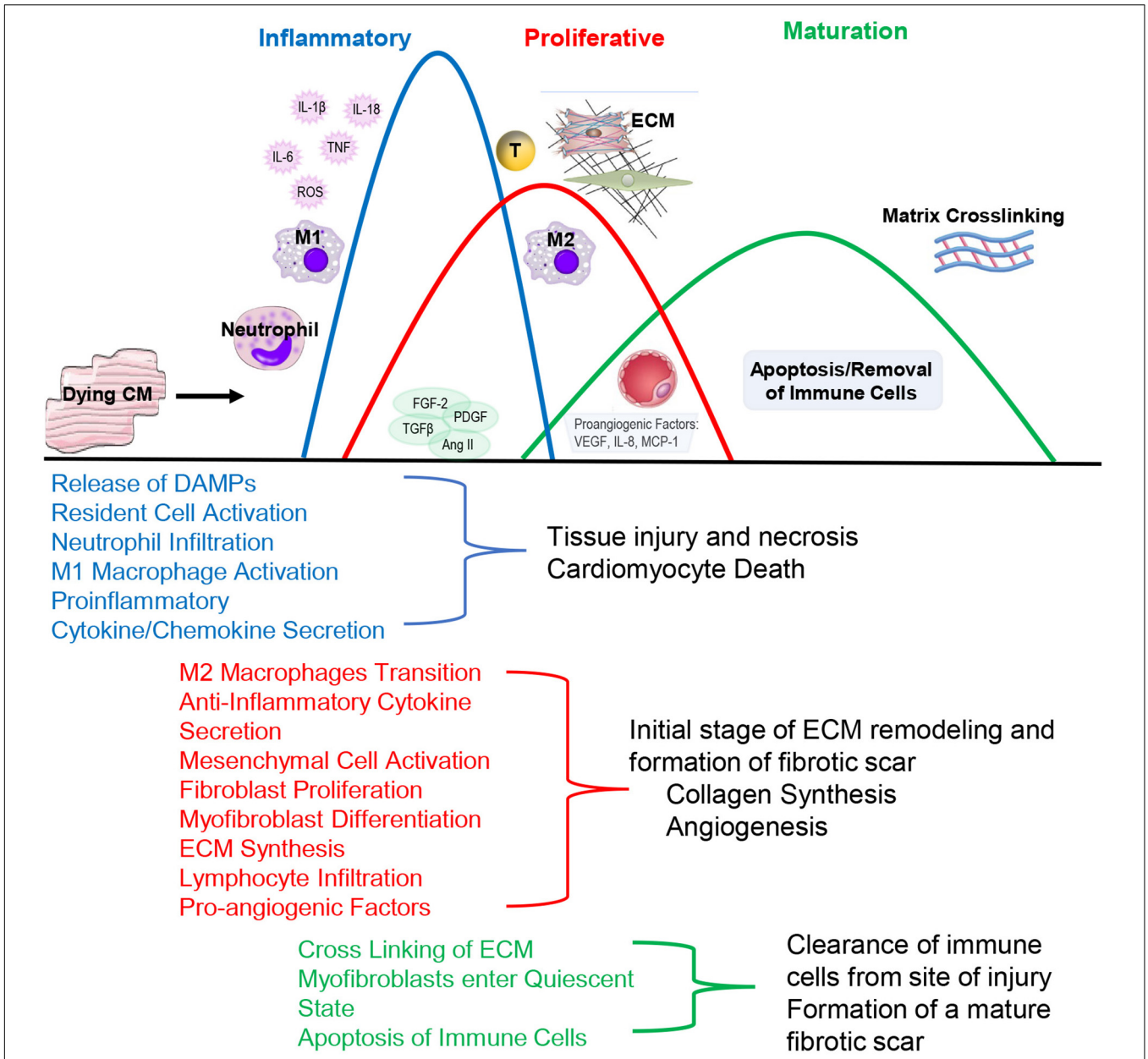

FIGURE 2 | During the Inflammatory Phase, damage or death of cardiomyocytes activates resident fibroblasts and other cell populations to produce cytokines and recruit pro-inflammatory leukocyte populations, primarily neutrophils and monocytes that differentiate into M1-like macrophages. This acute, pro-inflammatory response transitions into a reparative response during the Proliferative Phase with the recruitment of reparative lymphocyte and M2-like macrophages populations. Activated myofibroblasts secrete collagen and other extracellular matrix components. Pro-angiogenic factors are secreted that promote neovascularization. The events conclude during the Maturation Phase with the apoptosis of reparative immune cell and myofibroblast populations and matrix crosslinking, resulting in mature scar formation.

pro-inflammatory phenotype characterized by the secretion of cytokines/chemokines including IL-8, IL-1β, CCL2, eotaxin and TNF-α and the presence of matrix-degrading properties (Sandanger et al., 2013; Sandstedt et al., 2019). The inflammatory potential of cardiac fibroblasts has been extensively documented *in vitro* (Heim et al., 2000; Lafontant et al., 2006). Stimulation of cardiac fibroblasts with ATP results in a large release of pro-inflammatory cytokines (Lu et al., 2012). A number of different factors in addition to ATP are also known to cause fibroblast activation including reactive oxygen species (ROS) (Siwik et al., 2001; Lijnen et al., 2006; Lu et al., 2012) and cytokines (Lafontant et al., 2006; Zymek et al., 2007; Turner et al., 2009). Cytokines have been implicated in inducing an inflammatory phenotype in cardiac fibroblasts and potentiating cytokine and chemokine synthesis (Lafontant et al., 2006; Zymek et al., 2007; Turner et al., 2009). They have also been shown to

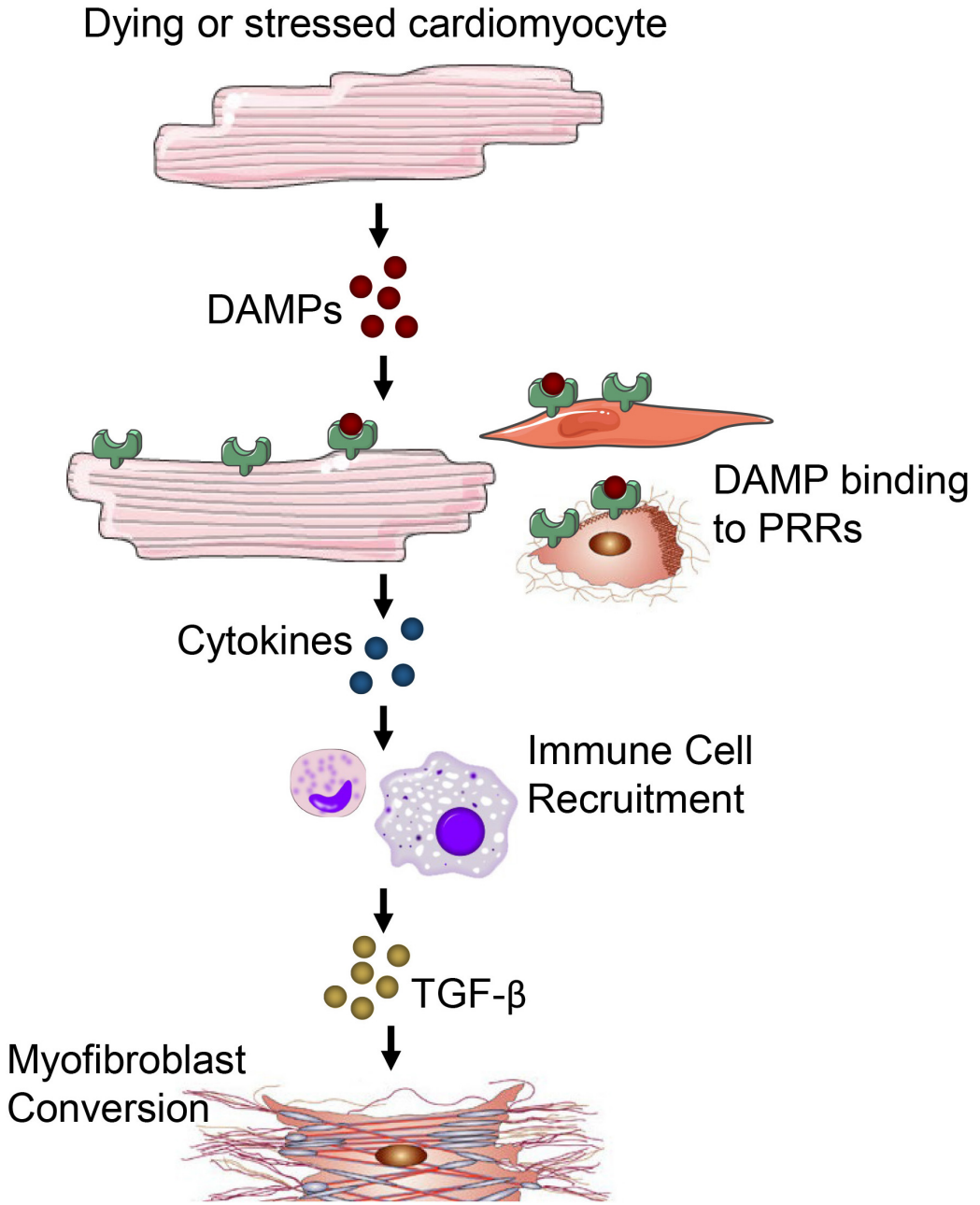

FIGURE 3 | Damage or death of cardiomyocytes leads to the release of DAMPs. DAMPs acting through PRRs on neighboring cardiomyocytes, fibroblasts, resident immune cells, endothelial cells and other parenchymal cells of the heart promote cytokine and chemokine release. Immune cells migrate in response to cytokine/chemokines in the heart and secrete TGF-β and other pro-fibrotic factors to promote fibrosis and myofibroblast conversion.

regulate expression of matrix-degrading proteases (Li et al., 2002; Siwik and Colucci, 2004). However, the contribution of cardiac fibroblasts in activating inflammatory cascades in pathological settings is less understood. *In vivo* studies have been limited due to the absence of specific markers for cardiac fibroblasts (Kong et al., 2013). As a result, studies have been largely descriptive. However, infarction models in mice show activation of the inflammasome in cardiac fibroblasts, an indication of the generation of active IL-1β (Kawaguchi et al., 2011; Sandanger et al., 2013).

Endothelial and resident mast cell populations have also been implicated in triggering the inflammatory cascade post-infarction (Lakshminarayanan et al., 1997, 2001; Frangogiannis et al., 1998a). As previously mentioned, there is a small population of resident mast cells that plays an important role in homeostasis in the normal myocardium and during

pathological events. Expansion of the mast cell population is associated with cardiac fibrosis in response to multiple pathological challenges (Frangogiannis et al., 1998b; Patella et al., 1998; Shiota et al., 2003; Wei et al., 2003). The mechanisms associated with this expansion is not well understood. Stem cell factor (SCF), which is known to be involved in the recruitment and differentiation of mast cell progenitors, is upregulated in hearts following myocardial infarction and may contribute to the proliferation of resident mast cells (Frangogiannis et al., 1998b). However, other studies suggest mast cell progenitors infiltrate the myocardium from outside sources (Bujak et al., 2008). Regardless of origin, mast cells are known to be vital in the pathogenesis of cardiac fibrosis. Mast cell deficiency results in attenuated perivascular fibrosis and reduced progression to decompensated heart failure in a mouse model of pressure overload (Hara et al., 2002). Pharmacological prevention mast cell product release in spontaneously hypertensive rats reduced fibrosis, reduced inflammatory cell recruitment and decreased pro-inflammatory cytokines (Levick et al., 2009).

How mast cells influence fibrosis is also poorly understood. Mast cells are known to have abundant numbers of granules that store a wide range of mediators. This includes many pro-fibrotic mediators including TNF-α (Frangogiannis et al., 1998a), TGF-β (Shiota et al., 2003), and platelet-derived growth factor (PDGF) (Nazari et al., 2016). However, these mediators are produced by many cell types and the relative contribution of mast cells has not been fully elucidated. Additionally, mast cells have abundant expression of chymase, a protease implemented in the angiotensin converting enzyme (ACE)-independent generation of angiotensin II (Urata et al., 1990a,b). This mechanism may represent an important mechanism in the progression of cardiac fibrosis in the presence of ACE inhibition.

The cytokine rich environment present in the heart following injury causes infiltration of pro-inflammatory immune cell populations including phagocytic neutrophils and mononuclear cells which clear the area of dead cells and ECM debris (Prabhu and Frangogiannis, 2016). These responses are facilitated by changes in the vasculature. Hypoxia compromises the vascular endothelial cell integrity and barrier function, increasing vessel permeability to facilitate leukocyte infiltration (Sansbury and Spite, 2016). Neutrophils are among the first immune cell types to infiltrate into the damaged heart in response to a number of pro-inflammatory mediators including DAMPs, cytokines, chemokines, endogenous lipid mediators (prostaglandins and leukotrienes), histamine and complement components (Yan et al., 2013; Puhl and Steffens, 2019). Neutrophils are continually produced from hematopoietic progenitors in the bone marrow through the process of granulopoiesis. They reside in specific niches in the bone marrow through the action of CXCL12 (Katayama et al., 2006; Russell et al., 2011). Maturation of immature neutrophils is regulated by granulocyte colony-stimulating factor (G-CSF), which is produced in response to IL-17 from γδT-cells and counteracted by IL-23 (Stark et al., 2005; Liao et al., 2012; Yan et al., 2012; Savvatis et al., 2014). In this way γδT-cells regulate neutrophil and macrophage infiltration and have detrimental effects on remodeling in myocardial infarction models (Yan et al., 2012). Following maturation, neutrophils remain in the bone marrow through the actions of CXCR4 or are release into the circulation by CXCR2-dependent signaling (Tarzami et al., 2003; Devi et al., 2013).

Extravasation of neutrophils into the heart is dependent on adhesion interactions between the neutrophils and endothelial cells. Endothelial cells activated by PRR-dependent mechanism rapidly upregulate pre-stored *P*-selectin. There is a slower upregulation of *E*-selectin that is generated *de novo* (Ley et al., 2007; Petri et al., 2008). Circulating neutrophils express selectin ligands, which causes them to interact with the endothelium and roll along the endothelial layer. The two selectins have partially overlapping functions and bind P-selectin glycoprotein ligand 1 (PSGL1) leading to tethering of neutrophils and initiate rolling (Ley et al., 2007). Lymphocyte function-associated antigen 1 (LFA1), which binds to intracellular adhesion molecule (ICAM) 1 and 2 on endothelium facilitates neutrophil rolling (Zarbock et al., 2011). Rolling neutrophils respond to chemokines bound to the endothelial surface to induce a conformational change of integrins and endothelial cell surface molecules such as ICAM1 and ICAM2, enhancing their adhesion and resulting in arrest (Detmers et al., 1990; Herter and Zarbock, 2013). It is thought that full activation requires a two-step process initiated by specific priming pro-inflammatory cytokines including TNFα and IL-1β however other chemoattractants and growth factors may also be involved (Summers et al., 2010). This priming is also important for maximal neutrophil degranulation and activation (Guthrie et al., 1984; Summers et al., 2010). Signaling initiated by CXCL8 in humans (CXCL1, CXCL2 and CXCL5 in mice) via CXCR2 further activates neutrophils and promotes their adhesion (Pruenster et al., 2009; Williams et al., 2011). The neutrophils transmigrate through the endothelial junctions and then the basement membrane through multiple effectors including VCAM1, PECAM1, and VLA4 (Wang et al., 2006). Many of these processes have been studied extensively in other tissues and are believed to be directly applicable to the heart, however, a careful examination of cardiac specific neutrophil extravasation and transmigration process have not been extensively investigated.

Once in the tissue, neutrophils release proteolytic enzymes such as myeloperoxidase (MPO) and play an important role in clearing the area of dead cells and matrix debris (Puhl and Steffens, 2019). They may also amplify the immune response through production of pro-inflammatory mediators (Boufenzer et al., 2015) and have been shown to regulate recruitment of pro-inflammatory monocyte populations to the heart (Alard et al., 2015). While these actions are critical for proper healing, neutrophils may also exert cytotoxic actions on cardiomyocytes to exacerbate the injury (Simpson et al., 1988; Entman et al., 1992; Ali et al., 2016). These cytotoxic effects occur through the release of reactive oxygen species (ROS) and also release of granules associated with adverse left ventricular remodeling (Vasilyev et al., 2005; Ciz et al., 2012).

Following injury, this resident macrophage populations expands (Yan et al., 2013). There are two distinct subsets of monocyte recruitment to the damaged heart (Nahrendorf et al., 2007). Pro-inflammatory, M1-like macrophages are recruited to the heart shortly after neutrophils. This initial population of

macrophages is derived from bone marrow progenitor cells and release from splenic reservoirs. They are recruited to the heart through the MCP-1(CCL2)/CCR2 axis (Swirski et al., 2009; Bajpai et al., 2018). The first subset is pro-inflammatory and recruited through the MCP-1(CCL2)/CCR2 axis. This pro-inflammatory population is characterized by high Ly-6C expression (Dewald et al., 2005). Infiltrating Ly-6C^{high} populations are derived from bone marrow progenitor cells and reservoirs of mononuclear cells in the spleen that can be deployed quickly to the site of inflammation (Swirski et al., 2009). These M1-like macrophages are proteolytic with increased expression of proteinases such as cathepsins and MMPs and are involved in ECM remodeling due to being a major source of MMPs and TIMPs (Huang et al., 2012; Khokha et al., 2013). Like fibroblasts, macrophages play a role in ECM remodeling through the secretion of ECM components. These classically activated macrophage populations serve as a major source of pro-inflammatory cytokines including IL-12, IL-23, IL-1, and IL-6 as well as being involved in phagocytosis.

THE PROLIFERATIVE PHASE

Suppression and resolution of inflammation is an active process. While the mechanisms contributing to the initiation of inflammation have been well characterized, resolution of inflammation is not as well understood. Neutrophils that are recruited initially during the inflammatory phase are short-lived cells and rapidly undergo cell death primarily through apoptosis, but also necrosis, which releases mediators that promote the resolution of inflammation including lipoxins and resolvins that suppress neutrophil transmigration and promote neutrophil apoptosis (Serhan et al., 2008; Mantovani et al., 2011; Geering et al., 2013). Dying neutrophils also express decoy and scavenging receptors that deplete the area of inflammatory mediators (Soehnlein and Lindbom, 2010; Penberthy and Ravichandran, 2016). Phagocytosis of necrotic neutrophils by macrophages clears the area of apoptotic cells and induces a pro-resolving M2 macrophage phenotype characterized by the secretion of suppressors of inflammation such as transforming growth factor (TGF)-β, IL-10, interleukin receptor associated kinase-M (Chen et al., 2012) and pro-resolving lipid mediators such as lipoxins and resolvins (Sansbury and Spite, 2016; Horckmans et al., 2017). An anti-inflammatory/reparative monocyte subpopulation is recruited to contribute to the M2-like macrophage pool and contributes to the resolution of inflammatory responses. Similarly, these pro-resolving, M2-like macrophages secrete anti-inflammatory, pro-fibrotic and pro-angiogenic cytokines including IL-10 and TGF-β to suppress inflammation and promote tissue repair.

Dendritic cells infiltrate the damaged heart predominantly during the reparative phase (Yan et al., 2013). They play an important role in the resolution of inflammation, scar formation and angiogenesis. Deletion of dendritic cells prolongs the accumulation of Ly-6C^{high} monocytes, pro-inflammatory macrophages and pro-inflammatory mediators (Anzai et al., 2012). Mice lacking dendritic cells have a reduction in endothelial cell proliferation and worsened cardiac function following myocardial infarction. Additionally, they have been shown to play a role in activation of T cell populations, which play a role in remodeling (Van der Borght et al., 2017). They also play an important role in phagocytosis of foreign or damaged material and antigen presentation making them an important link between the innate and adaptive immune response (Dieterlen et al., 2016; Van der Borght et al., 2017).

Lymphocytes migrate to the heart following injury and there is emerging evidence for an important role of lymphocyte populations in mediating cardiac fibrosis in both ischemic and non-ischemic heart failure (Laroumanie et al., 2014; Nevers et al., 2015; Bansal et al., 2017). The cause of T lymphocytes in the non-ischemic myocardium is uncertain but may be a result of mechanical-stress activation of neurohumoral pathways (Amador et al., 2014; Li et al., 2017). In the ischemic heart, T cells are recruited via chemokine-dependent mechanisms primarily during the reparative phase (Dobaczewski et al., 2010b). Cytotoxic T cells are activated after infarction and may exert cytotoxic actions on healthy cardiomyocytes in a mechanism that is thought to involve cross-reactive cardiac antigens (Varda-Bloom et al., 2000; Ilatovskaya et al., 2019). B cells are also recruited to the heart through poorly understood mechanisms (Wang et al., 2019). They are thought to have a negative impact on remodeling though their role is not well defined (Adamo et al., 2018, 2020). B cells promote mobilization of pro-inflammatory Ly-6C^{high} monocytes through the production of CCL7 and may affect the heart through their role in antibody deposition (Zouggari et al., 2013; Adamo et al., 2020). CD4+ helper T cells play an important role in response to cardiac injury. Following myocardial infarction, they are likely activated by cardiac autoantigens to promote wound healing, resolution of inflammation, proper collagen matrix and scar formation (Hofmann et al., 2012). Studies using CD4+ T-cell deficient mice, mice lacking the MHCII genes and OT-II mice that have defective T-cell antigen recognition, have augmented infiltrating leukocytes and disrupted collagen matrix formation Hofmann et al., 2012). Regulatory T cells (CD4+ Foxp3+) are also critical for favorable wound healing, scar formation and resolution of inflammation after myocardial infarction, in part, through modulating macrophage polarization toward an M2-like phenotype (Weirather et al., 2014). NKT cell activation reduces leukocyte infiltration and adverse remodeling following both non-perfused and reperfused myocardial infarction partially through enhanced expression of IL-10 and other anti-inflammatory cytokines (Sobirin et al., 2012; Homma et al., 2013).

Along with the repression of inflammation, there is induction of mediators that activate mesenchymal cells. During the proliferative phase there is abundant infiltration of fibroblasts and vascular cells. Suppression of pro-inflammatory signaling such as IL-1β and interferon-γ-inducible protein (IP)-10 allows for growth and infiltration of cardiac fibroblasts (Palmer et al., 1995; Koudssi et al., 1998). Fibroblast migration is a critical aspect of fibroblast biology in the damaged myocardium. Fibroblasts must migrate to the site of dead cardiomyocytes for optimal repair in a manner that is dependent on their ability to degrade and deposit matrix (Tschumperlin, 2013). Several factors have been

shown to mediate fibroblast migration including leukotrienes (Blomer et al., 2013), cytokines such as IL-1β and cardiotrophin-1 (Mitchell et al., 2007; Freed et al., 2011) and growth factors including fibroblast growth factor (FGF) and TGF-β (Detillieux et al., 2003; Liu et al., 2008).

Fibroblast proliferation also plays an important role during the proliferative phase. Studies demonstrate an intense proliferation of fibroblasts in the injured heart (Frangogiannis et al., 1998b; Virag and Murry, 2003). Many factors influence fibroblast proliferation including the growth factors fibroblast growth factor (FGF)-2 and platelet-derived growth factor (PDGF) (Booz and Baker, 1995; Zymek et al., 2006). Other factors including angiotensin II, mast cell-derived tryptase and chymase also play a role. However, the relative importance of these factors is not well defined.

Following infiltration and proliferation at the sight of injury, fibroblasts differentiate into myofibroblast. Myofibroblasts arise primarily through proliferation of resident fibroblasts (Fredj et al., 2005; Teekakirikul et al., 2010; Ali et al., 2014; Moore-Morris et al., 2014) and are characterized by the expression of contractile proteins and the ability to secrete large amounts of matrix proteins (Cleutjens et al., 1995b). While myofibroblasts may become activated through several potential mechanisms, transforming growth factor (TGF)-β is the best characterized mechanism of myofibroblast activation. TGF-β is upregulated in the damaged heart and induces transcription of myofibroblast genes through canonical Smad-dependent signaling (Dobaczewski et al., 2010a). Alternatively, non-canonical signaling through p38 mitogen-activated protein kinase (MAPK), also plays a role in myofibroblast conversion (Hashimoto et al., 2001; Sousa et al., 2007).

Activated myofibroblasts secrete ECM to form the fibrotic scar. Myofibroblasts are thought to represent the main source of ECM deposition (Cleutjens et al., 1995a; Squires et al., 2005). Secretion of structural proteins including collagens and fibronectin as well as matrix metabolism through the expression of MMPs and TIMPs are critical for fibrosis. At the end of the proliferative phase, there is an ECM composed primarily of collagen. Signals leading to the transition from the proliferative to the maturation phase are not well characterized. Regardless, fibrotic and angiogenic responses are halted, preventing the expansion of fibrosis and leading to the maturation phase.

THE MATURATION PHASE

The maturation phase follows the proliferative phase and is characterized by mature scar formation. During the maturation phase, cross-linking of the extra cellular matrix occurs. Reparative cells that are present during the proliferative phase become deactivated and may go through apoptosis. The mechanisms involved in the transition from the proliferative phase to the maturation phase are largely unknown. Myofibroblasts undergo quiescence, potentially due to a lessening of fibrotic growth factors and decreased TGF-β and angiotensin II signaling. They may also go through apoptotic death (Takemura et al., 1998).

INFLAMMATION IN MYOCARDITIS

Inflammatory cardiomyopathy or myocarditis occurs due to inflammation in the heart. Unlike other forms of heart failure, myocarditis is initiated by a pathogen or autoimmune response and may produce a unique type of inflammation depending on the causative agent. Myocarditis is commonly associated with viral infection (Caforio et al., 2007), the Coxsackie virus of group B (CVB) is the most studied, which leads to viral particle processing by innate immune cells followed by antigen presentation and activation of the antiviral cytotoxic CD8+ T cells and some CD4+ T cell populations. While viruses of the adenovirus, enterovirus, and parvovirus families are most commonly associated with myocarditis, other infectious events including bacterial causes such as staphylococcus, streptococcus and Clostridia infections, fungal diseases including aspergillosis and actinomycosis, protozoan illnesses such as Chagas disease and malaria and parasitic infections like in schistosomiasis. Toxins and autoimmune disorders can also give rise to myocarditis (Caforio et al., 2007). While the immune response is unique depending on the cause of myocarditis, common hallmarks include inflammatory cell infiltration, which can lead to fibrosis. Inflammation in myocarditis is highly linked to the severity of the disease (Kindermann et al., 2008). Most individuals who have inflammatory cardiomyopathy see a resolution of symptoms however, the type, extent and duration of the inflammatory response determines whether myocarditis will be resolved or progress to dilated cardiomyopathy and ultimately heart failure. Patients with an acute hypersensitive myocarditis seem to recover after a few days, while patients with giant cell myocarditis and eosinophilia myocarditis more often progress to heart failure (Fung et al., 2016).

Similar to other forms of injury, the noxious insult initiating myocarditis causes damage to cardiomyocytes, stimulating the recruitment of circulating immune cells. If the extent of damage results in a loss of cardiomyocytes, the heart repairs itself through the deposition of ECM and myocardial fibrosis. This process can be exacerbated by continued inflammation due to prolonged exposure to the pathogen or toxic agent, T lymphocyte responses to specific antigens and persistent immune responses due to antibodies against or similar to endogenous heart antigens (Cooper, 2009).

INFLAMMATION IN HYPERTENSION

Hypertension involves both the innate and adaptive immune system throughout the progression of the disease. Inflammation is believed to be a contributing factor to the diseased state of hypertension. T lymphocytes have been shown to have a role in the onset of the disease in an Angiotensin II (Ang II)-induced hypertension mouse model. In a RAG-$1^{-/-}$ mouse model null of T and B lymphocytes, mice display a dampened form of hypertension, while reintroduction of T cells recapitulated the classical hypertension readouts (Guzik et al., 2007). A more recent study closely investigated the role of B lymphocytes in Ang II-induced hypertension and found depletion of B cells

ablated the phenotype associated with the model and adoptive transfer of B cells recapitulated the hypertensive phenotype (Chan et al., 2015). In a similar Ang II infusion induced hypertensive mouse model, immune cells of the monocytic lineage were shown to be a key mediator in enabling vascular dysfunction (Wenzel et al., 2011; Harrison, 2014). Ablation of LysM+ monocytes in this model significantly dampened vascular macrophage infiltration, aortic macrophage populations, and inflammatory gene expression in vasculature. The common accepted mechanism follows enhancement of hypertension symptoms due to the stress put on vasculature and the release of damage associated molecular patterns (DAMPs) causing a secondary chronic inflamed state (Drummond et al., 2019). The involvement of the immune system in hypertension further exacerbates the disease state induced by high blood pressure.

CYTOKINES-MEDIATORS OF FIBROSIS

Many of the Th-2 cytokines were first recognized as having pro-fibrotic properties including IL-4, IL-5, IL-10, and IL-13. IL-4 has been shown to increase collagen and matrix protein synthesis in fibroblasts (Fertin et al., 1991; Postlethwaite et al., 1992) and deletion reduces myocardial fibrosis (Kanellakis et al., 2012; Peng et al., 2015). IL-4 is pleiotropic in nature and effects a variety of cell types including having immunosuppressive effects on pro-inflammatory mediators (Hart et al., 1989; Levings and Schrader, 1999). IL-13 has also been shown to directly activate fibroblasts (Oriente et al., 2000) and plays a role in fibrosis and deletion in mice aggravates healing after myocardial infarction (Hofmann et al., 2014).

While many immune responses are thought to be a reciprocal regulation between cell populations, Th-1 and Th-17 cytokines also promote fibrogenesis (Mosmann and Coffman, 1989; Choy et al., 2015). IL-17 has reported direct and indirect pro-fibrotic properties (Li et al., 2014). Some Th1 cytokines, including TNF-α, are pro-fibrotic while others, such as IFN-γ and IL-12, are anti-fibrotic (Zhang et al., 2011; Han et al., 2012; Li et al., 2012; Kimura et al., 2018; Lee et al., 2019).

INTERLEUKIN-1

IL-1α and IL-1β are upregulated in the injured heart and play an important role in inducing the expression of other cytokines, chemokines, adhesion molecules and growth factors (Guillen et al., 1995; Herskowitz et al., 1995). Most cell types in the heart are impacted by IL-1 family members, particularly IL-1β. It plays a large role in pro-inflammatory leukocyte recruitment to the heart following damage (Saxena et al., 2013). Notably, IL-1β has been found to be particularly important in regulating cardiac fibroblast function during the inflammatory phase. It is markedly upregulated in the infarcted myocardium (Herskowitz et al., 1995; Christia et al., 2013). Induction mediates inflammatory signaling and ECM metabolism through its effects on proteases (Bujak et al., 2008). IL-1β promotes fibroblast migration through increasing the expression of proteins involved in ECM turnover (Mitchell et al., 2007). IL-1β may also play a role in the conversion of fibroblasts into myofibroblasts (Saxena et al., 2013). It has also been linked to fibroblast proliferation where it has been shown to inhibit proliferation through the modulation of cyclins, cyclin-dependent kinases and their inhibitors (Palmer et al., 1995; Koudssi et al., 1998). However, many of these studies were performed *in vitro* and the actions of IL-1β *in vivo* is less clear.

In vivo studies assessing the role of IL-1β are more confounding. Viral overexpression of IL-1 receptor antagonist (IL-1ra) in the hearts of rats subjected to ischemia reperfusion injury was protective through the inhibition of inflammatory responses and decreased cardiomyocyte apoptosis (Suzuki et al., 2001). Global IL-1RI knockout mice have decreased inflammation and immune cell recruitment following myocardial infarction, which culminated in an attenuated fibrotic response (Bujak et al., 2008). Contrarily, neutralizing antibody administration for IL-1β in mice in the acute phase after myocardial infarction delayed the wound healing process leading to increased incidence of cardiac rupture and enhanced maladaptive remodeling long-term (Hwang et al., 2001). These confounding studies demonstrate the increasingly appreciated pleiotropic nature of many cytokines including the IL-1 family.

INTERLEUKIN-6

IL-6 has been extensively characterized for its role in increasing fibroblast proliferation and myocardial fibrosis (Banerjee et al., 2009). It is a member of a family of structurally related cytokines including oncostatin-M and cartotrophin-1 that have overlapping functions. IL-6 effects most cells of the heart. In cardiomyocytes, IL-6 protects cells from death and promotes hypertrophy (Sano et al., 2000; Smart et al., 2006). Inhibition of IL-6 diminishes acute immune cell recruitment (Muller et al., 2014). Lack of IL-6 protects the heart from fibrosis in several models of heart failure (Gonzalez et al., 2015; Zhang et al., 2016).

INTERLEUKIN-10

IL-10 is upregulated in the injured heart (Frangogiannis et al., 2000a). It is produced primarily by activated Th2 cells and monocytes that have anti-inflammatory properties (Frangogiannis et al., 2000a). In macrophages, IL-10 suppresses the synthesis of pro-inflammatory cytokines and chemokines such as IL-1, IL-6, and TNF-α (Fiorentino et al., 1991). It can also regulate ECM remodeling through the regulation of MMPs and TIMPs (Lacraz et al., 1995). IL-10 knockout mice have increased mortality and enhanced inflammation in response to ischemia/reperfusion injury (Yang et al., 2000). Since IL-10 is increased at later time points following myocardial infarction and has potent anti-inflammatory effects, it would be anticipated that IL-10 might play an important role in the resolution of inflammation. However, studies have been conflicting. Studies using IL-10 knockout mice showed that, while mice have augmented acute inflammatory responses, resolution of inflammation was unchanged (Zymek et al., 2007).

TUMOR-NECROSIS FACTOR

TNF-α is a pleiotropic cytokine capable of effecting all cell types involved in cardiac injury and repair. It is able to suppress cardiac contractility and augment cardiomyocyte apoptosis (Finkel et al., 1992; Yokoyama et al., 1993). Secretion by various cell types involved in remodeling enhances production of pro-inflammatory cytokines, chemokines and adhesion molecules by immune cells. TNF-α can also effect ECM metabolism through its ability to decreased collagen synthesis in fibroblasts and enhance MMP activity (Siwik et al., 2000). While these findings and studies showing that TNF-α knockout mice have decreased inflammation and improvements in cardiac remodeling and function following myocardial infarction suggest TNF-α neutralization would be beneficial in the injured heart, this has not been the case (Maekawa et al., 2002; Berthonneche et al., 2004; Sugano et al., 2004; Sun et al., 2004). Inhibiting TNF-α through gene therapy to express the soluble TNF receptor produced deleterious effects in a mouse model of myocardial infarction through increased incidence of cardiac rupture and augmented cardiac remodeling (Monden et al., 2007b). Genetic deletion of TNFR1/TNFR2 produced increased infarct size and enhanced cardiomyocyte apoptosis following myocardial infarction (Kurrelmeyer et al., 2000). These findings have been proposed to be due to distinct TNF-α effects through different receptor subtypes (Monden et al., 2007a), but may also be attributed to the complex nature of TNF-α signaling on biological processes in the heart.

INTERFERONS

Interferons (IFN) can be secreted by immune cells or fibroblasts to effect a wide array of biological responses (Noppert et al., 2007; Ivashkiv and Donlin, 2014). IFN-γ knockout mice have a reduction in the myofibroblast marker α-smooth muscle actin following angiotensin II administration (Han et al., 2012). Similarly, mice lacking the INF-γ receptor have decreased cardiac hypertrophy and fibrosis along with reductions in macrophage and T cell infiltration following angiotensin II infusion (Marko et al., 2012). However, these studies used global knockout mice and fail to determine the specific cardiac contribution of immune cells compared to fibroblasts.

TRANSFORMING GROWTH FACTOR FAMILY

TGF-β1 has been proposed to be a master regulator in the transition from inflammation to repair in the damaged heart (Dobaczewski et al., 2011). Neutralization of TGF-β1 worsens cardiac dysfunction and prolongs inflammation in a model of myocardial infarction (Ikeuchi et al., 2004). However, cardiomyocyte-specific knockout of TGF-β receptors is protective and promotes anti-inflammatory and cytoprotective signaling (Rainer et al., 2014). These studies suggest that the detrimental effects of loss of TGF-β1 signaling is not likely through directly impacting cardiomyocytes, but though loss of anti-inflammatory actions and fibrosis. In addition to its role in suppressing inflammation and promoting reparative immune responses, TGF-β1 is critical for myofibroblast transdifferentiation (Hashimoto et al., 2001; Wang et al., 2005; Dobaczewski et al., 2010a).

Growth differentiation factor-15 (GDF-15) is also a member of the TGF-β family that has been implicated in suppression of inflammation after myocardial infarction. GDF-15 counteracts integrin activation on leukocytes to curb pro-inflammatory responses (Kempf et al., 2011). Knockout of GDF-15 in mice augments inflammation and increases cardiac rupture following myocardial infarction (Kempf et al., 2011). This is also reflected in the patient population where patients with elevated plasma GDF-15 are prone to increased mortality (Kempf et al., 2007).

CLINICAL PERSPECTIVES

Currently approved heart failure therapies target the short-term clinical status to minimize symptoms and improve quality of life, but long-term prognosis remains poor (Machaj et al., 2019). Treatments aimed at preventing the progression of heart failure or reversing maladaptive remodeling are an attractive target, but have culminated in minimal success. Due to the involvement of inflammation in all stages of disease progression, targeting the immune response has been an ongoing area of interest to address this unmet clinical need. In the past two decades the field of cardiac inflammation has made numerous ventures into clinical trials targeting inflammatory pathways. To date, cytokine-targeted therapies have dominated with clinical trials targeting TNF-α and IL-1β (Murphy et al., 2020).

Early studies identified TNF-α as a potential therapeutic target due to its known role as a pro-inflammatory mediator in heart failure. To date, several randomized, placebo-controlled, anti-TNF-α studies have been performed. The RENEWAL trial (Randomized Etanercept Worldwide Evaluation), testing etanercept, and the ATTACH trial (Anti-TNF-α Therapy Against Congestive Heart Failure), involving infliximab, showed no indication of beneficial effects with treatment and the ATTACH trial exposed adverse effects of anti-TNF-α therapy (Bozkurt et al., 2001; Chung et al., 2003; Mann et al., 2004). These initial studies targeting the inflammatory response demonstrate our lack of understanding and under appreciation of the complexity of immune system involvement in heart failure. TNF-α is a widely expressed cytokine with pleotropic actions. This includes a protective role in cardiomyocytes by preventing death (Kurrelmeyer et al., 2000; Evans et al., 2018). Appropriate TNF-α levels may also be necessary for adequate tissue remodeling and repair (Anker and Coats, 2002).

IL-1β is another potential cytokine target for the treatment of heart failure due to its up-regulation in heart failure, role in pro-inflammatory responses and positive benefits from IL-1β inhibition in preclinical trials (Van Tassell et al., 2015). The CANTOS trial (Canakinumab Anti-Inflammatory Thrombosis Outcome Study) was a randomized, double-blinded, placebo-controlled, anti-IL-1β study investigating the use of the

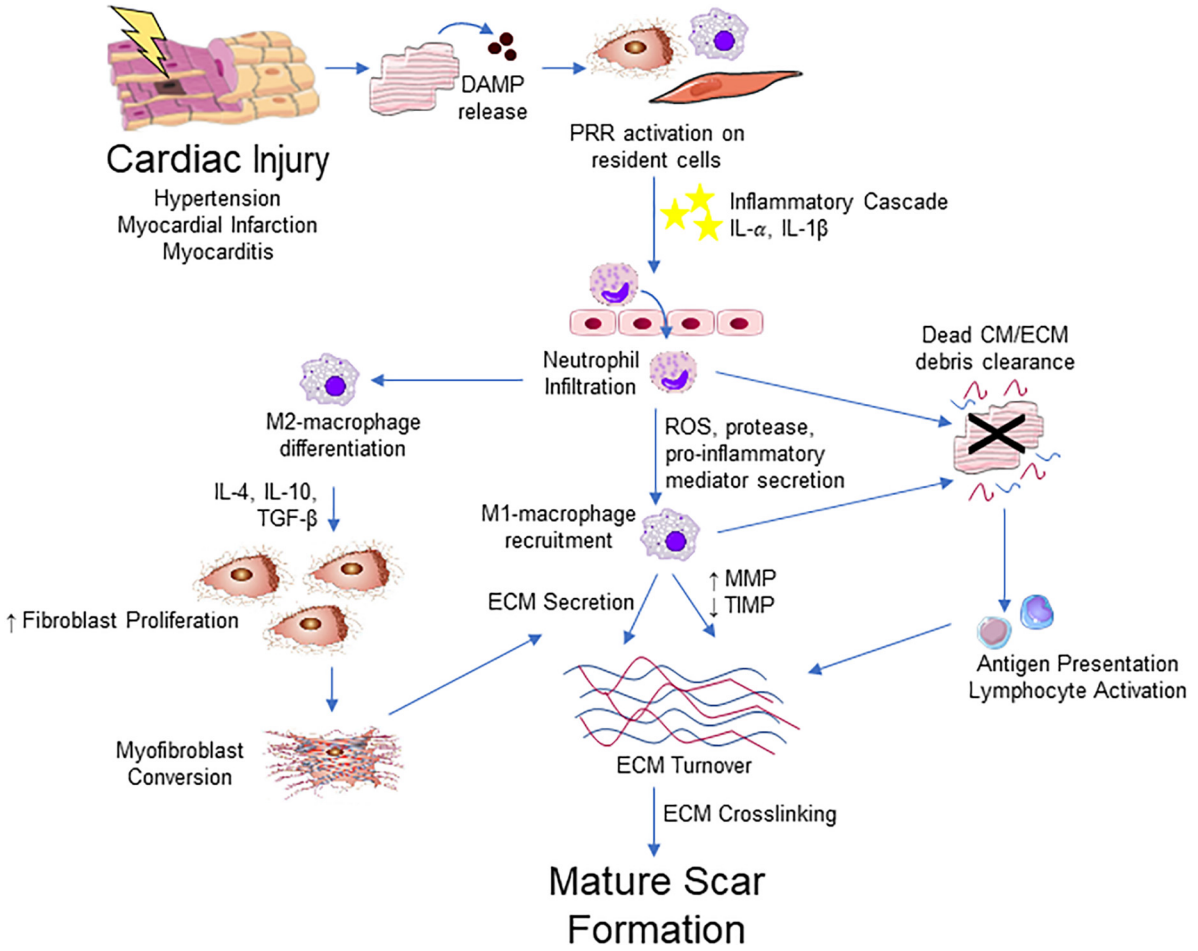

FIGURE 4 | Integrative schematic of inflammation and cardiac fibrosis. After a cardiac insult, the release of DAMPs from dying or damaged cardiomyocytes (CM) triggers an inflammatory cascade through PRRs expressed on resident fibroblast, endothelial, mast cell, macrophage and other immune cell populations in the heart. This results in the cytokine/chemokine-mediated infiltration of the immune cells, initially neutrophils then Ly-6C^{high} monocytes that contribute to an increase in M1-like macrophages into the myocardium. M1-like macrophages and neutrophils contribute to clearance of dead cells and ECM debris through phagocytosis. Macrophages also contribute to ECM remodeling through the production of collagen and other ECM components and ECM turnover though the regulation of MMPs and TIMPs. Macrophage engulfment of apoptotic neutrophils promotes and M2-like phenotype, which promotes the proliferation and migration of fibroblast and promotes differentiation into myofibroblast, primarily through the action of TGF-β. Antigen presentation by phagocytic cells activate T lymphocyte populations that contribute to fibrosis through poorly defined mechanisms. Myofibroblasts are the major source of ECM components and contribute to remodeling of the ECM. The fibrotic response concludes with ECM crosslinking and the apoptosis or quiescence of immune cells and myofibroblasts, producing a mature scar.

monoclonal antibody canakinumab (Ridker et al., 2017). All doses tested had a positive impact on inflammatory burden as indicated by C-reactive protein. However, only the highest dose examined (150 mg) was successful in reducing one of the primary end points of the study, reoccurrence of non-fatal MI, with no changes in other end points including stroke or cardiovascular death.

The ACCLAIM trial (Advanced Chronic Heart Failure Clinical Assessment of Immune Modulation Therapy) was a double-blinded, placebo-controlled study using a device-based non-specific immunomodulation therapy approach (Torre-Amione et al., 2008). This study did not find a significant reduction in cardiovascular hospitalization or mortality. However, in certain populations, those without a previous myocardial infarction and New York Heart Association (NYHA) II heart failure, significant reductions in primary endpoints were observed, suggesting that this approach may be beneficial in certain groups. Important to note, the mechanisms of immunomodulation are not well defined and the impact on cytokine levels were not measured making the findings difficult to interpret at a mechanistic level.

The clinical trials targeting inflammation for the treatment of heart failure, with the exception of the CANTOS trial (anti-IL-1β), have been largely disappointing (Van Tassell et al., 2015). However, to date, strategies have broadly targeted inflammation through either a generic approach or inhibition of cytokines that have an array of functions on many cell types. It is also important to note that these studies involve subsets of heart failure patients and it should not be discounted that these approaches may be valuable in certain patient populations such as inflammatory

cardiomyopathies. These findings highlight our need for a better understanding of how inflammation contributes to the pathogenesis of heart failure. More recent preclinicial studies targeting a specific signaling pathways and cell populations give hope for future immunomodulatory therapies for the treatment of heart failure. The CCL2/CCR2 axis that is important for infiltrating pro-inflammatory monocytes has be targeting using small molecular antagonists (Hilgendorf et al., 2014; Grisanti et al., 2016; Liao et al., 2018; Patel et al., 2018), antibodies (Patel et al., 2018), small interfering RNA (Leuschner et al., 2011), lipid micelles containing CCR2 antagonists (Wang et al., 2018), and microparticles (Getts et al., 2014). Antibody-depletion based approaches targeting lymphocyte populations including CD3 and CD4 antibodies for T cell (Nevers et al., 2015; Bansal et al., 2017), CD25 for regulatory T cell (Bansal et al., 2019) and CD22 for B cell (Cordero-Reyes et al., 2016) depletion all display promise. However, if these and other preclinical studies translate in humans remains to be seen.

THE IMPACT OF INFLAMMATION ON FIBROSIS

It should be apparent that inflammation is a major regulator of the reparative response after cardiac injury (**Figure 4**). Inflammatory cells, such as neutrophils and macrophages, infiltrate to the site of injury where they release numerous pro-inflammatory mediators including tumor necrosis factor (TNF)-α, interleukin (IL)-1β and IL-6. These cytokines play an important role in the induction of resident fibroblast proliferation and activation of myofibroblasts initiating the production of ECM components (Christia et al., 2013). In turn, activated cardiac fibroblasts upregulate various cytokine and growth factors to influence healing via autocrine and paracrine-dependent mechanisms (Zhao and Eghbali-Webb, 2001).

Monocytes/macrophages play an important role in the fibrotic response following injury. While it is now recognized that the historical view of macrophage polarization into M1 and M2 phenotypes is an oversimplification and there are several differentiation states that are dynamic in response to changes in the environmental milieu (Xue et al., 2014), these distinct populations play unique roles in their modulation of fibrosis. Macrophage-derived TGF-β induces migration, growth and activation of fibroblasts and promotes collagen synthesis (Fine and Goldstein, 1987; Clark et al., 1997; Acharya et al., 2008). Macrophages also represent an important source of MMPs and TIMPs that influence matrix degradation (Huang et al., 2012; Khokha et al., 2013). MMPs are also involved in the control of chemokines to influence inflammatory responses (Van den Steen et al., 2000; Dean et al., 2008; Song et al., 2013).

During the proliferative phase of cardiac repair, cardiac fibroblast populations undergo expansion and conversion to myofibroblasts (Travers et al., 2016). The conversion of macrophages to a reparative phenotype promotes the recruitment and expansion of fibroblasts through the secretion of pro-fibrotic factors (Bajpai et al., 2018). These macrophages and recruited lymphocyte populations contribute to the activation of fibroblasts into a myofibroblast phenotype through cytokine release of factors such as TGF-β (Dobaczewski et al., 2011). Myofibroblasts, in turn, generate large amounts of ECM to repair the damaged heart (Travers et al., 2016).

The interplay between the immune and fibrotic response is extremely interconnected. Immune cells regulate all aspects of fibroblast biology and fibroblasts, in turn, regulate immune cell recruitment, activation and function. Dissecting the role of the various mediators has proven to be difficult due to the pleiotropic nature of many of these factors and their context-dependent and cell type-dependent nature. Furthermore, lack of cell type specific markers has hampered progress. Understanding the relationship between inflammation and cardiac remodeling is an important avenue of study due to its importance for recovery and represent a significant potential area of therapeutic intervention.

AUTHOR CONTRIBUTIONS

TT and LG designed the topic, collected the references, wrote the text, and revised the manuscript. Both authors contributed to the article and approved the submitted version.

FUNDING

This work was supported by an American Heart Association Scientific Development Grant 17SDG33400114 (LG).

ACKNOWLEDGMENTS

Figures were created using Servier Medical Art templates, and are licensed under Creative Commons Attribution 3.0 Uniported License (https://smart.servier.com).

REFERENCES

Abe, R., Donnelly, S. C., Peng, T., Bucala, R., and Metz, C. N. (2001). Peripheral blood fibrocytes: differentiation pathway and migration to wound sites. *J. Immunol.* 166, 7556–7562. doi: 10.4049/jimmunol.166.12.7556

Acharya, P. S., Majumdar, S., Jacob, M., Hayden, J., Mrass, P., Weninger, W., et al. (2008). Fibroblast migration is mediated by CD44-dependent TGF beta activation. *J. Cell Sci.* 121(Pt 9), 1393–1402. doi: 10.1242/jcs.021683

Adamo, L., Rocha-Resende, C., and Mann, D. L. (2020). The emerging role of b lymphocytes in cardiovascular disease. *Annu. Rev. Immunol.* 38, 99–121. doi: 10.1146/annurev-immunol-042617-053104

Adamo, L., Staloch, L. J., Rocha-Resende, C., Matkovich, S. J., Jiang, W., Bajpai, G., et al. (2018). Modulation of subsets of cardiac B lymphocytes improves cardiac function after acute injury. *JCI Insight.* 3:e120137.

Akira, S., and Takeda, K. (2004). Toll-like receptor signalling. *Nat. Rev. Immunol.* 4, 499–511.

Alard, J. E., Ortega-Gomez, A., Wichapong, K., Bongiovanni, D., Horckmans, M., Megens, R. T., et al. (2015). Recruitment of classical monocytes can be inhibited by disturbing heteromers of neutrophil HNP1 and platelet CCL5. *Sci. Transl. Med.* 7:317ra196. doi: 10.1126/scitranslmed.aad5330

Ali, M., Pulli, B., Courties, G., Tricot, B., Sebas, M., Iwamoto, Y., et al. (2016). Myeloperoxidase inhibition improves ventricular function and remodeling

after experimental myocardial infarction. *JACC Basic Transl. Sci.* 1, 633–643. doi: 10.1016/j.jacbts.2016.09.004

Ali, S. R., Ranjbarvaziri, S., Talkhabi, M., Zhao, P., Subat, A., Hojjat, A., et al. (2014). Developmental heterogeneity of cardiac fibroblasts does not predict pathological proliferation and activation. *Circ. Res.* 115, 625–635. doi: 10.1161/circresaha.115.303794

Amador, C. A., Barrientos, V., Pena, J., Herrada, A. A., Gonzalez, M., Valdes, S., et al. (2014). Spironolactone decreases DOCA-salt-induced organ damage by blocking the activation of T helper 17 and the downregulation of regulatory T lymphocytes. *Hypertension* 63, 797–803. doi: 10.1161/hypertensionaha.113.02883

Anderson, K. R., Sutton, M. G., and Lie, J. T. (1979). Histopathological types of cardiac fibrosis in myocardial disease. *J. Pathol.* 128, 79–85. doi: 10.1002/path.1711280205

Anker, S. D., and Coats, A. J. (2002). How to RECOVER from RENAISSANCE? The significance of the results of RECOVER, RENAISSANCE, RENEWAL and ATTACH. *Int. J. Cardiol.* 86, 123–130. doi: 10.1016/s0167-5273(02)00470-9

Anzai, A., Anzai, T., Nagai, S., Maekawa, Y., Naito, K., Kaneko, H., et al. (2012). Regulatory role of dendritic cells in postinfarction healing and left ventricular remodeling. *Circulation* 125, 1234–1245. doi: 10.1161/circulationaha.111.052126

Bajpai, G., Schneider, C., Wong, N., Bredemeyer, A., Hulsmans, M., Nahrendorf, M., et al. (2018). The human heart contains distinct macrophage subsets with divergent origins and functions. *Nat. Med.* 24, 1234–1245. doi: 10.1038/s41591-018-0059-x

Banerjee, I., Fuseler, J. W., Intwala, A. R., and Baudino, T. A. (2009). IL-6 loss causes ventricular dysfunction, fibrosis, reduced capillary density, and dramatically alters the cell populations of the developing and adult heart. *Am. J. Physiol. Heart Circ. Physiol.* 296, H1694–H1704.

Banerjee, I., Fuseler, J. W., Price, R. L., Borg, T. K., and Baudino, T. A. (2007). Determination of cell types and numbers during cardiac development in the neonatal and adult rat and mouse. *Am. J. Physiol. Heart Circ. Physiol.* 293, H1883–H1891.

Bansal, S. S., Ismahil, M. A., Goel, M., Patel, B., Hamid, T., Rokosh, G., et al. (2017). Activated T lymphocytes are essential drivers of pathological remodeling in ischemic heart failure. *Circ. Heart Fail.* 10:e003688.

Bansal, S. S., Ismahil, M. A., Goel, M., Zhou, G., Rokosh, G., Hamid, T., et al. (2019). Dysfunctional and proinflammatory regulatory T-Lymphocytes are essential for adverse cardiac remodeling in ischemic cardiomyopathy. *Circulation* 139, 206–221. doi: 10.1161/circulationaha.118.036065

Benjamin, E. J., Muntner, P., Alonso, A., Bittencourt, M. S., Callaway, C. W., Carson, A. P., et al. (2019). Heart disease and stroke statistics-2019 update: a report from the american heart association. *Circulation* 139, e56–e528.

Berthonneche, C., Sulpice, T., Boucher, F., Gouraud, L., de Leiris, J., O'Connor, S. E., et al. (2004). New insights into the pathological role of TNF-alpha in early cardiac dysfunction and subsequent heart failure after infarction in rats. *Am. J. Physiol. Heart Circ. Physiol.* 287, H340–H350.

Bliksoen, M., Mariero, L. H., Torp, M. K., Baysa, A., Ytrehus, K., Haugen, F., et al. (2016). Extracellular mtDNA activates NF-kappaB via toll-like receptor 9 and induces cell death in cardiomyocytes. *Basic Res. Cardiol.* 111:42.

Blomer, N., Pachel, C., Hofmann, U., Nordbeck, P., Bauer, W., Mathes, D., et al. (2013). 5-Lipoxygenase facilitates healing after myocardial infarction. *Basic Res. Cardiol.* 108:367.

Booz, G. W., and Baker, K. M. (1995). Molecular signalling mechanisms controlling growth and function of cardiac fibroblasts. *Cardiovasc. Res.* 30, 537–543. doi: 10.1016/0008-6363(96)88507-5

Boufenzer, A., Lemarie, J., Simon, T., Derive, M., Bouazza, Y., Tran, N., et al. (2015). TREM-1 mediates inflammatory injury and cardiac remodeling following myocardial infarction. *Circ. Res.* 116, 1772–1782. doi: 10.1161/circresaha.116.305628

Bozkurt, B., Torre-Amione, G., Warren, M. S., Whitmore, J., Soran, O. Z., Feldman, A. M., et al. (2001). Results of targeted anti-tumor necrosis factor therapy with etanercept (ENBREL) in patients with advanced heart failure. *Circulation* 103, 1044–1047. doi: 10.1161/01.cir.103.8.1044

Bucala, R., Spiegel, L. A., Chesney, J., Hogan, M., and Cerami, A. (1994). Circulating fibrocytes define a new leukocyte subpopulation that mediates tissue repair. *Mol. Med.* 1, 71–81. doi: 10.1007/bf03403533

Bujak, M., Dobaczewski, M., Chatila, K., Mendoza, L. H., Li, N., Reddy, A., et al. (2008). Interleukin-1 receptor type I signaling critically regulates infarct healing and cardiac remodeling. *Am. J. Pathol.* 173, 57–67. doi: 10.2353/ajpath.2008.070974

Burt, J. R., Zimmerman, S. L., Kamel, I. R., Halushka, M., and Bluemke, D. A. (2014). Myocardial T1 mapping: techniques and potential applications. *Radiographics* 34, 377–395. doi: 10.1148/rg.342125121

Caforio, A. L., Calabrese, F., Angelini, A., Tona, F., Vinci, A., Bottaro, S., et al. (2007). A prospective study of biopsy-proven myocarditis: prognostic relevance of clinical and aetiopathogenetic features at diagnosis. *Eur. Heart J.* 28, 1326–1333. doi: 10.1093/eurheartj/ehm076

Camelliti, P., Borg, T. K., and Kohl, P. (2005). Structural and functional characterisation of cardiac fibroblasts. *Cardiovasc. Res.* 65, 40–51. doi: 10.1016/j.cardiores.2004.08.020

Chan, C. T., Sobey, C. G., Lieu, M., Ferens, D., Kett, M. M., Diep, H., et al. (2015). Obligatory role for B cells in the development of angiotensin II-dependent hypertension. *Hypertension* 66, 1023–1033. doi: 10.1161/hypertensionaha.115.05779

Chen, W., Saxena, A., Li, N., Sun, J., Gupta, A., Lee, D. W., et al. (2012). Endogenous IRAK-M attenuates postinfarction remodeling through effects on macrophages and fibroblasts. *Arterioscler. Thromb. Vasc. Biol.* 32, 2598–2608. doi: 10.1161/atvbaha.112.300310

Choy, D. F., Hart, K. M., Borthwick, L. A., Shikotra, A., Nagarkar, D. R., Siddiqui, S., et al. (2015). TH2 and TH17 inflammatory pathways are reciprocally regulated in asthma. *Sci. Transl. Med.* 7:301ra129.

Christia, P., Bujak, M., Gonzalez-Quesada, C., Chen, W., Dobaczewski, M., Reddy, A., et al. (2013). Systematic characterization of myocardial inflammation, repair, and remodeling in a mouse model of reperfused myocardial infarction. *J. Histochem. Cytochem.* 61, 555–570. doi: 10.1369/0022155413493912

Chung, E. S., Packer, M., Lo, K. H., Fasanmade, A. A., Willerson, J. T., and Anti, T. N. F. T. A. C. H. F. I. (2003). Randomized, double-blind, placebo-controlled, pilot trial of infliximab, a chimeric monoclonal antibody to tumor necrosis factor-alpha, in patients with moderate-to-severe heart failure: results of the anti-TNF therapy against congestive heart failure (ATTACH) trial. *Circulation* 107, 3133–3140. doi: 10.1161/01.cir.0000077913.60364.d2

Ciz, M., Denev, P., Kratchanova, M., Vasicek, O., Ambrozova, G., and Lojek, A. (2012). Flavonoids inhibit the respiratory burst of neutrophils in mammals. *Oxid. Med. Cell Longev.* 2012:181295.

Clark, R. A., McCoy, G. A., Folkvord, J. M., and McPherson, J. M. (1997). TGF-beta 1 stimulates cultured human fibroblasts to proliferate and produce tissue-like fibroplasia: a fibronectin matrix-dependent event. *J. Cell Physiol.* 170, 69–80. doi: 10.1002/(sici)1097-4652(199701)170:1<69::aid-jcp8>3.0.co;2-j

Cleutjens, J. P., Kandala, J. C., Guarda, E., Guntaka, R. V., and Weber, K. T. (1995a). Regulation of collagen degradation in the rat myocardium after infarction. *J. Mol. Cell. Cardiol.* 27, 1281–1292. doi: 10.1016/s0022-2828(05)82390-9

Cleutjens, J. P., Verluyten, M. J., Smiths, J. F., and Daemen, M. J. (1995b). Collagen remodeling after myocardial infarction in the rat heart. *Am. J. Pathol.* 147, 325–338.

Cooper, L. T. Jr. (2009). Myocarditis. *N. Engl. J. Med.* 360, 1526–1538.

Cordero-Reyes, A. M., Youker, K. A., Trevino, A. R., Celis, R., Hamilton, D. J., Flores-Arredondo, J. H., et al. (2016). Full expression of cardiomyopathy is partly dependent on B-cells: a pathway that involves cytokine activation, immunoglobulin deposition, and activation of apoptosis. *J. Am. Heart Assoc.* 5, e002484.

Dean, R. A., Cox, J. H., Bellac, C. L., Doucet, A., Starr, A. E., and Overall, C. M. (2008). Macrophage-specific metalloelastase (MMP-12) truncates and inactivates ELR+ CXC chemokines and generates CCL2, -7, -8, and -13 antagonists: potential role of the macrophage in terminating polymorphonuclear leukocyte influx. *Blood* 112, 3455–3464. doi: 10.1182/blood-2007-12-129080

Detillieux, K. A., Sheikh, F., Kardami, E., and Cattini, P. A. (2003). Biological activities of fibroblast growth factor-2 in the adult myocardium. *Cardiovasc. Res.* 57, 8–19. doi: 10.1016/s0008-6363(02)00708-3

Detmers, P. A., Lo, S. K., Olsen-Egbert, E., Walz, A., Baggiolini, M., and Cohn, Z. A. (1990). Neutrophil-activating protein 1/interleukin 8 stimulates the binding activity of the leukocyte adhesion receptor CD11b/CD18 on human neutrophils. *J. Exp. Med.* 171, 1155–1162. doi: 10.1084/jem.171.4.1155

Devi, S., Wang, Y., Chew, W. K., Lima, R., Gonzalez, N. A., Mattar, C. N., et al. (2013). Neutrophil mobilization via plerixafor-mediated CXCR4 inhibition arises from lung demargination and blockade of neutrophil homing to the bone marrow. *J. Exp. Med.* 210, 2321–2336. doi: 10.1084/jem.20130056

Dewald, O., Zymek, P., Winkelmann, K., Koerting, A., Ren, G., Abou-Khamis, T., et al. (2005). CCL2/monocyte chemoattractant Protein-1 regulates inflammatory responses critical to healing myocardial infarcts. *Circ. Res.* 96, 881–889. doi: 10.1161/01.res.0000163017.13772.3a

Diaz-Araya, G., Vivar, R., Humeres, C., Boza, P., Bolivar, S., and Munoz, C. (2015). Cardiac fibroblasts as sentinel cells in cardiac tissue: receptors, signaling pathways and cellular functions. *Pharmacol. Res.* 101, 30–40. doi: 10.1016/j.phrs.2015.07.001

Dieterlen, M. T., John, K., Reichenspurner, H., Mohr, F. W., and Barten, M. J. (2016). Dendritic cells and their role in cardiovascular diseases: a view on human studies. *J. Immunol. Res.* 2016:5946807.

Dobaczewski, M., Bujak, M., Li, N., Gonzalez-Quesada, C., Mendoza, L. H., Wang, X. F., et al. (2010a). Smad3 signaling critically regulates fibroblast phenotype and function in healing myocardial infarction. *Circ. Res.* 107, 418–428. doi: 10.1161/circresaha.109.216101

Dobaczewski, M., Xia, Y., Bujak, M., Gonzalez-Quesada, C., and Frangogiannis, N. G. (2010b). CCR5 signaling suppresses inflammation and reduces adverse remodeling of the infarcted heart, mediating recruitment of regulatory T cells. *Am. J. Pathol.* 176, 2177–2187. doi: 10.2353/ajpath.2010.090759

Dobaczewski, M., Chen, W., and Frangogiannis, N. G. (2011). Transforming growth factor (TGF)-beta signaling in cardiac remodeling. *J. Mol. Cell Cardiol.* 51, 600–606. doi: 10.1016/j.yjmcc.2010.10.033

Drummond, G. R., Vinh, A., Guzik, T. J., and Sobey, C. G. (2019). Immune mechanisms of hypertension. *Nat. Rev. Immunol.* 19, 517–532.

Entman, M. L., Youker, K., Shoji, T., Kukielka, G., Shappell, S. B., Taylor, A. A., et al. (1992). Neutrophil induced oxidative injury of cardiac myocytes. A compartmented system requiring CD11b/CD18-ICAM-1 adherence. *J. Clin. Invest.* 90, 1335–1345. doi: 10.1172/jci115999

Epelman, S., Lavine, K. J., Beaudin, A. E., Sojka, D. K., Carrero, J. A., Calderon, B., et al. (2014). Embryonic and adult-derived resident cardiac macrophages are maintained through distinct mechanisms at steady state and during inflammation. *Immunity* 40, 91–104. doi: 10.1016/j.immuni.2013.11.019

Evans, S., Tzeng, H. P., Veis, D. J., Matkovich, S., Weinheimer, C., Kovacs, A., et al. (2018). TNF receptor-activated factor 2 mediates cardiac protection through noncanonical NF-kappaB signaling. *JCI Insight.* 3:e98278.

Fertin, C., Nicolas, J. F., Gillery, P., Kalis, B., Banchereau, J., and Maquart, F. X. (1991). Interleukin-4 stimulates collagen synthesis by normal and scleroderma fibroblasts in dermal equivalents. *Cell Mol. Biol.* 37, 823–829.

Fildes, J. E., Shaw, S. M., Yonan, N., and Williams, S. G. (2009). The immune system and chronic heart failure: is the heart in control? *J. Am. Coll. Cardiol.* 53, 1013–1020.

Fine, A., and Goldstein, R. H. (1987). The effect of transforming growth factor-beta on cell proliferation and collagen formation by lung fibroblasts. *J. Biol. Chem.* 262, 3897–3902.

Finkel, M. S., Oddis, C. V., Jacob, T. D., Watkins, S. C., Hattler, B. G., and Simmons, R. L. (1992). Negative inotropic effects of cytokines on the heart mediated by nitric oxide. *Science* 257, 387–389. doi: 10.1126/science.1631560

Fiorentino, D. F., Zlotnik, A., Mosmann, T. R., Howard, M., and O'Garra, A. (1991). IL-10 inhibits cytokine production by activated macrophages. *J. Immunol.* 147, 3815–3822.

Frangogiannis, N. G., Burns, A. R., Michael, L. H., and Entman, M. L. (1999). Histochemical and morphological characteristics of canine cardiac mast cells. *Histochem. J.* 31, 221–229.

Frangogiannis, N. G., Lindsey, M. L., Michael, L. H., Youker, K. A., Bressler, R. B., Mendoza, L. H., et al. (1998a). Resident cardiac mast cells degranulate and release preformed TNF-alpha, initiating the cytokine cascade in experimental canine myocardial ischemia/reperfusion. *Circulation* 98, 699–710. doi: 10.1161/01.cir.98.7.699

Frangogiannis, N. G., Perrard, J. L., Mendoza, L. H., Burns, A. R., Lindsey, M. L., Ballantyne, C. M., et al. (1998b). Stem cell factor induction is associated with mast cell accumulation after canine myocardial ischemia and reperfusion. *Circulation* 98, 687–698. doi: 10.1161/01.cir.98.7.687

Frangogiannis, N. G., Mendoza, L. H., Lindsey, M. L., Ballantyne, C. M., Michael, L. H., Smith, C. W., et al. (2000a). IL-10 is induced in the reperfused myocardium and may modulate the reaction to injury. *J. Immunol.* 165, 2798–2808. doi: 10.4049/jimmunol.165.5.2798

Frangogiannis, N. G., Michael, L. H., and Entman, M. L. (2000b). Myofibroblasts in reperfused myocardial infarcts express the embryonic form of smooth muscle myosin heavy chain (SMemb). *Cardiovasc. Res.* 48, 89–100. doi: 10.1016/s0008-6363(00)00158-9

Franken, L., Schiwon, M., and Kurts, C. (2016). Macrophages: sentinels and regulators of the immune system. *Cell Microbiol.* 18, 475–487. doi: 10.1111/cmi.12580

Frantz, S., Kobzik, L., Kim, Y. D., Fukazawa, R., Medzhitov, R., Lee, R. T., et al. (1999). Toll4 (TLR4) expression in cardiac myocytes in normal and failing myocardium. *J. Clin. Invest.* 104, 271–280. doi: 10.1172/jci6709

Fredj, S., Bescond, J., Louault, C., and Potreau, D. (2005). Interactions between cardiac cells enhance cardiomyocyte hypertrophy and increase fibroblast proliferation. *J. Cell Physiol.* 202, 891–899. doi: 10.1002/jcp.20197

Freed, D. H., Chilton, L., Li, Y., Dangerfield, A. L., Raizman, J. E., Rattan, S. G., et al. (2011). Role of myosin light chain kinase in cardiotrophin-1-induced cardiac myofibroblast cell migration. *Am. J. Physiol. Heart Circ. Physiol.* 301, H514–H522.

Fung, G., Luo, H., Qiu, Y., Yang, D., and McManus, B. (2016). Myocarditis. *Circ. Res.* 118, 496–514.

Geering, B., Stoeckle, C., Conus, S., and Simon, H. U. (2013). Living and dying for inflammation: neutrophils, eosinophils, basophils. *Trends Immunol.* 34, 398–409. doi: 10.1016/j.it.2013.04.002

Getts, D. R., Terry, R. L., Getts, M. T., Deffrasnes, C., Muller, M., van Vreden, C., et al. (2014). Therapeutic inflammatory monocyte modulation using immune-modifying microparticles. *Sci. Transl. Med.* 6:219ra7. doi: 10.1126/scitranslmed.3007563

Gittenberger-de Groot, A. C., Vrancken Peeters, M. P., Mentink, M. M., Gourdie, R. G., and Poelmann, R. E. (1998). Epicardium-derived cells contribute a novel population to the myocardial wall and the atrioventricular cushions. *Circ. Res.* 82, 1043–1052. doi: 10.1161/01.res.82.10.1043

Gondokaryono, S. P., Ushio, H., Niyonsaba, F., Hara, M., Takenaka, H., Jayawardana, S. T., et al. (2007). The extra domain A of fibronectin stimulates murine mast cells via toll-like receptor 4. *J. Leukoc. Biol.* 82, 657–665. doi: 10.1189/jlb.1206730

Gonzalez, G. E., Rhaleb, N. E., D'Ambrosio, M. A., Nakagawa, P., Liu, Y., Leung, P., et al. (2015). Deletion of interleukin-6 prevents cardiac inflammation, fibrosis and dysfunction without affecting blood pressure in angiotensin II-high salt-induced hypertension. *J. Hypertens.* 33, 144–152. doi: 10.1097/hjh.0000000000000358

Grisanti, L. A., Traynham, C. J., Repas, A. A., Gao, E., Koch, W. J., and Tilley, D. G. (2016). beta2-Adrenergic receptor-dependent chemokine receptor 2 expression regulates leukocyte recruitment to the heart following acute injury. *Proc. Natl. Acad. Sci. U.S.A.* 113, 15126–15131. doi: 10.1073/pnas.1611023114

Guillen, I., Blanes, M., Gomez-Lechon, M. J., and Castell, J. V. (1995). Cytokine signaling during myocardial infarction: sequential appearance of IL-1 beta and IL-6. *Am. J. Physiol.* 269(2 Pt 2), R229–R235.

Guthrie, L. A., McPhail, L. C., Henson, P. M., and Johnston, R. B. Jr. (1984). Priming of neutrophils for enhanced release of oxygen metabolites by bacterial lipopolysaccharide. Evidence for increased activity of the superoxide-producing enzyme. *J. Exp. Med.* 160, 1656–1671. doi: 10.1084/jem.160.6.1656

Guzik, T. J., Hoch, N. E., Brown, K. A., McCann, L. A., Rahman, A., Dikalov, S., et al. (2007). Role of the T cell in the genesis of angiotensin II induced hypertension and vascular dysfunction. *J. Exp. Med.* 204, 2449–2460. doi: 10.1084/jem.20070657

Han, Y. L., Li, Y. L., Jia, L. X., Cheng, J. Z., Qi, Y. F., Zhang, H. J., et al. (2012). Reciprocal interaction between macrophages and T cells stimulates IFN-gamma and MCP-1 production in Ang II-induced cardiac inflammation and fibrosis. *PLoS One* 7:e35506. doi: 10.1371/journal.pone.035506

Hara, M., Ono, K., Hwang, M. W., Iwasaki, A., Okada, M., Nakatani, K., et al. (2002). Evidence for a role of mast cells in the evolution to congestive heart failure. *J. Exp. Med.* 195, 375–381. doi: 10.1084/jem.20002036

Harrison, D. G. (2014). The immune system in hypertension. *Trans. Am. Clin. Climatol. Assoc.* 125, 130–138.

Hart, P. H., Vitti, G. F., Burgess, D. R., Whitty, G. A., Piccoli, D. S., and Hamilton, J. A. (1989). Potential antiinflammatory effects of interleukin 4: suppression of

human monocyte tumor necrosis factor alpha, interleukin 1, and prostaglandin E2. *Proc. Natl. Acad. Sci. U.S.A.* 86, 3803–3807. doi: 10.1073/pnas.86.10.3803

Hashimoto, S., Gon, Y., Takeshita, I., Matsumoto, K., Maruoka, S., and Horie, T. (2001). Transforming growth Factor-beta1 induces phenotypic modulation of human lung fibroblasts to myofibroblast through a c-Jun-NH2-terminal kinase-dependent pathway. *Am. J. Respir. Crit. Care Med.* 163, 152–157. doi: 10.1164/ajrccm.163.1.2005069

Haudek, S. B., Xia, Y., Huebener, P., Lee, J. M., Carlson, S., Crawford, J. R., et al. (2006). Bone marrow-derived fibroblast precursors mediate ischemic cardiomyopathy in mice. *Proc. Natl. Acad. Sci. U.S.A.* 103, 18284–18289. doi: 10.1073/pnas.0608799103

Heidt, T., Courties, G., Dutta, P., Sager, H. B., Sebas, M., Iwamoto, Y., et al. (2014). Differential contribution of monocytes to heart macrophages in steady-state and after myocardial infarction. *Circ. Res.* 115, 284–295. doi: 10.1161/circresaha.115.303567

Heim, A., Zeuke, S., Weiss, S., Ruschewski, W., and Grumbach, I. M. (2000). Transient induction of cytokine production in human myocardial fibroblasts by coxsackievirus B3. *Circ. Res.* 86, 753–759. doi: 10.1161/01.res.86.7.753

Herskowitz, A., Choi, S., Ansari, A. A., and Wesselingh, S. (1995). Cytokine mRNA expression in postischemic/reperfused myocardium. *Am. J. Pathol.* 146, 419–428.

Herter, J., and Zarbock, A. (2013). Integrin regulation during leukocyte recruitment. *J. Immunol.* 190, 4451–4457. doi: 10.4049/jimmunol.1203179

Hilgendorf, I., Gerhardt, L. M., Tan, T. C., Winter, C., Holderried, T. A., Chousterman, B. G., et al. (2014). Ly-6Chigh monocytes depend on Nr4a1 to balance both inflammatory and reparative phases in the infarcted myocardium. *Circ. Res.* 114, 1611–1622. doi: 10.1161/circresaha.114.303204

Hofmann, U., Beyersdorf, N., Weirather, J., Podolskaya, A., Bauersachs, J., Ertl, G., et al. (2012). Activation of CD4+ T lymphocytes improves wound healing and survival after experimental myocardial infarction in mice. *Circulation* 125, 1652–1663. doi: 10.1161/circulationaha.111.044164

Hofmann, U., Knorr, S., Vogel, B., Weirather, J., Frey, A., Ertl, G., et al. (2014). Interleukin-13 deficiency aggravates healing and remodeling in male mice after experimental myocardial infarction. *Circ. Heart Fail.* 7, 822–830. doi: 10.1161/circheartfailure.113.001020

Homma, T., Kinugawa, S., Takahashi, M., Sobirin, M. A., Saito, A., Fukushima, A., et al. (2013). Activation of invariant natural killer T cells by alpha-galactosylceramide ameliorates myocardial ischemia/reperfusion injury in mice. *J. Mol. Cell Cardiol.* 62, 179–188. doi: 10.1016/j.yjmcc.2013.06.004

Horckmans, M., Ring, L., Duchene, J., Santovito, D., Schloss, M. J., Drechsler, M., et al. (2017). Neutrophils orchestrate post-myocardial infarction healing by polarizing macrophages towards a reparative phenotype. *Eur. Heart J.* 38, 187–197.

Huang, W. C., Sala-Newby, G. B., Susana, A., Johnson, J. L., and Newby, A. C. (2012). Classical macrophage activation up-regulates several matrix metalloproteinases through mitogen activated protein kinases and nuclear factor-kappaB. *PLoS One* 7:e42507. doi: 10.1371/journal.pone.0042507

Hulsmans, M., Clauss, S., Xiao, L., Aguirre, A. D., King, K. R., Hanley, A., et al. (2017). Macrophages facilitate electrical conduction in the heart. *Cell* 169, 510–522.e10.

Hwang, M. W., Matsumori, A., Furukawa, Y., Ono, K., Okada, M., Iwasaki, A., et al. (2001). Neutralization of interleukin-1beta in the acute phase of myocardial infarction promotes the progression of left ventricular remodeling. *J. Am. Coll. Cardiol.* 38, 1546–1553. doi: 10.1016/s0735-1097(01)01591-1

Ikeuchi, M., Tsutsui, H., Shiomi, T., Matsusaka, H., Matsushima, S., Wen, J., et al. (2004). Inhibition of TGF-beta signaling exacerbates early cardiac dysfunction but prevents late remodeling after infarction. *Cardiovasc. Res.* 64, 526–535. doi: 10.1016/j.cardiores.2004.07.017

Ilatovskaya, D. V., Pitts, C., Clayton, J., Domondon, M., Troncoso, M., Pippin, S., et al. (2019). CD8(+) T-cells negatively regulate inflammation post-myocardial infarction. *Am. J. Physiol. Heart Circ. Physiol.* 317, H581–H596.

Ivashkiv, L. B., and Donlin, L. T. (2014). Regulation of type I interferon responses. *Nat. Rev. Immunol.* 14, 36–49. doi: 10.1038/nri3581

Kai, H., Mori, T., Tokuda, K., Takayama, N., Tahara, N., Takemiya, K., et al. (2006). Pressure overload-induced transient oxidative stress mediates perivascular inflammation and cardiac fibrosis through angiotensin II. *Hypertens. Res.* 29, 711–718. doi: 10.1291/hypres.29.711

Kanellakis, P., Ditiatkovski, M., Kostolias, G., and Bobik, A. (2012). A pro-fibrotic role for interleukin-4 in cardiac pressure overload. *Cardiovasc. Res.* 95, 77–85. doi: 10.1093/cvr/cvs142

Katayama, Y., Battista, M., Kao, W. M., Hidalgo, A., Peired, A. J., Thomas, S. A., et al. (2006). Signals from the sympathetic nervous system regulate hematopoietic stem cell egress from bone marrow. *Cell* 124, 407–421. doi: 10.1016/j.cell.2005.10.041

Kawaguchi, M., Takahashi, M., Hata, T., Kashima, Y., Usui, F., Morimoto, H., et al. (2011). Inflammasome activation of cardiac fibroblasts is essential for myocardial ischemia/reperfusion injury. *Circulation* 123, 594–604. doi: 10.1161/circulationaha.110.982777

Kempf, T., Bjorklund, E., Olofsson, S., Lindahl, B., Allhoff, T., Peter, T., et al. (2007). Growth-differentiation factor-15 improves risk stratification in ST-segment elevation myocardial infarction. *Eur. Heart J.* 28, 2858–2865. doi: 10.1093/eurheartj/ehm465

Kempf, T., Zarbock, A., Widera, C., Butz, S., Stadtmann, A., Rossaint, J., et al. (2011). GDF-15 is an inhibitor of leukocyte integrin activation required for survival after myocardial infarction in mice. *Nat. Med.* 17, 581–588. doi: 10.1038/nm.2354

Khokha, R., Murthy, A., and Weiss, A. (2013). Metalloproteinases and their natural inhibitors in inflammation and immunity. *Nat. Rev. Immunol.* 13, 649–665. doi: 10.1038/nri3499

Kimura, A., Ishida, Y., Furuta, M., Nosaka, M., Kuninaka, Y., Taruya, A., et al. (2018). Protective roles of interferon-gamma in cardiac hypertrophy induced by sustained pressure overload. *J. Am. Heart Assoc.* 7:e008145.

Kindermann, I., Kindermann, M., Kandolf, R., Klingel, K., Bultmann, B., Muller, T., et al. (2008). Predictors of outcome in patients with suspected myocarditis. *Circulation* 118, 639–648. doi: 10.1161/circulationaha.108.769489

Kisanuki, Y. Y., Hammer, R. E., Miyazaki, J., Williams, S. C., Richardson, J. A., and Yanagisawa, M. (2001). Tie2-Cre transgenic mice: a new model for endothelial cell-lineage analysis in vivo. *Dev. Biol.* 230, 230–242. doi: 10.1006/dbio.2000.0106

Kong, P., Christia, P., Saxena, A., Su, Y., and Frangogiannis, N. G. (2013). Lack of specificity of fibroblast-specific protein 1 in cardiac remodeling and fibrosis. *Am. J. Physiol. Heart Circ. Physiol.* 305, H1363–H1372.

Kono, H., Chen, C. J., Ontiveros, F., and Rock, K. L. (2010). Uric acid promotes an acute inflammatory response to sterile cell death in mice. *J. Clin. Invest.* 120, 1939–1949. doi: 10.1172/jci40124

Koudssi, F., Lopez, J. E., Villegas, S., and Long, C. S. (1998). Cardiac fibroblasts arrest at the G1/S restriction point in response to interleukin (IL)-1beta. Evidence for IL-1beta-induced hypophosphorylation of the retinoblastoma protein. *J. Biol. Chem.* 273, 25796–25803. doi: 10.1074/jbc.273.40.25796

Kramann, R., Schneider, R. K., DiRocco, D. P., Machado, F., Fleig, S., Bondzie, P. A., et al. (2015). Perivascular Gli1+ progenitors are key contributors to injury-induced organ fibrosis. *Cell Stem Cell* 16, 51–66. doi: 10.1016/j.stem.2014.11.004

Kukielka, G. L., Hawkins, H. K., Michael, L., Manning, A. M., Youker, K., Lane, C., et al. (1993). Regulation of intercellular adhesion molecule-1 (ICAM-1) in ischemic and reperfused canine myocardium. *J. Clin. Invest.* 92, 1504–1516. doi: 10.1172/jci116729

Kumar, A. G., Ballantyne, C. M., Michael, L. H., Kukielka, G. L., Youker, K. A., Lindsey, M. L., et al. (1997). Induction of monocyte chemoattractant protein-1 in the small veins of the ischemic and reperfused canine myocardium. *Circulation* 95, 693–700. doi: 10.1161/01.cir.95.3.693

Kurrelmeyer, K. M., Michael, L. H., Baumgarten, G., Taffet, G. E., Peschon, J. J., Sivasubramanian, N., et al. (2000). Endogenous tumor necrosis factor protects the adult cardiac myocyte against ischemic-induced apoptosis in a murine model of acute myocardial infarction. *Proc. Natl. Acad. Sci. U.S.A.* 97, 5456–5461. doi: 10.1073/pnas.070036297

Lacraz, S., Nicod, L. P., Chicheportiche, R., Welgus, H. G., and Dayer, J. M. (1995). IL-10 inhibits metalloproteinase and stimulates TIMP-1 production in human mononuclear phagocytes. *J. Clin. Invest.* 96, 2304–2310. doi: 10.1172/jci118286

Lafontant, P. J., Burns, A. R., Donnachie, E., Haudek, S. B., Smith, C. W., and Entman, M. L. (2006). Oncostatin M differentially regulates CXC chemokines in mouse cardiac fibroblasts. *Am. J. Physiol. Cell Physiol.* 291, C18–C26.

Lakshminarayanan, V., Beno, D. W., Costa, R. H., and Roebuck, K. A. (1997). Differential regulation of interleukin-8 and intercellular adhesion molecule-1

by H2O2 and tumor necrosis factor-alpha in endothelial and epithelial cells. *J. Biol. Chem.* 272, 32910–32918. doi: 10.1074/jbc.272.52.32910

Lakshminarayanan, V., Lewallen, M., Frangogiannis, N. G., Evans, A. J., Wedin, K. E., Michael, L. H., et al. (2001). Reactive oxygen intermediates induce monocyte chemotactic protein-1 in vascular endothelium after brief ischemia. *Am. J. Pathol.* 159, 1301–1311. doi: 10.1016/s0002-9440(10)62517-5

Laroumanie, F., Douin-Echinard, V., Pozzo, J., Lairez, O., Tortosa, F., Vinel, C., et al. (2014). CD4+ T cells promote the transition from hypertrophy to heart failure during chronic pressure overload. *Circulation* 129, 2111–2124. doi: 10.1161/circulationaha.113.007101

Lee, J. W., Oh, J. E., Rhee, K. J., Yoo, B. S., Eom, Y. W., Park, S. W., et al. (2019). Co-treatment with interferon-gamma and 1-methyl tryptophan ameliorates cardiac fibrosis through cardiac myofibroblasts apoptosis. *Mol. Cell Biochem.* 458, 197–205. doi: 10.1007/s11010-019-03542-7

Lefebvre, J. S., Levesque, T., Picard, S., Pare, G., Gravel, A., Flamand, L., et al. (2011). Extra domain A of fibronectin primes leukotriene biosynthesis and stimulates neutrophil migration through activation of Toll-like receptor 4. *Arthrit. Rheum.* 63, 1527–1533. doi: 10.1002/art.30308

Leuschner, F., Dutta, P., Gorbatov, R., Novobrantseva, T. I., Donahoe, J. S., Courties, G., et al. (2011). Therapeutic siRNA silencing in inflammatory monocytes in mice. *Nat. Biotechnol.* 29, 1005–1010.

Levick, S. P., McLarty, J. L., Murray, D. B., Freeman, R. M., Carver, W. E., and Brower, G. L. (2009). Cardiac mast cells mediate left ventricular fibrosis in the hypertensive rat heart. *Hypertension* 53, 1041–1047. doi: 10.1161/hypertensionaha.108.123158

Levings, M. K., and Schrader, J. W. (1999). IL-4 inhibits the production of TNF-alpha and IL-12 by STAT6-dependent and -independent mechanisms. *J. Immunol.* 162, 5224–5229.

Ley, K., Laudanna, C., Cybulsky, M. I., and Nourshargh, S. (2007). Getting to the site of inflammation: the leukocyte adhesion cascade updated. *Nat. Rev. Immunol.* 7, 678–689. doi: 10.1038/nri2156

Li, C., Sun, X. N., Zeng, M. R., Zheng, X. J., Zhang, Y. Y., Wan, Q., et al. (2017). Mineralocorticoid receptor deficiency in T cells attenuates pressure overload-induced cardiac hypertrophy and dysfunction through modulating T-cell activation. *Hypertension* 70, 137–147. doi: 10.1161/hypertensionaha.117.09070

Li, J., Schwimmbeck, P. L., Tschope, C., Leschka, S., Husmann, L., Rutschow, S., et al. (2002). Collagen degradation in a murine myocarditis model: relevance of matrix metalloproteinase in association with inflammatory induction. *Cardiovasc. Res.* 56, 235–247. doi: 10.1016/s0008-6363(02)00546-1

Li, Y., Wu, Y., Zhang, C., Li, P., Cui, W., Hao, J., et al. (2014). gammadeltaT Cell-derived interleukin-17A via an interleukin-1beta-dependent mechanism mediates cardiac injury and fibrosis in hypertension. *Hypertension* 64, 305–314. doi: 10.1161/hypertensionaha.113.02604

Li, Y., Zhang, C., Wu, Y., Han, Y., Cui, W., Jia, L., et al. (2012). Interleukin-12p35 deletion promotes CD4 T-cell-dependent macrophage differentiation and enhances angiotensin II-Induced cardiac fibrosis. *Arterioscler. Thromb. Vasc. Biol.* 32, 1662–1674. doi: 10.1161/atvbaha.112.249706

Liao, X., Shen, Y., Zhang, R., Sugi, K., Vasudevan, N. T., Alaiti, M. A., et al. (2018). Distinct roles of resident and nonresident macrophages in nonischemic cardiomyopathy. *Proc. Natl. Acad. Sci. U.S.A.* 115, E4661–E4669.

Liao, Y. H., Xia, N., Zhou, S. F., Tang, T. T., Yan, X. X., Lv, B. J., et al. (2012). Interleukin-17A contributes to myocardial ischemia/reperfusion injury by regulating cardiomyocyte apoptosis and neutrophil infiltration. *J. Am. Coll. Cardiol.* 59, 420–429. doi: 10.1016/j.jacc.2011.10.863

Lijnen, P., Papparella, I., Petrov, V., Semplicini, A., and Fagard, R. (2006). Angiotensin II-stimulated collagen production in cardiac fibroblasts is mediated by reactive oxygen species. *J. Hypertens.* 24, 757–766. doi: 10.1097/01.hjh.0000217860.04994.54

Lipps, C., Nguyen, J. H., Pyttel, L., Lynch, T. L. T., Liebetrau, C., Aleshcheva, G., et al. (2016). N-terminal fragment of cardiac myosin binding protein-C triggers pro-inflammatory responses in vitro. *J. Mol. Cell Cardiol.* 99, 47–56. doi: 10.1016/j.yjmcc.2016.09.003

Liu, T., Song, D., Dong, J., Zhu, P., Liu, J., Liu, W., et al. (2017). Current understanding of the pathophysiology of myocardial fibrosis and its quantitative assessment in heart failure. *Front. Physiol.* 8:238. doi: 10.3389/fphys.2017.00238

Liu, Y. R., Ye, W. L., Zeng, X. M., Ren, W. H., Zhang, Y. Q., and Mei, Y. A. K. (2008). + channels and the cAMP-PKA pathway modulate TGF-beta1-induced migration of rat vascular myofibroblasts. *J. Cell Physiol.* 216, 835–843. doi: 10.1002/jcp.21464

Lotze, M. T., and Tracey, K. J. (2005). High-mobility group box 1 protein (HMGB1): nuclear weapon in the immune arsenal. *Nat. Rev. Immunol.* 5, 331–342. doi: 10.1038/nri1594

Lu, D., Soleymani, S., Madakshire, R., and Insel, P. A. (2012). ATP released from cardiac fibroblasts via connexin hemichannels activates profibrotic P2Y2 receptors. *FASEB J.* 26, 2580–2591. doi: 10.1096/fj.12-204677

Machaj, F., Dembowska, E., Rosik, J., Szostak, B., Mazurek-Mochol, M., and Pawlik, A. (2019). New therapies for the treatment of heart failure: a summary of recent accomplishments. *Ther. Clin. Risk Manag.* 15, 147–155. doi: 10.2147/tcrm.s179302

Maekawa, N., Wada, H., Kanda, T., Niwa, T., Yamada, Y., Saito, K., et al. (2002). Improved myocardial ischemia/reperfusion injury in mice lacking tumor necrosis factor-alpha. *J. Am. Coll. Cardiol.* 39, 1229–1235. doi: 10.1016/s0735-1097(02)01738-2

Mann, D. L. (2011). The emerging role of innate immunity in the heart and vascular system: for whom the cell tolls. *Circ. Res.* 108, 1133–1145. doi: 10.1161/circresaha.110.226936

Mann, D. L., McMurray, J. J., Packer, M., Swedberg, K., Borer, J. S., Colucci, W. S., et al. (2004). Targeted anticytokine therapy in patients with chronic heart failure: results of the randomized etanercept worldwide evaluation (RENEWAL). *Circulation* 109, 1594–1602. doi: 10.1161/01.cir.0000124490.27666.b2

Mantovani, A., Cassatella, M. A., Costantini, C., and Jaillon, S. (2011). Neutrophils in the activation and regulation of innate and adaptive immunity. *Nat. Rev. Immunol.* 11, 519–531. doi: 10.1038/nri3024

Marko, L., Kvakan, H., Park, J. K., Qadri, F., Spallek, B., Binger, K. J., et al. (2012). Interferon-gamma signaling inhibition ameliorates angiotensin II-induced cardiac damage. *Hypertension* 60, 1430–1436. doi: 10.1161/hypertensionaha.112.199265

McDonald, B., Pittman, K., Menezes, G. B., Hirota, S. A., Slaba, I., Waterhouse, C. C., et al. (2010). Intravascular danger signals guide neutrophils to sites of sterile inflammation. *Science* 330, 362–366. doi: 10.1126/science.1195491

Merline, R., Moreth, K., Beckmann, J., Nastase, M. V., Zeng-Brouwers, J., Tralhao, J. G., et al. (2011). Signaling by the matrix proteoglycan decorin controls inflammation and cancer through PDCD4 and MicroRNA-21. *Sci. Signal.* 4:ra75. doi: 10.1126/scisignal.2001868

Mitchell, M. D., Laird, R. E., Brown, R. D., and Long, C. S. (2007). IL-1beta stimulates rat cardiac fibroblast migration via MAP kinase pathways. *Am. J. Physiol. Heart Circ. Physiol.* 292, H1139–H1147.

Mollmann, H., Nef, H. M., Kostin, S., von Kalle, C., Pilz, I., Weber, M., et al. (2006). Bone marrow-derived cells contribute to infarct remodelling. *Cardiovasc. Res.* 71, 661–671. doi: 10.1016/j.cardiores.2006.06.013

Monden, Y., Kubota, T., Inoue, T., Tsutsumi, T., Kawano, S., Ide, T., et al. (2007a). Tumor necrosis factor-alpha is toxic via receptor 1 and protective via receptor 2 in a murine model of myocardial infarction. *Am. J. Physiol. Heart Circ. Physiol.* 293, H743–H753.

Monden, Y., Kubota, T., Tsutsumi, T., Inoue, T., Kawano, S., Kawamura, N., et al. (2007b). Soluble TNF receptors prevent apoptosis in infiltrating cells and promote ventricular rupture and remodeling after myocardial infarction. *Cardiovasc. Res.* 73, 794–805. doi: 10.1016/j.cardiores.2006.12.016

Monvoisin, A., Alva, J. A., Hofmann, J. J., Zovein, A. C., Lane, T. F., and Iruela-Arispe, M. L. (2006). VE-cadherin-CreERT2 transgenic mouse: a model for inducible recombination in the endothelium. *Dev. Dyn.* 235, 3413–3422. doi: 10.1002/dvdy.20982

Moore-Morris, T., Cattaneo, P., Guimaraes-Camboa, N., Bogomolovas, J., Cedenilla, M., Banerjee, I., et al. (2018). Infarct fibroblasts do not derive from bone marrow lineages. *Circ. Res.* 122, 583–590. doi: 10.1161/circresaha.117.311490

Moore-Morris, T., Guimaraes-Camboa, N., Banerjee, I., Zambon, A. C., Kisseleva, T., Velayoudon, A., et al. (2014). Resident fibroblast lineages mediate pressure overload-induced cardiac fibrosis. *J. Clin. Invest.* 124, 2921–2934. doi: 10.1172/jci74783

Mosmann, T. R., and Coffman, R. L. (1989). TH1 and TH2 cells: different patterns of lymphokine secretion lead to different functional properties. *Annu. Rev. Immunol.* 7, 145–173. doi: 10.1146/annurev.iy.07.040189.001045

Muller, J., Gorressen, S., Grandoch, M., Feldmann, K., Kretschmer, I., Lehr, S., et al. (2014). Interleukin-6-dependent phenotypic modulation of cardiac fibroblasts after acute myocardial infarction. *Basic Res. Cardiol.* 109:440.

Murphy, S. P., Kakkar, R., McCarthy, C. P., and Januzzi, J. L. Jr. (2020). Inflammation in heart failure: JACC State-of-the-art review. *J. Am. Coll. Cardiol.* 75, 1324–1340.

Mylonas, K. J., Jenkins, S. J., Castellan, R. F., Ruckerl, D., McGregor, K., Phythian-Adams, A. T., et al. (2015). The adult murine heart has a sparse, phagocytically active macrophage population that expands through monocyte recruitment and adopts an 'M2' phenotype in response to Th2 immunologic challenge. *Immunobiology* 220, 924–933. doi: 10.1016/j.imbio.2015.01.013

Nag, A. C. (1980). Study of non-muscle cells of the adult mammalian heart: a fine structural analysis and distribution. *Cytobios* 28, 41–61.

Nahrendorf, M., Swirski, F. K., Aikawa, E., Stangenberg, L., Wurdinger, T., Figueiredo, J. L., et al. (2007). The healing myocardium sequentially mobilizes two monocyte subsets with divergent and complementary functions. *J. Exp. Med.* 204, 3037–3047. doi: 10.1084/jem.20070885

Nazari, M., Ni, N. C., Ludke, A., Li, S. H., Guo, J., Weisel, R. D., et al. (2016). Mast cells promote proliferation and migration and inhibit differentiation of mesenchymal stem cells through PDGF. *J. Mol. Cell Cardiol.* 94, 32–42. doi: 10.1016/j.yjmcc.2016.03.007

Nevers, T., Salvador, A. M., Grodecki-Pena, A., Knapp, A., Velazquez, F., Aronovitz, M., et al. (2015). Left ventricular T-Cell recruitment contributes to the pathogenesis of heart failure. *Circ. Heart Fail.* 8, 776–787. doi: 10.1161/circheartfailure.115.002225

Noppert, S. J., Fitzgerald, K. A., and Hertzog, P. J. (2007). The role of type I interferons in TLR responses. *Immunol. Cell Biol.* 85, 446–457. doi: 10.1038/sj.icb.7100099

Oriente, A., Fedarko, N. S., Pacocha, S. E., Huang, S. K., Lichtenstein, L. M., and Essayan, D. M. (2000). Interleukin-13 modulates collagen homeostasis in human skin and keloid fibroblasts. *J. Pharmacol. Exper. Therap.* 292, 988–994.

Palmer, J. N., Hartogensis, W. E., Patten, M., Fortuin, F. D., and Long, C. S. (1995). Interleukin-1 beta induces cardiac myocyte growth but inhibits cardiac fibroblast proliferation in culture. *J. Clin. Invest.* 95, 2555–2564. doi: 10.1172/jci117956

Patel, B., Bansal, S. S., Ismahil, M. A., Hamid, T., Rokosh, G., Mack, M., et al. (2018). CCR2(+) Monocyte-derived infiltrating macrophages are required for adverse cardiac remodeling during pressure overload. *JACC Basic Transl. Sci.* 3, 230–244. doi: 10.1016/j.jacbts.2017.12.006

Patella, V., Marino, I., Arbustini, E., Lamparter-Schummert, B., Verga, L., Adt, M., et al. (1998). Stem cell factor in mast cells and increased mast cell density in idiopathic and ischemic cardiomyopathy. *Circulation* 97, 971–978. doi: 10.1161/01.cir.97.10.971

Penberthy, K. K., and Ravichandran, K. S. (2016). Apoptotic cell recognition receptors and scavenger receptors. *Immunol. Rev.* 269, 44–59. doi: 10.1111/imr.12376

Peng, H., Sarwar, Z., Yang, X. P., Peterson, E. L., Xu, J., Janic, B., et al. (2015). Profibrotic role for interleukin-4 in cardiac remodeling and dysfunction. *Hypertension* 66, 582–589. doi: 10.1161/hypertensionaha.115.05627

Petri, B., Phillipson, M., and Kubes, P. (2008). The physiology of leukocyte recruitment: an in vivo perspective. *J. Immunol.* 180, 6439–6446. doi: 10.4049/jimmunol.180.10.6439

Pinto, A. R., Ilinykh, A., Ivey, M. J., Kuwabara, J. T., D'Antoni, M. L., Debuque, R., et al. (2016). Revisiting cardiac cellular composition. *Circ. Res.* 118, 400–409. doi: 10.1161/circresaha.115.307778

Pinto, A. R., Paolicelli, R., Salimova, E., Gospocic, J., Slonimsky, E., Bilbao-Cortes, D., et al. (2012). An abundant tissue macrophage population in the adult murine heart with a distinct alternatively-activated macrophage profile. *PLoS One* 7:e36814. doi: 10.1371/journal.pone.0036814

Postlethwaite, A. E., Holness, M. A., Katai, H., and Raghow, R. (1992). Human fibroblasts synthesize elevated levels of extracellular matrix proteins in response to interleukin 4. *J. Clin. Invest.* 90, 1479–1485. doi: 10.1172/jci116015

Prabhu, S. D., and Frangogiannis, N. G. (2016). The biological basis for cardiac repair after myocardial infarction: from inflammation to fibrosis. *Circ. Res.* 119, 91–112. doi: 10.1161/circresaha.116.303577

Pruenster, M., Mudde, L., Bombosi, P., Dimitrova, S., Zsak, M., Middleton, J., et al. (2009). The Duffy antigen receptor for chemokines transports chemokines and supports their promigratory activity. *Nat. Immunol.* 10, 101–108. doi: 10.1038/ni.1675

Puhl, S. L., and Steffens, S. (2019). Neutrophils in Post-myocardial Infarction inflammation: damage vs. resolution? *Front. Cardiovasc. Med.* 6:25. doi: 10.3389/fphys.2017.00025

Rainer, P. P., Hao, S., Vanhoutte, D., Lee, D. I., Koitabashi, N., Molkentin, J. D., et al. (2014). Cardiomyocyte-specific transforming growth factor beta suppression blocks neutrophil infiltration, augments multiple cytoprotective cascades, and reduces early mortality after myocardial infarction. *Circ. Res.* 114, 1246–1257. doi: 10.1161/circresaha.114.302653

Ridker, P. M., Everett, B. M., Thuren, T., MacFadyen, J. G., Chang, W. H., Ballantyne, C., et al. (2017). Antiinflammatory therapy with canakinumab for atherosclerotic disease. *N. Engl. J. Med.* 377, 1119–1131.

Rienks, M., Papageorgiou, A. P., Frangogiannis, N. G., and Heymans, S. (2014). Myocardial extracellular matrix: an ever-changing and diverse entity. *Circ. Res.* 114, 872–888. doi: 10.1161/circresaha.114.302533

Rohde, D., Schon, C., Boerries, M., Didrihsone, I., Ritterhoff, J., Kubatzky, K. F., et al. (2014). S100A1 is released from ischemic cardiomyocytes and signals myocardial damage via Toll-like receptor 4. *EMBO Mol. Med.* 6, 778–794. doi: 10.15252/emmm.201303498

Russell, J. L., Goetsch, S. C., Gaiano, N. R., Hill, J. A., Olson, E. N., and Schneider, J. W. (2011). A dynamic notch injury response activates epicardium and contributes to fibrosis repair. *Circ. Res.* 108, 51–59. doi: 10.1161/circresaha.110.233262

Sandanger, O., Ranheim, T., Vinge, L. E., Bliksoen, M., Alfsnes, K., Finsen, A. V., et al. (2013). The NLRP3 inflammasome is up-regulated in cardiac fibroblasts and mediates myocardial ischaemia-reperfusion injury. *Cardiovasc. Res.* 99, 164–174. doi: 10.1093/cvr/cvt091

Sandstedt, J., Sandstedt, M., Lundqvist, A., Jansson, M., Sopasakis, V. R., Jeppsson, A., et al. (2019). Human cardiac fibroblasts isolated from patients with severe heart failure are immune-competent cells mediating an inflammatory response. *Cytokine* 113, 319–325. doi: 10.1016/j.cyto.2018.09.021

Sano, M., Fukuda, K., Kodama, H., Pan, J., Saito, M., Matsuzaki, J., et al. (2000). Interleukin-6 family of cytokines mediate angiotensin II-induced cardiac hypertrophy in rodent cardiomyocytes. *J. Biol. Chem.* 275, 29717–29723. doi: 10.1074/jbc.m003128200

Sansbury, B. E., and Spite, M. (2016). Resolution of acute inflammation and the role of resolvins in immunity, thrombosis, and vascular biology. *Circ. Res.* 119, 113–130. doi: 10.1161/circresaha.116.307308

Santiago, J. J., Dangerfield, A. L., Rattan, S. G., Bathe, K. L., Cunnington, R. H., Raizman, J. E., et al. (2010). Cardiac fibroblast to myofibroblast differentiation in vivo and in vitro: expression of focal adhesion components in neonatal and adult rat ventricular myofibroblasts. *Dev. Dyn.* 239, 1573–1584. doi: 10.1002/dvdy.22280

Savvatis, K., Pappritz, K., Becher, P. M., Lindner, D., Zietsch, C., Volk, H. D., et al. (2014). Interleukin-23 deficiency leads to impaired wound healing and adverse prognosis after myocardial infarction. *Circ. Heart Fail.* 7, 161–171. doi: 10.1161/circheartfailure.113.000604

Saxena, A., Chen, W., Su, Y., Rai, V., Uche, O. U., Li, N., et al. (2013). IL-1 induces proinflammatory leukocyte infiltration and regulates fibroblast phenotype in the infarcted myocardium. *J. Immunol.* 191, 4838–4848. doi: 10.4049/jimmunol.1300725

Schaefer, L., Babelova, A., Kiss, E., Hausser, H. J., Baliova, M., Krzyzankova, M., et al. (2005). The matrix component biglycan is proinflammatory and signals through Toll-like receptors 4 and 2 in macrophages. *J. Clin. Invest.* 115, 2223–2233. doi: 10.1172/jci23755

Scheibner, K. A., Lutz, M. A., Boodoo, S., Fenton, M. J., Powell, J. D., and Horton, M. R. (2006). Hyaluronan fragments act as an endogenous danger signal by engaging TLR2. *J. Immunol.* 177, 1272–1281. doi: 10.4049/jimmunol.177.2.1272

Serhan, C. N., Chiang, N., and Van Dyke, T. E. (2008). Resolving inflammation: dual anti-inflammatory and pro-resolution lipid mediators. *Nat. Rev. Immunol.* 8, 349–361. doi: 10.1038/nri2294

Shiota, N., Rysa, J., Kovanen, P. T., Ruskoaho, H., Kokkonen, J. O., and Lindstedt, K. A. (2003). A role for cardiac mast cells in the pathogenesis of hypertensive

heart disease. *J. Hypertens.* 21, 1935–1944. doi: 10.1097/00004872-200310000-00022

Simpson, P. J., Todd, R. F. III, Fantone, J. C., Mickelson, J. K., Griffin, J. D., and Lucchesi, B. R. (1988). Reduction of experimental canine myocardial reperfusion injury by a monoclonal antibody (anti-Mo1, anti-CD11b) that inhibits leukocyte adhesion. *J. Clin. Invest.* 81, 624–629. doi: 10.1172/jci113364

Siwik, D. A., Chang, D. L., and Colucci, W. S. (2000). Interleukin-1beta and tumor necrosis factor-alpha decrease collagen synthesis and increase matrix metalloproteinase activity in cardiac fibroblasts in vitro. *Circ. Res.* 86, 1259–1265. doi: 10.1161/01.res.86.12.1259

Siwik, D. A., and Colucci, W. S. (2004). Regulation of matrix metalloproteinases by cytokines and reactive oxygen/nitrogen species in the myocardium. *Heart Fail. Rev.* 9, 43–51. doi: 10.1023/b:hrev.0000011393.40674.13

Siwik, D. A., Pagano, P. J., and Colucci, W. S. (2001). Oxidative stress regulates collagen synthesis and matrix metalloproteinase activity in cardiac fibroblasts. *Am. J. Physiol. Cell Physiol.* 280, C53–C60.

Smart, N., Mojet, M. H., Latchman, D. S., Marber, M. S., Duchen, M. R., and Heads, R. J. (2006). IL-6 induces PI 3-kinase and nitric oxide-dependent protection and preserves mitochondrial function in cardiomyocytes. *Cardiovasc. Res.* 69, 164–177. doi: 10.1016/j.cardiores.2005.08.017

Sobirin, M. A., Kinugawa, S., Takahashi, M., Fukushima, A., Homma, T., Ono, T., et al. (2012). Activation of natural killer T cells ameliorates postinfarct cardiac remodeling and failure in mice. *Circ. Res.* 111, 1037–1047. doi: 10.1161/circresaha.112.270132

Soehnlein, O., and Lindbom, L. (2010). Phagocyte partnership during the onset and resolution of inflammation. *Nat. Rev. Immunol.* 10, 427–439. doi: 10.1038/nri2779

Sofat, N., Robertson, S. D., and Wait, R. (2012). Fibronectin III 13-14 domains induce joint damage via Toll-like receptor 4 activation and synergize with interleukin-1 and tumour necrosis factor. *J. Innate Immun.* 4, 69–79. doi: 10.1159/000329632

Somasundaram, P., Ren, G., Nagar, H., Kraemer, D., Mendoza, L., Michael, L. H., et al. (2005). Mast cell tryptase may modulate endothelial cell phenotype in healing myocardial infarcts. *J. Pathol.* 205, 102–111. doi: 10.1002/path.1690

Song, J., Wu, C., Zhang, X., and Sorokin, L. M. (2013). In vivo processing of CXCL5 (LIX) by matrix metalloproteinase (MMP)-2 and MMP-9 promotes early neutrophil recruitment in IL-1beta-induced peritonitis. *J. Immunol.* 190, 401–410. doi: 10.4049/jimmunol.1202286

Sousa, A. M., Liu, T., Guevara, O., Stevens, J., Fanburg, B. L., Gaestel, M., et al. (2007). Smooth muscle alpha-actin expression and myofibroblast differentiation by TGFbeta are dependent upon MK2. *J. Cell Biochem.* 100, 1581–1592. doi: 10.1002/jcb.21154

Sperr, W. R., Bankl, H. C., Mundigler, G., Klappacher, G., Grossschmidt, K., Agis, H., et al. (1994). The human cardiac mast cell: localization, isolation, phenotype, and functional characterization. *Blood* 84, 3876–3884. doi: 10.1182/blood.v84.11.3876.bloodjournal84113876

Squires, C. E., Escobar, G. P., Payne, J. F., Leonardi, R. A., Goshorn, D. K., Sheats, N. J., et al. (2005). Altered fibroblast function following myocardial infarction. *J. Mol. Cell Cardiol.* 39, 699–707. doi: 10.1016/j.yjmcc.2005.07.008

Stark, M. A., Huo, Y., Burcin, T. L., Morris, M. A., Olson, T. S., and Ley, K. (2005). Phagocytosis of apoptotic neutrophils regulates granulopoiesis via IL-23 and IL-17. *Immunity* 22, 285–294. doi: 10.1016/j.immuni.2005.01.011

Sugano, M., Tsuchida, K., Hata, T., and Makino, N. (2004). In vivo transfer of soluble TNF-alpha receptor 1 gene improves cardiac function and reduces infarct size after myocardial infarction in rats. *FASEB J.* 18, 911–913. doi: 10.1096/fj.03-1148fje

Summers, C., Rankin, S. M., Condliffe, A. M., Singh, N., Peters, A. M., and Chilvers, E. R. (2010). Neutrophil kinetics in health and disease. *Trends Immunol.* 31, 318–324. doi: 10.1016/j.it.2010.05.006

Sun, M., Dawood, F., Wen, W. H., Chen, M., Dixon, I., Kirshenbaum, L. A., et al. (2004). Excessive tumor necrosis factor activation after infarction contributes to susceptibility of myocardial rupture and left ventricular dysfunction. *Circulation* 110, 3221–3228. doi: 10.1161/01.cir.0000147233.10318.23

Suzuki, K., Murtuza, B., Smolenski, R. T., Sammut, I. A., Suzuki, N., Kaneda, Y., et al. (2001). Overexpression of interleukin-1 receptor antagonist provides cardioprotection against ischemia-reperfusion injury associated with reduction in apoptosis. *Circulation* 104(12 Suppl. 1), I303–I308.

Swirski, F. K., Nahrendorf, M., Etzrodt, M., Wildgruber, M., Cortez-Retamozo, V., Panizzi, P., et al. (2009). Identification of splenic reservoir monocytes and their deployment to inflammatory sites. *Science* 325, 612–616. doi: 10.1126/science.1175202

Takemura, G., Ohno, M., Hayakawa, Y., Misao, J., Kanoh, M., Ohno, A., et al. (1998). Role of apoptosis in the disappearance of infiltrated and proliferated interstitial cells after myocardial infarction. *Circ. Res.* 82, 1130–1138. doi: 10.1161/01.res.82.11.1130

Tarzami, S. T., Cheng, R., Miao, W., Kitsis, R. N., and Berman, J. W. (2002). Chemokine expression in myocardial ischemia: MIP-2 dependent MCP-1 expression protects cardiomyocytes from cell death. *J. Mol. Cell Cardiol.* 34, 209–221. doi: 10.1006/jmcc.2001.1503

Tarzami, S. T., Miao, W., Mani, K., Lopez, L., Factor, S. M., Berman, J. W., et al. (2003). Opposing effects mediated by the chemokine receptor CXCR2 on myocardial ischemia-reperfusion injury: recruitment of potentially damaging neutrophils and direct myocardial protection. *Circulation* 108, 2387–2392. doi: 10.1161/01.cir.0000093192.72099.9a

Teekakirikul, P., Eminaga, S., Toka, O., Alcalai, R., Wang, L., Wakimoto, H., et al. (2010). Cardiac fibrosis in mice with hypertrophic cardiomyopathy is mediated by non-myocyte proliferation and requires Tgf-beta. *J. Clin. Invest.* 120, 3520–3529. doi: 10.1172/jci42028

Torre-Amione, G., Anker, S. D., Bourge, R. C., Colucci, W. S., Greenberg, B. H., Hildebrandt, P., et al. (2008). Results of a non-specific immunomodulation therapy in chronic heart failure (ACCLAIM trial): a placebo-controlled randomised trial. *Lancet* 371, 228–236. doi: 10.1016/s0140-6736(08)60134-8

Travers, J. G., Kamal, F. A., Robbins, J., Yutzey, K. E., and Blaxall, B. C. (2016). Cardiac fibrosis: the fibroblast awakens. *Circ. Res.* 118, 1021–1040. doi: 10.1161/circresaha.115.306565

Tschumperlin, D. J. (2013). Fibroblasts and the ground they walk on. *Physiology* 28, 380–390. doi: 10.1152/physiol.00024.2013

Turner, N. A. (2016). Inflammatory and fibrotic responses of cardiac fibroblasts to myocardial damage associated molecular patterns (DAMPs). *J. Mol. Cell Cardiol.* 94, 189–200. doi: 10.1016/j.yjmcc.2015.11.002

Turner, N. A., Das, A., Warburton, P., O'Regan, D. J., Ball, S. G., and Porter, K. E. (2009). Interleukin-1alpha stimulates proinflammatory cytokine expression in human cardiac myofibroblasts. *Am. J. Physiol. Heart Circ. Physiol.* 297, H1117–H1127.

Urata, H., Healy, B., Stewart, R. W., Bumpus, F. M., and Husain, A. (1990a). Angiotensin II-forming pathways in normal and failing human hearts. *Circ. Res.* 66, 883–890. doi: 10.1161/01.res.66.4.883

Urata, H., Kinoshita, A., Misono, K. S., Bumpus, F. M., and Husain, A. (1990b). Identification of a highly specific chymase as the major angiotensin II-forming enzyme in the human heart. *J. Biol. Chem.* 265, 22348–22357.

van Amerongen, M. J., Bou-Gharios, G., Popa, E., van Ark, J., Petersen, A. H., van Dam, G. M., et al. (2008). Bone marrow-derived myofibroblasts contribute functionally to scar formation after myocardial infarction. *J. Pathol.* 214, 377–386. doi: 10.1002/path.2281

van Amerongen, M. J., Harmsen, M. C., van Rooijen, N., Petersen, A. H., and van Luyn, M. J. (2007). Macrophage depletion impairs wound healing and increases left ventricular remodeling after myocardial injury in mice. *Am. J. Pathol.* 170, 818–829. doi: 10.2353/ajpath.2007.060547

Van den Steen, P. E., Proost, P., Wuyts, A., Van Damme, J., and Opdenakker, G. (2000). Neutrophil gelatinase B potentiates interleukin-8 tenfold by aminoterminal processing, whereas it degrades CTAP-III, PF-4, and GRO-alpha and leaves RANTES and MCP-2 intact. *Blood* 96, 2673–2681. doi: 10.1182/blood.v96.8.2673

Van der Borght, K., Scott, C. L., Nindl, V., Bouche, A., Martens, L., Sichien, D., et al. (2017). Myocardial infarction primes autoreactive T cells through activation of dendritic cells. *Cell Rep.* 18, 3005–3017. doi: 10.1016/j.celrep.2017.02.079

Van Tassell, B. W., Raleigh, J. M., and Abbate, A. (2015). Targeting interleukin-1 in heart failure and inflammatory heart disease. *Curr. Heart Fail. Rep.* 12, 33–41. doi: 10.1007/s11897-014-0231-7

Varda-Bloom, N., Leor, J., Ohad, D. G., Hasin, Y., Amar, M., Fixler, R., et al. (2000). Cytotoxic T lymphocytes are activated following myocardial infarction and can recognize and kill healthy myocytes in vitro. *J. Mol. Cell Cardiol.* 32, 2141–2149. doi: 10.1006/jmcc.2000.1261

Vasilyev, N., Williams, T., Brennan, M. L., Unzek, S., Zhou, X., Heinecke, J. W., et al. (2005). Myeloperoxidase-generated oxidants modulate left ventricular

remodeling but not infarct size after myocardial infarction. *Circulation* 112, 2812–2820. doi: 10.1161/circulationaha.105.542340

Virag, J. I., and Murry, C. E. (2003). Myofibroblast and endothelial cell proliferation during murine myocardial infarct repair. *Am. J. Pathol.* 163, 2433–2440. doi: 10.1016/s0002-9440(10)63598-5

Wang, J., Duan, Y., Sluijter, J. P., and Xiao, J. (2019). Lymphocytic subsets play distinct roles in heart diseases. *Theranostics* 9, 4030–4046. doi: 10.7150/thno.33112

Wang, J., Seo, M. J., Deci, M. B., Weil, B. R., Canty, J. M., and Nguyen, J. (2018). Effect of CCR2 inhibitor-loaded lipid micelles on inflammatory cell migration and cardiac function after myocardial infarction. *Int. J. Nanomed.* 13, 6441–6451. doi: 10.2147/ijn.s178650

Wang, S., Voisin, M. B., Larbi, K. Y., Dangerfield, J., Scheiermann, C., Tran, M., et al. (2006). Venular basement membranes contain specific matrix protein low expression regions that act as exit points for emigrating neutrophils. *J. Exp. Med.* 203, 1519–1532. doi: 10.1084/jem.20051210

Wang, S., Wilkes, M. C., Leof, E. B., and Hirschberg, R. (2005). Imatinib mesylate blocks a non-Smad TGF-beta pathway and reduces renal fibrogenesis in vivo. *FASEB J.* 19, 1–11. doi: 10.1096/fj.04-2370com

Wei, C. C., Lucchesi, P. A., Tallaj, J., Bradley, W. E., Powell, P. C., and Dell'Italia, L. J. (2003). Cardiac interstitial bradykinin and mast cells modulate pattern of LV remodeling in volume overload in rats. *Am. J. Physiol. Heart Circ. Physiol.* 285, H784–H792.

Weirather, J., Hofmann, U. D., Beyersdorf, N., Ramos, G. C., Vogel, B., Frey, A., et al. (2014). Foxp3+ CD4+ T cells improve healing after myocardial infarction by modulating monocyte/macrophage differentiation. *Circ. Res.* 115, 55–67. doi: 10.1161/circresaha.115.303895

Wenzel, P., Knorr, M., Kossmann, S., Stratmann, J., Hausding, M., Schuhmacher, S., et al. (2011). Lysozyme M-positive monocytes mediate angiotensin II-induced arterial hypertension and vascular dysfunction. *Circulation* 124, 1370–1381. doi: 10.1161/circulationaha.111.034470

Williams, M. R., Azcutia, V., Newton, G., Alcaide, P., and Luscinskas, F. W. (2011). Emerging mechanisms of neutrophil recruitment across endothelium. *Trends Immunol.* 32, 461–469. doi: 10.1016/j.it.2011.06.009

Xu, J., Lin, S. C., Chen, J., Miao, Y., Taffet, G. E., Entman, M. L., et al. (2011). CCR2 mediates the uptake of bone marrow-derived fibroblast precursors in angiotensin II-induced cardiac fibrosis. *Am. J. Physiol. Heart Circ. Physiol.* 301, H538–H547.

Xue, J., Schmidt, S. V., Sander, J., Draffehn, A., Krebs, W., Quester, I., et al. (2014). Transcriptome-based network analysis reveals a spectrum model of human macrophage activation. *Immunity* 40, 274–288. doi: 10.1016/j.immuni.2014.01.006

Yan, X., Anzai, A., Katsumata, Y., Matsuhashi, T., Ito, K., Endo, J., et al. (2013). Temporal dynamics of cardiac immune cell accumulation following acute myocardial infarction. *J. Mol. Cell Cardiol.* 62, 24–35. doi: 10.1016/j.yjmcc.2013.04.023

Yan, X., Shichita, T., Katsumata, Y., Matsuhashi, T., Ito, H., Ito, K., et al. (2012). Deleterious effect of the IL-23/IL-17A axis and gammadeltaT cells on left ventricular remodeling after myocardial infarction. *J. Am. Heart Assoc.* 1:e004408.

Yang, Z., Zingarelli, B., and Szabo, C. (2000). Crucial role of endogenous interleukin-10 production in myocardial ischemia/reperfusion injury. *Circulation* 101, 1019–1026. doi: 10.1161/01.cir.101.9.1019

Yano, T., Miura, T., Ikeda, Y., Matsuda, E., Saito, K., Miki, T., et al. (2005). Intracardiac fibroblasts, but not bone marrow derived cells, are the origin of myofibroblasts in myocardial infarct repair. *Cardiovasc. Pathol.* 14, 241–246. doi: 10.1016/j.carpath.2005.05.004

Yokoyama, T., Vaca, L., Rossen, R. D., Durante, W., Hazarika, P., and Mann, D. L. (1993). Cellular basis for the negative inotropic effects of tumor necrosis factor-alpha in the adult mammalian heart. *J. Clin. Invest.* 92, 2303–2312. doi: 10.1172/jci116834

Ytrehus, K., Hulot, J. S., Perrino, C., Schiattarella, G. G., and Madonna, R. (2018). Perivascular fibrosis and the microvasculature of the heart. Still hidden secrets of pathophysiology? *Vascul. Pharmacol.* 107, 78–83. doi: 10.1016/j.vph.2018.04.007

Zarbock, A., Ley, K., McEver, R. P., and Hidalgo, A. (2011). Leukocyte ligands for endothelial selectins: specialized glycoconjugates that mediate rolling and signaling under flow. *Blood* 118, 6743–6751. doi: 10.1182/blood-2011-07-343566

Zeisberg, E. M., Tarnavski, O., Zeisberg, M., Dorfman, A. L., McMullen, J. R., Gustafsson, E., et al. (2007). Endothelial-to-mesenchymal transition contributes to cardiac fibrosis. *Nat. Med.* 13, 952–961.

Zhang, W., Chancey, A. L., Tzeng, H. P., Zhou, Z., Lavine, K. J., Gao, F., et al. (2011). The development of myocardial fibrosis in transgenic mice with targeted overexpression of tumor necrosis factor requires mast cell-fibroblast interactions. *Circulation* 124, 2106–2116. doi: 10.1161/circulationaha.111.052399

Zhang, W., Lavine, K. J., Epelman, S., Evans, S. A., Weinheimer, C. J., Barger, P. M., et al. (2015). Necrotic myocardial cells release damage-associated molecular patterns that provoke fibroblast activation in vitro and trigger myocardial inflammation and fibrosis in vivo. *J. Am. Heart Assoc.* 4:e001993.

Zhang, Y., Wang, J. H., Zhang, Y. Y., Wang, Y. Z., Wang, J., Zhao, Y., et al. (2016). Deletion of interleukin-6 alleviated interstitial fibrosis in streptozotocin-induced diabetic cardiomyopathy of mice through affecting TGFbeta1 and miR-29 pathways. *Sci. Rep.* 6:23010.

Zhao, L., and Eghbali-Webb, M. (2001). Release of pro- and anti-angiogenic factors by human cardiac fibroblasts: effects on DNA synthesis and protection under hypoxia in human endothelial cells. *Biochim. Biophys. Acta* 1538, 273–282. doi: 10.1016/s0167-4889(01)00078-7

Zouggari, Y., Ait-Oufella, H., Bonnin, P., Simon, T., Sage, A. P., Guerin, C., et al. (2013). B lymphocytes trigger monocyte mobilization and impair heart function after acute myocardial infarction. *Nat. Med.* 19, 1273–1280. doi: 10.1038/nm.3284

Zymek, P., Bujak, M., Chatila, K., Cieslak, A., Thakker, G., Entman, M. L., et al. (2006). The role of platelet-derived growth factor signaling in healing myocardial infarcts. *J. Am. Coll. Cardiol.* 48, 2315–2323. doi: 10.1016/j.jacc.2006.07.060

Zymek, P., Nah, D. Y., Bujak, M., Ren, G., Koerting, A., Leucker, T., et al. (2007). Interleukin-10 is not a critical regulator of infarct healing and left ventricular remodeling. *Cardiovasc. Res.* 74, 313–322. doi: 10.1016/j.cardiores.2006.11.028

Conflict of Interest: The authors declare that the research was conducted in the absence of any commercial or financial relationships that could be construed as a potential conflict of interest.

Advantages of publishing in Frontiers

OPEN ACCESS
Articles are free to read for greatest visibility and readership

FAST PUBLICATION
Around 90 days from submission to decision

HIGH QUALITY PEER-REVIEW
Rigorous, collaborative, and constructive peer-review

TRANSPARENT PEER-REVIEW
Editors and reviewers acknowledged by name on published articles

Frontiers
Avenue du Tribunal-Fédéral 34
1005 Lausanne | Switzerland

Visit us: www.frontiersin.org
Contact us: frontiersin.org/about/contact

REPRODUCIBILITY OF RESEARCH
Support open data and methods to enhance research reproducibility

DIGITAL PUBLISHING
Articles designed for optimal readership across devices

FOLLOW US
@frontiersin

IMPACT METRICS
Advanced article metrics track visibility across digital media

EXTENSIVE PROMOTION
Marketing and promotion of impactful research

LOOP RESEARCH NETWORK
Our network increases your article's readership